



Experimental study and modeling of hydrodynamic and heating characteristics of flighted rotary kilns

Alex Stéphane Bongo Njeng

► To cite this version:

Alex Stéphane Bongo Njeng. Experimental study and modeling of hydrodynamic and heating characteristics of flighted rotary kilns. Chemical and Process Engineering. Ecole des Mines d'Albi-Carmaux, 2015. English. NNT : 2015EMAC0009 . tel-01291791

HAL Id: tel-01291791

<https://theses.hal.science/tel-01291791>

Submitted on 22 Mar 2016

HAL is a multi-disciplinary open access archive for the deposit and dissemination of scientific research documents, whether they are published or not. The documents may come from teaching and research institutions in France or abroad, or from public or private research centers.

L'archive ouverte pluridisciplinaire **HAL**, est destinée au dépôt et à la diffusion de documents scientifiques de niveau recherche, publiés ou non, émanant des établissements d'enseignement et de recherche français ou étrangers, des laboratoires publics ou privés.



THÈSE

En vue de l'obtention du

DOCTORAT DE L'UNIVERSITÉ FÉDÉRALE DE TOULOUSE MIDI-PYRÉNÉES

Délivré par :

l'École Nationale Supérieure des Mines d'Albi-Carmaux conjointement avec l'INP Toulouse

Soutenue le 04/11/2015 par :

BONGO NJENG Alex Stéphane

**Experimental study and modeling of hydrodynamic and heating
characteristics of flighted rotary kilns.**

JURY

PATISSON FABRICE	Professeur des Universités, Ecole des Mines de Nancy	Rapporteur
HERZ FABIAN	Professeur des Universités, OvGU Magdebourg	Rapporteur
DIRION JEAN-LOUIS	Maitre-Assistant HDR, Ecole des Mines d'Albi-Carmaux	Directeur de thèse
CLAUSSE MARC	Professeur des Universités, INSA Lyon	Co-directeur de thèse
MARIAS FRÉDÉRIC	Professeur des Universités, ENSGTI Pau	Président
DEBACQ MARIE	Maitre des Conférences, CNAM Paris	Co-encadrante
VITU STÉPHANE	Maitre des Conférences, CNAM Paris	Invité
FLOQUET PASCAL	Professeur des Universités, INP-ENSIACET Toulouse	Invité

École doctorale et spécialité :

MEGEP : Énergétique et transferts

Unité de Recherche :

Centre RAPSODEE, CNRS - UMR 5302 de l'École des Mines d'Albi-Carmaux et le Laboratoire CMGPCE du Conservatoire National des Arts et Métiers Paris.

Directeur(s) de Thèse :

Dirion Jean-Louis et Clausse Marc

Rapporteurs :

Patissou Fabrice et Fabian Herz

Thesis conducted at RAPSODEE Center
Ecole des Mines d'Albi-Carmaux
Campus Jarlard, 81013 Albi

CMGPCE Laboratory
CNAM Paris
2 Rue Conté, 75003 Paris

Under the direction of Jean-Louis DIRION jean-louis.dirion@mines-albi.fr
Marc CLAUSSE marc.clausse@insa-lyon.fr

Co-supervisor Marie DEBACQ marie.debacq@cnam.fr
Stéphane VITU stephane.vitu@cnam.fr

Funding 2 short-term research contracts

EMOFOTOR

to my mother

Abstract

The present work addresses a fundamental study on flighted rotary kilns. They are gas-solid reactors, used in a variety of industries to process heterogeneous media. However, operating these kilns mainly relies on the know-how of operators due to insufficient fundamental understanding. The aim of this work is to provide engineers with relevant tools and models to assist in the design stage and the performance improvement of existing operating process units, in particular indirectly heated rotary kilns, inclined and equipped with lifters.

In the first part, we studied the effects of operating parameters on the flow of materials of differing properties and shape. For this purpose, residence time distribution measurements were performed through experimental stimulus response tests. Two pilot-scale rotary kilns with similar length-to-diameter ratios, but a dimension ratio of about two were used in this study. We focused on the effects of lifter shape and configurations. The effects of the rotational speed, the kiln slope, the mass flow rate and the exit dam height were also analyzed. The flow of solids was quantitatively characterized primarily by the experimental mean residence time, hold-up, and axial dispersion coefficient. Using a dimensional analysis, models were established to predict the mean residence time, the filling degree and the axial dispersion coefficient, providing basic information on the kiln design, solid particle properties and operating conditions.

In the second part, we studied the heat transfer mechanisms occurring in the flighted rotary kiln by measuring temperature profiles at the wall, the freeboard gas and the bulk of solids. Analysis of the temperature profiles focused on two main issues: assessment of the heat transfer coefficient between wall and gas, and assessment of the heat transfer coefficient between wall and solid particles. The lumped system analysis and a heat balance using the power supplied for the heating were applied to determine the experimental heat transfer coefficients. The effects of operating conditions and lifting flights were analyzed. Both heat transfer coefficients were then correlated through dimensional considerations. Lastly a global dynamic model mainly based on the models developed in this study can be used to determine wall, gas and bulk solids axial temperature profiles in an indirectly heated flighted rotary kiln. This global model needs to be completed with specific models related to a reaction so as to be used as a framework for the simulation of specific industrial rotary kilns.

Keywords: Rotary Kilns, Lifters, Dimensional Analysis, RTD, Heat Transfer Coefficient, Dynamic Model.

Acknowledgments

I feel an immense privilege and a real pleasure to express my deep sense of gratitude and I am indebted towards all those people who have encouraged, inspired and helped me during the thesis and its development. This thesis is the result of a collaborative work between two laboratories in France: the Laboratory CMGPCE from “Conservatoire National des Arts et Métiers” in Paris and the RAPSODEE Center from “Ecole des Mines d’Albi” located in Albi.

Foremost, I would like to thank my supervisory committee, constituted of Dr. M. DEBACQ, Dr. S. VITU and Pr. M. CLAUSSE from the Laboratory CMGPCE, and Dr. J-L. DIRION from the RAPSODEE center, for always finding the time in their busy schedules to attend work sessions mostly remote meetings because of the distance between the two laboratories. Through the entire course of this research, their fruitful suggestions, keen insight and encouragement were a real source of inspiration and driving force.

I am also indebted to the technicians from both laboratories for their contribution to the realization of the experimental aspect of the thesis work. In particular, sincere thanks are given to Mr. C. HAUSTANT for the technical assistance and cooperation in building, installation and testing of the experimental pilot-scale rotary dryer from the laboratory CMGPCE.

Deep appreciations are expressed to all faculty and staff members of both laboratories for their invaluable help, advice and true companionship all along the thesis preparation.

Finally, my acknowledgment would be incomplete if I did not include my loved ones. I would like to thank my friends and my family for their tremendous patience and their ever support without which this work would not have been possible.

Contents

Abstract	7
Acknowledgments	9
Contents	11
General introduction and thesis focus	15
Literature review	25
1 Literature review	27
1.1 Solid materials transport in rotary kilns	29
1.1.1 Characterization of solids transport in rotary kilns	29
1.1.2 Characteristics of flighted rotary kilns	38
1.1.3 Modeling the particle flow : the case of flighted rotary kilns	40
1.2 Heat transfer in rotary kilns	48
1.2.1 Heat transfer modes in rotary kilns	48
1.2.2 Heat transfer coefficients	50
1.3 Global models for rotary kilns	60
1.3.1 Non dynamic models	60
1.3.2 Dynamic models	61
1.4 Review Summary	62
Methodology	63
2 Methodology	65
2.1 Experimental apparatus	68
2.1.1 General characteristics	68
2.1.2 Thermal metrology	70
2.1.3 Internal and external fixtures, features or devices	71

2.2	Materials properties	73
2.2.1	Selected solids: physical properties	73
2.2.2	Thermo-physical properties	75
2.3	Experimental procedures	77
2.3.1	Hydrodynamics	77
2.3.2	Temperature profile measurements	85
2.4	Dimensional analysis	87
2.5	Methodology summary	88

Hydrodynamic characteristics of flighted rotary kilns: experiments and modeling 89

3 Effect of lifter shape and operating parameters on the flow of materials in a pilot rotary kiln : Part I. Experimental RTD and axial dispersion study 91

Abstract	92
3.1 Introduction	93
3.2 Materials and methods	94
3.2.1 Apparatus and materials	94
3.2.2 Experimental technique	96
3.3 Data processing	97
3.4 Results and discussion	99
3.4.1 Axial dispersion model	100
3.4.2 Influence of operating variables and nature of materials on the RTD	101
3.4.3 Influence of operating variables and nature of materials on the Pe and D .	106
3.5 Conclusions	109

4 Effect of lifter shape and operating parameters on the flow of materials in a pilot rotary kiln : Part II. Experimental hold-up and mean residence time modeling 113

Abstract	114
4.1 Introduction	115
4.2 Materials and methods	117
4.2.1 Apparatus and materials	117
4.2.2 Experimental technique	118
4.3 Results and discussion	118
4.3.1 Hold-up, volume fraction	118
4.3.2 Mean residence time	121
4.4 Conclusions	129
4.5 Appendices	131
4.5.1 Geometrical characteristics and operating conditions of some kilns	131

5 Effect of lifter shape and operating parameters on the flow of materials in a pilot rotary kiln : Part III. Up-scaling considerations and segregation analysis 133

Abstract	134
5.1 Introduction	135
5.2 Materials and methods	136
5.2.1 Apparatus and materials	136
5.2.2 Experimental procedure	137
5.2.3 Data processing	138

5.3	Results and discussion	140
5.3.1	Influence of operating variables on the experimental RTD, MRT, VRT and HU	140
5.3.2	Influence of operating variables on the experimental Pe and D	145
5.3.3	Modeling: MRT, HU and D	145
5.3.4	Analysis of particle segregation	149
5.3.5	Reproducibility of experiments	151
5.4	Conclusion	152
5.5	Appendices	155
5.5.1	Experimental Results: HU, MRT, VRT, Pe, D	155

Heat transfer in flighted rotary kilns: experiments and modeling 157

6 Evaluation of the wall-to-gas and wall-to-solid heat transfer coefficients in flighted rotary kilns: Lumped system analysis 159

Abstract	160
6.1 Introduction	161
6.2 Materials and methods	162
6.2.1 Apparatus and materials	162
6.2.2 Experimental procedure	164
6.3 Results and discussion	167
6.3.1 Lumped system analysis	167
6.3.2 Wall-to-gas heat transfer coefficient	168
6.3.3 Wall-to-solid heat transfer coefficient	173
6.3.4 Biot number	177
6.4 Conclusion	177
6.5 Appendices	180
6.5.1 Bulk bed conductivity model	180
6.5.2 Evaluation of the lifter effective heating length	180
6.5.3 Experimental matrix	181

7 Wall-to-solid heat transfer coefficient in flighted rotary kilns: experimental determination and modeling 183

Abstract	184
7.1 Introduction	185
7.2 Materials and methods	186
7.2.1 Apparatus and materials	186
7.2.2 Experimental procedure	188
7.3 Heat transfer	189
7.3.1 Heat transfer mechanisms	189
7.3.2 Heat balance	192
7.3.3 Convection and radiation modeling	193
7.3.4 Estimation of heat transfer areas	194
7.4 Results and discussion	197
7.4.1 Experimental wall-to-solid heat transfer coefficient	197
7.4.2 Modeling of the wall-to-solid heat transfer coefficient	200
7.5 Conclusion	203
7.6 Appendices	206
7.6.1 Calculation of the heat losses through the insulation	206

7.6.2	Bed depth profile measurements	207
7.6.3	Uncertainties calculations	208
7.6.4	Experimental results: wall-to-solid heat transfer coefficient	208
8	A simplified global model for the prediction of axial temperature profiles in flighted rotary kilns	211
	Abstract	212
8.1	Introduction	213
8.2	Model description	214
8.2.1	Description of the flow model	214
8.2.2	Description of the thermal model	218
8.3	Experimental data for validation of the global model	223
8.4	Results and discussion	224
8.4.1	Steady state simulation	225
8.4.2	Dynamic simulation	229
8.5	Conclusion	230
8.6	Appendices	233
8.6.1	Experimental apparatus characteristics	233
8.6.2	Model parameters	233
	Conclusions and recommendations	235
	Appendices	245
A	Experimental apparatus	247
B	Solids transport characterization	249
B.1	Dispersion models: analytical solutions	249
B.1.1	The «open» dispersion model	249
B.1.2	The «closed» dispersion model	249
B.2	Residence time distribution results	250
B.2.1	Results from RK1	250
B.2.2	Results from RK2	255
B.3	Bed depth measurements results	260
C	Heat transfer	261
C.1	Experiments with rectangular lifters	262
C.2	Experiments without lifters	265
C.3	Experiments with straight lifters	269
C.3.1	Experiments without solids flow	269
C.3.2	Experiments with solids flow	271
	Bibliography	281
	List of Figures	297
	List of Tables	305

General introduction and thesis focus

Background

Heterogeneous media are frequently encountered in different fields of science and industry. These systems are usually processed within gas-solid reactors that use specific contacting methods, such as moving bed, fluidized bed, bulk bed or entrained flow of solids. Among the existing reactors acting as gas-solid contactors, this study focuses on the rotary kiln, also known as rotary dryer when operated at low temperature. This type of reactor is one of the most widely used in industry, in particular for calcining, clinkering, reacting, mixing, heating or cooling particulate solids.

Rotary kilns provide a number of functions necessary for the processing of raw materials. In addition to serving as vessels for chemical reactions, they provide the conveyance of solids and a mechanism for heat exchange. These units are equally applicable to solids, sludges, and slurries and are even capable of receiving and processing simultaneously liquids and solids as reported by [Schaefer 1988]. This ability of rotary kilns to handle an extensive range of feedstock has promoted their use in a variety of basic industries, especially for coarse or free-flowing materials, initially in the cement and metallurgical ore industries, then in the mineral, chemical and pharmaceutical industries, and more recently in food, fertilizer and waste disposal industries.

Rotary kiln design varies greatly. However, the majority of rotary kilns consist of a straight cylindrical tube. Kiln sizes range from small bench-scale apparatus used mostly for low production rates, to large installations over 150 m long and 6 m in diameter for example in the cement industry. Fundamentally, rotary kilns are heat exchangers: the energy can be supplied either directly or indirectly. In directly heated rotary kilns, a hot gas generated usually by an axial-burner is introduced either co-currently or counter-currently to the solid flow, while indirectly heated rotary kilns are electrically heated or gas fired at the outer wall, in specific control zones; in this way a clean heating can be achieved, if contact between the heat source and material is undesirable. They may also be equipped with internal fixtures such as dams or baffles, used to increase the material residence time; lifters are also often used. Lifters of different shapes exist; they collect and carry the solids from the lower to the upper half of the kiln tube, and then cascade the solids across the width of the kiln tube. Lifters are also used in some cases to promote particle mixing [Boateng 2008]. The kiln slope may produce a slight forward axial displacement of solids toward the kiln exit end.

From the process engineering point of view, the design and the modeling of rotary kilns depends on the clear definition and understanding of the following issues: the flow of solids and gas, the heat transfer, the mass transfer and the reaction kinetic.

General framework and purpose

The present work addresses a fundamental study of solid transport characteristics and heat transfer mechanisms within rotary kilns. The aim of this work is to provide engineers with relevant tools and models to assist in the design stage and the performance improvement of existing operating process units, in particular indirectly heated rotary kilns, inclined and equipped with lifters. Developing such tools or models requires a significant amount of experimental data, which are quite long and sometimes very difficult to obtain, especially when operating industrial kilns, due to the slowdown in production and delays induced. In addition, most of the models developed in previous research are empirical or mechanistic, and therefore often lack predictive capabilities without smart preliminary fitting of parameters. Others are highly complex and system-specific in an attempt to take into account the large number of parameters controlling the process. In this study, the objective is to use dimensional analysis in order to design a suitable experimental campaign and set scaling rules, which can then be applied to a variety of kilns operating in different conditions.

As highlighted above, the purpose is to characterize the flow characteristics of solids, for example, the residence time distribution, the mean residence time, hold-up, or axial dispersion coefficient, by defining an experimental procedure to determine these quantities. Two pilot-scale rotary kilns with similar length-to-diameter ratios, but a dimension ratio of about two, were used to perform the experimental measurements. The effects of operating parameters on the flow of materials of differing properties and shapes are to be determined. A further aim, using dimensional analysis, is to establish models for the prediction of some important flow parameters such as the mean residence time, the filling degree or the axial dispersion coefficient.

The second main objective of this work is to investigate the heat transfer phenomena in rotary kilns. This is to be achieved through experimental determination of the heat transfer coefficient between wall and gas, and of the heat transfer coefficient between wall and solid particles. For this purpose, experimental procedures must be devised for the measurement of temperature profiles at the wall, the freeboard gas and the bulk of solids within a pilot-scale indirectly heated rotary kiln. The effects of operating conditions and lifting flights must be analyzed. Then for the purpose to be predicted, both heat transfer coefficients need to be correlated through dimensional considerations.

The final aim is to establish a global dynamic model, mainly based on the models developed in this study, that can be used to determine wall, gas and bulk solids axial temperature profiles in an indirectly heated flighted rotary kiln.

Structure of the thesis

The main body of this thesis contains six papers that are presented in the last six Chapters of the manuscript and separated into two parts. Among these papers, two have been published, one has been submitted and three will be submitted shortly for publication.

The *first part* of this thesis is dedicated to a literature review pertaining to solid transport and heat transfer in flighted rotary kilns; this is presented in **Chapter 1**. The experimental methods used to characterize the solids transport in terms of residence time distribution, along with some modeling of the distributions, are first presented. After a survey of the classifications of flighted rotary kilns and various lifter shapes, the main modeling approaches used to describe the solids transport characteristics are reported. This is followed by a description of the main paths of heat transfer within the kiln during heating operation. The experimental procedures used to determine the wall-to-solid and convective heat transfer coefficients, as well as some models used for their prediction, are then presented. Lastly, global models for rotary kilns are briefly described. Both dynamic and non dynamic models are reported.

The *second part* of this thesis describes in **Chapter 2** the overall methodology used in this study. The methodology is based on dimensional analysis, completed by systematic experimentation. Along with the research methodology developed, the experimental apparatus, in particular the two pilot-scale rotary kilns used, are described; the smaller kiln is installed at the CMGPCE laboratory and the larger one is at the RAPSODEE center. The properties of the materials and the experimental procedures used for the study of solids transport and heat transfer characteristics are also fully detailed. The dimensional analysis which is used several times in the study to model solids transport characteristics and heat transfer coefficients is also presented.

The *third part* of this thesis deals specifically with the experimental and modeling study of the hydrodynamic characteristics of the flighted rotary kilns, which is developed in Chapters 3 to 5. Using the experimental setup at the CMGPCE laboratory, a comprehensive experimental study of the residence time distribution (RTD) was conducted at room temperature for the continuous flow of sand and broken rice. Factors such as the rotational speed, the kiln slope, the solids flow rate and the exit dam height were studied. Furthermore, two lifter profiles were used: straight lifters (SL) and rectangular lifters (RL). From these experiments flow characteristics such as RTD curves, mean and variance of residence time (MRT and VRT), Peclet number (Pe) and axial dispersion coefficient (D), and the kiln hold-up (HU) were determined.

Chapter 3 focuses on the RTD curves, which are obtained through a typical stimulus response test using a tracer, and the corresponding axial dispersion coefficients. The validity of the axial dispersion model is assessed with regard to the experimental data, and the effects of operating parameters on the solids flow characteristics are analyzed. A correlation for the prediction of the axial dispersion coefficient of the solid particles within the kiln is established and tested against reported models.

Chapter 4 investigates the effects of operating parameters on the experimental HU and MRT of solid particles within the kiln. A model for the MRT is developed using dimensional analysis. The predictive performances of the correlation, which is established from the experimental data in this study, are tested against published experimental data of other rotary kilns.

Chapter 5 describes similar experiments carried out in the apparatus at the RAPSODEE center, which is twice as large as the kiln previously used; up-scaling tracer experiments were carried out while processing granular biomass materials (beech chips). Removable internal fixtures such as a grid, or a lifter structure arranged in 3 and 6 rows of single throughout lifters were used. The effects of these fixtures and other usual operating conditions, as given above, on the RTD, MRT and VRT, HU, Pe and corresponding D, were investigated. Then using the whole data set (including sand, rice, and beech chips), scaling-up rules were derived for the MRT, HU volume fraction and D; they are determined for application to inclined kilns that process materials in cascading (tumbling) motion, whether equipped with lifters or not or fitted with dams at the outlet end. The wide size distribution of the beech chips allows analysis of particle segregation whether the kiln is equipped with internal fixtures or not.

The *fourth part* of this thesis deals specifically with the experimental and modeling study of the heat transfer in flighted rotary kilns, presented in Chapters 6 to 8. The experiments carried out in this part were performed using the indirectly heated pilot-scale rotary kiln installed at the CMGPCE laboratory, which is equipped with thermocouples for high temperature metrology. Under varying operating conditions, temperature profiles of the gas phase, the bulk of solids particles and the wall were recorded following kiln wall tube heating at low to medium setpoint temperatures (100-500°C) for the continuous flow of sand particles; however, certain experiments were performed without solid flow. The overall experimental campaign primarily aims at investigating convective and wall-to-solid heat transfer coefficients. In accordance with the dimensional analysis of these coefficients, some operating conditions, namely rotational speed, filling degree, lifters and control temperature, were varied during the experiments.

In **Chapter 6**, the wall-to-gas and wall-to-solid heat transfer coefficients are determined from

the experimental data by applying the lumped system analysis to the gas and solid phase. A dimensional correlation based on experimental results is then presented for the Nusselt number relative to convective heat transfer, which may be used when there is no forced axial gas flow. The effect of operating conditions on both coefficients are analyzed, and notably the lifter design.

In **Chapter 7**, readings of the power supplied for the heating throughout the experiments allowed the determination of the experimental wall-to-solid heat transfer coefficient using an energy balance. These results are analyzed in relation to those from the lumped system analysis. A model based on dimensional analysis is proposed for the calculation of the wall-to-solid heat transfer coefficient for low to medium setpoint temperatures. The experimental results are also compared to the predictions of models selected from the literature.

Lastly, in **Chapter 8**, using the models developed in this study, a simple model for indirectly heated flighted rotary kilns is developed for the prediction of axial profiles and transient responses of the temperature of the solid bed, free-board gas, and kiln wall. The results from the simulation of the overall model are compared with experimental data. The model validation is performed in the absence of any chemical reaction in order to validate the sub-models used for the predictions of flow characteristics as well as the heat transfer fluxes, notably the convective heat transfer and the wall-to-solid heat transfer. A sensitivity analysis of the model was carried out. Dynamic simulations of the model were also investigated. The model presented is intended to serve as the backbone for the simulation of a kiln handling specific reactions.

Finally, the main conclusions of the experimental and modeling study achieved to further understand the mechanisms of solids transportation and heat transfer within flighted rotary kilns are summarized along with some perspectives and recommendations.

For Chapters 3 to 8, a nomenclature is provided at the end of each Chapter.

Introduction et objectifs de la thèse

Contexte

Les matériaux granulaires ou plus généralement les milieux hétérogènes sont très souvent rencontrés dans différents domaines des sciences et de l'industrie. Ces matériaux sont généralement traités dans des contacteurs gaz/solide tels que des réacteurs à lits fixe, mobile ou fluidisé. Parmi les solutions technologiques existantes, les fours tournants ou rotatifs, aussi connus sous le nom de séchoirs rotatifs lorsqu'utilisés à faible température, seront considérés dans cette étude. Ce type de contacteur est largement utilisé dans l'industrie, en particulier pour effectuer des traitements tels que la calcination, la clinkérisation, le chauffage, le séchage ou le refroidissement des particules solides, ou tout simplement pour effectuer un mélange.

Les fours tournants offrent une certaine facilité pour le traitement des matériaux solides divisés. En plus de servir de contenant pour le déroulement des réactions chimiques, ils jouent le rôle d'échangeur de chaleur et assurent le transport de la charge solide. Ces équipements s'appliquent aussi bien aux particules solides qu'aux mélanges de boues ou de pâtes. Ils peuvent ainsi traiter simultanément des mixtures de liquides et solides [Schaefer 1988]. Leur grande flexibilité et la diversité des matériaux pouvant être traités a favorisé l'utilisation des fours tournants dans de nombreux domaines telles que la cimenterie, la métallurgie, la chimie et la pharmacie, mais aussi dans l'alimentaire, les fertilisants ou le traitement des déchets.

La conception des fours tournants varie d'un équipement à l'autre. Cependant, dans la majorité des cas les fours tournants sont constitués d'un cylindre droit, dont les dimensions vont du banc de laboratoire, principalement utilisé pour les faibles flux de production, aux grandes installations industrielles de plus de 150 m de long et 6 m de diamètre en cimenterie par exemple. Les fours tournants sont en premier lieu des échangeurs de chaleur, en mode de chauffage direct ou indirect. Dans les fours rotatifs à chauffage direct, un gaz chaud généralement issu d'un brûleur est introduit à co-courant ou à contre-courant de l'écoulement des particules solides ; tandis que les fours rotatifs à chauffage indirect sont chauffés par des résistances électriques ou un flux de gaz chaud circulant à la paroi externe, sur une ou plusieurs zones pouvant être indépendamment chauffées. De cette manière, un chauffage "propre" peut être obtenu, en particulier lorsque le contact entre la source de chaleur et la matière à traiter est indésirable. Les fours tournants peuvent également être équipés d'installations internes tels que des diaphragmes ou chicanes, utilisés pour augmenter le temps de séjour des particules solides ; des releveurs sont également très souvent utilisés. Il existe de nombreuses formes de releveurs ; ces derniers permettent de collecter et transporter les particules solides du lit, de la partie inférieure à la moitié supérieure du tube, et ensuite les solides sont déversés à nouveau dans le lit de particules. Les releveurs

sont également utilisés dans certains cas, afin d'améliorer le mélange des solides [Boateng 2008]. La faible inclinaison des fours tournants est principalement à l'origine du déplacement axial des solides vers la sortie.

Du point de vue du génie des procédés, la conception et la modélisation des fours tournants dépend de la définition claire et la compréhension des points suivants : l'écoulement des phases solide et gazeuse, le transfert de chaleur, le transfert de matière et la cinétique des réactions en jeu.

Objectifs

L'objectif de ces travaux est de réaliser une étude fondamentale des caractéristiques du transport des particules solides et des mécanismes de transfert de chaleur dans les fours tournants. Ces travaux permettront de fournir aux ingénieurs des outils et modèles pertinents pour les accompagner de la conception de nouvelles unités à l'optimisation des performances des appareils existants, en particulier les fours tournant à chauffage indirect, inclinées et équipés de releveurs. Le développement de tels outils ou modèles nécessite une quantité importante de données expérimentales, très souvent couteuse en temps et difficile de mise en œuvre, en particulier en industrie, en raison du ralentissement de la production et des retards induits. En outre, la plupart des modèles développés dans les travaux précédents sont empiriques, et manquent donc de capacités prédictives ; une paramétrisation est généralement nécessaire au préalable. On trouve aussi des modèles très complexes et prenant en compte un grand nombre de paramètres se restreignant ainsi à des systèmes spécifiques. Dans cette étude, l'analyse dimensionnelle est utilisée afin de concevoir d'une part des campagnes expérimentales appropriées, et d'autre part mettre en place aux travers de modèles des extrapolations raisonnées, applicables à une variété de fours rotatifs fonctionnant dans des conditions opératoires différentes.

Comme indiqué ci-dessus, l'un des objectifs est de caractériser l'écoulement des solides divisés, en analysant entre autre, la distribution de temps de séjour, le temps de séjour moyen, le taux de remplissage du four, ou le coefficient de dispersion axiale ; cela est mis en oeuvre en définissant un protocole expérimental permettant de déterminer ces quantités. Deux fours rotatifs à l'échelle pilote avec des ratios longueur sur diamètre similaires, mais un rapport de dimension ou de taille d'environ deux, ont été utilisés pour effectuer les mesures expérimentales. Les effets des paramètres opératoires sur l'écoulement de particules solides de propriétés physiques différentes sont analysés. A l'aide de l'analyse dimensionnelle, sont établis des modèles pour la prédiction de certaines caractéristiques importantes de l'écoulement des particules solides telles que le temps de séjour moyen, le taux de remplissage ou le coefficient de dispersion axiale.

Le second objectif principal de ce travail est l'étude des phénomènes de transfert de chaleur dans les fours tournants. Le focus est mis en particulier sur la détermination expérimentale du coefficient de transfert de chaleur entre la paroi et la phase gazeuse, et celle du coefficient de transfert de chaleur entre la paroi et le lit de particules solides. Pour ce faire, dans un four tournant à chauffage indirect, des procédures expérimentales sont mises au point pour la mesure des profils de température à la paroi, dans la phase gazeuse et le lit de particules solides. L'impact des releveurs et des conditions opératoires utilisés, est analysé. Enfin, dans le but d'estimer les valeurs des deux coefficients de transfert de chaleur, ces derniers sont corrélés par analyse dimensionnelle.

L'objectif final de ce travail est d'établir un modèle global dynamique de fours tournants, principalement basé sur les sous-modèles développés dans cette étude, et ayant pour but de déterminer les profils de température axiale en particulier dans le cas de fours rotatifs à chauffage indirect et équipés de releveurs.

Organisation de la thèse

Le corps principal de cette thèse est composé de six articles de recherche qui sont contenus dans les six derniers chapitres du manuscrit, séparés en deux parties. Parmi ces articles, deux ont été publiés (Chapitres 3 et 4), l'un a été soumis (Chapitre 5) et trois seront soumis sous peu pour publication (Chapitres 6, 7 et 8).

La *première partie* de cette thèse est consacrée à un état de l'art concernant le transport des particules solides et le transfert de chaleur dans les fours tournants équipés de releveurs ; cela est présenté dans le **Chapitre 1**. Les méthodes expérimentales utilisées pour caractériser le transport de particules solides en terme de distribution de temps de séjour, ainsi que les modèles utilisés pour représenter ces distributions, sont tout d'abord présentés. Après une présentation de quelques profils de releveurs utilisés couramment ainsi que celle de la classification des fours tournants lorsqu'équipés de releveurs, les principaux modèles utilisés pour décrire les caractéristiques du transport des particules solides sont abordés. Ceci est suivi par une description des principaux phénomènes de transfert de chaleur se produisant au cours du chauffage des fours tournants. Les procédures expérimentales utilisées pour déterminer les coefficients de transfert de chaleur paroi/solide et de convection entre la paroi et la phase gazeuse, ainsi que les modèles prédictifs existants, sont ensuite présentés. Enfin, les modèles globaux pour les fours tournants sont brièvement décrits. Les deux types de modèles, dynamiques et non dynamiques sont présentés.

La *deuxième partie* de cette thèse décrit dans le **Chapitre 2** la méthodologie générale utilisée dans cette étude. Cette méthodologie basée sur l'analyse dimensionnelle intègre de nombreux essais expérimentaux. Sont ici explicités : la méthodologie de recherche employée, le dispositif expérimental utilisé, en particulier les deux fours tournants à l'échelle pilote sont décrits ; le four de plus petite taille est installé au laboratoire CMGPCE et le second est au centre RAPSODEE. Les propriétés des matériaux ainsi que les procédures expérimentales utilisés tout au long de l'étude des caractéristiques du transport de particules solides et du transfert de chaleur sont également entièrement détaillées. L'analyse dimensionnelle qui est utilisée plusieurs fois au cours de ce travail pour modéliser les caractéristiques de transport des particules solides et des coefficients de transfert de chaleur est également succinctement présentée.

La *troisième partie* de cette thèse traite spécifiquement de l'étude expérimentale et la modélisation des caractéristiques hydrodynamiques des fours tournants équipés de releveurs, ceci est développé dans les Chapitres 3 à 5. Le dispositif installé au laboratoire CMGPCE, est utilisé pour réaliser une étude expérimentale de la distribution de temps de séjour (DTS) pour l'écoulement de sable et de riz à température ambiante. Les effets de la vitesse de rotation et l'inclinaison du four, le débit massique en entrée et la hauteur du diaphragme en sortie ont été étudiés. Par ailleurs, deux profils de releveurs ont été testés : des releveurs plats (RP) et des releveurs rectangulaires (RR). Les résultats de ces expériences permettent de déterminer certaines caractéristiques de l'écoulement telles que les courbes de DTS, le temps de séjour moyen (TSM) et la variance de la distribution (VD), le nombre de Péclet (Pe) et le coefficient de dispersion axiale (D), et le taux de remplissage du four (TR).

Le **Chapitre 3** met l'accent sur les courbes de DTS et les coefficients de dispersion axiale correspondants, qui sont obtenus pour différentes conditions opératoires suite à une injection impulsion de traceurs dans le pilote installé au laboratoire CMGPCE. La validité du modèle de dispersion axiale sélectionné est évaluée, et les effets des paramètres opératoires sur les caractéristiques d'écoulement des solides sont analysés. Une corrélation est proposée pour la prédiction du coefficient de dispersion axiale des particules solides et une comparaison de ses résultats avec ceux de modèles existants dans la littérature est rapportée.

Le **Chapitre 4** étudie les effets des paramètres opératoires sur le taux de remplissage et le temps de séjour moyen des particules solides dans le pilote installé au laboratoire CMGPCE. Un

modèle est développé pour le temps de séjour moyen en utilisant l'analyse dimensionnelle. Les performances prédictives de la corrélation obtenue et paramétrée à l'aide des données expérimentales mesurées dans cette étude, sont évaluées par rapport aux données expérimentales publiées d'autres fours tournants.

Le **Chapitre 5** reprend les expériences effectuées précédemment, mais cette fois-ci dans le pilote installé au centre RAPSODEE qui est deux fois plus grand que le four utilisé précédemment ; ces expériences ont consisté à effectuer des mesures de DTS sur de la biomasse (copeaux de bois). Des éléments internes amovibles tels qu'une grille, ou une structure équipée de 3 ou 6 rangées de relevateurs ont été utilisés. Les effets de ces équipements amovibles et des conditions opératoires, comme indiqués ci-dessus, sur la distribution du temps de séjour, le temps de séjour moyen et la variance de la distribution, le taux de remplissage du four, le nombre de Pécelet et le coefficient de dispersion axiale pour l'écoulement de plaquettes de bois de hêtre ont été étudiés. Sur la base d'analyse dimensionnelle, et en tenant compte de l'ensemble des résultats y compris ceux issus du sable et du riz, des corrélations ont été proposées pour la prédiction du temps de séjour moyen, du taux de remplissage et du coefficient de dispersion axiale. Ces corrélations pourront être appliquées au cas de fours tournants inclinés, équipés ou non de relevateurs et/ou de diaphragme en sortie, et traitant des matériaux solides s'écoulant notamment en régime d'avalanche. La dispersion de taille des particules de bois utilisées a permis l'étude de phénomènes de ségrégation, en particulier en présence de relevateurs.

La *quatrième partie* de cette thèse traite spécifiquement de l'étude expérimentale et la modélisation du transfert de chaleur dans les fours tournants équipés de relevateurs, ceci est développé dans les Chapitres 6 à 8. Les expériences menées dans ce cadre ont été effectuées en utilisant le four tournant installée au laboratoire CMGPCE fonctionnant en chauffage indirect, et équipé de thermocouples pour la mesure de haute température. Pour diverses conditions opératoires, les profils de température de la phase gazeuse, du lit de particules solides et de la paroi du tube du four ont été enregistrés à la suite du chauffage du tube du four à des températures de consigne de douce à chaude (100-500 ° C) pour un écoulement continu de particules de sable. Cependant, certaines expériences ont été réalisées à vide. La campagne expérimentale vise dans son ensemble principalement à déterminer d'une part le coefficient de transfert convectif paroi/gaz, et d'autre part le coefficient de transfert de chaleur de paroi/solide. Conformément à l'analyse dimensionnelle appliquée en vue de la détermination de ces coefficients, les valeurs de certaines conditions opératoires, à savoir la vitesse de rotation du tube, le taux de remplissage, les relevateurs et de la température de chauffage, ont été variées au cours de ces essais.

Dans le **Chapitre 6**, le coefficient de transfert convectif entre la paroi et le gaz et le coefficient de transfert entre la paroi et les particules solides ont été déterminés à partir des relevés de température en utilisant une analyse globale supposant des systèmes minces. Basée sur les résultats expérimentaux, une corrélation sous la forme d'un produit de nombres sans dimension est ensuite proposée et représente un nombre de Nusselt relatif au transfert de chaleur par convection, en absence de convection forcée de gaz à l'intérieur du tube. L'effet des conditions opératoires sur les deux coefficients sont analysés, et notamment l'impact du design des relevateurs.

Dans le **Chapitre 7**, les relevés de puissance fournie tout au long des expériences pour le chauffage du four rotatif ont permis la détermination expérimentale du coefficient d'échange paroi/solide à partir de bilans énergétiques. Ces résultats sont analysés par rapport à ceux obtenus préalablement par l'analyse des systèmes minces. Un modèle basé sur l'analyse dimensionnelle est proposé pour l'estimation du coefficient d'échange paroi/solide pour des températures comprises entre 100 et 500°C. Les résultats expérimentaux sont également comparés aux prédictions de modèles existants et sélectionnés à partir de la littérature.

Enfin, au **Chapitre 8**, en utilisant l'ensemble des modèles développés au cours de cette étude, un modèle global simplifié a été développé pour simuler le fonctionnement de fours tournants à chauffage indirect, équipés ou non de relevateurs, et dans le but d'obtenir les profils axiaux et les

réponses transitoires de la température à la paroi du tube du four et celle des phases gazeuse et solide. Les résultats de la simulation du modèle global sont comparées avec les données expérimentales. Pour la validation du modèle, les données expérimentales sont obtenues en l'absence de réactions chimiques afin de limiter la validation aux seuls modèles utilisés pour la description du transport de la charge et pour le transfert de chaleur, notamment, le coefficient d'échange convectif et le coefficient d'échange paroi/solide. Une analyse de sensibilité du modèle a été réalisée. Des simulations en régime dynamique du modèle ont été effectuées. Ainsi le modèle pourrait être utilisé à des fins d'optimisation des procédures opératoires mais aussi de design.

Pour terminer, les principales conclusions de cette étude expérimentale et de modélisation réalisée en vue d'améliorer les connaissances sur les mécanismes de transport des particules solides et de transfert de chaleur dans les fours tournants équipé de releveurs, sont résumées avec des perspectives et recommandations.

En ce qui concerne les Chapitres 3 à 8, une nomenclature est fournie en fin de chaque chapitre.

Literature review

"I found that I was fitted for nothing so well as the study of Truth; as having a nimble mind and versatile enough to catch the resemblance of things (which is the chief point), and at the same time steady enough to fix and distinguish their subtle differences..."

(Francis Bacon, 1561-1628)

Chapter 1

Literature review

1.1 Solid materials transport in rotary kilns	29
1.1.1 Characterization of solids transport in rotary kilns	29
1.1.2 Characteristics of flighted rotary kilns	38
1.1.3 Modeling the particle flow : the case of flighted rotary kilns	40
1.2 Heat transfer in rotary kilns	48
1.2.1 Heat transfer modes in rotary kilns	48
1.2.2 Heat transfer coefficients	50
1.3 Global models for rotary kilns	60
1.3.1 Non dynamic models	60
1.3.2 Dynamic models	61
1.4 Review Summary	62

With the broadening of the scope of applications of rotary kilns in recent decades, many experimental and modeling studies have been carried out to gain a better understanding of their behavior. Rotary kilns are usually inclined tubes, equipped with a heating system. While this unit may sound very simple in theory, in fact it is quite complex. Although various models have been proposed to describe the operations of these units, critical challenges still remain, in particular when studying transport of solids and heat transfer at the wall in flighted rotary kilns.

In the following sections, is first reviewed the state of the art of solids transport in rotary kilns, particularly when equipped with lifters, is first reviewed. The main characteristics and the different transverse bed motions are presented. The experimental methods used to characterize the solids transport in terms of residence time distribution, along with some modeling of the distributions are also presented. This is followed by an examination of the classification of kilns and various lifter shapes or profiles with respect to the solids transport within flighted rotary kilns. The main modeling approaches, namely, empirical, mechanistic, and compartment models are presented. Finally, lifter hold up models are described.

The second section reviews the modeling of heat transfer mechanisms. The main paths of heat transfer within the kiln during heating operation are presented. Attention will be paid in particular to the heat transfer coefficient between wall and solids and the convective and radiative heat transfer coefficients. When available, the experimental procedures used in previous studies are reported, along with the data analysis chosen to estimate these coefficients. Some of the most widely used correlations proposed to model convective, radiative and wall-to-solids heat transfer

are presented.

In the last section, global models for rotary kilns are briefly presented. Dynamic and non dynamic models are reported. They mainly consist of solid transport models, coupled to heat and mass transfer models.

Utilisés à échelle industrielle depuis plus d'un siècle, les fours tournants ont vu leurs domaines d'application s'élargir ces dernières décennies, ainsi de nombreuses études expérimentales et de modélisation ont été effectuées pour acquérir une meilleure compréhension de leurs comportements. Les fours tournants sont généralement des tubes inclinés, et munis d'un système de chauffage. Bien que ces unités puissent sembler assez simples en théorie, dans la pratique, elles sont beaucoup plus complexes. Et si différents modèles ont été proposés pour décrire les opérations de ces appareils, il demeure cependant des points d'ombre, en particulier lorsqu'il s'agit du transport de solides divisés et du transfert de chaleur dans les fours tournants équipés de releveurs.

Dans les paragraphes qui suivent, dans la première section, il sera tout d'abord fait un état de l'art du transport des particules solides dans des fours tournants, en particulier lorsqu'équipés de releveurs. Les principales caractéristiques et les différentes formes d'écoulement de la charge sont présentées. Les méthodes expérimentales utilisées pour caractériser le transport de la charge solide en terme de distribution de temps de séjour, ainsi que les modélisations développées pour ces distributions sont également présentées. Ensuite, la classification des fours tournants lorsqu'équipés de releveurs sera précisée et quelques uns des profils de releveurs couramment utilisés seront présentés. Les principaux types de modèles mis en place, à savoir, les modèles empiriques, ceux basés sur des considérations physiques, et les modèles à compartiments sont présentés. Enfin, les modèles établis pour le taux de chargement des releveurs sont décrits.

La deuxième section porte sur la modélisation des mécanismes de transfert de chaleur dans les fours tournants. Les principaux modes de transfert de chaleur pendant le chauffage sont présentés. L'accent sera porté en particulier sur le coefficient de transfert de chaleur paroi/solide, et les coefficients de transfert de chaleur par convection et par rayonnement. Lorsque possible, les procédures expérimentales utilisées dans les études antérieures sont rapportées, ainsi que l'analyse de données mise en œuvre pour estimer ces coefficients. Certaines des corrélations plus largement utilisées pour modéliser la convection, le rayonnement et le transfert de chaleur paroi/solide sont présentés.

Dans la dernière section, les modèles globaux pour les fours tournants sont brièvement présentés. Les deux types de modèles, dynamique et non dynamique sont évoqués. Ils sont principalement constitués de sous-modèles pour le transport des particules solides, couplés à des modèles de transfert de chaleur et de masse.

1.1 Solid materials transport in rotary kilns

As stated in the introduction, rotary kilns are used in a wide range of processes, and depending on the application, the rotary drum may be equipped with internal fixtures or not. In the high temperature treatment of cement as well as in metallurgical processes, there are usually no lifters inside the kiln, whereas lifters are employed in the drying and mixing of fertilizers or agricultural products, etc. Therefore several research investigations have been carried out on the motion of solid particles through rotary kilns. In view of the different fields of industrial applications, some investigations concerned rotary kilns without any internal fixtures while others focused on rotary kilns (dryers) equipped with lifters or miscellaneous internal fixtures. In the following sub-sections, a brief review of solids behavior in rotary kilns without lifters and some models used to represent the flow behavior will be first presented. The case of rotary kilns equipped with lifters will then be considered. Some of the points that will be addressed include existing lifter profiles, methods for the characterization of solids transport and modeling approaches of the flow of solid particles.

1.1.1 Characterization of solids transport in rotary kilns

The bed motion within the kiln rotating tube can be described as a movement comprising two components. The first movement in the transverse plane, perpendicular to the kiln axis, influences most of the primary bed process phenomena (material mixing, heat transfer, reaction rate, etc.). The second movement toward the axial direction mainly governs the residence time or the bed profile of the solid particles in the rotary kiln.

1.1.1.1 Transverse bed motion

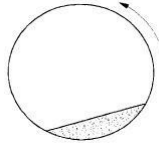
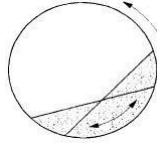
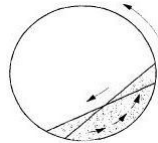
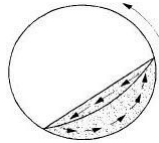
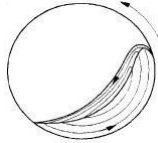
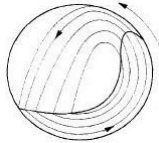
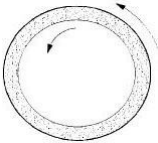
The transverse bed motion occurring when a rotary kiln turns on its axis has been extensively studied experimentally by [Rutgers 1965, Henein 1983, Mellmann 2001]. Depending on variables such as rotational speed, kiln diameter or bed particle characteristics, different forms of bed motion can occur, as classified in Table 1.1.

[Mellmann 2001] subdivided these bed motions into three basic forms:

- Slipping motion. This motion includes sliding and surging. There is no particle mixing. In the first case the bed takes up a stationary position as the tube rotates; in the second case the solid bed adheres on the rotating wall up to a certain angle of deflection then slides back en masse on the wall surface.
- Cascading (tumbling) motion. This motion includes slumping, rolling and cascading. Slumping motion occurs when a segment of the bulk of materials at the shear wedge becomes unstable then yields and empties down the incline. By increasing the rotational speed, rolling motion, which is characterized by a steady discharge onto the bed surface (active layer) while the bottom part of the bed (passive or plug flow region) is transported upwards with the rotational speed of wall, will occur. This type of motion maximizes particle mixing. A further increase in the rotational speed may bring about cascading motion where the bed surface starts to arch.
- Cataracting motion. This motion includes cataracting and centrifuging which are not usually found in rotary kiln operations.

Industrial rotary kilns, in particular those without lifters, are usually operated in rolling motion so as to promote homogeneity and uniformity of treatments.

Table 1.1: Forms of transverse motion of solids in rotating cylinders [Mellmann 2001].

Basic form	Slipping motion		Cascading (“tumbling”) motion			Cataracting motion	
Subtype	Sliding	Surging	Slumping	Rolling	Cascading	Cataracting	Centrifuging
Schematic							
Physical process	Slipping		Mixing			Crushing	Centrifuging
Froude number Fr [-]	$0 - 10^{-4}$		$10^{-5} - 10^{-3}$	$10^{-4} - 10^{-2}$	$10^{-3} - 10^{-1}$	$0.1 - 1$	$Fr \geq 1$
Filling degree f [-]	$f < 0.1$	$f > 0.1$	$f < 0.1$	$f > 0.1$		$f > 0.2$	
Wall friction coeff. μ_W [-]	$\mu_W < \mu_{W,c}$	$\mu_W \geq \mu_{W,c}$	$\mu_W > \mu_{W,c}$			$\mu_W > \mu_{W,c}$	
Application	No use		Rotary kilns and reactors; rotary dryers and cooler; mixing drum			Ball mills	No use

The main criteria for the determination of the solid bed motion within a rotating kiln were summarized by [Mellmann 2001]:

- the Froude number ($Fr = \omega^2 R/g$, where ω is the angular rotation speed, R is the kiln tube radius, g is the gravitational constant) and the filling degree ($f = \left(\frac{\psi}{2} - \sin\left(\frac{\psi}{2}\right) \cos\left(\frac{\psi}{2}\right)\right) / \pi$, where ψ is the bed angle of circular segment occupied with solids),
- the coefficient of wall friction and the internal frictional coefficient,
- the dynamic and static angle of repose of the bulk solids,
- the ratio of particles to the rotating kiln tube internal diameter.

No influence of kiln length or inclination was reported. Both these parameters determine the axial motion as presented in the following sections. Hence the experimental study of the transverse motion behavior can be conducted batchwise in a short horizontal drum or cylinder.

1.1.1.2 Solids transport: experimental methods

There are several methods to characterize the solids transport behavior in rotary kilns. These methods focus on the knowledge of the distribution of the times that solid particles will undergo. [Sullivan 1927, Saeman 1951] and other researchers used one of the simplest approaches to gain some understanding of the solids transport, namely the average time of passage of solid particles through the kiln. [Sullivan 1927] described the experimental method to determine that time as follows. First of all, the kiln should be fed at a uniform rate until the whole system reaches a steady state condition with a constant discharge rate. Usually the rotary kiln is operated at room temperature in most published studies [Kramers 1952, Chatterjee 1983c, Chatterjee 1983b, Li 2002b, Liu 2006b]. Then the weight m of solids discharged at the exit end of the kiln during a time t can be measured. The remaining solids in the kiln can then be discharged. Depending on the global installation, for that purpose, the kiln can be stopped and the feeding system disconnected or disabled. The weight HU of these remaining solids constitutes the hold up within the unit. From these measurements, the time of passage is estimated as follows:

$$t_p = HU \frac{t}{m} \quad (1.1)$$

Some researchers such as [Cao 1999, Liu 2006a, Hwan 2009] confused the mean residence time with the time of passage. Indeed this later is quite simple to measure but does not give a clear insight into the kiln behavior, whereas the mean residence time derives from the experimental measurement of the residence time distribution of solid particles within the kiln. The time of passage represents only the average amount of time that a particle will spend inside a unit assuming plug flow and no dispersion. However it can be used to assess the level of dispersion when compared to the mean residence time. A significant discrepancy between these two is indicative of the presence of short-circuiting or dead volume.

A more accurate and realistic approach to describe the particle dispersion and rate of transport, thus assessing the underlying transport mechanism in the rotary kiln, is through the use of the residence time distribution (RTD). The residence time distribution, also called the exit age distribution, E , has been described by [Levenspiel 1999]. It is obvious that solid particles entering the kiln will follow different trajectories when cascaded or when kilning at the bottom; these several paths may require different durations to pass through the kiln. The RTD describes the distribution of these times spent by the solid particles in the kiln. However, [Levenspiel 1999] pointed out one restriction on the RTD curve: the fluid only enters and only leaves the unit one time. This is known as the closed vessel boundary condition, implying that there should not be

any flow, or diffusion or up flow eddies at the entrance or exit of the unit. The simplest and most common way of determining the RTD is to add a physical or nonreactive tracer at the feed inlet end of the kiln (assuming steady conditions) and measure the concentration of the tracer at the discharge end. From the tracer concentration measurements, [Levenspiel 1999] showed how to develop the RTD curve for a vessel. Figure 1.1 presents typical RTD curves plotted as $E(t)$ curves by [Hehl 1978], when operating soda in a small rotary kiln, 25 cm in diameter and 60 cm in length at rotational speeds between 1 and 10 rpm, and a constant flow rate.

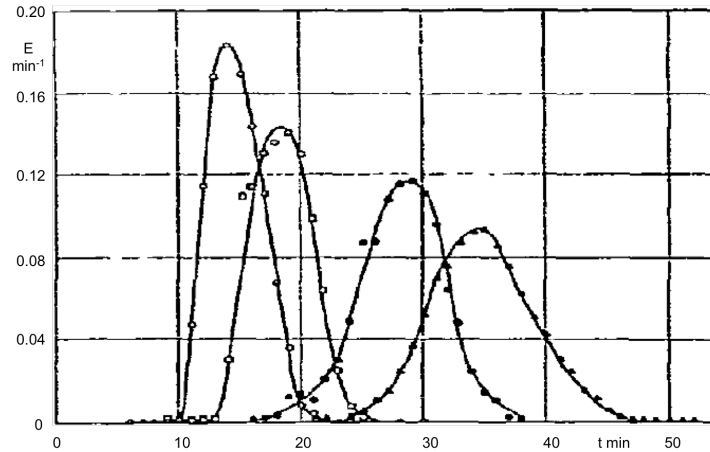


Figure 1.1: Typical residence time distribution for different rotational speeds at a constant feed rate [Hehl 1978].

The shape of RTD curves depends on the combined effect of the flow behavior and mixing performance inside the process equipment [Makokha 2011], which are usually related to a number of statistical RTD parameters, i.e., mean residence time (MRT) and variance (VRT): the first and second moments of the RTD. While rotary kilns usually behave as plug flow reactors with lower dispersion, the dispersion can be significant as shown in Figure 1.1 and in other published RTD studies in the literature [Karra 1977, Abouzeid 1980, Sai 1990, Li 2002a, Gao 2013]. RTD curves in rotary kilns are characterized by two mean features highlighted by [Lee 2008]:

- an initial steep increase of the tracer concentration, which may indicate a slight forward dispersion of the solids since the tracer elements usually arrive in a concentrated front. As there is only one increase of tracer concentration, and so a single peak, this implies that there is no short-circuiting of solid particles.
- an extended tail of the distribution, which may indicate some backwards dispersion of materials. Several reasons can explain this phenomenon: it can be due for example to the presence of some dead volumes [Levenspiel 1999] or of a counter-current airflow driving solid particles backwards in the kiln.

1.1.1.2.1 Residence time distribution experiments

As explained in the preceding Subsection, it is important to take into account the fact that not all the solid particles remain exactly the same length of time within the kiln. It is quite difficult to predict the distribution of residence time in advance. However as shown in Subsections 1.1.3 and 1.1.1.3 below, some models and correlations have been proposed but lack the requisite degree of generality (type of materials being processed and equipment characteristics) to be used for other systems than those they were derived from. Hence, this information must be obtained experimentally.

The stimulus response test is a common method used when measuring the residence time distribution. In this test, the injection of either a step change or a pulse of a tracer or salt is performed at the inlet end (at time=0) and the tracer concentration is recorded continuously or discretely at the outlet in terms of concentration or conductivity.

These tests have to be carried out when steady-state flow conditions are achieved.

1.1.1.2.1.1 Tracer characteristics

Almost all RTD studies use tracers. The selected tracer is expected to share similar properties with the bulk solids, thus introducing as few disturbances as possible on the bulk flow. In past studies [Venkataraman 1986, Hatzilyberis 1999b, Li 2002b], dyed tracer particles were used. Thus except for the color, the tracer material is identical to the bulk. In other studies [Duchesne 1996, Renaud 2000, Sheehan 2002] dealing with wet solids feed, the tracer material used was a salt such as lithium, potassium or sodium chloride. In that case tracers must be carefully selected with regards to individual particle properties (shape, size, particle density) and physical properties of these particles en masse (bulk density, angle of repose,...). The experiments by [Sheehan 2002], for example, showed that lithium chloride was the best tracer compared with water and potassium chloride in an industrial sugar rotary dryer. Some bulk bed materials and associated tracer materials used in previous RTD studies conducted in rotary kilns equipped with internal fixtures are presented in Table 1.2.

Table 1.2: Bulk bed and tracer materials used in rotary kiln equipped with internal fixtures from the literature.

Researchers Kiln size [m]	Bulk Materials		Tracer Materials	
	Type	Size [mm]	Type	Size [mm]
[Duchesne 1996] [Renaud 2000] L=15; D=2	Zinc sulphides	NA	Lithium Chloride	
	Straight 15 cm lifters			
[Hatzilyberis 1999a] L=3; D=0.12	Moist Lignite	-11.2+8	Alumina cylindrical pellets	-11.2+8
			Porcelain	4.5;6.5;8;9;14
	RA - EAD - EHD (see Figure 1.5)			
[Li 2002b] L=1.8 D=0.3m	Municipal Solid Waste: wood, paper, tyres	NA	Dyed MSW	
	Sand	-2+1	Dyed sand	-2+1
	12 axial ribs (20 mm) -4 circular ribs (30 mm)			+
	12 axial ribs (20 mm) -7 circular ribs (30 mm)			smooth wall
	12 axial ribs (10 mm) -4 circular ribs (50 mm)			Finer emery cloth setting
12 axial ribs (20 mm) -4 circular ribs (50 mm)			Coarser emery cloth setting	
[Sheehan 2002] L=15 m D=2 m	Wet raw sugar	NA	Lithium Chloride	
			Potassium Chloride	
			Water	
Straight 15 cm lifters				
[Abouzeid 2010] L=0.25 m D=0.08 m	Dolomite, hematite, magnetite, galena, glass beads, gopper shot	1.07; 0.75; 0.54; 0.43; 0.31; 0.23	Dolomite, hematite, magnetite, galena, glass beads, gopper shot	1.07; 0.75; 0.54; 0.43; 0.31; 0.23
	8 straight 3 mm lifters			

1.1.1.2.1.2 Tracer detection techniques

Tracer detection techniques have been sorted as either inline or offline [Gao 2012]. Inline detections directly record the optical, thermal or electrical signals of the tracer concentration from inline probes. After having been converted, these signals are usually stored for further data analysis. However it is not usually possible to install such detection systems in rotary kilns: solid sampling is usually invasive and cannot be achieved very quickly. Moreover, the analysis of solid samples, sometimes requiring dissolution of dye or salt tracers, is time-consuming. For all these reasons, offline detection techniques are mostly used in rotary kilns and particulate solid processes in general.

Depending on the tracer selected, tracer detection can be performed optically or by conductivity measurements. Optical detection systems include: colorimetry and digital image processing, fluorescence analysis, and spectroscopy analysis (near infrared and ultraviolet). Conductive detection systems are based on the difference of electrical conductivity between the tracer and the bulk flow. Some studies [Debacq 2001, Sherritt 2003] also used radioactive tracer techniques when appropriate to measure the residence time of particles.

1.1.1.2.1.3 Data evaluation of stimulus response test

The criteria and assumptions needed for a reliable data set have already been underlined and are summarized here:

- Steady state flow conditions are required within the rotary kiln;
- The tracer material must not generate hydrodynamic flow disturbance in the bulk flow;
- The system is assumed to have closed inlet and outlet boundaries; however in rotary kilns with open-open boundaries, boundary dispersion can be neglected since axial transport is usually much faster than the dispersion (with large Peclet number).

1.1.1.2.1.4 Pulse experiment

Pulse experiments are simple to operate and do not need a large amount of tracer per experiment. Thus they are the most commonly performed. Besides the stimulus pulse test, particle tracking is reported as an alternative RTD measurement method [McTait 1998].

In this case the tracer is injected as a pulse. The amount of injected tracer should be defined cautiously to ensure sufficient accuracy for analysis. The fraction of tracer that remains in the system at anytime is described by the distribution function $E(t)$ as follows [Levenspiel 1999]:

$$E(t) = \frac{C(t)}{\int_0^\infty C(t)dt} \quad (1.2)$$

where $C(t)$ represents the tracer concentration at the kiln exit end and the integral of $C(t)dt$ defines the area under the curve. In practice, this relation changes each of the tracer concentration values to a normalized tracer concentration value by simply dividing the tracer concentration by the total amount of tracer used. For the discrete sample, $i=1, \dots, N_s$, with N_s the number of samples in total, and the associated sampling time Δt_i , the RTD curve can be determined as follows [Levenspiel 1999]:

$$E(t_i) \cong \frac{C(t_i)}{\sum_{i=1}^{N_s} C(t_i)\Delta t_i} \quad (1.3)$$

Interpretation of the RTD curves is based on moment analysis which provides various aspects of flow in the unit. The first moment of the RTD function gives the mean residence time (MRT) τ which is defined as follows [Levenspiel 1999]:

$$\tau = \frac{\int_0^\infty tC(t)dt}{\int_0^\infty C(t)dt} \cong \frac{\sum_{i=1}^{N_s} t_i C(t_i) \Delta t_i}{\sum_{i=1}^{N_s} C(t_i) \Delta t_i} \quad (1.4)$$

The second moment of the RTD function gives the variance of residence times (VRT) about the MRT, σ^2 . The latter indicates the width or scatter of the distribution: the greater the value of this moment, the greater the distribution spread. This moment is defined as follows [Levenspiel 1999]:

$$\sigma^2 = \frac{\int_0^\infty (t - \tau)^2 C(t)dt}{\int_0^\infty C(t)dt} \cong \frac{\sum_{i=1}^{N_s} t_i^2 C(t_i) \Delta t_i}{\sum_{i=1}^{N_s} C(t_i) \Delta t_i} - \tau^2 \quad (1.5)$$

The $E(t)$ function and variance of residence time can also be expressed in dimensionless form [Levenspiel 1999]:

$$E(\theta) = \tau E(t) \quad (1.6)$$

$$\sigma_\theta^2 = \sigma^2 / \tau^2 \quad (1.7)$$

respectively the mean residence time and variance of residence time, where the dimensionless time is defined as $\theta = t/\tau$.

1.1.1.2.1.5 Step experiment

In this case the bulk flow switches from ordinary solid particles at time = 0 to solid particles with tracer of concentration C_{max} . The fraction of tracer material in the outlet at time t later, is given by the function $F(t)$. The F curve is the dimensionless form of the tracer concentration curve versus time t . It is found by having the tracer concentration rise from zero to unity.

The mean residence time of the tracer is obtained by [Levenspiel 1999]:

$$\tau = \frac{\int_0^{C_{max}} t dC}{\int_0^{C_{max}} dC} = \frac{1}{C_{max}} \int_0^{C_{max}} t dC \quad (1.8)$$

The F and E curves can be related at time t as follows [Levenspiel 1999]:

$$F = \int_0^t E dt \quad (1.9)$$

All these relationships show how stimulus response tests, using either step or pulse inputs, can give the RTD and its parameters for a better understanding of the solids flow through the unit.

1.1.1.2.2 Dynamic response experiments

Studying the dynamic response of a system may provide valuable information on the solids transport characteristic by achieving a step change of an operating parameter. As highlighted by [Lee 2008], if performed alone it cannot give insight into the RTD, but when coupled with a tracer study (see the preceding Section 1.1.1.2.1.5), results of the experiments can give satisfactory information on the solids transport through the time distribution and can be used to develop realistic models of the system.

The experimental procedure is quite simple and can be easily performed during filling (start-up) and discharging (shut-down) procedures without affecting productivity, in contrast to a tracer study. The experimental procedure consists in the continuous measurement of outlet and/or inlet flow rates [Ding 2001, Sherritt 2003, Song 2003].

1.1.1.3 Solids transport: modeling

Several models have been developed to describe the flow and mixing behaviors of solid materials along a rotary kiln. These models are generally classified into two categories [Li 2002b]: the axial dispersion model (ADM) which assumes the solid particles as ideal fluid; and the particulate trajectory model (PTM) which considers solid particles as granular substances. However some of these approaches will be further detailed in Subsection 1.1.3 for the quantification of the axial solids transport variables in the specific case of flighted rotary kilns.

1.1.1.3.1 Axial dispersion models

Among pioneers of the axial dispersion model are [Danckwerts 1952, Fan 1961].

Using an appropriate Pe number (experimentally determined), [Danckwerts 1952] managed to build an ADM by means of F-diagrams (see Figure 1.2) and age-distribution functions. It was then possible to predict distribution functions so that this first model could give meaningful information about the behavior of the fluid flowing through beds of solids or a vessel. Later [Fan 1961] first applied a similar unidirectional diffusion model to analyze the axial dispersion of solid particles flowing through a rotary solid flow system. They were able to predict the residence time distribution as well as the dispersion coefficient of solid materials.

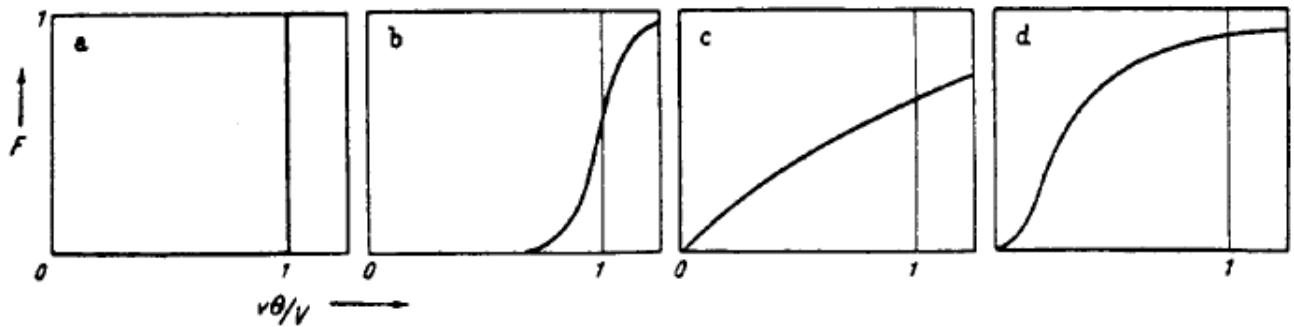


Figure 1.2: [Danckwerts 1952] F-diagrams : a) piston flow, b) piston flow with some longitudinal mixing, c) complete mixing, d) dead water.

The application of that model was validated by [Rutgers 1965] for the continuous flow of granular solids through a rotating cylinder, providing a uniform radial mixing. The axial dispersion coefficient was determined under varying filling degrees, rotational speeds, slopes, bed motions, shapes of kiln entrance and exit end restrictions, and solid bulk bed characteristics. [Abouzeid 1974] also assessed the validity of the axial dispersion model in rotary kilns. He noted that a few assumptions must be satisfied: steady state flow conditions and constant axial velocity in order to ensure a constant flow rate, radial mixing large enough to smooth the concentration at any cross-section, and at fixed operating conditions, a constant axial dispersion coefficient.

[Sai 1990] considered the other mono dimensional model of N tanks-in-series to fit experimental residence time distribution profiles. [Mu 1980] developed a four-parameter model to describe the particle movement pattern in various regions. This model simulated the flow of solids by N rolling steps. Each step represented a selected cross-section of the kiln and consisting of a flow through a tubular vessel followed by a well-mixed vessel with by-pass and recycling. Similar models were developed by [Duchesne 1996, McTait 1998, Dinesh V 2004] for the residence time distribution of solids in rotary kilns.

1.1.1.3.2 Particulate trajectory models

[Saeman 1951] originally developed a mathematical model from the geometrical analysis of a single particle trajectory to predict time of passage in a rotary kiln following the work by [Sullivan 1927]. This model also enables the calculation of the bed profiles (Equation 1.10), the axial velocity and flow rate of solid particles along the kiln under the steady-state regime. It has been further examined by [Kramers 1952, Descoins 2003, Liu 2006b, Colin 2013] .

$$Q_v^E = \frac{4\pi NR^3}{3} \left(\frac{\tan(S)}{\sin(\theta)} + \cot(\theta) \frac{dh(z)}{dz} \right) \times \left(\frac{2h(z)}{R} - \frac{h^2(z)}{R^2} \right)^{3/2} \quad (1.10)$$

where Q_v^E is the volumetric flow rate, $h(z)$ is the bed depth at the axial position z , N is the rotational speed, R is the kiln radius, S and θ are respectively the kiln slope and angle of repose of the solids.

[Descoins 2005] developed a dynamic model described in the following system of equations:

$$F_h^{1/2} \frac{\partial h(z, t)}{\partial t} - \frac{U^T \tan(S)}{\sin(\theta)} F_h^{1/2} (1 - F_h)^{1/2} \frac{\partial h(z, t)}{\partial z} = \frac{\partial}{\partial z} \left(\frac{U^T}{3} R \cot(\theta) F_h^{3/2} \frac{\partial h(z, t)}{\partial z} \right) \quad (1.11)$$

$$\text{Outlet end boundary :} \quad h(z = 0, t) = h_{exit} \quad (1.12)$$

$$\text{Inlet end boundary :} \quad \frac{\partial h(z, t)}{\partial z} \Big|_{z=L, t} = \frac{3Q_v^E|_t \tan(\theta)}{2U^T R^2} (F_h^{-3/2})_{z=L, t} - \frac{\tan(S)}{\cos(\theta)} \quad (1.13)$$

$$\text{Initial condition :} \quad \frac{\partial h(z, t)}{\partial z} \Big|_{z, t_0} = \frac{3Q_v^E|_{t_0} \tan(\theta)}{2U^T R^2} (F_h^{-3/2})_{L, t_0} - \frac{\tan(S)}{\cos(\theta)} \quad (1.14)$$

where $F_h = \frac{2h(z, t)}{R} - \frac{h^2(z, t)}{R^2}$, $U^T = 2\pi NR$ and h_{exit} is the height in exit (equal to the dam height or the particle size). This model aims at predicting the bed profile evolution following a step change of any operating parameter(s), for example it can simulate the filling phase of the kiln. The dynamic model developed by [Spurling 2001] can also be mentioned in the same field.

Using a Monte Carlo simulation, [Rogers 1979] extended [Vàhl 1952]'s originally simple physical model by defining a cumulative probability function describing the particle random re-entry point (position) in the bed. The dispersion could then be taken into account, allowing predictions of RTD and axial dispersion. [Das Gupta 1991]'s particle trajectory model, derived from the particle kinematics, appeared as a breakthrough. This model included a stochastic evaluation equation for the probability of rolling distance of a particle within the active layer in the [Saeman 1951] model. The model predictions of volumetric flow rate, mean residence time and axial dispersion coefficient were successfully validated with the experimental results of [Hehl 1978]. In the same trend, [Kohav 1995] developed stochastic algorithms in order to predict the axial dispersion in rolling or slumping flow in a continuous rotary kiln. An important advantage of this model is that radial segregation is also accounted for. However, the validity of the model is limited to the filling level of solids. Then [Wightman 1998] used a discrete element model to simulate the flow of granular material in a cylindrical vessel undergoing rotational and rocking motions; their simulations matched the experimental results well. Later on [Li 2002b] developed a novel stochastic PTM based on the vector analysis of a particle's gravity-induced axial displacement in a single excursion. He introduced a statistical-averaged analysis on PTM for lightly filled kilns, and for a rotary kiln in which bed depth varies, he developed a stochastic PTM incorporating the trajectory segregation of municipal solid wastes to predict detailed residence time distribution curves.

Nevertheless one must bear in mind that most of these models require long calculation times along with the need for some parameter estimations. The determination of these parameters may often require performing experiments on the system considered.

1.1.2 Characteristics of flighted rotary kilns

A key aspect in understanding rotary kiln operation, as stated by [Wang 1995], is knowledge of the solids transport behavior including the residence time distribution and the axial solids flow rate as mentioned before, but also the discharge rate from lifters, the geometry and voidage of curtains, as well as the particle hold up in lifters.

Several kiln designs include lifters or flights. Lifters are usually longitudinally disposed and arranged uniformly around the inner wall. Their shape varies from one application to another depending on the flow characteristics. In the rotary kiln, lifters carry the solid particles into the upper half and then cascade them in a more or less continuous curtain, as illustrated in Figure 1.3. Solid particles cascading from the lifters can be displaced axially due to the kiln slope and/or a gas stream if present.

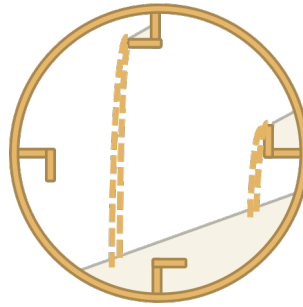


Figure 1.3: Cross section of an operating rotary kiln equipped with lifters.

1.1.2.1 Classification

Rotary kilns equipped with lifters are classified into three categories namely under-loaded, design-loaded and over-loaded (kilning) based on the hold-up of the lifters [Sheehan 2005, Lee 2008, Sunkara 2013b].

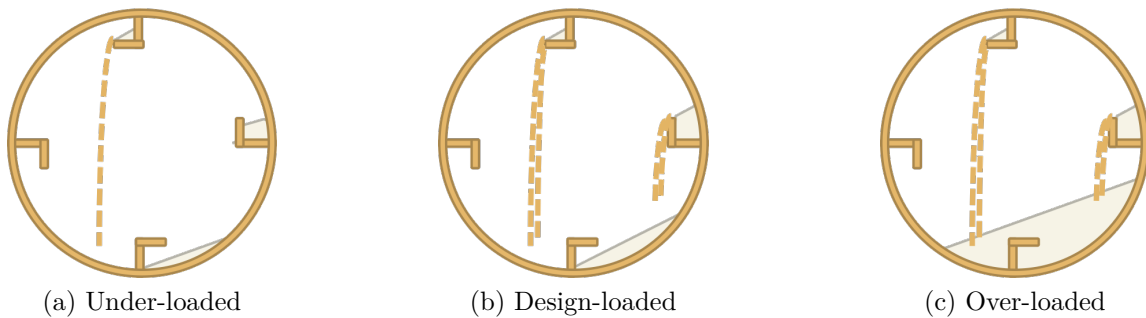


Figure 1.4: Load conditions within rotary kiln equipped with lifters.

In cases where lifters are not completely filled with solid particles when leaving the bulk bed, the kiln is under-loaded (see Figure 1.4a); when there are just enough solid particles at the bottom of the kiln to fill every lifter to its maximum capacity, the kiln is design-loaded (see Figure 1.4b); lastly, when there are more solid particles than the lifter can carry so that its surface is completely submerged then the kiln is over-loaded (see Figure 1.4c).

1.1.2.2 Lifter profiles

There are several lifter designs. The selected lifters must take into account the angle of repose of the solid materials being operated. The radial height of the lifter is chiefly responsible for

the quantity of material carried per lifter ([Miller 1942]) and so, will determine the thickness or “particle density” of the falling curtains. Several lifter profiles can be found in the literature. The most basic ones are straight one-section (flat) lifters, straight two-section lifters and three-section lifters. Some lifters may be serrated with curved edges. Whilst in many cases lifters are attached perpendicularly to the inner wall of the kiln, it may not always be the case.

[Kelly 1968] designed and used equal angular distribution (EAD) lifters. In the upper half of the kiln, these lifters should give a constant quantity cascaded per unit angle of lifter rotation, especially for free flowing solids. [Kelly 1992] also designed equal horizontal distribution (EHD) lifters, which should achieve an equal distribution of falling particles across the horizontal diameter of the rotary kiln. [Hatzilyberis 1999a] used the latter two designs and also rectangular lifters, which are two-section lifters with a right angle cross section, to carry out a residence time distribution study. These lifter profiles are illustrated in Figure 1.5.

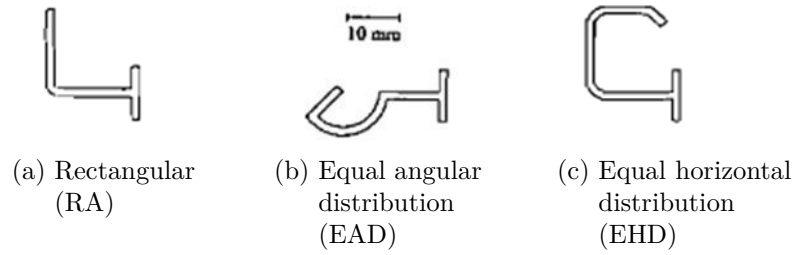


Figure 1.5: Lifter profiles used by [Hatzilyberis 1999a].

[Debacq 2001] characterized twelve lifter profiles with U_3O_8 , a cohesive powder. These lifters are shown in Figure 1.6, numbered from I to XII. Two main criteria were used to analyze their performance:

- The effective fraction of powder carried, defined as the lifter hold up in horizontal position,
- The final unloading angle.

The higher these criteria are, the better the lifter performance is with regard to the unloading regularity. Results of the study showed that the best lifter profiles were the shapes II, III, X and XI; shapes III and XI were among the most effective.

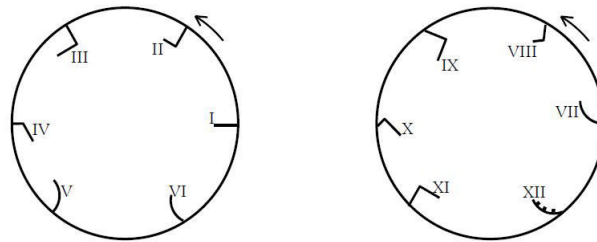


Figure 1.6: Lifter profiles studied by [Debacq 2001]

A study by [Hwan 2009] analyzed the design and configurations of removable segmented lifters in a horizontal rotating kiln. The study considered a number of lifter designs, shown in Figure 1.7, in order to investigate the effect of the lifter configurations, folded lifter section, lifter slope and number of lifters per row. This study showed a strong dependence of bed depth profile, volumetric filling fraction and Peclet numbers on solid loading, lifter design and configurations.

[Ablitzer 2000] characterized the basic functions of lifters (and other internal fixtures) as follows:

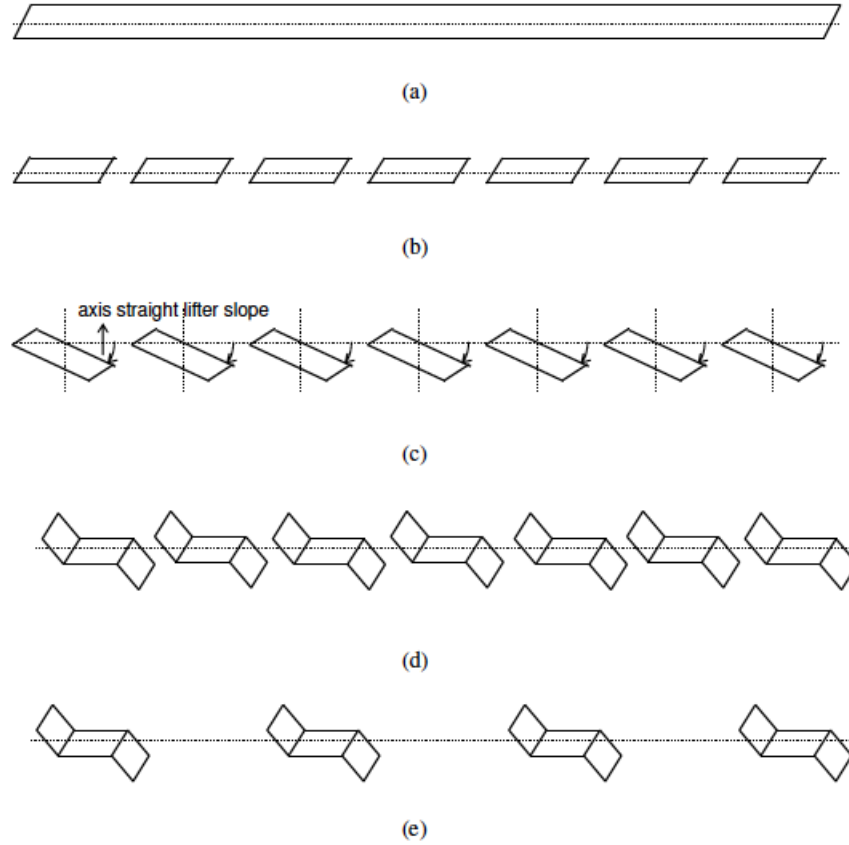


Figure 1.7: Designs and configurations of lifters per row used by [Hwan 2009] in a horizontal rotating kiln with L/D ratio of 7: a) single lifters, b) horizontal straight lifters, c) inclined straight lifters, d) and e) folded lifters.

- the first is to alter the trajectory of solid particles from the regular bed motion (see Subsection 1.1.1.1) achieved within the kiln; however [Grajales 2012], referring to the work by [Chaudhuri 2010], stated that (straight) baffles (or lifters) do not alter the flow regimes but only reduce the area of the central core in the case of rolling motion;
- the second is to increase friction between the bed and the kiln wall;
- the third is to cascade the solid particles to a “controlled degree” with or without an axial component to the trajectory;
- the fourth suggests that lifters (and other internal fixtures) increase the wall surface area and so may enhance wall-to-solids heat transfer. However, it may depend upon whether these internal fixtures are welded to the internal wall or not and possibly upon the type of heating system.

1.1.3 Modeling the particle flow : the case of flighted rotary kilns

The movement of particles is mostly dependent on lifters and kiln designs as well as on the operating conditions. One of the most challenging aspects in the theoretical modeling of rotary kilns is to address the complex motion of particles being lifted, and cascaded by the lifters, then re-entering the bed at the bottom, with the possibility of bouncing and rolling. In the following section some of the existing models used to predict the solid transport characteristics in rotary kilns are presented, along with the modeling of solid hold up (profile) within a lifter.

1.1.3.1 Modeling approach

There have been several studies aiming to model the solids transport within rotary kilns equipped with lifters, due to their extensive use in industry. These models mostly attempted to predict key parameters such as the hold up (HU), mean residence time (MRT) or residence time distribution (RTD) of solid particles within the kiln. Assuming no or small axial dispersion, the time of passage, \bar{t} , must be close to the mean residence time, τ , and thus the results from time of passage estimations are usually exploited for the modeling of the mean residence time in some studies. The models developed in the literature range from relatively simple empirical equations to fully mechanistic models and can be sorted into three main groups: empirical models, mechanistic models and compartment models.

1.1.3.1.1 Empirical Models

The earliest equation was developed by [Sullivan 1927] as mentioned before for rotary kilns not equipped with lifters. The MRT was correlated as follows:

$$\tau = \frac{1.77L\sqrt{\theta}}{SDN} \times factor \quad (1.15)$$

where θ is the angle of repose, S is the kiln slope, N is the rotational speed, L and D respectively the length and internal diameter of the kiln, and factor is a parameter accounting for the operating conditions; it is unity for a simple kiln without obstructions or constrictions.

Among the earliest models developed for rotary kilns equipped with lifters is the correlation proposed by [Prutton 1942] to predict the mean residence time:

$$\tau = \frac{kL}{SDN} + mV_f \quad (1.16)$$

where V_f is the volume of solids inside a lifter, k is a constant depending on the number and shape of the lifters, and m is a constant which depends on gas flow. This model does not consider the effect of changing the solid or gas flow rates through the rotary kiln. Moreover the constants k and m must be determined by fitting the model to experimental data of a specific rotary kiln.

Certainly the most commonly used model is the [Friedman 1949] relation which is derived from [Sullivan 1927] with an additional term to allow for air drag on the solid particles; the following equation was obtained through the study of hold up of a range of materials under overloaded conditions:

$$\tau = L \left[\frac{\alpha}{SDN^{0.9}} \pm \frac{\beta G}{d_p^{0.5} \dot{M}} \right] \quad (1.17)$$

where d_p is the average particle diameter, and \dot{M} and G are respectively the feed rate of the solid particles and the flow rate of the gas. The second term in this equation expresses the air drag; thus the negative sign is used for counter-current flow and the positive sign is used for co-current flow. Compared to the model by [Prutton 1942] model, [Friedman 1949] correlation can account for variation in solid and gas feed rate. However, by increasing the solid and gas feed rate by proportional amounts the predicted mean residence time will remain constant. Moreover the geometric features of lifters are not taken into account in this formulation.

[Shahhosseini 2000] modified the [Friedman 1949] model in order to better represent the dynamic of the system. An additional term, γ , was introduced to account for variation of solid hold up under zero gas flow rate conditions:

$$\tau = L \left[\frac{\alpha}{\tan(S)DN^{0.9}} + \frac{\beta(G + \gamma)}{d_p^{0.5} \dot{M}} \right] \quad (1.18)$$

Even if this model attempted to address some of the shortcomings of the [Friedman 1949] model, it still does not consider internal fixtures of the kiln.

[Alvarez 1994] presented an empirical relationship for residence time estimation. It was derived from experimental data concerning solid particles of biological and mineral origin. This equation requires up to six constants namely, A_i , $i = \{1, \dots, 6\}$:

$$\tau = \frac{A_1 d_p^{0.032} \rho^{0.956}}{N\dot{M}(A_2 S + 1)} + \frac{A_3 d_p^{-0.065} \rho^{0.002}}{A_4 S + 1} - \frac{A_5 G^{0.5}}{A_6 S + 1} \quad (1.19)$$

where d_p is the average particle diameter, ρ is the density of the bulk solids. This formulation allows prediction of residence times even when the kiln is horizontal and can be applied to a wide range of solid materials. However due to the large number of model parameters, the model has to be fitted to the system prior to its utilization.

The correlations developed by [Hwan 2009] for horizontal flighted rotary kilns can be mentioned. They are based on dimensional analysis similarly to the correlation of [Chatterjee 1983b] (see Eq. 1.20). [Chatterjee 1983b] carried out tracer experiments within inclined rotary kilns not equipped with lifters but fitted with a variety of exit dams. By applying conditions of dimensional homogeneity, [Chatterjee 1983b] obtained the following correlation:

$$\bar{t} = 0.1026 \frac{L^3}{\dot{M}} \left(\frac{\theta}{S} \right)^{1.054} \left(\frac{L^3 N}{\dot{M}} \right)^{-0.981} \left(\frac{L}{D} \right)^{1.1} \quad (1.20)$$

Though the effect of the exit dam height was studied, it was not taken into account in the proposed correlation. Following this lead, and based on systematic experiments performed in a variety of horizontal rotary kilns with different L/D ratios (between 5 and 10), and equipped with segmented lifters and different solid materials (10 in total), [Hwan 2009] proposed the following equations respectively for the volumetric filling degree, f , the time of passage, τ , and the axial dispersion coefficient, D :

$$f = 10.91 \theta^{1.14} \left(\frac{d_p}{D} \right)^{-0.15} \left(\frac{\rho \omega D^2}{F/D} \right)^{-0.90} \left(\frac{\omega^2 D}{g} \right)^{-0.03} \left(\frac{h_l}{D} \right)^{-0.52} \left(\frac{L}{D} \right)^{-0.40} \quad (1.21)$$

$$\tau = 8.57 \frac{\rho L D^2}{F} \theta^{1.14} \left(\frac{d_p}{D} \right)^{-0.15} \left(\frac{\rho \omega D^2}{F/D} \right)^{-0.90} \left(\frac{\omega^2 D}{g} \right)^{-0.03} \left(\frac{h_l}{D} \right)^{-0.52} \left(\frac{L}{D} \right)^{-0.40} \quad (1.22)$$

$$D^2 = 0.12 \frac{F}{\rho u} \theta^{-1.14} \left(\frac{d_p}{D} \right)^{0.15} \left(\frac{\rho \omega D^2}{F/D} \right)^{0.90} \left(\frac{\omega^2 D}{g} \right)^{0.03} \left(\frac{h_l}{D} \right)^{0.52} \left(\frac{L}{D} \right)^{0.40} \quad (1.23)$$

where ω is the kiln angular rotational velocity, h_l is the lifter height, g the acceleration of gravity and u is the axial solid velocity. However, by using the same set of parameters for the exponent, these models suggest that the three solids transport coefficients f , $\frac{\tau \dot{M}}{\rho L D^2}$, and $\frac{F}{\rho u D^2}$ vary in exactly the same way for each set of dimensionless groups identified, and thus differ only by a multiplication factor.

More recently [Thibault 2010] proposed two empirical models for the prediction of the mean residence time. The models consist of the multiplication of three factors as follows:

$$\bar{t} = \rho f_1(1/N\dot{M}) f_2(S) f_3(G) \quad (1.24)$$

The three functions f_1 , f_2 and f_3 account for the influence of the product $N\dot{M}$, the slope of the rotary kiln, and the impact of the gas flow rate on the mean residence time. The definition of f_2 and f_3 as first order functions in the models, makes it possible to carry out calculations for horizontal kilns with no gas flow rate. The main difference between the two models proposed is the definition of the function f_1 which can be either a second-order polynomial with the inverse of $N\dot{M}$ or a simple function with \dot{M} and N each with an exponent.

1.1.3.1.2 Mechanistic Models

While empirical models are usually simple, they may sometimes lack predictive capabilities without smart preliminary fitting of parameter(s). In order to address these limitations, there have been several studies based on physical and mathematical approaches to model the solids transport in rotary kilns. These mechanistic models are usually very complex and very system-specific in order to take into account the large number of parameters controlling the process as well as their possible interactions.

[Saeman 1954] was the first to break away from the empirical approach. By assuming a linear relationship between horizontal displacement of the particles due to the air flow and its velocity, the following equation was obtained for the mean residence time:

$$\bar{t} = \frac{L}{f_H(\tan(S) \pm k_m U_G) DN} \quad (1.25)$$

where f_H is a “cascade factor” varying between 2 and π , and increasing as solid hold up increases, k_m is an empirical constant (dimensional) for a given material, and U_G is the superficial gas velocity through the empty drum. One can find some similarities with previous formulae but this model is mainly based on a study of the cascades and the airborne phase. However, like the model proposed by [Prutton 1942], this formula contains two empirical parameters, f_H and k_m which are not readily available.

[Schofield 1962], based on a forward step method, analyzed particle motion from lifter and airborne drag. Knowing the average axial displacement of a particle in a single cascade and the length of the kiln, the number of steps required for a particle to leave the kiln can be obtained. Then if the time taken for a fall is known, the residence time can be calculated. From that physical analysis the following equation is derived:

$$\bar{t} = \frac{L}{\bar{y} \sin(S) - x_l} \left(t_f - \frac{1}{\bar{\theta} N} \right) \quad (1.26)$$

where \bar{y} is the average length of fall of particles, x_l is the longitudinal displacement of falling particles, $\bar{\theta}$ is the average angle move by particles in lifters, and t_f is the time of fall of a particle.

[Matchett 1987] provided a detailed analysis of particle motions. They treated separately the airborne phase of particles falling through air and the dense phase of particles in the lifters or the rolling bed at the bottom. Using a range of physical and geometric relationships they obtained:

$$HU = \frac{\dot{M}L(2Nt_a + 1)}{2Nt_a \left(U_S + \frac{aD\tan(S)}{2t_a} \right)} \quad (1.27)$$

$$\bar{t} = \bar{t}_G + \bar{t}_S \quad (1.28)$$

$$L = \bar{t}_G U_{S_1} + \bar{t}_S U_{S_2} \quad (1.29)$$

where t_a is the average time a solid particle spends in the airborne phase, \bar{t}_G and \bar{t}_S are residence times in the airborne and dense phases, U_{S_1} and U_{S_2} are respectively the particle velocity in the airborne phase and the axial velocity of solids in the dense phase, and a is a dimensionless velocity number given by the equation:

$$a = \frac{U_{S_2}}{ND\tan(S)} \quad (1.30)$$

[Kemp 2004] tried to recast the [Matchett 1987] “parallel form” analysis to a correlation giving the relationship between \bar{t} and L and obtained:

$$\bar{t} = \frac{L \left(1 + \frac{K_{fl}}{N} \sqrt{\left(\frac{g}{D} \right)} \right)}{\left(\sqrt{gD} \tan(S) \left(\frac{K_K}{\sqrt{2}} + K_{fl} a \right) + U_{S_1}^d \right)} \quad (1.31)$$

This is a straightforward equation with only known parameters or physically significant constants such as K_K and K_{fl} whose values are defined within a relatively narrow range. However the model does not consider the effects of number of flights or the solids characteristics and it was noted that the kiln hold up per unit length was constant along the unit. Note that [Matchett 1990] also proposed a number of modifications to the original model to account for the effect of kiln geometry and number of lifters, but they noted that the model lacked a mechanism for including variations in the model parameters.

Along similar lines, [Sherritt 1993] proposed another two-particle phases model mainly based on the discharging rate of lifters. Application of the model to other published experimental data showed that its performance depended on the kiln geometry and its loading condition. Even if there was no significant improvement in the predictive capacity, [Sherritt 1993] underlined that this model could be applied to a variety of drum configurations with no need for experimentally derived parameters to determine the dense phase flow rate.

[Wang 1995] also developed a generalized model for the solids transport in rotary kilns equipped with lifters using differential equations. This mechanistic model aimed at partly filling identified gaps existing in previous attempts. [Wang 1995] proposed a model to estimate the discharge rate of solids from lifters and then deduce the axial solid flow rate. Using extreme value theory, the geometrical feature of curtains formed could be determined as well. The comparison of results with experimental data showed that the predicted discharge rate of lifters deviated significantly. However predicted mean residence times were in good agreement with experimental data within a 10% margin; errors were attributed to the effects of kilning and bouncing at the kiln bottom.

1.1.3.1.3 Compartment Models

Compartment models assume that the unit can be divided into a number of slices, where each slice can be described by an ideal reactor or a combination of ideal reactors, which are either the continuous stirred tank reactor (CSTR) or the plug flow reactor (PFR). As each ideal reactor can be defined by a differential equation, one can get a distribution for the model parameters. Whilst the empirical and mechanistic models presented above mostly lump the solids and predict average parameters, compartment models can give also information such as residence time distribution.

There have been several one-dimensional model types designed to characterize deviations from the two ideal reactors. The ones most usually encountered are the “open” and “closed” dispersion models ([Fan 1961, Karra 1977, Bensmann 2010]) as well as the tank in series (TIS) model ([Venkataraman 1986, Ang 1998, Debacq 2001]).

The “open” and “closed” dispersion models consider the axial motion of fluid elements as two components [Martin 2000]: a convective component arising from the bulk motion of the fluid and a diffusive component arising from the random motion of elements in response to the decay of turbulent eddies. This is represented by the following one-dimensional diffusion equation:

$$\frac{\partial C}{\partial \theta} = \frac{D}{uL} \frac{\partial^2 C}{\partial z^2} - \frac{\partial C}{\partial z} \quad (1.32)$$

$$\frac{D}{uL} = \frac{1}{Pe} \quad (1.33)$$

$$\theta = \frac{t}{\tau} = \frac{ut}{L} \quad (1.34)$$

where D is the axial dispersion coefficient, and Pe the Peclet number.

The “open” and “closed” boundary conditions, from which both these models draw their name, define the flow condition at the unit inlet and outlet. The “open” boundary condition

is achieved when the flow is undisturbed at the inlet and outlet, whereas the “closed” boundary condition is achieved when the flow approaches the unit inlet as an idealized plug flow, transforms into a dispersed flow in the unit, and returns to an idealized plug flow at the exit. [Thomas 1944, Levenspiel 1999] gave an analytical solution to Equation 1.32 for the “open” and “closed” boundary conditions respectively. These solutions are presented in Appendix B.1.

Another common approach in compartment modeling is the TIS model. In this model the unit is represented by a series of N_T equal-sized hypothetical CSTRs. This approach does not require a precise definition of the inlet and outlet boundary conditions. Furthermore it has the advantage of being easy to follow and to compute. However, it requires an integer value for N_T , which is a significant problem when N tends to 1. The RTD equation is also the definition of the Erlang distribution:

$$E(\theta) = \frac{N_T^{N_T}}{(N_T - 1)!} \theta^{(N_T-1)} \exp(-N_T \theta) \quad (1.35)$$

with mean and variance of the distribution defined as follows: $\bar{t}_T = 1$, $\sigma_T^2 = \frac{1}{N_T}$.

In order to address the quantization issue arising in the analysis of high-dispersion systems [Martin 2000] proposed an extended tanks in series (ETIS) model which allows a non-integer number of hypothetical TIS. The RTD obtained is given by:

$$E(\theta) = \frac{N_T^{N_T}}{\Gamma(N_T)} \theta^{(N_T-1)} \exp(-N_T \theta) \quad (1.36)$$

[Duchesne 1996] used two compartment models to simulate the solids transport through a rotary kiln equipped with lifters. The first model used was the simple tank in series model. The model is described by two single parameters: the number of CSTRs N_T and the conductance k that modulates the flow of solid particles from one tank to the next and is assumed to be constant. A schematic representation of this model is presented in Figure 1.8. The second model is a modified Cholette-Cloutier model which accounts for the presence of dead zones. Each slice is composed of two CSTRs exchanging solids. Only one of them exchanges solids with neighboring slices contributing to the axial transport in the active zone, and the other simulates dead zones (see Figure 1.9). Here two additional parameters are required: α , the fraction of total volume of solids occupied by the active zone and β , which is the ratio of the exchange rate between the active and dead zones to the slice cell mass feed rate. Comparison of the predictions of the two models with experimental RTD shows that the TIS model failed to accurately represent the RTD extended tail while the modified Cholette-Cloutier model gave a good fit to experimental data. [Renaud 2000] expanded the validity of this model by defining the parameters (k , α and β) as a function of solid and gas flow rates; the MRT calculated with the model was compared with those of empirical correlations available in the literature using experimental data from an industrial ore rotary kiln. The model gave good results while empirical correlations under-predicted the MRT. [Renaud 2000] suggested that empirical correlations failed to incorporate the varying characteristics of wet materials. [Sheehan 2005] also mentioned that the expression for the axial transport, that moderates the flow between tanks in this model, leads to an improbable distribution of solids along the length of the kiln. The lack of relations between the model parameters and the physical and operational characteristics of the process is also pointed out.

Following the lead of [Schneider 2003], [Sheehan 2005] presented two compartment models. Both models split the kiln into a series of twin tanks, and denote airborne solids as active phase and the solids at the bottom and within lifters as passive phase. The first model extends the [Schneider 2003] compartment model by introducing in a kilning flow for overloaded conditions and also a constant air phase, based on the MRT correlation by [Friedman 1949]. That first model is predominately statistical and was used as a basis to illustrate the methodology to develop a

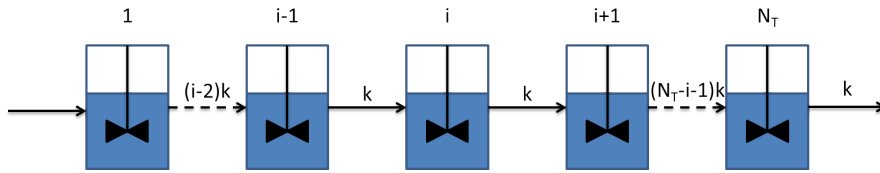


Figure 1.8: Tank in series model

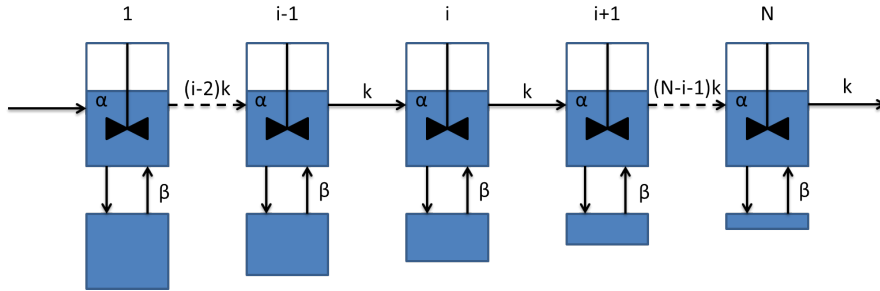


Figure 1.9: Modified Cholette - Cloutier model

more physical model. The second model is illustrated in Figure 1.10. The structure is similar to the first: each slice here is designed to better reflect the physics of a rotary kiln equipped with lifters. Therefore key parameters may be defined in terms of physical properties and transport behavior. The number of estimated parameters was reduced from 4 to 2 by implementing an empirical model along with physical and mechanical properties of the rotary kiln. It was reported that the model could accurately reproduce experimental RTD, but still some parameters required mechanistic description.

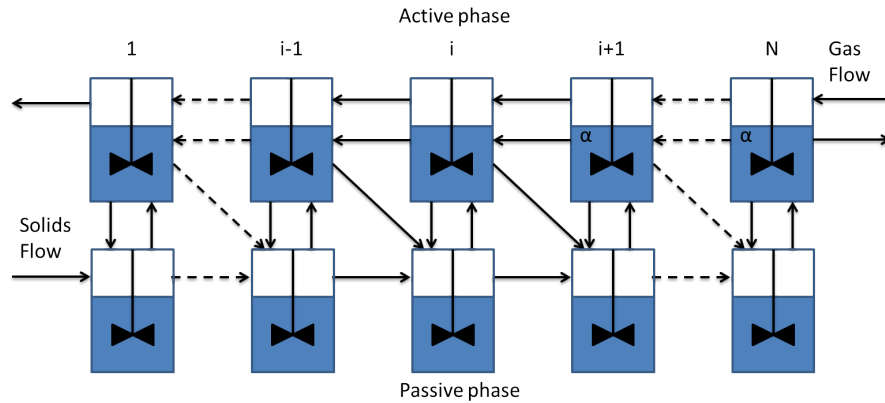


Figure 1.10: Model proposed by [Sheehan 2005]

More recently [Makokha 2011] proposed an improved mixing cell (IMC) model to study the slurry transport and mixing characteristics in a large overflow ball mill. The layout of the model is shown in Figure 1.11. This model assumes some short-circuiting (bypass) to the outlet, and similarly to the previous presented models a non-flowing zone exchanging material with an adjacent flowing zone. The IMC model was found to predict the experimental RTD with good agreement for different levels of load volume and slurry fraction. However results show that IMC and the simple mixing cell model may predict the mean residence time with similar accuracy.

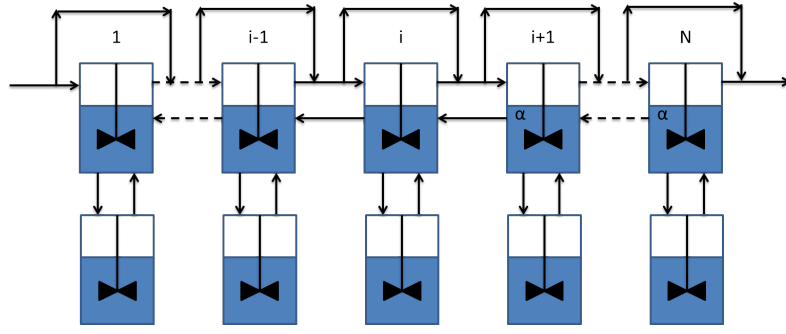


Figure 1.11: Model proposed by [Makokha 2011]

1.1.3.2 Modeling of the lifter hold up

It is essential to know the quantity of solids held in the lifters in order to understand the solids transport, thus a large amount of research has focused on modeling the hold up profile within a lifter as it moves around the circumference of the kiln. In other words the question to answer concerns prediction of the amount of solids carried by a lifter at any time.

The particles within the lifters will show a kinetic angle of repose with the horizontal plane. This angle also depends on the angular position of the lifter. [Schofield 1962] developed an equation to evaluate the dynamic angle of repose of solid particles as a function of its dynamic coefficient of friction and the radial position of the lifter. [Kelly 1977] reviewed equations relating the drum loading and lifter loading and also provided a measurement procedure for the dynamic friction coefficient; then [Baker 1983] calculated the solids hold up and rate of discharge of a lifter at any angular position by using the dynamic angle of repose. [Sherritt 1993] determined separately the hold up and axial flow rate of particles in the airborne phase (falling curtains) and dense phase (loaded onto the lifter), when the kiln equipped with straight two-section lifters is either underloaded or overloaded. [Lisboa 2007] proposed equations predicting straight two-section lifter hold up and length of fall of particles for a design-loaded rotary dryer. Good agreement was found between predictions and experimental data. Working with straight three-section lifters, [Fernandes 2009] validated equations for the prediction of the load of lifters proposed by [Revol 2001] as well as for the average particle length of fall proposed by [Glikin 1978].

More recently, [Van Puyvelde 2009] studied hold up profiles of five different lifters, i.e. a flat horizontal lifter, a flat inclined lifter and three lifters to which other segments are added to produce a hook formation. Results showed that the more complex lifters had higher hold up and larger range but the rate of material lost from these lifters was generally less than with simple perpendicular lifters. [Cronin 2011] developed a probabilistic model to analyze the motion of solid particles in a relatively simple system of four straight lifters. [Lee 2010] developed and validated a geometrical model for the unloading profile of a generic two-section lifter, whereas [Sunkara 2013b] provided a geometrical model to predict the discharge characteristics of rectangular lifters (arranged every 90° around the kiln circumference), and found that the lifters' length ratios have a great influence on the hold up and the cascading rate. [Debacq 2013b] developed a model which is assumed to be possibly extended to other lifter profiles and provided an equation for the lifter discharge as a function of the angular position. The study was based on geometrical calculations and showed good agreement with experimental results of the unloading of cohesive particles.

Lastly, [Sunkara 2015] extended the model of the dynamic angle of repose developed by [Schofield 1962]. The new geometrical approach considers inertial forces, therefore accounting for the flowing region existing at the lifter surface. Despite some deviations of the predicted results from the measurements, compared with the model from [Schofield 1962], there is better agreement between the extended model predictions and experimental data.

1.2 Heat transfer in rotary kilns

Rotary kilns used in industry can be classified into two main heating modes; they can be either directly heated or indirectly heated, depending on the heating source position with respect to the kiln wall. In the case of a direct heated kiln, usually a combustion furnace burning oil, gas or coal is used to generate a hot gas inside the kiln. The gas flows through the kiln either co-currently or counter-currently with regard to the solid flow. Co-current operations are often preferred to avoid high temperature of the final product which may result in handling problems or deterioration of sensitive products. In the case of an indirect rotary kiln, the heat source which can be electrical or hot gas, is external to the kiln, while the solids are operated inside the kiln. The indirect heating mode allows the compartmentalization of the kiln in temperature controlled zones. Therefore, indirectly heated kilns are used when there is a need for tight control and clean heating.

1.2.1 Heat transfer modes in rotary kilns

Heat transfer in rotary kilns involves the exchange of energy via all the fundamental physical transfer mechanisms, i.e. conduction, convection, and radiation. The heat transfer modes can be classified into three categories, corresponding to three zones, outside, inside, and across the kiln wall. Each mode may encompass one or more heat transfer mechanisms. The basic equations for the heat transfer flux of each transfer mechanism are:

Conduction: $\Phi = -kA \frac{dT}{dr}$, with k the thermal conductivity, A the contact area, T the temperature.

Convection: $\Phi = hA\Delta T$, h is the heat transfer coefficient.

Radiation: $\Phi = \sigma AT^4$, σ is the Stephan-Boltzmann constant.

The dominant mechanism in supplying heat to the solid bed depends on: the kiln operating conditions, notably the operating temperature, the kiln design and internal fixtures, thermal and physical properties of the solid particles, gas and the kiln wall.

As presented in Figure 1.12, the following heat fluxes may occur in rotary kilns equipped with lifters (without being exhaustive):

1. Φ_{cw-cb} , heat transfer flux between the covered wall and the covered lower bulk bed, including conduction and radiation.
2. Φ_{eb-g} , heat transfer flux between the exposed upper bed and the freeboard gas, including convection and radiation terms.
3. Φ_{ew-g} , heat transfer flux between the exposed wall and the freeboard gas, including convection and radiation terms.
4. Φ_{ew-eb} , heat transfer flux between the exposed upper bed and the exposed wall, only in terms of radiation.
5. Φ_{g-fs} , heat transfer flux between the freeboard gas and the falling solid particles by convection and radiation for kilns equipped with lifters.
6. S_o , heat supplied by the heating system.
7. Φ_{loss} , heat loss from the kiln wall to the ambient for a directly heated rotary kiln by convection and radiation.

Heat transfer between the outer wall and the inner wall occurs by conduction, and the direction depends on the kiln heating mode. Lifters can be regarded as part of the internal wall and therefore increase the contact areas. In Table 1.3, [Boateng 2008] presents some energy-saving percentages, presumably obtained following the installation of lifters in some industrial kilns. Still these advantages are not obvious or even certain, and they are mostly reliant on the process heating mode.

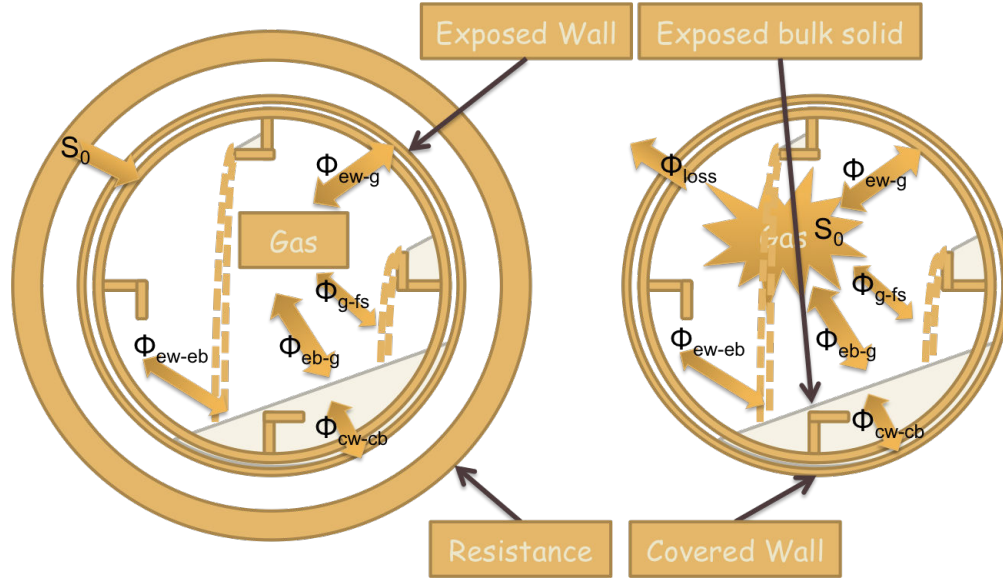


Figure 1.12: Heat transfer mechanisms in the cross section of indirectly (left) and directly (right) heated rotary kilns equipped with lifters.

Table 1.3: Advantages of using lifters [Boateng 2008].

Unit	Before lifters installed	After lifters installed	Percent change
3.6×76.2 m LWA kiln			
Added 3 rows of lifters + 3 dam			
Product rate [STPD]	650	970	47
Specific heat consumption [kWh/ton]	0.76-0.82	0.59	-35
Exit gas temperature [K]	922	661	39
Kiln speed [rpm]	1.6	2.7	70
3.4×53.3 m LWA kiln			
Added 3 rows of lifters + 1 dam			
Capacity [TPD]	550	625	14
Specific heat consumption [kWh/ton]	2.53	2.24	-12
Exit gas temperature [K]	839	728	19
Kiln speed [rpm]	1.75	2.3	31

[Cook 1995] reported that when operating at relatively low temperature, i.e. gas and wall temperatures around 300°C, the heat transfer between the covered wall and bulk bed is the dominant mechanism. [Gorog 1981, Gorog 1982, Ding 2001] specified that at temperatures below 600-700°C, the contribution of radiation is less than 10%, around 700-900°C, radiative and convective heat transfer contributions are comparable, and above 1000°C the radiative transfer becomes dominant. [Li 2005] forecast similar trends.

1.2.2 Heat transfer coefficients

A significant amount of research has been completed over the past years to determine the heat transfer coefficient or heat flux related to the differing mode of heat transfer occurring in rotary kilns; unfortunately the heat transfer mechanisms have not been fully clarified. Among papers available on the subject, most of them focused on the axial heat transfer and presented some correlations developed with the use of experimental measurements to calculate the heat transfer coefficient or heat flux. However most of the authors mainly used the experimental results from the work by [Brimacombe 1978], [Tscheng 1979] and [Barr 1989a]. Recently [Ding 2001] conducted a comprehensive review and investigation of heat transfer focusing on directly heated kilns operating at low to medium temperature. Theoretical and empirical correlations extracted from the literature, some of which are presented below, were used in the later work. Results showed that the wall to solid heat transfer is dominant at low to medium temperatures, and can be estimated from penetration theory and contact resistance, whereas heat transfer from free-board gas to the solid bed contribution was found to be small.

1.2.2.1 Experimental setups and measurement procedures

Although a considerable amount of work has been carried out on heat transfer in rotary kilns, only a few papers have reported on experimental measurements of heat transfer coefficients. The experimental setups are rarely well detailed and the measurement procedures not always fully explained. However, it is possible to classify the experimental setups into the following categories: continuous feed rotary kilns equipped with either stationary or rotating thermocouple probes, and batch rotary kilns with fixed and/or rotating thermocouple probes. Table 1.4 gives the available process details of previous studies relevant to the topic.

1.2.2.1.1 Continuous fed rotary kilns with stationary thermocouples

[Wes 1976a] studied the heat transfer in an industrial rotary kiln measuring 0.6 m in diameter and 9 m in length, equipped with 9 lifters and externally heated by steam. The purpose of the study was to measure heat transfer coefficients in order to predict temperature profiles. Thermocouples were placed along the kiln at 4 axial positions to measure the gas and solids temperature, and another thermocouple was placed flush with the outer wall to record the wall temperature. Temperatures were recorded every 46 s and all the measurements were made in the steady state.

The measurement of the wall to solid heat transfer was achieved following the given procedure. The kiln was operated until the filling degree reached the desired value, at room temperature and without a forced air flow. The kiln was then stopped and heated to approximately 100°C. When the wall reached the desired temperature, rotation and temperature recording were started. Providing some assumptions, the wall to solid heat transfer coefficient could be determined from the analytical solution of the heat balance obtained (a differential equation) defined as follows:

$$m_b c_{pb} \frac{dT_b}{dt} = h_{cw-cb} A_{cw-cb} (T_w - T_b) \quad (1.37)$$

$$\ln \frac{T_w - T_b}{T_w - T_b^0} = - \frac{h_{cw-cb} A_{cw-cb} L}{m_s c_{ps}} t \quad (1.38)$$

where m_b is the mass of solid materials, c_{pb} the heat capacity, A_{cw-cb} the contact surface between the solid particle and the wall and h_{cw-cb} the related heat transfer coefficient. T_w and T_b are respectively the wall and solid particles temperature, and t is time.

Table 1.4: Summary of experimental studies on heat transfer in rotary kilns.

Authors	Kiln design			Kiln Features		Kiln operating conditions			Solids characteristics				Exp. measurements	
	Heating mode	Kiln diam., mm	L/D ratio, -	Lifters	Exit dam height, mm	Rotational speed, rpm	Kiln slope, °	Feed rate, kg.h ⁻¹	Solids	Heat diffus., 10 ⁻⁶ m ² .s ⁻¹	Particle size, mm	Bulk density, kg.m ⁻³	Temp. range, °C	Measured temp.
[Wachters 1964]	Indirect	152	3.1	No	No	0.48-43.2	0	Batch	Dry sand	0.274	N/A	N/A	90	Solids
[Wes 1976a]	Indirect	600	15	9	N/A	1.6-6.5	N/A	N/A	Carbo-hydrates	N/A	0.015-0.1	N/A	~100	Wall, gas, solids
[Lehmberg 1977]	Indirect	250	2.4	No	No	N/A	0	Batch	Sand Soda	0.218-0.224 0.158	0.16-1.04 0.137	1240-1480 675	200	Wall, solids
[Tscheng 1979]	Direct	190	13.2	N/A	29-51	0.4-6	1.36-4.1	11-50	Sand Limestone	0.210 N/A(?)	0.73 0.51-1.26	1650 1680	317	Wall, gas, solids
[Brimacombe 1978]	Direct	406	13.6	N/A	Yes	1-5	2.4	70-135	Sand	N/A	0.58	1587	~827	Wall, gas, solids
[Lybaert 1987]	Indirect	250-485	1.2-2.4	0-8	No	1-40	0	Batch	Glass Sand Steel	N/A	0.194-4	N/A	90	Wall
[Dhanjal 2004]	Direct	400	2.3	No	100	1-3	0	Batch	Sand	N/A	1.2-3	N/A	775	Wall, solids
[Suzuki 2008b] [Suzuki 2008a]	Indirect	1000	1.5	Yes	N/A	2.7-4	N/A	Batch	Model wastes	N/A	N/A	N/A	630	Wall, gas, solids
[Thammavong 2011]	Indirect	101	19	No	23.5	1-3	2.4	2.4-3.6	Sand	0.226	0.54	1220	600	Wall, gas, solids
[Herz 2012]	Indirect	600	0.75	No	No	1-6	0	Batch	Glass Sand Cooper	0.186 0.174 1.572	0.7-2 0.2 0.8	1680 1590 5580	200	Wall, gas, solids

The measurements of the heat transfer coefficient from wall to air were made with the kiln empty. The kiln was heated to approximately 90°C, an air flow was introduced at a constant rate.

The temperatures were measured and the coefficient was established with the use of a heat balance and logarithmic mean temperature difference:

$$h_{ew-g}A_{ew}\Delta T_{log} = \dot{M}_g c_{pg} (T_g^{out} - T_g^{in}) \quad (1.39)$$

where h_{ew-g} is the heat transfer coefficient from wall to gas, A_{ew} is the surface of exposed wall, ΔT_{log} is the logarithmic mean temperature, \dot{M}_g is the gas mass flow rate, and c_{pg} its heat capacity, T_g^{out} and T_g^{in} are respectively gas temperature before entering and upon leaving the kiln.

For the measurements of the gas to solid heat transfer, the kiln was partially filled with solids and a cold air flow was generated. Both temperatures of air and solids were measured at steady state, but the heating temperature is not mentioned. The latter coefficient was determined through a heat balance on the solids, requiring the wall to solid heat transfer coefficient:

$$h_{cw-cb}A_{cw-cb}(T_w - T_b) = h_{g-eb}A_{eb}(T_w - T_g) \quad (1.40)$$

where A_{eb} is the surface between solids and freeboard gas, and h_{g-eb} is the corresponding heat transfer coefficient.

[Wes 1976a] found that the gas to wall heat transfer coefficient was in the magnitude expected for natural convection coefficients, whereas the gas to solids heat transfer coefficient was found to be approximately an order of magnitude greater.

[Tscheng 1979] studied the convective heat transfer in a pilot scale rotary kiln measuring 0.19 m in diameter and 2.5 m in length, directly heated by a counter-current preheated air flow. The study aimed at determining the effects on the convection heat of gas velocity and temperature, kiln slope and rotational speed, solid hold up and mass flow rate, and particle size. Thermocouples were placed at four fixed positions inside the kiln to measure solids and gas temperature. Another set of thermocouples was positioned along the kiln wall and in the insulation. No specific procedure was applied to determine the heat transfer coefficient; the gas, solids, wall and insulation temperatures were recorded under varying conditions. Preliminary investigations showed that gas to wall radiation could be neglected (at around 300°C). The heat transfer coefficients were obtained from gas and solids temperature measurements with the use of heat balances. Some assumptions such as planar bulk bed upper surface, uniform wall temperature, uniform temperature at axial position and plug flow of gas and solid phases, were made. The following heat balances were established:

$$\dot{M}_b c_{pb} \frac{dT_b}{dz} = h'_{g-eb} l_{g-eb} (T_g - T_b) - h'_{cw-cb} l_{cw-cb} (T_b - T_w) \quad (1.41)$$

$$\dot{M}_g c_{pg} \frac{dT_g}{dz} = h'_{g-eb} l_{g-eb} (T_g - T_b) + h'_{g-ew} l_{g-ew} (T_g - T_w) \quad (1.42)$$

In these equations the different terms can be measured or determined from the temperature records, except for the three heat transfer coefficients. There is a need for either a third equation or an expression to determine the value of one of the unknown heat transfer coefficients per unit length h' . Thus [Tscheng 1979] developed a semi-empirical correlation based on the penetration theory to determine h_{cw-cb} using published data (see Equation 1.54 in Table 1.5). In the range of values tested by [Tscheng 1979], no significant effect of kiln slope, solid feed rate or particle size was observed on the convective coefficient. However the gas to solids transfer coefficient was found to be about 10 times higher than that of gas to wall.

[Thammavong 2011] designed an experimental setup for the study of heat transfer which is also used in the present study: the pilot scale rotary kiln is 0.1 m in diameter and 1.95 m in length, and

is indirectly heated. The study investigated the effects of solids flow rate and rotational speed on the heat transfer coefficient between the wall and solid particles. Stationary thermocouples placed in and outside along the kiln cylinder, 36 altogether, were used. The experimental procedure used is as follows: the operating parameters (feed rate, slope and rotational speed of the kiln, exit dam height) were set to the desired value, the process temperature was applied and the temperature recording was started. Temperature measurements showed that the steady state was reached within 5 h in the range of operating conditions studied. The wall-to-solid heat transfer coefficient was determined from a heat balance in the heated zone; radiative and convective heat transfer were taken into account for the calculation using the following correlation from the literature:

$$h_{cw-cb} = \frac{\dot{M}_b c_{pb} (T_b^{exit} - T_b^{entry}) + h_{g-eb} (T_b - T_g) + A_{eb} \sigma \varepsilon_b \varepsilon_w (1 - \varepsilon_g) F (T_b^4 - T_w^4)}{A_{cw-cb} (T_w - T_b)} \quad (1.43)$$

where the correction factor is defined by: $F = \frac{1}{\frac{1-\varepsilon_s}{\varepsilon_s} + 1 + \frac{1-\varepsilon_w}{\varepsilon_w} \frac{A_{eb}}{A_{ew}}}$. For the calculations only the data at steady state conditions were used. [Thammavong 2011] found that the wall-to-solid heat transfer coefficient linearly increased with the feed rate, and within the range of kiln rotational speeds investigated no significant effect was observed.

1.2.2.1.2 Continuous fed rotary kilns with rotating thermocouples

[Brimacombe 1978] designed a pilot scale rotary kiln, 0.4 m in diameter and 5.5 m in length, processing under counter-current direct-firing conditions. The study aimed at measuring the heat transfer fluxes from gas to wall and gas to solids, under varying conditions including kiln rotational speed, degree of fill and firing rate. The kiln was heavily equipped with thermocouples evenly distributed radially and along the kiln: 16 suction pyrometers (for gas temperature), 10 bare thermocouples (for solids temperature), 19 refractory thermocouples and 7 shell surface thermocouples were used. The central zone of the kiln considered as the test section, comprised 4 axial locations for the measurements and was the most heavily instrumented. All the thermocouples (52 in total) were fixed to the kiln and thus rotated with the kiln. Their signals were transferred to the recorder through a slip ring and a fixed brush contact. The operating procedure was as follows: (1) the empty kiln was preheated at half of the desired firing rate over the night, (2) the solids feed and firing rate were set at the desired value, (3) the temperatures (gas, wall and shell) were monitored until steady state conditions were reached, (4) the gas, solids, refractory wall and shell temperatures were recorded and the solids discharge rate was measured, (5) the temperatures were rechecked and a gas sample collected before stopping the kiln. With a similar hypothesis to that of [Tscheng 1979] presented above, the following heat balance was obtained over a section:

$$\frac{(\Phi_{g-ew} + \Phi_{g-eb})}{L} = \dot{M}_g \frac{dT_g}{dz} \left[c_{pg} + (T_g - T_{reference}) \frac{dc_{pg}}{dT_g} \right] \quad (1.44)$$

$$\frac{(\Phi_{g-eb} + \Phi_{ew-eb})}{L} = \dot{M}_b \frac{dT_b}{dz} \left[c_{pb} + (T_b - T_{reference}) \frac{dc_{pb}}{dT_b} \right] \quad (1.45)$$

Heat transfer fluxes were determined from the enthalpy balances using experimental data. [Watkinson 1978] provided a further analysis and obtained the following equation to determine the convective heat transfer coefficient between gas and solids:

$$h_{cs} = \frac{(\Phi_{g-eb} + \Phi_{ew-eb}) - \Phi_{g-eb}^{rad}}{A_{g-eb} (T_g - T_s)} \quad (1.46)$$

The main results from that study showed that at the working temperature investigated (between 200 and 800°C) convection played a minor role compared to radiation in the gas to solids heat flux. However under certain conditions of gas side-control (at high rotational speed), radiation represented less than 30% of the total gas to solids heat flux.

[Barr 1989a] instrumented extensively the rotary kiln used primarily by [Brimacombe 1978] for greater accuracy. Experiments were conducted to measure the heat transfer flux among the freeboard gas, the bulk materials, and refractory wall. The radial heat flux at the inside refractory surface was studied as a function of the circumferential position. The experimental procedure remained approximately the same as the one used by [Brimacombe 1978]. However the solids discharge rate was measured after 6 hours of operation and during 2 hours, then in the case of steady state conditions the thermocouple output data were recorded for 1.5 hours. The kiln rotation speed was mainly 1.5 rpm and the filling degree maintained at 12%. Operating temperatures were between 200 and 1500°C. It was found that the maximum rate of heat transfer from covered wall to the bed was 60% of the rate of heat transfer from freeboard gas to the exposed bed surface. These experimental results were used by [Boateng 1996] for verification of their one-dimensional model for heat transfer in rotary kilns.

1.2.2.1.3 Batch fed rotary kilns with stationary and/or rotating thermocouples

[Wachters 1964] demonstrated, providing some assumptions, that the heat transfer from the wall to the solid particles can be described by non steady heat conduction while studying the cooling of dry sand. One of the three average heat transfer coefficients that was determined could also be obtained directly from the penetration theory. The experimental setup consisted of a horizontal copper cylinder with an inside diameter of 0.152 m and length of 0.475 m that was partially filled with dry sand. Three thermocouples, placed inside the granular material along circular arcs of differing radii, were used. The cylinder was first heated up to about 90°C using gas burners, then it was rotated to homogenize the sand temperature, finally it was cooled down and the decrease in the temperature of the sand was recorded.

A similar procedure was followed by [Lehmberg 1977] who studied the cooling process of sand and sodium carbonate (soda) in a copper cylinder 0.25 m in diameter and 0.6 m in length. However some differences should be mentioned: (1) the cylinder was fitted with an adjustable half cylinder filled with insulating material, (2) the cylinder was heated up to 200°C while being rotated, (3) during cooling, the wall temperature was maintained constant and measured along with the solids temperature. The heat transfer coefficient between the wall and solid particles was then estimated similarly to [Wes 1976a]. It was shown that without taking into account the film resistance between wall and bulk bed (by adjusting the value of the contact resistance), correct calculation of the coefficient was not possible.

[Lybaert 1987] investigated the effect of different parameters on the wall-to-solid heat transfer coefficient. An externally heated (by electrical resistance) batch fed pilot scale rotary kiln 0.6 m long and with varying diameters (0.25 - 0.485 m), was used. 6 thermocouples were used to measure the wall temperature: 4 of them were evenly distributed around the tube at the mid-length of the kiln, and the other two were placed at 25 and 75% of the kiln length. The experimental procedure was as follows: (1) the empty kiln was heated at constant power until steady-state wall temperature, (2) a fixed quantity of solids at room temperature was fed into the kiln, and the transient evolution of the wall temperature was measured. During the whole procedure the heat power Q was maintained. The heat transfer coefficient was determined from the transient heat balance of the system, with some assumptions such as constant wall to solids heat transfer and heat loss, or uniform solids and wall temperatures:

$$m_b c_{pb} \frac{dT_b}{dt} + m_w c_{pw} \frac{dT_w}{dt} = h_{loss} (T_w^0 - T_w) \quad (1.47)$$

$$m_b c_{pb} \frac{dT_b}{dt} = h_{cw-cb} A_{cw-cb} (T_w - T_b) \quad (1.48)$$

where h_{loss} is the heat loss coefficient. The wall to solids heat transfer coefficient was obtained by fitting the measured data with the analytical solution of the system of Equations 1.47 and 1.48. It was found that the coefficient increased with the kiln rotational speed, but decreased with the particle size (especially at high rotation speed), and with the filling degree.

[Suzuki 2008b] set up experiments to measure the wall-to-solid heat transfer in an indirectly heated (by hot gas) batch-type rotary kiln 1 m in diameter and 1.5 m in length. The kiln was used for the pyrolysis of solid waste. Thermocouples were placed at the inner wall, in the solid waste, in the pyrolysis gas, in the heating gas and in the insulator. They were spaced in 3 series along the kiln, and except for the pairs of thermocouples attached to the inner and outer kiln wall, the thermocouples were stationary. [Suzuki 2008a] investigated the effects of kiln rotational speed, and number and height of lifters on the wall-to-solid heat transfer coefficient. The experimental procedure was described as follows: (1) temperature recording was started, and the kiln was heated to a predetermined temperature, (2) the solid waste was then fed into the kiln, (3) the heating stopped when no pyrolysis gas was detected. Assuming that the heat flux going through the wall Q_w was equal to the heat flux from the inner wall to the solid waste Q_{cw-cb} , the heat transfer coefficient was determined by:

$$h_{cw-cb} = \frac{Q_{cw-cb}}{A_{cw-cb} (T_w^{in} - T_w)} \quad (1.49)$$

$$Q_{cw-cb} = Q_w = \lambda_w \frac{(T_w^{out} - T_w^{in})}{\frac{D^{in}}{2} \ln \frac{D^{out}}{D^{in}}} \quad (1.50)$$

They found that during pyrolysis the heat transfer coefficient from wall to solids rises with an increase in the solid waste temperature, and significantly increases with the kiln rotational speed, and also with the number and height of lifters.

[Dhanjal 2004] studied the radial thermal gradients within the bed particles in a batch rotary kiln 0.4 m in internal diameter and 0.9 m long. 9 thermocouples were used to determine the refractory temperature at the blanket interface and hot face. A probe consisting of 4 thermocouples was placed approximately at the mid-length of the kiln and at different radial depths in the bulk bed. The kiln was directly heated using a natural gas burner. The procedure established was as follows: (1) the empty rotary kiln was rotated and heated, and as soon as the refractory hot face temperature reached 1100°C, rotation and heating were stopped, (2) when the hot face temperature dropped to about 1000°C, materials were uniformly fed in the kiln and the temperature recording started, (3) the bed temperature probe was positioned to be in the middle plane of the kilning bed, (4) Rotation was started and maintained for the duration of the run. Recording started at step 3 and the temperature acquisition lasted 20 min in total. Steps 3 and 4 lasted less than 2 min, so for uniformity step 4 was started at 3 min. Results showed that radial thermal gradients were likely due to inadequate particle mixing rather than to particle segregation that may exist.

[Herz 2012] conducted a systemic investigation of the heat transfer between the covered wall and bulk bed. An indirectly heated (by 3 electric radiant heaters) rotary kiln 0.6 m in internal diameter and 0.45 m in length was used. A rotating measuring rod of 16 thermocouples was used. One of these thermocouples was fixed to the inner wall, and the others were installed at different distances along the wall in a rotating measuring rod, so as to measure the solids temperature as well as the gas temperature. An additional stationary measuring rod was used to allow measurement of temperature at a defined radius. No specific experimental procedure was described. However, it seems likely that the solids were fed into the kiln to the desired filling degree, and the kiln rotational speed set, then the heating and temperature recording

were started. Measurements were stopped when steady state conditions were achieved. The wall to solids heat transfer coefficient was determined from an energy balance similar to the one given in Equation 1.48, assuming that the total energy supply at the wall is transferred to the solid materials and therefore neglecting the possible enthalpy transport in the wall. The transfer coefficient was found to increase with the kiln rotational speed (at constant filling degree), but decrease with the filling degree and the particle size.

1.2.2.2 Correlations

1.2.2.2.1 Heat transfer coefficient between wall and bulk solids

The heat transfer coefficient between wall and bulk bed of material plays an important role in the heat transfer model of a rotary kiln. Table 1.5 gives some of the correlations that are available in the literature. The penetration theory, widely used in the case of fluidized beds and fixed beds [Schlünder 1984a], has also been applied several times in previous investigations to determine the overall coefficient of heat transferred between the kiln wall and the bulk bed.

[Wachters 1964] developed a model (see Equation 1.51) assuming a thin layer at the wall, consisting always of the same particles mixing only with each other. However that hypothesis was not validated by the transverse mixing investigations conducted by [Lehmberg 1977] or [Wightman 1998]. [Wes 1976a] was among the first to use the penetration theory in a rotary kiln (see Equation 1.52) with the assumption of equal temperature at the contact point between wall and bulk bed. They mainly considered the transfer coefficient of the bed surface to bulk solid and thus neglected that of the wall surface to bed surface. [Lehmberg 1977] assumed the presence of a thin layer at the contact between covered wall and bulk materials, and so incorporated into the penetration theory an equation of heat flux to account for the thin gap as given in Equation 1.53. There have been other attempts by [Tscheng 1979, Ferron 1991, Ding 2001, Le Guen 2014, Li 2005] resulting in sometimes very complex equations. [Li 2005] proposed an extended model of the penetration theory for the wall-to-solid heat transfer coefficient, encompassing the heat transfer coefficient from the bed surface to the bulk materials, and the advection heat coefficient within the bulk materials. Note that [Malhotra 1990] extended the first particle heat transfer coefficient (inverse of the thermal contact resistance) to account for different particle geometries. Equation 1.54 by [Tscheng 1979] has been used several times [Gorog 1982, Owens 1991, Martins 2001, Herz 2012] and can be regarded as quite reliable. However, as shown by [Debacq 2001, Thammavong 2011, Herz 2012], there were often quantitatively significant differences between the models presented here. In addition, [Debacq 2001] conducted a sensitivity analysis clearly demonstrating that variations in the wall to solids heat transfer coefficient significantly impact the predicted bed temperature profiles.

1.2.2.2.2 Convective heat transfer coefficients

In rotary kilns the convective heat transfer includes the heat transfer from the freeboard gas to the exposed wall and to the exposed bulk solids surfaces. [Tscheng 1979] developed correlations for the gas to solids and gas to wall heat transfer coefficients from experimental data covering the effects of rotational speed, gas flow rate and filling degree, in a direct heated rotary kiln. The proposed correlations are as follows:

$$h_{g-ew}^{cv} = 1.54 \frac{k_g}{D_e} Re_g^{0.575} Re_w^{-0.292} \quad (1.58)$$

$$h_{g-eb}^{cv} = 0.46 \frac{k_g}{D_e} Re_g^{0.535} Re_w^{0.134} \eta^{-0.341} \quad (1.59)$$

Table 1.5: Summary of wall-to-solid heat transfer coefficient correlations.

Authors	Heat transfer coefficient equations
[Wachters 1964]	$h_{cw-cb} = \left(\frac{\sqrt{\pi a_b t_c}}{2k_b} + \frac{\sqrt{\pi} d'}{2k_b} \right)^{-1}, \quad (1.51)$ $n < 10rpm, d = 0.00112\sqrt{\phi_0}$
[Wes 1976a]	$h_{cw-cb} = 2\sqrt{\frac{k_b \rho_b c_{pb}}{\pi t_c}} \quad (1.52)$
[Lehmberg 1977]	$h_{cw-cb} = \sqrt{\frac{k_b \rho_b c_{pb}}{\pi t_c}} \left(\frac{2}{\sqrt{\pi}} - \frac{1}{h\sqrt{a_b t_c}} + \frac{1}{h\sqrt{a_b t_c}} \exp(h^2 a_b t_c) \operatorname{erfc}(h a_b t_c) \right), \quad (1.53)$ $h = \alpha_g / \lambda_b$
[Tscheng 1979]	$h_{cw-cb} = 11.6 \frac{k_b}{l'_w} \left(\frac{n R^2}{a_b \phi_0} \right)^{0.3} \quad (1.54)$
[Ferron 1991]	$h_{cw-cb} = \frac{k_b}{l'_w} \frac{2\sqrt{2}Pe^{1/2}}{1 + \sum_{j=1}^{\infty} \left[\frac{B_j(\phi_0)}{\pi a_1} \left(1 - \exp\left(\frac{-j^2 \pi \phi_0^2}{2Pe a_2^2}\right) \right) \right]}, \quad (1.55)$ $Pe = \frac{n R^2 \phi_0}{a_b}$
[Li 2005]	$h_{cw-cb} = \left(\frac{\chi d_p}{k_g} + \frac{1}{2} \sqrt{\frac{\phi_0}{2k_b \rho_b c_{pb} n}} \right)^{-1}, \quad (1.56)$ $0.096 < \chi < 0.198$
[Le Guen 2014]	$h_{cw-cb} = 0.032 Re^{0.8} St^{0.3} \left(1 + \left(\frac{D}{L} \right)^{0.7} \right) \left(\frac{\dot{m}_{b,cold} c_{pb,cold}}{\dot{m}_{b,hot} c_{pb,hot}} \right) \quad (1.57)$

Within $1600 < Re_g < 7800$ and $20 < Re_w < 800$, where $Re_g = V_g D_e / \nu$ is the gas flow Reynolds number, $Re_w = D_e^2 \omega / \nu$ is the rotational Reynolds number, $\eta = (\phi_0 - \sin \phi_0) / 2\pi$ is the percent fill, and $D_e = \frac{0.5D(2\pi - \phi_0 + \sin \phi_0)}{(\pi - \frac{\phi_0}{2} + \sin \frac{\phi_0}{2})}$ is the equivalent diameter. These correlations have been used in the literature by [Wild 1993, Martins 2001], for the modeling of heat transfer in rotary kilns.

Other correlations recommended by [Gorog 1982] were used in the literature, notably in the work by [Yang 1997, Silcox 1990, Patisson 2006]. [Gorog 1982] suggested using the following expression from [Kreith 1980] which is valid for the case of a not fully turbulent flow developed and $10 < L/D < 400$, to determine the convective heat transfer at the exposed wall:

$$h_{g-ew}^{cv} = 0.036 \frac{k_g}{D} Re_g^{0.8} Pr^{0.33} \left(\frac{D}{L} \right)^{0.055} \quad (1.60)$$

[Gorog 1982] developed a correlation from experimental studies for the convective heat transfer coefficient from the freeboard gas to the solids:

$$h_{g-eb}^{cv} = 0.4G_g^{0.62}, \quad G_g = \frac{\dot{M}_g}{A_g} \quad (1.61)$$

where G_g is the gas mass flux expressed in $\text{kg.m}^{-2}.\text{h}^{-1}$.

It must be mentioned that, in the case of natural convection of the gas phase inside the kiln, no correlation was found in the literature to model the free convection that may occur in the rotary kilns.

1.2.2.2.3 Radiative heat transfer coefficient

[Gorog 1981] developed charts which may be used for the evaluation of radiative heat transfer for any combination of kiln diameter, gas composition, temperature and filling degree. These charts were developed from the determination of the radiative exchange between free-board gas and the kiln wall, gas and solids, and kiln wall and solids. Radiative heat transfer occurred between the gas volume and boundary surfaces, i.e., the exposed wall and bulk bed. [Gorog 1983] proposed some of the following assumptions to simplify the radiative conditions: (1) both solids and wall exposed surfaces are taken to be radiatively gray, (2) inlet or outlet surfaces of the kiln are adiabatic, (3) the gas is taken to be radiantly gray (error must be about 20%), (4) uniform temperature of gas, wall and solid bed surfaces, (5) the effects of axial gradient in solids, wall and gas are neglected. On the basis of the above assumptions, the one-zone wall model for the radiative heat transfer flux within the free-board area can be determined.

[Oppenheim 1956] developed an electrical analogy for gray body heat exchange. The following two quantities were defined:

1. Irradiance E , the flux of energy that irradiates the surface, per unit area per unit time.
2. Radiosity J , the total radiation energy streaming from the surface, per unit area per unit time. It is the summation of the irradiated energy that is reflected and the emitted radiation by the surface as follows :

$$J = \varepsilon\sigma T^4 + (1 - \varepsilon)E \quad (1.62)$$

The net heat flux leaving any particular surface can be written as the difference between J and E , giving with Equation 1.62:

$$\frac{\phi}{A} = J - E = \frac{\varepsilon}{1 - \varepsilon} (\sigma T^4 - J) \quad (1.63)$$

Considering a surface i reflecting on n surfaces referred to as j , it is possible to write [Sacadura 1993]:

$$J_i = \varepsilon_i\sigma T_i^4 + (1 - \varepsilon_i) \sum_{j=1}^n F_{i,j} \tau_g J_j + (1 - \varepsilon_i) \varepsilon_g \sigma T_g^4 \quad (1.64)$$

where $F_{i,j}$ is the view factor between the surface areas A_i and A_j . The view factor (or shape factor) is a purely geometrical parameter that accounts for the effects of orientation on radiation between surfaces. $\tau_g = 1 - \varepsilon_g$ is the fraction of irradiation transmitted through the gas. Considering A_i and A_j , Eq.1.64 can be written as a system with two unknowns J_b and J_w :

$$\begin{bmatrix} Z_{bb} & Z_{bw} \\ Z_{wb} & Z_{ww} \end{bmatrix} \begin{bmatrix} J_b \\ J_w \end{bmatrix} = \begin{bmatrix} B_b \\ B_w \end{bmatrix} \quad (1.65)$$

with:

$$\begin{aligned}
&\succ Z_{bb} = 1 - (1 - \varepsilon_b)F_{bb}(1 - \varepsilon_g), \\
&\succ Z_{bw} = -(1 - \varepsilon_b)F_{bw}(1 - \varepsilon_g), \\
&\succ Z_{wb} = -(1 - \varepsilon_w)F_{wb}(1 - \varepsilon_g), \\
&\succ Z_{ww} = 1 - (1 - \varepsilon_w)F_{ww}(1 - \varepsilon_g), \\
&\succ B_b = \varepsilon_b \sigma T_b^4 + (1 - \varepsilon_b)\varepsilon_g \sigma T_g^4, \\
&\succ B_w = \varepsilon_w \sigma T_w^4 + (1 - \varepsilon_w)\varepsilon_g \sigma T_g^4.
\end{aligned}$$

The view factor ranges between zero and one. [Gorog 1981] defined the view factors for the one-zone wall model as follows:

$$F_{bb} = 0 \quad (1.66)$$

$$F_{bw} = F_{wg} = F_{bg} = 1 \quad (1.67)$$

$$F_{wb} = \frac{A_{eb}}{A_{ew}} \quad (1.68)$$

$$F_{ww} = 1 - F_{wb} \quad (1.69)$$

When using Eq. 1.63, the radiant heat transfer flux from the bed surface is expressed as:

$$\Phi_b^r = \frac{\varepsilon_b}{1 - \varepsilon_b} (\sigma T_b^4 - J_b) A_{eb} \quad (1.70)$$

The radiant heat transfer flux from the exposed wall, with the use of Eq. 1.63, is given by:

$$\Phi_w^r = \frac{\varepsilon_w}{1 - \varepsilon_w} (\sigma T_w^4 - J_w) A_{ew} \quad (1.71)$$

Using the one-zone wall model [Gorog 1982] defined the heat transfer coefficient as follows:

\succ at the exposed wall:

$$h_w^r = \frac{\varepsilon_w}{1 - \varepsilon_w} \frac{(J_w - E_w)}{(T_g - T_w)} \quad (1.72)$$

\succ at the exposed bed:

$$h_{eb}^r = \frac{\varepsilon_b}{1 - \varepsilon_b} \frac{(J_b - E_b)}{(T_g - T_b)} \quad (1.73)$$

Following this lead, [Li 2005] defined the radiant heat transfer coefficients in the case of internal heating as follows:

\succ from the gas to the bed surface:

$$h_{g-eb}^r = \frac{\Phi_{g-eb}^r}{A_{eb}(T_g - T_b)} = \frac{(E_g - J_b)/R_{g-eb}}{A_{eb}(T_g - T_b)}, \quad R_{g-eb} = \frac{1}{\varepsilon_g F_{bg} A_{eb}} \quad (1.74)$$

\succ from the gas to the exposed wall:

$$h_{g-ew}^r = \frac{\sum \Phi_{g-ew}^r}{A_{ew}(T_g - T_w)} = \frac{\sum (E_g - J_w)/R_{g-ew}}{A_{ew}(T_g - T_w)}, \quad R_{g-ew} = \frac{1}{\varepsilon_g F_{wg} A_{ew}} \quad (1.75)$$

\succ from the exposed wall to the exposed bed surface:

$$h_{w-eb}^r = \frac{\sum \Phi_{w-eb}^r}{A_{wb}(T_w - T_b)} = \frac{\sum (E_w - J_b)/R_{w-eb}}{A_{wb}(T_w - T_b)} \quad (1.76)$$

1.3 Global models for rotary kilns

As stated previously, rotary kilns are used in a wide range of processes. The global models developed and proposed in the literature mainly depend on the type of application and are thus very specific to a system, so as to take into account the reactions involved (specific geometry, operating conditions, etc.). However, all these models aim at a better understanding of the solids transport, heating and reaction behaviors or processes in order to improve and optimize the design or the control of the industrial unit. They are usually based on solids transport, mass and heat transfer equations for transient or steady state conditions. The global models can then be sorted in two categories: dynamic and non dynamic models. In the following sections the most recent research on this topic is presented. Most of these global models combine the transport and heat transfer models presented in preceding sections.

1.3.1 Non dynamic models

A variety of steady state models were established for directly or indirectly heated rotary kilns. Following the studies for example by [Wes 1976a, Brimacombe 1978], they are mostly based on the earlier models for solids transport by [Friedman 1949, Saeman 1951, Matchett 1987] and heat transfer by [Tscheng 1979, Jenkins 1981, Gorog 1981, Gorog 1982, Gorog 1983, Schlünder 1984a].

[Silcox 1990] developed a model to study of the effects of operating conditions and kiln design on solids bulk temperature. Results showed that higher bulk temperatures were obtained when operating the gas and solids in co-current flows.

[Boateng 1993] developed a quasi three-dimensional rotary kiln model. The model is a combination of a two-dimensional thermal model of a transverse plane and a one-dimensional plug flow type thermal model considering the transverse slice of the rotary kiln. Results from the model were compared to the temperature measurements of [Barr 1989b], and good agreement was found.

The study in a batch pilot scale rotary kiln by [Leger 1993] can also be mentioned. Solids were loaded in a preexisting hot bed, and a model was developed to predict the bed thermal histories from the mixing time constant. The model developed by [Lebas 1995a] for the pyrolysis of petroleum coke and those develop later by [Nicole 1996, Debacq 2001] in the field of uranium oxides preparation can also be mentioned.

[Martins 2001] presented a model to describe petroleum coke calcination in rotary kilns. The solid transport was based on the study by [Perron 1990]. The model predictions were validated using [Bui 1993] and compared to the predictions by the model of [Perron 1992] for the composition of the kiln exhaust gas. Except for a large deviation in the case of hydrogen, the model prediction was in good agreement with the experiment and better than the predictions of the [Perron 1992] model. The temperature profiles for the solids bed were also compared and showed some deviations.

[Li 2005] developed a model for a directly heated counter-current rotary kiln. The experiments by [Barr 1989b] were used for the model validation. Comparison of the predicted temperature profiles with experiments showed good agreement. While some discrepancies appeared when comparing predictions and measurements for heat transfer rates, they were small for the steady values.

[Zheng-ming 2013] developed a model for the simulation of an alumina rotary kiln based on the analysis of gas and solid bed motions as well as heat transfer and mass transport processes. The reliability of the model predictions was assessed only against the gas temperature measurements. Good agreement was found between experiments and predictions. Optimal excess air coefficient and coal amount in dry weight of raw material were found to improve the alumina yield.

1.3.2 Dynamic models

[Rovaglio 1998] developed a dynamic model to describe the behavior of a rotary kiln in a typical incineration plant. The model takes into account the primary combustion chamber, the after-burner and the heat recovery system. The empirical correlation by [Sullivan 1927] was used to determine the time of passage of solids. In addition, assumptions were made so that both gas and solids flows were considered faster with respect to mass and energy dynamic balances. The reaction scheme was based on the work of [Niessen 1978]. The bulk flow temperature variation with time was described by the lumped model, which assumes a uniform temperature within the bulk bed at any time. The model predictions were compared to the experimental data obtained during start-up procedures and unit operations. Results showed reasonable estimations of the heat of combustion, and the discrepancies observed in temperature profiles were attributed to fast changes in the waste feed rate, composition or heat of combustion.

[Cao 2000] developed a dynamic global model for a directly heated rotary kiln equipped with lifters. The model is based on fundamental mass and energy balances, and the kiln was divided into a number of equal-sized control volumes. A linear falling rate curve was used to describe the drying kinetic and the models by [Matchett 1987, Ranz 1952] were used respectively to describe the retention time and the wall-to-solids heat transfer coefficient. For the model validation, predicted parameters were compared to the measurements obtained while processing sorghum grains. Discrepancies lower than 10% were reported for the outlet solids moisture content and temperature.

[Shahhosseini 2001] developed a dynamic modeling methodology for a rotary kiln drying sugar. The heat and mass transfer rates were determined from on-line measurements. The dynamic model for the solids transport developed by [Shahhosseini 2000] from the work by [Friedman 1949] was used. Therefore the system was represented as a series of interconnected lumped parameter systems. However for better accuracy of dynamic processes, it is reported that the kiln must be axially discretized into 10 slices. With regard to the field of application, comparison of the model predictions with experimental data indicated accurate estimation of the sugar moisture content but less accurate predictions of the temperature at the outlet.

[Iguaz 2003] proposed a dynamic model for the dehydration of vegetable by-products in a rotary kiln. This model also sliced the kiln into a number of control volumes. The solids transport was described by [Friedman 1949]. The heat transfer within the control volume was considered with the use of the volumetric transfer coefficient defined by [Myklestad 1963]. Specific models were used to describe the drying rate. The model successfully predicted the steady state conditions, the outlet moisture content, and the temperature of air and product. Dynamic simulations were performed but the results were not confronted with experimental results.

[Descoins 2003] developed a dynamic model to describe a pyrolysis pilot scale rotary kiln. From the model of [Saeman 1951] a dynamic model was derived for the solids motion. The reaction scheme for the wood pyrolysis was based on the work by [Miller 1996, Mousques 2001]. The heat transfers were described with the use of the models proposed by [Lybaert 1985, Tscheng 1979, Sacadura 1993]. The dynamic solids motion model predictions were in good agreement with the experiments. However the global model was not validated by experiments, only results from simulations were presented.

[Ginsberg 2011a] developed a dynamic model of a rotary kiln for calcination of titanium dioxide white pigment. They used the chemical reactions as presented in [Ginsberg 2011b]. The solids transport was described by differential molar balances for all species in the axial direction, and the heat transfer was described using the models proposed by [Gnielinski 1975, Jeschar 1975, Schlünder 1984b, Barr 1989b]. The model was validated using dynamic and steady state experiments performed in an industrial plant. The overall agreement between the predicted and measured clinker temperature was good regarding the uncertainties of the model parameters.

1.4 Review Summary

With a view to developing a global model for flighted rotary kilns, the literature review has highlighted the following points:

1. The importance of understanding the main variable parameters influencing the solids transport behavior (kiln and internal fixtures design, solids characteristics, and operating conditions), in particular through the study of residence time of solids in the unit to be able to achieve representative modeling of the main transport characteristics such as mean residence time, hold up and axial dispersion.
2. The importance of accurate modeling of the heat transfer mode by convection, conduction and radiation within the rotary kiln. Models presented in the literature for the convective coefficient are scarce and none of them are appropriate for the case of natural convection of the gas inside the kiln. Concerning the wall-to-solid heat transfer coefficient models described in the literature, there is little or no consensus on the predictions.
3. The need to develop a dynamic model for flighted rotary kilns, sufficiently simple and accurate enough to be readily used across a wide range of applications. Up to now most of the global models presented are steady state models and usually related to a specific application, only a few dynamic models are reported.

Finally this critical analysis of the previous work achieved reveals a few key research gaps, which are useful for the definition of the main objectives in the present study as follows:

- Through a comprehensive RTD experimental study at room temperature:
 - investigate quantitatively the effect of lifter shape and number of rows, exit dam height, and usual operating parameters such as rotational speed, inclination, feed rates on solids transport characteristics, mean residence time and filling degree, but also axial dispersion and Peclet number which assess the mixing behavior, considering two kiln designs and various free-flowing solids.
 - correlate the solids transport characteristics namely, the mean residence time, the filling degree, and the axial dispersion coefficient, using dimensional considerations, taking into account identified variable parameters affecting the phenomena of interest and considering kiln design.
- Through a comprehensive experimental study investigating heating of the flighted rotary kiln at low to medium temperatures:
 - determine and characterize the convective heat transfer between the wall and gas, in the case of a non forced air flow. Develop a dimensionless correlation to describe the natural convection heat transfer coefficient in indirectly heated rotary kilns.
 - determine and characterize the wall-to-solids heat transfer coefficient with respect to experimental conditions, notably the rotational speed and the filling degree. Also develop with the use of dimensionless groups a correlation to describe the corresponding heat transfer mechanisms in indirectly heated rotary kilns.
- Through computation, develop a global dynamic model to determine gas, wall and solids temperature profiles when operating in indirectly heated rotary kilns equipped with lifters, with the aim of being simple in use for design, scaling or control purposes.

Methodology

“... all knowledge starts from experience and ends in it. Propositions arrived at by purely logical means are completely empty as regards reality.”

(Albert Einstein, 1879-1955)

Chapter 2

Methodology

2.1	Experimental apparatus	68
2.1.1	General characteristics	68
2.1.2	Thermal metrology	70
2.1.3	Internal and external fixtures, features or devices	71
2.2	Materials properties	73
2.2.1	Selected solids: physical properties	73
2.2.2	Thermo-physical properties	75
2.3	Experimental procedures	77
2.3.1	Hydrodynamics	77
2.3.2	Temperature profile measurements	85
2.4	Dimensional analysis	87
2.5	Methodology summary	88

The main objectives of this thesis have been outlined in the introduction and put in context by an analysis of the state of the art within the field of rotary kilns. In order to achieve the defined objectives, a research methodology was set up. The methodology involves both aspects of the study: experiments and modeling. This systematic research methodology is summarized in Figure 2.1.

The experimental campaign initiated in the study involves experiments at room temperature, and experiments in a rotary kiln heated at low to medium temperatures. The solids transport characteristics were investigated at room temperature in particular through impulse response tests using tracers, but not exclusively. Three free flowing granular solids having different shapes and sizes were selected, as well as the corresponding tracers. Comprehensive experimental matrices were designed with regard to the dimensional analysis. These experiments consider: kiln and lifter design, operating conditions such as kiln rotational speed and slope, flow rate or exit dam height. The measured variables are: the tracer concentration, the hold-up, but also the bed depth and the time elapsed to obtain steady flow conditions.

The thermal study is achieved using a pilot scale rotary kiln implemented with thermocouples connected to a fast temperature logging system. It was then possible to measure the temperature profiles of the heating zones, the free-board gas and the bulk of solids. The effects of lifters and of the above-mentioned operating conditions except the kiln slope were investigated.

Correlations were established through dimensional considerations and adjusted with experimental results to describe the solids transport behavior but also the heat transfer mechanisms. The predictive performance of these correlations was also compared to experimental studies from the literature when possible.

Finally these correlations were used to develop a global model to be used as a toolkit for the design, process control and scaling for a wide range of applications.

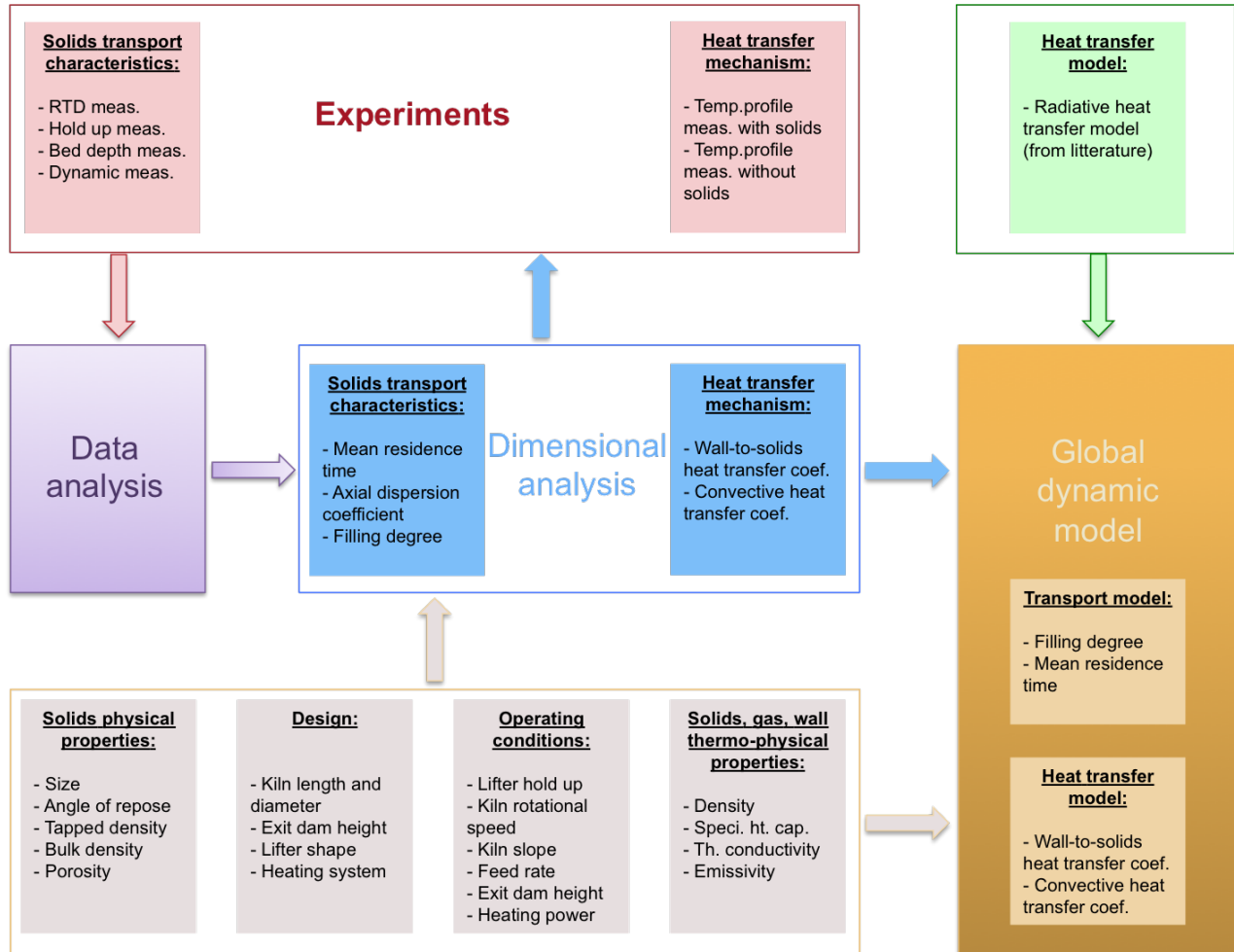


Figure 2.1: Research methodology.

Les principaux objectifs de cette thèse ont été abordés dans l'introduction et ensuite ont été mis en contexte davantage par une analyse de l'état de l'art dans le domaine des fours tournants. Afin d'atteindre les objectifs définis, une certaine méthodologie de recherche a été utilisée. Cette méthodologie implique les deux aspects majeurs de ce travail en mettant en œuvre des études expérimentales et de la modélisation. Cette méthodologie de recherche systématiquement appliquée est résumée dans la Figure 2.1.

Les travaux expérimentaux initiés dans cette étude impliquent des expériences dans des fours tournants à échelle laboratoire à température ambiante, ainsi qu'à des températures élevées. Les caractéristiques du transport des particules solides ont été étudiées à température ambiante, en particulier grâce à des tests d'injection impulsion (ou Dirac) de traceurs, mais pas exclusivement. Trois types de particules solides caractérisées par leur écoulement libre ou fluide, avec des propriétés physiques (formes et tailles) différentes ont été choisis, ainsi que les traceurs correspondants. En fonction de l'analyse dimensionnelle effectuée, des matrices expérimentales assez complètes ont été conçues. Les essais réalisés tiennent en compte la présence ou non de relevés, ainsi que différentes conditions opératoires pour la vitesse de rotation et l'inclinaison du four,

le débit d'entrée ou la hauteur du diaphragme en sortie. Les variables mesurées sont alors : la concentration de traceurs en sortie, la charge du four, mais aussi le profil de charge (hauteur du lit de particules solides) et le temps écoulé pour obtenir des conditions d'écoulement stable.

L'étude thermique est réalisée dans un four tournant à échelle pilote équipé de thermocouples reliés à un système d'acquisition rapide permettant de relever et d'enregistrer les données de température. Les profils de température dans les zones de chauffage ont pu être déterminés, en particulier ceux de la phase gazeuse et du lit de particules solides. Les effets des releveurs et des conditions opératoires mentionnées ci-dessus à l'exception de l'inclinaison du four ont été étudiés.

Des corrélations ont été établies en tenant compte de considérations dimensionnelles et elles ont été paramétrées à l'aide des données expérimentales, afin de décrire le comportement de la charge solide au cours de son transport, mais aussi les mécanismes de transfert de chaleur. Les performances prédictives de ces corrélations ont également été analysées et comparées lorsque cela était possible aux résultats des études expérimentales issues de la littérature.

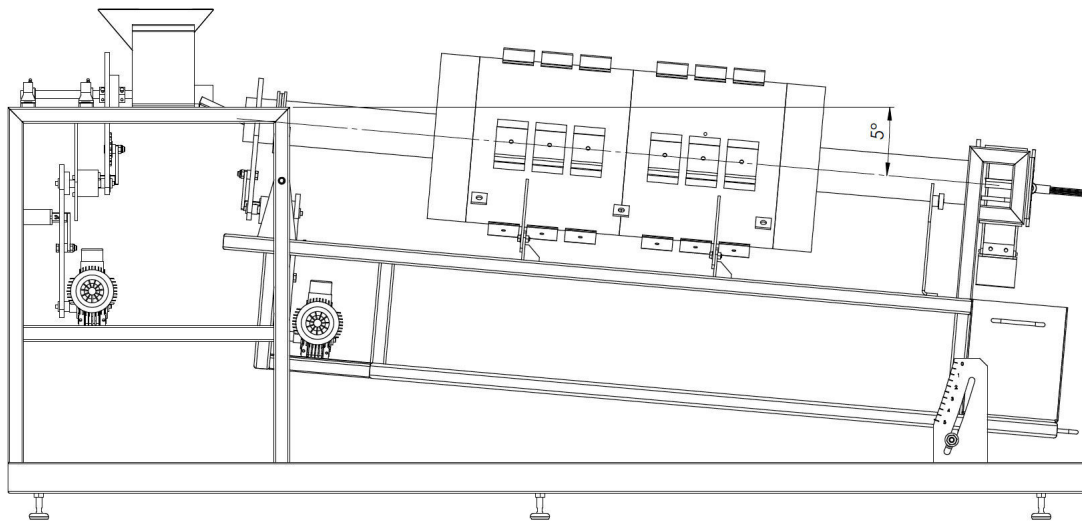
Enfin, ces corrélations développées, constituent des sous-modèles d'un modèle global de four tournant faisant office d'outils pertinent et performant pour la conception, le changement d'échelle ou l'optimisation des conditions opératoires de fours tournants pour une large gamme d'application.

2.1 Experimental apparatus

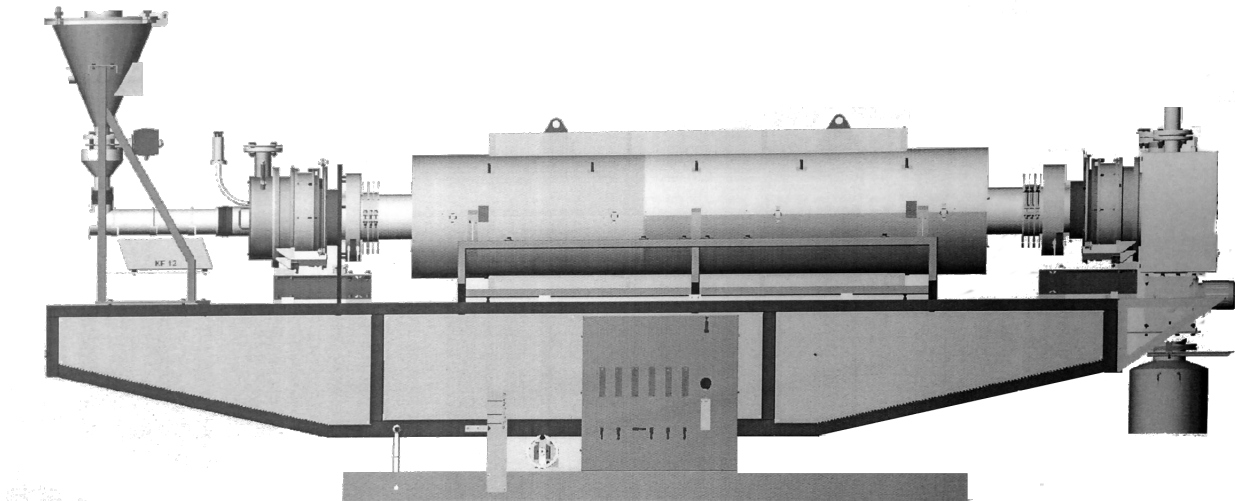
The experiments reported in this study were performed using two pilot scale rotary kilns. The smaller kiln referred to as RK1 was installed at the LCMGPCE (CNAM Paris), and the larger one, referred to as RK2, was installed at the RAPSODEE center (Mines d'Albi). The main characteristics of these rotary kilns are summarized in Table A.1 in Appendix A.

2.1.1 General characteristics

The layouts of the experimental apparatus are presented in Figure 2.2. Both systems mainly consist of a feeding system, a counter-clockwise rotating kiln and a recovery zone.



(a) LCMGPCE rotary kiln (RK1)

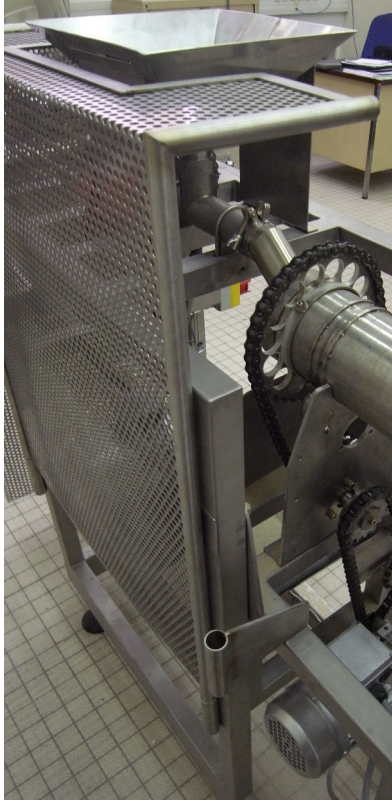


(b) RAPSODEE rotary kiln (RK2)

Figure 2.2: Side views of the experimental apparatus.

Considering Figure 2.3, the feeding systems of RK1 and RK2 may seem similar at first sight, but they differ by the mechanical solution adopted to feed the kiln. The feeding system of RK1 is a combination of a 5 dm³ hopper, from which solids flow through a motor-driven screw, and a feed chute, from which the solid particles are delivered to the kiln inlet. The feeding system

of RK2 consists of a 30 dm³ hopper, followed by a vibrating cylindrical conveyor. The feed rate is set by adjusting the rotational frequency of the screw feeder for RK1, and for RK2 by adjusting the vibration frequency of the conveyor. RK2 is equipped with an electronic balance allowing continuous measurements of the inlet mass flow rate. These measurements are used by a controller to adjust the vibration frequency of the conveyor to obtain the desired feed rate (PID adjustment loop).



(a) RK1



(b) RK2

Figure 2.3: Feeding systems.

The RK1 rotary tube is made of an Incoloy alloy 800, and measures 1.95 m in length and 0.101 m in (internal) diameter. The RK2 rotating tube is 4.2 m long and 0.21 m (internal) diameter, and is made of nickel-chrome. The internal wall of both kiln tubes is smooth. The kiln tubes are supported on rollers. In addition these tubes are driven from the inlet end through chains and sprockets, and a variable speed motor. Depending on the sprockets installed, RK1 and RK2 can be respectively operated at speeds between 0.5-12 rpm, and 0.5-21 rpm. Using hydraulic pumps and an electronic level, the RK1 and RK2 units can be tilted respectively to an angle of 5 and 7°.

Both kilns are indirectly heated by furnaces comprising independent heating zones placed side by side as shown in Figure 2.4. Each heating zone is composed of heating resistors and insulation. The RK1 furnace is made of 2 heating zones designed to heat the kiln wall up to 1000°C. The RK1 heating elements can each deliver a maximum power of 5 kW. The RK2 furnace is made of 5 heating zones also designed to heat the kiln wall up to 1000°C. The two heating devices placed at the ends (Zones 1 and 5) can each deliver a power up to 10.8 kW, whereas in the central zones 2, 3 and 4, they are limited to a power of 5.4 kW.

After being processed, the solids exiting the kiln tube are collected in a storage tank. In the case of RK2, a tank (30 dm³) can be attached in a sealed manner to the exit chamber. Unlike RK1 which is operated at atmospheric pressure, RK2 can be operated under a positive working pressure using air or nitrogen.

2.1.2 Thermal metrology

Adequate instrumentation is required for the study of heat transfer within rotary kilns. Therefore the experimental apparatus are equipped with thermocouples (TC) for the measurement of wall, gas and bed temperature profiles as shown in Figure 2.4.

2.1.2.1 RK1 instrumentation

Temperatures in the solids bed and the free-board gas are measured by 20 TC of type N, 1.5 mm in diameter. An additional set of 16 TC of type K 3 mm in diameter are used to measure temper-

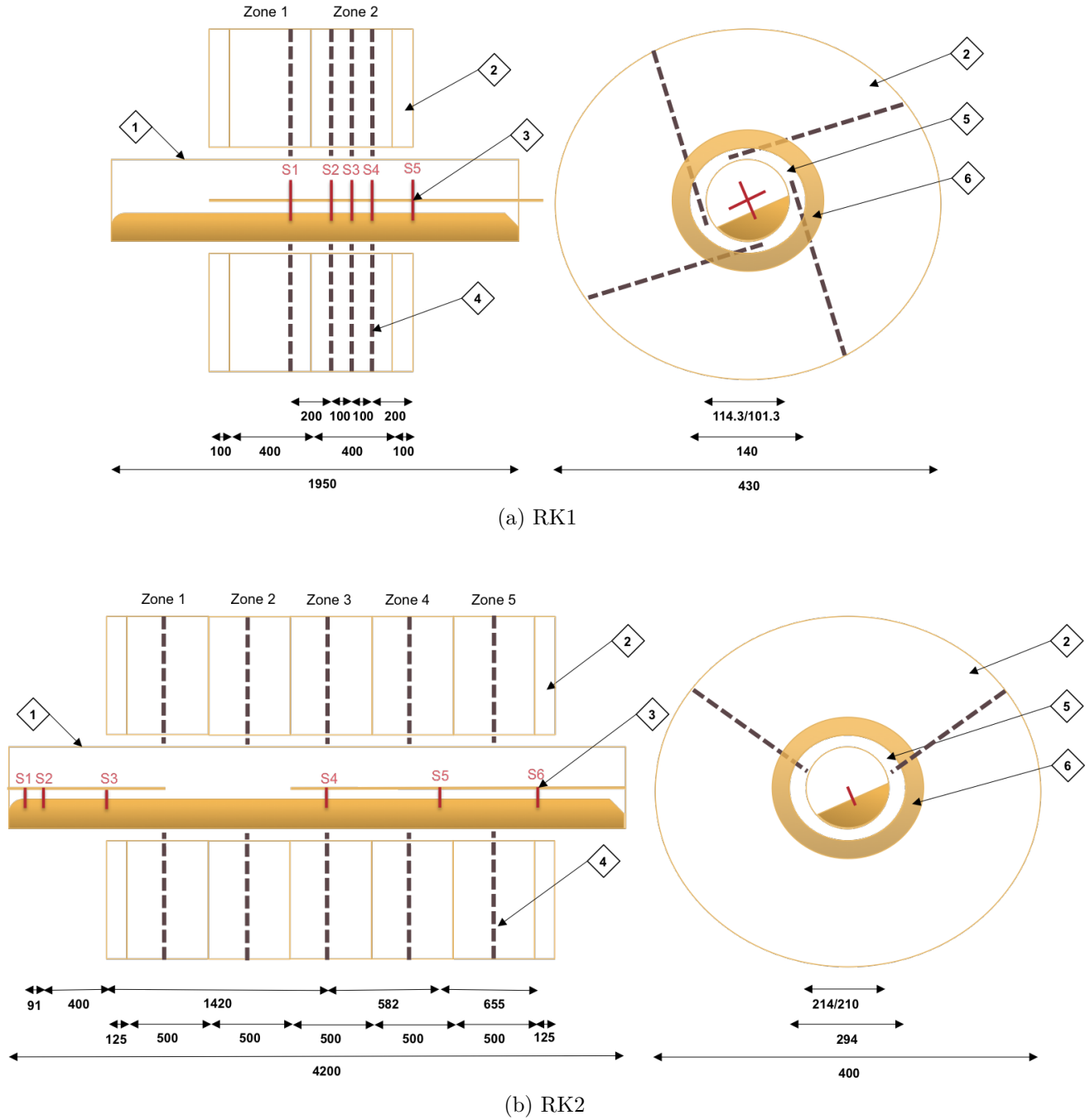


Figure 2.4: Layout of the experimental apparatus heating zones, longitudinal (left side) and transverse (right side) sections: (1) kiln tube, (2) Insulation, (3) Measuring rod with thermocouples, (4) external thermocouples, (5) air, (6) heating resistors.

atures at the outer wall. The thermocouples were calibrated with a tolerance of $\pm 1.5^{\circ}\text{C}$ according to the manufacturer. Uncertainty calculations from repeated experimental measurements show that type N and K TC have respectively an uncertainty of $\pm 1^{\circ}\text{C}$ and $\pm 1^{\circ}\text{C}$.

The 20 type N TC used are installed in a measuring rod, and arranged in a series of 5 sections. At each section, 4 TC are installed; 3 of them are placed so as to be in the free-board gas and the remaining TC is embedded in the case of solids flow. The measuring rod is placed inside the kiln tube. The axial and radial locations of the TC are shown in Figure 2.4a. These TC were radially positioned so as to avoid contact with lifters when present.

The 16 type K TC used to measure the kiln wall temperature are installed at the outer wall and arranged in a series of 4 sections. To protect the TC from the radiation emitted by the heating resistors, their tips are sheathed in ceramic. The measured temperature can be assumed to be either the resistance temperature or virtually the wall temperature. As shown in Figure 2.4a, at each section 4 TC are placed around the outer wall in the air between the tube and resistors. The first section of TC namely S1 is located in the heating zone 1 and the 3 other sections namely S2, S3 and S4 are located in the heating zone 2. In each zone one TC is used by the temperature controller. It is possible to measure the wall temperature directly using a pyrometer via a hole in the heating unit, in order to validate measurements of the type K TC.

2.1.2.2 RK2 instrumentation

Temperatures in the solids bed are measured using 6 type K TC 2 mm in diameter, and additional 10 type K TC are used to measure the heating resistors temperature.

The TC used to measure the resistors or virtually the wall temperature are intended to feed the temperature controllers of the heating zones. They are arranged in a series of 5 sections. Each section is positioned at the center of a heating zone and is equipped with 2 TC spaced by an angle of 100° around the kiln, as shown in Figure 2.4b.

Two measuring rods are used to support the 6 TC intended to be embedded as presented in Figure 2.4b. The first rod, which holds half of the TC, is installed at the inlet end before the heating zone, but is not readily accessible. The axial positions given at S1, S2 and S3 are only estimated positions. The remaining TC are installed in the second rod which is inserted from the outlet end. For the latter, the positions S4, S5 and S6 are precisely defined.

Unlike the instrumentation of RK1, there are no thermocouples for the measurement of the free-board gas in the RK2 instrumentation.

2.1.3 Internal and external fixtures, features or devices

The rotary kilns can be equipped with specific fixtures or linked to some devices or other apparatus.

In order to limit back spillage outside of solids flow at the kiln entrance, RK2 is fitted with a dam at the inlet end. Unlike RK2, RK1 can be fitted at the outlet end with a dam of a specific open diameter as presented in Figure 2.5. This makes it possible to set the exit bed depth to a given value.

Lifter structures can be fitted to the smooth inner wall of both kilns. Two structures fitted with 4 identical non removable single throughout lifters equally distributed in the periphery were designed for RK1. These structures differ by the shape of the lifters: straight one-section 10 mm lifters referred to as straight lifters (SL), and two-section 10 mm lifters with a right angle cross section referred to as rectangular lifters (RL), as shown in Figure 2.6a and 2.6b. For RK2, one lifter structure was designed. The structure can be fitted with up to 36 identical removable straight lifters of 30 mm each, that can be longitudinally arranged either as single throughout lifters or as segmented lifters, and also equally distributed in the periphery. 3 configurations were

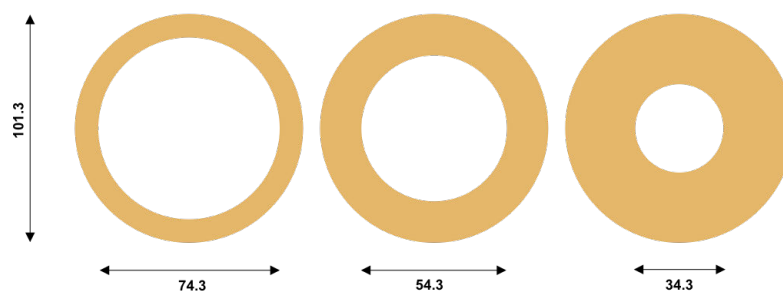


Figure 2.5: Exit dams available for RK1.

used: 1) no lifters, 2) 3 rows of single throughout lifters (see Figure 2.6c), and 3) 6 rows of single throughout lifters (see Figure 2.6d). Instead of the lifter structure, as shown in Figure 2.7, RK2 can be fitted with a grid to avoid slipping motion by increasing the friction between the solids bed and the kiln wall.



Figure 2.6: Shapes and configurations of lifters used.



Figure 2.7: RK2 fitted with the grid.

RK2 can be equipped with an additional electronic balance allowing continuous measurements of the outlet flow rate.

RK1 can be equipped with a chamber at the kiln outlet to monitor the gas inflow during the heating phase; in addition, the gas flow rate can be varied up to $7 \text{ Nm}^3 \cdot \text{h}^{-1}$. However this setup is not readily connected to a gas network.

When operated under positive pressure, the gas concentration along RK2 can be regulated through flowmeters, and bursting disks intended to limit damage in the event of unexpected high pressure, are installed at the kiln ends. Finally, possible gases released during a reaction and which may contain volatile organic compounds, are discharged and destroyed through a thermal oxidizer following the exit chamber.

2.2 Materials properties

2.2.1 Selected solids: physical properties

For the purposes of this study, three granular solids were selected. The selection criteria are based on physical characteristics such as the size, or angle of repose, but also on the thermal characteristics. In particular, for the study of heat transfer mechanisms in a hot rotary kiln, the selected solids must be non-reactive at the chosen operating temperatures.

The main physical properties of the selected granular solids, namely, sand, broken rice, and beech chips, operated at ambient temperature are presented in Table 2.1.

Table 2.1: Selected granular material to be operated at room temperature.

Product	Shape	ρ_{true} [kg.m ⁻³]	ρ_{bulk} [kg.m ⁻³]	ρ_{tapped} [kg.m ⁻³]	Hausner ratio [-]	Size [mm]	θ [°]	Remarks
Sand	Nodular	2636	1422	1543	1.085	0.55	39	-
Broken rice	Cylindrical	1463	889	934	1.051	3.8×1.9	36	-
Beech chips	Parallelepiped	1506	260	284	1.092	10×4.5×2	42	-
NaCl	Nodular	-	1087	1184	1.089	0.6	35.4	Sand tracer
Dyed sand	Nodular	-	1422	1543	1.085	0.55	39	Sand Tracer
Dyed broken rice	Cylindrical	-	824	867	1.053	3.8×1.9	37.6	Rice tracer
Dyed beech chips	Parallelepiped	-	260	284	1.092	10×4.5×2	42	Beech chips tracer

The true (or skeletal) density of solids, ρ_{true} , is determined by pycnometry, by measuring changes in pressure with gas displacement.

The bulk (or pour) density of solids, ρ_{bulk} , is determined by weighing a known volume of solids simply poured into a measuring cylinder.

The tapped density of solids, ρ_{tapped} , is determined by:

1. placing a known weight of solids in a measuring cylinder,
2. “hand tapping” the measuring cylinder until a consistent volume, assumed to be the maximum packing density of the solids, is reached. However the raising and lowering of the cylinder were done without reference to the height and arbitrary acceleration in both directions (upward and downward).

A jolting volumeter was also used, and the results were very similar.

The solids angle of repose, θ , which is defined as the angle between the free surface of a pile of solid particles on a horizontal board to the horizontal plane [McGlinchey 2008], is calculated by means of the fixed cone method similarly to [Thammavong 2011]. The solid particles were poured into a funnel, centered over a grid sheet. The solids falling onto the sheet formed a heap, whose diameter and height were measured to estimate the angle of repose.

The Hausner ratio is determined from the ratio of the tapped density to the bulk density. Note that free flowing materials are characterized by a Hausner ratio below 1.25.

The three solids namely, sand, broke rice and beech chips, were chosen for the study at room temperature in particular for their differing properties in size and repose angle. Note that these

solids are all classified as free flowing materials. They are mostly used for RTD measurements, except for the sand which is also used for bed depth and dynamic measurements. For that reason tracer characteristics are also given in Table 2.1. Except for the salt used for the sand bulk bed, the other tracers were prepared from samples of the selected granular materials by coloring, using red dye. Therefore the dyed tracers were expected to share similar properties with the bulk materials, thus introducing as few disturbances as possible on the bulk flow.

Note that the presented densities have an uncertainty about $\pm 30 \text{ kg.m}^{-3}$; the angle of repose is determined within $\pm 1^\circ$. Regarding the particle size, the figures are averaged values. Using granulometric analysis, the sand grain size ranges between 0.4 and 0.8 mm as specified by the supplier as shown in Figure 2.8a. Sand diameter was found to be on average 0.55 mm from sieve analysis (with a maximum at 0.63-0.8 mm), and about 0.64 mm using the MasterSizer 3000 system (Malvern). An amount of 122 g of broken rice grains was measured using a sliding caliper. It can be seen in Figure 2.8b that the broken rice length was found to be within 2.5-4.4 mm, with an average diameter of 1.9 mm. 250 beech chips, randomly chosen among tracers, were measured using a sliding caliper. As illustrated in Figure 2.9, beech chip particles measured about 5-17 mm in length, 2-8 mm in width and 1-4 mm in thickness.

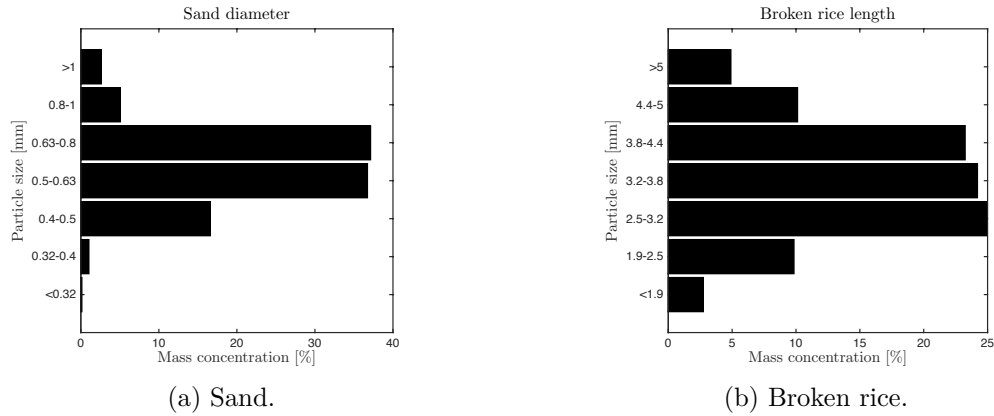


Figure 2.8: Particle size distribution: sand and rice.

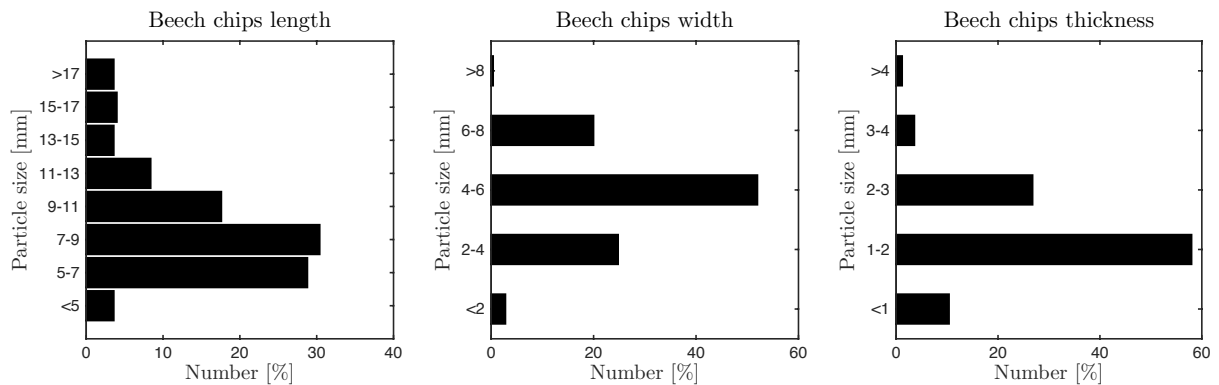


Figure 2.9: Beech chips size distribution in length, width and thickness.

2.2.2 Thermo-physical properties

Table 2.2 shows the thermo-physical properties of solids, gas and wall at an operating temperature of 300°C. Details of the thermal properties calculations, values or assumptions are given in the following paragraphs.

Table 2.2: Thermal properties of materials at 300°C.

Material	Sand	Air	Inconel	Remarks
ρ [kg.m ⁻³]	1422	0.616	7950	Density
c_p [J.kg ⁻¹ .K ⁻¹]	835	1045	514	Specific heat capacity
k [W.m ⁻¹ .K ⁻¹]	0.1836	0.0449	18.75	Thermal conductivity
α [m ² s ⁻¹]	1.5 10 ⁻⁷	696.9 10 ⁻⁷	0.5 10 ⁻⁷	Thermal diffusivity
ε [-]	0.76	0.01	0.9	Emissivity
ϵ_0 [%]	43.36	-	-	Measured porosity

Bulk Bed: Sand

Sand was also chosen for the study of heat transfer essentially for its non-reactive properties.

- $\rho_b = 1422$ kg/m³. The measured density is assumed invariant with temperature.
- $c_{pb} = 835$ J/kg.K [Thammavong 2009]. The specific heat capacity is assumed invariant with temperature.
- $k_b = k_{cb} + k_{rb}$, the thermal conductivity of the bed is determined using correlations presented by [Bauer 1977]:

$$- \frac{k_{cb}}{k_g^{int}} = 1 - (1 - \epsilon_0)^{1/2} + (1 - \epsilon_0)^{1/2} \left(\frac{2}{1-B/Z} \right) \left(\frac{(1-1/Z)B}{(1-B/Z)^2} \ln(Z/B) \right) - \frac{B+1}{2} - \frac{B-1}{1-B/Z}, \quad k_{cb} \text{ is the thermal conductivity through contact area.}$$

$$* B = 1.25 \left(\frac{1-\epsilon_0}{\epsilon_0} \right)^{10/9}, \quad \epsilon_0 = 0.43 \text{ is the bulk porosity.}$$

$$* Z = \frac{k_{pa}}{k_g^{int}}, \quad k_{pa} = 2 \text{ W/m.K is the particle thermal conductivity, } k_g^{int} = 0.01 \text{ W/m.K is the gas thermal conductivity.}$$

$$- \frac{k_{rb}}{k_g^{int}} = \left(1 - (1 - \epsilon_0)^{1/2} \right) fr + \frac{(1-\epsilon_0)^{1/2}}{\left(\frac{1}{fr} + \frac{k_g^{int}}{\lambda_0} \right)}, \quad k_{rb} \text{ is the thermal conductivity due to radiation.}$$

$$* fr = \frac{4\sigma T_b^3}{\left(\frac{2}{\epsilon_{pa}} - 1 \right)} \frac{D_{pa}}{k_g^{int}}, \quad \epsilon_{pa} = 1 \text{ is the particle emissivity, } D_{pa} = 0.55 \cdot 10^{-3} \text{ m is the particle diameter, } \sigma = 5.6703 \cdot 10^{-8} \text{ W/m}^2 \cdot \text{K}^4.$$

ϵ_0 is the sand porosity and was determined within $\pm 2\%$ by picnometry measurements.

$$➤ a_b = \frac{k_b}{\rho_b c_{pb}} \text{ m}^2/\text{s}, \text{ the bed thermal diffusivity.}$$

The thermal constants analyser TPS 2500 S by Hot Disk was used to determine both sand thermal conductivity and thermal diffusivity. The measurements were performed by applying a power of 0.03 W, during 20 s, and with the use of a sensor of 3.2 mm in radius. As shown in Figure 2.10, for the measured sand porosity of 0.43, the measurements and the predictions do not agree well for thermal conductivity and thermal diffusivity. To achieve the measurement, the sand was compacted, and so its porosity is modified and this may affect the thermal constants measured. As given in Figure 2.10, with a lower porosity of about 0.23, the predictions are significantly better.

$$➤ \varepsilon_b = 0.76 \text{ [Thammavong 2009], the bed thermal emissivity.}$$

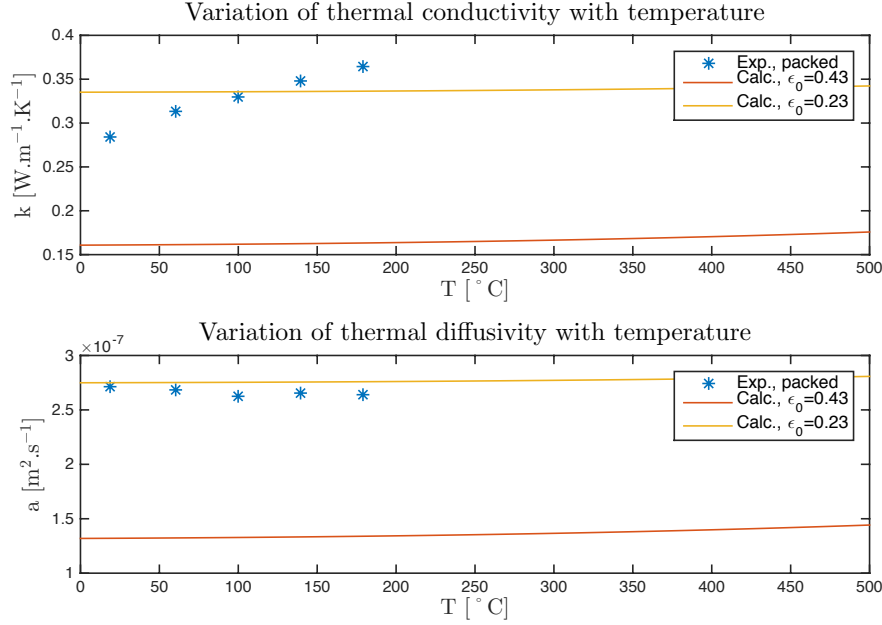


Figure 2.10: Thermal conductivity and diffusivity: experiments vs. [Bauer 1977] model predictions.

Gas: Air

➤ $\rho_g = 1.293 \frac{273.15}{T_g} \text{ kg/m}^3$, the gas density. (Derived from the ideal gas law)

The following correlations are derived respectively for the air specific heat capacity, thermal conductivity, cinematic and dynamic viscosity from the results by [White 1988]:

➤ $c_{pg} = 1.9327 \cdot 10^{-10} T_g^4 - 7.9999 \cdot 10^{-7} T_g^3 + 1.1407 \cdot 10^{-3} T_g^2 - 4.4890 \cdot 10^{-1} T_g + 1.0575 \cdot 10^3 \text{ J/kg.K.}$

➤ $k_g = 1.5207 \cdot 10^{-11} T_g^3 - 4.857 \cdot 10^{-8} T_g^2 + 1.0184 \cdot 10^{-4} T_g - 3.9333 \cdot 10^{-4} \text{ W/m.K.}$

➤ $\nu_g = -1.363528 \cdot 10^{-14} T_g^3 + 1.00881778 \cdot 10^{-10} T_g^2 + 3.452139 \cdot 10^{-8} T_g - 3.400747 \cdot 10^{-6} \text{ m}^2/\text{s.}$

➤ $\mu_g = 8.8848 \cdot 10^{-15} T_g^3 - 3.2398 \cdot 10^{-11} T_g^2 + 6.2657 \cdot 10^{-8} T_g + 2.3543 \cdot 10^{-6} \text{ Pa/s.}$

➤ $a_g = \frac{k_g}{\rho_g c_{pg}} \text{ m}^2/\text{s}$, the air thermal diffusivity.

➤ $\epsilon_g = 0.01$ [Thammavong 2009], the air emissivity.

Wall: Inconel 800

➤ $\rho_w = 7940 \text{ kg/m}^3$ [Corporation 2014] is the wall density and is assumed invariant with temperature.

The following correlations are derived respectively for the air specific heat capacity, and thermal conductivity from the results by [Corporation 2013] and [Corporation 2014]:

➤ $c_{pw} = 4.7374 \cdot 10^{-7} T_w^3 - 1.0958 \cdot 10^{-3} T_w^2 + 9.9514 \cdot 10^{-1} T_w + 2.1441 \cdot 10^2 \text{ J/kg.K.}$

➤ $k_w = 2.5285 \cdot 10^{-8} T_w^3 - 5.1235 \cdot 10^{-5} T_w^2 + 4.8213 \cdot 10^{-2} T_w + 9.220 \cdot 10^{-1} \text{ W/m.K.}$

➤ $a_w = \frac{k_w}{\rho_w c_{pw}} \text{ m}^2/\text{s}$ is the wall thermal diffusivity.

➤ $\epsilon_w = 0.9$ (from manufacturer), the wall emissivity.

2.3 Experimental procedures

The experimental procedures used to achieve the study of solid materials transport and heat transfer in flighted rotary kilns are detailed step-by-step in the following sections. Sufficient details are given so that other researchers in the field can duplicate exactly the experiments. While it was not possible to repeat every single experiment to verify the consistency of results, chosen experiments were repeated to assess reproducibility and uncertainties.

2.3.1 Hydrodynamics

The solids transport characteristics of flighted rotary kilns were investigated through the study of residence time distribution (RTD), solids bed profile, and solids flow behavior following a step change of an operating parameter of the system.

2.3.1.1 RTD measurements

These experiments aim not only to characterize the effect of lifter shape and operating parameters on the RTD of solids particles but also on the corresponding mean and variance of residence time, Peclet number and axial dispersion coefficient. Solids hold up, time of passage, and segregation are also within the scope of these experiments.

The RTD of particulate solids were determined from an experimental stimulus response test performed at room temperature using tracers. The experimental procedure is primarily a function of the kiln used. The following operating parameters were varied: shape or number of rows of lifters, kiln slope (S) and rotational speed (N), solids mass flow rate (\dot{M}), and insofar as possible, exit dam height (h).

2.3.1.1.1 RK1 experimental procedure and matrix

Sand and broken rice particles were processed in RK1. Depending on the bulk materials, the procedure may differ in a few points as follows:

Step 1: Before starting the run, the following operating parameters must be set:

- a) the suitable lifter structure, either straight (SL) or rectangular (RL) lifters, or none (NL),
- b) the exit dam of either 13.5, 23.5 or 33.5 mm, or none,
- c) the kiln must be tilted to the desired slope,
- d) the kiln rotational speed N and solids mass flow rate \dot{M} are set to the desired value by adjusting the corresponding motor rotational frequency.

The rotary kiln is then started and the feed hopper regularly filled with the operating solids to keep it topped up till the end of the run.

Step 2: The system is run until it reaches steady-state conditions, usually after 2 to 4 hours. The steady state is assumed to be reached when at least three consecutive measurements of the flow rate at the kiln outlet are equal within a margin of $\pm 0.05 \text{ kg}\cdot\text{h}^{-1}$.

Step 3: *In the case of a bulk of sand:*

- a) A preliminary test is performed with dyed sand tracer to visually estimate the beginning and ending time of the sampling.

- b) Then a known amount of NaCl tracer is injected in the inlet flow at the feed chute at an arbitrary zero time. Tracer injections lasted about 2 s, which is assumed short enough (with regard to the measured residence times) to approximate an impulse input.
- c) Samples of 5 g are collected at the kiln outlet at constant time intervals of 30 s.

In the case of a bulk of broken rice:

- a) A known amount of dyed broken rice is injected in the inlet flow at the feed chute at an arbitrary zero time.
- b) Samples are continuously collected at the kiln exit end with a sampling time of 30 s. until all tracer materials are visually discharged.

Step 4: The rotary kiln rotation is stopped and the screw feeder disabled at the same time. If present, the exit dam is removed. Then only the kiln rotation is started again and the solids are discharged. The collected solids which constitute the kiln hold-up are weighed.

Step 5: Lastly, *in the case of a bulk of sand*, each collected sample is weighed, then mixed with 20 mL of distilled water in order to dissolve the NaCl particles if present. The sample conductivity, which is proportional to the concentration of diluted NaCl tracer, is then measured.

In the case of a bulk of broken rice, the tracer concentration in each sample is determined by weighing on the one hand the collected sample and on the other hand the dyed tracer manually extracted from the sample.

Note that the flow rate is measured by weighing the materials collected at the kiln outlet during a period of 15 min.

Preliminary experiments were performed to assess the amount of tracer to be injected so as to provide sufficient accuracy for analysis. Therefore experiments were conducted with different amounts of dyed broken rice and the resulting dimensionless RTD were compared. As shown in Figure 2.11 for amounts of tracer varying from 7.4 g to 15 g, the dimensionless RTD was not significantly affected. Since the sampling analysis lasted longer with increasing amount of tracer, 7.4 g of tracer were used for the experiments involving broken rice. To keep approximately a similar volume of tracer in all experiments performed within RK1, for the bulk of sand, 10-12 g of tracer were needed. For accurate data 12 g of tracer were used for the experiments involving sand.

Table 2.3 presents the experimental matrix designed for the RTD measurements in RK1. For each set of operating conditions investigated the given number represents all the runs including repetition. Note that runs intended to assess reproducibility were not all performed in the exact operating conditions of the runs presented in Table 2.3; however, they were performed within the same range. It must be pointed out that the average mass flow rate measured was within a margin of $\pm 0.1 \text{ kg.h}^{-1}$ of the reported values. Note that in runs where the kiln was equipped with lifters, when the steady state was achieved, the kiln was either design-loaded or over-loaded, i.e. there were always enough solids at the bottom of the kiln to fill lifters to their maximum capacity.

The experimental RTD curves obtained when operating RK1 with a bulk of sand or broken rice, within the range of operating parameters given in Table 2.3, are shown in Section B.2.1 in the Appendices.

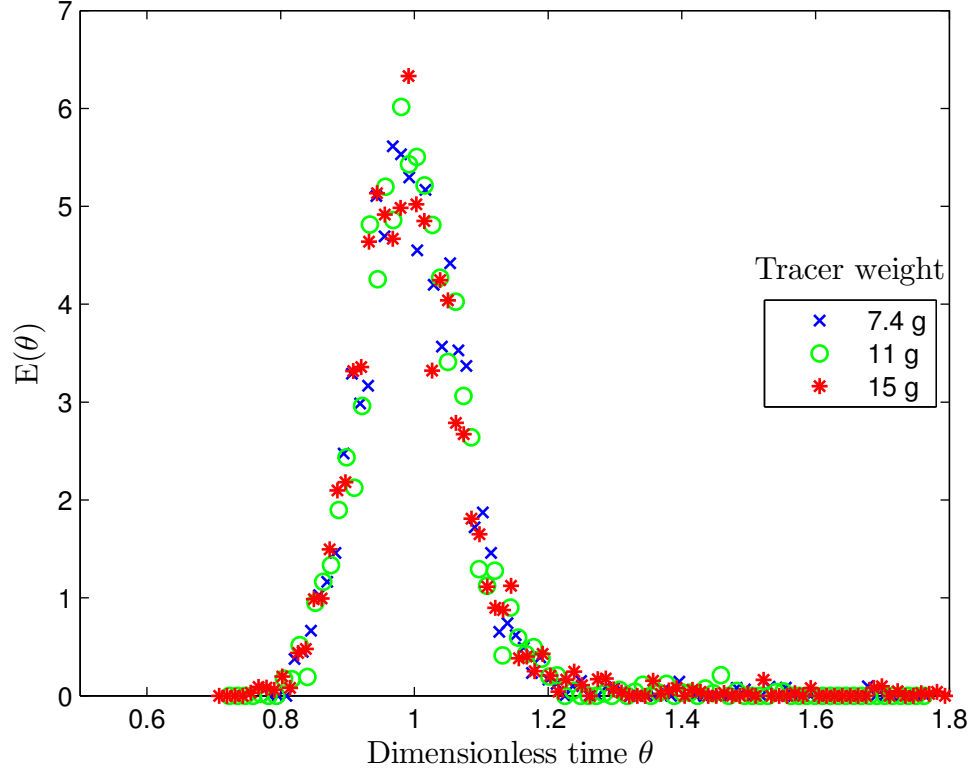


Figure 2.11: Effect of the amount of tracer (dyed broken rice) upon the dimensionless RTD in a bulk of broken rice. Operating conditions: 3 rpm rotation speed, 2° slope, 2.5 kg.h⁻¹ mass flow rate, 23.5 mm exit dam height with rectangular lifters.

Table 2.3: RK1 Experimental matrix for the RTD measurements using rectangular lifters (RL), straight lifters (SL) and no lifters (NL).

Operating conditions				RL		SL		NL
N [rpm]	S [°]	M [kg.h ⁻¹]	h [mm]	Rice	Sand	Rice	Sand	Rice
3	2	2.5	23.5	5	1	3	4	1
2	2	2.5	23.5	2	1	1	1	-
4	2	2.5	23.5	1	1	-	1	-
6	2	2.5	23.5	1	1	1	1	1
8	2	2.5	23.5	1	1	-	1	-
10	2	2.5	23.5	3	1	3	1	3
12	2	2.5	23.5	1	1	-	1	-
3	2.5	2.5	23.5	2	1	-	1	-
3	3	2.5	23.5	1	1	2	1	1
3	4	2.5	23.5	1	1	1	1	-
3	5	2.5	23.5	1	1	1	1	-
3	2	0.68	23.5	1	1	1	1	-
3	2	1.3	23.5	1	1	1	1	1
3	2	1.9	23.5	1	1	1	1	-
3	2	2.5	0	1	1	1	1	-
3	2	2.5	13.5	1	1	-	1	-
3	2	2.5	33.5	3	1	3	1	1

2.3.1.1.2 RK2 experimental procedure and matrix

Beech chip particles were chosen for processing with RK2. The following experimental procedure was used:

Step 1: Before starting the run, the following operating parameters must be set:

- a) the grid, or the lifter structure equipped with either 3 or 6 rows of straight lifters (SL), or no internal fixtures (NL) is fitted to the inner wall,
- b) the kiln must be tilted to the desired slope,
- c) the kiln rotational speed N and solids mass flow rate \dot{M} must be indicated on the user interface.

In addition to the inlet electronic balance, another balance is placed at the outlet and connected to the user interface. The rotary kiln is then started and the feed hopper regularly filled with the beech chips to keep it topped up till the end of the run. The rotary kiln is operated at atmospheric pressure. There is no gas flow and the exit chamber is open so as to have a visual overview of the flow motion of solid particles within the kiln.

Step 2: The system is run until it reaches steady-state conditions, usually after 2 to 4 hours. The steady state is assumed to be reached when inlet and outlet flow rate at the kiln ends are equal within a margin of $\pm 0.05 \text{ kg.h}^{-1}$. In practice, in the user interface the steady state can be graphically established when the slopes of the resulting straight lines obtained by plotting the measured weight at inlet and outlet versus time are equal.

Step 3: When flow steady state is achieved:

- a) The system is run until the hopper is completely empty. Then as soon as the vibrating conveyor is empty, the whole system is stopped.
- b) While the system is stopped, a known amount of dyed beech chips is injected at the kiln inlet end through the hopper and the vibrating conveyor. The feed hopper is then refilled with the beech chips.
- c) The system is then started again (feeding system and kiln rotation, etc.) at an arbitrary zero time.
- d) Samples are continuously collected at the kiln exit end with a sampling time of 30 s until all tracer materials are discharged. In some runs where the solids in the bulk bed were visually in the slipping motion, the tracer particles tended to exit the kiln in a very short time, so the sample time was reduced to 15 s.

Step 4: Then, the rotary kiln rotation is stopped and the vibrating conveyor disabled at the same time. Only the kiln rotation is started again and the solids are discharged. The collected solids which constitute the kiln hold-up are weighed.

Step 5: Lastly, tracer concentration in each sample is determined by weighing on the one hand the collected sample and on the other hand the dyed tracer, manually extracted from the sample. While analyzing the collected samples, the number of dyed tracer particles extracted is also determined for each sample.

Preliminary experiments were also performed here to assess the minimum amount of tracers to be injected in the bulk bed to provide sufficient accuracy for RTD analysis. As shown in Figure 2.12, experiments were conducted with different amounts of dyed beech chips varying from 5 g to 30 g. Comparison of the resulting dimensionless RTDs showed that amounts of 20 and 30 g of tracers

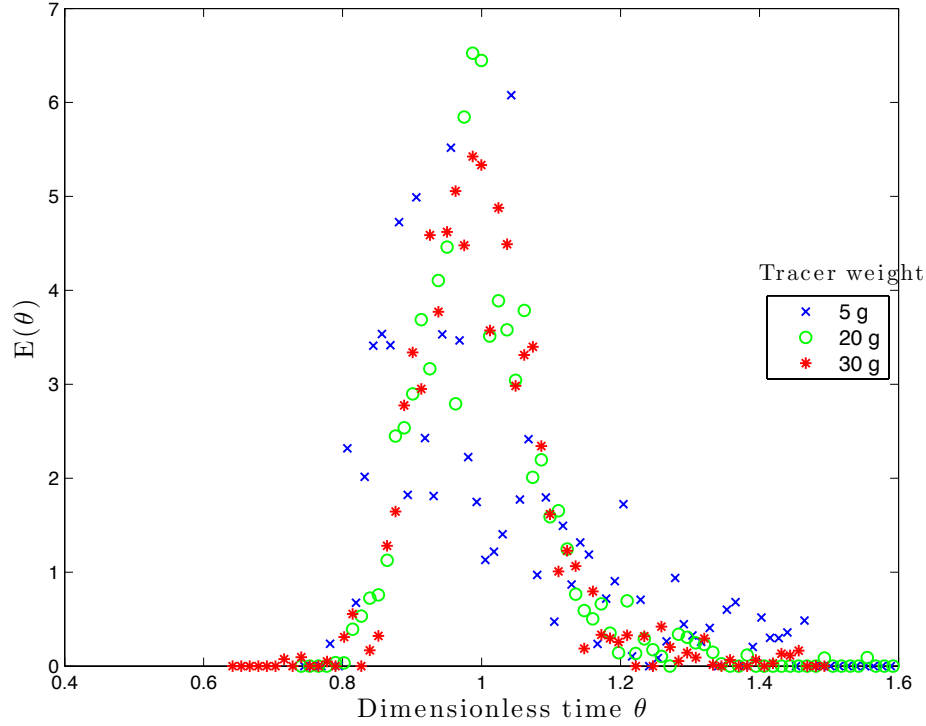


Figure 2.12: Effect of the amount of tracer (dyed beech chips) upon the dimensionless RTD in a bulk of beech chips. Operating conditions: 3 rpm rotation speed, 2° slope, 2.5 kg.h⁻¹ mass flow rate, with only the lifter structure without lifters.

are enough to ensure good accuracy. To shorten the sampling analysis time, 20 g of tracers were used in these experiments.

Table 2.4: RK2 Experimental matrix for the RTD measurements using no internal fixtures (NL), a grid, 3 rows of straight lifters (3SL), and 6 rows of straight lifters (6SL).

Operating conditions			Beech chips			
N [rpm]	S [°]	M [kg.h ⁻¹]	NL	Grid	3SL	6SL
3	2	5	2	1	2	2
2	2	5	1	1	1	1
6	2	5	2	1	1	1
3	1	5	1	1	1	1
3	3	5	1	1	2	1
3	2	2.5	1	1	1	2
3	2	7.5	1	1	1	1

Table 2.4 presents the experimental matrix designed for the RTD measurements in RK2. For each set of operating conditions investigated the given number represents the number of runs including repetition. It must be pointed out that the average mass flow rate measured was within a margin of ± 0.1 kg.h⁻¹ of the reported values. Note that in runs where the kiln was equipped with lifters, when the steady state was achieved, the kiln was either design-loaded or over-loaded. When operating RK2 without internal fixtures, visual observations show that the solids bed was in the slipping motion.

The experimental RTD curves obtained when operating RK2 with a bulk of sand or broken rice, within the range of operating parameters given in Table 2.4, are shown in Section B.2.2 in the Appendices.

2.3.1.1.3 Difficulties encountered

Notwithstanding the fact that such procedures are time consuming, the difficulties encountered were mostly linked with the rotary kilns operation. In particular back spillage at the inlet end of RK1 due to the absence of a dam, or flowing problems at the feeding system section of RK2 mainly due to bridging of solids in the hopper.

2.3.1.2 Bed depth profile measurements

The aim of the bed depth profile measurements was to measure precisely the bed depth in particular within the heating zone 2 of RK1. For that purpose a measuring rod was designed. The rod is equipped with ten stems measuring 50 mm in length and 5 mm in diameter, and it can be easily fitted inside the kiln using the existing system used to hold the TC measuring rod. The stems are attached to the rod using boss-heads. The measuring rod and the stems' positions (numbered from 1 to 10) are shown in Figure 2.13. Note that positions 1, 3, 5, 7 and 9 highlighted in gray color correspond respectively to the sections S1 to S5 identified in Figure 2.4. The following operating parameters were varied: the solids mass flow rate (\dot{M}) and the exit dam height (h).

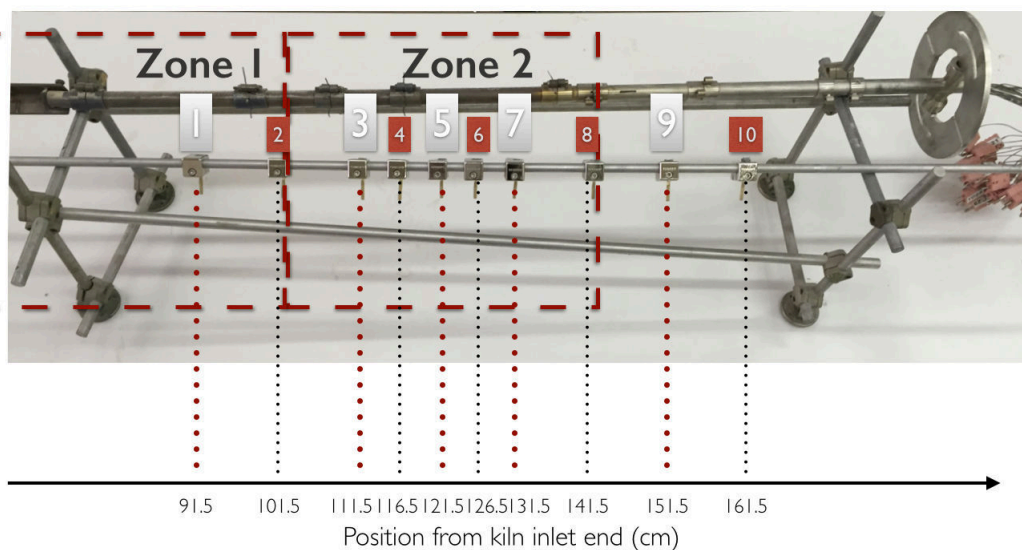


Figure 2.13: Bed depth measuring rod and position of the stems.

2.3.1.2.1 Experimental procedure and matrix

Figure 2.14 sums up the main steps of the procedure. The following experimental procedure was used to measure the bed depth:

- Step 1: The stems are cleaned and coated with glue over the whole length.
- Step 2: The measuring rod is then installed inside the kiln and its support fixed to the kiln frame.
- Step 3: Steady flow conditions are achieved following steps 1 and 2 as given in Section 2.3.1.1.1 above.

Step 4: The bed burden is discharged and weighed following step 4 as given in Section 2.3.1.1.1 above.

Step 5: The measuring rod is removed from the kiln and the height of particles clinging to the stems are measured using a slipping caliper.



Figure 2.14: Experimental procedure for the bed depth measurement.

Note that even though the measuring rod was fixed to the kiln frame so as to be centered, it could still rotate with the kiln tube. This is the main reason why as shown in Table 2.5, experiments were performed without lifters. Each run was repeated 2 or 3 times. The measured bed depth profiles are given in Section B.3 in the Appendices. The stems made of copper were coated using Pattex Contact Adhesive, which offers superior sticking power and is flexible once cured.

Table 2.5: RK1 Experimental matrix for the bed depth measurements without internal fixtures (NL).

Operating conditions				Sand
N	S	\dot{M}	h	NL
[rpm]	[°]	[kg.h ⁻¹]	[mm]	
2	3	0.9	23.5	3
2	3	1.8	23.5	3
2	3	2.5	23.5	3
2	3	0.9	33.5	3
2	3	1.8	33.5	3
2	3	2.5	33.5	3

2.3.1.2.2 Difficulties encountered

No major difficulties were encountered during the experimental campaign. However, while running the preliminary experiments, it was found that the stems could easily get out of the boss-head. Therefore, the stems were first fitted into rubber caps to improve fixation.

2.3.1.3 Dynamic measurements

The aim of the dynamic response experiments was to observe and characterize the dynamic response of the system following step changes of the system operating parameters. They may provide valuable information of the solids transport through the rotary kiln. These experiments were performed using RK1. Step changes either in the rotational speed (N) or in the feed rate (\dot{M}) were made.

2.3.1.3.1 Experimental procedure and matrix

The steps for the dynamic response measurements are:

- Step 1: From the start-up (step 2) to the shut-down (step 4) procedures, achieve continuous measurement of the flow rate. The mass flow rate is measured by weighing the solids collected at the kiln outlet during a period of 20 min.
- Step 2: Following steps 1 and 2 as given in Section 2.3.1.1.1, achieve steady state of the initial flow condition.
- Step 3: When 4 consecutive measurements of the flow rate are equal within a margin of $\pm 0.05 \text{ kg.h}^{-1}$:
- perform a step change of the relevant operating parameter,
 - achieve steady flow conditions.
- Step 4: When 4 consecutive measurements of the flow rate are equal within a margin of $\pm 0.05 \text{ kg.h}^{-1}$, discharge and weigh the bed burden following step 4 as given in Section 2.3.1.1.1.

The experimental matrix for these experiments is given in Table 2.6. Note that the start-up and discharging procedures can be regarded and analyzed as step changes comparable to those presented in Table 2.6.

Table 2.6: RK1 Experimental matrix for the dynamic response measurements using rectangular lifters (RL), straight lifters (SL) and no lifters (NL).

Operating conditions:				Final conditions										
Sand, S= 3°, h= 33.5 mm				NL			RL			SL				
Initial conditions	N [rpm]		2	2	2	2	2	2	2	2	2	4	8	12
		\dot{M} [kg.h ⁻¹]	0.9	1.8	2.5	0.9	1.8	2.5	0.9	1.8	2.5	2.5	2.5	2.5
	2	0.9	-	2	1	-	1	1	-	2	2	-	-	-
	2	1.8	-	-	1	-	-	1	1	-	2	-	-	-
	2	2.5	-	-	-	-	-	-	1	1	-	2	2	1
	4	2.5	-	-	-	-	-	-	-	-	1	-	2	-
	8	2.5	-	-	-	-	-	-	-	-	1	-	-	1
	12	2.5	-	-	-	-	-	-	-	-	1	-	-	-

2.3.2 Temperature profile measurements

In this study, the temperature profile measurements aimed primarily to determine the wall-to-solid heat transfer coefficient within flighted rotary kilns operated at low to medium temperature. More generally, these measurements allow investigations on the heat transfer mechanisms occurring in indirectly heated rotary kilns.

2.3.2.1 Experimental procedure and matrix

In order to study the heat transfer mechanisms, the following experimental procedure was set up using RK1:

Step 1: The desired values of the operating parameters are set:

- a) Depending on the run, rectangular, straight or no lifters are installed inside the kiln.
- b) The measuring rod with thermocouples is installed inside the kiln.
- c) The desired exit dam is fixed if needed, the kiln slope is adjusted to 3° (same angle for all runs).
- d) The rotational speed and the feed rate are set in the control box to the desired value.

Then the kiln is operated at room temperature until steady state conditions of the flow (as defined in step 2 given in Section 2.3.1.1.1).

Some experiments were performed without a flow of solids. In that case, RK1 was simply started with no need for the operator to wait for flow steady state conditions.

Step 2: Temperature recording is started at an arbitrary zero time. From that time until the end (step 4), the following parameters are measured every half hour:

- a) the power supplied to the installation,
- b) the ambient temperature around the kiln,
- c) the free-board gas temperature at the inlet end of the kiln.

Step 3: Half an hour after starting recording the temperature, the temperature set point is adjusted on the controller and the heating source is turned on either in zone 2 or both zones

Step 4: When the supply power, wall, gas, and solids temperatures are stabilized, the steady state conditions are considered to be attained. The thermal steady state is assumed to be reached when the temperatures and the supply power are both stable during 2 consecutive hours, respectively with variations within 2°C or 0.01 kW. The logging is then stopped.

Step 5: After the experiments, the solids are discharged following step 4 as given Section 2.3.1.1.1. The empty kiln is cooled down by natural convection over at least a night before starting a new run.

The heating usually lasted between 6 to 8 hours. Most of the time the runs were performed in two days, the first to achieve flow steady conditions and the second to achieve thermal steady state of the bulk bed. A summary of the experimental conditions for the solids flow and no solids flow runs is given in Table 2.7. As shown in the table, the kiln was operated at low and medium temperatures 100°C , 300°C , and 500°C . The effects of the presence and geometry of lifters, as well as the influence of the feed rate of solids, the filling degree or the kiln rotational speed can be investigated upon heat transfer mechanisms. The temperature profiles obtained from these runs are presented in Appendix C.

Table 2.7: Experimental conditions of experiments within RK1 for the study of heat transfer using rectangular lifters (RL), straight lifters (SL) and no lifters (NL).

Operating conditions: Sand, S = 3°				Zone 2						Zone 1&2		Zone 2			Zone 1&2	
Setpoint T.	N	\dot{M}	HU	Lifters	NL		SL		RL		SL	Lifters	NL	SL	RL	SL
[°C]	[rpm]	[kg.h ⁻¹]	[%]	h[mm]	23.5	33.5	23.5	33.5	23.5	33.5	33.5	h[mm]	33.5	33.5	33.5	33.5
100	2	0.7-0.9	3.97 - 6.7	Solids flow	1	1	1	1	1	1	1	No solids flow	-	-	-	-
	2	1.7-1.9	6.89 - 9.5		1	1	1	1	1	2	-		-	-	-	-
	2	2.4-2.6	10.43 - 13.30		1	1	1	1	1	2	1		1	1	1	1
300	2	0.7-0.9	3.97 - 6.7		1	1	1	1	-	-	1		-	-	-	-
	2	1.7-1.9	6.89 - 9.5		2	1	3	3	-	-	-		-	-	-	-
	2	2.4-2.6	10.43 - 13.30		1	1	3	1	-	-	2		1	2	-	1
500	2	0.7-0.9	3.97 - 6.7		-	-	-	1	-	-	1		-	-	-	-
	2	1.7-1.9	6.89 - 9.5		-	-	1	1	-	-	-		-	-	-	-
	2	2.4-2.6	10.43 - 13.30		-	-	1	1	-	-	1		-	1	-	1
100	4	1.9	6.7		-	-	-	-	-	-	1		-	-	-	-
100	4	2.4-2.6	8		-	-	-	-	-	-	2		-	-	-	-
300	4	1.9	6.7		-	-	-	-	-	-	1		-	1	-	-
500	4	1.9	6.7		-	-	-	-	-	-	1		-	-	-	-
500	4	2.4-2.6	8		-	-	-	-	-	-	1		-	-	-	-
100	8	3.2	6.7		-	-	-	-	-	-	1		-	-	-	-
100	8	2.4-2.6	6		-	-	-	-	-	-	1		-	-	-	-
300	8	3.2	6.7		-	-	-	-	-	-	1		-	1	-	-
500	8	2.4-2.6	6		-	-	-	-	-	-	1		-	-	-	-
500	8	3.2	6.7		-	-	-	-	-	-	1		-	-	-	-
100	12	2.4-2.6	5		-	-	-	-	-	-	1		-	-	-	-
300	12	2.4-2.6	5		-	-	-	-	-	-	1		-	1	-	-
500	12	2.4-2.6	5		-	-	-	-	-	-	1		-	-	-	-

2.3.2.2 Difficulties encountered

A major problem encountered in these experiments was a failure of the support system, holding and centering the TC measuring rod, causing material damage that was most of the time irreversible. The failure occurred twice, damaging several TC fitted in the measuring rod and twisting the lifter structure. The first time the lifter structure was irreversibly damaged and a new one was ordered. The second time it was repaired.

The embedded thermocouples were placed almost tangent to the lifters thereby plunging in the solid bed. The friction between the thermocouple tips and the lifter edges supposedly causes wear and tear. Therefore, while operating RK1 in presence of lifters, some TC were eroded and then damaged, giving random and large temperature values, despite the fact that a reasonable space was left between lifter edges and thermocouple tips, a space that was sufficient to keep the TC inside the solids bed but away from the lifters even at low filling degree. Fortunately, having a sufficiently large number of thermocouples in stock, it was always possible to replace broken or eroded TC.

Another issue, related to the operating conditions is that regarding the bulk bed the position of the embedded thermocouples was not fixed. Indeed, the bed depth varied depending on the operating conditions. Unfortunately, as it was not possible to keep the TC tips at the same depth with respect to the bed depth, this may have had an impact on the experimental results to a certain extent.

2.4 Dimensional analysis

Dimensional analysis has a long history, and was developed by most of the greatest scientists such as Fourier, Vaschy, Buckingham or Einstein. As stated by [Gibbings 2011], combining great utility with demanding intellectual rigor, it is remarkable for its universality of application. In particular it has been used increasingly in recent times as guidance in experimental design, similarity laws or data correlation in order to tackle scaling up issues in chemical and process engineering, as shown by some examples in [Delaplace 2014].

In the present study dimensional analysis was used with the aim of proving a correlation that may apply to a wide range of rotary kilns equipped with lifters, and so may be used as a toolkit for design and scaling. This analysis requires the knowledge at least of the most important variables influencing the phenomena to be described. In this study the phenomena of interest investigated in flighted rotary kilns are:

- the mean residence time of granular solids,
- the axial dispersion coefficient,
- the volumetric hold up (or filling degree),
- the heat transfer coefficients from wall to solids,
- the convective heat transfer coefficient.

The variables influencing these phenomena were determined with the use of the existing literature and by setting up an experimental campaign. The most challenging part is to identify an appropriate reduced set of dimensionless groups from the determined variable parameters. Using the conservation law of dimensions these dimensionless groups can be used to represent the phenomena of interest. A more detailed description of the steps of the dimensional analysis process followed in this study can be found in [Delaplace 2014].

2.5 Methodology summary

This chapter has depicted the methodology employed to investigate on the one hand the solids transport characteristics and on the other hand the heat transfer mechanisms. The methodology is based on dimensional considerations, completed by systematic experimentation. The pilot scale rotary kilns used, the different solids selected, and the experimental procedures achieved, are also well described.

In particular, the pilot scale rotary kilns used in the study can be considered to assess and address scaling up issues. Both pilots were used for the quantitative characterization of the solids transport. The selected solids, namely sand, broken rice and beech chips were not uniform in density, but they all behave as free-flowing systems and mainly differed in size and angle of repose. The smallest pilot unit, well suited to perform heat transfer studies was operated at low to medium temperatures with a bulk of sand. Some difficulties were encountered but most of them were easily tackled.

The techniques and steps defined in the experimental procedures must provide results with reasonable confidence in terms of accuracy and reproducibility. To achieve a comprehensive study and quantitative analysis of both solids transport and heat transfer issues, the minimum number of runs performed was about 170 and 90 respectively. This huge amount of experiments will certainly help to provide a better understanding of heat transfer mechanisms and solids transport behavior in flighted rotary kilns.

Hydrodynamic characteristics of flighted rotary kilns: experiments and modeling

“...what a man means by a term is to be found by observing what he does with it, not by what he says about it.”

(Percy W. Bridgman, 1882-1961)

Chapter 3

Effect of lifter shape and operating parameters on the flow of materials in a pilot rotary kiln : Part I. Experimental RTD and axial dispersion study

Abstract	92
3.1 Introduction	93
3.2 Materials and methods	94
3.2.1 Apparatus and materials	94
3.2.2 Experimental technique	96
3.3 Data processing	97
3.4 Results and discussion	99
3.4.1 Axial dispersion model	100
3.4.2 Influence of operating variables and nature of materials on the RTD	101
3.4.3 Influence of operating variables and nature of materials on the Pe and D	106
3.5 Conclusions	109

The research described in this Chapter has been published in: [Bongo Njeng 2015c]

Bongo Njeng, A.S., Vitu, S., Clausse, M., Dirion, J.-L., Debacq, M., 2015. Effect of lifter shape and operating parameters on the flow of materials in a pilot rotary kiln: Part I. Experimental RTD and axial dispersion study. Powder Technology 269, 554–565.

DOI:10.1016/j.powtec.2014.03.066

Abstract

Abstract:

Experiments on the residence time distribution (RTD) and axial dispersion for the continuous flow of sand and broken rice, through a pilot scale rotary kiln at room temperature and equipped with lifters, are reported. Factors such as the rotational speed, the kiln slope, the materials flow rate and the exit dam height have been studied. Furthermore, two profiles of lifters were used: straight lifters (SL) and rectangular lifters (RL). Thus, under varying conditions the RTDs were obtained by the typical stimulus response test using a tracer and the corresponding axial dispersion coefficients were determined. The validity of the axial dispersion model was assessed in this study, and the model was found to match well with the experimental data. A large number of experiments was conducted, so that, a correlation could be developed to predict the axial dispersion coefficient of the solid particles within the kiln. Comparisons with reported models are also discussed. The second part of this study will be concerned with the experimental kiln hold-up and the mean residence time (MRT) of solid particles.

Résumé :

On a mené des expériences avec du sable et des brisures de riz, dans un four tournant à l'échelle pilote, équipé de releveurs et à température ambiante, en vue d'étudier la distribution du temps de séjour (DTS) et la dispersion axiale des particules solides. On a étudié en particulier l'influence de paramètres opératoires tels que la vitesse de rotation du four, son inclinaison, le débit des particules solides et la hauteur du diaphragme en sortie du four. Deux formes de releveurs ont été considérées : des releveurs plats (RP) et des releveurs rectangulaires (RR). En procédant à des injections impulsion (Dirac) de traceurs, des courbes de DTS ont pu être établies et les coefficients de dispersion axiale déterminés. Le modèle piston-dispersion a été testé pour représenter les résultats expérimentaux ; ce modèle s'est révélé adéquat pour représenter la DTS. On propose une corrélation pour prédire le coefficient de dispersion axiale des particules solides, les prédictions de cette nouvelle corrélation sont comparées à celles d'autres corrélations de la littérature. Dans la deuxième partie de cette étude, on s'intéressera au taux de chargement du four et on continuera l'exploitation des résultats de DTS, en particulier on examinera le temps de séjour moyen des particules solides.

3.1 Introduction

Through the years, rotary kilns have become an inescapable benchmark in several industrial sectors. This is because they offer special possibilities regarding the wide range of materials which can be continuously processed with little or no labor to operate, especially when they are under automatic control. As wider are the scopes of applications as wider are the kilns design and size. Rotary kilns range from small cylinders with length-to-diameter ratio (L/iD) below 5 [Abouzeid 2010, Cronin 2011] used mostly for mixing granular materials in the pharmaceutical manufacture; medium cylinders with L/iD up to 20 [Duchesne 1996, Bensmann 2010, Li 2002a, Chen 2009], used for the drying or cooling of solid particles, for instance in the food processing industry when dealing with wet or dry granular materials; and long cylinders with L/iD above 20 [Sai 1990, Hatzilyberis 1999a, Hatzilyberis 1999b, Sudah 2002], often used at high temperature for calcination of limestone, petroleum coke, or production of cement. Other applications include: regeneration of spent catalyst, hazardous waste reclamation, defluorination and reduction of uranyl difluoride and so on. Kilns are usually equipped with internal fixtures such as lifters, baffles, constrictions or exit dam.

The complex hydrodynamic behavior of the granular materials within rotary kilns has led to extensive research over the years. Among the first to investigate this subject, [Sullivan 1927], followed by others [Prupton 1942, Saeman 1951, Kramers 1952, Schofield 1962], focused on the factors affecting the time of passage of solid particles and derived an empirical correlation for a range of small and medium inclined rotary kilns. Studying the time of passage is one of the simplest ways to get some understanding of the solids transport. However, this method can be inaccurate with regard to the distribution of the times that solid particles will undergo inside the kiln. Variations of times which may be observed are therefore represented by the residence time distribution (RTD) at steady state flow. Because the knowledge and a good characterization of the RTD are necessary for the design, improvement and scale-up of manufacturing process, there have been some recent published works on the experimental and theoretical analysis of the solids transport using the RTD notion. Most of these publications report on the influence of operating parameters (rotational speed, kiln slope, mass flow rate or exit dam height) [Rutgers 1965, Abouzeid 1974, Karra 1977, Hehl 1978, Venkataraman 1986, Sai 1990, Lebas 1995b, Ang 1998, Hatzilyberis 1999a, Hatzilyberis 1999b, Sudah 2002, Li 2002a, Chen 2009, Abouzeid 2010, Gao 2011] and others on the influence of the bulk or tracer materials properties [Sai 1990], or segregation phenomena [Hatzilyberis 1999a, Bensmann 2010, Abouzeid 2010]. Fewer are those analyzing the effect of presence of lifters, their number or shape [Venkataraman 1986, Li 2002a, Hatzilyberis 1999a]. However, some authors have focused on the study of lifters hold-up and discharging rate [Schofield 1962, Baker 1988, Matchett 1990, Sherritt 1993, Sherritt 1994, Wang 1995, Lisboa 2007, Cronin 2011, Ajayi 2012, Sunkara 2013b, Sunkara 2013a].

RTD experiments usually involve tracer detection techniques. The stimulus response test is a common method used for measurements of the RTD [Gao 2012, Martin 2000]. In this test, the injection of either a step change or a pulse of tracer is performed at the inlet end. The tracer materials must share similar physical properties with the bulk materials. The tracer detection can be either inline by means of inline probes, therefore requiring fast sample acquisition, or offline, in which case the detection is performed either optically (fluorescence analysis, spectroscopy, near infrared and ultraviolet), by measuring the conductivity, or by counting and weighing.

Several models have been used and developed to describe the experimental RTD of solid particles through the kiln. The most popular used is the axial dispersion model. In addition to the mean residence time, this model provides a dispersion parameter, able to characterize the material transport behavior. A similar model is the tank in series model. These two models are usually called one-parameter models, as opposed to the multi-parameter models. Among the

multi-parameter models are: the modified Cholette-Cloutier model used by [Duchesne 1996], and the models developed by [Mu 1980, Sheehan 2002, Dinesh V 2004, Sheehan 2005, Britton 2006]. Generally these one-parameter or multi-parameter models can give quantitative predictions about the materials transport behavior, thus giving an insight on the deviation from the two ideal extremes. The flow in rotary kilns are likely closed to that of plug flow reactors.

This paper is concerned with the effects of kiln rotational speed, kiln slope, mass flow rate, exit dam height, lifters shape and bulk materials properties on:

- the RTD of solid particles, determined from experimental stimulus response test;
- the Peclet number as well as the corresponding axial dispersion coefficient, which characterizes the materials transport and mixing within the system.

In previous literature, such a comprehensive systematic experimental investigation of RTD, Peclet number and axial dispersion coefficient is very seldom. Earlier studies [Venkataraman 1986, Hatzilyberis 1999a, Hatzilyberis 1999b] may differ from the present work with regard to the use of lifters of different shapes and materials of different properties. Furthermore the apparatus operated, the experimental procedures and operating conditions carried out in this study may differ from published works. In the following section, the experimental results are interpreted in light of the axial dispersion model for the RTD, and the validity of the model is assessed on the full set of data. After checking the experiments reproducibility, the RTDs and the corresponding variances, Peclet numbers and axial dispersion coefficients are analyzed in terms of the operating parameters. Eventually a correlation to predict the axial dispersion coefficient is given for kiln equipped with lifters and the calculated coefficients are compared with the experimental results. Predictions of other published correlations are also compared to the experimental results.

3.2 Materials and methods

3.2.1 Apparatus and materials

A pilot scale rotary kiln was used to carry out the investigation of solid particles motion. The layout of the experimental system is shown in Figure 3.1. The main parts of this set up are the feeding system and the rotating kiln followed by a recovery zone [Thammavong 2011].

The feeding system is mainly a combination of a hopper and a feed screw. The hopper acts as a storage where the bulk materials are manually poured. The solid particles flow by gravity from the bottom of the hopper through a feed screw. This later delivers the solid particles to a feed chute ending up at the kiln inlet end. There is no possible access to recover the solids at the kiln inlet end. Therefore the feed rate is controlled at the kiln outlet and regulated by adjusting the rotational frequency of a 180W DC motor, which drives the screw feeder by means of a belt drive. Thus the feed rate measurements were achieved when steady-state flow conditions were established.

The rotary kiln is a tube made of an Incoloy alloy 800 and measures 1.95 m in length and 0.101 m in (internal) diameter. For the purpose of the residence time distribution study, the smooth inner wall can be equipped with a network or a structure of lifters when necessary. Each structure is fitted with 4 identical lifters equally distributed in the periphery. Two shapes of lifters were used: straight one-section lifters of 10 mm refer to as straight lifters (SL) and two-section lifters of 10 mm each, with a right angle cross section refer to as rectangular lifters (RL) as shown in Figure 3.1. The kiln tube is supported on 4 rollers, and is driven through chain and sprocket and a variable speed 180W DC motor. This setting allows kiln operation at speeds ranging from 2 to 12 rpm. At the discharged end, constriction dams of different height can be installed in order to restrict the flow of solids, so that the filling degree within the kiln varies

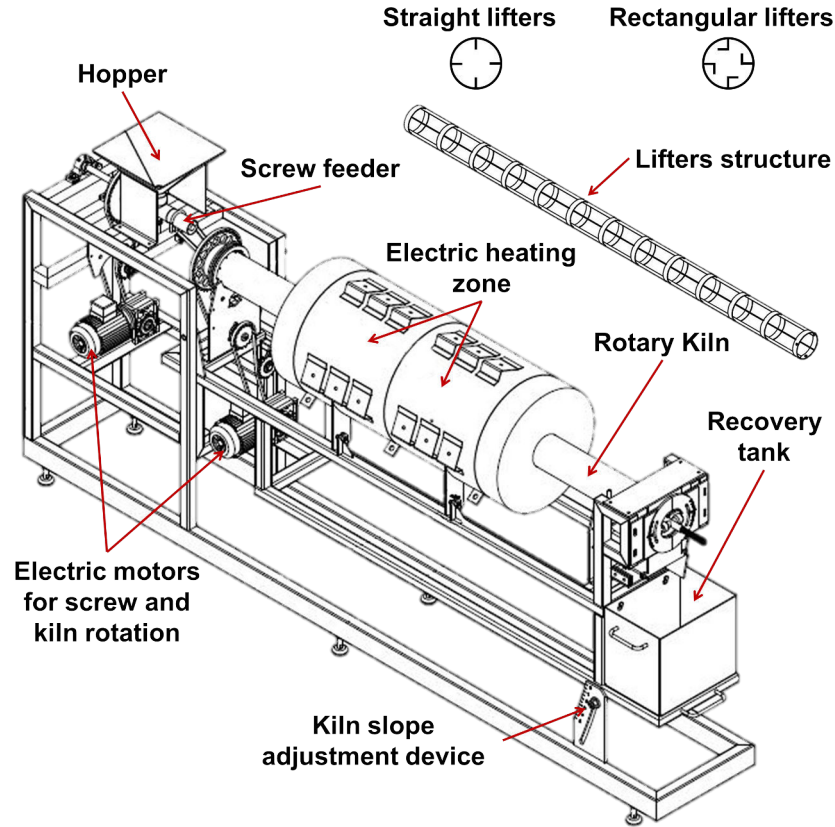


Figure 3.1: Layout of the experimental apparatus, including the structure and shapes of lifters.

irrespectively of the solids flow rate or kiln rotational speed. The kiln slope is measured using an electronic level. The slope can be modified by means of an hydraulic jack with manual pump and an adjustment device. So, the kiln unit can be tilted to an angle of 5° . Table 3.1 summarizes the geometrical and operational characteristics of the kiln in this study.

Table 3.1: Geometrical characteristics of the rotary kiln

Subsets	Parameters	Order of magnitude
Rotary Kiln	iD [m]	0.1013
	L [m]	1.95
	Exit dam height [mm]	0-33.5
	Lifters shape	None, SL, RL
Operating conditions	N [rpm]	2-12
	S [$^\circ$]	2-5
	\dot{M} [kg.h $^{-1}$]	0.68-2.5

In order to investigate the motion of solid particles of different properties within the kiln, two granular solids were used as bulk materials: (1) dry nodular sand characterized by a 1422 kg.m^{-3} bulk density, a mean particle size of 0.55 mm and an angle of repose of 39° ; (2) broken rice characterized by a 889 kg.m^{-3} bulk density, a mean particle size of 3.8 mm in length and 1.9 mm in diameter, and an angle of repose of 36° . Table 3.2 shows some of the most important properties of the materials used. The bulk density was determined by measuring the weight of materials which occupied a volume of 100 mL in a graduated cylinder. In order to determine the tapped density this latter was compacted by “hand tapping” the measuring cylinder, from 10 to 20 mm

height until the variation of volume is less than 1 %, and the new volume was measured. However the raising and lowering of the cylinder were done without reference to the height and arbitrary acceleration in both directions (upward and downward). The solids angle of repose were determined by means of the fixed cone method similarly to [Thammavong 2011]. The solid particles were poured into a funnel and formed a heap from which the angle of repose could be estimated.

Table 3.2: Physical properties of materials

Product	Shape	ρ_{bulk} [kg.m ⁻³]	ρ_{tapped} [kg.m ⁻³]	d_p [mm]	θ [°]
Sand	Nodular	1422	1543	0.55	39
NaCl	Nodular	1087	1184	0.6	35.4
Broken rice	Cylindrical	889	934	3.8×1.9	36

3.2.2 Experimental technique

The experiments performed in this study were conducted at ambient temperature with a procedure mostly similar to [Abouzeid 1974]. The RTDs were determined by stimulus response tests using dyed sand and sodium chloride as tracers for sand bulk flow, and dyed rice as tracer for rice bulk flow. Depending on the bulk materials, the procedure may differ in few points as follows:

- Step 1: Before starting a run, the suitable lifters and exit dam are installed for the experiment, the variable parameters (N, S, M) are set to the desired values. The rotary kiln, operating at atmospheric pressure, is then started and the feed hopper regularly fulfilled with the operating solids to keep it topped up till the end of the run.
- Step 2: The system is run until it reaches steady-state conditions, usually after 4 hours. The steady state is assumed to be reached when at least three consecutive measurements of the flow rate at the kiln outlet are almost equal within a margin of $\pm 0.05 \text{ kg.h}^{-1}$. The flow rate was measured by weighing the materials collected at the kiln outlet during a period of 15 min.
- Step 3: *In the case of a bulk of sand*, a preliminary test was performed with dyed sand tracer to visually estimate the starting and stopping time of the sampling. Then a known amount of NaCl tracer was injected in the feed chute at an arbitrary zero time. Tracer injections lasted about 2 sec, which have been assumed short enough (with regard to measured residence times) to approximate an impulse input. Samples of 5 g were collected at the kiln outlet at constant time intervals of 30 sec. *In the case of a bulk of broken rice*, a known amount of dyed broken rice was injected in the feed chute at an arbitrary zero time. Samples were continuously collected at the kiln exit end with a sampling time of 30 sec until all tracer materials had discharged.
- Step 4: The rotary kiln rotation was stopped and the screw feeder disabled at the same time. Only the kiln rotation was started again and the solids could be discharged. The collected solids which constitute the kiln hold-up were weighted.
- Step 5: Eventually, *in the case of a bulk of sand*, each collected sample was weighted, then mixed with 20 mL of distilled water in order to dissolve the NaCl particles if present. The sample conductivity, which is proportional to the concentration of diluted NaCl tracer, was then measured. Whereas *in the case of a bulk of broken rice*, tracer concentration in each sample was determined by weighting on one hand the sample and, on the other hand the dyed tracer manually extracted from the sample.

The choice of tracer is important. Indeed, selected tracers were expected to share similar properties with the bulk materials, thus introducing as few disturbances as possible on the bulk flow. For the bigger particles size (broken rice) dyed particles were chosen, otherwise except for the color the tracer materials were identical to the bulk. And for the small particle size (sand), the tracers were sodium chloride particles of same size rather than dyed particles due to time consuming samples analysis. No less importantly, the amount of tracer to be injected should be well defined to provide the desired accuracy for analysis [Abouzeid 1974]. Therefore experiments were conducted with different amount of dyed broken rice. Figure 3.2 presents effect on the RTD of the amount of injected tracer in a bulk of broken rice. As shown in Figure 3.2 for amount of tracer varying from 7.4 g to 15 g the dimensionless RTD was not significantly affected, making easier the decision. Since the sampling analysis lasted longer with increasing amount of tracer, 7.4 g of tracer were used in experiments involving broken rice. To keep approximately a similar volume of tracer in all experiments, in the case of sand 10-12 g of tracer were needed. For a more accurate data 12 g of tracer were used in experiments involving sand.

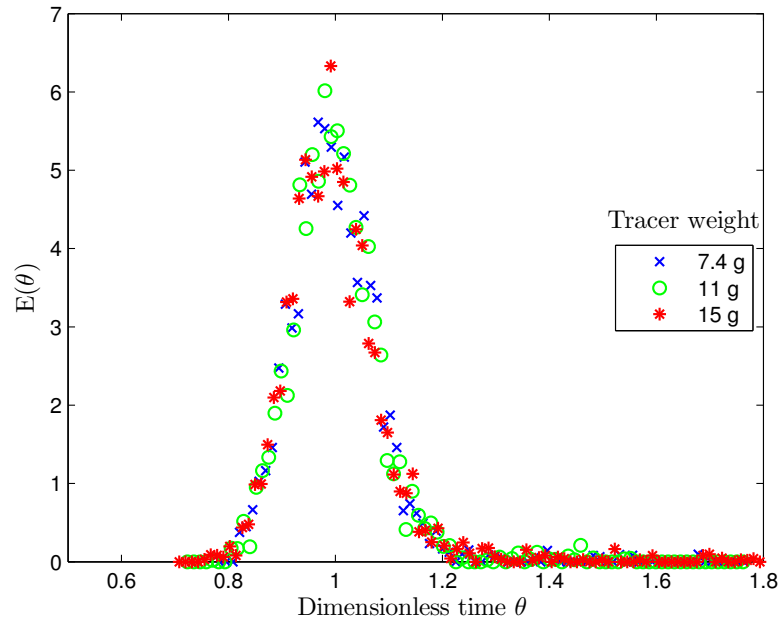


Figure 3.2: Effect of the amount of tracer (dyed broken rice) upon the dimensionless RTD in a bulk of broken rice. Operating conditions: 3 rpm rotation speed, 2° slope, 2.5 kg.h⁻¹ MFR , 23.5 mm exit dam height with rectangular lifters.

3.3 Data processing

Data evaluation

When performing a stimulus test, the fraction of tracer that remains in the system at any time is described by the distribution function $E(t)$ as follows :

$$E(t) = \frac{C(t)}{\int_0^\infty C(t)dt} \quad (3.1)$$

where $C(t)$ represents the tracer concentration at the kiln exit end and the time integral of $C(t)$ represents the total tracer concentration. In this study, for each sample the tracer concentration

(or conductivity) was yielded, so that from the discrete sample, and associated sampling time Δt_i , $i=\{1, 2, 3, \dots, N_s\}$, the RTD curve or E-curve of each experiment can be determined as follows [Levenspiel 1999]:

$$E(t_i) \cong \frac{C(t_i)}{\sum_i^{N_s} C(t_i) \Delta t_i} \quad (3.2)$$

The interpretation of the RTD curves is based on moment analysis which provides various aspect of the flow in the unit. The first moment of the RTD function gives the mean residence time (MRT) \bar{t} which is defined by [Levenspiel 1999]:

$$\bar{t} = \frac{\int_0^\infty tC(t)dt}{\int_0^\infty C(t)dt} \cong \frac{\sum_i^{N_s} t_i C(t_i) \Delta t_i}{\sum_i^{N_s} C(t_i) \Delta t_i} \quad (3.3)$$

The second moment of the RTD function, σ^2 , gives the variance of residence times (VRT) about the MRT. It indicates the width or scatter of the distribution: the greater the value of this moment, the greater the distribution spread. This moment is defined as follows [Levenspiel 1999]:

$$\sigma^2 = \frac{\int_0^\infty (t - \bar{t})^2 C(t) dt}{\int_0^\infty C(t) dt} \cong \frac{\sum_i^{N_s} t_i^2 C(t_i) \Delta t_i}{\sum_i^{N_s} C(t_i) \Delta t_i} - \bar{t}^2 \quad (3.4)$$

Since the sampling time was constant and equal in all experiments, the sampling intervals in Eq.3.3 and Eq.3.4 can be simplified. The presented $E(t)$ function and VRT can also be expressed in dimensionless form:

$$\theta = \frac{t}{\bar{t}} \quad (3.5)$$

$$E(\theta) = \bar{t} E(t) \quad (3.6)$$

$$\sigma_\theta^2 = \frac{\sigma^2}{\bar{t}^2} \quad (3.7)$$

respectively the dimensionless time, mean residence time and variance of residence time.

Axial dispersion model

The axial dispersion model is used to represent the RTDs. Originally used by [Danckwerts 1952], this model considers the axial motion of fluid element as two components [Martin 2000]: a convective component arising from the bulk motion of the fluid and a diffusive component arising from the random motion of the element in response to the decay of turbulent eddies. This is represented by the following one-dimensional Fokker-Planck equation, which describes the evolution of particle distribution in continuous systems [Risken 1996, Sherritt 2003]:

$$\frac{\partial C}{\partial \theta} = \frac{1}{Pe} \frac{\partial^2 C}{\partial z^2} - \frac{\partial C}{\partial z} \quad (3.8)$$

$$\frac{D}{uL} = \frac{1}{Pe} \quad (3.9)$$

$$\theta = \frac{t}{\bar{t}} = \frac{ut}{L} \quad (3.10)$$

where D is the axial dispersion coefficient in $\text{m}^2.\text{s}^{-1}$, Pe is the dimensionless Peclet number, z is dimensionless and defined as the ratio of the axial position to the kiln length L , t and \bar{t} are respectively the time and the MRT in s, u is the velocity in m.s^{-1} . This continuum

model has been applied in rotary kilns [Venkataraman 1986, Abouzeid 1974, Das Gupta 1991, Lebas 1995b, Sudah 2002, Sherritt 2003, Gao 2011] to describe the transport of granular solids providing that some assumptions are satisfied. Among the most important [Abouzeid 1974, Sudah 2002, Sheehan 2002]:

- (i) Steady-state conditions must be achieved and maintained over the tracer stimulus test.
- (ii) A delta-dirac tracer pulse insuring that tracer concentration is only function of time and axial position.
- (iii) Constant axial convective velocity and axial dispersion coefficient of tracer for stable operating conditions.

Analytical solutions for the RTD were published by several authors [Thomas 1944, Abouzeid 1974, Karra 1977, Levenspiel 1999] for the different type of boundary conditions. In this study the flow of materials was undisturbed at the inlet and outlet, so that the open-open boundary condition is considered for the system.

The analytical solution for Eq.3.8, acknowledging the open-open boundary condition, published by [Levenspiel 1999] is given in a dimensionless form as follows:

$$E(\theta) = \frac{1}{2} \sqrt{\frac{Pe}{\pi\theta}} \exp \left\{ -\frac{Pe(1-\theta)^2}{4\theta} \right\} \quad (3.11)$$

The mean and variance of this distribution are defined as:

$$\bar{t}_{oo} = 1 + \frac{2}{Pe} \quad (3.12)$$

$$\sigma_{\theta,oo}^2 = \frac{2}{Pe} + \frac{8}{Pe^2} \quad (3.13)$$

There are two main methods to evaluate the Peclet number: the simplest one is to match the measured variance (Eq.3.4) to theory (Eq.3.13), the other one imply to fit the experimental E-curve using the dispersion model (Eq.3.11). These two methods are considered in the coming section to evaluate the Peclet numbers and resulting axial dispersion coefficients for varying experimental conditions.

3.4 Results and discussion

In this study, benchmark values of a range of operating conditions were defined, so that every operating parameter was kept constant except the one being studied. Whatever the materials being processed, in presence or not of lifters (SL or RL), the benchmark values were a rotational speed of 3 rpm, a kiln slope of 2°, a mass flow rate of 2.5 kg.h⁻¹ (±0.05 kg.h⁻¹) and a 23.5 mm exit dam height. The rotary kiln was either over-loaded or design-loaded during the experiments. Hence a set of 69 experiments was performed. The main purposes of these latter being to investigate: (1) the residence time entire distribution, (2) the mean residence time of the distribution which is discussed elsewhere separately [Bongo Njeng 2015a], (3) the variance of residence time, (4) the validity of the axial dispersion model, (5) the Peclet number and axial dispersion coefficient.

In order to test the reproducibility, an additional 20 experiments were performed. Some of these experiments are reported in Table 3.3. Repeated experiments at 10 rpm with a bulk of broken rice while using straight, rectangular, or no lifters with other parameters kept at the benchmark values are presented in Figure 3.4. From these results, it is clear that the reproducibility is good, but greater variations were observed at high rotational speed, thereby supporting the

chosen benchmark value. These variations derived from a variety of sources [Abouzeid 1974] ranging from the feeding system to the sampling analysis and including the tracer injection and discharge sampling procedures. Results from the overall replicated experiments showed that the coefficients of variation of the mean residence time and the variance of RTD are on average 1.2% and 16.2%, respectively. In light of this, results from the experimental campaign were considered as sufficiently reliable for the analysis of the influence of operating parameters upon the materials transport in a rotary kiln equipped with lifters.

Table 3.3: Reproducibility of experiments

Materials - Lifters	Operating conditions	\bar{t} [min]	Cv [%]	σ^2 [min ²]	Cv [%]
Sand - SL	3 rpm , 2.1° , 2.5	43.39		6.91	
	kg.h ⁻¹ MFR , 23.5	43.64	0.76	6.72	11.2
	mm exit dam height	42.99		8.22	
Broken rice - RL	3 rpm , 2.5° , 2.5	31.77		8.57	
	kg.h ⁻¹ MFR , 23.5		0.67		5.9
	mm exit dam height	31.47		7.88	
Broken rice - NL	10 rpm , 2° , 2.5	13.38		2.98	
	kg.h ⁻¹ MFR , 23.5	13.14	2.1	3.37	19.2
	mm exit dam height	12.83		2.28	

3.4.1 Axial dispersion model

The axial dispersion model presented above was used to represent the time dependent E-curves. Therefore, to determine the RTD equation, Eq.3.11 is rewritten in dimensional form using Eq.3.5 and Eq.3.6 as follows:

$$E(t) = \frac{1}{2} \sqrt{\frac{Pe}{\pi \bar{t} t}} \exp \left\{ -\frac{Pe(\bar{t} - t)^2}{4\bar{t}t} \right\} \quad (3.14)$$

While the dimensionless form of the model needs only a unique parameter namely the Peclet number, in its dimensional form there is a second parameter to determine: the mean residence time of the distribution. As explained before there are two methodologies. Both of them are considered:

- Case 1: The MRT is obtained from experimental data using Eq.3.3. The Peclet number is obtained from the theoretical expression described in Eq.3.13 using the dimensionless VRT obtained from experimental data using Eq.3.7.
- Case 2: The parameters are determined to minimize the mean sum of square error between the experimentally determined RTD values using Eq.3.2 and the predicted values from Eq.3.14. Parameters for the best fitted curve were calculated through a MatLab script using the curve fitting tool function.

Parameters deriving from the above methodologies are used in Figure 3.7, which shows the influence of operating parameters on the RTD of broken rice, to investigate the validity of the axial dispersion model. The simulated curves using the case 1 parameters, referred to as theoretical parameters, are dashed lines. The simulated curves using the case 2 parameters, referred to as fitted parameters, are solid lines. It appears clearly that both sets of parameters give good agreement with experimental data; that was the case for experiments of the whole campaign.

However, as one would have expected, fitted parameters lead to better results than theoretical parameters. Although theoretical parameters are simple to obtain, they are not necessarily the best choice. A comparison of theoretical and fitted parameters is given in Figure 3.3. Experimental and fitted MRT are perfectly correlated (see Figure 3.3a), whereas theoretical and fitted Peclet numbers exhibit some discrepancy. Consequently, it is recognized that the theoretical Peclet numbers reported in this study are likely underestimating the actual Peclet numbers as suggested in Figure 3.3b. However, with regard to the validity of the chosen model, one may keep in mind that some irregularities can occur at inlet and outlet ends of the kiln, reducing the model accuracy. The observed discrepancies could be presumably due to some of the model's assumptions that have not been completely fulfilled.

The Peclet number expressed the ratio of the axial convection forces to the dispersion forces as given in Eq.3.9. Subsequently it is possible to obtain the axial dispersion coefficient from theoretical and fitted Peclet number. The calculated axial dispersion numbers were found in the range of 10^{-7} to $10^{-4} \text{ m}^2.\text{s}^{-1}$ highlighted by [Sherritt 2003] for kiln diameters ranging from 0.076 to 0.144 m not always equipped with lifters and/or exit dam (from published data). Axial dispersion coefficients calculated from theoretical Peclet numbers were found in general higher than those obtained from fitted Peclet numbers (see Figure 3.3c). This is a direct consequence of both the underestimation of theoretical Peclet number and definition of the axial dispersion as inverse of the Peclet number as given in Eq.3.9. From now on, only results obtained from the fitted parameters are considered.

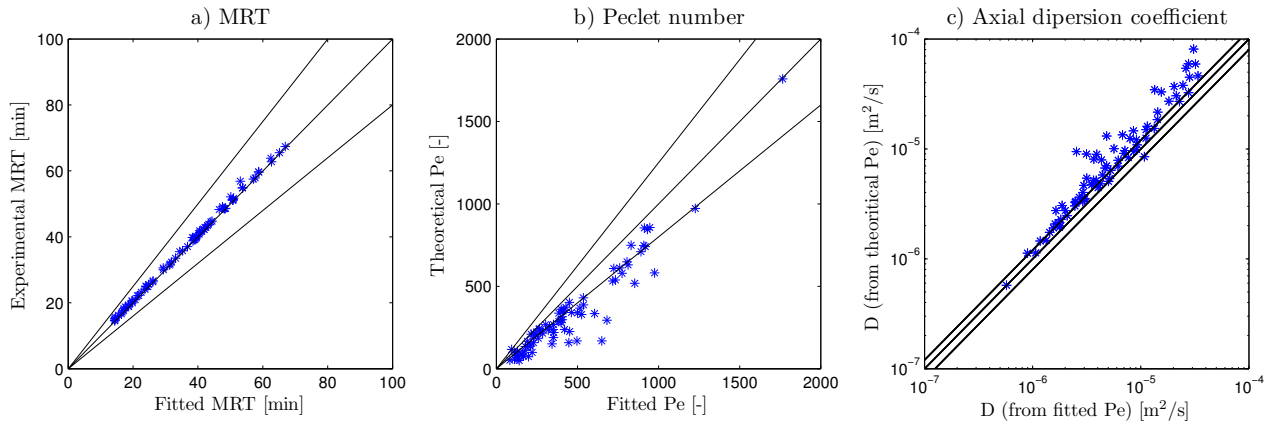


Figure 3.3: Comparison of experimental/theoretical and fitted values of the axial dispersion model parameters, i.e MRT, Pe, and resulting D. Solids lines are $\pm 20\%$ margins.

3.4.2 Influence of operating variables and nature of materials on the RTD

There have been several research works investigating the same scope of this study. However very few experiments on residence time using materials of different physical properties, were performed in rotary kiln equipped with different shape of lifters to study transport of particulate solids. Earlier studies [Venkataraman 1986, Hatzilyberis 1999a, Hatzilyberis 1999b] differ from the present investigation with regard to the design of apparatus, the operating conditions, the experimental procedures, or the materials used.

Effect of lifters profile

Figure 3.4 presents RTDs obtained while processing broken rice, with the kiln equipped with straight, rectangular and no lifters. The three curves are overlapping, but still a distinction can

be found with regards to values of the MRT and the VRT, which are adequate for the analysis. Notably, as previously stated, the VRT gives an indication about the spread of the distribution.

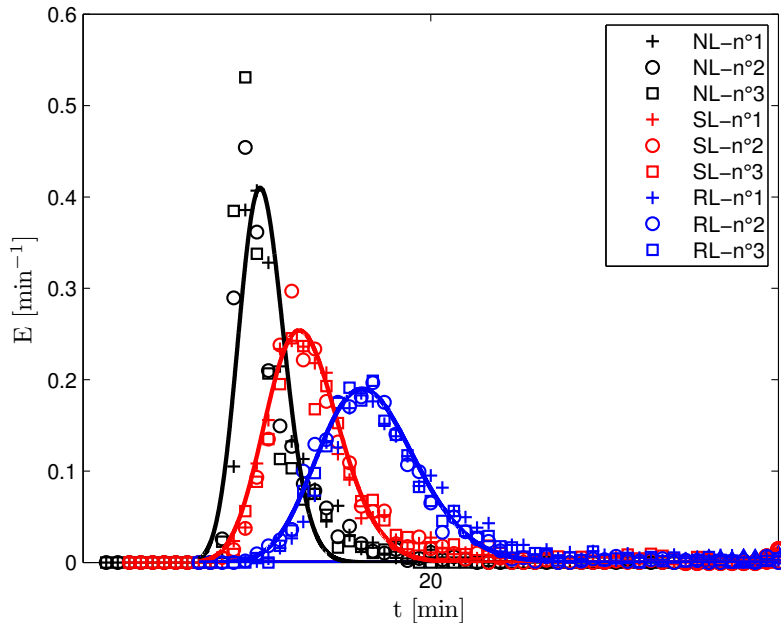


Figure 3.4: Effect of presence and shape of lifters on the RTD for the flow of broken rice. Operating conditions: 10 rpm rotation speed, 2° slope, 2.5 kg.h⁻¹ MFR, 23.5 mm exit dam height. In each case (NL, SL and RL), the experiment was repeated three times. Solid lines are the axial dispersion model of the n°1 replicated run with fitted parameters.

The following orders apply in these experiments:

$$\bar{t}_{NL} < \bar{t}_{SL} < \bar{t}_{RL} \text{ and } \sigma_{NL}^2 < \sigma_{SL}^2 < \sigma_{RL}^2.$$

The experiments performed in this study, for a given type of materials when all operating parameters but the shape of the lifters are kept constant, showed the exact same trend here observed for MRT and VRT of the distribution. Regarding the MRT: RL experiments always have higher MRT than those of SL experiments or NL experiments. This may first be explained by the maximum hold-up of loading lifters. As stated before, the kiln was either over-loaded or design-loaded during the experiments, so that lifters could be filled to their maximum capacity. Let's calculate the volume of solids in a loading lifter for both geometries at horizontal position following [Debacq 2013b] calculations. Assuming the slope drawn by solids in the lifters is equal to the static angle of repose, $V_{SL} = 75.8 \text{ cm}^3$ and $V_{RL} = 242 \text{ cm}^3$, if the bulk materials are sand particles. One may assume that while being regularly kept inside lifters, solid particles are somehow delayed until being cascaded from the lifters with respect to solids inside the kilning bed (which are not taking extra routes or trajectories). Hence the axial transport of particles occurs mainly in the kilning bed. This may be the simple reason why in the presence of lifters, the residence times of solids are increased. But this must not be a sufficient analysis to understand the effect of the lifters' shape or profile. For that, it is necessary to study the discharge rate of lifters. Since there have been recent studies reporting on that field [Debacq 2013b, Sunkara 2013b], such a study was not necessary, but still it was possible to observe the angular position γ_f of a lifter at the end of discharge (with respect to the horizontal). It was found that $\gamma_{fSL} < \gamma_{fRL}$. γ_{fSL} was within the range of 20° to 40° whereas γ_{fRL} was within the range of 120° and 140°.

This implies that on average the SL were totally discharged before RL, every other operating parameter remaining constant. Thus, solid particles were less delayed when using straight lifters, explaining why residence times were higher when the kiln was equipped with rectangular lifters. It was observed that SL were already empty above 40° , while RL were still cascading solids. It is therefore recognized that RL produce more effect of mixing than SL, because they discharge through almost the whole kiln cross section with a relatively sustained rate. This explains why results showed $\sigma_{SL}^2 < \sigma_{RL}^2$ as displayed in Figure 3.6, which presents variation of the VRT with operating parameters when the kiln is equipped with either SL or RL.

Effect of materials of differing physical properties

The two materials used in the study, namely sand and rice, are very different as indicated by their properties given in Table 3.2. Figure 3.5 presents examples of distribution curves obtained while processing these materials in similar operating conditions.

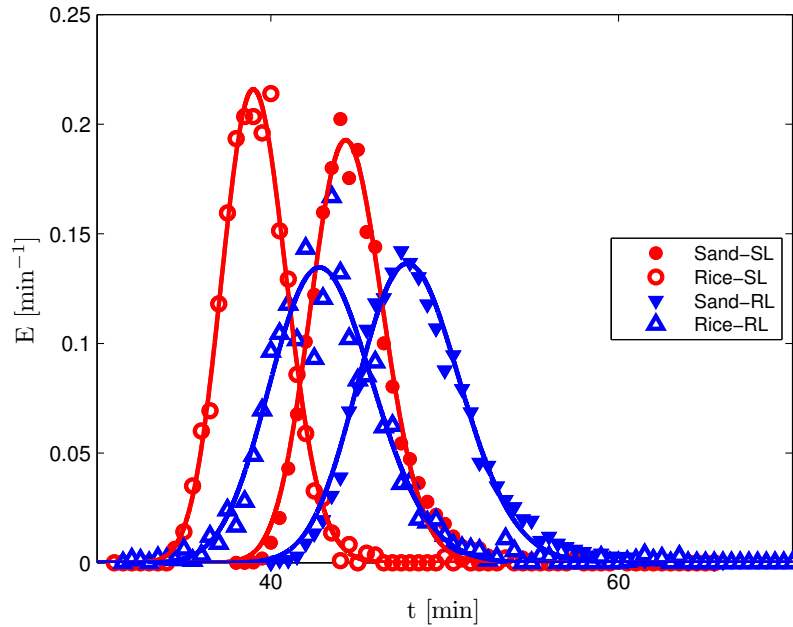


Figure 3.5: Effect of the bulk materials characteristics on the RTD. Operating conditions for both SL and RL: 3 rpm rotation speed, 2° slope, 2.5 kg.h^{-1} MFR, 23.5 mm exit dam height. Solid lines are the axial dispersion model with fitted parameters.

A first remark to be made is that larger solid particles (broken rice) always have smaller residence times compared to the smaller solids particles (sand). In the presence of lifters, rolling motions were observed in the kilning bed. Assuming that lifters, in particular straight lifters, do not affect the flow regimes but only reduce the area of the central core in the bed at the bottom of the kiln as suggested by [Grajales 2012] analysis of [Chaudhuri 2010] experiments and simulations, the main physical property responsible for the differing residence times is likely to be the angle of repose. That is because in this type of motion, as explained by [Mellmann 2001], the larger part of the bed is transported as a solid body upwards with the rotational speed of the wall to the surface layer where particulates roll on themselves from the apex, between or over the lifters. As mentioned by [Friedman 1949] the kilning effect decreases with increasing angle of repose of the materials. Thus, the higher the angle of repose, the higher the time for solid particles to roll down at the surface layer. This latter, combined with effects of gravity, can explain why the rice residence times are shorter compared to those of the sand particles.

Secondly the RTD curves displayed in general nearly the same width: over the whole experimental campaign the VRT obtained were generally of the same order of magnitude for both materials at equivalent operating conditions (see Figure 3.6) except when varying the kiln slope and the feed rate. In the latter cases significant deviations were observed.

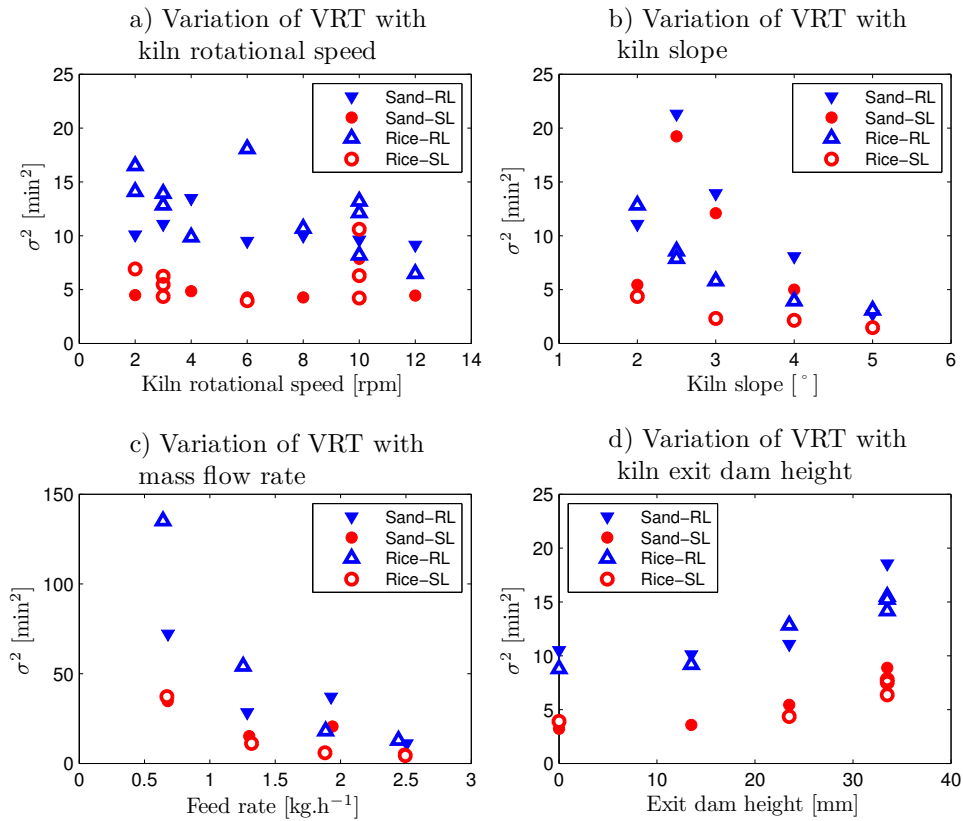


Figure 3.6: Influence of operating parameters (N, S, \dot{M} and exit dam height) on the VRT for the flow of sand and broken rice, when the kiln is equipped with either straight or rectangular lifters.

Effect of operating parameters: rotational speed, kiln slope, flow rate and exit dam height

Effects of profile of the lifters and nature of the bulk materials have been previously discussed, therefore Figure 3.7 shows the influence of the remaining operating parameters in this study in the case of a bulk of broken rice when the kiln is equipped with rectangular lifters.

Rotational speed

As shown in Figure 3.7a, an increase of the kiln rotational speed from 2 to 12 rpm has caused a remarkable shift of the RTD towards lower and lower residence times, while the shape (width and height of the peak) of these RTD curves remains approximately unchanged. Within this range of rotational speed a rolling motion coupled with the mixing effect of the lifters was visually verified. Moreover the rolling motion was theoretically verified by mean of [Mellmann 2001] criteria. These results agreed with [Abouzeid 1974] experiments ranging from rolling to cataracting bed in a small cylinder, but industrial applications are usually within the rolling motion. For a given type of materials and shape of lifters, the VRT remained approximately steady (see Figure 3.6a) as implied by the similar width displayed by the corresponding RTD curves.

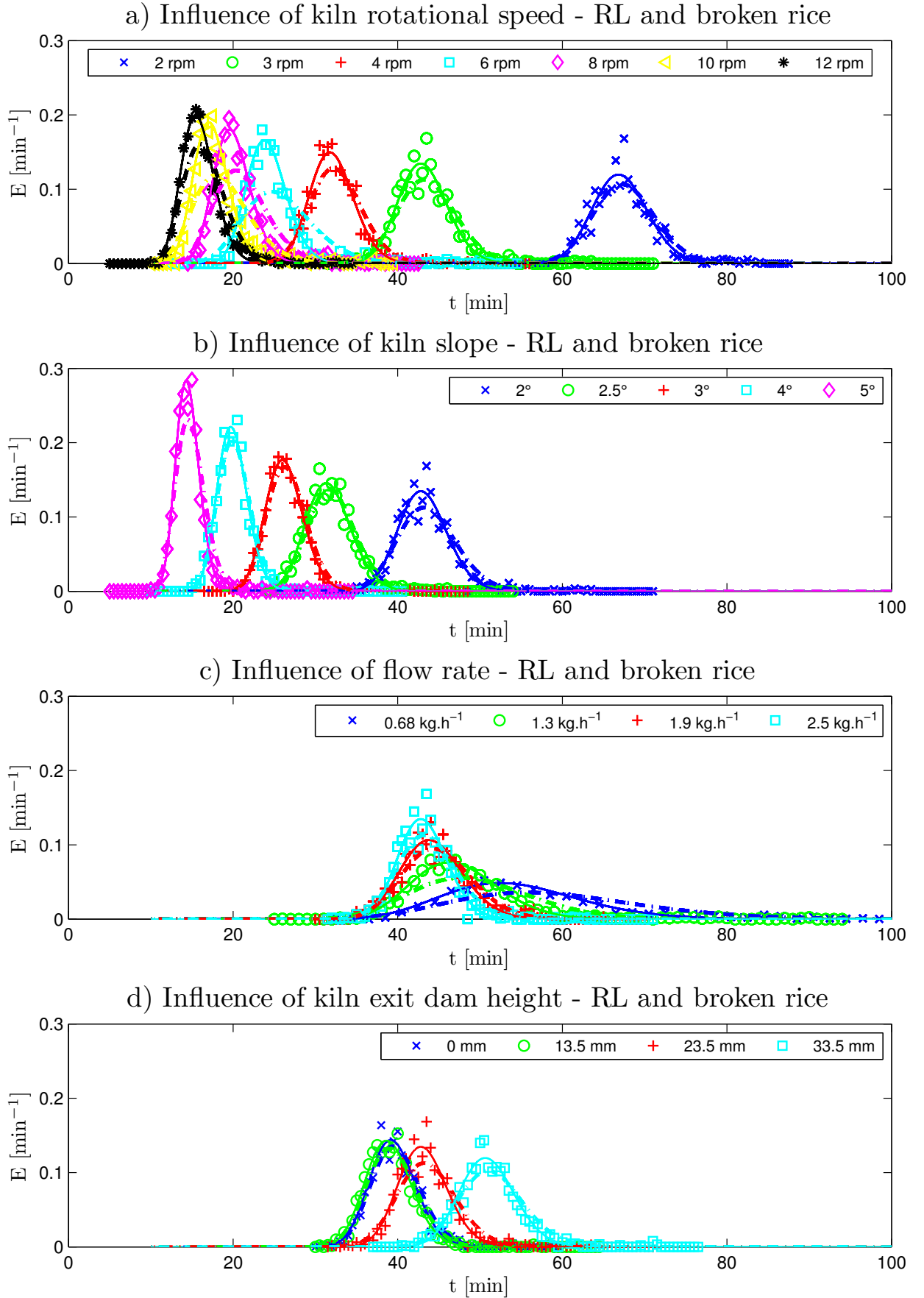


Figure 3.7: Influence of operating parameters (N , S , \dot{M} and exit dam height) on the RTD for the flow of broken rice, when the kiln is equipped with rectangular lifters. Solid lines represent the axial dispersion model using fitted parameters. Dashed lines represent the axial dispersion model using theoretical parameters.

Kiln slope

Even though that some industrial applications have used horizontal rotary kiln [Hehl 1978, Das Gupta 1991, Pan 2006], most kilns are designed to operate in an inclined position. Therefore our investigations extended from 2 to 5 degrees slope. Figure 3.7b shows that RTD curves shift left towards lower residence time regions, while demonstrating gradual changes in their shape. These latter changes may be explained by the gradual decrease observed on the VRT from 2.5° kiln slope. Results also show in Figure 3.6b that sand VRT are slightly higher to those of broken rice.

Mass flow rate

It may be seen from Figure 3.7c, that RTD curves are overlapping. When the solid flow rate decreases from 2.5 to 0.68 kg.h⁻¹, RTD curves gradually spread and flatten, while slowly moving forward so that the residence time of the particles increases. The VRT were found to diminish with increasing feed rate (see Figure 3.6c). By qualitative comparison, these results agreed well with those published previously [Abouzeid 1974, Hehl 1978].

Exit dam height

Eventually it was found that RTD curves shift on the right side (i.e toward region of higher residence time) and become flatter and broader as the exit dam height increases from 0 to 33.5 mm. RTD curves of experiments with a 13.5 mm exit dam height or nothing installed at the kiln outlet, were completely overlapping, in fact nearly the same. This is shown in Figure 3.7d. Thus, results suggest that dams covering less than 45% of the area at the kiln outlet will not have a significant impact on the residence time of solid particles. However, that conclusion should likely apply to kilns having similar L/iD ratios to the one used in this study. The VRT exhibits a plateau before slowly increase with the exit dam height as shown in Figure 3.6d.

3.4.3 Influence of operating variables and nature of materials on the Pe and D

The Peclet numbers obtained in this study are very high usually larger than 100. This is generally common when the flow behavior of the stream in a unit tends toward plug flow, as is usually the case for rotary kilns. Figure 3.8 presents the Peclet numbers obtained by the fitting method, as function of operating parameters. The first observation is that the Peclet numbers obtained with rectangular lifters are always lower compared with those obtained while using straight lifters. This implies that rectangular lifters introduce more back-mixing into the system, confirming previous observations. The Peclet number was found to decrease with increasing kiln rotational speed and slope. However, a plateau seems to be reached in both cases for higher parameter values. As it has been previously observed while using straight lifters as well as forward and reverse spiraling lifters [Venkataraman 1986], the Peclet number also increases with feed rate in the present study. It was found that the Peclet number remains quite constant, unlike [Karra 1977] who have detected a maximum value for the Peclet number, while varying the exit dam height. Regarding the materials used, no significant tendency was found: at similar operating conditions the Peclet numbers are in general of the same order of magnitude.

The axial dispersion coefficient was calculated using the Peclet number and the axial convective velocity in Eq.3.9. The effects of operating parameters on the dispersion coefficient are shown in Figure 3.9. It can be seen that the effect of the profile of lifters on the dispersion coefficient are highly pronounced with increasing kiln rotational speed and slightly significant for higher kiln slope or smaller flow rate. Otherwise the axial dispersion coefficient seemed to

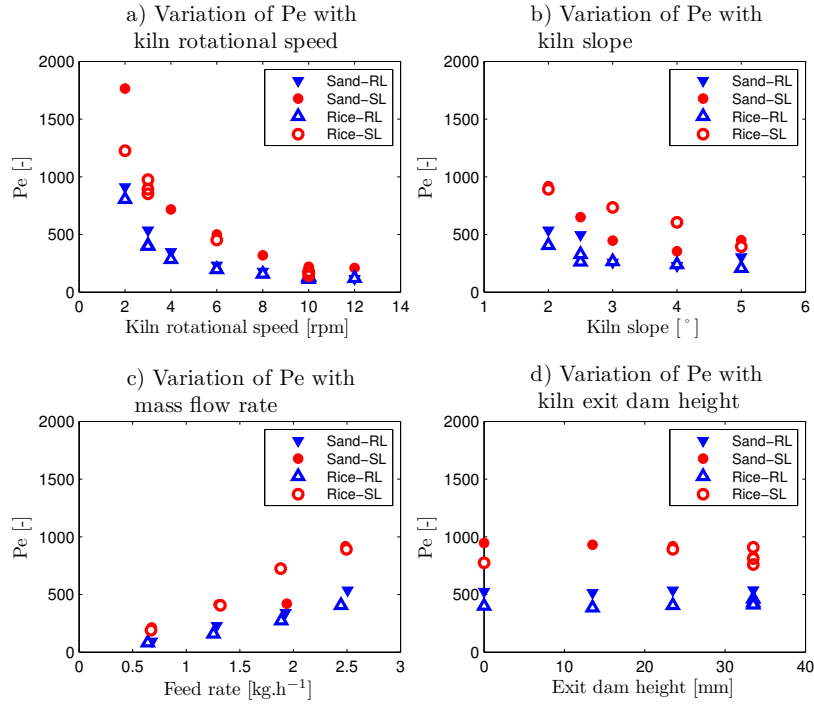


Figure 3.8: Influence of operating parameters (N , S , \dot{M} and exit dam height) on the experimental Peclet number for the flow of sand and broken rice, when the kiln is equipped with either straight or rectangular lifters.

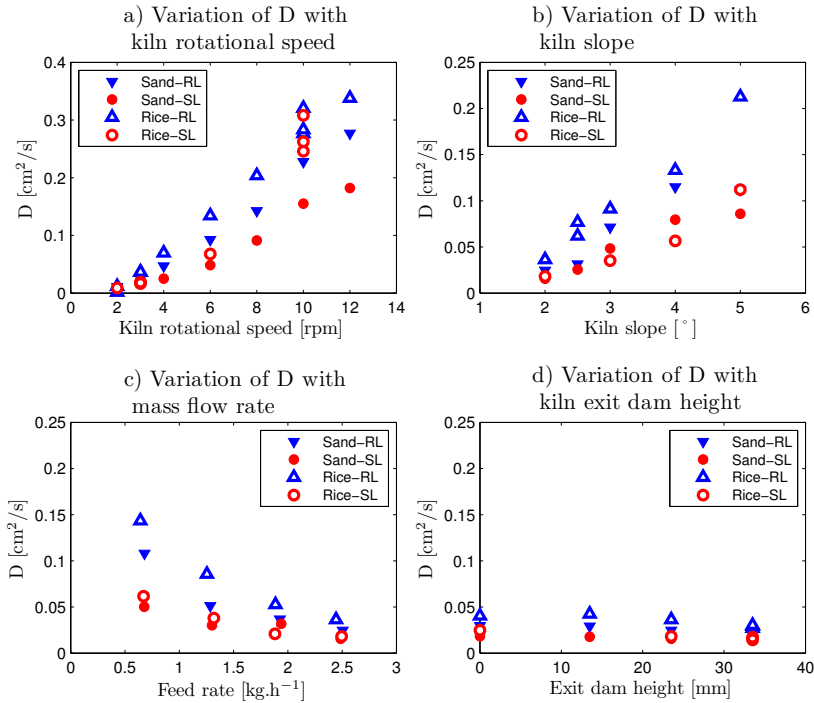


Figure 3.9: Influence of operating parameters (N , S , \dot{M} and exit dam height) on the experimental axial dispersion coefficient for the flow of sand and broken rice, when the kiln is equipped with either straight or rectangular lifters. The axial dispersion coefficients are obtained from the fitted Pe .

have relatively little direct dependence on the lifters shape. If the axial dispersion coefficient values with straight and rectangular lifters are sometimes closed while keeping all other operating parameters constant, experiments with rectangular lifters always have the highest value, confirming previous observations. Variations of the axial dispersion coefficient with the other parameters, namely the kiln rotational speed, the kiln slope, and the flow rate, are the opposite of those mentioned for the Peclet number: it increases with an increase in the two first (N, S) in agreement with [Rutgers 1965] works, and decreases with the last parameter (\dot{M}) contrary to [Venkataraman 1986] tendency for that parameter. The dispersion coefficient was quite stable when varying the exit dam height. Eventually, except for scarce cases, it appears that the axial dispersion coefficient is higher in the case of larger particles: broken rice. This may be linked to the bouncing backward or forward at the bottom of the kiln of these particles after having been cascaded from a lifter, as observed during experiments.

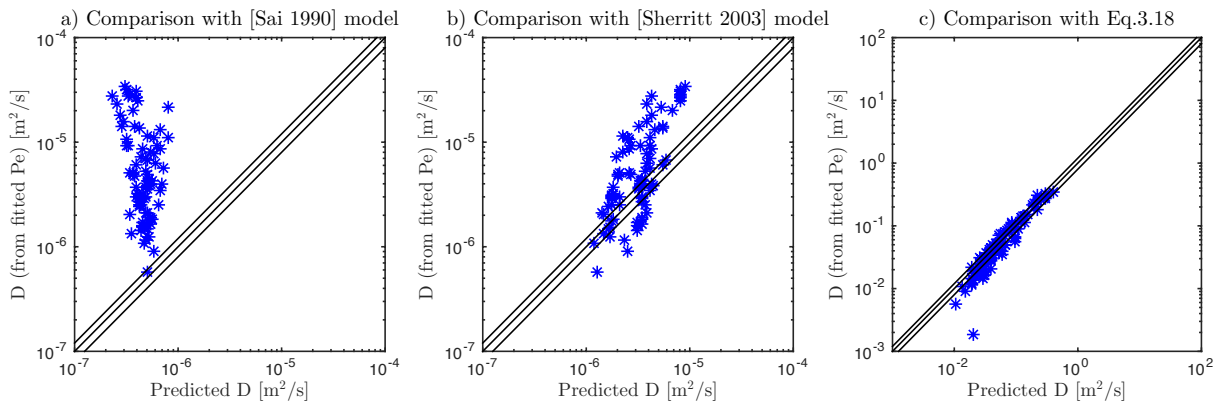


Figure 3.10: Comparison of axial dispersion coefficient values obtained in the present study with predicted values from a) [Sai 1990], b) [Sherritt 2003], c) Present authors Eq.3.18. Solids lines are $\pm 20\%$ margins.

Some correlations intended to predict the axial dispersion coefficient have been published previously [Ang 1998, Fan 1961, Sherritt 2003, Sai 1990].

[Sai 1990] correlated the axial dispersion coefficient with operating parameters as follows:

$$D/uL = 0.000562\theta_t^{0.79}/S^{0.67}N^{1.06}\rho_t^{0.25} \quad (3.15)$$

Tracer properties were considered of major importance along with the kiln rotational speed and slope.

[Sherritt 2003] proposed the following equation to correlate the axial dispersion coefficient with operating parameters when the hold-up volume fraction is less than 0.5:

$$D = 0.0011(N/N_c)^{0.39}(iD)^{1.15}(d_p)^{0.46}X^{-0.43} \quad (3.16)$$

$$N_c = \frac{60}{2\pi} \sqrt{\frac{2g}{iD}} \quad (3.17)$$

with fitting parameters determined for all modes of bed behavior from a set of published data. N_c is the critical speed defined in Eq.3.17, and X is the hold-up, volume fraction.

The two correlations above allow one to determine the axial dispersion coefficient. They are used to calculate the axial dispersion coefficients for the operating conditions achieved in this study. Figures 3.10a and 3.10b show comparison of predictions with experimental axial dispersion coefficient values. Results do not fairly agree with the experimental data especially when using Eq.3.15. However both correlations results are mostly under-predicting. Therefore the axial

dispersion coefficient is correlated in terms of operating parameters. Acknowledging that the geometrical properties of the kiln [Sherritt 2003], and as discussed previously N , S , and \dot{M} , as well as the bulk materials properties, have stronger influence on the axial dispersion coefficient, the following correlation is proposed for kiln equipped with lifters:

$$D = k \left(\frac{\dot{M}}{\rho_{bulk}} \right)^a (N \cdot S)^b (\theta \cdot d_p)^c (Ls)^d \quad (3.18)$$

$$Ls = \frac{n_{lift} - 1}{2} S_{horlift} \quad (3.19)$$

The variables being expressed in the International System of Units, the axial dispersion coefficient D is obtained in $\text{m}^2 \cdot \text{s}^{-1}$, Ls accounts for the area occupied by solid particles contained in loading lifters m^2 , n_{lift} is the total number of lifters, and $S_{horlift}$ represents the section of materials in a lifter at horizontal position in m^2 . The values of the fitted parameters k , a , b , c , and d were optimized using a MatLab program fitting experimental and theoretical data. Results of the calculations are presented in Table 3.4. Predictions are in good agreements with experimental data as shown in Figure 3.10c. As previously mentioned models of [Sherritt 2003] and [Sai 1990] appeared to be not truly realistic for the case of rotary kiln equipped with lifters while the model hereby presented should be valid and give acceptable results for that case as illustrated in Figure 3.10c.

Table 3.4: Parameters for the axial dispersion coefficient in Eq.3.18.

Parameters	Value	Confidence interval	
$k \times 10^7$	1.2023	0.1612	2.2434
a	-0.8714	-0.9348	-0.8081
b	1.6736	1.6329	1.7144
c	0.4349	0.4120	0.4578
d	0.2062	0.1834	0.2290

3.5 Conclusions

From the results obtained in this work, it is possible to draw the following conclusions:

- The axial dispersion model used to represent the experimental data was found to be in very good agreement with the data set. There were no particular effects of segregation or dead volume, since RTD curves do not showed extended tails. The fitted parameters were considered reasonably accurate to characterize the materials transport behavior within the system.
- The RTD curves were found to shift towards lower residence time regions with an increase in either the rotational speed, the kiln slope, or the mass flow rate, or a decrease in the exit dam height. Changes in the shape of the curve were linked to the VRT value, which remained quite stable while varying the rotational speed and exit dam height. The smaller the VRT, the higher the peak of corresponding RTD curves. Broken rice used as the largest materials has generally lower residence time than sand particles. For a given type of bulk materials the VRT are always bigger when using rectangular lifters.
- The Peclet numbers were often greater than 100, as usually observed in rotary kiln unit. They were found to be higher in the case of straight lifters. There was no significant

difference between the two materials except when varying the kiln slope. The exit dam height has no incidence on the Peclet number, whereas an increase in either the rotational speed or the kiln slope induces a decrease of the Peclet number. The Peclet number increases with the feed rate. Regarding the axial dispersion coefficient, results tendencies are the inverse of those reported for the Peclet number. A correlation applicable to rotary kilns equipped with lifters is presented and showed a reasonable degree of quantitative accuracy with regard to the experimental data, compared to other published correlations regarding rotary kilns without lifters.

List of symbols

a,b,c,	Fitted parameters	-
d, k		
C	Tracer concentration, sample conductivity	g/g, $\mu\text{S.cm}^{-1}$
Cv	Coefficient of variation	-
D	Axial dispersion coefficient	$\text{m}^2.\text{s}^{-1}$
d_p	Average particle size	m
E(t)	Distribution function	min^{-1}
E(θ)	Dimensionless distribution function	-
g	Gravitational acceleration	m.s^{-2}
iD	Kiln internal diameter	m
L	Kiln Length	m
Ls	Area occupied by solid particles contained in loading lifters	m^2
\dot{M}	Mass flow rate	kg.h^{-1}
MFR	Mean Flow rate	kg.h^{-1}
MRT	Mean residence time	min
N	Kiln rotational speed	rpm
N_c	Critical speed	-
NL	No lifters	-
n_{lifter}	Total number of lifters	-
N_S	Total number of samples	-
Pe	Peclet number	-
RL	Rectangular lifters	-
rpm	Rotation per minute	-
RTD	Residence Time Distribution	-
S	Kiln slope	degrees
SL	Straight lifters	-
$S_{\text{horlifter}}$	Area covered by solid particles in a lifter at horizontal position	m^2
std	Standard deviation	-

t	Time	min
\bar{t}	MRT	min
u	Velocity	m.s ⁻¹
V	Lifter volumetric hold-up	cm ³
VRT	Variance of the RTD	min ²
X	Hold-up volume fraction	-
z	Dimensionless axial position	-

Greek letters

γ_f	Angular position of the lifter at the end of discharge	degrees
Δt_i	Sampling times	s
θ	Angle of repose, dimensionless time	degrees, -
ρ_{bulk}	Bulk density	kg.m ⁻³
ρ_{tapped}	Tapped density	kg.m ⁻³
σ^2	Variance of residence time	min ²
σ_θ^2	Dimensionless variance of residence time	-

Subscripts

NL	No lifters	-
oo	Open-open	-
RL	Rectangular lifters	-
SL	Straight lifters	-
t	Tracer	-

Chapter 4

Effect of lifter shape and operating parameters on the flow of materials in a pilot rotary kiln : Part II. Experimental hold-up and mean residence time modeling

Abstract	114
4.1 Introduction	115
4.2 Materials and methods	117
4.2.1 Apparatus and materials	117
4.2.2 Experimental technique	118
4.3 Results and discussion	118
4.3.1 Hold-up, volume fraction	118
4.3.2 Mean residence time	121
4.4 Conclusions	129
4.5 Appendices	131
4.5.1 Geometrical characteristics and operating conditions of some kilns	131

The research described in this Chapter has been published in: [Bongo Njeng 2015b]

Bongo Njeng, A.S., Vitu, S., Clausse, M., Dirion, J.-L., Debacq, M., 2015. Effect of lifter shape and operating parameters on the flow of materials in a pilot rotary kiln: Part II. Experimental hold-up and mean residence time modeling. Powder Technology 269, 566–576.

DOI:10.1016/j.powtec.2014.05.070

Abstract

Abstract:

Experiments were carried out on a pilot scale rotary kiln equipped with lifters at room temperature to investigate the effects of the kiln slope, rotational speed, mass flow rate of materials, and exit dam height on the hold-up and the mean residence time (MRT). The MRT was determined from the residence time distribution measurements as detailed in Part I of this work. Two granular solids having different properties were used: sand and broken rice. Furthermore, two shapes of lifters were compared to determine the influence of lifter geometry: straight lifters (SL) and rectangular lifters (RL). A new model to predict the MRT was established by means of a dimensional analysis. The correlation not only gave good agreement with the experimental data from the present study, but also demonstrated good predictive performances when applied to published experimental data of other kilns; the model is applicable for inclined kilns that process materials in cascading (tumbling) motion, whether or not equipped with lifters or fitted with dams at the outlet end.

Résumé :

On a mené des expériences dans un four tournant à l'échelle pilote, équipé de releveurs et à température ambiante, afin d'examiner l'influence de la vitesse de rotation du four, son inclinaison, le débit des particules solides et la hauteur du diaphragme en sortie du four sur le taux de chargement et le temps de séjour moyen des particules solides. Le temps de séjour moyen est déterminé à partir des mesures de distribution du temps de séjours réalisées dans la première partie de cette étude. Les deux solides considérés pour cette étude sont : du sable et des brisures de riz. De plus, afin d'évaluer l'impact du design des releveurs, deux formes de releveurs ont été considérées : des releveurs plats (RP) et des releveurs rectangulaires (RR). On propose un nouveau modèle basé sur l'analyse dimensionnelle pour prédire le temps moyen de séjour des particules solides. On montre d'une part que les prédictions du modèle sont en bon accord avec les résultats expérimentaux de cette étude, et d'autre part que l'application du modèle à d'autres fours de la littérature donne des résultats très satisfaisants. Ce modèle est applicable aux fours tournants, inclinés, équipés ou non de releveurs et ou de diaphragme en sortie, et opérant en régime d'avalanche.

4.1 Introduction

Rotary kilns are gas-solid reactors widely used in mineral process applications and other processes applied to specific granular materials. Due to their extensive use in industry, there have been several studies aimed at modeling the transport of the solids through the kiln cylinder [Sullivan 1927, Prutton 1942, Saeman 1951, Shahhosseini 2000, Chatterjee 1983b, Chatterjee 1983a, Abouzeid 1974, Das Gupta 1991, Descoins 2005, Liu 2006b, Boateng 2008, Liu 2009, Zhu 2011], which is usually equipped with lifters [Hatzilyberis 1999b, Hatzilyberis 1999a, Li 2002a, Britton 2006]. Most of these studies attempted to understand and predict key parameters such as the hold-up, the mean residence time (MRT) or, as shown in Part I of this study [Bongo Njeng 2015c], the residence time distribution of solid particles.

Most of the substantial earlier body of scientific literature that exists in the field assumed no axial dispersion through the kiln, such that the time of passage τ was analyzed instead of the mean residence time \bar{t} . Others simply conflated the two and assumed the mean residence time to be equal to the time of passage. Indeed the time of passage is very easy to determine; it results from the ratio of the weight of the kiln hold-up to the mass flow rate. However, it should not be forgotten that the time of passage might fail to reflect the flow of solids, especially when there is some axial dispersion, which is increased when using lifters.

One of the earliest equations was developed by [Sullivan 1927] for the calculation of the time of passage of particles in rotary kilns which do not have lifters, as follows:

$$\tau = \frac{1.77L\sqrt{\theta}}{SDN} \times factor \quad (4.1)$$

where θ is the angle of repose, S is the kiln slope, N is the rotational speed, L and D respectively the length and internal diameter of the kiln, and *factor* is a parameter accounting for the operating conditions and is equal to one for a simple kiln without obstructions or constrictions.

[Chatterjee 1983b] used a semi-empirical correlation to predict the mean residence time of solid particles. Their model was built on a dimensional analysis taking into account parameters influencing the flow of materials. However, some parameters were missing such as the exit dam height, which did not appear in the list of parameters, though its effect was studied in their experimental matrix. By applying conditions of dimensional homogeneity, they deduced the following correlation:

$$\bar{t} = k \frac{L^3}{F} \left(\frac{\theta}{S} \right)^a \left(\frac{L^3 N}{F} \right)^e \left(\frac{L}{D} \right)^{-c} \quad (4.2)$$

where F is the volumetric feed rate, k is a constant equal to 0.1026 and exponents {a,e,c} are evaluated as {1.054,-0.981,-1.1} [Chatterjee 1983a]. It can be noted in this correlation that the effect of the kiln slope and the angle of repose of solid particles are strongly linked.

In the literature, models for the mean residence time or time of passage, developed for kilns both with and without lifters, range from relatively simple empirical equations to fully mechanistic models. However, we will focus here on some of the simple empirical models developed for kilns equipped with lifters, since the so-called mechanistic models are not suitable for control purposes [Shahhosseini 2000].

Among the earliest models developed for rotary kilns equipped with lifters is the relation of [Prutton 1942] to predict the time of passage:

$$\tau = \frac{kL}{SDN} + mV_f \quad (4.3)$$

where V_f is the volume of solids inside a lifter, k is a constant depending on the number and shape of lifters, and m is a constant depending on the gas flow direction and the properties of

the materials. This model does not consider the effect of any changes in the flow rate of the solid particles and/or gas through the rotary kiln. Moreover the constants k and m must be determined by fitting the model to experimental data from the rotary kiln in use, thus making the model impossible to use for design purposes.

Certainly the most commonly used model, is the correlation of [Friedman 1949], which is derived from the model of [Sullivan 1927] with an additional term to allow for air drag on the solid particles. The [Friedman 1949] equation was obtained through the study of hold-up of a range of materials under overloaded conditions:

$$\tau = L \left[\frac{0.3344}{SDN^{0.9}} \pm \frac{0.6085G}{d_p^{0.5}F} \right] \quad (4.4)$$

where d_p is the average particle diameter, and F and G are respectively the feed rate of the solid particles and the flow rate of the gas. The second term in this equation expresses the air drag; thus the negative sign is used for counter-current flow and the positive sign is used for co-current flow. Compared to the the model of [Sullivan 1927], this model may account for variations in solid and gas feed rates. However, by increasing the solid and gas feed rate by proportional amounts, the predicted residence time will remain constant. Furthermore, the geometric features of lifters are not taken into account in this formulation.

[Shahhosseini 2000] modified the model of [Friedman 1949] in order to better represent the dynamic of the system, the main objective being to determine the hold-up through the use of the retention time of sugar in the rotary kiln. An additional term was introduced to account for changes in the flow rate of the solid particles under zero gas flow rate conditions:

$$\tau = L \left[\frac{8.5}{\tan(S)DN^{0.8}} + \frac{0.41(G + 0.14)}{d_p^{0.5}F} \right] \quad (4.5)$$

This model attempted to address some of the shortcomings of the [Friedman 1949] model, but still did not consider internal fixtures of the kiln.

[Alvarez 1994] presented an empirical relationship for residence time estimation. It was derived from experimental data concerning solid particles of biological and mineral origin. Their correlation requires up to six constants and five other exponents, leading to a total of 11 parameters to be determined:

$$\tau = \frac{\alpha d_p^{0.032} \rho_{bulk}^{0.956}}{NF(\beta S + 1)} + \frac{\gamma d_p^{-0.065} \rho_{bulk}^{0.002}}{\delta S + 1} - \frac{\epsilon G^{0.5}}{\varepsilon S + 1} \quad (4.6)$$

where ρ_{bulk} is the density of the bulk materials. This formulation allows prediction of residence times even when the kiln is horizontal and may apply to a wide range of solid materials. However, due to the large number of model parameters there might be a need to fit the model with the system experimental data prior to its utilization.

Recently [Thibault 2010] proposed two empirical models for the prediction of the mean residence time with the use of a data-set of different types of solids. The models consist of three functions as follows:

$$\bar{t} = \rho_p f_1(1/FN) f_2(S) f_3(G) \quad (4.7)$$

The three functions f_1 , f_2 and f_3 account for the influence of the product FN , the slope of the rotary kiln, and the impact of the gas flow rate on the mean residence time. The definition of f_2 and f_3 as first order functions in the models makes it possible to calculate MRT for horizontal kilns with no gas flow rate. The main difference between the two models proposed is the definition of the function f_1 which can be either a second-order polynomial with the inverse of FN or a simple function with F and N each with an exponent.

This paper is concerned with the study of the effects of usual operating parameters, shape of lifters, and type of materials on the mean residence time of solid particles as well as on the kiln hold-up. A semi-empirical model obtained from dimensional consideration of the mean residence time of solid particles is also presented. Compared to the other published correlations, this new one should be applicable to a wide range of kilns and operating conditions, and could also be useful for design purposes. Therefore this paper will compare the predictions obtained with this model when applied to experimental data from the literature to the corresponding experimental MRT, and will also present the predictions of published models using the present experimental data.

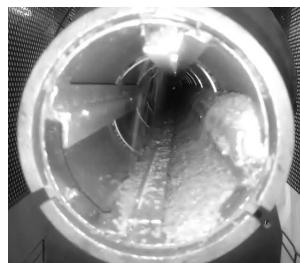
4.2 Materials and methods

4.2.1 Apparatus and materials

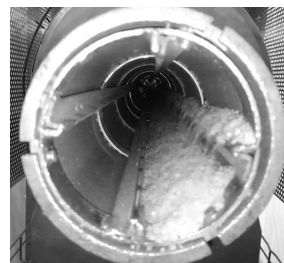
The apparatus and materials have been described in Part I of this work. Therefore only their main characteristics are given here. The rotary kiln is a 0.101 m diameter and 1.95 m long tube, which can be tilted to a maximum angle of 5° . Its rotational speed can be adjusted by a driven motor between 2 and 12 rpm. The flow rate of the solid particles was adjusted by regulating the rotational speed of a screw feeder. Different dam heights were used as given in Table 4.1. In order to study the effect of internal flights, 4 straight one-section lifters of 10 mm (inside length), referred to as straight lifters (SL), and 4 two-section lifters of 10 mm (inside length), referred to as rectangular lifters (RL) due to their right angle cross section as shown in Figure 4.1, were used.

Table 4.1: Details of the circular dams at the kiln outlet end

Exit Dam Height [mm]	Open Diameter [mm]	Diameter Covered [%]	Area Covered [%]
0	101.3	0.00	0.00
13.5	74.3	13.33	46.20
23.5	54.3	23.20	71.27
33.5	34.3	33.07	88.54



(a) Rectangular lifters



(b) Straight lifters

Figure 4.1: Experimental Rotary kiln equipped with lifters: a) Rectangular lifters b) Straight lifters. The bulk materials are broken rice.

Quartz sand (average size 0.55 mm) with a narrow distributed size fraction and broken rice (average size 3.8 mm in length, 1.9 mm in diameter) were employed as experimental materials. The physical properties of these materials are listed in Table 3.2.

Table 4.2: Physical properties of materials

Materials	Shape	ρ_{bulk} [kg.m ⁻³]	ρ_{tapped} [kg.m ⁻³]	d_p [mm]	θ [°]
Sand	Nodular	1422	1543	0.55	39
NaCl	Nodular	1087	1184	0.6	35.4
Broken rice	Cylindrical	889	934	3.8×1.9	36

4.2.2 Experimental technique

The experimental mean residence time was determined from the residence time distribution (RTD) measurement data. The MRT \bar{t} is defined by [Levenspiel 1999]:

$$\bar{t} = \frac{\int_0^\infty tC(t)dt}{\int_0^\infty C(t)dt} \simeq \frac{\sum_i^{N_S} t_i C(t_i) \Delta t_i}{\sum_i^{N_S} C(t_i) \Delta t_i} \quad (4.8)$$

where $C(t_i)$ represents the tracer concentration at the kiln exit end at the discrete time t_i , $i=\{1, 2, 3, \dots, N_S\}$, and Δt_i the associated sampling time.

The kiln hold-up was obtained after the RTD measurement. The feeding system was disabled, and then the solid materials within the kiln were discharged into the recovery tank and weighed. Thus, it was possible to assess the time of passage of particles in the rotary kiln by dividing the weight of solid materials measured by the mean flow rate at steady state.

Part I of this work provides further details on the whole experimental procedure.

4.3 Results and discussion

Table 4.3 gives the results of the hold-up and the mean residence time for a number of experiments where sand and broken rice were operated, with either straight, rectangular or no lifters. The details of these runs are also given. It must be pointed out that the average mass flow rate measured was within a margin of ± 0.05 kg.h⁻¹ of the reported values. Note that in runs where the kiln was equipped with lifters, when the steady state was achieved, the kiln was either design-loaded or over-loaded, i.e. there were always enough solids at the bottom of the kiln to fill lifters to their maximum capacity. Repeated experiments are not reported in Table 4.3. This part of the paper will discuss the effects of kiln rotational speed, kiln slope, mass flow rate, exit dam height, lifter shape and bulk material properties on the fractional volumetric hold-up and the mean residence time. Next, a model for the prediction of the MRT will be proposed.

4.3.1 Hold-up, volume fraction

As shown in Table 3.2, the particulate solids used as bulk materials have varying properties. It was convenient to use the fractional volumetric hold-up (or elsewhere the degree of filling) for the analysis of the results. Fractional volumetric hold-up is defined as the ratio of the volume of the solids loading to the volume of the kiln cylinder. The volume of solids was determined by dividing the hold-up of the solid particles by the bulk density. The effects of operating parameters on the volumetric hold-up are illustrated in Figure 4.2. Note that only experiments with lifters are presented in Figure 4.2. At given operational conditions, experiments processing broken rice filled a higher volume than those with sand, even though the values of the hold-up weight were very close. This is a direct consequence of the materials' differing bulk density properties.

Table 4.3: Experimental results

Operating conditions				RL				SL				NL	
				Rice		Sand		Rice		Sand		Rice	
N	S	\dot{M}	h	MRT	HU	MRT	HU	MRT	HU	MRT	HU	MRT	HU
[rpm]	[°]	[kg.h ⁻¹]	[mm]	[min]	[kg]	[min]	[kg]	[min]	[kg]	[min]	[kg]	[min]	[kg]
3	2	2.5	23.5	43.4	1.953	48.6	1.959	39.2	1.736	44.8	1.886	29.5	1.214
2	2	2.5	23.5	67.4	2.953	65.5	2.808	57.9	2.505	62.7	2.488	-	-
4	2	2.5	23.5	32.3	1.391	39.7	1.536	-	-	35.8	1.508	-	-
6	2	2.5	23.5	25.1	1.033	30.0	1.143	21	0.932	26.7	1.124	18.0	0.724
8	2	2.5	23.5	20.6	0.849	25.5	0.973	-	-	22.2	0.892	-	-
10	2	2.5	23.5	18.2	0.704	22.2	0.831	15.2	0.684	19.3	0.791	13.4	0.532
12	2	2.5	23.5	16.2	0.653	20.5	0.774	-	-	17.1	0.736	-	-
3	2.5	2.5	23.5	31.8	1.305	41.9	1.631	-	-	39.8	1.621	-	-
3	3	2.5	23.5	26.4	1.137	35.5	1.333	24.9	0.919	30.6	1.198	18.8	0.774
3	4	2.5	23.5	20	0.858	24.9	0.937	18.9	0.705	23.2	0.918	-	-
3	5	2.5	23.5	14.6	0.625	18.9	0.734	14.5	0.625	16.6	0.693	-	-
3	2	0.68	23.5	56.9	0.573	63.9	0.676	54.9	0.570	59.7	0.670	-	-
3	2	1.3	23.5	48.3	1.028	54.8	1.105	41.6	0.967	51.7	1.085	34.9	0.758
3	2	1.9	23.5	44.5	1.415	52.1	1.541	42.2	1.276	49.1	1.503	-	-
3	2	2.5	0	39.6	1.685	41.3	1.646	33.5	1.478	37.0	1.539	-	-
3	2	2.5	13.5	39.1	1.713	42.9	1.720	-	-	38.8	1.619	-	-
3	2	2.5	33.5	51.1	2167.5	59.6	2.489	48.6	2.122	57.5	2478	42.1	1.742

It is also important to note the effect of lifters: the experimental results show that the presence of lifters significantly increased the hold-up (see Table 3.2). The results also show that the use of rectangular lifters slightly increased the hold-up within the kiln compared to the use of straight lifters. This may be related to the lifters' hold-up capacity, which is higher in the case of rectangular lifters. Hence the loading of a kiln will be partly dependent on the presence, size and shape of the lifters as previously suggested by [Pruyton 1942] and [Afacan 1990].

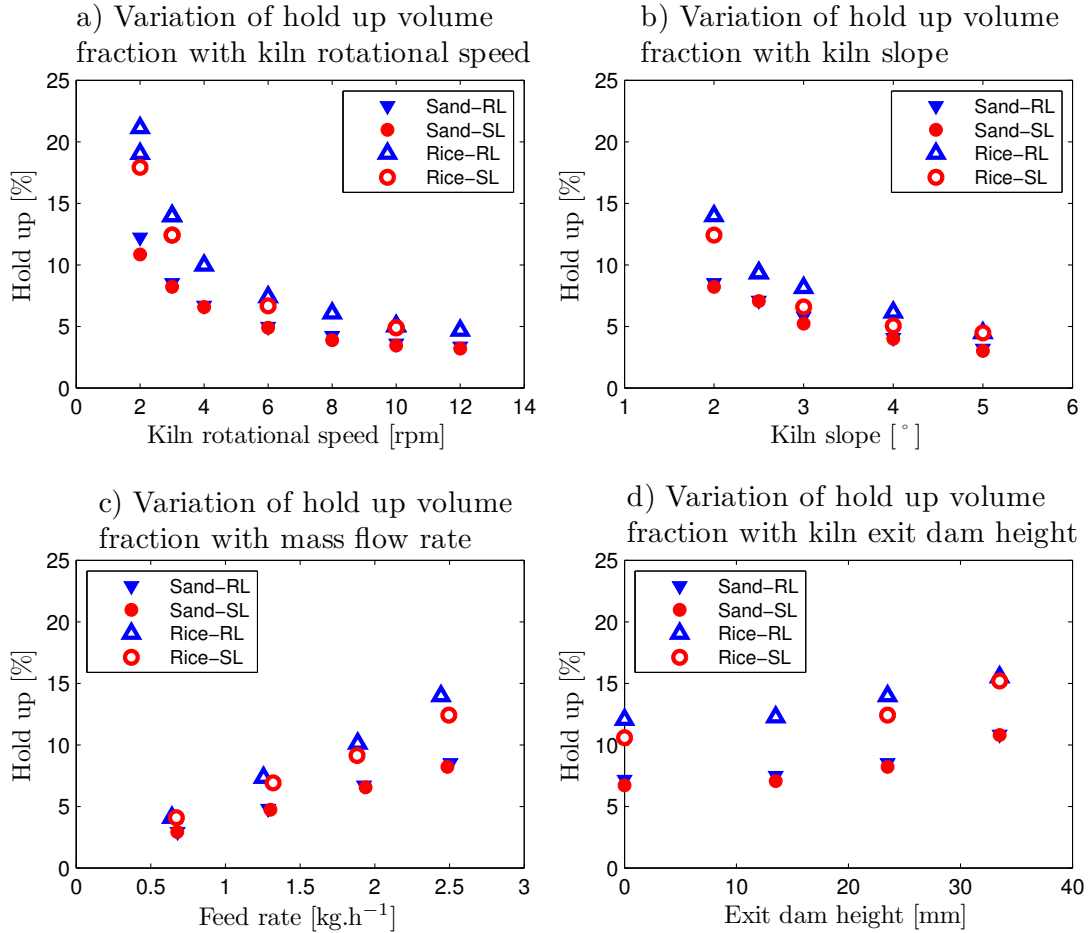


Figure 4.2: Influence of operating parameters (N, S, \dot{M} and exit dam height) on the hold-up volume fraction for the flow of sand and broken rice, when the kiln is equipped with either straight or rectangular lifters.

The classical operational parameters also significantly influence the volumetric hold-up. The fractional volumetric hold-up sharply decreased at smaller rotational speed values before slowing down at higher speed values, as if a bottom had been reached (see Figure 4.2a). Indeed the hold-up must be at the lowest possible level when the motion is starting to centrifuge. This usually happens at very high speed. The fractional volumetric hold-up gradually fell as the kiln slope increased (see Figure 4.2b). On the contrary, the volumetric hold-up steadily increased with the feed rate (see Figure 4.2c). This is not obvious but still can be understood if one extrapolates the work of [Saeman 1951] followed by [Descoins 2005] on the bed depth profiles. These studies show that in a kiln without lifters any increase in the feed rate will result in an increase in the bed depth and hence an increase in the fractional volumetric hold-up. Even if their models are not directly applicable to kilns equipped with lifters, the results remain the same with respect to the effect of the flow rate on the volumetric hold-up. It was observed that the volumetric hold-up increased slightly with increasing exit dam height (see Figure 4.2d). The higher the dam height,

the higher the kilning bed depth, which explains the obtained results.

4.3.1.1 Time of passage

The time of passage can be calculated from the hold-up measurements, as follows:

$$\tau = \frac{HU}{\dot{M}} \quad (4.9)$$

Most of the previous studies focus on this simple relation to investigate the transport of solid particles through a rotary kiln, sometimes conflating it with the MRT, as previously stated. In the present study, therefore, we compared the time of passage and the MRT results over the whole experimental campaign as shown in Figure 4.3. It must be said that, not surprisingly, quite good agreement was found between the MRT and corresponding time of passage in general. This is because the dispersion coefficients observed in the system are quite low, as shown in Part I of this work. Contrary to the MRT, this method does not offer insight into dispersion related issues, which are linked to the residence time distribution of the solid particles. This is why some deviations are still observable. The time of passage estimates the mean residence time only with a certain degree of accuracy depending on the installation.

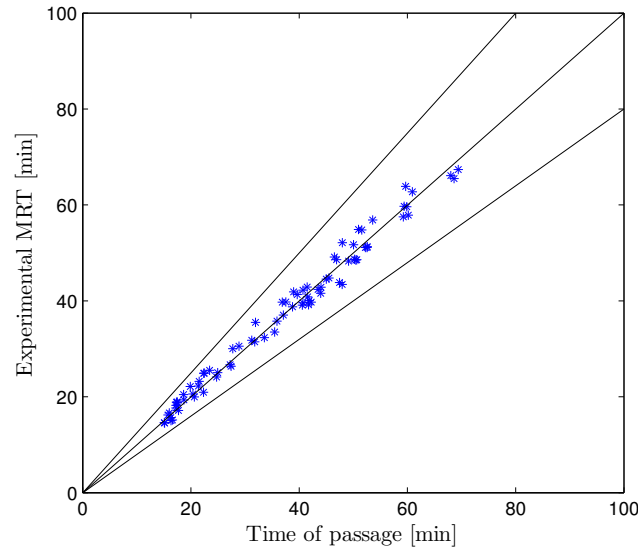


Figure 4.3: Comparison of experimental MRT and time of passage of solid particles. Solid lines are $\pm 20\%$ margins.

4.3.2 Mean residence time

4.3.2.1 Influence of operating conditions

The mean residence times of sand particles were found to be higher than those of broken rice particles, mainly due to the effect of gravity and their differing angle of repose. For a given type of material and fixed operating parameters, the MRT obtained while using rectangular lifters was higher than that obtained while using straight lifters, due to the differing loading capacity of the lifters. These trends, as shown in Figure 4.4, were previously discussed in detail by [Bongo Njeng 2015c]. Note that only experiments with lifters are presented in Figure 4.4.

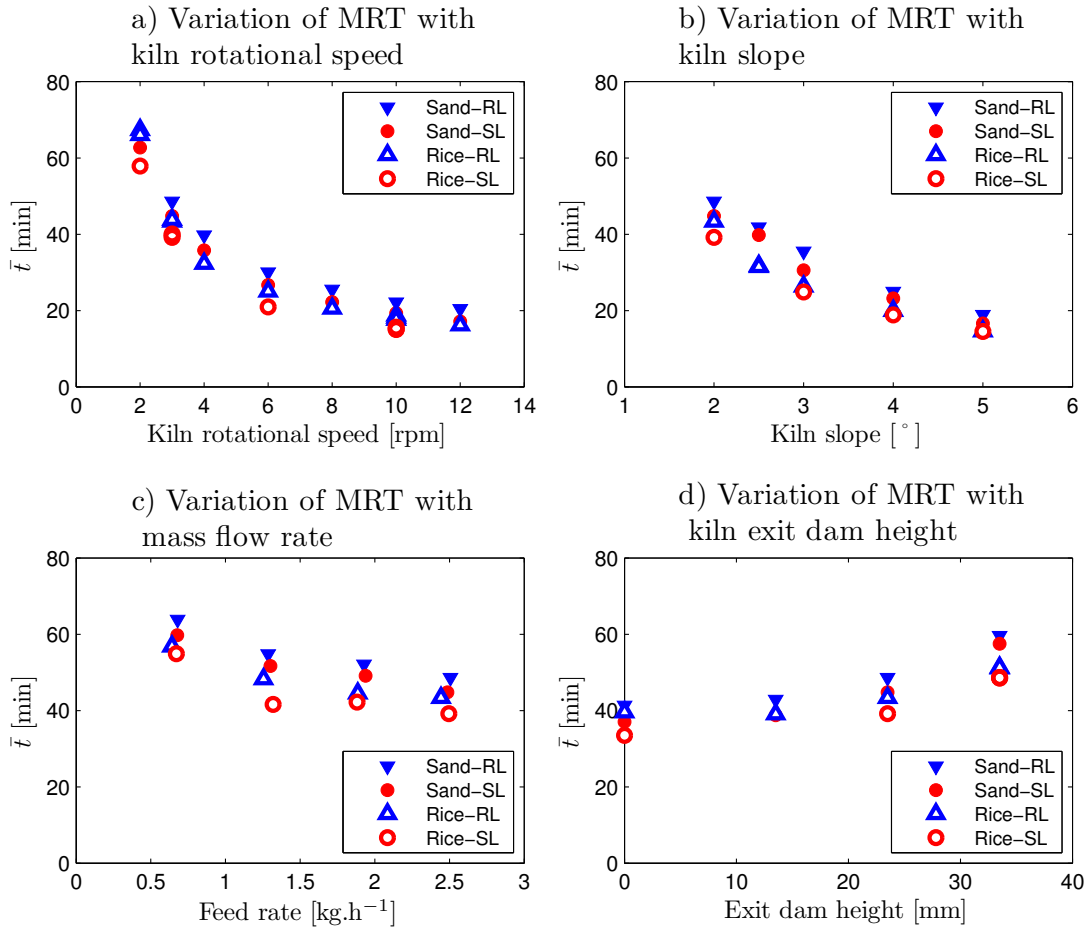


Figure 4.4: Influence of operating parameters (N, S, \dot{M} and exit dam height) on the MRT for the flow of sand and broken rice, when the kiln is equipped with either straight or rectangular lifters.

The MRT significantly decreased by about 69% as the rotational speed increased 6 times, as shown in Figure 4.4a. These results also agreed well with the findings of [Abouzeid 1974] while varying the rotational speed over a wide range of values. [Abouzeid 1974] found in their experiments that the MRT declined when increasing the rotational speed up to 20 rpm. With a further increase in speed the MRT remained approximately unchanged between 40 and 80 rpm. Above 80 rpm, when particles were cataracting, they found that the MRT significantly increased. Figures 4.4b and 4.4c show that the MRT decreased with the kiln slope and the mass flow rate. But it must be further specified in the case of the inclination that there was a sharp decrease between 2 and 4 degrees followed by a slow decrease for higher slopes, whereas the MRT slowly decreased when the mass flow rate increased from 0.68 to 2.5 kg.h⁻¹ (see Figure 4.4c). This tendency is similar to the one observed by some other researchers [Abouzeid 1974, Hehl 1978, Chatterjee 1983b, Chatterjee 1983a]. When increasing the exit dam height the MRT slightly increased (see Figure 4.4d) as observed previously by [Chatterjee 1983b]. However, in our experiments, a maximum increase of only 5% was observed on MRT by using a 13.5 mm exit dam height compared to the case where no exit dam was fitted at the kiln outlet end. It has been observed that these two experimental conditions, all in all, led to similar bed profiles. The only difference which can be mentioned is that in the first case the bed depth was kept constant till the outlet end with the use of the dam, while in the second case it started displaying a slope assumed to be close to the angle of repose approximately 20 mm from the exit. Hence the design of a kiln and its exit dam should give careful consideration to the aspects mentioned here to

optimize the production objectives. For a dam to have a significant impact on the transport characteristics of the materials, its height must be higher than the bed depth observed when the kiln has a clear exit.

4.3.2.2 Model

The main purpose of this model is to come up with a prediction of the MRT of solid particles defined as a function of the kiln design, the properties of the bulk materials, and the operating parameters, namely the kiln rotational speed, the kiln slope, the mass flow rate and the exit dam height. For the purpose of application to other kiln design and operating conditions, and thus to meet scaling-up issues, the model for the prediction of the MRT is based on a dimensional analysis as described below.

4.3.2.2.1 Dimensional analysis

In dimensional analysis, a certain functional form is assumed to relate the varying parameters. All the possible parameters are commonly present with their own exponent. In this study the main operating, geometrical, and physical parameters which can affect the MRT are listed below along with their dimensions:

N	rotational speed	T^{-1}
\dot{M}	mass flow rate	MT^{-1}
S	kiln slope	-
D_{open}	effective exit open diameter	L
S_{lift}	cross section of materials in lifters	L^2
L	length of the kiln	L
D	internal diameter of the kiln	L
ρ_{bulk}	bulk density of materials	ML^{-3}
ρ_{tapped}	tapped bulk density of materials	ML^{-3}
θ	angle of repose of the bulk materials	-
g	gravitational acceleration	LT^{-2}

The analysis involves the fundamental dimensions MLT: mass, length and time. It follows from the above that the relation being sought can be summarized as:

$$F(\bar{t}, N, \dot{M}, S, D_{open}, S_{lift}, L, D, \rho_{bulk}, \rho_{tapped}, \theta, g) \quad (4.10)$$

It is convenient to rewrite Eq.4.10 so that the dependent variable \bar{t} appears directly. Whatever the function F may be, Eq.4.10 can be written in the form:

$$F(N, \dot{M}, S, D_{open}, S_{lift}, L, D, \rho_{bulk}, \rho_{tapped}, \theta, g) \cdot \bar{t} = 1 \quad (4.11)$$

Assuming that Eq.4.11 is dimensionally homogeneous, the parameters of function F must be subject to the power dependence. According to Buckingham's theorem, the formula connecting the set of parameters can be expressed as a function of dimensionless arguments. And each of these arguments is a dimensionless product of a combination of the original parameters raised to integer power. Having in Eq.4.11 a number of variables $r=12$ and a number of fundamental units $n=3$, the number of dimensionless groups p is, according to Buckingham's second theorem:

$$p = r - n = 12 - 3 = 9$$

A collection of 9 dimensionless groupings formed from the parameters in Eq.4.11 were defined as follows:

$$\frac{\bar{t}\dot{M}}{\rho_{bulk}LD^2} = F\left[\frac{N^2D}{g}, \frac{D_{open}}{D}, \theta, S, \frac{\dot{M}}{\rho_{bulk}NLD^2}, \frac{4S_{lift}}{\pi D^2}, \frac{\rho_{bulk}}{\rho_{tapped}}, \frac{L}{D}\right] \quad (4.12)$$

Table 4.4: Calculated values of exponents and constant k for the MRT dimensional correlation

Exp. data	k	α	β	γ	δ	ϵ	ε	ζ	η^1
Sand	0.1363	0.0508	-0.4008	0.8749	-0.9814	0.8115	-4.5285	0.7723	1.1
Rice	0.0792	-0.0218	-0.3387	0.8749	-1.2277	0.8184	-8.0175	0.7723	1.1
Sand & Rice	0.2611	0.0842	-0.3649	0.8749	-1.1243	0.8350	-5.5283	0.7723	1.1

In the literature, some of these dimensionless expressions have been defined, i.e. the Froude number, the length-to-diameter ratio, or the (inverse of the) Hausner ratio. $\frac{D_{open}}{D}$ is the fractional open diameter at the kiln outlet end. $\frac{4S_{lift}}{\pi D^2}$ estimates the fraction of tube cross section not covered by solid particles in loading lifters, where $S_{lift} = \frac{\pi D^2}{4} - \frac{n_{lift}-1}{2} S_{horlift}$ with n_{lift} being the total number of lifters and $S_{horlift}$ being the section of materials in a lifter at horizontal position. When there are no lifters fitted inside the kiln tube, $S_{horlift} = 0$ and $\frac{4S_{lift}}{\pi D^2} = 1$. The two dimensionless groupings $\frac{\dot{M}}{\rho_{bulk} L D^2}$ and $\frac{\dot{M}}{\rho_{bulk} N L D^2}$ are very similar to those found by [Chatterjee 1983b] in their correlation. However, in this work, contrary to what [Chatterjee 1983b] proposed, the bulk materials' angle of repose and the slope of the kiln are taken as separate factors rather than combined as an angular ratio (see Eq.4.2). Eq.4.12 can be written as specified by Buckingham's theorem so that an expression of the MRT is obtained from the defined dimensionless numbers as given in Eq.4.13.

$$\bar{t} = k \frac{\rho_{bulk} L D^2}{\dot{M}} \left(\frac{N^2 D}{g} \right)^\alpha \left(\frac{D_{open}}{D} \right)^\beta (\theta)^\gamma (S)^\delta \left(\frac{\dot{M}}{\rho_{bulk} N L D^2} \right)^\epsilon \left(\frac{4S_{lift}}{\pi D^2} \right)^\varepsilon \left(\frac{\rho_{bulk}}{\rho_{tapped}} \right)^\zeta \left(\frac{L}{D} \right)^\eta \quad (4.13)$$

The variables in Eq.4.13 are expressed in the international system of units, therefore the mean residence time obtained is in seconds. The exponents $\alpha, \beta, \dots, \zeta$ and the constant k are to be determined with the use of experimental data. The length-to-diameter ratio was not varied in our experimental matrix, therefore the exponent η was fixed to the value of 1.1, which was determined by [Chatterjee 1983a] when varying the dimensionless group $\frac{L}{D}$ from 3.3 to 16. To determine the other exponents and the constant k, a MatLab script was written. The program sought to determine the parameters by minimizing the sum of square errors between the experimental and predicted values of the MRT. The program was first run with the whole experimental data matrix, i.e. that which resulted from the flow of both sand and broken rice, then it was run with the sand and broken rice experimental data separately. The angle of repose and the (inverse of the) Hausner ratio are strongly dependent on the materials' properties; for this reason, when determining the parameters with experimental data from either sand or broken rice, γ and ζ were fixed to the values obtained from the whole experimental data matrix. Thus, three sets of parameters best fitting the experimental data using the presented model were obtained as given in Table 4.4.

It should be noted that the aforementioned correlation for the MRT is applicable in the case of inclined rotary kilns, whether or not they are equipped with lifters or fitted with a dam at the outlet end. Using one of the proposed set of parameters in Table 4.4, the kiln must be operated with solid particles in cascading motion [Mellmann 2001].

¹[Chatterjee 1983a]

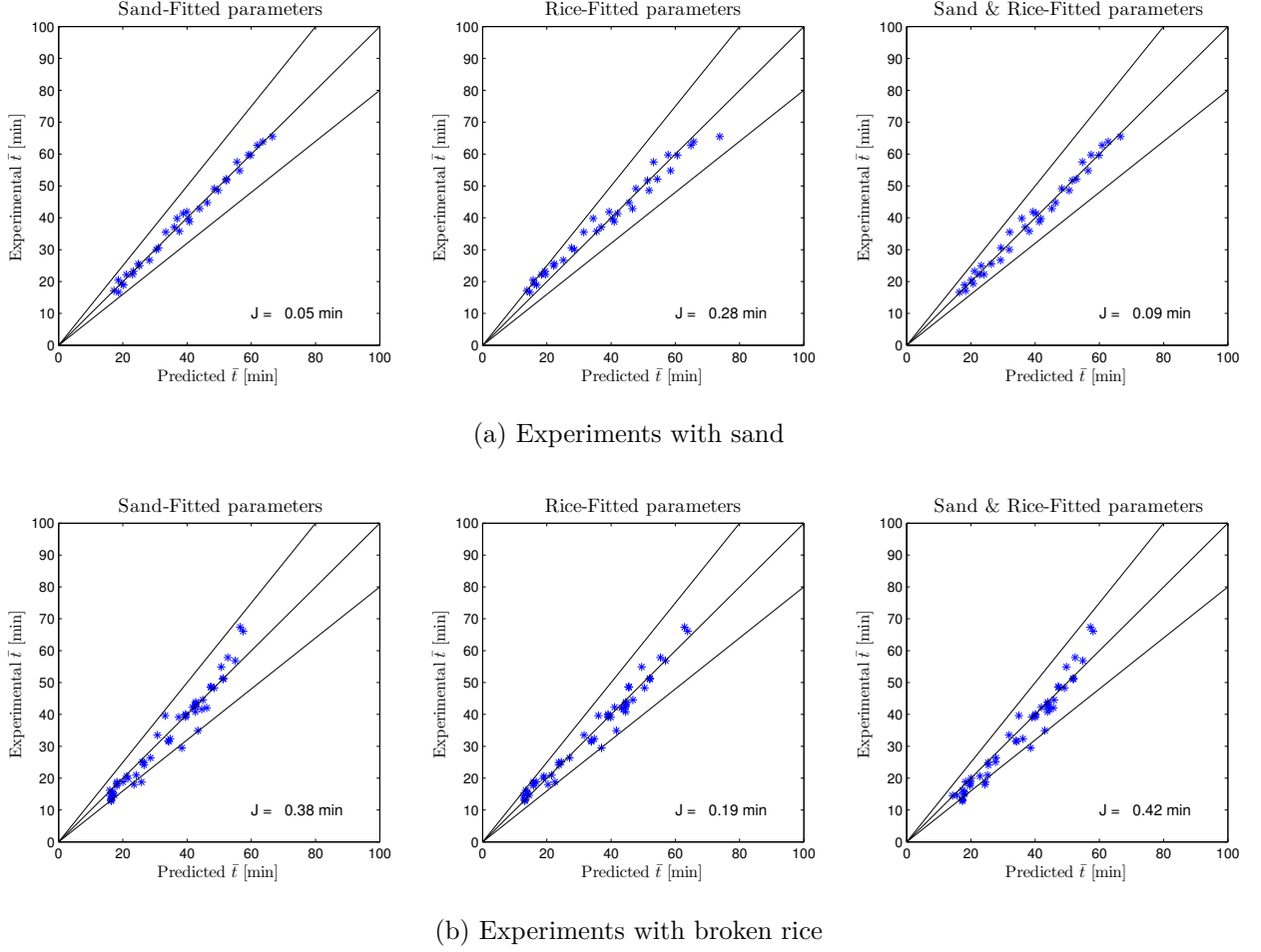


Figure 4.5: Comparison of the experimental MRT while using a) a bulk of sand and b) a bulk of broken rice with predicted values from Eq.4.13 using the 3 sets of parameters as given in Table 4.4. Solid lines are $\pm 20\%$ margins.

4.3.2.2 Predictive performance of the model

The performance of the model was assessed using the three sets of optimal parameters separately on the experimental results. For reasons of clarity, a criterion in performance assessments J was defined as follows:

$$J = \frac{1}{N_T} \sum_{i=1}^{i=N_T} \frac{(\bar{t}_{i_{exp}} - \bar{t}_{i_{calc}})^2}{\bar{t}_{i_{exp}}} \quad (4.14)$$

This criterion can be defined as the sum of the relative square errors between predicted and experimentally determined values of the MRT divided by the number of experiments. It will be used to determine which one among the three sets of optimal parameters gives the best predictions. The lower the value of this criterion, the better the predictions.

The performance of the proposed model was first tested on the experimental data from this study as given in Figure 4.5. Very good agreement was found between the experimental MRT obtained while processing sand and the predictions in general. However, as one may expect, the best predictions were obtained with the “sand-fitted parameters” which displayed the lowest value of the criterion J as shown in Figure 4.5a. Similar remarks can be made when looking at the experiments processing broken rice. There as well, good agreement was found between the experimental and predicted values of the MRT, and the “rice-fitted parameters” gave the least deviations from experimental values according to the criterion value (see Figure 4.5b). In both

cases the “sand & rice-parameters” give some good results, with values of the criterion sometimes very close to the minimum observed.

The predictive capacity of the proposed model was then tested on some experimental data from the literature. Kilns of different geometries and processing a range of materials at varying conditions were chosen. Only a few researchers investigating the residence time of particles through rotary kilns have published their experimental data along with sufficient details on properties of the bulk materials. This is even truer for kilns equipped with lifters. The results from the work by [Debacq 2001] were used in this case. The results from kilns equipped with dams and no lifters were also tested. The latter are from the work by [Sai 1990] and [Chatterjee 1983b]. The results from the kiln used by [Colin 2013], which was equipped with neither lifters nor exit dam, were also used in this study. The experimental results of the aforementioned kilns were used to evaluate the predictive performance of the model for kilns of varying geometries with differing types of material properties and operating conditions. Details about the geometry of the kilns and the properties of the materials are specified in Appendix 4.5.1. However, it should be pointed out that the mass flow rates achieved in most of these experiments extracted from the literature are (between 2 to 300 times) higher than those achieved in the present study.

Figure 4.6 shows a comparison of the experimental MRT reported in [Debacq 2001] with corresponding predictions. The model predictions are very good and the values of the criterion are very close for the three sets of parameters, but the “rice-fitted parameters” proved to be the best in this case with the lowest value of the criterion. The results are even better given that this industrial kiln was equipped with six rectangular lifters and processed a high mass flow rate of cohesive particles .

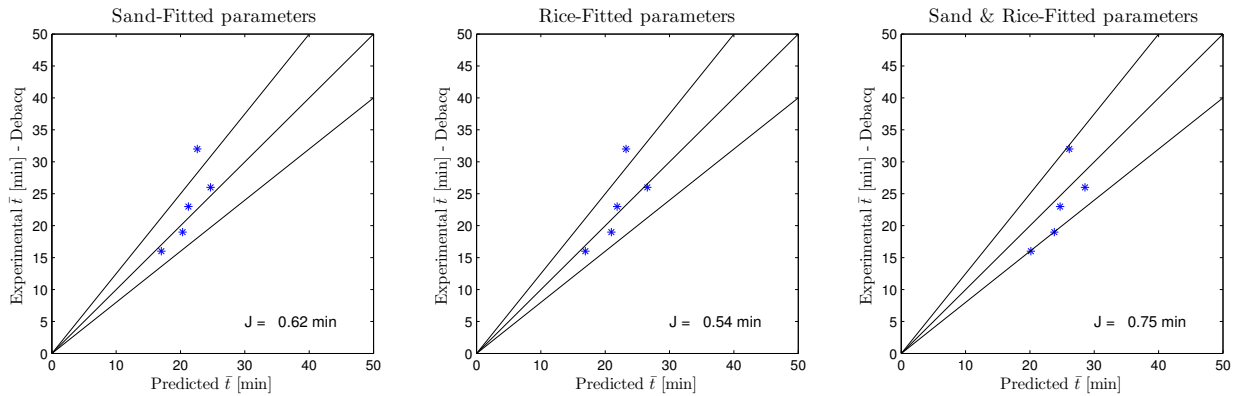


Figure 4.6: Comparison of experimental MRT from [Debacq 2001] with predicted values from Eq.4.13 using the 3 sets of parameters as given in Table 4.4. Solid lines are $\pm 20\%$ margins.

The correlation was then used to calculate the MRT of beech chips flowing through the kiln used by [Colin 2013], and operating without any internal fixtures or exit dam. It should be mentioned that this kiln is twice as big as the one used in the present study. Hence, these kilns have similar length-to-diameter ratios. The comparisons of predicted and experimental values of the MRT are given in Figure 4.7. Results show good agreement between the experimental and calculated MRT regardless of the set of parameters used. However, it should be noted that results obtained while using the “sand-fitted parameters” give the lowest value of the performance criterion followed by the “rice-fitted parameters.”

Other tests were carried out with data from rotary kilns equipped with dams of differing heights at their outlet ends. These rotary kilns were those used by [Sai 1990] and [Chatterjee 1983b] as previously mentioned. Figure 4.8 shows the results of the comparison of the experimental and predicted values of the MRT. In the results obtained from the data of [Sai 1990], the correlation

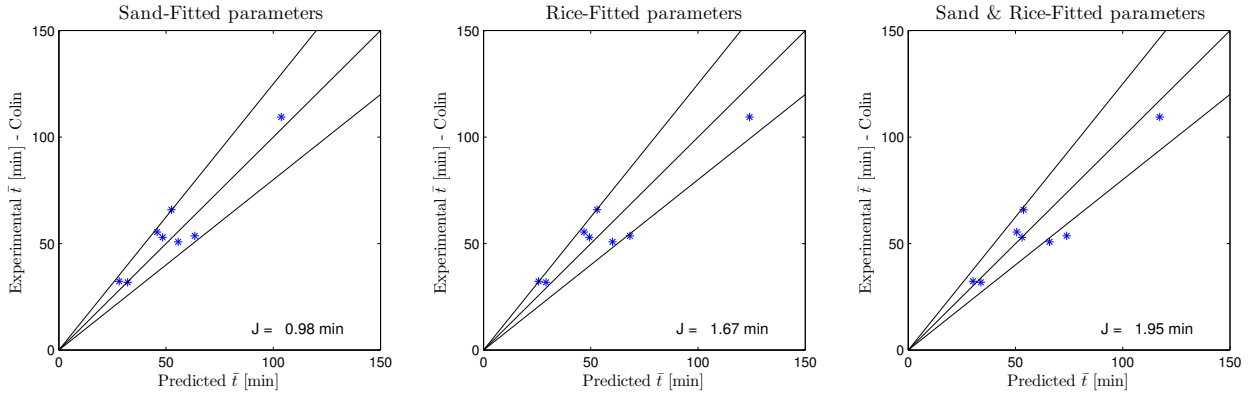
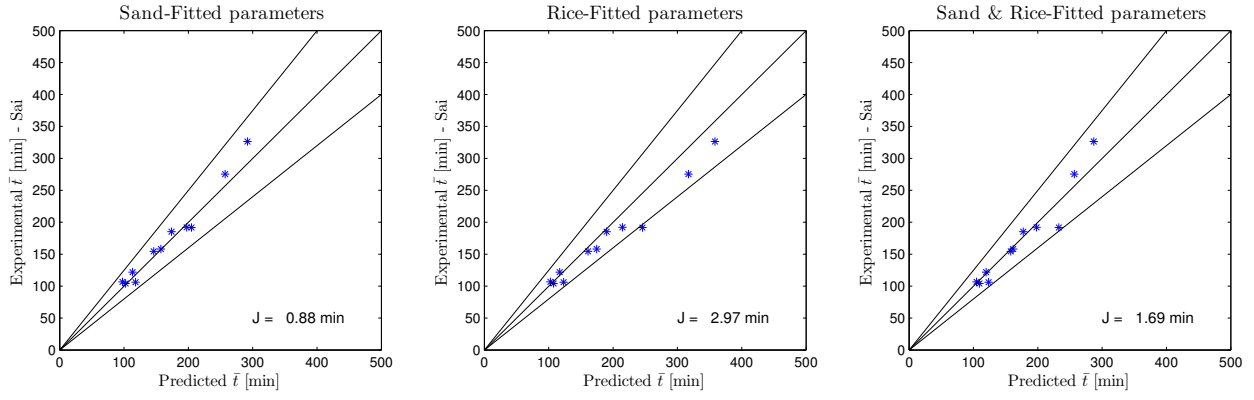


Figure 4.7: Comparison of experimental MRT from [Colin 2013] with predicted values from Eq.4.13 using the 3 sets of parameters as given in Table 4.4. Solid lines are $\pm 20\%$ margins.

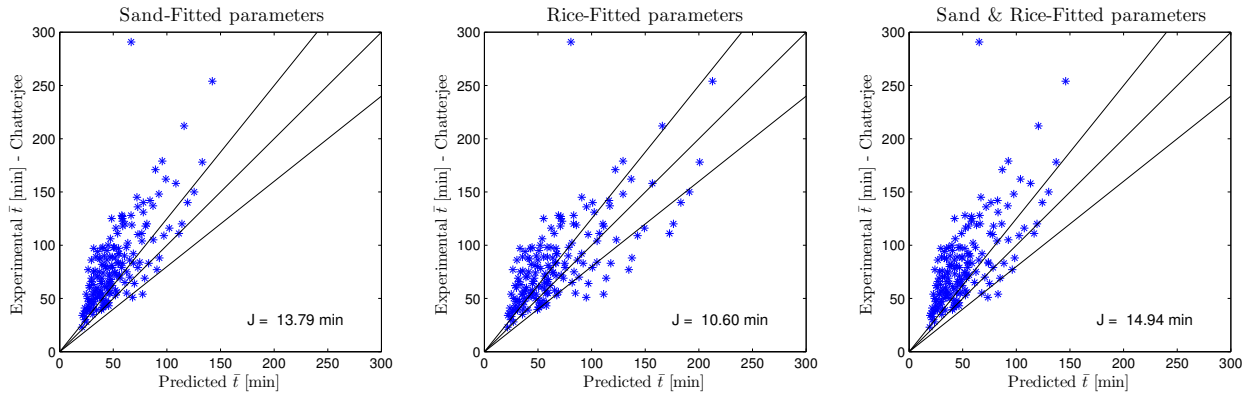
gives a good predictive performance when using either the “rice-fitted parameters” or “sand & rice-fitted parameters,” but revealed an even better agreement with the experimental MRT with the “sand-fitted parameters,” which gives a significantly low criterion compared with the other results. [Chatterjee 1983b] achieved a huge experimental matrix including 5 types of dam, but their correlation for the MRT was not adapted for kilns fitted with exit dams (see Eq.4.2). The comparisons of the predicted and experimental values of the MRT show some deviations. In this case the predictive performance of the model seems to be somewhat diminished, as suggested by the elevated values obtained for the criterion J . Nonetheless, about 30 to 50% of the results are within reasonable margins of the MRT experimentally measured. These poor results of the model can be attributed to (i) the difficulties in extrapolating to kilns with a rotational speed lower than 2 rpm, leading most of time to small Froude numbers characteristic of beds in slipping motion [Mellmann 2001], or perhaps (ii) the wide range of variation of the effective exit open diameter achieved by [Chatterjee 1983b] even if the results obtained in the case of [Sai 1990]’s experiments were quite acceptable.

To complete the analysis of the predictive capacity of the proposed model, other models developed for rotary kilns were applied in order to compare the MRT predictions. The correlation proposed by [Chatterjee 1983a] (see Eq.4.2) which does not account for the presence of lifters or an exit dam was used. The correlation of [Shahhosseini 2000] (see Eq.4.5) which may apply to kilns equipped with lifters was also used. The predictions of these models are presented in Figure 4.9, along with predictions obtained from Eq.4.13 with the use of “sand & rice-fitted parameters.” The predictions from [Chatterjee 1983a]’s correlation underestimate the experimental MRT by almost half, while those from [Shahhosseini 2000]’s correlation largely overestimate them. Furthermore, the predictions from Eq.4.5 display two patterns that are associated with the two types of solid particles used in this study. These results give a large value of the performance criterion, whereas the predictions from Eq.4.2 and Eq.4.13 are more uniformly distributed, with a relatively lower value of the criterion. However, predictions from Eq.4.2 display a vertical pattern linked to its incapacity to take into account the presence of lifters and exit dam. As shown in Figure 4.9, predictions from Eq.4.13 give the lowest value of the criterion compared to the other two models, failing to give good predictions of the experimental MRT.

It appears, in accordance with the results of the present study, that the correlation proposed in this work for the MRT is also valid when applied to kilns with materials and operating conditions different from those used in the study. This confirms the excellent predictive capacity of Eq.4.13 compared to similar semi-empirical models which are often limited to a small range of conditions and operating variables. Regardless of the set of parameters, the predictions of the correlation



(a) [Sai 1990]



(b) [Chatterjee 1983b]

Figure 4.8: Comparison of experimental MRT from a) [Sai 1990] and b) [Chatterjee 1983b] with predicted values from Eq.4.13 using the 3 sets of parameters as given in Table 4.4. Solid lines are $\pm 20\%$ margins.

are usually within reasonable margins of the experimental MRT. For that reason the authors recommend the use of the “sand & rice-fitted parameters.”

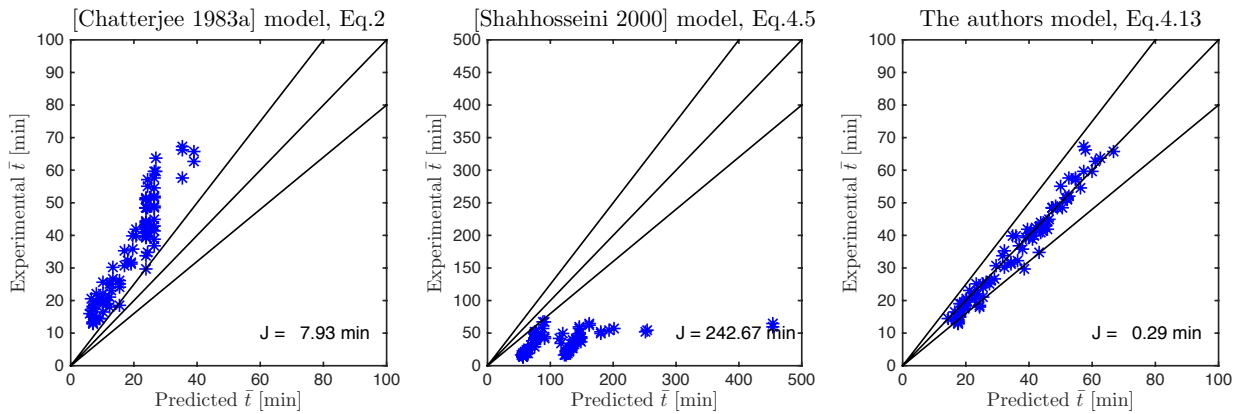


Figure 4.9: Comparison of the experimental MRT with predicted values from Eq.4.2, Eq.4.5 and Eq.4.13 (using "sand & rice-fitted parameters").

4.4 Conclusions

The effects of operating parameters, namely, the rotational speed, the kiln slope, the mass flow rate, the exit dam height, the type of materials and shape of lifters, on the hold-up and mean residence time have been investigated. As far as these parameters are concerned, in this work it was observed that:

- Increasing either the rotational speed or the kiln slope decreased the kiln hold-up and the MRT of the charge.
- Increasing the feed rate tended to increase the hold-up while the MRT of particles decreased. With an increase in the exit dam height the latter two increased slightly.
- The use of rectangular lifters slightly increased the kiln hold-up and the MRT of particulate solids compared with straight or no lifters.
- Sand and broken rice bulks have similar Hausner ratios though they have different bulk and tapped densities and different particle sizes. Their MRT were relatively close but the sand MRT were always higher whereas the rice hold-ups were usually higher.

A semi-empirical model was developed in order to predict the mean residence time of solid materials under steady state conditions in inclined rotating kilns, whether equipped or not with lifters and exit dams, as follows:

$$\bar{t} = k \frac{\rho_{bulk} L D^2}{\dot{M}} \left(\frac{N^2 D}{g} \right)^\alpha \left(\frac{D_{open}}{D} \right)^\beta (\theta)^\gamma (S)^\delta \left(\frac{\dot{M}}{\rho_{bulk} N L D^2} \right)^\epsilon \left(\frac{4S_{lift}}{\pi D^2} \right)^\varepsilon \left(\frac{\rho_{bulk}}{\rho_{tapped}} \right)^\zeta \left(\frac{L}{D} \right)^\eta$$

The correlation consists of dimensionless factors accounting for (i) the basic operational parameters of the kiln, (ii) the properties of the bulk solids, (iii) the geometry of the kiln, (iv) the number, shape and presence of lifters, (v) the height of the exit dam. The parameters, namely $k, \alpha, \beta, \dots, \zeta$ have been determined from experimental data. The authors recommend the use of the “sand & rice-fitted parameters” as given in Table 4.4, which give good agreement with experimental data from this study as well as from published data. However, the sets of parameters proposed here are only applicable to beds in cascading (tumbling) motion as defined by [Mellmann 2001]. Therefore, possible directions for further work could be (i) to extend the validity of the model to other types of bed motion with an adequate set of parameters, (ii) to enrich the experimental data matrix with results from the use of new types of solid materials to reaffirm the set of parameters determined.

List of symbols

C	Tracer concentration,	g/g,
	sample conductivity	$\mu\text{S.cm}^{-1}$
D_{open}	Effective exit open	m
	diameter	
d_p	Average particle size	mm
D	Kiln internal diameter	m
$F,$	Function	-
f_1, f_2, f_3		
F	Solids feed rate	kg.s^{-1}

<i>factor</i>	Fitting parameters	-
G	Gas flow rate	kg.s ⁻¹
g	Gravitational acceleration	m.s ⁻²
HU	Hold-up	kg
k	Fitting parameters	-
J	Performance criterion	min
L	Kiln Length	m
Ls	Area occupied by solid particles contained in loading lifters	m ²
\dot{M}	Mass flow rate	kg.h ⁻¹
MRT	Mean residence time	min
N	Kiln rotational speed	rpm
NL	No lifters	-
n_{lift}	Total number of lifters	-
N _S	Total number of samples	-
N _T	Total number of experiments	-
RL	Rectangular lifters	-
rpm	Rotation per minute	-
RTD	Residence Time Distribution	-
S	Kiln slope	degrees
SL	Straight lifters	-
S_{lift}	Area covered by solid particles in a lifter at horizontal position	m ²
$S_{horlift}$	Area covered by solid particles in a lifter at horizontal position	m ²
t	Time	min
\bar{t}	MRT	min
V _f	Volume of solids inside a lifter	m ³
X	hold-up volume fraction	-

Greek letters

$\alpha, \beta, \gamma,$	Fitting parameters	-
$\delta, \epsilon, \varepsilon,$		
ζ, η		
Δt_i	Sampling times	s
θ	Angle of repose	degrees
ρ_{bulk}	Bulk density	kg.m ⁻³
ρ_p	Particle density	kg.m ⁻³
ρ_{true}	Tapped density	kg.m ⁻³
τ	Time of passage	min

4.5 Appendices

4.5.1 Geometrical characteristics and operating conditions of some kilns

Table 4.7 gives the characteristics of different kilns from the literature, along with the range of their operating conditions and characteristics of the materials used. For some materials the tapped density was missing in the published papers (those marked with * in Table 4.2). For these cases a literature review was done to determine the ability of the solid particles to flow. The flow ability is influenced by the particle size; fine particles (< 0.1 mm) tend to be more cohesive and thus less free-flowing, whereas larger, denser particles tend to be free-flowing. It was decided to used a Hausner ratio of 1.05, characteristic of a free flowing bulk, for both Ilmenite and Iron ore.

Table 4.7: Characteristics of differing kilns with their operating parameters range of variation as given in literature.

Authors	L [m]	D [m]	L/D [-]	Materials [-]	Size [mm]	θ [°]	ρ_{bulk} [kg.m ⁻³]	ρ_{tapped} [kg.m ⁻³]	N [rpm]	S [°]	\dot{M} [kg.h ⁻¹]	h [mm]	S_{lift} [m ²]
[Bongo Njeng 2015c]	1.95	0.10	19.50	Sand	0.4-0.8	39	1422	1543	2-12	2-5	0.69-2.5	0-33.5	0-0.008
				Rice	1.8-4.4	36	889	934					
[Debacq 2001]	6.85	0.75	9.13	UO ₂ F ₂	0.02-0.5	42	400	500	1.6-2.1	1.43	508-895	0	0.438
				U ₃ O ₈	0.01-0.05	33	1000	1300					
[Colin 2013]	4.2	0.21	20.00	Beech	5-15	42	260	284	2-4	1-2	4-8	0	0
[Sai 1990]	5.9	0.15	39.33	Ilmenite	1.1	27.4	4200	4410*	1-3	0.78-1.37	6-36	15-28	0
[Chatterjee 1983b]	2	0.3	6.67	Iron ore	3-6	35	2500	2625*	0.3-0.7	1-3	15-60	0-75	0

Chapter 5

Effect of lifter shape and operating parameters on the flow of materials in a pilot rotary kiln : Part III. Up-scaling considerations and segregation analysis

Abstract	134
5.1 Introduction	135
5.2 Materials and methods	136
5.2.1 Apparatus and materials	136
5.2.2 Experimental procedure	137
5.2.3 Data processing	138
5.3 Results and discussion	140
5.3.1 Influence of operating variables on the experimental RTD, MRT, VRT and HU . . .	140
5.3.2 Influence of operating variables on the experimental Pe and D	145
5.3.3 Modeling: MRT, HU and D	145
5.3.4 Analysis of particle segregation	149
5.3.5 Reproducibility of experiments	151
5.4 Conclusion	152
5.5 Appendices	155
5.5.1 Experimental Results: HU, MRT, VRT, Pe, D	155

The research described in this Chapter is to be submitted for publication to Powder Technology.

Abstract

Abstract:

Up-scaling tracer experiments were carried out in a pilot-scale rotary kiln twice as big as the kiln used in the first two Parts of this study. Internal fixtures such as grid, or lifter structure arranged in 3 and 6 rows of single throughout lifters were used. The effects of these removable fixtures and other usual operating conditions, namely, mass flow rate of granular biomass materials, rotational speed and slope of the kiln on the residence time distribution (RTD), the mean and variance of residence time (MRT and VRT), the hold-up (HU), the Peclet number (Pe) and corresponding axial dispersion coefficient (D), were investigated. Scaling-up rules were derived for the MRT, HU volume fraction and D from the results of a comprehensive experimental work. Good agreement was found between the experimental data and the calculated values. The wide size distribution of the beech chips used in the present study allows analysis of particle segregation, which may further increase understanding of the flow characteristics of granular materials, notably within flighted rotary kilns. The results show that while significantly increasing the dispersion, ipso facto, enhancing the mixing, the lifters limit the extent of particle segregation.

Résumé :

Afin de proposer des règles générales pouvant s'appliquer à d'autres fours, on a mené des expériences dans un four tournant deux fois plus grand que celui précédemment utilisé dans les deux premières parties de cette étude. Ces expériences ont consisté à effectuer des mesures de distribution du temps de séjour (DTS). Des éléments internes amovibles tels qu'une grille, ou une structure équipée de 3 ou 6 rangées de releveurs ont été utilisés. Les effets de ces équipements amovibles et des conditions opératoires (débit de matière solide, vitesse de rotation et inclinaison du four) sur la distribution du temps de séjour, le temps de séjour moyen et la variance de la distribution, la rétention de solide dans le four, le nombre de Peclet et le coefficient de dispersion axiale pour l'écoulement de plaquettes de bois de hêtre ont été analysés. Sur la base d'analyse dimensionnelle, des corrélations ont été proposées pour la prédiction du temps de séjour moyen, du taux de remplissage et du coefficient de dispersion axiale; la paramétrisation de ces modèles a été réalisée à l'aide des résultats expérimentaux de cette étude dans son ensemble. La dispersion de taille des particules de bois utilisées a permis l'étude de phénomènes de ségrégation, en particulier en présence de releveurs. Les résultats montrent qu'en présence de releveurs la dispersion augmente significativement, de fait l'effet de mélange est accentué, et les phénomènes de ségrégation sont limités.

5.1 Introduction

Rotary kilns have become over the years among the most commonly used gas-solid reactors in a variety of applications in metallurgical and chemical manufacturing, but also in the waste disposal. They are equally applicable to a wide range of materials ranging from granular solids to sludge and slurry. In the processing of solids, the particle size distribution is only a function of the handling capacity of the feeding system.

The focus of this study, initiated in [Bongo Njeng 2015a, Bongo Njeng 2015b], is the characterization of solids transport within flighted rotary kilns. If there have been several studies in that field up-to-date, most of these studies have generally focused on the bare kiln [Chatterjee 1983c, Bandopadhyay 1986, Sai 1990, Chen 2009] to model through empirical or mechanistic correlations some of the main solids transport variables such as the hold-up, mean residence time or the bed depth profile. A few studies have characterized effect of the lifters on the flow of solids particles [Miller 1942, Kelly 1968, Kelly 1992, Hatzilyberis 1999b, Ablitzer 2000].

The correlations developed by [Hwan 2009] for horizontal flighted rotary kilns can be mentioned. They are based on dimensional analysis similar to the correlation by [Chatterjee 1983b], which was adjusted using residence time distribution (RTD) measurements conducted in an inclined rotary kiln without lifters but equipped with an exit dam. [Hwan 2009] performed systematic experiments carried out in horizontal rotary kilns of different length-to-diameter ratios (between 5 and 10), using segmented lifters and different solid materials. From these results, the following equations were established respectively for the prediction of the volumetric filling degree, f , the time of passage, τ , and the axial dispersion coefficient, D :

$$f = 10.91\theta^{1.14} \left(\frac{d_p}{D_i}\right)^{-0.15} \left(\frac{\rho\omega D_i^2}{\dot{M}/D_i}\right)^{-0.90} \left(\frac{\omega^2 D_i}{g}\right)^{-0.03} \left(\frac{h_l}{D_i}\right)^{-0.52} \left(\frac{L}{D_i}\right)^{-0.40} \quad (5.1)$$

$$\tau = 8.57 \frac{\rho L D_i^2}{\dot{M}} \theta^{1.14} \left(\frac{d_p}{D_i}\right)^{-0.15} \left(\frac{\rho\omega D_i^2}{\dot{M}/D_i}\right)^{-0.90} \left(\frac{\omega^2 D_i}{g}\right)^{-0.03} \left(\frac{h_l}{D_i}\right)^{-0.52} \left(\frac{L}{D_i}\right)^{-0.40} \quad (5.2)$$

$$D^2 = 0.12 \frac{\dot{M}}{\rho u} \theta^{-1.14} \left(\frac{d_p}{D_i}\right)^{0.15} \left(\frac{\rho\omega D_i^2}{\dot{M}/D_i}\right)^{0.90} \left(\frac{\omega^2 D_i}{g}\right)^{0.03} \left(\frac{h_l}{D_i}\right)^{0.52} \left(\frac{L}{D_i}\right)^{0.40} \quad (5.3)$$

where θ is the angle of repose, d_p is the particle mean diameter, ω is the angular speed, h_l is the lifter height, and u is the axial solids velocity. Unsurprisingly these models suggest that the three solids transport coefficients f , $\frac{\tau \dot{M}}{\rho L D^2}$, and $\frac{\dot{M}}{\rho u D^2}$ are dependent of same parameters, however, in the present case they may vary exactly in the same way for the identified set of dimensionless groups, only differing by a multiplication factor.

To further understanding of the flow of materials in inclined flighted rotary kiln units started in Parts I and II, in the present work, granular materials (biomass) of wider size distribution, and a rotary kiln of larger scale were used. As will be presented in the following sections, the present study aims at investigating the effects of lifter shape and configurations, kiln rotational speed and slope, and mass flow rate on:

- the RTD of solid particles, determined from experimental stimulus response test; and the corresponding mean and variance of residence time (MRT and VRT);
- the hold-up (HU) of solid particles;
- the Peclet number (Pe) as well as the corresponding axial dispersion coefficient (D);
- the segregation of solid particles.

A set of models are proposed for the prediction of the MRT, HU (volume fraction) and D. These models, established on the basis of dimensional considerations, can be used either for design or control purposes.

5.2 Materials and methods

5.2.1 Apparatus and materials

The pilot scale rotary kiln considered to carry out this study consists of a tube made of an nickel-chromium alloy. The tube, supported on rollers, is 4.2 m in length and 0.21 m in diameter. It can be tilted from 0° and downward to an angle of 7° . The kiln tube can be rotated between 0.5 and 21 rpm through chains and sprockets coupled to a variable speed motor. At the upper end of the tube, the feeding system comprising a 30 L hopper and a vibrating cylindrical conveyor is set up. At the lower end, it is possible to install (in a sealed manner, if necessary) a tank (30 L) for storage. Notice that the feed rate is adjusted by regulating the vibration frequency of the conveyor on the basis of continuous weight measurements of the feeding system by an electronic balance. A second electronic balance is installed at the kiln end, so that both inlet and outlet mass flow rates can be continuously determined.

The smooth inner wall of the kiln tube can be equipped with a grid or a lifter structure. These features are illustrated in Figure 5.1. The grid consists of 16 rows of thin rods (5 mm in diameter) equally distributed in the periphery as shown in Figure 5.1a. The lifter structure can hold, depending on the desired configuration, a maximum of 36 one-section lifters (30 mm), referred to as straight lifters (SL). The lifters can be longitudinally arranged in a maximum of six rows equally distributed in the periphery: either as single throughout lifters or segmented lifters. The configurations used in this study are represented in Figure 5.1b: 3 and 6 rows of single throughout lifters. The main characteristics of the rotary kiln and the order of magnitude of operating conditions investigated in the present work are summarized in Table 5.1.

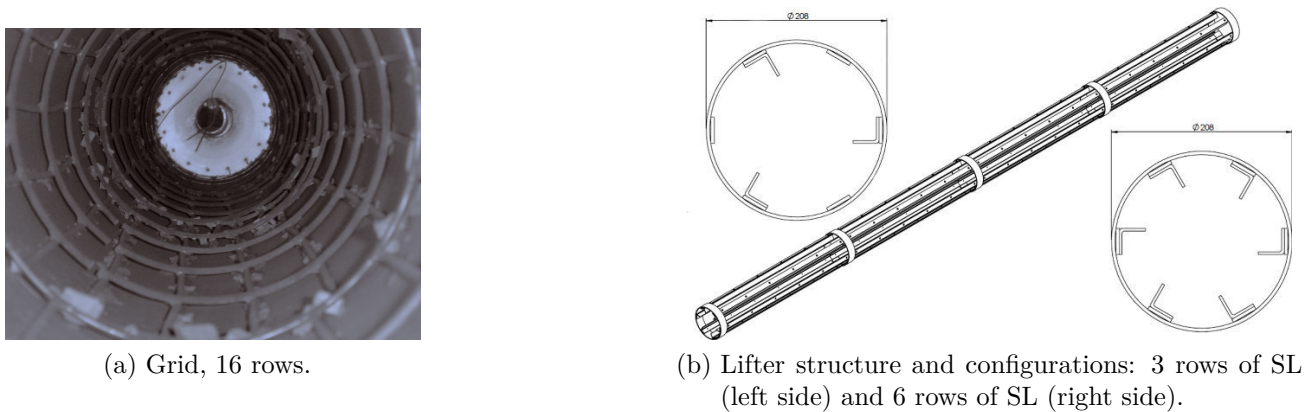


Figure 5.1: Kiln internal fixtures: a) lifter structure and b) grid.

Biomass materials are selected to run the experiments; specifically, beech chips are chosen. A characterization of the size distribution of these particles is achieved using 250 particles randomly chosen among tracer particles used for the RTD experiments. The size distribution of these free flowing parallelepiped chips is quite wide as illustrated in Figure 5.2: 5-17 mm in length, 2-8 mm in width and 1-4 mm in thickness. In addition, as shown in Table 5.2, the materials used are characterized by a bulk density, ρ_{bulk} , about $260 \pm 30 \text{ kg.m}^{-3}$ and a repose angle, θ , about $42 \pm 1^\circ$ measured through the fixed cone method [Woodcock 1987].

A comparison with the rotary kiln used in [Bongo Njeng 2015a, Bongo Njeng 2015b] shows that the two pilot-scale rotary kilns share a very similar length-to-diameter ratio. However, looking at their dimension ratio, there is a factor about two. The particles size used in the present study is an order of magnitude higher and of a wider distribution compared to those of the sand (0.55 mm) and broken rice (3.8 mm \times 1.9 mm) particles used in the first Parts [Bongo Njeng 2015a, Bongo Njeng 2015b].

Table 5.1: Geometrical characteristics of the rotary kiln and order of magnitude of operating conditions achieved in this study.

Subsets	Parameters	Order of magnitude	Remarks
Rotary kiln	D_i [m]	0.21	Internal diameter
	L [m]	4.20	Kiln length
Operating conditions	N [rpm]	2-6	Rotational speed
	S [°]	1-3	Kiln slope
	\dot{M} [kg.h ⁻¹]	2.5-7.5	Mass flow rate
	Lifters shape	None	Smooth wall
	and	Grid (16 rows)	5 mm height
	configurations	3 SL, 6SL	30 mm height

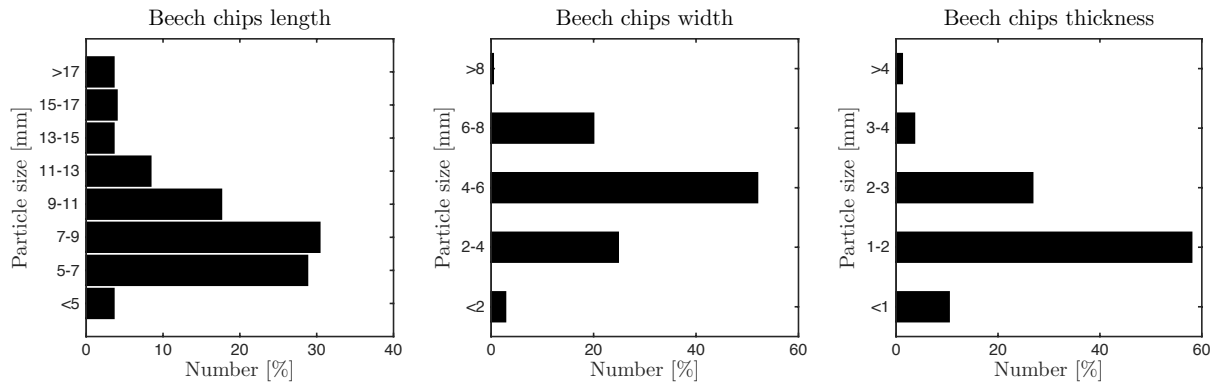


Figure 5.2: Beech chips size distribution in length, width and thickness.

Table 5.2: Physical properties of granular materials.

Product	Shape	ρ_{true} [kg.m ⁻³]	ρ_{bulk} [kg.m ⁻³]	ρ_{tapped} [kg.m ⁻³]	Size [mm]	θ [°]
Beech chips	Parallelepiped	1506	260	284	10 \times 4.5 \times 2	42
Beech chips tracer	Parallelepiped	-	279	310	10 \times 4.5 \times 2	42

5.2.2 Experimental procedure

The experiments conducted in the present study were performed at ambient temperature and atmospheric pressure. The RTD measurement procedure was kept as close as possible to the one presented in [Bongo Njeng 2015a]. However, the feeding systems of these units being different, the impulse injection was carried out differently. In order to characterize the flow of beech chips, stimulus response tests are performed using dyed beech chip tracers as emphasized above, following the procedure outlined below:

- Step 1: The desired internal fixture is installed at the inner wall, if necessary. The kiln tube is then tilted to the desired angle value. Then the rotational speed and mass flow rate are indicated on the user interface of the operating unit. The rotary kiln is then started and the feed hopper regularly filled with biomass materials to keep it topped up, when needed.
- Step 2: Steady-state conditions of the flow are reached, usually after 2-4 hours. The steady-state conditions are assumed to be reached when: the slopes of the lines obtained by plotting the mass variations with time at inlet and outlet, are equal. In addition, the measured inlet and outlet mass flow rates must be equal within a margin of $\pm 0.05 \text{ kg.h}^{-1}$.
- Step 3: The unit is then run until emptying the hopper. The kiln tube inlet end is not readily accessible. Hence, when the vibrating conveyor was empty, the system was stopped to perform the tracer injection. A known amount of dyed beech chips is injected at the kiln inlet end through the hopper and the vibrating conveyor, while the system is stopped. The feed hopper is then refilled with the beech chips and the whole unit is started again at an arbitrary zero time.
- Step 4: Samples are then continuously collected at the kiln outlet end with a sampling time of 30 s until all tracer materials are (visually) discharged. The sample time was reduced to 15 s when the tracer particles tended to exit the kiln in a very short time.
- Step 5: Then, the kiln rotation is stopped and the vibrating conveyor disabled at the same time. Only the kiln rotation is started again and the solids are discharged. The collected solids which constitute the kiln hold-up are weighed.
- Step 6: Lastly, the tracer concentration in each sample is determined by weighing on the one hand the collected sample and on the other hand the dyed tracer, manually extracted from the sample. While analyzing the collected samples, the number of dyed tracer particles extracted from each sample is also determined.

It is important to assess the amount of tracers required to provide sufficient accuracy for the RTD analysis. Therefore, preliminary experiments were performed using amounts of dyed beech chips varying from 5 g to 30 g. It was found that amounts of 20 and 30 g of tracers are enough to get a good accuracy. To shorten the sampling analysis time, 20 g of tracers (about 720 particles) are used to perform the RTD measurements.

5.2.3 Data processing

Data evaluation

The RTD curve or E-curve, $E(t)$, the mean residence time (MRT), \bar{t} , and the variance of residence times (VRT), σ^2 , are determined as follows [Levenspiel 1999]:

$$E(t_i) = \frac{C(t)}{\int_0^\infty C(t)dt} \cong \frac{C(t_i)}{\sum_i^{N_s} C(t_i)\Delta t_i} \quad (5.4)$$

$$\bar{t} = \frac{\int_0^\infty tC(t)dt}{\int_0^\infty C(t)dt} \cong \frac{\sum_i^{N_s} t_i C(t_i)\Delta t_i}{\sum_i^{N_s} C(t_i)\Delta t_i} \quad (5.5)$$

$$\sigma^2 = \frac{\int_0^\infty (t - \bar{t})^2 C(t)dt}{\int_0^\infty C(t)dt} \cong \frac{\sum_i^{N_s} t_i^2 C(t_i)\Delta t_i}{\sum_i^{N_s} C(t_i)\Delta t_i} - \bar{t}^2 \quad (5.6)$$

where t is the time, $C(t)$ represents the tracer concentration at the kiln exit end, the time integral of $C(t)$ represents the total tracer concentration, and Δt_i is the sampling time with $i=\{1, 2, 3, \dots, N_s\}$, N_s is the total number of collected samples.

The presented $E(t)$ function and VRT can also be expressed in dimensionless form using the dimensionless time, $\theta = \frac{t}{\bar{t}}$, as follows: $E(\theta) = \bar{t}E(t)$, and $\sigma_\theta^2 = \frac{\sigma^2}{\bar{t}^2}$.

Axial dispersion model

As shown in [Bongo Njeng 2015a], the axial dispersion model can be used to represent the time dependent E -curves. This model is used to fit the RTD measurements assuming open-open boundary condition. In dimensionless form, the model is given as follows [Levenspiel 1999]:

$$E(\theta) = \frac{1}{2} \sqrt{\frac{Pe}{\pi\theta}} \exp \left\{ -\frac{Pe(1-\theta)^2}{4\theta} \right\} \quad (5.7)$$

The variance of this distribution is defined as:

$$\sigma_\theta^2 = \frac{2}{Pe} + \frac{8}{Pe^2} \quad (5.8)$$

The Peclet number, Pe , is then determined by a fitting method that consists in minimizing the deviation between the experimental E -curve and the prediction. The fitted Peclet numbers obtained, and the theoretical Peclet numbers determined from Eq.5.8, are compared in Figure 5.3. Except in isolated cases (2 in total), where the least-square algorithm used failed to find the actual Peclet number that represents the experiment, it was found that the theoretical Peclet Number underestimates the actual Peclet number. A similar observation was previously made in [Bongo Njeng 2015a] while processing sand and broken rice; however in this case the discrepancy observed is smaller. Nevertheless, for the analysis, only results obtained from the fitting method are considered.

Figure 5.3 also displays a comparison of the experimental MRT from Eq.5.5 versus the fitted MRT, which is obtained when fitting the experimental data using the dimensional form of Eq.5.7, i.e., $E(t) = \frac{1}{2} \sqrt{\frac{Pe}{\pi t \bar{t}}} \exp \left(-\frac{Pe(\bar{t}-t)^2}{4t\bar{t}} \right)$. Very good agreement is found. Lastly, in Figure 5.3 is presented a comparison of the axial dispersion determined from the theoretical and fitted Peclet number using the following expression: $D = uL/Pe$, where $u = L/\bar{t}$ estimates the solids axial velocity. D is inversely proportional to Pe , so that the observed discrepancies show this time an overestimation of the actual axial dispersion coefficient by the theoretical coefficient.

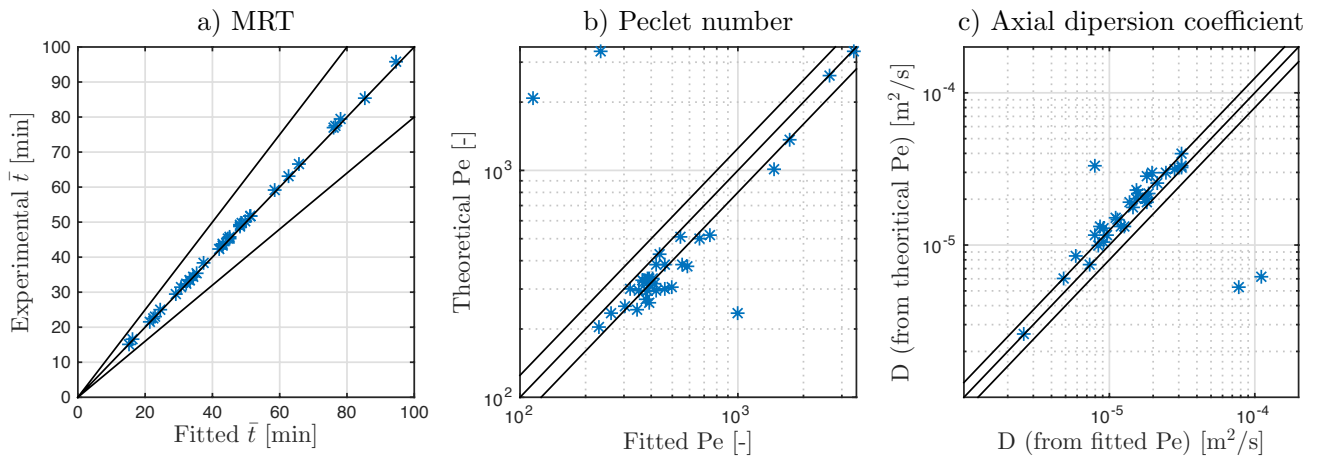


Figure 5.3: Comparison of experimental/theoretical and fitted values of the axial dispersion model parameters, i.e MRT, Pe , and resulting D . Solids lines are $\pm 20\%$ margins.

5.3 Results and discussion

The experimental matrix was derived from a set of benchmark values of the operating parameters defined as follows: a rotational speed of 3 rpm, a kiln slope of 2° and a mass flow rate (MFR) of 5 kg.h^{-1} ($\pm 0.05 \text{ kg.h}^{-1}$). While using the grid, the straight lifters, or even without any internal fixtures, the operating conditions were set to the given values except the one whose effect is being evaluated on the beech chips flow. Note that no exit dam was fitted at the kiln exit end, unlike the kiln used in Parts I and II of this study. Moreover, compared with preceding Parts, the benchmark value of the mass flow rate is doubled, so that the actual kiln can be operated design-loaded or over-loaded depending on the other operating conditions. In addition, the present paper investigates in particular effect of the configuration of lifters, arranged as 3 or 6 rows of single throughout lifters; effect of the grid on the flow behavior is also considered. Effect of the operating parameters on the flow characteristics of materials are qualitatively and quantitatively studied through: (1) the residence time distribution (RTD), (2) the mean residence time (MRT), (3) the variance of residence time (VRT), (4) the hold-up (HU), (5) the Peclet number (Pe) and axial dispersion coefficient (D), and (6) the segregation of solids. For this purpose, 28 different runs are performed. The detailed results of the experimental campaign are summarized in Table 5.8 in the Appendix 5.5.1.

5.3.1 Influence of operating variables on the experimental RTD, MRT, VRT and HU

5.3.1.1 Effect of lifters configuration

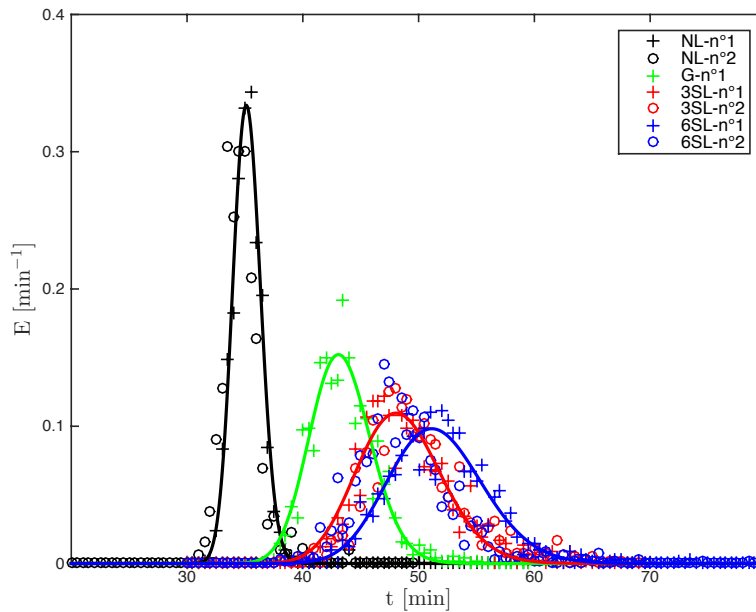


Figure 5.4: Effect of lifters configurations on the RTD: no lifters (NL), grid (G), 3 and 6 rows of straight lifters (3SL, 6SL). Operating conditions: 3 rpm rotation speed, 2° slope, 5 kg.h^{-1} MFR. For the runs using NL, 3SL and 6SL, there are 2 replicates. Solid lines are the axial dispersion model of the n°1 replicate.

Effect of the lifter shape has been previously established while comparing the flow characteristics in a smaller kiln operated with 4 straight and 4 rectangular lifters equally spaced around

the kiln tube internal wall periphery. The lifters with higher hold up capacity were found to generate more dispersion and longer residence times. Here the lifters used are similar but two configurations are tested: 3 and 6 rows of single throughout straight lifters. In addition, the effects of a grid are also considered. Figure 5.4 presents the variations of the residence time distribution when operating at the given benchmark values with and without internal fixtures; the replicated runs are plotted. The RTD curves overlap; in particular, those corresponding to 3SL and 6SL are nearly superimposing. Notice that in the absence of internal fixtures the flow behaves as a plug flow as suggested by the narrow RTD obtained.

Figure 5.6 presents the variations of mean residence time, filling degree and variance of residence time with the kiln operating conditions for different internal fixtures or without. From the latter, it is clear, except when varying the mass flow rate, that the following order can apply to the experiments considering uncertainties as presented later on:

$$\bar{t}_{NL} < \bar{t}_G < \bar{t}_{3SL} \lesssim \bar{t}_{6SL}, \sigma_{NL}^2 < \sigma_G^2 < \sigma_{3SL}^2 \lesssim \sigma_{6SL}^2 \text{ and } HU_{NL} < HU_G < HU_{3SL} \lesssim HU_{6SL}.$$

It must be specified that very little or no significant differences were observed in the results obtained with the 3SL and 6SL. However, using lifters significantly increased the kiln hold-up and thus the filling degree, but also the MRT and VRT, as shown in Figure 5.6. Still, unlike what might be expected, the results are more or less equal with small discrepancies, especially when the kiln was over-loaded in both 3SL and 6SL configurations. The kiln was over-loaded usually for filling degree higher than 8-10%. In fact, it appears that in the latter condition the amount of solids lifted out of the bulk bed by the lifters is virtually the same while using 3SL or 6SL, and probably would have not been increased much even with 12SL as illustrated in Figure 5.5. Hence, it is not so much the number of rows of lifters that will affect the flow characteristic but rather the overall hold up capacity of these lifters. Using lifters of (1) higher holding capacity and (2) higher angular position at the end of discharge, such as rectangular lifters, theoretically must have shown greater differences between the lifters configurations mainly because of the overall hold up capacity.

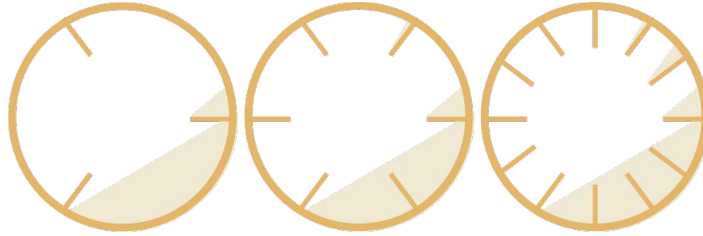


Figure 5.5: Lifters hold-up for three configurations, from left to right side: 3SL, 6SL and 12SL.

Aside from the evident benefit of increasing the friction at the kiln smooth wall, using a grid helps to promote rolling motion into the bulk bed. This latter motion, well characterized by [Henein 1983], is most commonly found in kiln operation. It is observed that in runs where no internal fixtures are installed at the kiln internal wall, the bulk bed is in the slipping mode as described by [Henein 1983, Mellmann 2001], especially when the filling degree is lower than 8%. Experiments show that using a grid at similar operating conditions will set a rolling motion within the bulk bed. In fact, the grid can be considered as a structure of small flights, which continuously scrape off the solids from the bottom of the bulk bed to the upper part of the bed surface. Therefore, the grid imposes a motion en masse at the bottom part of the bed at the kiln rotational speed and generates at the bed surface a steady discharge of solids. This has a significant impact on the HU, MRT and VRT, which are all increased compared to the case of a smooth internal wall. However, this is still a moderate increase compared to the large increase induced by the use of lifters because of differences in size and holding capacity.

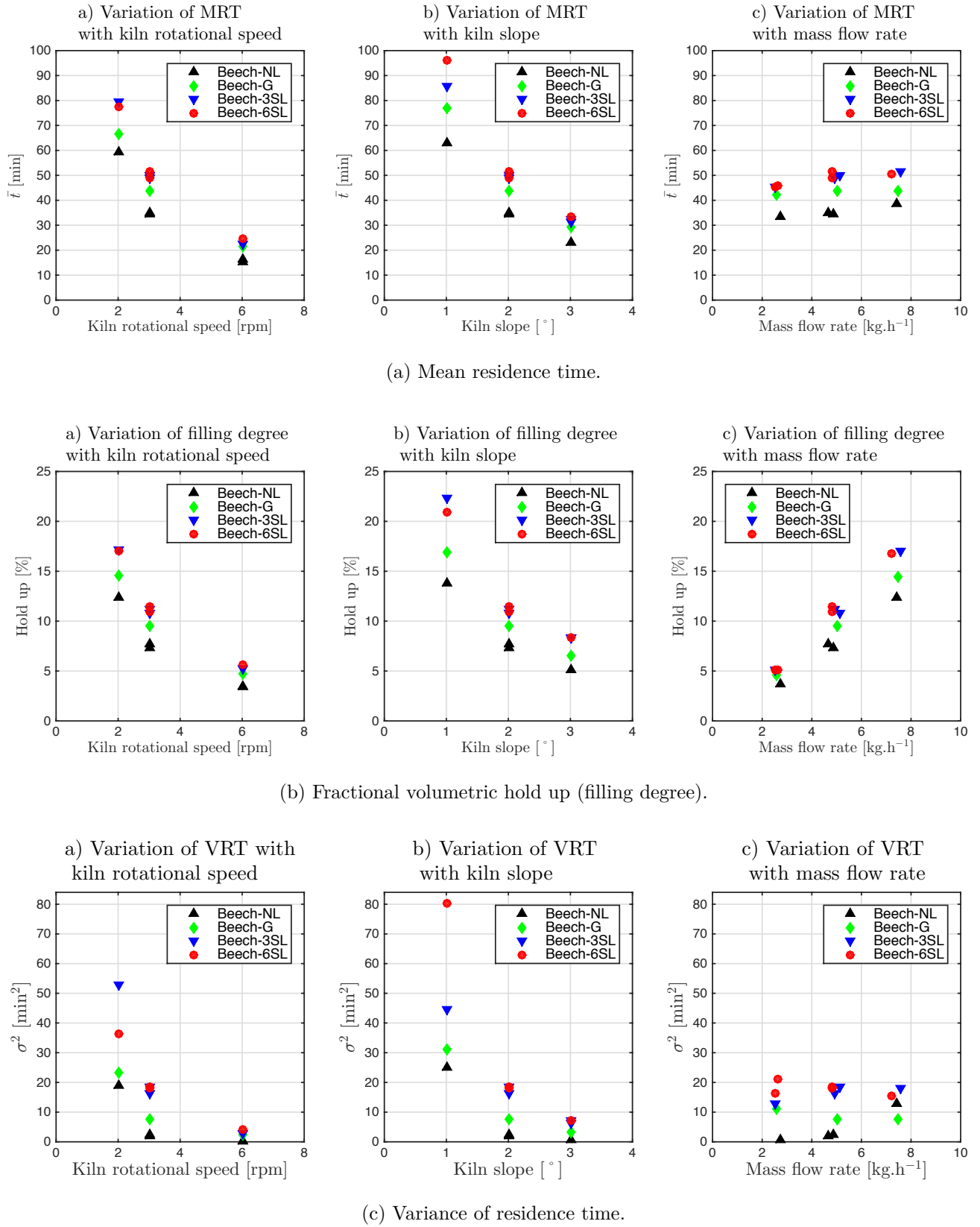


Figure 5.6: Influence of operating parameters (N, S and M) on the MRT, HU[%] and VRT, for the flow of beech chips, when the kiln is equipped without lifters, with a grid, or with 3 and 6 rows of straight lifters.

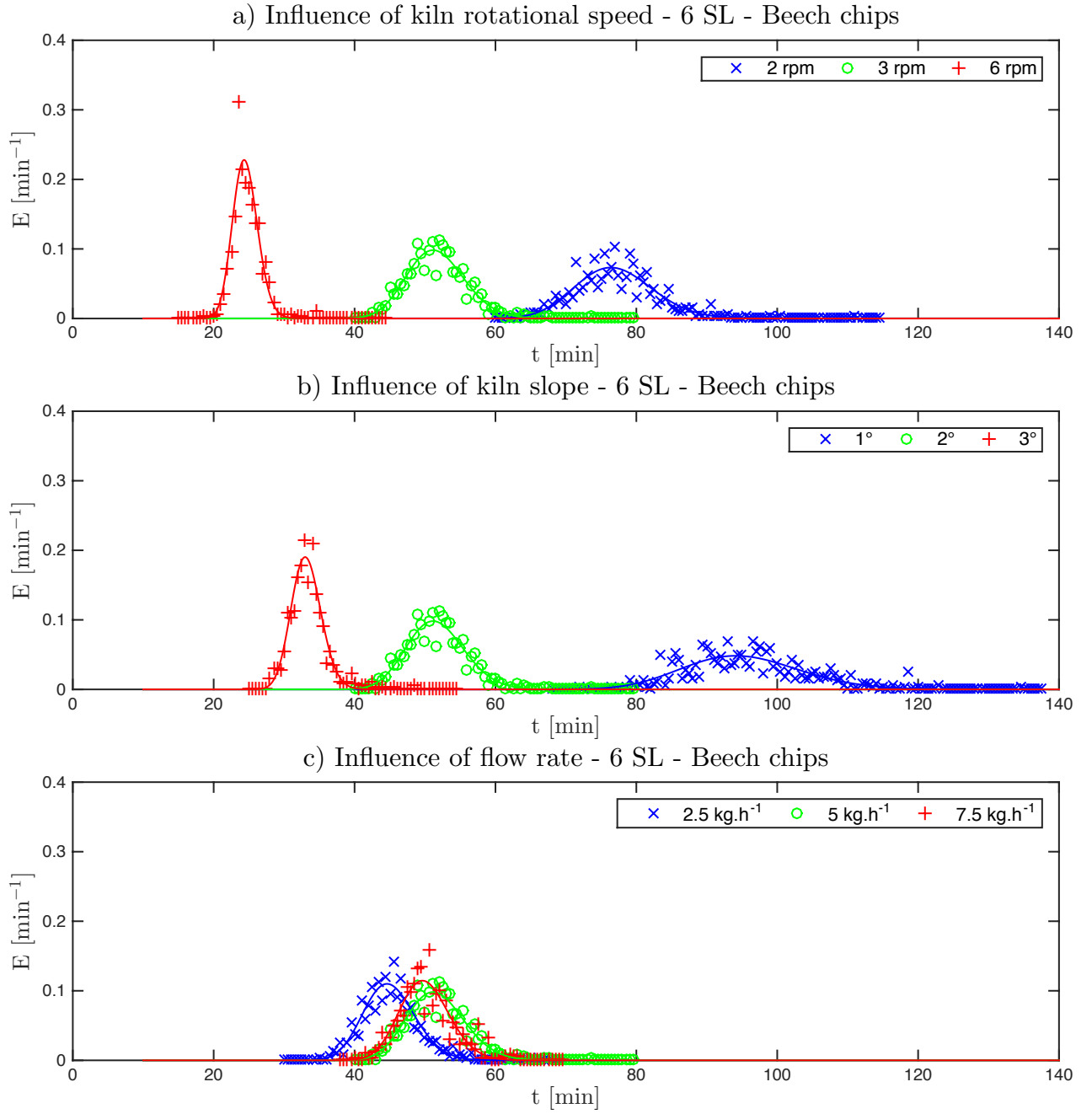


Figure 5.7: Influence of operating parameters (N , S and \dot{M}) on the RTD for the flow of beech chips, when the kiln is equipped with 6 rows of straight lifters. Solid lines represent the axial dispersion model using fitted parameters.

5.3.1.2 Effect of operating parameters: rotational speed, kiln slope and mass flow rate

Figure 5.7 shows the influence of the operating parameters on the residence time distribution of beech chips when the kiln is equipped with 6 rows of single throughout lifters. A general remark that can be made on the obtained RTD curves over the whole experimental campaign is the presence of small peaks extending the tail of the distributions. This can be due to some particle segregation phenomena occurring in the bulk bed as discussed later. The results presented in the following sections are also analyzed in the scope of previous observations made on the flow characteristics of sand and broken rice.

5.3.1.2.1 Kiln rotational speed

Similar to previous observations, there is a sharp decrease of the MRT by about 70% as the rotational speed is increased from 2 to 6 rpm (see Figure 5.6a). That increase is also suggested by the shifting of the RTD curves toward lower residence times (see Figure 5.7). However, unlike previous observations, the shape of the curves significantly changes from a spread distribution with a low peak to a very narrow distribution with a high peak. This is confirmed by the sharp decrease in the VRT (see Figure 5.6c). Finally, the kiln hold up is also decreased, actually divided by 3 to 4, when the kiln rotational speed varies from 2 to 6 rpm (see Figure 5.6b). Indeed with higher rotational speed the solids flow in the kilning bed or through lifters is faster, so that the accumulation of solids in the burden is reduced.

5.3.1.2.2 Kiln slope

The kiln slope has a similar effect to that of the kiln rotational speed on the flow of beech chips. The same trends were previously observed while operating sand or broken rice. When increasing the kiln slope, whether the motion within the bulk bed is slipping or rolling, the forward axial displacement of solids is significantly increased due to gravity. In the first case, it is observed that the bed adheres to the rotating wall, up to a certain angle of deflection as described by [Mellmann 2001], and then en masse, the bed slides back and forward along the kiln slope. In the second case, when rolling motion is achieved, the particles thrown off the apex of the bed flow down along the bed inclination but also forward following the kiln slope. The higher the kiln slope, the higher the particles forward displacement. As a result an increase in the kiln slope reduce the MRT and filling degree, as illustrated respectively in Figures 5.6a and 5.6b. As shown in Figure 5.7, the RTD shapes also vary much from widespread distribution to narrow distribution with increasing kiln slope, as indicated by the decrease of the VRT in Figure 5.6c.

5.3.1.2.3 Mass flow rate

Surprisingly, the mass flow rate has little effect on the flow of beech chips, as implied by the quasi overlapping RTD curves (see Figure 5.7). Even if a similar trend was observed previously while using broken rice, the rate of increase of the MRT with flow rate was higher than that of the present materials (see Figure 5.6a). In addition, significant changes in the shape of RTD curves were reported for the flow of sand and broken rice. The observed divergence can be related to the materials properties, rather than a difference in the tracer pulse experiment procedure, or even the amount of tracer with regard to the bulk burden. Notice that the VRT is strongly influenced by the type of motion of the bulk bed (see Figure 5.6c). Large discrepancies can be observed with regard to runs in slipping mode (without lifters or grid). When operating in rolling motion, if the MRT and VRT remain almost constant, the filling degree significantly increases linearly with the mass flow rate (see Figure 5.6b). This latter results are important for kiln operation,

since they imply that the bulk burden can be significantly increased, without, this requiring much more residence time within the kiln.

5.3.2 Influence of operating variables on the experimental Pe and D

Figure 5.8 represents the variations of the Peclet number and resulting axial dispersion coefficient with the kiln operating conditions, when equipped with internal fixtures. The runs without internal fixtures, which display slipping motion, are not represented in order to focus only on the results referring to the rolling motion.

The Peclet numbers, determined by fitting the RTD curves, are large and comprise between 200 and 800 for runs in rolling motion, and even higher in case of slipping motion (see NL in Table 5.8). Indeed the higher the Peclet number, the smaller the dispersion, which thereby promotes plug flow. The Peclet number and axial dispersion have been previously investigated by several authors [Rutgers 1965, Abouzeid 1974, Sai 1990, Sudah 2002], concluding most of the time that the Peclet number increased with rotational speed and slope of the kiln, and remained constant with the flow rate. However the present results do not all agree with these previous findings. Among the internal fixtures, the grid, which induces lower filling degree, shows higher Peclet number, and thus generates lower longitudinal back-mixing compared to the 3SL and 6SL configurations. It can be seen that when using the grid, the Peclet number decreases with the rotational speed, but that it remains fairly constant within the experimental error for the 3SL and 6SL configurations. A previous analysis of the flow of sand and broken rice shows, in accordance with the actual results, that the Peclet number increases with the mass flow rate; but unlike previous results, it is observed in this case while investigating the flow of beech chips that the Peclet number increases with the kiln slope.

The values reported in the present study for the axial dispersion coefficient are in the order of magnitude of those reported for the sand and broken rice in Part I, but also with those reported by [Wes 1976b] ($4 \cdot 10^{-5} \text{m}^2 \cdot \text{s}^{-1}$) or [Sai 1990] ($2 \cdot 10^{-5} \text{m}^2 \cdot \text{s}^{-1}$). Furthermore the observed trends are similar to those previously described: the axial dispersion coefficient is found to increase with rotational speed and slope of the kiln, but to decrease with the mass flow rate. It can be added that higher dispersion coefficient values are obtained for the 3SL and 6SL configurations, as expected. Note that the axial dispersion coefficient increases as the filling degree decreases for a given internal fixture. Indeed, the mixing effect is much more powerful in a lower bulk burden than in a large one.

5.3.3 Modeling: MRT, HU and D

In this section are presented some scale-up rules for flighted rotary kilns. Models are determined from dimensional considerations for the prediction of the mean residence time, the filling degree and the axial dispersion. The dimensionless groups presented in the following sections may not account for inter-particle forces that may occur between cohesive particles. They may primarily be appropriated for free-flowing particles whose size may vary between 0.4 and 15 mm. In addition, they may likely be applicable to the rolling mode. The following scale-up rules are derived from previous findings in the literature as well as from experimental results obtained in this study while processing sand, broken rice and beech chips. The main operating parameters, geometrical characteristics and physical properties, that may affect the MRT, the HU volume fraction and D are listed as follows: the rotational speed (N), the mass flow rate (\dot{M}), the kiln slope (S), the exit diameter (D_{ex}), the cross section of materials in lifters (S_{lift}), the length of the kiln (L), the internal diameter of the kiln (D_i), the bulk density of materials (ρ_{bulk}), the tapped density of materials (ρ_{tapped}), the angle of repose of the bulk materials (θ), the particle equivalent size (d_p), and the gravitational acceleration (g). Note that: (1) $S_{lift} =$

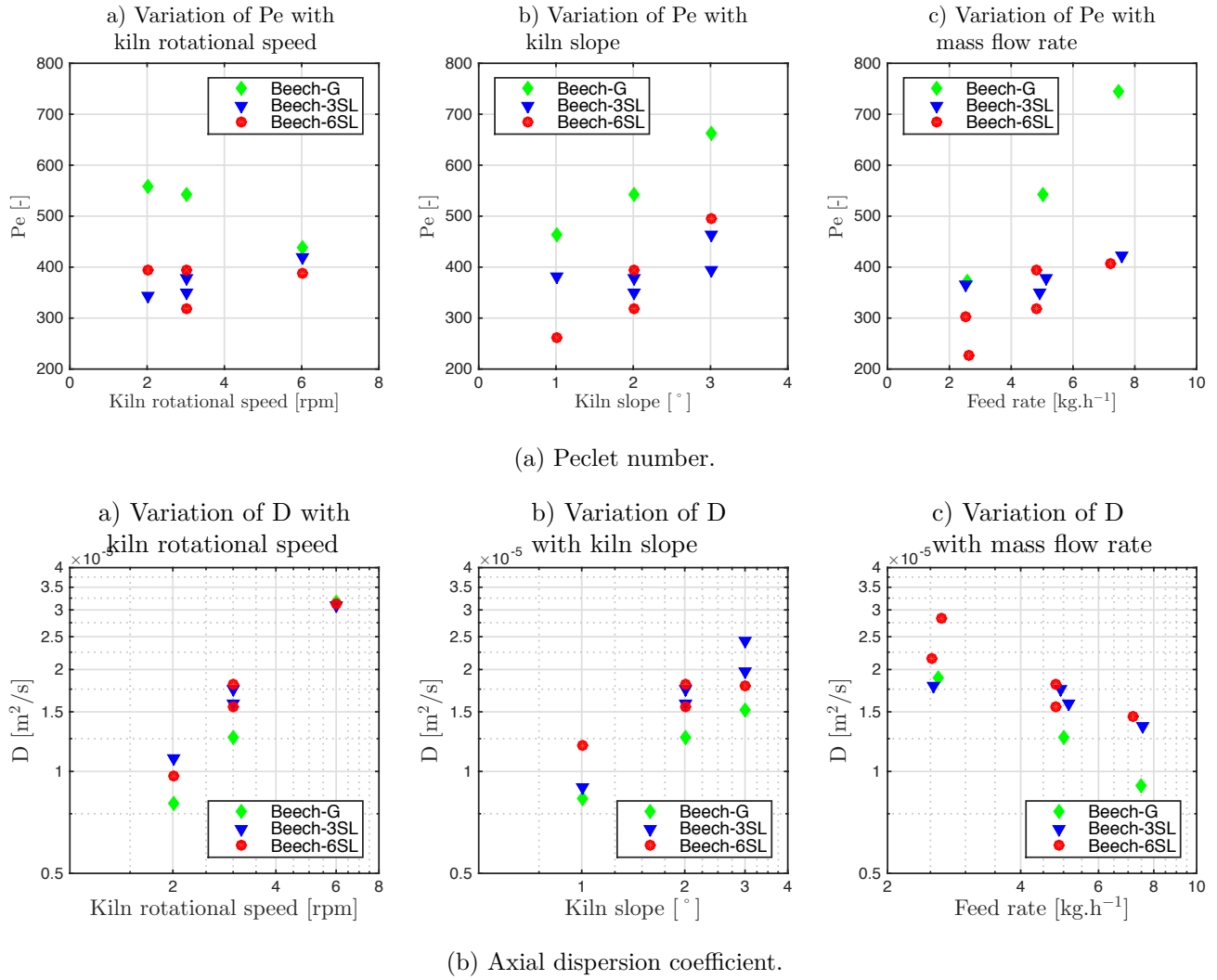


Figure 5.8: Influence of operating parameters (N, S and M) on the Pe and D, for the flow of beech chips, when the kiln is equipped with a grid, or with 3 and 6 rows of straight lifters.

$\frac{\pi D_i^2}{4} - \frac{n_{lift}-1}{2} S_{horlift}$ with n_{lift} the total number of lifters and $S_{horlift}$ the section of materials in a lifter at horizontal position, which can be determined using the materials angle of repose and lifters dimensions [Van Puyvelde 2000, Sunkara 2013b, Debacq 2013b], (2) $d_p = \sqrt[3]{l_l l_w l_t}$ with l_l , l_w and l_t respectively the particles average length, width and thickness.

From the defined variables, following a procedure that can be found in [Delaplace 2014], dimensionless groups are set to correlate the MRT, HU[%] and D as follows. Table 5.3 summarizes the values of the model parameters determined with the use of experimental data at the 95% confidence level, while Figure 5.9 presents the comparison of the calculated model predictions with experimental results.

5.3.3.1 MRT

The model established for the mean residence time is presented in Eq.5.9. This might be very similar to the previous proposition in Part II, but there are a few differences. In order to define the dimensionless groups, it is necessary to choose a set of parameters to represent the fundamental dimensions. In this study the involved dimensions are mass, length and time. To achieve the dimensional analysis in this paper ρ_{bulk} , D_i and g are selected, instead of ρ_{bulk} , D_i and N in Part II of this study. This allows the impact of the operating parameter N to be set

Table 5.3: Determined parameters for the models proposed for the mean residence time, the filling degree and the axial dispersion, with associated confidence intervals.

Model	\bar{t}	Confid. interval		HU[%]	Confid. interval		D	Confid. interval	
parameters	Value	Inf.	Sup.	Value	Inf.	Sup.	Value	Inf.	Sup.
k	0.0026	-0.0023	0.0074	45.65	5.74	85.56	1.52 10⁻⁴	-8.92 10 ⁻⁴	0.0012
α	-0.4422	-0.5367	-0.3478	-0.4439	-0.5506	-0.3372	0.7483	0.3033	1.1933
β	-0.3597	-0.4715	-0.2478	-0.3987	-0.5229	-0.2745	0.2996	-0.1362	0.7354
γ	0.9276	0.7730	1.0822	0.7780	0.6296	0.9263	1.9859	0.6477	3.3240
δ	-0.1130	-0.1574	-0.0686	0.9584	0.7814	1.1354	-0.4511	-1.2280	0.3259
ϵ	-8.8835	-11.459	-6.3081	-3.8197	-6.5517	-1.0878	1.2185	-13.809	16.246
ζ	-2.4641	-5.3569	0.4286	16.763	14.275	19.252	5.5513	-4.7868	18.889
η	1.1¹	NA	NA	0	-	-	0	-	-

in only one dimensionless group: the Froude number. The dimensionless parameters, θ and S , are gathered in one group. Finally, the model parameters presented in Table 5.3 are determined from experimental results obtained from the 3 granular materials used: sand, broken rice and beech chips. Notice that these parameters are determined within narrow confidence intervals.

$$\bar{t} = k\sqrt{gL} \left(\frac{N^2 D_i}{g} \right)^\alpha \left(\frac{D_{ex}}{D_i} \right)^\beta \left(\frac{\theta}{S} \right)^\gamma \left(\frac{\dot{M}}{\rho_{bulk} D_i^2 \sqrt{gL}} \right)^\delta \left(\frac{4S_{lift}}{\pi D_i^2} \right)^\epsilon \left(\frac{\rho_{bulk}}{\rho_{tapped}} \right)^\zeta \left(\frac{L}{D_i} \right)^\eta \quad (5.9)$$

Unlike previous results in Part II or by [Hwan 2009] in the literature, it is found that the Froude number has a significant impact on the MRT. As illustrated in Figure 5.9a, the predictions from Eq.5.9 are in good agreement with the experimental data irrespective of the kiln or the materials used. For the calculations, the variables forming the dimensionless groups must be filled in SI units, therefore the unit of the obtained predictions for the MRT is second. Notice that in the present study the length-to-diameter ratio varies only slightly and could not be used for parameter fitting, therefore the value of η is set to 1.1, which has been previously determined by [Chatterjee 1983b].

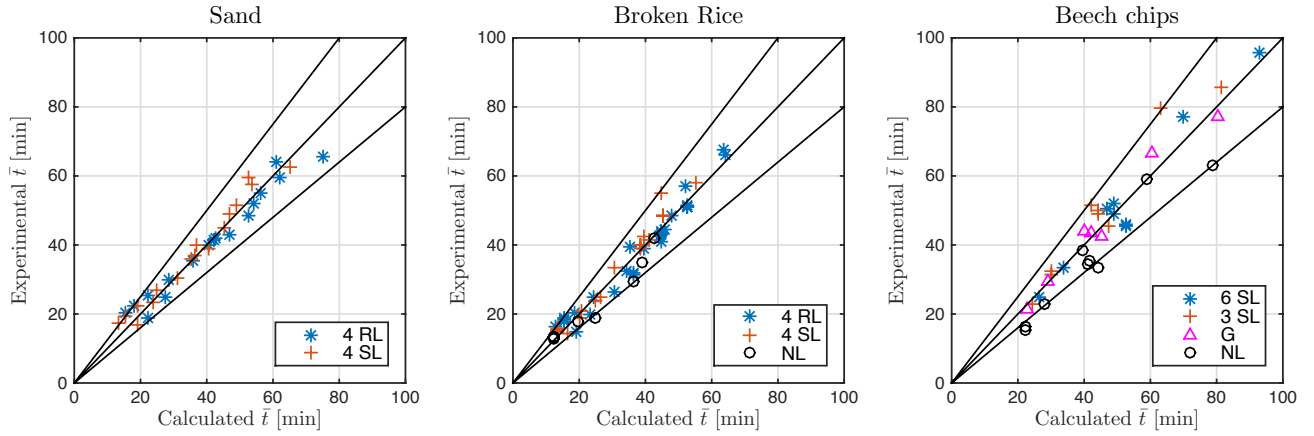
5.3.3.2 HU

The model defined for the filling degree is presented in Eq.5.10. It is very similar to the one proposed for the MRT. Indeed a direct correlation can be found between these two, especially when the dispersion is very negligible, the time of passage and the mean residence time are very close, yet the time of passage is defined as $\tau = HU/\dot{M}$. This also explains why some parameters of both models are very close, such as α , β , and γ , as shown in Table 5.3.

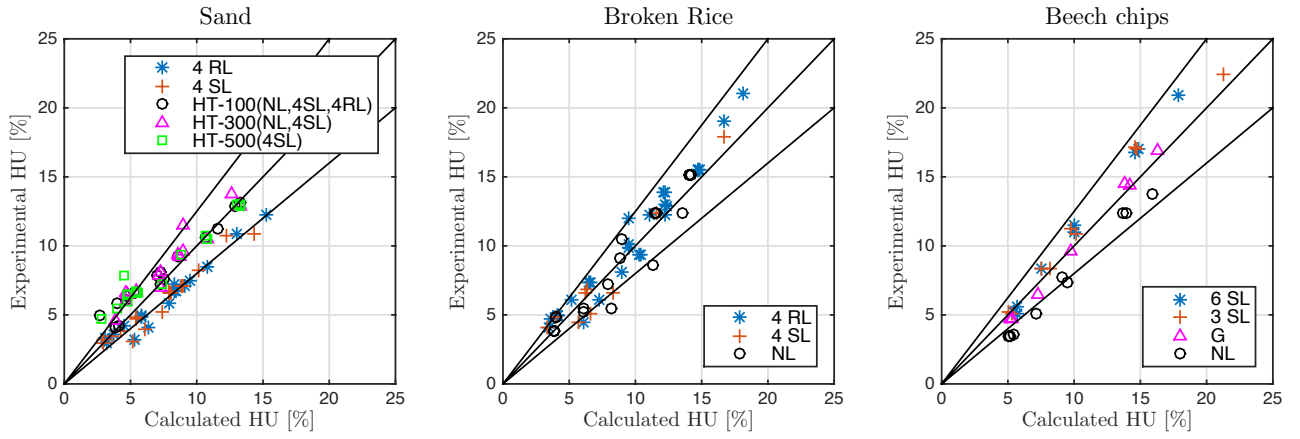
$$HU[\%] = k \frac{\rho_{bulk} L \pi D_i^2}{4} \left(\frac{N^2 D_i}{g} \right)^\alpha \left(\frac{D_{ex}}{D_i} \right)^\beta \left(\frac{\theta}{S} \right)^\gamma \left(\frac{\dot{M}}{\rho_{bulk} D_i^2 \sqrt{gL}} \right)^\delta \left(\frac{4S_{lift}}{\pi D_i^2} \right)^\epsilon \left(\frac{\rho_{bulk}}{\rho_{tapped}} \right)^\zeta \left(\frac{L}{D_i} \right)^\eta \quad (5.10)$$

Note that the model parameters were not only determined using the hold-up measurements from this hydrodynamic study; the hold-up measurements obtained while performing experiments

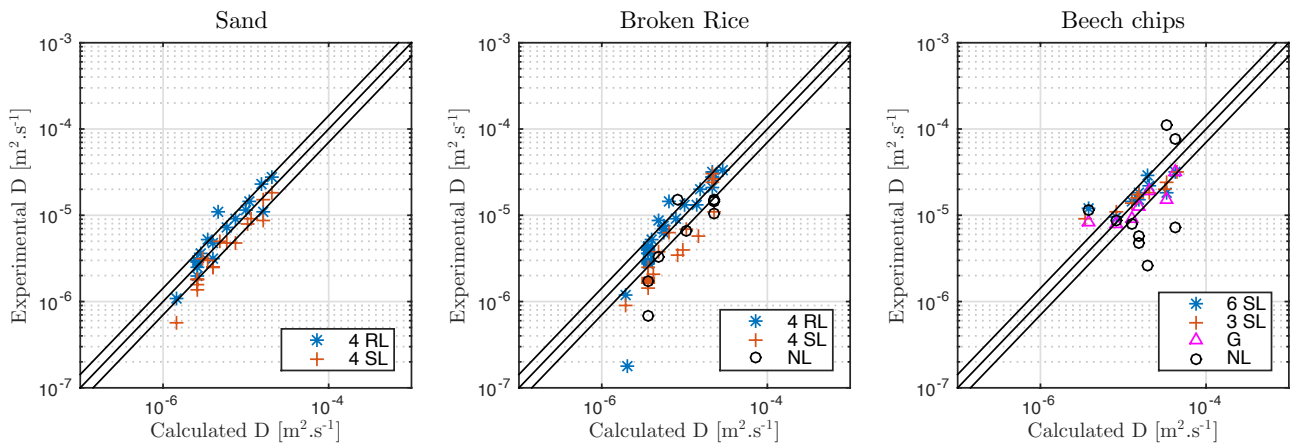
¹ [Chatterjee 1983b]



(a) Mean Residence time.



(b) Fractional volumetric hold up (filling degree).



(c) Axial dispersion coefficient.

Figure 5.9: Comparison of the experimental MRT, HU[%] and D, while using sand (left), broken rice (middle), and beech chips (right), with the calculated values from Eq.5.9 using the sets of parameters given in Table 5.3. Solid lines are $\pm 20\%$ margins.

at hot temperatures with sand were also used [Bongo Njeng 2015d], as illustrated in Figure 5.9b. The model parameters were defined within narrower confidence intervals, and good agreements were found between the calculated and experimental filling degree. To obtain the filling degree, the variable parameters must be filled using SI units; the model directly produces a percentage. Note that the value of the parameter η is fixed to 0, since no fitting value was found in the literature that was defined with sufficient accuracy for the length-to-diameter ratio.

5.3.3.3 D

The proposed model for the axial dispersion coefficient is given in Eq.5.11. The materials physical properties have been reported to significantly affect the axial dispersion coefficient. They are represented in the given model by the Hausner ratio, as well as a ratio of the particle equivalent size to the kiln diameter. The model parameters are determined within reasonable confidence intervals as given in Table 5.3.

$$D = k\sqrt{D_i^2 g L} \left(\frac{N^2 D_i}{g} \right)^\alpha \left(\frac{d_p}{D_i} \right)^\beta (S)^\gamma \left(\frac{\dot{M}}{\rho_{bulk} D_i^2 \sqrt{g L}} \right)^\delta \left(\frac{4S_{lift}}{\pi D_i^2} \right)^\epsilon \left(\frac{\rho_{bulk}}{\rho_{tapped}} \right)^\zeta \left(\frac{L}{D_i} \right)^\eta \quad (5.11)$$

Figure 5.9c shows that all experimental data do not agree well with the predicted value within the $\pm 20\%$ margins. However, as shown later on, these predictions are mostly within the experimental uncertainty which is about 30%. Except scarce cases in particular for beech chips, the experimental data obtained without internal fixture are not well predicted by the model, certainly because of a bed flowing in the slipping mode. Note that η is fixed to 0. Therefore the effect of the length-to-diameter ratio is taken into account within the value of the model parameter k .

5.3.4 Analysis of particle segregation

Segregation is a property of dry granular solids, which tend to separate spatially by size, shape or density under varying flow conditions [Cantelaube 1997, Khan 2004]. This phenomenon has been observed in industrial processing involving granular materials, and it has been widely studied within rotating drums.

In this study, there are a few elements that may indicate possible phenomena of segregation. Firstly, the wide size distribution of beech chips, as illustrated in Figure 5.2, indeed implies not only larger or smaller particles but also heavier and lighter particles. Generally, the larger the chip size, the heavier the chip weight. Secondly, while analyzing the beech chips RTD curves, an extended tail can be observed due to small peaks of tracer concentration, implying a possible higher concentration due to particle segregation.

[Bensmann 2010] has been able to investigate the particle segregation through tracer experiments using several fractions of tracers particles. With such a straightforward approach, the effects of segregation can be easily observed and analyzed. However as previously demonstrated by [Colin 2015] such experiments are not mandatory. Instead, a tracer of wide distribution size (see Figure 5.2) can be used to achieve this purpose. As stated before, while analyzing the samples collected after the tracer injection, the number of tracer particles contained in each sample was determined. From the number of tracer particles collected and their weight, an average particle weight can be determined and is used for the analysis of particle segregation. The present analysis is therefore less in terms of particle size and more in terms of particle weight, due to the direct relationship. Note that there have been good tracer mass recoveries as follows, for NL

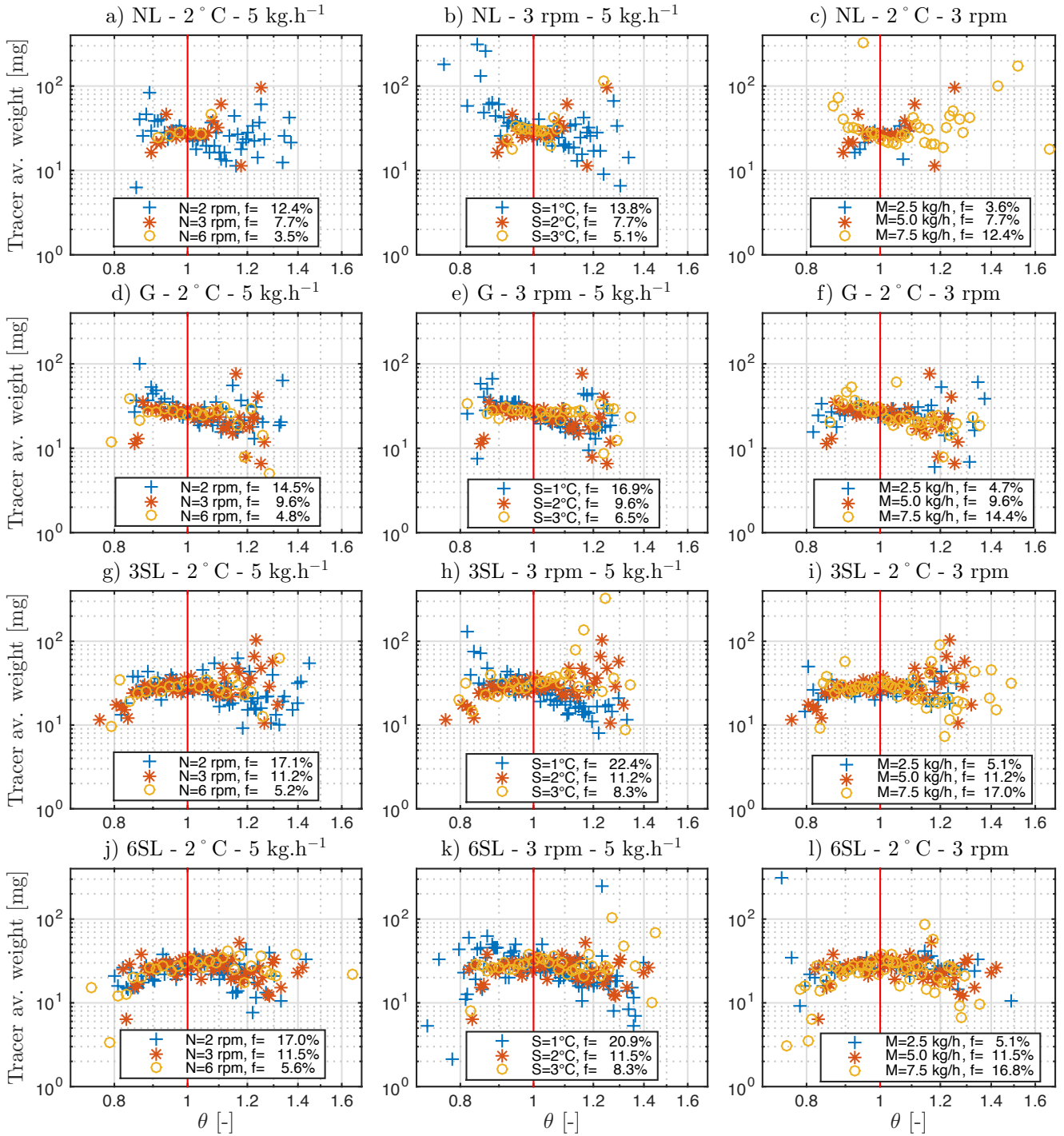


Figure 5.10: Influence of operating parameters N (a-d-g-j), S (b-e-h-k) and \dot{M} (c-f-i-l) on the tracer average weight (function of dimensionless time) for the flow of beech chips, when the kiln is equipped with: NL (1st row), G (2nd row), 3SL (3rd row) and 6SL (4th row). The dimensionless time is defined as $\theta = t/\bar{t}$ and so the red lines represent the time when $t = \bar{t}$.

experiments $99.5\% \pm 0.5$, for G experiments $99.4\% \pm 0.7$, for 3SL experiments $99.3\% \pm 0.6$ and for 6SL experiment $99.9 \pm 0.6\%$.

Figure 5.10 presents the (dimensionless) time variations of the average tracer weight for a variety of operating conditions when using a grid, 3SL, 6SL and no internal fixtures. A first preliminary general observation concerns the unbalanced distribution of tracer around the mean residence time symbolized by the red line, which furthers understanding of the presence of an extended tail on the RTD curves. It is also observed that the average weight of tracer particles is mainly between 20 and 30 mg. Out of this interval the particles can be considered lighter or heavier and by extension smaller or larger. Assuming a beech chip of parallelepiped shape, about $10 \text{ mm} \times 4.5 \text{ mm} \times 2 \text{ mm}$, and a density of 279 kg.m^{-3} , the particle weight is about 25.1 mg.

A more detailed look in Figure 5.10 demonstrates that when varying only one operating condition and keeping the other constant, the obtained weight distribution differed primarily in function of the filling degree as highlighted by [Colin 2015]. Secondly it is also observed that the tracer average weight distribution varies depending on presence and type of internal fixtures.

In Figures 5.10a, b and c, where there is no internal fixtures, there is no significant effect of segregation at low filling degree (below 8%): distributions are more centered, with a tracer weight remaining nearly constant in spite of few lighter and heavier particles respectively at lower and larger residence times. Whereas at higher filling degree, the tracer average weight distribution is more dispersed and the heavier particles tend to have significantly lower residence time compared to lighter particles. This can be explained by the differing mode of motion observed at lower and higher filling degree, respectively, slipping motion and rolling motion. From the literature [Cantelaube 1997], it is well known that especially in the rolling motion, radial segregation may appear very quickly, causing concentration of smaller particles toward the core of the bed, while larger particles may roll in the active layer following the incline at the bed surface. Knowing that the axial transport is highly promoted by the continuous flow at the bed surface, this may explain the preceding observations.

When a grid is used as shown in Figures 5.10d, e and f, the tracer average weight decreases slowly with time, implying higher concentration of heavier particles at low residence time and higher concentration of lighter particles at high residence time as previously observed in case of rolling motion. It seems that the grid tends in a way to homogenize the bulk of particles. That homogenization can also be observed when using 3SL or 6SL. In both latter cases, except at higher residence times, the weight distribution is not widespread, and there is no more a decrease in the tracer average weight. These observations may be related with [Grajales 2012] statements implying that straight lifters do not affect the flow regimes of the kilning bed but only reduce the area of the central core in the rolling motion. Hence, the concentration of small particles in the core at the bed center is reduced, and the small particles are allowed to flow with the bigger particles in the active layer. This reduces the time of residence of smaller particles, therefore lowering the tracer average weight at lower residence times, and by scarcity effect (of lighter particles) automatically increases the tracer average weight at higher residence times, as shown in Figures 5.10g, h and i when using 3SL, and in Figures 5.10j, k and l when using 6SL.

However, the presence of heavier particles at higher residence time can be possibly due to effect of axial segregation [Khan 2004], which unlike radial segregation is reported to develop after hundreds of kiln rotations. Therefore the axial segregation, happening after radial segregation, splits the existing core into periodic axial band along the kiln axis. This may also explained in some cases the extensive presence of heavier particles at higher residence time.

5.3.5 Reproducibility of experiments

Reproducibility of the experimental results was investigated through replicates of some runs. Table 5.4 shows the experimental hold-up, mean residence time, variance of residence time, Peclet

Table 5.4: Reproducibility of experiments: experimental hold-up, mean residence time, variance of residence time, Peclet number and axial dispersion.

Operating conditions	HU Values	[kg] $\frac{\Delta HU}{HU}$ [%]	\bar{t} Values	[min] $\frac{\Delta \bar{t}}{\bar{t}}$ [%]	σ^2 Values	[min ²] $\frac{\Delta \sigma^2}{\sigma^2}$ [%]	Pe Values	[-] $\frac{\Delta Pe}{Pe}$ [%]	D Values	[m ² /s] $\frac{\Delta D}{D}$ [%]
3 rpm, 2°, 5 kg.h ⁻¹ , NL	2.920 2.785	±4.47	35.20 34.64	±1.51	1.81 2.38	±25.51	1370 1013	±28.38	0.0610 0.0838	±29.86
3 rpm, 2°, 5 kg.h ⁻¹ , 3SL	4.235 4.105	±2.95	49.06 49.84	±1.48	16.42 18.50	±11.28	297.2 272.5	±8.21	0.2016 0.2165	±6.73
3 rpm, 2°, 5 kg.h ⁻¹ , 6SL	4.345 4.145	±4.45	51.78 48.81	±5.57	18.19 18.46	±1.38	298.7 262.1	±12.33	0.1901 0.2298	±17.86

number and axial dispersion coefficient determined. Figure 5.11 illustrates the reproducibility of the segregation of particles. Both Table 5.4 and Figure 5.11 gather the results of the replicates of some runs carried out at selected benchmark values for the operating conditions, when the kiln was equipped with 3 and 6 rows of straight lifters, and without internal fixture.

In Table 5.4, the given values of the relative uncertainty for the hold up and MRT are lower than 6%, implying very good reproducibility of these two flow characteristics. The reported relative uncertainties for the VRT, Pe and D are higher, reaching 30% at maximum. For decision making in industry, even if these uncertainties are relatively high, they are sufficiently low to consider the experimental values as consistent. Note that the relative uncertainties derived from the replicates are determined at the 80% confidence level.

In Figure 5.11, the reproducibility of the experiments is very good in terms of uniform repartition of more and less dense tracer particles along the dimensionless time. This confirms also the reproducibility of RTD experiments as illustrated in Figure 5.4.

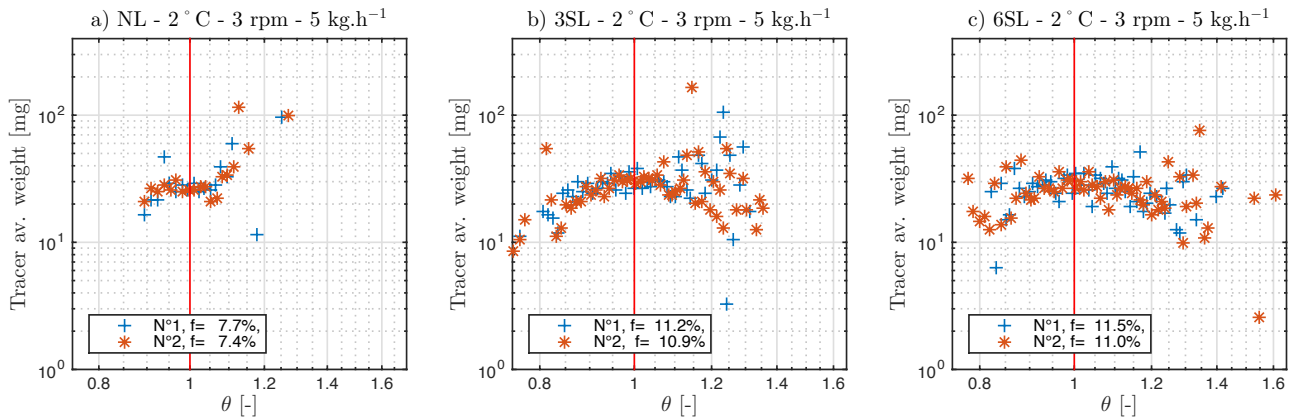


Figure 5.11: Reproducibility of segregation of beech chips when the kiln is operated within the defined benchmark value for the operating parameter, and equipped with 3 or 6 rows of straight lifters or without lifters.

5.4 Conclusion

The flow characteristics of materials are significantly impacted by the internal fixtures. Therefore, in the design stage or for improvement purposes, the choice of lifters' configuration as well as their overall holding capacity, mostly dependent on the shape, must be carefully selected. The use of lifters increases the burden and the residence time of solid particles. They promote the

mixing of particles as suggested by the increase of the axial dispersion coefficient. In regard to the flow of materials of wide size distribution, by their mixing effect, lifters reduce the segregation phenomena that may occur, causing different residence time for the different size fractions.

The flow characteristics of solids through flighted rotary kilns are also affected by the operating conditions as demonstrated by the experimental results:

- Increase in the mean residence time may result from a decrease of the rotational speed and slope of the kiln, but also to a lesser extent, from an increase in the mass flow rate of solids;
- The mass flow rate has a remarkable influence on the filling degree. As the flow rate is increased, or the kiln rotational speed and slope are decreased, the hold-up increased.
- The axial dispersion is increased with the kiln rotational speed and slope, but decreased with the mass flow rate. The higher the filling degree the smaller the axial dispersion.

Three models were developed for the prediction of the mean residence time, the filling degree, and the axial dispersion coefficient under steady-state conditions in inclined rotating kilns, whether equipped with lifters and exit dams or not, and operated in the rolling mode. These correlations consist of dimensionless factors accounting for (1) the basic operational parameters of the kiln, (2) the properties of the bulk solids, (3) the geometry of the kiln, (4) the overall lifters' holding capacity, (5) the height of exit dam. The model parameters, namely $k, \alpha, \beta, \dots, \zeta$ as given in Table 5.3, have been determined from experimental data of the flow of sand, broken rice and beech chips, at varying operational conditions and through different rotary kilns. The predictions and experimental data were in good agreement.

The segregation analysis made on the flow of beech chips revealed a possible effect of radial segregation. However, it was found that the segregation was lessened in some operating conditions, in particular when using lifters, depending on the filling degree of solids within the kiln.

List of symbols

av.	Average	-
C	Tracer concentration	g/g,
D	Axial dispersion coefficient	$\text{m}^2.\text{s}^{-1}$
D_{ex}	Effective exit diameter	m
d_p	Particle equivalent size, particle mean diameter	mm
D_i	Kiln internal diameter	m
f	volumetric filling degree	-
g	Gravitational acceleration	m.s^{-2}
HU	Hold-up	kg
HU[%]	hold-up volume fraction or filling degree	-
k	Model parameter	-
L	Kiln Length	m
l	Particle size	m

Ls	Area occupied by solid particles contained in loading lifters	m ²
\dot{M} , MFR	Mass flow rate	kg.h ⁻¹
MRT	Mean residence time	min
N	Kiln rotational speed	rpm
NL	No lifters	-
n_{lifter}	Total number of lifters	-
N _S	Total number of samples	-
N _T	Total number of experiments	-
Pe	Peclet number	-
RL	Rectangular lifters	-
rpm	Rotation per minute	-
RTD	Residence Time Distribution	-
S	Kiln slope	degrees
SL	Straight lifters	-
S_{lifter}	Area covered by solid particles in a lifter at horizontal position	m ²
$S_{horlifter}$	Area covered by solid particles in a lifter at horizontal position	m ²
t	Time	min
\bar{t}	MRT	min
VRT	Variance of the RTD	min ²

Greek letters

α, β, γ ,	Fitting parameters	-
$\delta, \epsilon, \zeta, \eta$		
Δt_i	Sampling times	s
θ	Angle of repose, dimensionless time	degrees, -
ρ_{tapped}	Tapped density	kg.m ⁻³
ρ_{bulk}	Bulk density	kg.m ⁻³
ρ_{true}	Particle density	kg.m ⁻³
σ^2	Variance of residence time	min ²
σ_θ^2	Dimensionless variance of residence time	-
τ	Time of passage	min
ω	Kiln rotational speed	rad/s

Subscripts

G	Grid	-
l	Length	-
NL	No lifters	-
3SL	3 rows of straight lifters	-
6SL	6 rows of straight lifters	-
t	Thickness	-
w	Width	-

5.5 Appendices

5.5.1 Experimental Results: HU, MRT, VRT, Pe, D

The experimental matrix achieved and the experimental hold up, mean residence time, and variance of residence time, the fitted Peclet number, and resulting axial dispersion coefficient are resumed in Table 5.8.

Table 5.8: Results of the experimental matrix set for the RTD measurements.

Operating conditions			NL					Grid					3SL					6SL				
N	S	M	HU	\bar{t}	σ^2	Pe	D	HU	\bar{t}	σ^2	Pe	D	HU	\bar{t}	σ^2	Pe	D	HU	\bar{t}	σ^2	Pe	D
[rpm]	[°]	[kg.h ⁻¹]	[kg]	[min]	[min ²]	[-]	[m ² /s]	[kg]	[min]	[min ²]	[-]	[m ² /s]	[kg]	[min]	[min ²]	[-]	[m ² /s]	[kg]	[min]	[min ²]	[-]	[m ² /s]
3	2	5	2.920	35.20	1.81	1728	0.0484	3.615	43.54	7.49	541.4	0.1258	4.235	49.06	16.42	349.6	0.1745	4.345	51.78	18.19	318.3	0.1801
3	2	5	2.785	34.64	2.38	1467	0.0582	-	-	-	-	-	4.105	49.84	18.50	377.8	0.1591	4.145	48.81	18.46	394	0.1549
2	2	5	4.690	59.07	18.77	590	0.0853	5.490	66.52	23.30	557.5	0.0805	6.470	79.56	52.91	344.8	0.1095	6.440	77.26	36.48	394.3	0.0974
6	2	5	1.310	15.34	0.18	2629	0.0728	1.805	21.47	2.19	437.5	0.315	1.985	22.71	2.70	418.8	0.3109	2.135	24.76	4.21	387.5	0.3111
6	2	5	1.310	16.38	0.16	233.1	0.7721	-	-	-	-	-	-	-	-	-	-	-	-	-	-	-
3	1	5	5.215	62.95	25.12	416.4	0.1126	6.390	76.98	31.29	463.5	0.0833	8.470	85.61	44.78	382.7	0.0902	7.905	95.98	80.40	260.8	0.1193
3	3	5	1.940	23.00	0.51	114.8	0.1126	2.450	29.42	3.47	662	0.1525	3.150	31.33	6.34	393.1	0.3426	3.150	33.40	7.35	495.9	0.1794
3	3	5	-	-	-	-	-	-	-	-	-	-	-	32.50	7.14	464.8	0.1970	-	-	-	-	-
3	2	2.5	1.375	33.54	0.68	3392	0.0259	1.760	42.34	11.31	373	0.1882	1.935	45.29	12.75	365.3	0.1787	1.930	45.81	21.11	228.2	0.2842
3	2	2.5	-	-	-	-	-	-	-	-	-	-	-	-	-	-	-	1.950	45.26	16.53	303.7	0.2163
3	2	7.5	4.675	38.53	12.96	996.8	0.0785	5.450	43.73	7.46	746.3	0.0912	6.425	51.73	18.25	422.4	0.1363	6.340	50.37	15.42	407.5	0.145

Heat transfer in flighted rotary kilns: experiments and modeling

“The effects of heat are subject to constant laws which cannot be discovered without the aid of mathematical analysis. The object of the theory which we are about to explain is to demonstrate these laws; it reduces all physical researches on the propagation of heat to problems of the calculus whose elements are given by experiment.”

(J. Fourier, 1768-1830)

Chapter 6

Evaluation of the wall-to-gas and wall-to-solid heat transfer coefficients in flighted rotary kilns: Lumped system analysis

Abstract	160
6.1 Introduction	161
6.2 Materials and methods	162
6.2.1 Apparatus and materials	162
6.2.2 Experimental procedure	164
6.3 Results and discussion	167
6.3.1 Lumped system analysis	167
6.3.2 Wall-to-gas heat transfer coefficient	168
6.3.3 Wall-to-solid heat transfer coefficient	173
6.3.4 Biot number	177
6.4 Conclusion	177
6.5 Appendices	180
6.5.1 Bulk bed conductivity model	180
6.5.2 Evaluation of the lifter effective heating length	180
6.5.3 Experimental matrix	181

The research described in this Chapter is to be submitted for publication to the International Journal of Heat and Mass Transfer.

Abstract

Abstract:

A series of experiments were carried out on a pilot scale rotary kiln at atmospheric pressure, whether or not equipped with lifters and fitted with a dam at the outlet end. The experimental apparatus, 1.95 m in length and 0.1 m in (internal) diameter, can be externally heated in two independent consecutive zones by electrical resistance up to 1000°C. Under varying operating conditions, temperature profiles of the gas phase, the bulk of solids particles and the wall were recorded following kiln wall tube heating at low to medium setpoint temperature (100-500°C). The wall-to-gas and wall-to-solid heat transfer coefficients are determined from the experimental data by applying the lumped system analysis to the gas and solids phase. A dimensional correlation based on experimental results is presented for the Nusselt number relative to the convective heat transfer in the case of no forced axial gas flow. Both coefficients are found to be affected by the operating conditions, and particularly the wall-to-solid heat transfer is found to be increased in presence of a specific lifter shape, implying existence of a critical lifter design adequate for enhancing the heat transfer.

Résumé :

On a mené des expériences à pression atmosphérique dans un four tournant équipé ou non de releveurs et diaphragme (en sortie). Le dispositif expérimental est constitué d'un tube ayant un diamètre de 0.1 m et une longueur de 1.95 m ; ce tube peut être chauffé par des résistances électriques, réparties en 2 zones de chauffe indépendantes. Dans ces zones non séparées physiquement, la température peut atteindre 1000°C. Les profils de température des phases gazeuse et solide, et à la paroi du tube ont été enregistrés pour diverses conditions opératoires et à des températures comprises entre 100 et 500°C. Le coefficient de transfert convectif entre la paroi et le gaz et le coefficient de transfert entre la paroi et les particules solides ont été déterminés à partir des relevés de température en utilisant une analyse globale supposant des systèmes minces. Pour estimer la valeur du coefficient d'échange convectif en absence de convection forcée de gaz dans le tube, on a établi une corrélation pour le nombre de Nusselt sous la forme d'un produit de nombres sans dimension. Par ailleurs, les résultats montrent que les deux coefficients d'échange dépendent des conditions opératoires, en particulier, le coefficient d'échange paroi/solide augmente pour un certain type de releveurs, ce qui suggère l'existence d'un design optimal des releveurs permettant d'amplifier les échanges de chaleur.

6.1 Introduction

Rotary kilns are gas-solid reactors commonly used in industry to achieve a wide range of operations such as mixing, heating, cooling, or reacting of coarse, free-flowing or cohesive solid materials. Therefore rotary kilns are used in several applications [Boateng 2008], for example: reduction of oxide ore [Chatterjee 1983c, Atmaca 2014], pyrolysis of hazardous solid waste or of biomass [Suzuki 2008a, Colin 2015], calcining of petroleum coke [Bui 1993, Bui 1995, Martins 2001], conversion of uranium fluoride for the manufacture of nuclear fuel [Debacq 2013a, Debacq 2013b], and so on. When operated at atmospheric pressure, these units consist of a cylindrical shell that can be inclined, into which the solid burden is fed continuously at one end and discharged at the other. They are usually equipped with lifting flights or lifters, and/or exit dam at the kiln outlet end. These units can be classified into two main heating modes. They can be either directly heated or indirectly heated, depending on the location of the heating source with respect to the kiln tube wall. They are convenient reactors with relatively intensive heat and mass transfer, capable of treating large quantities of material.

Heat transfer in rotary kilns is very complex and may involve the exchange of energy via all the fundamental transfer mechanisms, i.e conduction, convection, and radiation. A significant amount of research has been completed over the past years to determine heat transfer coefficients or the heat fluxes related to the differing mode of heat transfer occurring in rotary kilns; unfortunately the heat transfer mechanisms have not been fully clarified. Most of the experimental apparatus used to study the heat transfer mechanisms in particular from wall-to-solid are batch-fed and indirectly heated, as reported in the previous works [Wachters 1964, Lehmberg 1977, Lybaert 1987, Suzuki 2008b, Herz 2012]. These rotary kilns are also quite small with length-to-diameter ratios lower than 5, which is not usual in the industry except when there is a special need of mixing rather than heating. However, it is reported that in rotary kilns the heat transfer is dependent on the rotational speed and the kiln tube diameter, but also the thermo-physical properties and type of motion of the solids.

Very few studies [Wes 1976a, Tscheng 1979, Le Guen 2013] focused on the experimental determination of the convective heat transfer occurring between gas and wall or gas and solids. [Wes 1976a] found that the gas-to-wall heat transfer coefficient was in the magnitude expected for natural convection coefficients, whereas the gas to solids heat transfer coefficient was found to be approximately an order of magnitude larger. In the range of values tested by [Tscheng 1979], no significant effect of kiln slope, solid feed rate or particle size was observed on the convective coefficient. However, gas-to-solid heat transfer coefficient was found to be about 10 times higher than that of gas-to-wall. Notice that all these studies involve a forced axial flow of gas.

Two main procedures were described in previous studies in order to determine experimentally the wall-to-solid heat transfer coefficient: earlier studies [Wachters 1964, Wes 1976a, Lehmberg 1977] recorded the cooling of solids from a predetermined wall temperature, while recent investigations [Lybaert 1987, Suzuki 2008b, Thammavong 2011, Herz 2012] mostly recorded the transient evolution of temperatures (wall, gas, and solids). The coefficient was determined through heat balances providing some assumptions. However, results from these kilns especially the small kilns, cannot be used with a sufficiently high degree of confidence to study heat transfer in industrial kilns.

The goal of the present paper is to describe an experimental procedure for the determination of the wall-to-gas and wall-to-solid heat transfer coefficients in indirectly heated rotary kilns. The kiln used was operated at varying operating conditions, namely rotational speed, solid mass flow rate, temperature (100-500°C); it was fitted with exit dam of different heights and equipped or not with lifters of different shapes. It was found that the kiln inclination has no significant influence on the heat transfer [Tscheng 1979], this parameter was kept constant in this study. [Cook 1995] reported that when operating at relatively low temperature, i.e. gas and wall temperatures

around 300°C, the heat transfer between the covered wall and bulk bed is the dominant mechanism. [Gorog 1981, Gorog 1982] specified that at temperatures below 600-700°C, the contribution of radiation is less than 10%. Therefore, radiation was not included in this work. The lumped system formulation, which provides a great simplification in regards to the analysis of transient heat transfer, is used to determine the convective and wall-to-solid heat transfer coefficients. A correlation based on dimensional consideration is provided for the prediction of the convective heat transfer coefficient in the particular case of no forced axial flow of the gas, which differs from existing correlations. The wall-to-solid heat transfer coefficient evaluated in the present study, distinguished from similar previous investigations by [Suzuki 2008b, Suzuki 2008a], where the coefficient was determined in batch heated rotary drum. After presenting the experimental procedure, the lumped system analysis is detailed and applied to the gas and solid phases. For each case, the effect of the operating conditions on both experimental heat transfer coefficients are analyzed. Lastly, the corresponding Biot numbers are assessed.

6.2 Materials and methods

6.2.1 Apparatus and materials

An indirectly heated pilot scale rotary kiln was used to carry out the investigation of the convective heat transfer between wall and gas, as well as the contact heat transfer between wall and solids. It consists of a feeding system, a rotating tube surrounded by a heating system and followed by a recovery zone, in accordance with the layout presented in Figure 6.1.

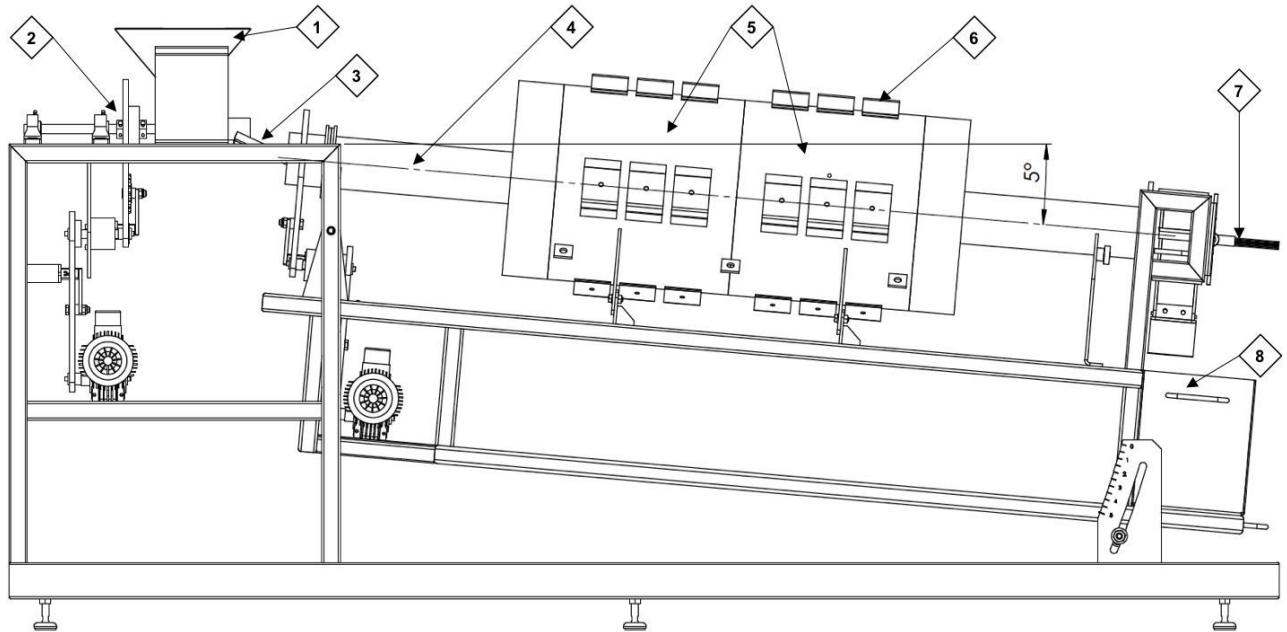


Figure 6.1: Layout of the experimental apparatus: (1) feed hopper, (2) screw feeder, (3) feed chute, (4) kiln tube, (5) heating system, (6) external thermocouples, (7) measuring rod with thermocouples, (8) storage tank.

The feeding system is a combination of a 5 dm³ hopper and a feed screw, followed by a feed chute, which conveys the solids at a desired mass flow rate up to the kiln inlet end.

Supported on four rollers and made of an Incoloy alloy 800, the rotating tube is 1.95 m in length, 0.101 m in (internal) diameter, and 6.5 mm in thickness. The smooth internal wall can be equipped with a structure constituted of 4 rows of lifters equally distributed in the periphery.

Two shapes of lifters are used, straight one-section 10 mm lifters referred to as straight lifters (SL), and two-section 10 mm lifters with a right angle cross section referred to as rectangular lifters (RL), as shown respectively in Figures 6.2a and 6.2b. The bed depth height can be set at the kiln outlet end by fitting the tube with a dam. Different exit dam heights are used as given in Figure 6.3. The kiln can be operated at speeds between 0.5 and 12 rpm, and tilted to a maximum angle of 5° .

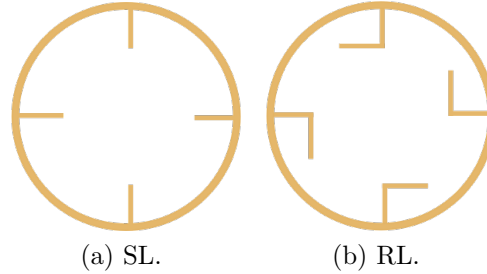


Figure 6.2: Lifters profiles: a) straight lifters (SL) and b) rectangular lifters (RL).

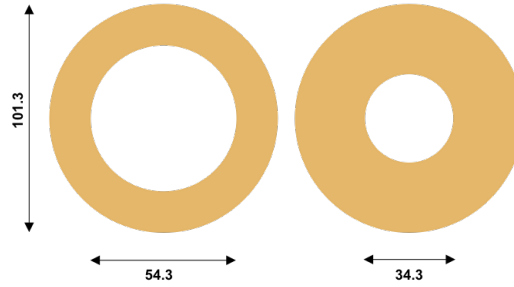


Figure 6.3: Exit dam designs.

The kiln is indirectly heated by furnaces comprising independent heating zones arranged in-line as shown in Figure 6.4. Each heating zone is constituted of heating resistors surrounded with a thick layer of insulation. The kiln furnace is made of 2 heating zones of 0.4 m long designed to heat the kiln tube wall up to 1000°C . The heating elements can each deliver a power of 5 kW. Figure 6.4 also illustrates the experimental setup of the thermocouples (TC) used for the thermal metrology, which is of importance in determining the temperature profiles of the bulk bed, the free-board gas and at the wall.

Temperatures in the bulk bed and the free-board gas are measured by 20 N-type TC, 1.5 mm in diameter. An additional set of 16 K-type TC 3 mm in diameter are used to measure temperatures at the outer wall. These thermocouples were calibrated with a tolerance of $\pm 1.5^\circ\text{C}$ according to the supplier.

- The 20 N-type TC used are installed in a measuring rod, and arranged in a series of 5 sections. At each section, 4 TC are installed; 3 of them are placed so as to be in the free-board gas and the remaining TC is embedded in the case of a solids flow. The measuring rod is placed inside the kiln tube and remains stationary during the kiln operation. The TC were radially positioned so as to avoid contact with lifters when present. Their axial and radial locations are shown in Figure 6.4. The first section of TC namely S1 is located in the heating zone 1 and the 3 other sections namely S2, S3 and S4 are located in the heating zone 2.
- The 16 K-type TC used to measure the kiln wall temperature are installed at the outer wall and arranged in a series of 4 sections as shown in Figure 6.4. The measured temperature

can be assumed to be virtually the wall temperature. As shown by the kiln transverse section in Figure 6.4, at each section 4 TC are placed around the outer wall in the air between the tube and resistors.

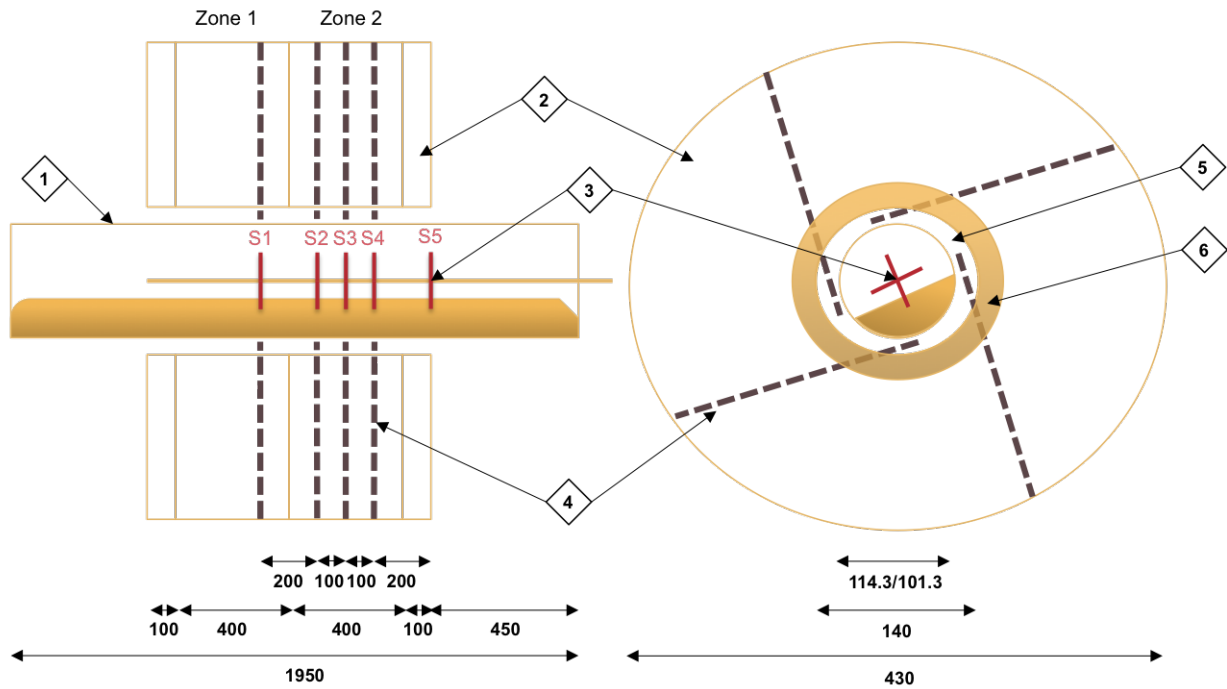


Figure 6.4: Layout of the experimental apparatus heating zones, longitudinal (left side) and transverse (right side) sections: (1) kiln tube, (2) insulation, (3) measuring rod with N-type thermocouples, (4) outer wall K-type thermocouples, (5) air, (6) heating resistors. The given dimensions in the drawing are in mm.

The experiments are performed at atmospheric pressure using nodular sand, 0.55 mm average particle size. The thermo-physical properties of the materials used are given in Table 6.1 (at 300°C). Regarding the sand, notice that the density and specific heat capacity are assumed constant, the thermal conductivity is determined after the model by [Bauer 1977] presented in Appendix 6.5.1. For the air, the density is determined from the ideal gas law; the specific heat capacity and conductivity are determined from model set using the results by [White 1988]. The Inconel thermal properties are extracted from [Corporation 2014, Corporation 2013]. The emissivities are provided by [Thammavong 2009] who designed the actual rotary kiln.

Table 6.1: Thermal properties of materials at 300°C.

Materials	Sand	Air	Inconel	Remarks
ρ [kg.m ⁻³]	1422	0.616	7950	Density
c_p [J.kg ⁻¹ .K ⁻¹]	835	1045	514	Specific heat capacity
k [W.m ⁻¹ .K ⁻¹]	0.1836	0.0449	18.75	Thermal conductivity
ε [-]	0.76	0.01	0.9	Emissivity
ϵ_0 [%]	43.36	-	-	Measured porosity

6.2.2 Experimental procedure

Experiments were performed with and without solids flow in order to investigate respectively the convective and wall-to-solid heat transfer coefficients as follows:

- Step 1: The operating parameters are set to the desired values: the kiln slope is adjusted to 3° (same angle for all runs); rectangular, straight or no lifters are installed at the kiln tube inner wall; the measuring rod is then installed inside the kiln; if necessary, an exit dam is fixed; the rotational speed and the feed rate are set in the control box to the desired value. Then, *in the case of solids flow*, the hopper was filled, the kiln was operated at room temperature until steady-state conditions of the flow. *In the case of no solids flow*, the kiln was simply started.
- Step 2: At an arbitrary zero time, the temperature recording is started. From that time until the end (step 4), the following parameters are measured every half hour: the power supplied to the installation, the ambient temperature around the kiln, the free-board gas temperature at the inlet end of the kiln.
- Step 3: Half an hour after starting recording the temperatures, the heating setpoint is adjusted on the controller and the heating source is turned on either in zone 2 or both zones 1 and 2.
- Step 4: When the supplied power, and temperature profiles of the wall, the gas, and the solids bed are stabilized, steady state conditions are established. The thermal steady state is assumed to be reached when the temperatures and the supply power are both stable during at least 2 consecutive half hours, respectively with variations within 2°C or 0.01 kW. The logging is then stopped.
- Step 5: The solids are then discharged to assess the kiln hold up. The empty kiln is cooled down by natural convection over at least a night before starting a new run.

The heating usually lasted between 6 to 8 hours. Notice that the wall temperatures are averaged over the 4 TC in each of the 4 series of TC at the wall. Therefore, the wall temperatures along the kiln are represented by Tw1 in the heating zone 1, and by Tw2, Tw3 and Tw4 in the heating zone 2. Inside the kiln as presented above, 5 series of 4 TC are installed, in the case of solids flow, at each section, one of these TC is immersed in the bulk bed, the resulting temperature profiles are noted: Ts1, Ts2, Ts3, Ts4 and Ts5. The remaining 3 TC measured at each section the freeboard gas temperatures (see Figure 6.5): at the top, Tgu in left side and Tgbu in right side, and at the bottom Tgbd in left side. In the case of no solids flow, the measured temperatures in the freeboard gas are averaged (when possible) at each section giving: Tg1, Tg2, Tg3, Tg4 and Tg5.

Examples of measured temperature profiles are presented in Figures 6.6 and 6.7, respectively for the case of no solids flow and the case of a solids flow, when the kiln is equipped with straight lifters, rotated at a speed of 2 rpm and heated in zone 2 at 300°C . It is shown that the temperatures measured at the wall rise steeply from the ambient to reach a plateau about the given heating setpoint. Following the heating of the kiln tube wall, the gas, and the solids bulk bed temperatures rise at a lower rate and then remain constant. Figure 6.7 shows that a thermal gradient may exist within the free board gas especially between the upper and bottom zones at a section of the hot kiln tube.

A summary of the whole experimental conditions of the runs with and without solids flow is given in Table 6.7 in the Appendix 6.5.3. As shown in that table, the kiln has been operated at low to medium temperatures ($100\text{--}500^\circ\text{C}$), varying filling degree (3-14%) and in presence of lifters of different shape.

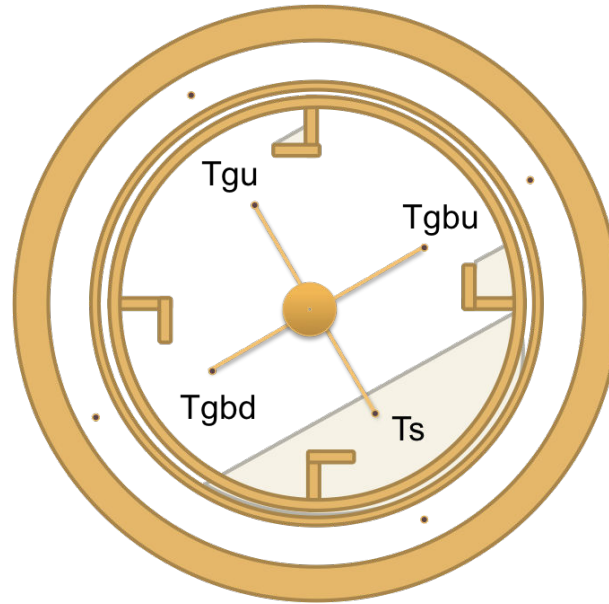


Figure 6.5: Location of thermocouples in a cross section of the kiln.

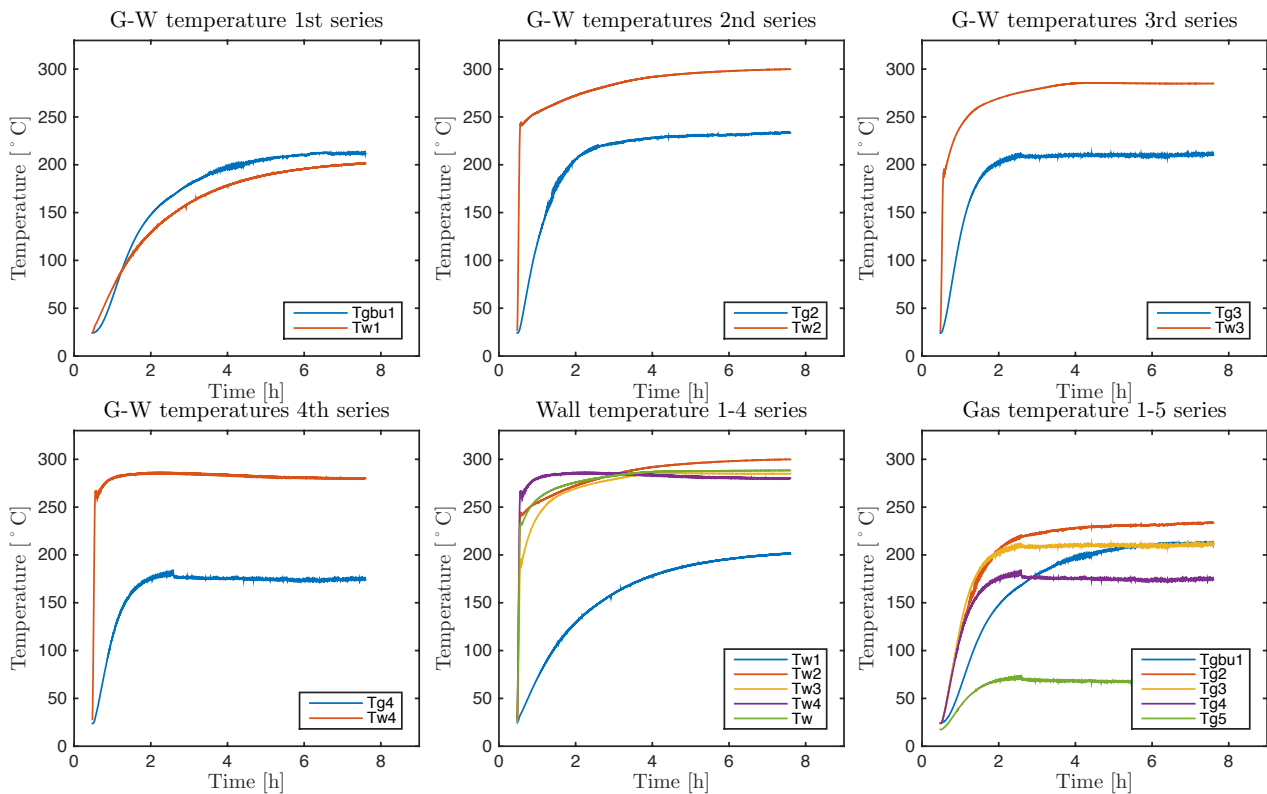


Figure 6.6: Experimental temperature profiles measured at the kiln outer wall and in the free-board gas. Operating conditions: 2 rpm rotation speed, 3° slope, no solids flow, 33.5 mm exit dam height with straight lifters, and a setpoint temperature of 300° C in zone 2. The presented wall and gas temperature profiles are the average of measurements within the sections (S1-S5) defined in Figure 6.4.

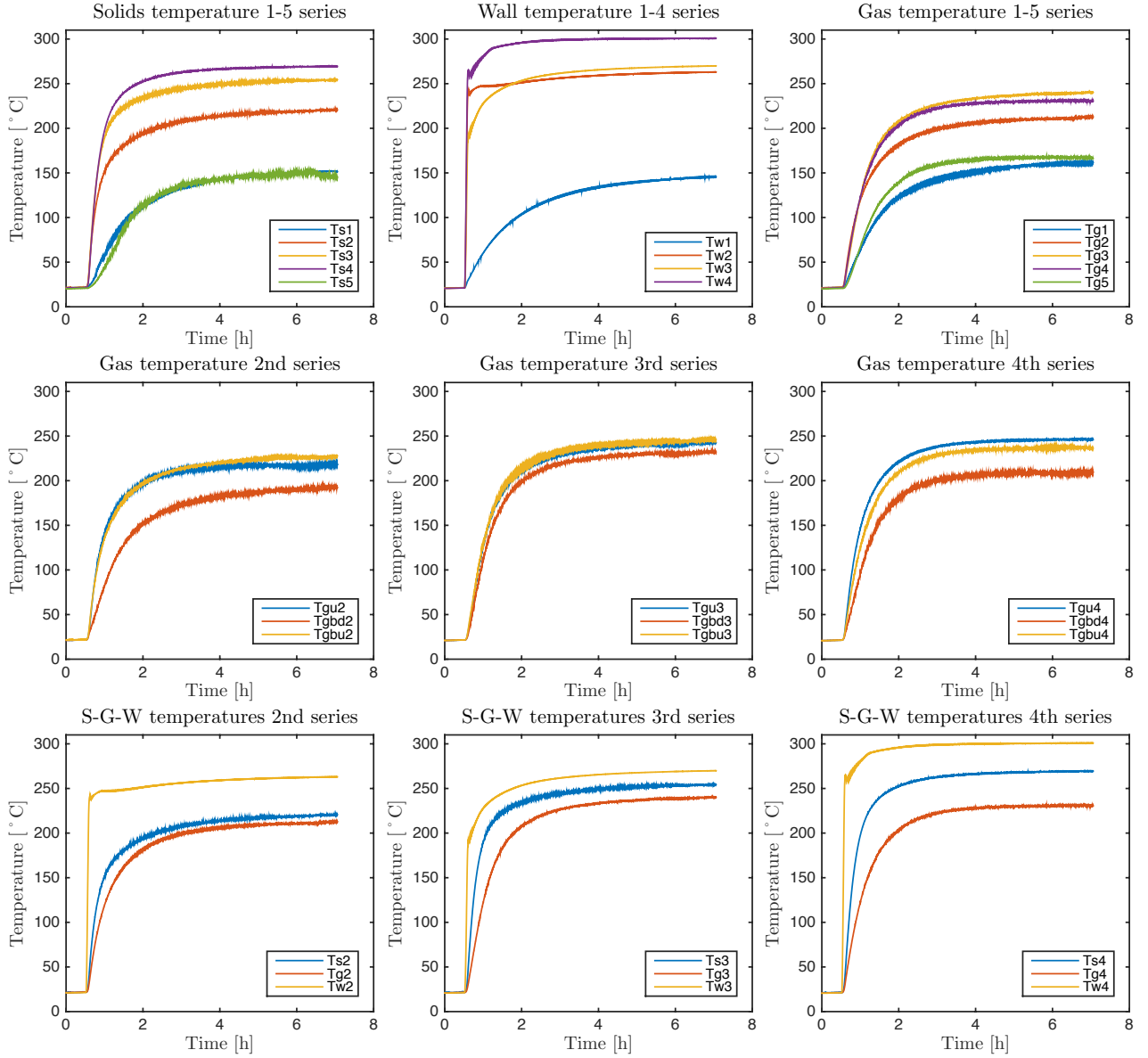


Figure 6.7: Experimental temperature profiles measured at the kiln outer wall, in the solids bed and in the freeboard gas. Operating conditions: 2 rpm rotation speed, 3° slope, 2.5 kg.h⁻¹ MFR, 33.5 mm exit dam height with straight lifters, and a setpoint temperature of 300° C in zone 2. The presented wall and gas temperature profiles are the average of measurements within the sections (S1-S5) defined in Figure 6.4.

6.3 Results and discussion

6.3.1 Lumped system analysis

The lumped system analysis is mainly based on the assumption of negligible gradient of temperature within the considered medium, that is, the temperature distribution may remain sufficiently uniform during the transients [Hahn 2012]. Therefore, the temperature, T , is considered to be only a function of time. Consider a medium initially at a temperature T^0 suddenly put in contact with a hot surface maintained at a uniform temperature T^∞ . Let h be the heat transfer coefficient between the medium and the hot surface through the contact surface, Ω be the volume, A be the contact surface area, ρ be the density, and c_p be the specific heat capacity of the medium.

Assuming a uniform temperature within the medium at any time, the energy balance equation can be stated as follows within a defined control volume comprising the medium [Hahn 2012]:

$$\left(\begin{array}{c} \text{Rate of heat flow from the} \\ \text{medium through its boundaries} \end{array} \right) = \left(\begin{array}{c} \text{Rate of change of the} \\ \text{internal energy of the medium} \end{array} \right) \quad (6.1)$$

The above heat transfer analysis is applied in the following sections to investigate and quantitatively estimate the convective and wall-to-solid heat transfer coefficients, the considered medium being successively the gas and the bulk bed.

6.3.2 Wall-to-gas heat transfer coefficient

The medium considered within this section is the gas, that is air. Indeed, the experiments performed to carry out this study were operated on ambient air without a forced axial flow. However, it should be noted that a gas flow can be induced by the rotation of the kiln tube and by chimney effect.

6.3.2.1 Energy balance

Considering a control volume Ω_g delimited inside the kiln tube by two sections within the heating zone(s), and assuming convection transfer as the only means for heat to enter or leave the defined control volume during a differential time interval dt , from Eq.6.1, the energy balance in the case of stand still gas phase can be expressed as follows:

$$- h_{ew-g} A_{ew} (T_g(t) - T^\infty) dt = \rho_g c_{pg} \Omega_g dT_g(t) \quad (6.2)$$

Rearranging Eq.6.2, and assuming the temperature set at the kiln tube internal wall T^∞ to be equal to the temperature reached by the gas at steady state T_g^∞ , the following ordinary differential equation (ODE) is obtained:

$$\text{for } t > 0, \quad \frac{dT_g(t)}{dt} + \frac{1}{\tau_g} (T_g(t) - T_g^\infty) = 0, \quad \tau_g = \frac{\rho_g c_{pg} \Omega_g}{h_{ew-g} A_{ew}} \quad (6.3)$$

$$IC : t = 0, \quad T_g(t = 0) = T_g^0 \quad (6.4)$$

where τ_g is the thermal time constant which characterizes the rate of change of the gas temperature variation. The above ODE is readily solved as given:

$$\ln \left(\frac{T_g^\infty - T_g(t)}{T_g^\infty - T_g^0} \right) = -\frac{t}{\tau_g} \quad (6.5)$$

or in a more explicit formulation:

$$T_g(t) = T_g^\infty - (T_g^\infty - T_g^0) \exp \left(-\frac{t}{\tau_g} \right) \quad (6.6)$$

6.3.2.2 Data evaluation

From the measured temperature profiles and the given analytical expressions of the gas temperature function of time (see Eqs. 6.5 and 6.6), the convective heat transfer coefficient (HTC) can be deduced through graphical and numerical methods of calculation as follows:

- Method 1. A non linear least square solver from Matlab® is used to minimize the deviations between the experimental gas temperature profile and the theoretical value as given by Eq.6.6, by fitting the thermal time constant. The convective HTC is then determined from the fitted thermal time constant.
- Method 2. The time constant of a first order system, corresponds to the time at which the system variable being followed, here T_g , reached 63.2% of its total variation, that is $63.2\% \times (T_g^\infty - T_g^0)$. The thermal time constant, τ_g , is calculated in this way from the experimental temperature profiles, using a Matlab® script. From these results the convective HTC can be assessed.
- Method 3. As implies by Eq.6.5, plotting the experimental values of $(T_g^\infty - T_g)$ against time on semi-log graph may result in a linear curve of slope $-1/\tau_g$. A Matlab® script is used (1) to evaluate the slope of the linear curve obtained from the experimental data during the transient period between 0 and 3 h (depending on the setpoint temperature), and (2) to deduce the thermal constant in order to determine the convective HTC.

Notice that the contact area between wall and gas includes the kiln tube internal wall and, if present, the effective lifters transfer area within the control volume. Details of the expression of the effective lifter heat transfer length are given in the Appendix 6.5.2. In the case of heating in zone 2 only, the control volume is delimited by the sections S2 and S3, and when heating both zones it is delimited by the sections S1 and S2. The considered gas temperature is the average of the measured temperature of the sections limiting the control volume.

6.3.2.3 Results of the methods of calculation

In the few previous studies focused on the subject [Tscheng 1979, Gorog 1982, Silcox 1990, Owens 1991, Le Guen 2013], the convective heat transfer has been always analyzed in the case of forced convection through a rotary kiln, most of the time directly heated. However, in some cases the forced axial flow was neglected due to small gas flow rate [Colin 2015]. Sometimes there is simply no need of a forced axial flow of the gas above the bulk bed in particular in the recent applications using indirectly heated kiln to better control the wall temperature along the kiln. In the present study, there is no forced flow of the air along the kiln axial direction. The results from the 3 methods of calculation presented above for the determination of the convective HTC are given in Table 6.2. From the latter Table, it is found that the HTC is of an order of magnitude about $10^{-3} \text{ W.m}^{-2}.\text{K}^{-1}$, within the range of variation of the operating parameters.

Using Eq.6.6 with the results presented in Table 6.2, it is possible to draw a theoretical gas temperature profile for the different runs achieved. For example, in Figure 6.8, the experimental wall and gas temperatures, and the theoretical gas temperature obtained from the results of the 3 methods of calculation, are plotted function of time for the run 7 in Table 6.2, which experimental data are illustrated in Figure 6.6. It can be seen that the graphs resulting from the convective HTC determined from the graphical methods give better predictions of the gas temperature profile compared to the graph resulting from the fitting method. In order to better assess the predictive performance of the coefficients resulting from the 3 methods and used to plot the temperature profile, a criterion in performance assessments, J , is defined as follows:

$$J = \frac{1}{N_T} \sum_{i=1}^{i=N_T} \frac{(\bar{T}_{i_{exp}} - \bar{T}_{i_{calc}})^2}{\bar{T}_{i_{exp}}} \quad (6.7)$$

As shown in Figure 6.8, the value of the criterion is lower for the Method 2, that is, the best representation of the experimental gas temperature profile is obtained when plotting Eq.6.6

Table 6.2: Results of the experimental wall-to-gas heat transfer coefficient determined from Methods 1, 2 and 3. NC stands for non convergence, when the numerical fitting from method 1 did not converged.

Run	Operating conditions: Sand, S=3°			$h_{ew-g} \times 10^3 [\text{W.m}^{-2}.\text{K}^{-1}]$		
	Setpoint Temp. [°C]	N [rpm]	Lifters	Method 1	Method 2	Method 3
1	100°C - Zones 1 & 2	2	SL	3.6	5.6	7.7
2	100°C - Zone 2	2	NL	4.6	7.4	9.0
3	100°C - Zone 2	2	RL	2.9	4.7	6.5
4	100°C - Zone 2	2	SL	2.1	2.5	4.9
5	300°C - Zones 1 & 2	2	SL	NC	6.3	8.7
6	300°C - Zone 2	2	NL	4.6	9.2	8.1
7	300°C - Zone 2	2	SL	3.3	5.7	7.0
8	300°C - Zone 2	4	SL	3.2	6.0	6.4
9	300°C - Zone 2	8	SL	3.3	5.6	7.0
10	300°C - Zone 2	12	SL	3.2	4.0	6.1
11	300°C - Zone 2	2	SL	3.2	4.0	6.3
12	300°C - Zone 2	8	SL	3.2	4.7	6.2
13	500°C - Zones 1 & 2	2	SL	2.2	7.5	9.2
14	500°C - Zone 2	2	SL	NC	6.0	6.9

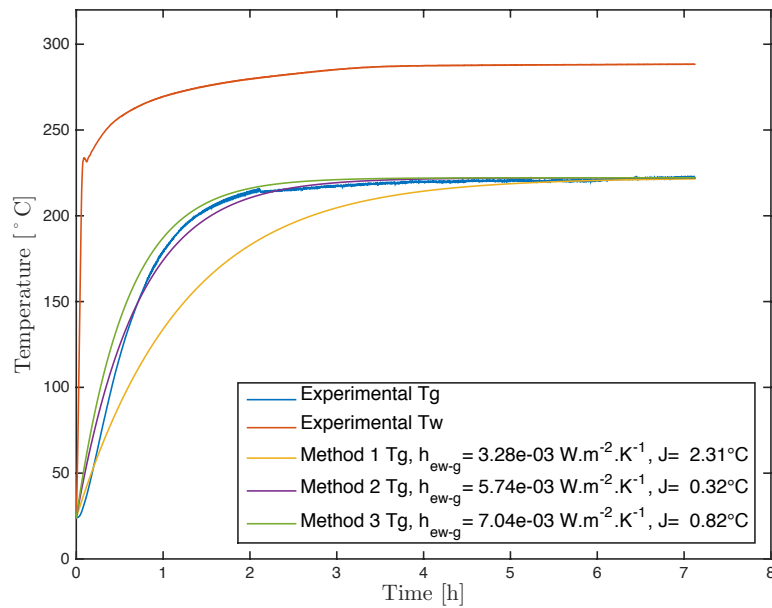


Figure 6.8: Comparison of the experimental gas temperature profile, with the predictions by Eq.6.6 using the convection HTC resulting from methods 1, 2 and 3.

function of time using the convective HTC from Method 2. Indeed, the lower the value of J , the better the predictions. J can be defined as the sum of relative square errors between experimental and predicted value of the measured temperature, relative to the number of measurements, N_T . Figure 6.9 shows the value of the criterion J for the runs achieved. A general observation is that the criterion seem to increase with the temperature, which may be the consequence of neglecting any modes of heat transfer other than convection. If over the whole experimental campaign the lower criteria are obtained for Methods 2 and 3 used for the calculation of the convective HTC, the values of the criterion are the lowest in general for the Method 2. Therefore, in the following section, only the results from Method 2 are considered to analyze the influence of the operating parameters, and to correlate the convective HTC.

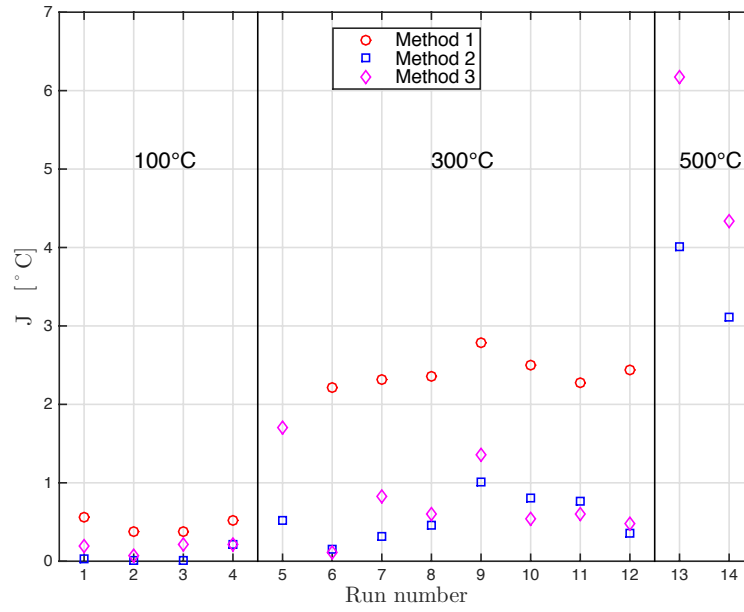


Figure 6.9: Values of J , the criterion in performance assessments, for the experimental runs presented in Table 6.2.

6.3.2.4 Effect of operating conditions on the wall-to-gas heat transfer coefficient

The influence of the lifters, the kiln rotational speed and the temperature on the wall-to-gas heat transfer coefficient are illustrated in Figure 6.10. The coefficient decreases significantly in presence of lifters, in particular, as shown in Figure 6.10a the higher the effective heat transfer area per unit length, the lower the heat transfer coefficient. The rate of heat transfer is governed by the thermal time constant. Indeed smaller value of that constant will provide faster heat transfer. Thus, within a given control volume, in theory, an increase in the surface of contact area may lower the thermal time constant by definition (see Eq.6.3). However, results show that the heat transfer does not seem to be enhanced in presence of lifter, which may in theory increase the contact area surface. A possible cause may be that the lifters are removable and so not sealed at the wall, therefore they must be heated with some delay with regard to the wall.

One may observe that the coefficient slightly decreases with increasing rotational speed as displayed in Figure 6.10b, certainly due to the rate of heating of the rotary kiln tube which changes following the increase of convection at the external wall of the kiln tube.

The temperature also influenced the wall-to-gas heat transfer coefficient as presented in Figure 6.10c; the coefficient increases with the temperature. However some discrepancies are found

between the results obtained when heating both zones and only zone 2. It was observed that the final temperature reached in the freeboard gas was higher when heating both zones.

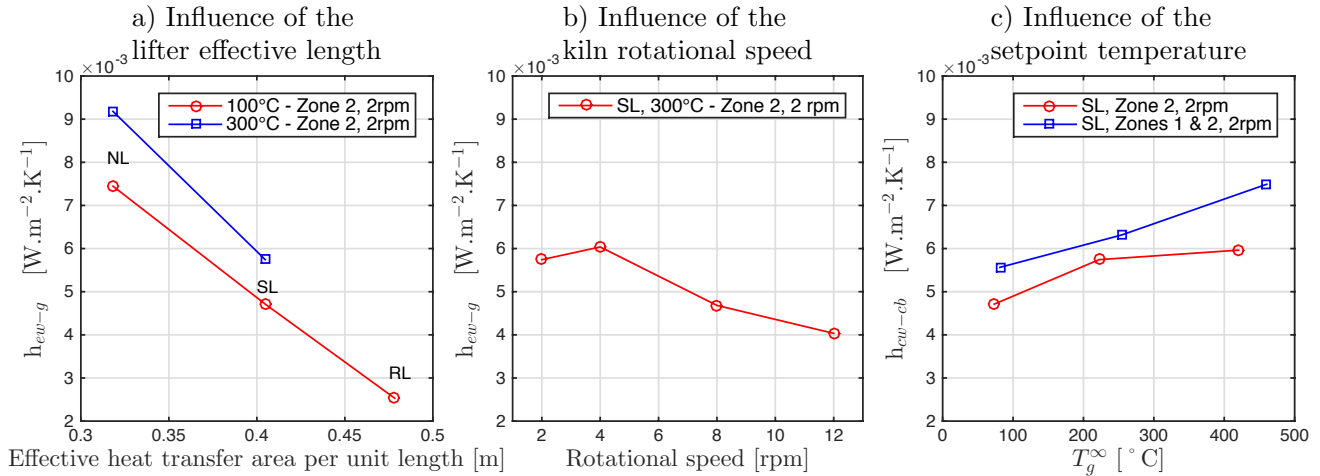


Figure 6.10: Variation of the wall-to-gas heat transfer coefficient with: a) lifter effective length (involves in the heat transfer), b) kiln rotational speed, c) temperature.

6.3.2.5 Modeling the wall-to-gas heat transfer coefficient

The heat transfer coupled to the convective motion of the freeboard gas at the cross-section of the rotary kiln has seldom been correlated. For the prediction of the convective heat transfer between wall and gas, using the methodology presented by [Delaplace 2014], a dimensionless correlation is developed as follows:

$$Nu_{ew-g} = \frac{h_{ew-g}D}{k_g} = K Re_\omega^\alpha Pr^\beta \left(\frac{l_g}{D} \right)^\gamma \left(K_\delta \frac{c_{pg}\rho_g T_g^\infty}{\omega \mu_g} \right)^\delta \quad (6.8)$$

where K , K_δ , α , ..., δ are the model parameters, $Re_\omega = \frac{\omega \rho D^2}{\mu_g}$ is the rotational Reynolds number with $\omega = \frac{2\pi}{60}N$, $Pr = \frac{c_{pg}\mu_g}{k_g}$ is the Prandtl number, l_g is the effective contact length along the cross section also taking into account lifters. Notice that (1) the constant K_δ is 10^{-10} (to facilitate the model parameter determination), (2) the temperature dependent properties such as the effective bed conductivity, k_g , the specific heat capacity, c_{pg} , the density, ρ_g , and the dynamic viscosity, μ_g , can be determined at the setpoint temperature, or the final gas temperature reached when known. In the case of solids flow, the correlation may be applied using the equivalent diameter $De = \frac{1}{2} \frac{2\pi - \psi + \sin \psi}{2\pi - \psi/2 + \sin \psi/2}$ instead of the internal diameter, D . This may allow calculations of the convective heat transfer between wall and gas as well as between gas and solids.

Table 6.3: Estimated parameters for the model proposed for the Nusselt number, with associated confidence intervals.

Model parameters		Confid. intervals	
		Inf.	Sup.
K	0.1085	-0.7314	0.9485
α	0.0275	-0.2518	0.3067
β	-0.4839	-16.188	15.220
γ	-1.9284	-2.5904	-1.2665
δ	-0.2208	-0.1369	0.5785

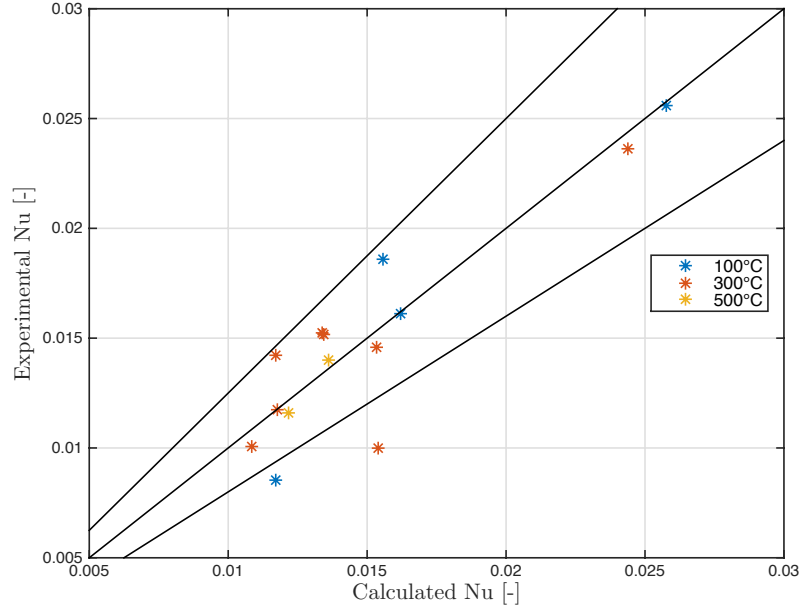


Figure 6.11: Comparison of experimental Nusselt number with predicted values from Eq.6.8 using the set of parameters given in Table 6.3. Solid lines are $\pm 20\%$ margins.

The model parameters are determined with the use of a nonlinear method based on iterative least squares estimation. Table 6.3 summarizes values of the model parameters determined with the use of experimental data at the 95% confidence level, while Figure 6.11 presents the comparison of the calculated model predictions with experimental results.

In spite of the few number of experiment used to build this model, only a few discrepancies with regard to the 20% margins can be found in Figure 6.11. In general, there is good agreement between the experimental and the calculated value of the Nusselt number relative to the wall-to-gas convective heat transfer. However as more data become available, the correlation can be suitably modified.

6.3.3 Wall-to-solid heat transfer coefficient

6.3.3.1 Energy balance

If the gas was virtually standstill within the pilot-scale unit used, the bulk bed was moving at a constant rate. The wall-to-solid heat transfer can be quantified through a unique coefficient, h_{cw-cb} , taking into account both contact resistance between the wall and solids bed and the penetration coefficient through the bulk bed. Let l_{ctrl} be the length between two sections defined within the heating zone(s). The bulk bed temperature is assumed uniform within a given section. Applying Eq.6.1 in the case of solids flowing at a mass flow rate, \dot{M} , gives the following energy balance for the bulk bed at any time:

$$-h_{cw-cb} \frac{A_{cw-cb}}{l_{ctrl}} (T_b(z) - T^\infty) dz = \dot{M} c_{pb} dT_b(z) \quad (6.9)$$

Rearranging Eq.6.9, and assuming the imposed heating temperature at the kiln tube internal wall, T^∞ , to be equal to the temperature measured at the outer wall at steady-state T_w^∞ , the following ODE is obtained:

$$\text{for } z > 0, \quad \frac{dT_b(z)}{dz} + \frac{1}{\lambda_b} (T_b(z) - T_w^\infty) = 0, \quad \lambda_b = \frac{\dot{M}c_{pb}l_{ctrl}}{h_{cw-cb}A_{cw-cb}} \quad (6.10)$$

$$IC : z = 0, \quad T_b(z = 0) = T_b^0 \quad (6.11)$$

herein λ_b is the thermal length constant which characterizes the rate of change of the bulk bed temperature variation. In addition, the given system must be valid only when thermal steady-state of the system is achieved otherwise the time also must have been taken into account. The above ODE is solved as given:

$$\ln \left(\frac{T_w^\infty - T_b(z)}{T_w^\infty - T_b^0} \right) = -\frac{z}{\lambda_b} \quad (6.12)$$

6.3.3.2 Data evaluation

If for a given run there are a large number of temperature measurements recorded over time, these temperature profiles are measured at only 4 positions within the heated zone(s) at sections S1, S2, S3 and S4 as given in Figure 6.4. The methods of calculation presented above to determine the convective heat transfer coefficient can also be employed in this case since the analytical solution is similar. However, due to the small number of data relative to the position, only Method 3 can be utilized. Indeed, measurements at a minimum of two positions are needed to be able to perform the calculations. At a given time when thermal steady state conditions are achieved, plotting the experimental values of $(T_w^\infty - T_b)$ against axial position on semi-log graph may result in a linear curve of slope $-1/\lambda_b$. A Matlab script is then used (1) to evaluate the slope of the linear curve obtained from the experimental data out of the transient period, and (2) to deduce the thermal constant used to determine the wall-to-solid HTC.

In general for the calculations:

- 4 positions (maximum) when heating only zone 2, specifically $z=\{0, 100(\text{S2}), 200(\text{S3}), 300(\text{S4})\}$ mm, with the origin located at the inlet section of zone 2;
- 5 positions (maximum) when heating zones 1 and 2, specifically $z=\{0, 300(\text{S1}), 500(\text{S2}), 600(\text{S3}), 700(\text{S4})\}$ mm, with the origin located at the inlet section of zone 1.

In both cases the temperature at the origin, T_b^0 , has been approximated. When heating only zone 2, a part of the kiln tube wall in zone 1 is heated by conduction, so that the solid particles are preheated when entering the heated zone 2. Therefore it is assumed for the calculations that the solid particles entering the heated zone 2 are at the temperature measured at S1, which is certainly a minimum but sufficiently accurate. When heating both zones 1 and 2, solid particles are also preheated. It has been observed that out of the heating zones, solid and gas temperatures were comparable. Hence, for the solid particles entering at the zone 1, the temperature has been approximated by the one measured in the gas at the kiln entrance. Notice that sometimes data were not available at all given positions, so that the calculations were performed with the remaining available data.

Several assumptions are made for the calculations, which may possibly affect the quantitative interpretation of the results, however, the order of magnitude and qualitative interpretation of the results must not be affected much. Figure 6.12 presents results of the calculation of the wall-to-solid heat transfer coefficient out of the transient for the experiment, of which the temperature profiles are shown in Figure 6.7. The heat transfer coefficient remains constant as expected. For the interpretation of the results in the coming section, the experimental coefficient is averaged over 2 hours in the period of thermal steady state. For example the results in Figure 6.12 yield

a wall-to-solid heat transfer coefficient about $51.5 \text{ W.m}^{-2}.\text{K}^{-1}$. Overall, the actual (or likely) results for the wall-to-solid heat transfer coefficient lie within $0.5\text{-}70 \text{ W.m}^{-2}.\text{K}^{-1}$.

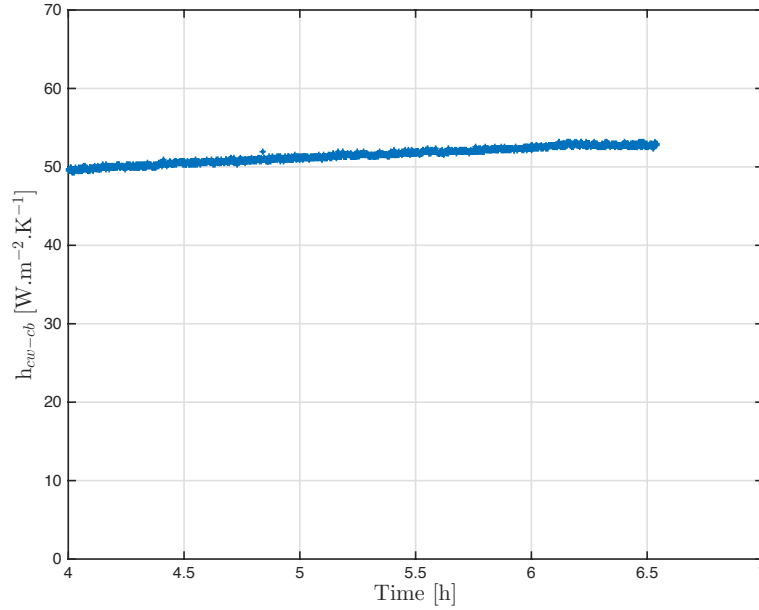


Figure 6.12: Experimental results obtained for the wall-to-solid heat transfer coefficient for the run which experimental temperature profiles are presented in Figure 6.7.

6.3.3.3 Effect of operating parameters on the wall-to-solid heat transfer coefficient

As highlighted above, the wall-to-solid heat transfer coefficient (HTC) has been seldom identified within continuously fed rotary kilns. The effect of operating parameters are analyzed with the use of the filling degree. Indeed, in previous studies [Bongo Njeng 2015a, Bongo Njeng 2015b, Bongo Njeng 2015c], it has been established that the filling degree increases with increasing mass flow rate, exit dam height or lifter hold-up capacity. Therefore, as presented in Figure 6.13, the only parameter, that is filling degree, is used to analyzed the influence of the three given operating parameters on the wall-to-solid HTC. Notice that the range of variation of the filling degree (HU[%]) for given operating conditions, in particular the mass flow rate, is shown in Table 6.7 in the Appendix 6.5.3. From Figure 6.13 it is clear that at a given kiln slope and rotational speed, in general the wall-to-solid HTC increases with the filling degree, and thus with the three given operating parameters (mass flow rate, exit dam height or lifter hold-up capacity). However, in the case of lifters, straight lifters displayed lower values of the wall-to-solid HTC compared to the case without lifters, which yield higher values (see Figures 6.13a and 6.13b), or with rectangular lifters, which yield the highest values (see Figure 6.13a). This brings to light a possible existence of critical lifter geometrical characteristics (or design) above which the lifters may be able to enhance the heat transfer. This may explain why there is no consensus in previous investigations about the use of lifters in rotary kilns to promote the heat transfer. It must be mentioned that the finding in the present study related to the variation of the heat transfer coefficient with the filling degree does not all agree with some previous results obtained in batch drum [Lybaert 1987, Herz 2012]. Notice that as previously observed by [Suzuki 2008b] the higher the temperature, the higher the heat transfer coefficient.

In presence of straight lifters and exit dam (33.5 mm in height), the effect of the kiln rotational speed on the wall-to-solid HTC is investigated in Figure 6.14, while keeping the solids flow rate

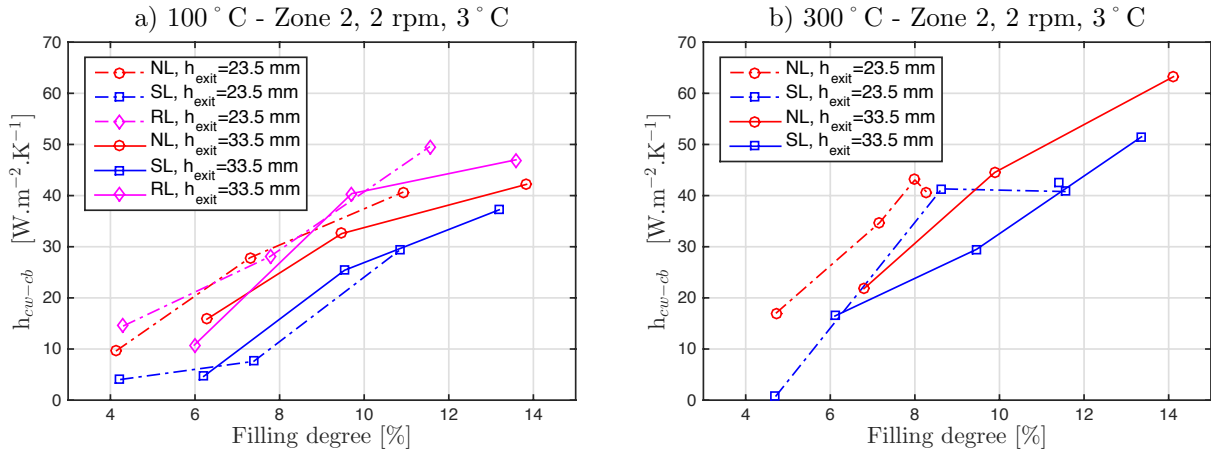


Figure 6.13: Variation of the wall-to-solid heat transfer coefficient with the filling degree for different temperatures: a) 100°C and b) 300°C.

constant on the one hand and the kiln filling degree constant on the other hand. At constant flow rate the wall-to-solid HTC tends to increase with the kiln rotational speed. However, this may seem incompatible with previous observations, it was previously found that an increase of the rotational speed must result in a decrease of the kiln filling degree. In Figure 6.14a, the filling degree decreases from 13 to 5% between 2 and 12 rpm, so in accordance with previous results the heat transfer must have decreased as well. Therefore, another mechanism must be involved, in order to promote the heat transfer as observed. To better understand the effect of the kiln rotational speed on the heating, in Figure 6.14b the rotational speed is varied while keeping a constant filling degree about 6.7% by adjusting the mass flow rate. The results show that the wall-to-solid HTC is significantly increased as the rotational speed is increased by a factor 4. The missing mechanism can then be easily identified with regard to the motion of the burden, namely the mixing effect resulting from the increase of the axial dispersion following the increase of rotational speed, in particular in the presence of lifters as found previously [Bongo Njeng 2015a, Bongo Njeng 2015c]. Similar trends are observed for the wall-to-solid HTC by [Lybaert 1987, Suzuki 2008b, Herz 2012, Nafsun 2015] in indirectly heated rotary batch kilns, whereas [Thammavong 2011] did not observe significant effect of the rotational speed in a continuously fed rotary kiln.

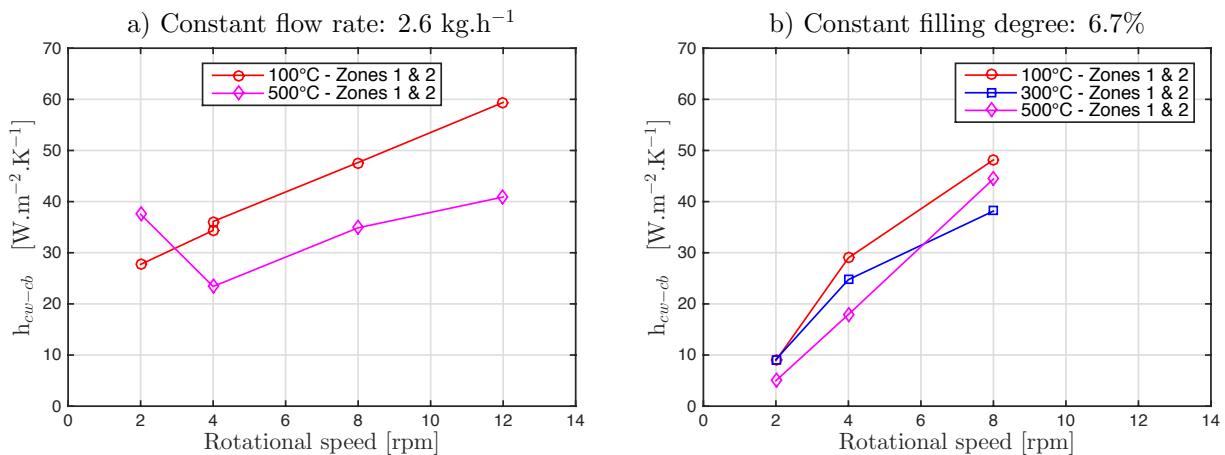


Figure 6.14: Variation of the wall-to-solid heat transfer coefficient with the kiln rotational speed at a) constant flow rate and b) constant filling degree, while using straight lifters and an exit dam (33.5 mm in height).

6.3.4 Biot number

The Biot number, Bi , is defined as hL/k , where L is the characteristic length of the medium, k is the thermal conductivity of the medium and h is the heat transfer coefficient. The biot number has been determined for the wall-to-gas and wall-to-solid heat transfer coefficients given above. For the calculation, the characteristic length used for the gas is the ratio of the gas volume to the wall-to-gas contact area within the control volume, and for the solids it is the ratio of the solids volume to the wall-to-solid contact area within the control volume of length l_{ctrl} . Figure 6.15 presents the calculated Biot numbers. In Figure 6.15a for the results corresponding to the wall-to-gas heat transfer, it is found that $Bi \ll 1$, which means that the temperature of the air is almost constant at any time as supposed. Whereas in Figure 6.15b for the results corresponding to the wall-to-solid heat transfer, it is found that Bi is of the order of 1, which means that the initial assumption of uniform temperature within the bulk bed may not be completely satisfied: the conduction process within the bed offers some resistance to the heat transfer from the wall. However, as stated by [Imber 1962], in the analysis of the overall performance of rotary kiln units, due to the complexity of exact analytical expressions for the bulk temperature, it has usually been assumed for practical use uniform bed temperature at any cross-section thanks to the kilning effect, that is tumbling, even if this assumption may not be always completely satisfied as shown here.

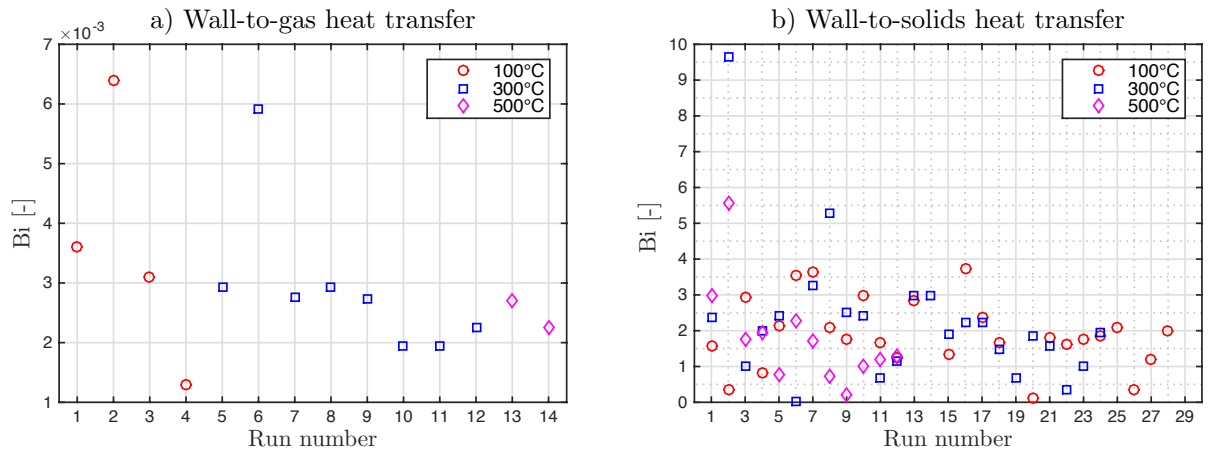


Figure 6.15: Biot number calculated for each run using the determined a) wall-to-gas and b) wall-to-solid heat transfer coefficient.

6.4 Conclusion

The lumped system analysis, which assumes a uniform temperature of the considered medium at any time has been applied for the determination of the wall-to-gas and wall-to-solid heat transfer coefficients (HTC). These coefficients are experimentally investigated using an indirectly heated rotary kiln equipped with lifters and operated with a continuous flow of solids (quartz sand) in the case of the wall-to-solid HTC, and without solids flow in the case of the wall-to-gas HTC. There was no forced axial flow of gas (air). The results shows that the wall-to-gas HTC was of the order of $10^{-2} \text{ W.m}^{-2}.\text{K}^{-1}$, whereas the wall-to-solid was of the order of $100 \text{ W.m}^{-2}.\text{K}^{-1}$. In particular for the prediction of the wall-to-solid HTC, a model based on dimensional analysis and accounting for the operating conditions and solid materials thermo-physical properties is proposed. Good agreements are found between experimental data and the predictions.

It was also found from the analysis of the effect of operating conditions within the flighted rotary kiln:

- the wall-to-gas HTC increased with the temperature, but decreased with the kiln rotational speed and in presence of lifters;
- the wall-to-solid HTC increased the temperature and the rotational speed. This coefficient was also found to increase with an increase of the filling degree following a variation of the solids mass flow rate, exit dam height or lifter capacity; however in the case of lifters this result has been validated only for rectangular lifter, raising the existence of a critical lifter design adequate to better promote the heat transfer. The lifter design thus becomes for the heat transfer an open-ended matter of optimizing.

List of symbols

A	Contact area	m^2
Bi	Biot number	$[-]$
c_p	Specific heat capacity	$J.kg^{-1}.K^{-1}$
D	Kiln internal diameter	m
D_e	Equivalent diameter	m
h	Heat transfert coefficient	$W.m^{-2}.K^{-1}$
h	Exit dam height	m
HTC	Heat transfert coefficient	$W.m^{-2}.K^{-1}$
HU[%]	hold-up volume fraction or filling degree	-
J	Performance criterion	K
k	Thermal conductivity	$W.m^{-1}.K^{-1}$
K, K_δ	Model parameter	-
L	Characteristic length	m
l_{ctrl}	Length between two sections within the kiln	m
l_g	Effective wall-to-gas contact length along the cross section between	m
\dot{M}	Mass flow rate	$kg.h^{-1}$
N	Kiln rotational speed	rpm
NC	No convergence	-
NL	No lifters	-
Nu	Nusselt number	-
N_T	Total number of experiments	-
ODE	Ordinary differential equation	-
Pr	Prandtl number	-
Re_w	Rotational Renolds number	-
rpm	Rotation per minute	-

RL	Rectangular lifters	-
S	Kiln slope	degrees
SL	Straight lifters	-
t	Time	h
T	Temperature	K
TC	Thermocouple	-
z	Axial position	m

Greek letters

α, β, γ	Fitting parameters	-
δ		
ϵ_0	Solid bulk porosity	-
ε	Emisivity	-
λ_b	Thermal length constant	m
μ	Dynamic viscosity	$\text{kg.m}^{-1}.\text{s}^{-1}$
ρ	Density	kg.m^{-3}
τ_g	Thermal time constant	h
ψ	Filling angle	rad
Ω	Volume	m^3
ω	Kiln rotational speed	rad/s

Subscripts

b	Bulk bed of solids	-
calc	Calculated	-
cb	Covered bed	-
cw	Covered wall	-
ew	Exposed wall	-
exp	Experimental	-
G,g	Gas	-
	Gas at the bottom in	
gbd	the left side of the kiln cross section	-
	Gas at the top in the	
gbu	right side of the kiln cross section	-
	Gas at the top in the	
gu	left side of the kiln cross section	-
S	Bulk bed of solids	-
W,w	Wall	-

6.5 Appendices

6.5.1 Bulk bed conductivity model

The effective bed thermal conductivity, k_b , is the summation of the conductivity due to solid particles and gas thermal conduction plus the conductivity due to the radiation between the solid particles:

$$\succ k_b = k_{cb} + k_{rb},$$

It is determined using the model presented by [Bauer 1977]:

$$- \frac{k_{cb}}{k_g^{int}} = 1 - (1 - \epsilon_0)^{1/2} + (1 - \epsilon_0)^{1/2} \left(\frac{2}{1-B/Z} \right) \left(\frac{(1-1/Z)B}{(1-B/Z)^2} \ln\left(\frac{Z}{B}\right) \right) - \frac{B+1}{2} - \frac{B-1}{1-B/Z}, \text{ with } k_{cb}$$

the thermal conductivity through gas-solids contact area.

$$* B = C \left(\frac{1-\epsilon_0}{\epsilon_0} \right)^{10/9}, \text{ with the bulk porosity } \epsilon_0 = 0.43, \text{ with } C = 1.25 \text{ for spheres and } C = 2.5 \text{ for cylinders.}$$

$$* Z = \frac{k_{pa}}{k_g^{int}}, \text{ with the particle thermal conductivity } k_{pa} = 2 \text{ W/m.K, and the gas thermal conductivity } k_g^{int} = 0.01 \text{ W/m.K.}$$

$$- \frac{k_{rb}}{k_g^{int}} = \left(1 - (1 - \epsilon_0)^{1/2} \right) Fr + \frac{(1-\epsilon_0)^{1/2}}{\left(\frac{1}{Fr} + \frac{k_g^{int}}{\lambda_0} \right)}, \text{ with } k_{rb} \text{ the thermal conductivity due to radiation.}$$

$$* Fr = \frac{4\sigma T_b^3}{\left(\frac{2}{\epsilon_{pa}} - 1 \right)} \frac{D_{pa}}{k_g^{int}}, \text{ with the particle emissivity } \epsilon_{pa} = 1, \text{ the particle diameter } D_{pa} = 0.55 \cdot 10^{-3} \text{ m, and } \sigma = 5.6703 \cdot 10^{-8} \text{ W/m}^2 \cdot \text{K}^4.$$

6.5.2 Evaluation of the lifter effective heating length

The lifters which are from the same material than the wall can be regarded as fin protrudes of the wall. Here, both lifters (straight and rectangular) are considered as one-section lifter of equivalent length, d , and width, e .

When heating the wall, the lifters may also be heated by the wall. However the existing temperature difference between the lifter and its environment may influence the heat transfer, in particular the efficiency of the lifter may diminish with increasing width. This efficiency is governed by the rate of heat transfer by conduction in the lifter in relation to the quantity of heat transfer to environment. In the steady state condition the temperature profile of the lifter along its width, T_{lift} , can be obtained from the following differential equation:

$$\frac{d^2 T_{lift}}{dy^2} + \frac{2h}{k_{lift}e} (T_e - T_{lift}) = 0 \quad (6.13)$$

Herein h is the mean heat transfer coefficient from lifter to environment (either h_{ew-g} in the gas or h_{cw-cb} in the bulk bed), k_{lift} is the thermal conductivity of the lifter, e the width of the lifter, T_e is the temperature of surrounding environment and T_{lift} the temperature of the lifter at a distance y from the wall.

Providing the following boundary conditions:

$$\begin{aligned} y = 0 \quad T_{lift} &= T_w \\ y = d \quad \frac{dT_{lift}}{dy} &= 0 \end{aligned}$$

Integration of Eq.6.13 then yields:

$$T_{lift} = A \exp(\lambda_1 y) + B \exp(\lambda_2 y) + T_e \quad (6.14)$$

Herein $\lambda_{1,2} = \pm \sqrt{\frac{2h}{k_{lift}e}}$, $A = T_w - T_e - B$, and $B = \frac{(T_e - T_w)\lambda_1 \exp(\lambda_1 d) - T_e}{\lambda_2 \exp(\lambda_2 d) - \lambda_1 \exp(\lambda_1 d)}$.

The effective length of the lifter transferring the heat, d_{eff} , is determined by integrating the temperature profile given in Eq.6.14 as follows:

$$\int_0^d (T_{lift} - T_e) dy = d_{eff} (T_w - T_e) \quad (6.15)$$

Thus

$$d_{eff} = \frac{1}{T_w - T_e} \left[\frac{A}{\lambda_1} (\exp(\lambda_1 d) - 1) + \frac{B}{\lambda_2} (\exp(\lambda_2 d) - 1) \right] \quad (6.16)$$

Notice that the lifter temperature near the contact with the kiln wall was not exactly equal to the wall temperature as shown by the measured temperature profiles presented in Figure 6.16, for the calculation we considered 85% of the actual wall temperature.

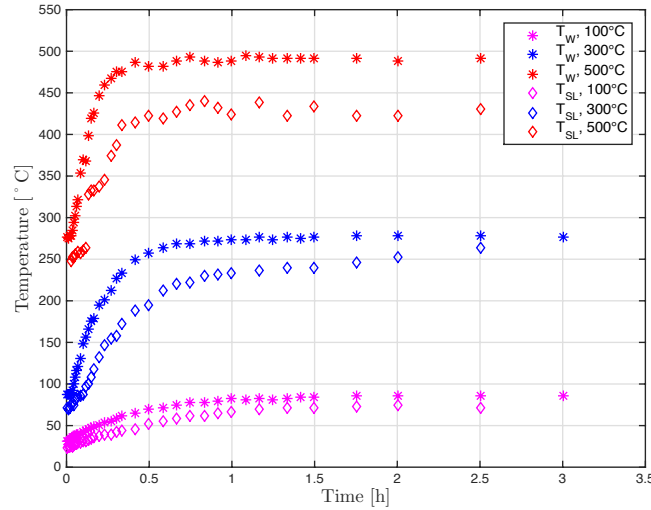


Figure 6.16: Temperature profile of the internal wall and of the root of straight lifters measured using a pyrometer.

6.5.3 Experimental matrix

The experimental matrix achieved with and without solids flow is summarized in Table 6.7. The given numbers represent the number of repetition of a run.

Table 6.7: Experimental conditions of the experiments for the study of heat transfer using rectangular lifters (RL), straight lifters (SL) and no lifters (NL).

Operating conditions: Sand, S = 3°				Zone 2						Zone 1&2		Zone 2			Zone 1&2	
Setpoint T.	N	M	HU	Lifters	NL		SL		RL		SL	Lifters	NL	SL	RL	SL
[°C]	[rpm]	[kg.h ⁻¹]	[%]	h[mm]	23.5	33.5	23.5	33.5	23.5	33.5	33.5	h[mm]	33.5	33.5	33.5	33.5
100	2	0.7-0.9	3.97 - 6.7	Solids flow	1	1	1	1	1	1	1	No solids flow	-	-	-	-
	2	1.7-1.9	6.89 - 9.5		1	1	1	1	1	2	-		-	-	-	-
	2	2.4-2.6	10.43 - 13.30		1	1	1	1	1	2	1		1	1	1	1
300	2	0.7-0.9	3.97 - 6.7		1	1	1	1	-	-	1		-	-	-	-
	2	1.7-1.9	6.89 - 9.5		3	1	3	3	-	-	-		-	-	-	-
	2	2.4-2.6	10.43 - 13.30		1	1	2	1	-	-	1		1	2	-	1
500	2	0.7-0.9	3.97 - 6.7		-	-	-	1	-	-	1		-	-	-	-
	2	1.7-1.9	6.89 - 9.5		-	-	1	1	-	-	-		-	-	-	-
	2	2.4-2.6	10.43 - 13.30		-	-	1	1	-	-	1		-	1	-	1
100	4	1.9	6.7		-	-	-	-	-	-	1		-	-	-	-
100	4	2.4-2.6	8		-	-	-	-	-	-	2		-	-	-	-
300	4	1.9	6.7		-	-	-	-	-	-	1		-	1	-	-
500	4	1.9	6.7		-	-	-	-	-	-	1		-	-	-	-
500	4	2.4-2.6	8		-	-	-	-	-	-	1		-	-	-	-
100	8	3.2	6.7		-	-	-	-	-	-	1		-	-	-	-
100	8	2.4-2.6	6		-	-	-	-	-	-	1		-	-	-	-
300	8	3.2	6.7		-	-	-	-	-	-	1		-	2	-	-
500	8	3.2	6.7		-	-	-	-	-	-	1		-	-	-	-
500	8	2.4-2.6	6		-	-	-	-	-	-	1		-	-	-	-
100	12	2.4-2.6	5		-	-	-	-	-	-	1		-	-	-	-
300	12	2.4-2.6	5		-	-	-	-	-	-	-		-	1	-	-
500	12	2.4-2.6	5		-	-	-	-	-	-	1		-	-	-	-

Chapter 7

Wall-to-solid heat transfer coefficient in flighted rotary kilns: experimental determination and modeling

Abstract	184
7.1 Introduction	185
7.2 Materials and methods	186
7.2.1 Apparatus and materials	186
7.2.2 Experimental procedure	188
7.3 Heat transfer	189
7.3.1 Heat transfer mechanisms	189
7.3.2 Heat balance	192
7.3.3 Convection and radiation modeling	193
7.3.4 Estimation of heat transfer areas	194
7.4 Results and discussion	197
7.4.1 Experimental wall-to-solid heat transfer coefficient	197
7.4.2 Modeling of the wall-to-solid heat transfer coefficient	200
7.5 Conclusion	203
7.6 Appendices	206
7.6.1 Calculation of the heat losses through the insulation	206
7.6.2 Bed depth profile measurements	207
7.6.3 Uncertainties calculations	208
7.6.4 Experimental results: wall-to-solid heat transfer coefficient	208

The research described in this Chapter is to be submitted for publication to the International Journal of Heat and Mass Transfer.

Abstract

Abstract:

A series of experiments are carried out on a pilot scale rotary kiln indirectly heated. These experiments aim at recording, while the solids flow, the temperature profiles of the freeboard gas, the bulk of solid particles and the wall, as well as the power supplied for the heating, over a range of operating conditions. With the use of these data, the experimental wall-to-solid heat transfer coefficient is determined through an energy balance. The effect of operating conditions, namely rotational speed, filling degree, lifter shape and control temperature on the heat transfer coefficient are discussed and analyzed in relation to results from preliminary analysis achieved in a separate paper [Bongo Njeng 2015d]. A model based on dimensional analysis is proposed for the calculation of the wall-to-solid heat transfer coefficient for low to medium heating temperatures (100-500°C). The experimental and calculated results are in good agreement. The experimental results are also compared to the predictions of some existing models. If the predictions are within a reasonable order of magnitude with regard to the experimental results, these models fail to represent well the actual variations with operating conditions.

Résumé :

On a mené des expériences dans un four tournant à chauffage indirect et à l'échelle laboratoire, en vue d'enregistrer pour diverses conditions opératoires, les profils de température des phases gazeuse et solide, et à la paroi du tube, ainsi que la puissance fournie pour la chauffe. A partir de bilans d'énergie, et en se servant des relevés de température (gaz, solide et paroi) et de puissance fournie au système, la valeur du coefficient d'échange paroi/solide a pu être déterminée. L'influence des paramètres opératoires, tels que, la vitesse de rotation du four, le taux de remplissage, la forme des releveurs ou la chauffe sur le coefficient d'échange a été étudiée et analysée au regard de résultats préliminaires obtenus et présenté par ailleurs [Bongo Njeng 2015d]. Une corrélation est proposée pour l'estimation du coefficient d'échange paroi/solide pour des températures comprises entre 100 et 500°C. La comparaison des prédictions du modèle avec les résultats expérimentaux est assez satisfaisante. Une comparaison est aussi faite avec des modèles existants ; bien que l'ordre de grandeur des prédictions est cohérent avec les valeurs expérimentales, ces modèles ne permettent pas de prendre en compte les variables opératoires.

7.1 Introduction

Indirect heated rotary kilns are widely used as heat exchangers, calciners, incinerators, coolers or dryers. They are usually designed for applications needing tight control and clean heating of materials. The possible applications include [Boateng 2008]: calcination, reduction, controlled oxidation, carburization, solid-state reaction or waste disposal. Typical industrial indirectly heated rotary kilns are usually smaller than those directly heated. The device consists generally of an inclined cylinder, rotated axially and which can be equipped with internal fixtures or exit dam. The heating system installed at the outer wall of the cylindrical shell can be either electrical or gas fired, and usually it is designed so that the heating can be achieved in different zones of the kiln at different controlled temperatures.

The heat transfer coefficient between wall and solids plays an important role in the heat transfer, especially when modeling operations of rotary kilns. There have been a few correlations proposed in the literature. The penetration theory, widely used in the case of fluidized and fixed beds [Schlünder 1984a], has been applied several times in previous investigations to determine the overall coefficient of heat transferred between the kiln wall and the bulk bed.

[Wes 1976a] was among the first to use the penetration theory in a rotary kiln with the assumption of equal temperature at the contact point between wall and bulk bed, and considering the heat conduction only in the radial direction. The calculations achieved proved that the following analytical formulation is applicable for the determination of the wall-to-solid heat transfer coefficient:

$$h_{cw-cb} = 2\sqrt{\frac{k_b \rho_b c_{pb}}{\pi t_c}} \quad (7.1)$$

where k_b , ρ_b and Cp_b are respectively the thermal conductivity, the density and the heat capacity of the bulk. t_c is the time during which a point on the kiln wall is in contact with the solids. [Wes 1976a] validated the applicability of the penetration theory by plotting experimental results against the square root of the kiln rotational speed at constant filling degree, which displayed straight lines, implying a proportionality in accordance with the theory. [Lehmberg 1977] assumed the presence of a thin layer at the contact between covered wall and bulk materials, and so incorporated into the penetration theory an equation of heat flux to account for the thin gap. There have been other attempts by [Tscheng 1979, Ferron 1991, Ding 2001, Le Guen 2014, Li 2005] resulting in sometimes very complex equations.

[Tscheng 1979] proposed a model established from rewriting the penetration theory in dimensionless form, with the use of published experimental data, from which the following equation is obtained:

$$h_{cw-cb} = 11.6 \frac{k_b}{l_\psi} \left(\frac{NR^2}{a_b \psi} \right)^{0.3} \quad (7.2)$$

where l_ψ is the arc length of the covered wall, ψ is the filling angle, a_b is the bed thermal diffusivity, R is the kiln internal radius and N is the rotational speed.

[Li 2005] proposed an extended model of the penetration theory for the wall-to-solid heat transfer coefficient, encompassing the heat transfer coefficient from the bed surface to the bulk materials, and the advection heat coefficient within the bulk materials. The correlation proposed is as follows:

$$h_{cw-cb} = \left(\frac{\chi d_p}{k_g} + \frac{1}{2} \sqrt{\frac{\psi}{2k_b \rho_b c_{pb} N}} \right)^{-1}, \quad 0.096 < \chi < 0.198 \quad (7.3)$$

where χ is the thickness of the gas film, d_p is the particle size, k_g is the gas thermal conductivity. This approach eliminates the need for a contact resistance at the wall. It can be noted that [Malhotra 1990] has extended the wall surface to single particle contact heat transfer coefficient known as the first particle heat transfer coefficient to account for different particle geometries.

Equation 7.2 has been used several times [Gorog 1982, Owens 1991, Martins 2001, Herz 2012] and can be regarded as quite reliable. However, as shown by [Debacq 2001, Thammavong 2011, Herz 2012], there were often quantitatively significant differences between the models' predictions. In addition, [Debacq 2001] conducted a sensitivity analysis clearly demonstrating that variations in the wall to solids heat transfer coefficient significantly impact the predictions of bed temperature profiles.

This paper aims at providing a correlation applicable for a wide range of kiln operating conditions for the determination of the wall-to-solid heat transfer. For this purpose, measurements were performed within a continuously fed pilot scale rotary kiln indirectly heated. In a separate paper [Bongo Njeng 2015d], the authors have discussed preliminary results about the wall-to-solid heat transfer coefficient determined through the lumped analysis method, and described the main effects of the operating parameter on the coefficient. This paper presents and discusses the experimental wall-to-solid heat transfer coefficient obtained from an energy balance using the power supplied to the unit. Then a model based on dimensional consideration is proposed for the heat transfer coefficient. This model may account for the operating conditions, namely rotational speed, filling degree, lifters and temperature at the wall. Eventually the experimental results are compared to the predictions of 3 existing models.

7.2 Materials and methods

7.2.1 Apparatus and materials

The main characteristics of the pilot scale rotary kiln indirectly heated, which is used to investigate the wall-to-solid heat transfer coefficient in the present study, are summarized in Table 7.1. Its main part consists of an Incoloy alloy rotating tube supported on 4 rollers and measuring 1.95 m in length, 0.101 m in (internal) diameter, and 6.5 mm in thickness. The tube is surrounded by heating elements (resistors) arranged in two zones in line (each 0.4 m in length) and designed to heat the tube wall up to 1000°C. The heating elements are covered with a thick layer of insulation. In addition, upstream of the kiln tube are installed a hopper and screw feeder followed by a feed chute, and downstream of the kiln tube is set a recovery tank.

The kiln tube rotational speed can be adjusted within 0.5-12 rpm and its slope set at a maximum angle of 5°. Some features such as lifters and dam can be fitted respectively at the kiln tube internal wall, and at its outlet end. Figure 7.1 represents these features which may equip the kiln. Straight one-section 10 mm lifters (see Figure 7.1a) referred to as straight lifters (SL) and two-section lifters 10 mm with a right angle cross section (see Figure 7.1b) referred to as rectangular lifters (RL), are used.

For the thermal metrology, the experimental unit is equipped with thermocouples (TC) placed at different positions as illustrated in Figure 7.2 to measure the temperature profiles in the bulk bed, free-board gas and at the wall. Temperatures of the solids and the free-board gas are measured by 20 N-type TC 1.5 mm in diameter. These thermocouples are installed in a measuring rod and arranged in a series of 5 sections, S1 to S5. At each section, one TC is

Table 7.1: Characteristics of the experimental setup and order of magnitude of operating conditions.

Subsets	Parameters	Order of magnitude	Remarks
Rotary kiln design	D [m]	0.101	Internal Diameter
	L [m]	1.95	Kiln length
	Feed hopper [m ³]	5	Capacity
	Heating zones, length [m]	2, 0.4	In a row
	Outer wall TC	16	K-type
	Measuring rod TC	20	N-type
Operating conditions	N [rpm]	2-12	Rotational speed
	S [°]	3	Kiln slope
	\dot{M} [kg.h ⁻¹]	0.5-3.2	Mass flow rate
	h [mm]	23.5-33.5	Exit dam height
	Heating temperature [°C]	100-500	Low to medium
	Lifters shape	NL	No lifter, smooth wall
	(configuration),	SL (4 rows), 10	Straight lifter
	height [mm]	RL (4 rows), 10	Rectangular lifter

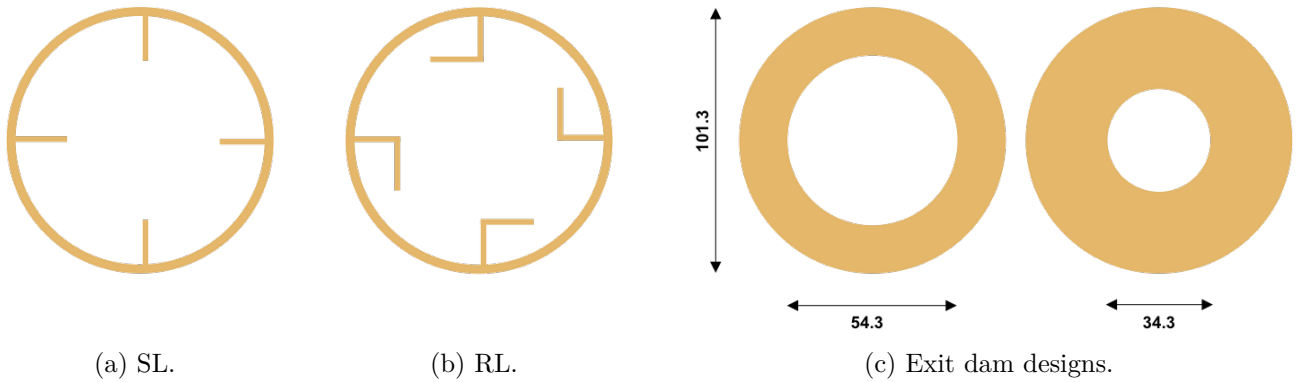


Figure 7.1: Features equipping the kiln: a) straight lifters (SL), b) rectangular lifters (RL) and c) exit dams.

embedded and measures the bulk temperature, T_s ; the 3 remaining TC are placed in the gas phase and their measurements are averaged to yield the gas temperature T_g . An additional set of 16 K-type TC 3 mm in diameter are used to measure temperatures at the outer wall. As shown in Figure 7.2, they are inserted through the kiln insulation and placed around the outer wall in a series of 4 sections, S1 to S4 along the kiln. The average of the temperatures measured at a given section yields the wall temperature, T_w , at the corresponding position. The whole set of TC was calibrated with a tolerance of $\pm 1.5^\circ\text{C}$ according to the supplier.

The experiments are performed at atmospheric pressure using nodular sand of 0.55 mm average particle size and without axial forced flow of air. The thermo-physical properties of the materials used are given in Table 7.2 (at 300°C). Regarding the sand, notice that the density and specific heat capacity are assumed constant, and the thermal conductivity is determined after the model by [Bauer 1977]. For the air, the density is determined from the ideal gas law, and the specific heat capacity and conductivity are determined from model set with the use of the results by [White 1988]. The Inconel thermal properties are extracted from [Corporation 2014, Corporation 2013]. The emissivities are provided by [Thammavong 2009], who designed the actual pilot rotary kiln.

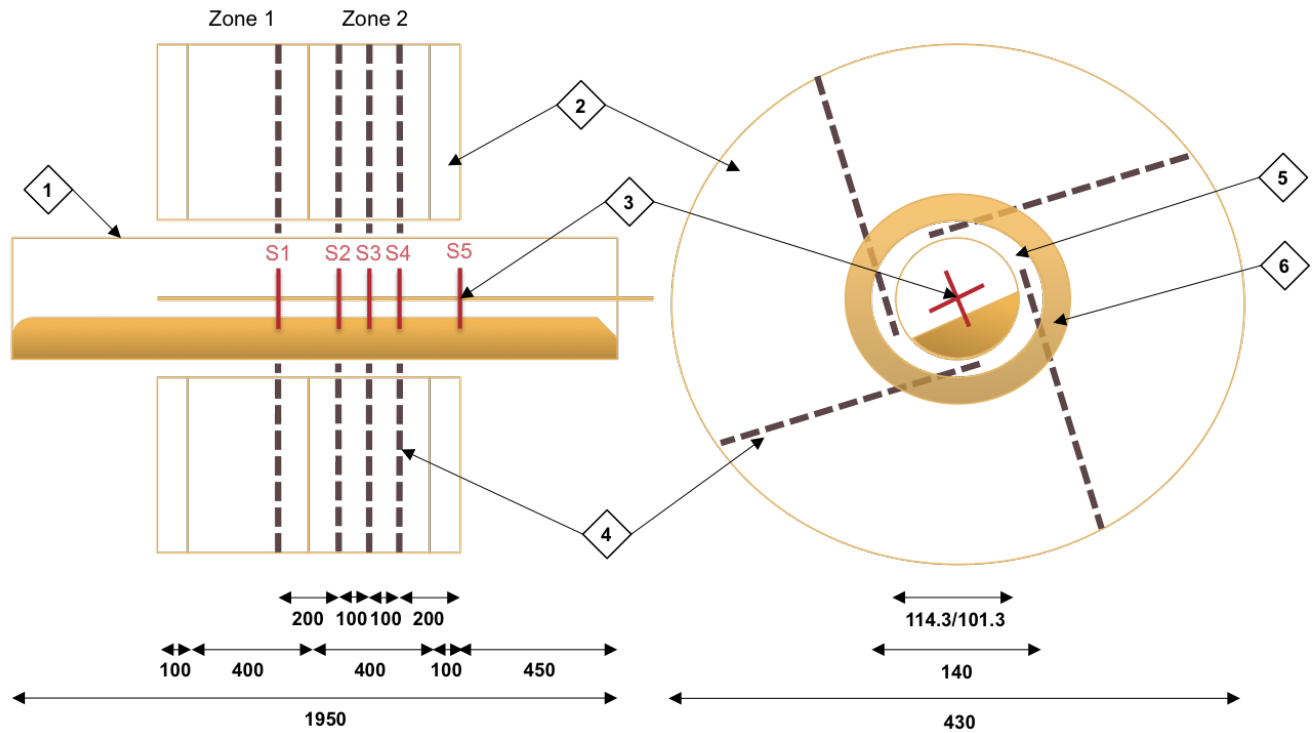


Figure 7.2: Layout of the experimental apparatus heating zones, longitudinal (left side) and transverse (right side) sections: (1) kiln tube, (2) insulation, (3) measuring rod with N-type thermocouples, (4) outer wall K-type thermocouples, (5) air, (6) heating resistors. The given dimensions in the drawing are in mm.

Table 7.2: Thermal properties of materials at 300°C.

Materials	Sand	Air	Inconel	Remarks
ρ [kg.m ⁻³]	1422	0.616	7950	Density
c_p [J.kg ⁻¹ .K ⁻¹]	835	1045	514	Specific heat capacity
k [W.m ⁻¹ .K ⁻¹]	0.1836	0.0449	18.75	Thermal conductivity
ϵ [-]	0.76	<0.01	0.9	Emissivity
ϵ_0 [%]	43.36	-	-	Measured porosity

7.2.2 Experimental procedure

The following experimental procedure is set to investigate the wall-to-solid heat transfer coefficient:

- Step 1: The operating parameters are set to the desired value: the kiln slope is adjusted at 3° (same angle for all runs); rectangular, straight or no lifters are installed at the kiln tube internal wall; the measuring rod is then installed inside the kiln; the desired exit dam is fixed; the rotational speed and the feed rate are set in the control box to the desired value. The hopper is filled and kept topped up, while the kiln is operated at room temperature until steady-state conditions of the flow.
- Step 2: The temperature recording is started at an arbitrary zero time. Until the end of the run, the power supplied to the installation, the ambient temperature around the kiln, and the freeboard gas temperature at the inlet end of the kiln are measured every half hour.

- Step 3: 30 min. after starting the recording, the temperature is adjusted on the controller and the heating source is turned on either in zone 2 or in both zones 1 and 2.
- Step 4: When the supplied power, and temperature profiles (wall, gas, and bed) are stabilized, steady state conditions are established. The thermal steady state is assumed to be reached when the temperatures and the supplied power are both stable during at least 2 consecutive half hours, respectively with variations within 2°C or 0.01 kW. The logging is then stopped. The solids are discharged to assess the kiln hold up.

Examples of measured temperature profiles are given in Figures 7.3 and 7.4, when the kiln is equipped with straight lifters, rotated at a speed of 2 rpm and heated about 300°C in zone 2 and in both zones 1 and 2. It is shown that the temperatures measured at the wall rise steeply from the ambient to reach a plateau at about the given setpoint temperature. Following the heating of the kiln tube wall, the gas, and the solids bulk bed temperatures rise but at a lower rate and then remain constant. Figures 7.3 and 7.4 show that a thermal gradient may exist within the free-board gas especially between the upper and lower zones at a section of the hot kiln tube.

7.3 Heat transfer

7.3.1 Heat transfer mechanisms

Heat transfer in rotary kilns involves the exchange of energy via all the fundamental physical transfer mechanisms, i.e. conduction, convection and radiation. The heat transfer modes can be classified into three categories, corresponding to three zones, outside, inside, and across the kiln wall. Each mode may encompass one or more heat transfer mechanisms.

The dominant mechanism in supplying heat to the solid bed depends on: the kiln operating conditions, notably the heating temperature, the kiln tube design (mainly its diameter) and internal fixtures, and the thermal and physical properties of the solid particles, gas and the kiln wall.

As shown in Figure 7.5 which represents cross-sections of directly and indirectly heated rotary kilns equipped with lifters, the following heat fluxes may occur (without being exhaustive):

1. Φ_{cw-cb} , heat transfer flux between the covered wall and the bulk bed, including conduction and radiation.
2. Φ_{eb-g} , heat transfer flux between the exposed bed surface and the freeboard gas, including convection and radiation terms.
3. Φ_{ew-g} , heat transfer flux between the exposed wall and the freeboard gas, including convection and radiation terms.
4. Φ_{ew-cb} , heat transfer flux between the exposed bed surface and the exposed wall, only in terms of radiation.
5. Φ_{g-fs} , heat transfer flux between the freeboard gas and the falling solid particles by convection and radiation for kilns equipped with lifters.
6. S_0 , heat supplied by the heating system, either at the inner or outer kiln wall.
7. Φ_{loss} , heat loss at the kiln wall especially to the ambient for a directly heated rotary kiln by convection and radiation.

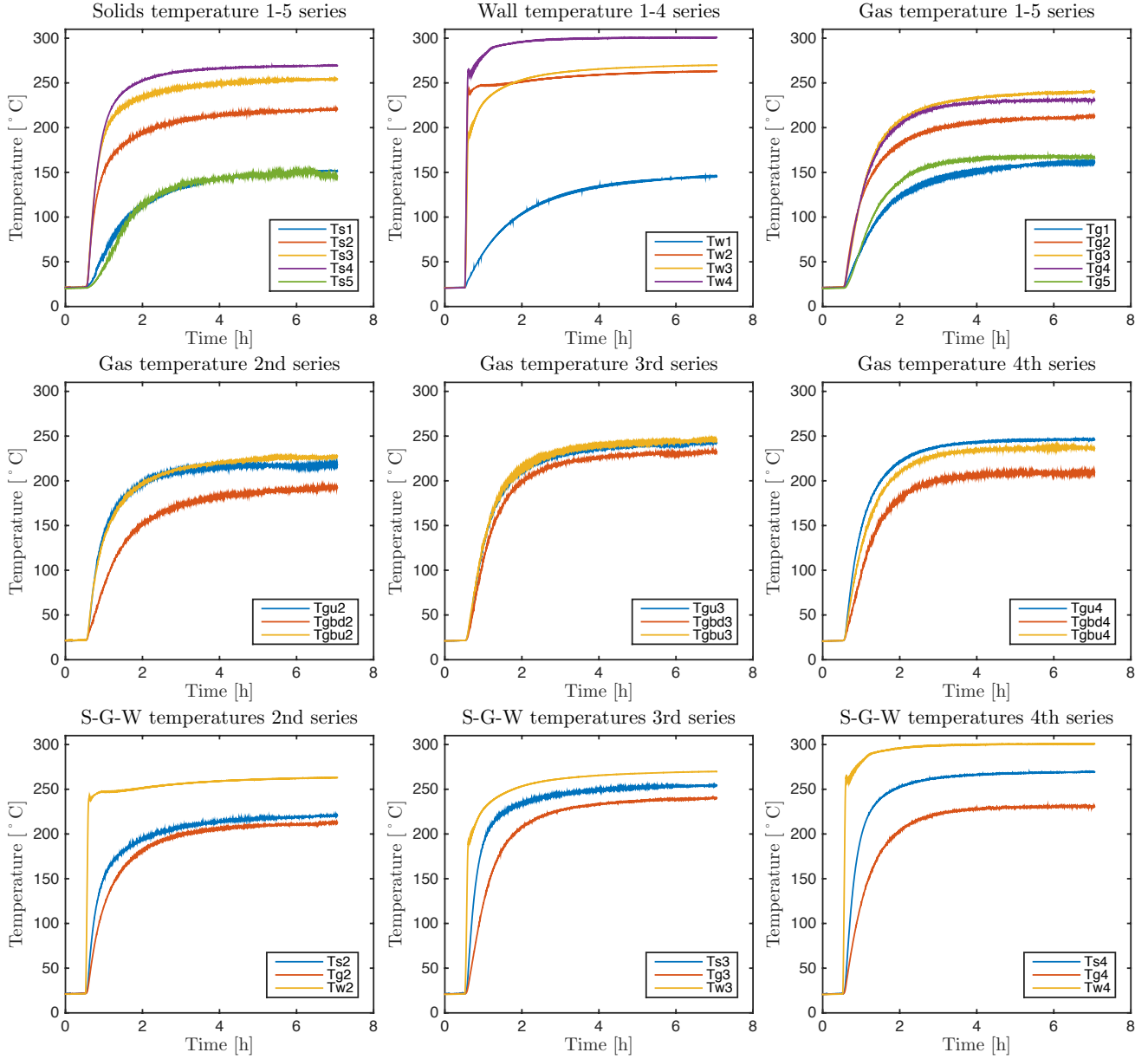


Figure 7.3: Experimental temperature profiles measured at the kiln outer wall, in the solids bed and in the freeboard gas. Operating conditions: 2 rpm rotation speed, 3° slope, 2.5 kg.h⁻¹ MFR, 33.5 mm exit dam height with straight lifters, and a setpoint temperature of 300°C in zone 2. The given wall and gas temperature profiles are the average of measurements within the sections S1 to S5 defined in Figure 7.2.

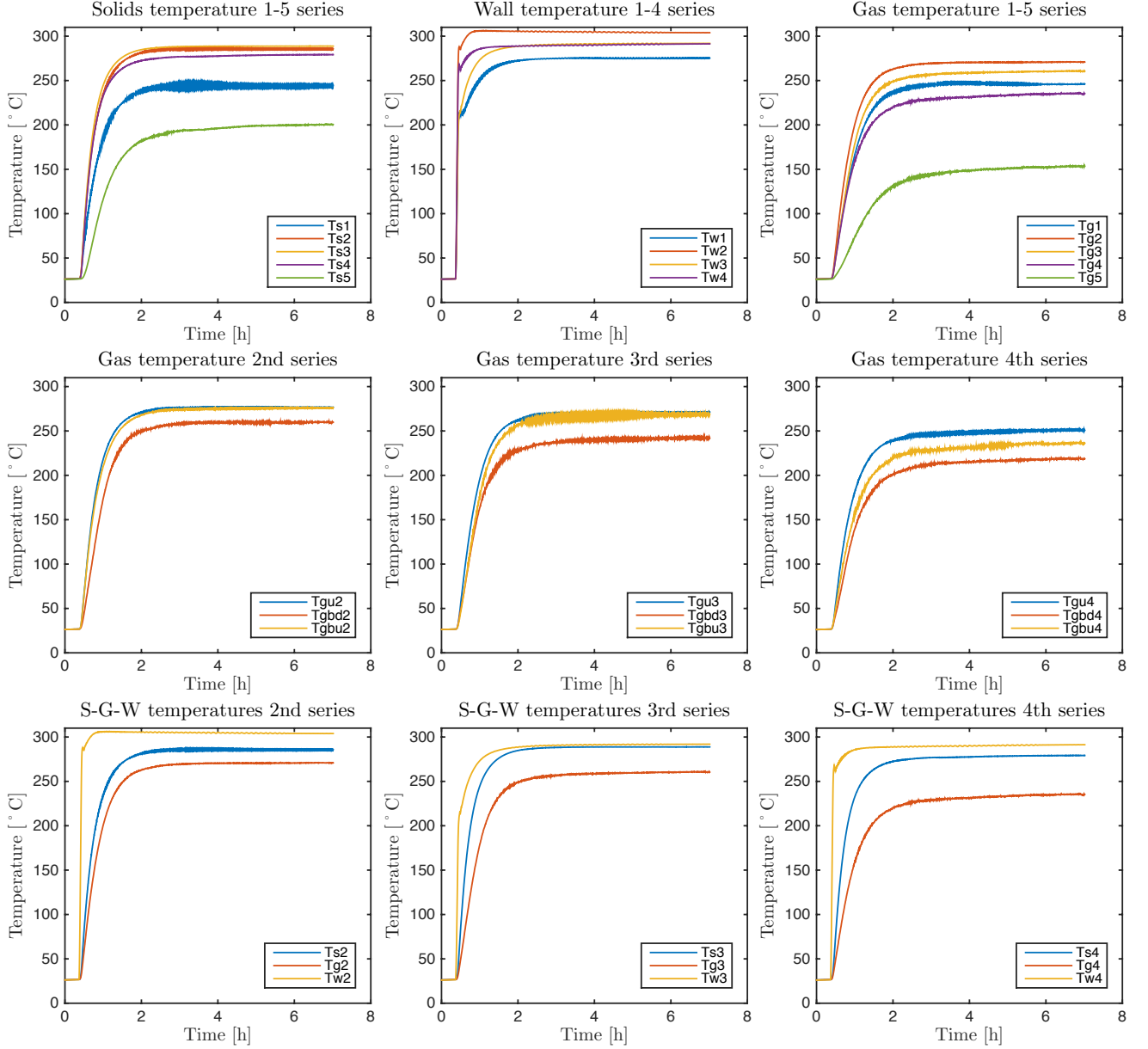


Figure 7.4: Experimental temperature profiles measured at the kiln outer wall, in the solids bed and in the freeboard gas. Operating conditions: 2 rpm rotation speed, 3° slope, 2.5 kg.h⁻¹ MFR, 33.5 mm exit dam height with straight lifters, and a setpoint temperature of 300°C in zone 1 and 2. The given wall and gas temperature profiles are the average of measurements within the sections (S1-S5) defined in Figure 7.2.

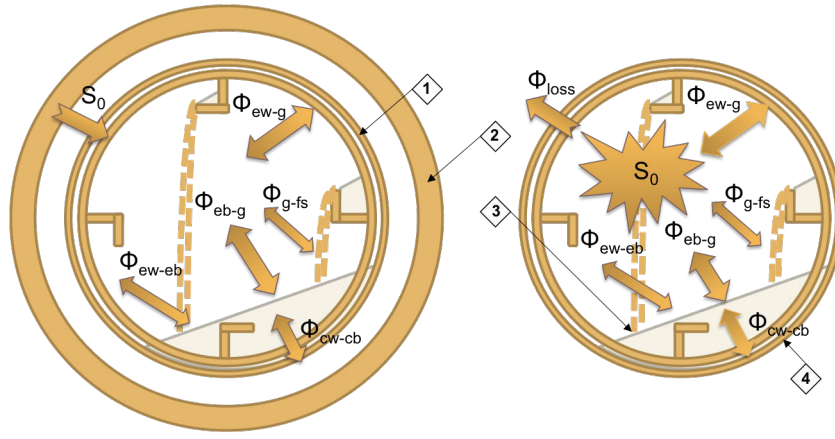


Figure 7.5: Heat transfer mechanisms in the cross section of indirectly (left) and directly (right) heated rotary kilns equipped with lifters. Herein: 1) exposed wall (ew), 2) heating elements, 3) exposed bed (eb), 4) covered wall (cw), covered bed (cb). In addition: g stands for gas, and fs for falling solids.

In this work, the following heat transfer paths are considered for the evaluation of the wall-to-solid heat transfer coefficient: wall to solid bed, wall to gas, solid bed to gas and conduction axially through the kiln wall (within non heated zone). Notice that in the absence of temperature recordings, the solids in the gas or in the lifters are not explicitly included.

7.3.2 Heat balance

Within the heating zone(s), a control volume is chosen between two sections at which the bed, gas and wall temperatures are recorded. As the bed and gas temperature variations between the selected sections is small, usually less than 15°C, the bed and gas temperature are assumed uniform in the control volume. The averaged gas and bed temperature between the two sections are considered. Notice that the control volume is positioned between S2 and S3 when heating both zones 1 and 2, and between S3 and S4 when heating only zone 2. The selected control volume can be regarded as a slice of the kiln tube wall; in the case of constant conductivity for steady conduction and no generation of heat, the heat balance at the wall assuming one dimensional heat conduction, convection and radiation is:

$$\rho_w c_{pw} \frac{\partial T_w}{\partial t} = \frac{\partial}{\partial z} \left(k_w \frac{\partial T_w}{\partial z} \right) + \frac{\Phi_w}{\Omega_w} \quad (7.4)$$

The heating of the wall is assumed uniform within the control volume, Ω_w^{ctrl} , so that there is no axial variation in the wall temperature, thus over a period $\Delta t = t_f - t_i$, Eq.7.4 simplifies as:

$$\rho_w c_{pw} \Omega_w^{ctrl} \frac{\Delta T_w}{\Delta t} = \Phi_w \quad (7.5)$$

$$\Phi_w = \Phi_{ew}^r + h_{ew-g}^{cv} A_{ew} LMTD_{ew-g} + h_{cw-cb} A_{cw} LMTD_{cw-cb} + S_0^{\Delta t} + \Phi_{loss}^{\Delta t} \quad (7.6)$$

Similar to heat-exchangers' problems, the logarithmic mean temperature differences (LMTD) are defined as follows:

$$LMTD_{ew-g} = \frac{(T_g^i - T_w^f) - (T_g^f - T_w^i)}{\ln \left(\frac{T_g^i - T_w^f}{T_g^f - T_w^i} \right)}, \quad LMTD_{cw-cb} = \frac{(T_b^i - T_w^f) - (T_b^f - T_w^i)}{\ln \left(\frac{T_b^i - T_w^f}{T_b^f - T_w^i} \right)} \quad (7.7)$$

The wall-to-solid heat transfer was then determined with the use of measured supplied power and temperature recordings through:

$$h_{cw-cb} = \frac{(\rho_w c_{pw} \Omega_w^{ctrl} \Delta T_w / \Delta t) - (\Phi_{ew}^r + h_{cw-g}^{cv} A_{ew} LMTD_{ew-g} + S_0^{\Delta t} + \Phi_{loss}^{\Delta t})}{A_{cw} LMTD_{cw-cb}} \quad (7.8)$$

Notice that the supplied power measured, Φ_{kiln} , includes the power delivered to the 2 motors driving the kiln tube and the screw feeder rotationally. These contributions are determined from measurements performed before starting the heating. The effective heating power at the heated zone(s), Φ_{eff} can then be deduced. Assuming that power uniformly and totally transferred to the wall by the resistors through radiation over the length, l_{Zone} , the heating power within the control volume of length, l_{ctrl} , is $S_0 = \Phi_{eff} \frac{l_{ctrl}}{l_{Zone}}$.

The losses are determined differently depending on whether both zones 1 and 2 are heated or only zone 2 is heated. In the former case, the heat losses include the heating of the measuring rod and the heat losses through the insulation. The temperature of the rod is assumed to be virtually equal to the gas temperature for the calculation. Hence, $\Phi_{loss} = \rho_{rod} c_{prod} \Omega_{rod}^{ctrl} \frac{\Delta T_{rod}}{\Delta t} + \phi_{ins} l_{ctrl}$; note that the rod is of the same material than the kiln tube and lifters. In the latter case, the heat losses include in addition the heat transfer within the wall by conduction toward the insulated zone 1 as well as the heat losses through the insulation. Indeed it can be seen in Figure 7.3 that the wall temperature increases also at the section S1 in the zone 1. For the calculation the losses are determined up to S1 using the temperature measured at that section giving: $\Phi_{loss} = \rho_{rod} c_{prod} \Omega_{rod}^{ctrl} \frac{\Delta T_{rod}}{\Delta t} + \rho_w c_{pw} \Omega_w^{S1-Zone2} \frac{l_{ctrl}}{l_{Zone}} \frac{\Delta T_w}{\Delta t} + \phi_{ins} l_{ctrl}$. Notice that the heat losses through the insulation covering the heating elements have been estimated for each heating temperature. When heating at 100, 300 and 500°C, the heat losses through the insulation per unit length, ϕ_{ins} , are respectively estimated about 50, 195 and 390 W.m⁻¹; details of the calculations are given in Appendix 7.6.1.

7.3.3 Convection and radiation modeling

7.3.3.1 Convective heat transfer

The convective heat transfer may occur between the freeboard gas and the boundaries limiting the gas volume. There is no axial forced flow of the gas, the heat transfer coefficient between the exposed wall and the gas can therefore be estimated with the use of the correlation presented in a companion paper [Bongo Njeng 2015d]:

$$Nu_{ew-g} = \frac{h_{ew-g} D_e}{k_g} = 0.1085 Re_\omega^{0.0275} Pr^{-0.4839} \left(\frac{l_g}{D} \right)^{-1.9284} \left(10^{-10} \frac{c_{pg} \rho_g T_g^\infty}{\omega \mu_g} \right)^{-0.2208} \quad (7.9)$$

herein, the Nusselt number is based on the equivalent diameter, $D_e = \frac{D(2\pi - \psi + \sin \psi)}{2(\pi - \psi/2 + \sin \psi/2)}$, which is a function of the filling angle (see Figure 7.6). Within the range of variation of the operating parameters set for the experiments, the application of Eq.7.9 yields coefficients higher than, or about, 10⁻² W.m⁻².K⁻¹.

7.3.3.2 Radiation heat transfer

For the calculation of the heat fluxes exchanged by radiation, [Oppenheim 1956] developed an electrical analogy for gray body where the following two quantities were defined:

1. Irradiance, E, the flux of energy that irradiates the surface, per unit area per unit time.

2. Radiosity, J , the total radiation energy streaming from the surface, per unit area per unit time. The radiosity is the summation of the irradiated energy that is reflected and the emitted radiation by the surface as follow:

$$J = \varepsilon \sigma T^4 + (1 - \varepsilon)E \quad (7.10)$$

The net heat flux leaving any particular surface can be written as the difference between J and E , giving with Eq.7.10:

$$\frac{\phi}{A} = J - E = \frac{\varepsilon}{1 - \varepsilon} (\sigma T^4 - J) \quad (7.11)$$

Considering a surface i reflecting on n surfaces referred to as j , it is possible to write [Sacadura 1993]:

$$J_i = \varepsilon_i \sigma T_i^4 + (1 - \varepsilon_i) \sum_{j=1}^n F_{i,j} \tau_g J_j + (1 - \varepsilon_i) \varepsilon_g \sigma T_g^4 \quad (7.12)$$

where $F_{i,j}$ is the view factor between the surface areas A_i and A_j . The view factor (or shape factor) is a purely geometrical parameter that accounts for the effects of orientation on radiation between surfaces. The view factor ranges between zero and one. [Gorog 1981] defined the view factors for the one-zone wall model as follows: $F_{bb} = 0$, $F_{bw} = F_{wg} = F_{bg} = 1$, $F_{wb} = \frac{A_{eb}}{A_{ew}}$, $F_{ww} = 1 - F_{wb}$. $\tau_g = 1 - \varepsilon_g$ is the fraction of irradiation transmitted through the gas. Considering A_i and A_j , Eq.7.12 can be written as a system of two unknowns, J_b and J_w :

$$\begin{bmatrix} Z_{bb} & Z_{bw} \\ Z_{wb} & Z_{ww} \end{bmatrix} \begin{bmatrix} J_b \\ J_w \end{bmatrix} = \begin{bmatrix} B_b \\ B_w \end{bmatrix} \quad (7.13)$$

with: $Z_{bb} = 1 - (1 - \varepsilon_b)F_{bb}(1 - \varepsilon_g)$, $Z_{bw} = -(1 - \varepsilon_b)F_{bw}(1 - \varepsilon_g)$, $Z_{wb} = -(1 - \varepsilon_w)F_{wb}(1 - \varepsilon_g)$, $Z_{ww} = 1 - (1 - \varepsilon_w)F_{ww}(1 - \varepsilon_g)$, $B_b = \varepsilon_b \sigma T_b^4 + (1 - \varepsilon_b) \varepsilon_g \sigma T_g^4$, and $B_w = \varepsilon_w \sigma T_w^4 + (1 - \varepsilon_w) \varepsilon_g \sigma T_g^4$.

When using Eq.7.11, the radiant heat transfer flux from the bed surface is expressed as:

$$\Phi_b^r = \frac{\varepsilon_b}{1 - \varepsilon_b} (\sigma T_b^4 - J_b) A_{eb} \quad (7.14)$$

The radiant heat transfer flux from the exposed wall, with the use of Eq.7.11, is given by:

$$\Phi_w^r = \frac{\varepsilon_w}{1 - \varepsilon_w} (\sigma T_w^4 - J_w) A_{ew} \quad (7.15)$$

Solving Eq.7.13 allows the determination of both radiosities J_b and J_w , and thus the estimation of the corresponding heat transfer flux.

7.3.4 Estimation of heat transfer areas

Accurate definition of the heat transfer areas is essential for the calculation of the heat fluxes (convective or radiative) on the one hand and the wall-to-solid heat transfer coefficient on the other hand. The knowledge of the bed depth, h_{bed} , or the kiln filling angle, ψ , is required for the determination of the main heat transfer areas, namely, A_{ew} , the interfacial area between the exposed wall (including lifters) and the free-board gas, A_{eb} , the interfacial area between the exposed wall and the free-board gas, and A_{cw} the interfacial area between the covered wall (including lifters) and the bed of solid particles, within the control volume of length l_{ctrl} . Figure 7.6 illustrates the bed depth, h_{bed} , and the kiln filling angle, ψ , as well as the main heat transfer areas presented above.

The bed depth is assumed almost flat along the kiln, even though it may not be the case at the kiln edges at the ends. Providing this assumption, the filling angle is determined from the measured kiln hold-up as follows:

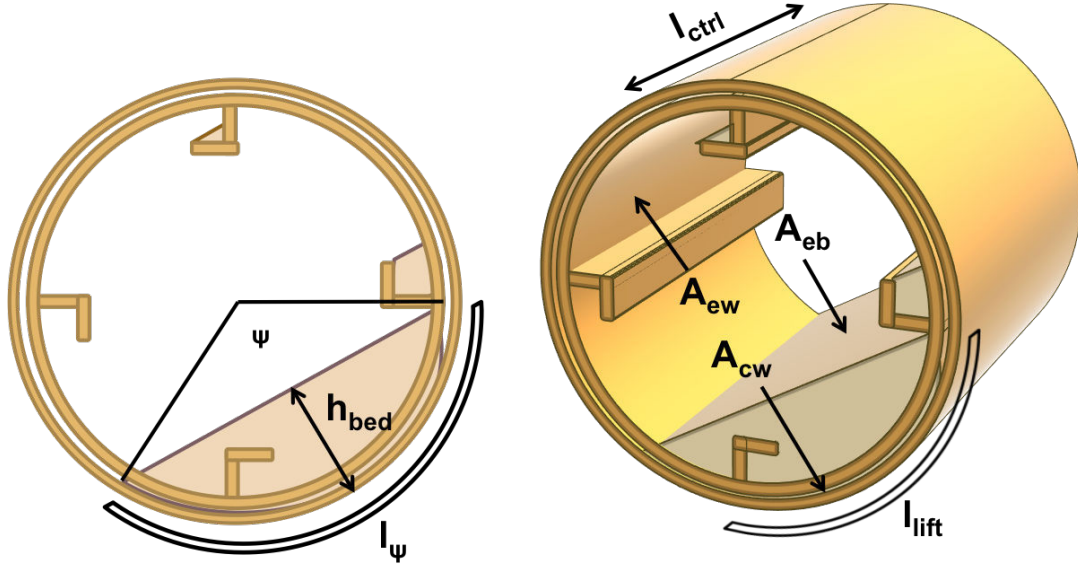


Figure 7.6: Kiln sections with nomenclature of the heat transfer areas, the bed depth and the filling angle.

$$\frac{HU}{\rho_b} = \Omega_b^{kilm} = R^2 \frac{\psi - \sin \psi}{2} L \quad (7.16)$$

With the use of the filling angle, the bed depth is then determined as follows:

$$h_{bed} = R \left(1 - \cos \frac{\psi}{2} \right) \quad (7.17)$$

Bed depth profile measurements have been performed for varying experimental conditions without lifters. These measurements are intended primarily to assess the experimental bed depth within the heating zone 2, where the control volume for the calculations is located. Therefore the measurements of bed depth were mainly located between the sections S1 and S5 (see Figure 7.2). For this purpose, a measuring rod equipped with 10 thin stems 50 mm in length and 5 mm in diameter, and rotating with the kiln is used. The stems were coated with glue, so that the bed depth could be assessed by measuring the height of hooked particles once steady flow conditions are achieved. Details about the set up and the experimental procedures are given in Appendix 7.6.2. Figure 7.7 displays the resulting bed depth profiles in zone 2 determined either by experimental measurements or with the use of Eqs. 7.16 and 7.17. As it can be seen in Figure 7.7, except in one case, the experimental bed depth measurements and the calculated bed depth agree well. It can also be mentioned that the bed depth increases with the mass flow rate or the exit dam height; these variations can be related to those of the hold-up with the operating parameters. The hold-up and the bed depth are linked, as suggested by Eqs. 7.16 and 7.17, higher hold-up may result in higher bed depth. These two last equations are then utilized for the determination of the bed depth and filling angle with the use of measured hold-up.

The identified heat transfer areas can then be determined as follows:

$$A_{ew} = \alpha \left(R(2\pi - \psi) + 2d_{eff}^{ew} n_{lift}^{ew} \right) l_{ctrl}, \quad n_{lift}^{ew} = n_{lift}^{total} - \frac{l_\psi}{l_{lift}} \quad (7.18)$$

$$A_{eb} = \beta \left(2\sqrt{h_{bed}D - h_{bed}^2} \right) l_{ctrl}, \quad (7.19)$$

$$A_{cw} = \gamma \left(R\psi + 2d_{eff}^{cw} n_{lift}^{cw} \right) l_{ctrl}, \quad n_{lift}^{cw} = \frac{l_\psi}{l_{lift}} \quad (7.20)$$

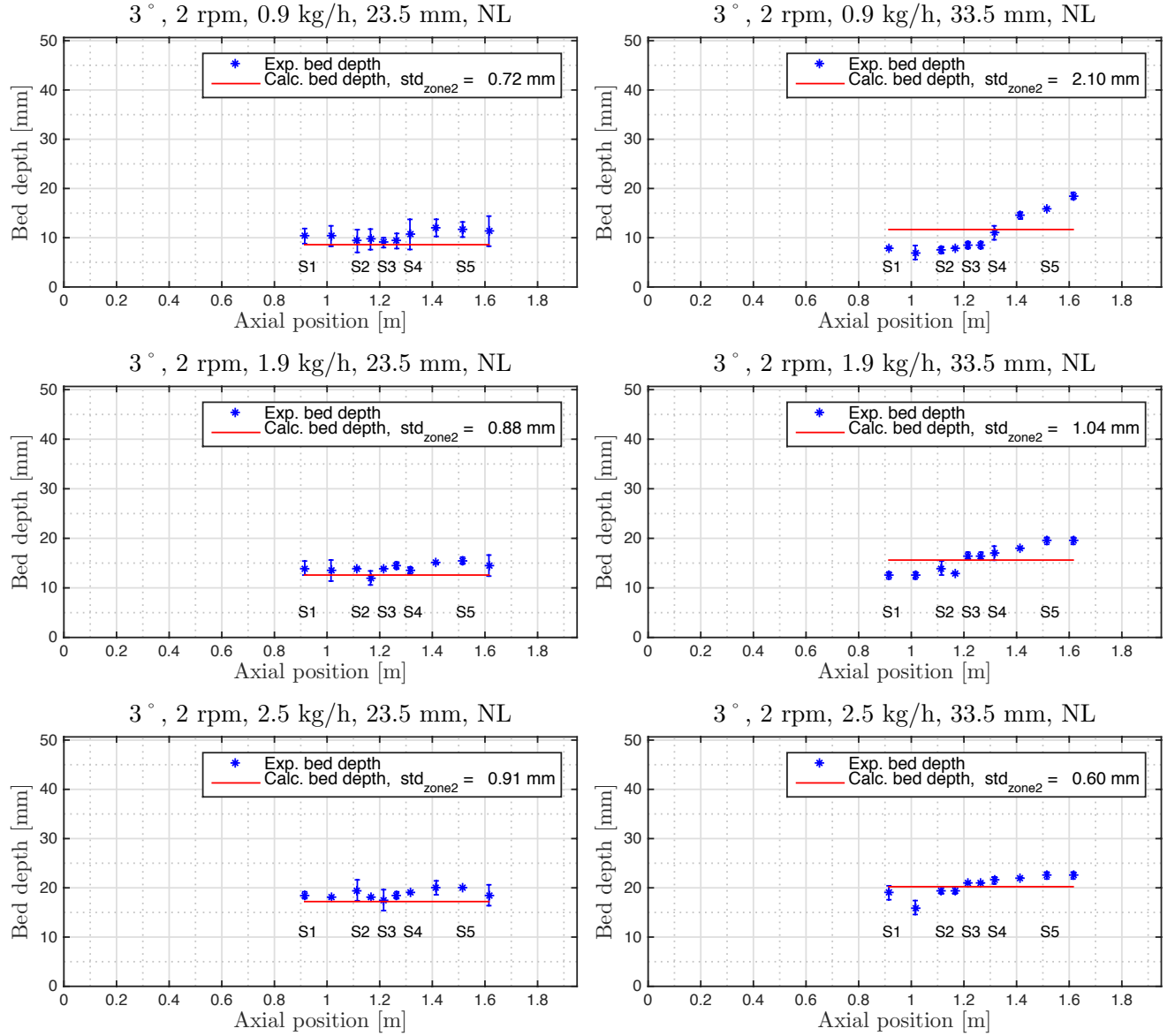


Figure 7.7: Experimental and calculated bed depth profiles in zone 2 for varying operating conditions without lifters. Eq.7.17 is used for the determination of the kiln bed depth. The standard deviation of the calculated bed depth with respect to the experimental measurements is also given.

The coefficients α , β and γ account for the smoothness of the surfaces. The internal kiln tube wall and the lifters can be considered as smooth surfaces, but this may not be the case for the surfaces at the exposed bed of solids or the contacting surface with the wall at the bottom of the bed. Therefore the coefficient α is set to 1, and measurement are performed to determine the coefficients β and γ . Using the AltiSurf 520 system, 3D micro-topography is performed over planar surfaces of solids 10 mm by 5 mm (3 replicates). The profilometric measurements shows that the heights of peaks and valleys along the surface are lower than 15% of the particle diameter on average, so that the surface at the exposed bed can be considered plane, and β can be taken as 1. Finally, γ , which accounts for the gas gap between the wall and solid particles, is determined by considering the percentage area filled with solid particles above the determined zero altitude; it is estimated about $84.83\% \pm 8.76$. This value is of the order about 80%, as given in the previous literature [Schl nder 1984a].

Both surface areas, A_{ew} and A_{cw} , account respectively for the fraction of the kiln wall circumference including lifters exposed or covered, within the control volume of length l_{ctrl} . The number of lifters within the covered wall, n_{lift}^{cw} , is estimated by the ratio of the arc length of the covered wall, l_{ψ} (see Figure 7.6), to the arc length between two consecutive lifters, l_{lift} (see Figure 7.6). The number of lifters, n_{lift}^{ew} , at the exposed wall is determined by subtracting n_{lift}^{cw} from the total number of lifters, n_{lift}^{total} . Regarding the lifters, instead of their actual length, the effective length for the heat transfer, d_{eff} , is used. An expression for the lifter effective length has been presented in a companion paper [Bongo Njeng 2015d].

7.4 Results and discussion

The evaluation of the wall-to-solid (w-t-s) heat transfer coefficient is achieved over a period Δt . This period is imposed by the time required for the measurement of the electrical power supplied to the unit. The measurement is performed using a multifunction meter, which displays the measured power every 30 min. The coefficient is then evaluated every half hour over the duration of the run from the temperature profiles and the supplied power.

7.4.1 Experimental wall-to-solid heat transfer coefficient

7.4.1.1 Time variation of the coefficient

Figure 7.8 represents the time variation of the w-t-s heat transfer coefficient for both runs, of which the experimental temperature profiles are shown in Figures 7.3 and 7.4. These experiments have similar experimental conditions except for the heating zone. For both, the results show a rapid increase of the coefficient during the two first hours and then it remains virtually constant, similar to the temperature profiles. One may expect very similar trends of the profiles, but there are some discrepancies between the two profiles with higher values of the coefficient for the experiment heating both zones 1 and 2. The difference observed can possibly be due to the hypothesis made while taking into account the losses. However the calculated error bars of the coefficients of these runs are mostly overlapping. Regarding the calculation of the uncertainties more details are given in the Appendix 7.6.3. For the global analysis of the results, the coefficient is averaged over the 4 last values determined, that is the last two hours of each run. For example, as given in Figure 7.8, the averaged w-t-s heat transfer coefficients are $293 \pm 32 \text{ W.m}^{-2}.\text{K}^{-1}$ and $249 \pm 29 \text{ W.m}^{-2}.\text{K}^{-1}$, respectively when heating the kiln in zone 2 and in both zones 1 and 2. The experimental results are summarized in Table 7.8 in the Appendix 7.6.4. These results are on average an order of magnitude higher than those found in a preliminary analysis of the wall-to-solid heat transfer coefficient using the lumped system analysis [Bongo Njeng 2015d].

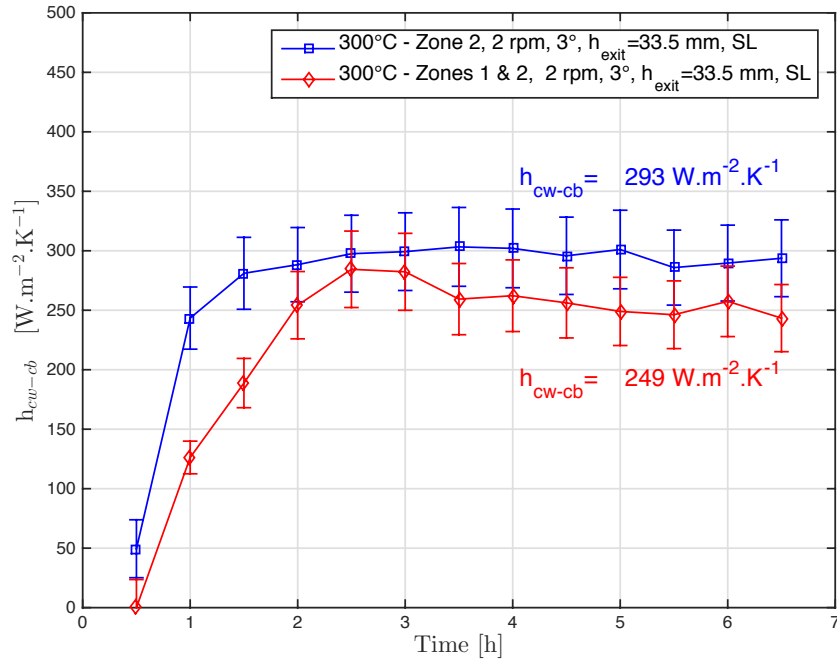


Figure 7.8: Time variation of the wall-to-solid heat transfer coefficient for both runs, of which the experimental temperature profiles are represented in Figures 7.3 and 7.4.

The reason for the difference can be attributed to the different methods (energy balance) and assumptions used for calculating the coefficient.

7.4.1.2 Effect of convection and radiation

Convective heat transfer has been mostly considered in literature for the case of directly heated kilns with turbulent conditions of the gas flow. If the order of magnitude for the wall-to-gas (w-t-g) heat transfer coefficient, in the case of no axial forced flow of the gas, determined above about $10^{-2} \text{ W.m}^{-2}.\text{K}^{-1}$ may seem quite small, it must be mentioned that while using a correlation recommended by [Incropera 1985], [Owens 1991] found for low gas flow within an industrial kiln of length-to-diameter 6.6, a w-t-g heat transfer coefficient about $1 \text{ W.m}^{-2}.\text{K}^{-1}$.

Radiation within the kiln may be very important and may dominate the heat transfer at high operating temperatures. [Ding 2001] specified that, in general, at temperature below 300-400°C, contribution of radiation is negligible, around 700-900°C, radiative and convective heat transfers are comparable, and above 1000°C the radiative transfer becomes dominant. In this study, experiments were achieved at low to medium temperature: 100-500°C.

Figures 7.9 shows the variation of the w-t-s heat transfer coefficient when assuming neither convection nor radiation, then only convection and finally both convection and radiation, at 100, 300 and 500°C setpoint temperatures. The results show that the convective heat transfer has no significant effect on the calculations of the w-t-s heat transfer coefficient. Indeed, whatever the setpoint temperature the error introduced by making the assumption of negligible convection is very small, about 0.05%. Whereas the effect of the radiative heat exchange at the wall on the heat transfer coefficient grows as the setpoint temperature increases. Had the radiation (and convection) been neglected, the calculations may have led to an overestimation of the heat transfer coefficient about 7% at 100°C, 13% at 300°C and 16% at 500°C on average.

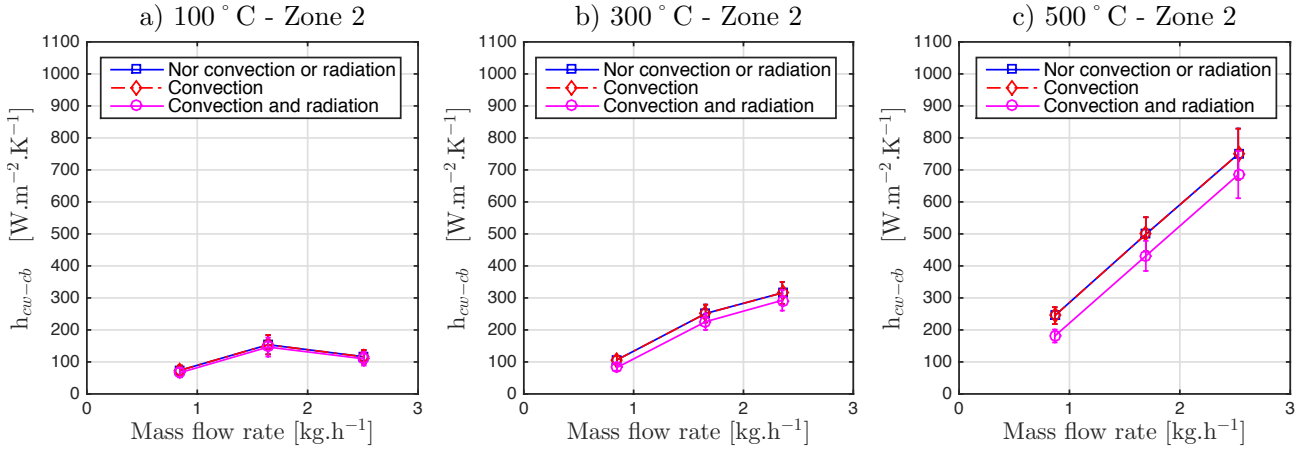


Figure 7.9: Effect of the convection and radiation heat transfers on the calculated value of the wall-to-solid heat transfer coefficient at different setpoint temperatures in zone 2: a) 100°C, b) 300°C and c) 500°C, while varying the mass flow rate, and operating at a rotational speed of 2 rpm, a kiln slope of 3°, an exit dam height of 33.5 mm and with straight lifters.

7.4.1.3 Effect of operating parameters

The influence of the operating parameters, namely the mass flow rate, the exit dam height and the lifter hold-up capacity on the w-t-s heat transfer coefficient are analyzed with the use of the filling degree similarly to [Bongo Njeng 2015d]. The filling degree has been found to increase with these operating parameters [Bongo Njeng 2015a, Bongo Njeng 2015b, Bongo Njeng 2015c]. Figure 7.10 shows the variation of the w-t-s heat transfer coefficient with the filling degree following a variation of the mass flow rate, the exit dam height and the lifter hold-up capacity. The results do not display a clear trend upward or downward contrary to what has been observed in a preliminary analysis. However these results confirm a preceding finding showing that the heat transfer can be enhanced depending on the lifter profile being used. Higher values of the heat transfer coefficient are obtained when using rectangular lifters while the coefficient is lower in the case of runs without lifter and even lower when using straight lifters.

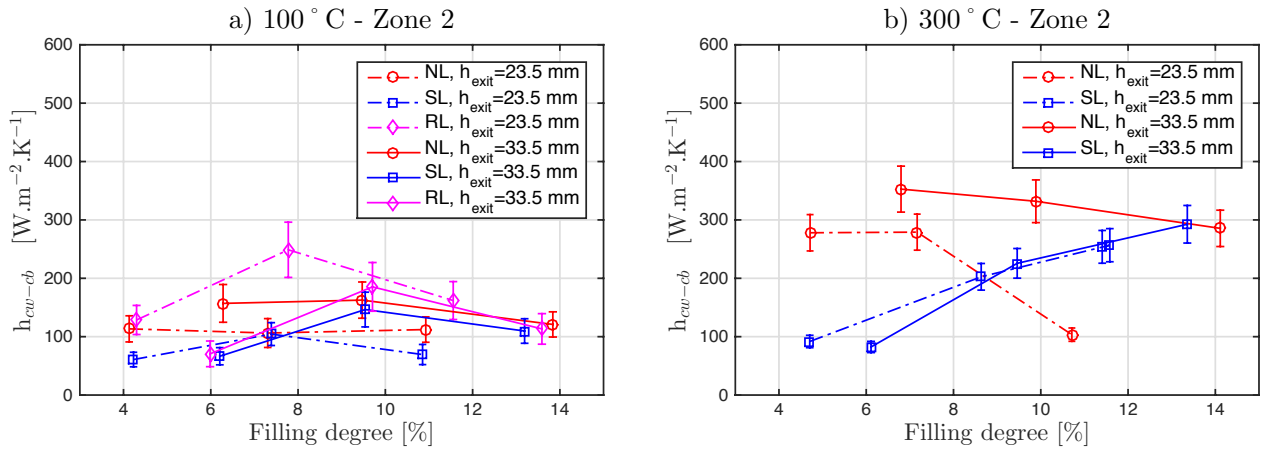


Figure 7.10: Variation of the wall-to-solid heat transfer coefficient with the filling degree at different setpoint temperatures in zone 2: a) 100°C and b) 300°C, while varying the lifters, the exit dam and the mass flow rate, and operating at a rotational speed of 2 rpm, a kiln slope of 3°.

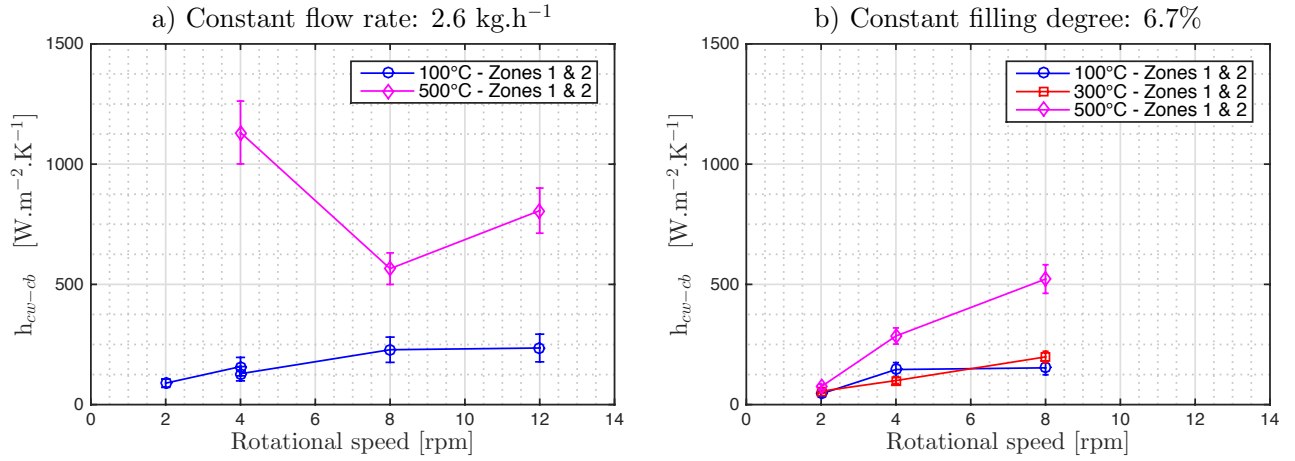


Figure 7.11: Variation of the wall-to-solid heat transfer coefficient with the kiln rotational speed at a) constant flow rate and b) constant filling degree, while heating in both zones 1 and 2, and operating a slope of 3° , with straight lifters and an exit dam (33.5 mm in height).

The effect of the rotational speed on the w-t-s heat transfer coefficient is shown in Figure 7.11. The rotational speed was varied while keeping a constant flow rate on the one hand and then a constant filling degree on the other hand. Except for the results obtained at a setpoint temperature of 500°C when varying the rotational speed at constant flow rate, the coefficient increases with the rotational speed. A similar trend has been found in a preliminary analysis [Bongo Njeng 2015d]. Hence, the rotational speed which promotes the mixing effect within the rotary kiln as well as the temperature set point can be identified as possible parameters that might be optimized in order to enhance the heat transfer, while also taking into account the whole set of operating parameters.

7.4.2 Modeling of the wall-to-solid heat transfer coefficient

Modeling the wall-to-solid heat transfer is a complex task in particular due to the strong non-linearity of the radiation heat transfer. As presented below, the wall-to-solid heat transfer has been correlated following a dimensional analysis. Then a comparison of the experimental results with predictions of models from literature is achieved.

7.4.2.1 Model

The main purpose of this model is to come up with a prediction of the heat transfer coefficient between wall and solid particles, to be used in a global model of rotary kiln. Within a heated zone, this model may take into account the kiln design, in particular the internal diameter, the bulk thermal properties, and the operating conditions, namely rotational speed, presence of lifters, filling degree and temperature set at the wall. Considering the Buckingham (II) theorem, the coefficient is expressed in terms of dimensionless numbers as follows [Delaplace 2014]:

$$h_{cw-cb} = K \frac{k_b}{l_\psi} \left(K_\alpha \frac{\omega D^2}{a_b} \right)^\alpha \left(K_\beta \frac{l_\psi}{D} \right)^\beta (K_\gamma [HU]\%)^\gamma \left(K_\delta \frac{T_w k_b^{0.4} c_{pb}^{0.6}}{\rho_b^{0.4} D^{2.8}} \right)^\delta \quad (7.21)$$

In Eq. 7.21, K , K_α , ..., K_δ , α , ..., δ are the model parameters, $\omega = \frac{2\pi}{60}N$ is the kiln angular speed, $a_b = \frac{k_b}{\rho_b c_{pb}}$ is the bulk diffusivity, $[HU]\%$ is the kiln filling degree in percent. Notice that: (1) the constant K_α , K_α , K_β , and K_δ , used to facilitate the model parameters determination,

are respectively set at 10^{-3} , 10, 10^{-2} , and 10^{-4} , (2) the effective bed conductivity, k_b , can be determined at the heating temperature at the wall, T_w , if the solids temperature is unknown. The model parameters given in Table 7.3 are determined through a Matlab script with the use of a nonlinear method based on iterative least squares estimation to minimize the discrepancy between the experimental results and the model calculations. These parameters are given with a confidence level of 95%. Figure 7.12 shows a comparison of the experimental results with the model calculations. Even though there are a few discrepancies, in general there is a good agreement between model calculations and experimental results within the 20% margins. If the model aims to be applied beyond its limits of validity, this must be done with a great deal of caution. At this point, let us mention that this model is mainly valid out of radiation dominated heat transfer, which is usually the case at low to medium heating temperatures. However, in the future the presented correlation can be suitably modified to better take into account effect of the radiation at very high temperature. This may require extending the experimental matrix to higher heating temperature at the wall, while at the same time varying the other parameters studied.

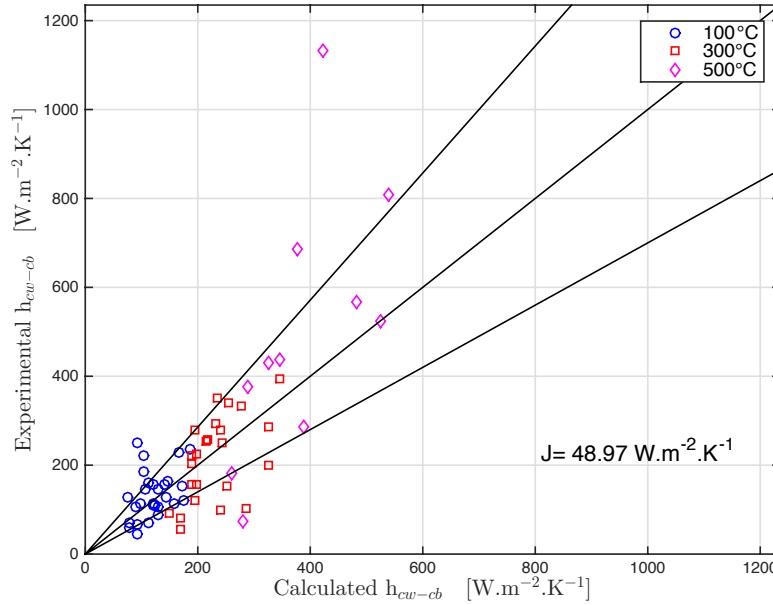


Figure 7.12: Comparison of experimental wall-to-solid heat transfer coefficients with predictions from Eq.7.21 using the set of parameters given in Table 7.3. Solid lines are $\pm 20\%$ margins.

Table 7.3: Estimated parameters for the model proposed for the wall-to-solid heat transfer coefficient, with associated confidence intervals.

	Model parameters	Confid. intervals	
		Inf.	Sup.
K	2.1371	-3.8809	8.1551
α	0.4531	0.2336	0.6725
β	-0.3507	-1.2654	0.5641
γ	0.9693	0.5039	1.4347
δ	1.4177	1.0082	1.8273

The set of parameters determined for Eq. 7.21 from the experimental results implies that the wall-to-solid heat transfer increases with the kiln rotational speed, the filling degree, and the heating temperature at the wall. Eventually, the coefficient also increases following an increase of the wall-to-solid contact area, possibly due to the presence of lifters. These later trends, even if not strictly established while analyzing the actual results, have been clearly established in a preliminary analysis in a companion paper [Bongo Njeng 2015d].

7.4.2.2 Predictive performance of selected models from literature

In this section, the experimental results are compared to the predictions of the models defined by [Wes 1976a, Tscheng 1979, Li 2005] as given respectively in Eqs. 7.1, 7.2 and 7.3. Figure 7.13 shows the comparison between experimental results and model predictions. In order to better assess the predictive performance of the different models, a criterion in performance assessments, J , is defined as follows:

$$J = \frac{1}{N_T} \sum_{i=1}^{i=N_T} \frac{(h_{cw-cb}^{i_{exp}} - h_{cw-cb}^{i_{calc}})^2}{h_{cw-cb}^{i_{exp}}} \quad (7.22)$$

This criterion can be defined as the sum of the relative square errors between predictions and experimental results, relative to the number of experiments, N_T . The lower the value of this criterion, the better the predictive performance of the model. Although it must be admitted that the 3 selected models give results in about the same order of magnitude as the experimental results, these results are significantly scattered across the 20% margins. In general these models failed to represent the variation of the coefficient with the operating parameters. None of these correlations explicitly accounts for the operating temperature; indeed the bed thermal conductivity varies very little as the temperatures is increased to 500°C. As a result, the predictions are virtually constant; this is notably the case for the predictions calculated from [Wes 1976a] correlation, which mostly vary with the rotational speed and nothing else. It must be noted, however, that at 100°C there is quite good agreement between the predicted and experimental results. In the case of the predictions obtained from [Tscheng 1979] correlation, the dispersal around the parity line appears greater than that previously observed; indeed Eq.7.2 takes account of the filling degree, rotational speed and temperature through the thermal diffusivity. The predictions calculated from [Li 2005] correlation display 3 patterns that are associated with the 3 heating

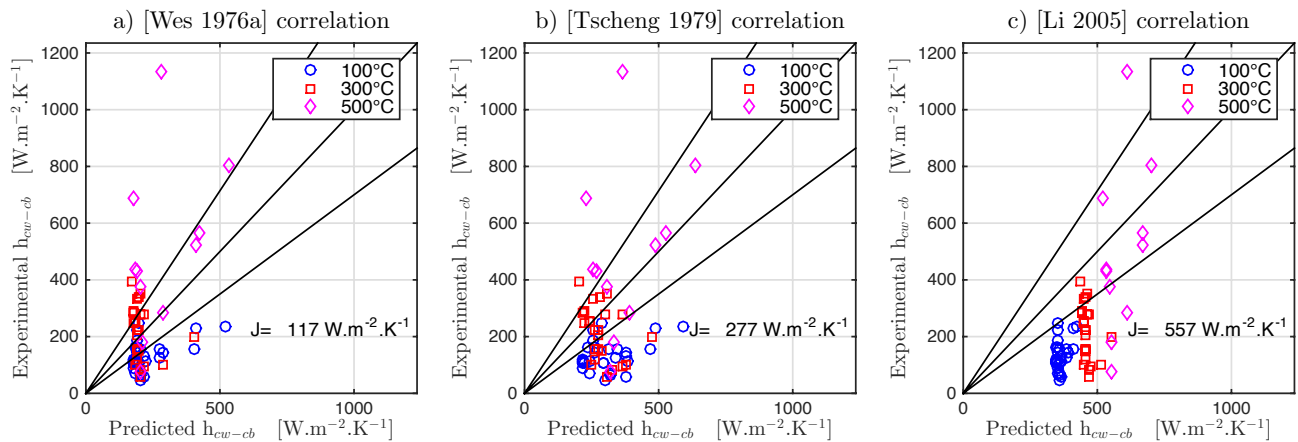


Figure 7.13: Comparison of the experimental wall-to-solid heat transfer coefficients with the predicted values from the correlations of: a) [Wes 1976a], b) [Tscheng 1979], c) [Li 2005]. Solid lines are $\pm 20\%$ margins.

temperatures set at wall in this study, very similar to the results from the correlation proposed by [Wes 1976a]; no other variation is observed. Among the 3 selected models, as shown in Figure 7.13, the lowest value of the criterion J is obtained from Eq.7.1 by [Wes 1976a]. Nonetheless, as given in Figure 7.12, let us mention that these criteria are 2 to 10 times higher than that obtained from Eq.7.21 while using the set of parameters given in Table 7.3.

7.5 Conclusion

In this study, the heat transfer coefficient between the wall and solids was investigated. The coefficient is determined from a heat balance with the use of experimental data comprising power supplied for the heating and temperature profiles measured within a continuously fed rotary kiln. The contact areas, through which the heat transmission occurs, have been defined so that the lifters presence, as well as surface roughness are taken into account. The main results of the above study can be summarized as follows:

- The wall-to-solid heat transfer coefficient was found to be of the order of magnitude about $10^3 \text{ W.m}^{-2}.\text{K}^{-1}$. It may be affected up to 24%, over the range of temperature set at the wall examined in this study, if the radiative heat transfer is neglected. The convection has little or no effect on this coefficient, in this case where there is no axial forced flow of gas.
- The effect of the operating parameters on the coefficient are not always obvious. However, in this study as also shown in [Bongo Njeng 2015d], the effect of the lifter design on the coefficient suggests a critical lifter design that may be well-suited in order to enhance the heat transfer. The coefficient is also found to increase with the rotational speed, especially at constant filling degree.
- From the experimental results, a model based on dimensional analysis is set for the prediction of the wall-to-solid heat transfer coefficient within rotary kilns. The correlation must be valid for a wide range of operating conditions. However, it should be applied to kilns operated at low to medium temperatures for a better confidence in the results. The proposed correlation successfully represents the majority of experimental results, at least better than the set of correlations selected to represent the experimental heat transfer coefficient.

List of symbols

A	Heat transfer area	m^2
a	thermal diffusivity	$[\text{m}^2.\text{s}^{-1}]$
c_p	Specific heat capacity	$\text{J.kg}^{-1}.\text{K}^{-1}$
d_{eff}	Length of lifter transferring heat	m
D	Kiln internal diameter	m
D_e	Equivalent diameter	m
d_p	Particle diameter	m
E	Irradiance	W.m^{-2}
F	View factor	-
h	Heat transfert coefficient	$\text{W.m}^{-2}.\text{K}^{-1}$
h_{exit}	Exit dam height	m

h_{bed}	Bed depth	m
HTC	Heat transfert coefficient	$\text{W.m}^{-2}.\text{K}^{-1}$
HU[%]	hold-up volume fraction or filling degree	-
J	Performance criterion	K
J	Radiosity	W.m^{-2}
k	Thermal conductivity	$\text{W.m}^{-1}.\text{K}^{-1}$
$K, K_{\alpha}, K_{\beta}, K_{\gamma}, K_{\delta}$	Model parameter	-
L	Kiln length	m
l_{ψ}	circumference of the covered wall	m
l_{ctrl}	Length between two sections within the kiln	m
l_g	Effective wall-to-gas contact length along the cross section between	m
l_{lift}	circumference between 2 consecutive lifters	m
LMTD	Logarithmic mean temperature difference	K
\dot{M}	Mass flow rate	kg.h^{-1}
N	Kiln rotational speed	rpm
NA	Not available	-
NL	No lifters	-
N_T	Total number of experiments	-
Pr	Prandtl number	-
R	Kiln radius	m
Re_w	Rotational Renolds number	-
rpm	Rotation per minute	-
RL	Rectangular lifters	-
S	Kiln slope	degree
S_0	Power supplied	W
SL	Straight lifters	-
t	Time	h
T	Temperature	K
TC	Thermocouple	-
t_c	wall-to-solid contact time	s
w-t-g	Wall-to-gas	-
w-t-s	wall-to-solid	-
z	Axial position	m

Greek letters

$\alpha, \beta, \gamma, \delta$	Fitting parameters	-
α, β, γ	Coefficients relative to the smoothness of surface	-
Δt	$t_f - t_i$	s
ϵ_0	Solid bulk porosity	-
ϵ	Emissivity	-
μ	Dynamic viscosity	$\text{kg.m}^{-1}.\text{s}^{-1}$
ρ	Density	kg.m^{-3}
τ_g	Fraction of irradiation transmitted through the gas	-
Φ	Heat transfer flux	W
ϕ	Heat transfer flux per unit length	W.m^{-1}
χ	Gas film thickness for that purpose a measuring rod was designed.	mm
ψ	Filling angle	rad
Ω	Volume	m^3
ω	Kiln rotational speed	rad/s

Subscripts and superscript

a	Ambiant	-
b	Bulk bed of solids	-
calc	Calculated	-
cb	Covered bed	-
ctrl	Control (volume)	-
cv	Convection	-
cw	Covered wall	-
eff	Effective	-
ew	Exposed wall	-
exp	Experimental	-
ext	External wall (insulation)	-
f	Final	-
fs	Falling solids particle	-
G,g	Gas	-
i	Initial	-
ins	Insulation	-
int	Internal wall (insulation)	-

gbd	Gas at the bottom in the left side of the kiln cross section	-
gbu	Gas at the top in the right side of the kiln cross section	-
gu	Gas at the top in the left side of the kiln cross section	-
lift	Lifters	-
loss	Losses	-
r	Radiation	-
S	Bulk bed of solids	-
W,w	Wall	-

7.6 Appendices

7.6.1 Calculation of the heat losses through the insulation

The heating zones are thermally isolated from surroundings using a 110 mm multilayer insulation constituted of alumina-based fiber. The heat loss per unit length of isolated kiln tube within heated zone(s) is estimated as follows:

$$\phi_{ins} = \pi D_{ins}^{ext} \frac{(T_w - T_a)}{R_{total}}$$

with the heat transfer resistance defined as follows:

$$R_{total} = R_{ins} + \frac{1}{h_{air}},$$

The thermal conductivity for insulation material is found in the literature [LANGLAIS 2004], a value of $k_{ins} = 0.125 \text{ W.m}^{-1}.\text{K}^{-1}$ is used for the calculations. The heat transfer resistance due to insulation is determined as follows:

$$R_{ins} = \frac{D_{ins}^{ext}}{2k_{ins}} \ln \left(\frac{D_{ins}^{ext}}{D_{ins}^{int}} \right)$$

The air side heat transfer coefficient is determined as follows:

$$h_{air} = h^r + h^{cv}$$

The heat transfer coefficient due to radiation at the insulation external wall is determined as follows:

$$h^r = \sigma \varepsilon_{ins}^{ext} \frac{(\bar{T}^4 - T_a^4)}{(\bar{T} - T_a)}$$

where the average temperature is $\bar{T} = \frac{T_a + T_{ins}^{ext}}{2}$, with T_{ins}^{ext} the temperature at the insulation cladding surface, and the value used in the calculation for the emissivity of the later surface is $\varepsilon_{ins}^{ext} = 0.05$.

The convective heat transfer coefficient is calculated based on a correlation by Churchill and Chu for the free convection from horizontal cylinders, but restricted to the laminar range of $10^{-6} < Gr Pr < 10^9$:

$$Nu_d = 0.36 + \frac{0.518 (Gr_d Pr)^{1/4}}{[1 + (0.0559/Pr)^{9/16}]^{4/9}}, \quad h^{cv} = \frac{Nu_d k_{air}}{D_{ins}^{ext}}$$

7.6.2 Bed depth profile measurements

The aim of the bed depth profile measurements was to measure precisely the bed depth in particular within the heating zone 2 of the kiln. For that purpose a measuring rod was designed. The rod is equipped with ten stems measuring 50 mm in length and 5 mm in diameter, and it can be easily fitted inside the kiln using the existing system used to hold the TC measuring rod. The stems are attached to the rod using boss-heads. The measuring rod and the stems' positions (numbered from 1 to 10) are shown in Figure 7.14. Note that positions 1, 3, 5, 7 and 9 highlighted in gray color correspond respectively to the sections S1 to S5 identified in Figure 7.2.

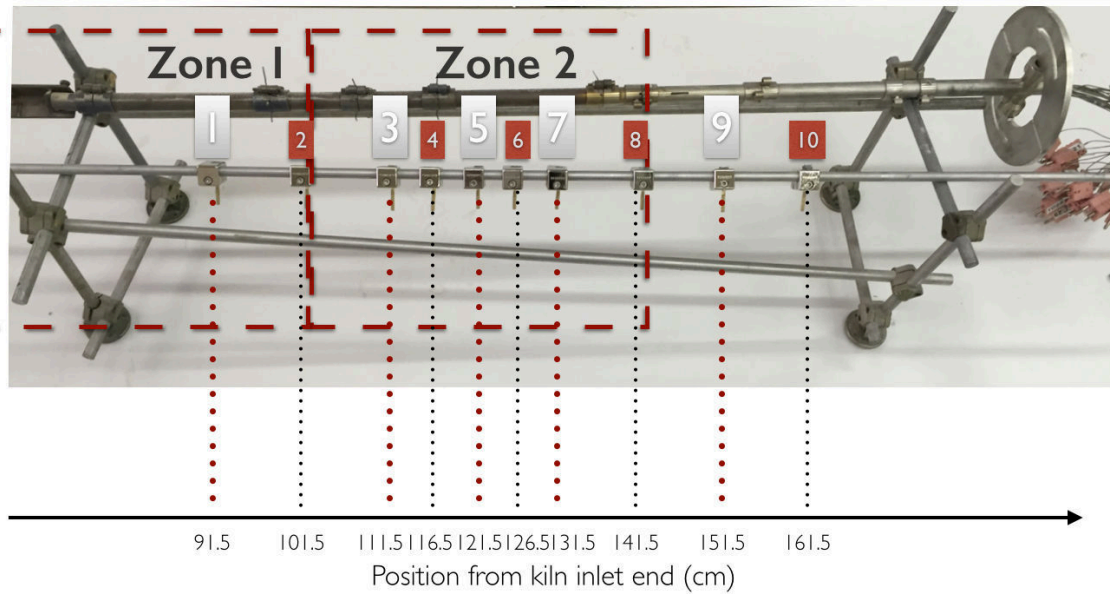


Figure 7.14: Bed depth measuring rod and position of the stems.

Figure 7.15 sums up the main steps of the procedure. Each run was repeated 2 or 3 times. The following experimental procedure was used to measure the bed depth:

- Step 1: The stems are cleaned and coated with glue over the whole length.
- Step 2: The measuring rod is then installed inside the kiln and its support fixed to the kiln frame.
- Step 3: Steady flow conditions are achieved following steps 1 and 2 as given in Section 2.3.1.1.1 above.
- Step 4: The bed burden is discharged and weighed following step 4 as given in Section 2.3.1.1.1 above.
- Step 5: The measuring rod is removed from the kiln and the height of particles clinging to the stems are measured using a slipping caliper.

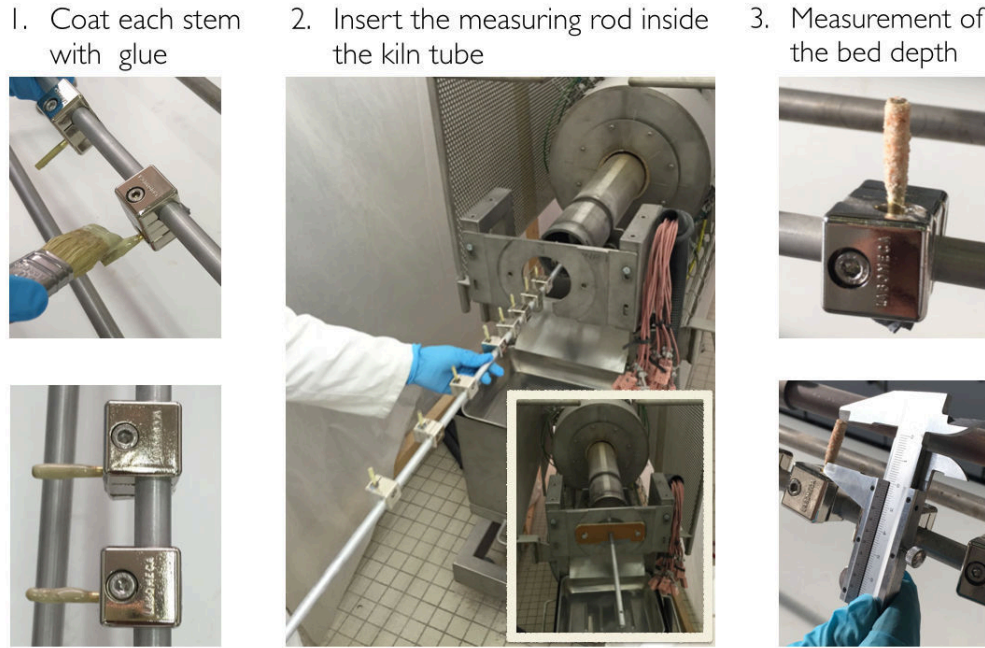


Figure 7.15: Experimental procedure for the bed depth measurement.

7.6.3 Uncertainties calculations

Let f be a function dependent on p independent variables: $f(x_1, x_2, \dots, x_j, \dots, x_p)$.

The uncertainty of the function f can be determined as follows [Rouaud 2013]:

$$(\Delta f)^2 = \sum_{j=1}^p \left[\left(\frac{\partial f}{\partial x_j} \right)^2 (\Delta x_j)^2 \right]$$

where Δx_j is the uncertainty of the independent variable. In our case the independent variables are measured, the value of their uncertainties were determined from the two existing approaches [Rouaud 2013]: Type A and Type B evaluations. The Type A estimates the uncertainty using statistics; this was used when repeated readings were available. The Type B estimates the uncertainty from calibration certificates, manufacturer's specifications, or calculations.

The uncertainties of variables used have been determined to calculate the uncertainty of the heat transfer coefficient in this study. The uncertainty of variables are given in Table 7.7.

Table 7.7: Calculated uncertainties.

Temperature	Power	Angular	Length	
$\Delta T_{g,b,w}$ [°C]	ΔS_o [kW]	$\Delta \psi$ [rad]	Δh_{bed} [mm]	$\Delta Length$ [mm]
0.1325	0.0058	0.0876	0.0011	$5.77 \cdot 10^{-5}$
$\Delta D, \Delta R, \Delta l_{ctrl}, \dots$				

7.6.4 Experimental results: wall-to-solid heat transfer coefficient

The experimental results for the wall-to-solid heat transfer coefficient are summarized in Table 7.8.

Table 7.8: Wall-to-solid heat transfer coefficients ($\text{W.m}^{-2}.\text{K}^{-1}$) calculated from Eq.7.8.

Operating conditions: Sand, S = 3°				Zone 2						Zone 1&2	
Setpoint T.	N	M	HU	Lifters	NL		SL		RL		SL
[°C]	[rpm]	[kg.h ⁻¹]	[%]	<i>h_{exit}</i> [mm]	23.5	33.5	23.5	33.5	23.5	33.5	33.5
100	2	0.7-0.9	3.97 - 6.7		113	157	61	67	129	71	45
	2	1.7-1.9	6.89 - 9.5		106	163	104	147	249	185	-
	2	2.4-2.6	10.43 - 13.30		112	121	69	110	162	113	89
300	2	0.7-0.9	3.97 - 6.7		278	353	92	82	-	-	56
	2	1.7-1.9	6.89 - 9.5		279	332	203	226	-	-	-
	2	2.4-2.6	10.43 - 13.30		104	286	257	293	-	-	249
500	2	0.7-0.9	3.97 - 6.7		-	-	-	181	-	-	74
	2	1.7-1.9	6.89 - 9.5		-	-	376	431	-	-	-
	2	2.4-2.6	10.43 - 13.30		-	-	436	685	-	-	NA
100	4	1.9	6.7		-	-	-	-	-	-	128
100	4	2.4-2.6	8		-	-	-	-	-	-	146
300	4	1.9	6.7		-	-	-	-	-	-	100
500	4	1.9	6.7		-	-	-	-	-	-	285
500	4	2.4-2.6	8		-	-	-	-	-	-	1132
100	8	3.2	6.7		-	-	-	-	-	-	228
100	8	2.4-2.6	6		-	-	-	-	-	-	153
300	8	3.2	6.7		-	-	-	-	-	-	198
500	8	3.2	6.7		-	-	-	-	-	-	522
500	8	2.4-2.6	6		-	-	-	-	-	-	565
100	12	2.4-2.6	5		-	-	-	-	-	-	235
500	12	2.4-2.6	5		-	-	-	-	-	-	807

Chapter 8

A simplified global model for the prediction of axial temperature profiles in flighted rotary kilns

Abstract	212
8.1 Introduction	213
8.2 Model description	214
8.2.1 Description of the flow model	214
8.2.2 Description of the thermal model	218
8.3 Experimental data for validation of the global model	223
8.4 Results and discussion	224
8.4.1 Steady state simulation	225
8.4.2 Dynamic simulation	229
8.5 Conclusion	230
8.6 Appendices	233
8.6.1 Experimental apparatus characteristics	233
8.6.2 Model parameters	233

Abstract

Abstract:

Rotary kilns are gas-solid reactors widely used in mineral process applications and other processes applied to specific granular materials in fields such as pharmaceutical or food-processing industries. The operation of such kilns or even their design can lead to some problems which may require accurate model simulations to be solved. In this paper, a simple model for indirectly heated flighted rotary kilns is developed for the prediction of axial profiles and transient responses of the temperature of the bulk bed, free-board gas, and kiln wall. The model validation was conducted in the absence of any chemical reactions in order to validate the sub-models used for the predictions of flow characteristics as well as the heat transfer fluxes, notably the convective heat transfer and the wall-to-solid heat transfer. Comparison of the results from the simulation of the global model with experimental data indicates mixed results. However, a good definition of the model parameters may significantly increase the accuracy of results. Therefore, the present model can serve as the backbone for the simulation of a kiln handling specific reactions. Dynamic simulations of the model are also investigated. Such a model can then be used in understanding and optimizing kiln operation or design.

Résumé :

Les fours tournants sont des contacteurs gaz/solide utilisés comme réacteur dans le domaine du ciment mais aussi dans les industries pharmaceutique et agroalimentaire à titre d'exemple. La mise en œuvre de ces équipements ainsi que leur conception peuvent occasionner des problèmes nécessitant le recours à la simulation de procédés pour être dénoués. Dans cette étude, un modèle simplifié a été développé pour simuler le fonctionnement de fours tournants à chauffage indirect, équipés ou non de rehausseurs, et pour déterminer les profils axiaux et les réponses transitoires de la température des phases gazeuse et solide, et à la paroi. Pour la validation du modèle, les données expérimentales sont obtenues en l'absence de réactions chimiques afin de limiter la validation aux seuls modèles utilisés pour la description du transport de la charge et pour le transfert de chaleur, notamment, le coefficient d'échange convectif et le coefficient d'échange paroi/solide. La comparaison des résultats de simulation avec les relevés expérimentaux reste assez mitigée. Cependant, une meilleure définition des paramètres sensibles du modèle permettrait d'améliorer significativement la précision des simulations. Ce modèle pourrait servir de base pour la simulation de fours tournants en présence d'une ou plusieurs réactions chimiques. Des simulations en régime dynamique du modèle ont été effectuées. Ainsi le modèle pourrait être utilisé à des fins d'optimisation des procédures opératoires mais aussi de design.

8.1 Introduction

Rotary kilns are complex systems whose operation may involve a significant number of processes within the bulk bed, the free-board gas and the wall, irrespective of the industrial application in which they are used. However in most cases, specific chemical reactions may take place within the kiln, sometimes at temperatures higher than 1000°C. In order to understand the underlying mechanisms and propose optimal operating conditions for existing installations as well as to optimize the design of new units, several models have been proposed in the literature. As presented below, they are either steady state models or dynamic models.

A variety of steady state models have been established for directly and indirectly heated rotary kilns. Following the studies for example by [Wes 1976a, Brimacombe 1978], they are mostly based on the earlier models for the flow described by [Friedman 1949, Saeman 1951, Matchett 1987] and the heat transfer models developed by [Tscheng 1979, Jenkins 1981, Gorog 1981, Gorog 1982, Gorog 1983, Schlünder 1984a]. [Boateng 1993] developed a quasi three-dimensional rotary kiln model. The model is a combination of a two-dimensional thermal model of a transverse plane and a one-dimensional plug flow type thermal model considering the transverse slice of the rotary kiln. Results from the model were compared to the temperature measurements of [Barr 1989b], and good agreement was found. Later, [Li 2005] developed a model for a directly heated counter-current rotary kiln. The experiments by [Barr 1989b] were also used for the model validation. Comparison of the predicted temperature profiles with experiments showed good agreement, although some discrepancies appeared when comparing predictions with experimental measurements for heat transfer rates; these discrepancies were small, however, for the steady values.

[Cao 2000] developed a dynamic global model for a directly heated rotary kiln (dryer) equipped with lifters. The model was based on fundamental mass and energy balances, and the kiln was divided into a number of equally sized control volumes. A linear falling rate curve was used to describe the drying kinetic and the models by [Matchett 1987, Ranz 1952] were used respectively to describe the retention time and the wall-to-solid heat transfer coefficient. For the model validation, predicted parameters were compared to the measurements obtained while processing sorghum grains. Discrepancies lower than 10% were reported for the outlet solids moisture content and temperature. [Descoins 2003] developed a dynamic model used to describe the operation of a pilot rotary kiln, indirectly heated, and processing wood. From the model of [Saeman 1951], a dynamic model was derived for the solids motion. The reaction scheme for the wood pyrolysis was based on the work by [Miller 1996, Mousques 2001]. The heat transfer mechanisms were described with the use of the models proposed by [Lybaert 1985, Tscheng 1979, Sacadura 1993]. The dynamic solids motion predictions were in good agreement with the experiments. However the global model was not validated by experiments, only results from simulations were presented.

All these models have in common: 1) a flow model which describes the solids motion, notably the bed depth within the kiln and 2) a heat transfer model which describes the basic heat transfer mechanisms occurring within solids and gas phases, and the kiln wall. In the present study, the focus is on the definition of a simple global model for an indirectly heated rotary kiln, processing a bulk of solids in the absence of any chemical reactions so as to validate the flow and heat transfer sub-models used for the determination of the axial profiles and transient response of the bulk bed, free-board gas and wall temperature; the results of interest are notably those related to the bulk bed within the heated zone.

In the next section, the model is fully described, beginning with the flow model. A 0-dimension model was used. Bed depth profiles from this model are compared to the dynamic Saeman model by [Descoins 2005], and experimental data; secondly the heat transfer model is detailed. Then simulation results are analyzed and compared with experimental data; a sensitivity analysis of the model to its parameters is achieved for the bulk bed temperature; results of dynamic simulations are also presented. Key conclusions based on this work are discussed at the end.

8.2 Model description

The knowledge of heat transfer phenomena and solids hydrodynamics are essential for the operation of rotary kilns. Mathematical modeling coupled to computer simulation are relevant tools for the analysis of the effects of changes in operating conditions with the aim of improving the process knowledge and supporting scale up. Therefore a basic global model for the prediction of the transient behavior of indirectly heated rotary kilns is developed in this section, notably for the prediction of the bulk bed temperature profile.

The kiln model consists of one-dimensional unsteady heat transfer equations for the bulk bed, free-board gas and wall; the bed depth of solid particles is assessed from the kiln filling degree in given process conditions and is considered constant along the kiln. Additional equations are used: on the one hand for the convective and radiative heat transfers, and the wall-to-solid heat transfer; and on the other hand for the materials thermo-physical properties. Chemical reactions taking place within the bulk of solids flowing through the kiln are not taken into account. The case study focused solely on the heat transfer phenomena within the kiln at low to medium heating temperatures (up to 500°C).

8.2.1 Description of the flow model

The behavior of the solids within the apparatus, notably the bed depth shapes by the solid particles flowing at the bottom of the kiln, has a significant influence on the heat transfer. This is due to the dependency of the heat transfer areas on the bed depth or filling degree, as shown in [Bongo Njeng 2015e]. The simplification assumed in this basic model as highlighted before is a constant bed depth and thus a constant filling degree along the kiln. This is more likely to happen far from the kiln edges.

The filling degree can be estimated from the operating conditions using the following correlation [Bongo Njeng 2015c]:

$$HU[\%] = k \frac{\rho_b L \pi D_i^2}{4} \left(\frac{N^2 D_i}{g} \right)^\alpha \left(\frac{D_{ex}}{D_i} \right)^\beta \left(\frac{\theta}{S} \right)^\gamma \left(\frac{\dot{M}}{\rho_b D_i^2 \sqrt{gL}} \right)^\delta \left(\frac{4S_{lift}}{\pi D_i^2} \right)^\epsilon \left(\frac{\rho_b}{\rho_{tapped}} \right)^\zeta \left(\frac{L}{D_i} \right)^\eta \quad (8.1)$$

where ρ_{bulk} is the bulk density of materials, L is the length of the kiln, D_i is the internal diameter of the kiln, N is the rotational speed, g is the gravitational acceleration, D_{ex} is the exit diameter, θ is the angle of repose of the bulk materials, S is the kiln slope, \dot{M} is the mass flow rate, S_{lift} is the cross section of solids in lifters and ρ_{tapped} is the tapped density of the solid bed. The values of the model parameters k , α , β , γ , δ , ϵ and ζ are given in Table 8.1. The hold up can then be calculated as follows:

$$HU = \frac{HU[\%]}{100} \cdot \pi R^2 L \rho_b \quad (8.2)$$

where R is the kiln radius. Assuming a flat bed with a constant depth along the kiln length, the volume of solids within the kiln can be determined as follows:

$$\Omega_{bulk}^{kiln} = R^2 \frac{\psi - \sin \psi}{2} L \quad (8.3)$$

where ψ is the filling angle. The filling angle is then determined from Eqs.8.2 and 8.3 by solving the following equation:

$$\frac{HU}{\rho_b} = R^2 \frac{\psi - \sin \psi}{2} L \quad (8.4)$$

The bed depth is then defined by:

$$h = R \left(1 - \cos \frac{\psi}{2} \right) \quad (8.5)$$

Otherwise the ordinary differential equation established by [Descoins 2005] based on the work by [Saeman 1951] can also be used to compute the bed depth:

$$F_h^{1/2} \frac{\partial h(z, t)}{\partial t} - \frac{U^T \tan(S)}{\sin(\theta)} F_h^{1/2} (1 - F_h)^{1/2} \frac{\partial h(z, t)}{\partial z} = \frac{\partial}{\partial z} \left(\frac{U^T}{3} R \cot(\theta) F_h^{3/2} \frac{\partial h(z, t)}{\partial z} \right) \quad (8.6)$$

$$\text{Outlet end boundary} \quad h(z = L, t) = h_{exit} \quad (8.7)$$

$$\text{Inlet end boundary} \quad \left. \frac{\partial h(z, t)}{\partial z} \right|_{z=0, t} = \frac{3Q_v|_t \tan(\theta)}{2U^T R^2} (F_h^{-3/2})_{z=0, t} - \frac{\tan(S)}{\cos(\theta)} \quad (8.8)$$

$$\text{Initial condition} \quad \left. \frac{\partial h(z, t)}{\partial z} \right|_{z, t_0} = \frac{3Q_v|_{t_0} \tan(\theta)}{2U^T R^2} (F_h^{-3/2})_{z, t_0} - \frac{\tan(S)}{\cos(\theta)} \quad (8.9)$$

where $F_h = \frac{2h(z, t)}{R} - \frac{h(z, t)^2}{R^2}$, and $U^T = 2\pi NR$ is the transverse rotation speed of the cylinder, and $Q_v = \frac{\dot{M}}{\rho_b}$ is the volumetric flow rate.

Table 8.1: Parameters for the models used to calculate of the filling degree and the mean residence time [Bongo Njeng 2015c].

Model	HU[%]	\bar{t}
parameters	Value	Value
k	45.65	0.0026
α	-0.4439	-0.4422
β	-0.3987	-0.3597
γ	0.7780	0.9276
δ	0.9584	-0.1130
ϵ	-3.8197	-8.8835
ζ	16.763	-2.4641
η	0	1.1

8.2.1.1 Comparison of bed depth predictions with experimental measurements at steady state conditions

The experimental bed depth profile measurements presented in [Bongo Njeng 2015e] and achieved at steady flow conditions were used to assess the accuracy of the predictions of the presented models. Three methods of calculation were used for the determination of the bed depth, the first two assume a constant bed depth as described above. In both cases, the bed depth is obtained from Eqs.8.4 and 8.5; the only difference between the two is that in one case the experimental HU is used whereas in the other case the HU is estimated from Eq.8.1. The third method is based on the model by [Saeman 1951] which can determine the bed depth as a function of the axial position by solving the following ordinary differential equation for given operating conditions:

$$\frac{dh(z)}{dz} = \frac{3Q_v \tan(\theta)}{4\pi NR^3} \left(\frac{2h(z)}{R} - \frac{h(z)}{R^2} \right)^{-3/2} - \frac{\tan(S)}{\cos(\theta)} \text{ and } h(z=L) = h_{exit} \quad (8.10)$$

In Figure 8.1, the experimental bed depth profiles obtained for varying operating conditions without lifters, are compared with the predicted values determined from experimental HU, predicted HU and the [Saeman 1951] model. In general, the predictive performance of these 3 methods of calculation is low, as can be seen from the discrepancies observed between the measured bed profiles and the predictions. The experimental bed depth profile measurements were achieved with an exit dam fitted at the kiln outlet end. Therefore, depending on the experimental conditions, specifically the exit dam height, the bed profiles display an incline near the kiln outlet end, which is fairly well represented by the [Saeman 1951] model. Away from the kiln tube edges, the predicted bed depth value from experimental HU agrees quite well with the measurements, while the predictions obtained from calculated HU (Eq.8.1) and the [Saeman 1951] model are slightly lower than experimental values and quasi superimposed most of the time.

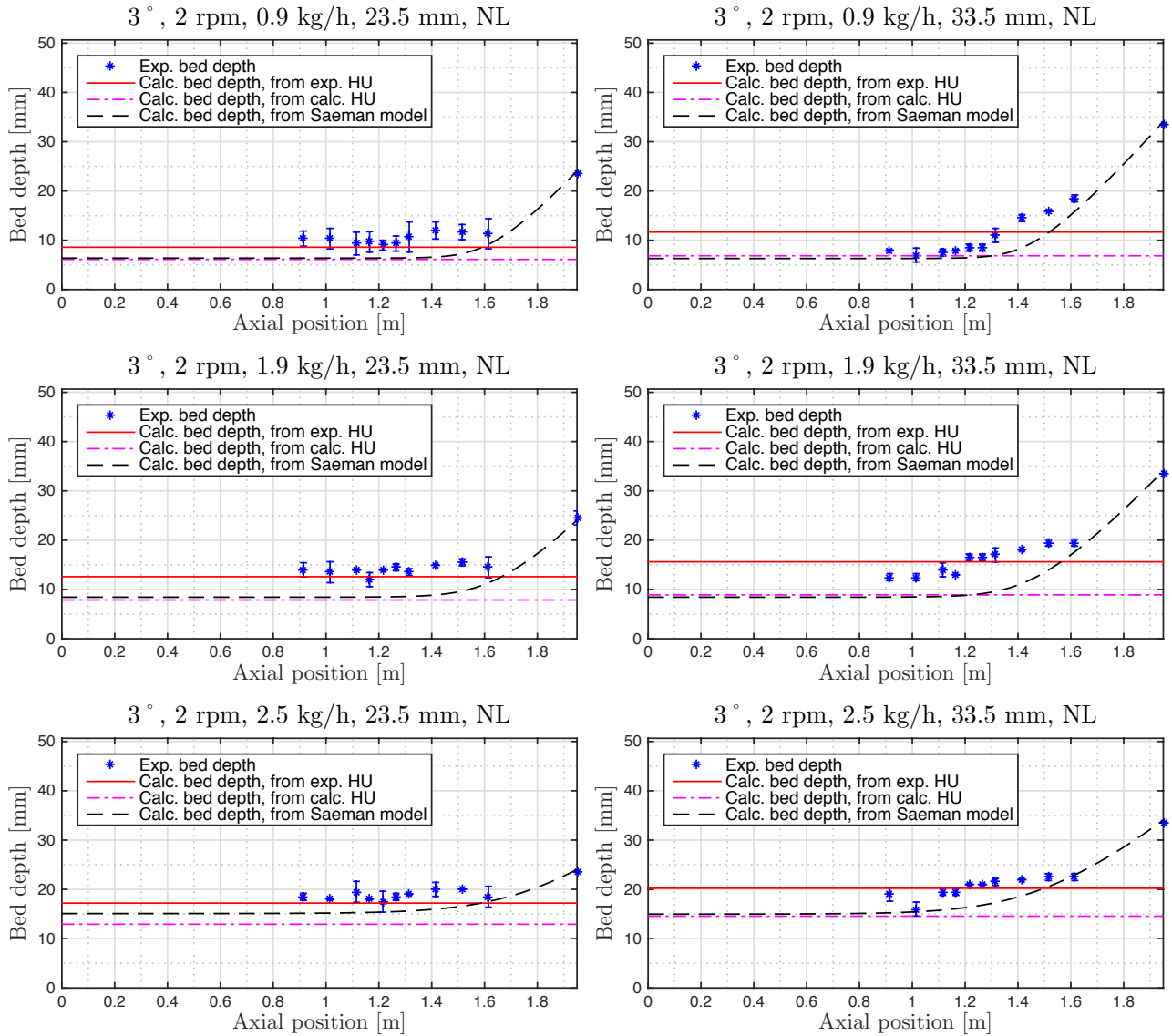


Figure 8.1: Comparison of bed depth predictions with experimental measurements. Notice that the mass flow rate is determined within $\pm 0.3 \text{ kg} \cdot \text{h}^{-1}$.

8.2.1.2 Transient response to a step change in operating parameters: mass flow rate and rotational speed

If the bed depth is considered constant along the kiln length at steady state conditions, it must nevertheless vary with time when the value of an operating parameter changes. An equation for the transitory regime can be established from the differentiation with respect to time of Eqs.8.5 and 8.4. Noting further that $HU = \tau \dot{M}$, with τ the time of passage, the derivative of these two equations is as follows:

$$\frac{dh}{dt} = \frac{R}{2} \sin\left(\frac{\psi}{2}\right) \frac{d\psi}{dt} \text{ and } \frac{\tau}{\rho_b} \frac{d\dot{M}}{dt} = \frac{R^2 L}{2} (1 - \cos(\psi)) \frac{d\psi}{dt} \quad (8.11)$$

From Eq.8.5, it comes that $\psi = 2 \arccos(1 - h/R)$ and noticing that $(1 - \cos(\psi)) = 2 \sin^2\left(\frac{\psi}{2}\right)$, combining these later equations yields:

$$\frac{dh}{dt} = \frac{\tau}{2RL\rho_b \sin(\arccos(1 - h/R))} \frac{d\dot{M}}{dt} \quad (8.12)$$

For the simulation of a step change in the value of an operating parameter, the initial bed depth is determined from Eq.8.5, for the resolution of the given ordinary differential equation. When solids pass through the kiln in plug flow, the time of passage can then be estimated by the following correlation for the mean residence time [Bongo Njeng 2015c]:

$$\bar{t} = k\sqrt{gL} \left(\frac{N^2 D_i}{g}\right)^\alpha \left(\frac{D_{ex}}{D_i}\right)^\beta \left(\frac{\theta}{S}\right)^\gamma \left(\frac{\dot{M}}{\rho_b D_i^2 \sqrt{gL}}\right)^\delta \left(\frac{4S_{lift}}{\pi D_i^2}\right)^\epsilon \left(\frac{\rho_b}{\rho_{tapped}}\right)^\zeta \left(\frac{L}{D_i}\right)^\eta \quad (8.13)$$

where k, α, \dots, η the parameters of this model are given in Table 8.1.

Similar to the experiments carried out in [Descoins 2005], the response of the exit flow rate following a step change in one of the operating parameters is measured. These experiments aim at evaluating the term $\frac{d\dot{M}}{dt}$ in Eq.8.12, and if possible at correlating this term with operating conditions. Following the work by [Ammarcha 2012], a preliminary analysis showed that it must be possible, considering the rotary kiln at a macroscopic level, to simulate the flow dynamic through a simple stochastic approach based on a Markov chain model. During the experiments the mass flow rate was continuously measured about every 20 min. The procedure set consisted in achieving steady state conditions of the flow for a given set of operating parameters, then performing at an arbitrary zero time a positive or negative step change in either the mass flow rate or the rotational speed, and then running the kiln operation again until steady state conditions. The experimental matrix for these experiments, which were conducted using sand (see Table 8.2) in a pilot scale rotary kiln, is given in Table 8.3. More details about the experimental apparatus characteristics can be found in Table 8.11 in Appendix 8.6.1.

Table 8.2: Physical properties of bulk materials

Materials	Shape	ρ_b [kg.m ⁻³]	ρ_{tapped} [kg.m ⁻³]	d_p [mm]	θ [°]
Sand	Nodular	1422	1543	0.55	39

Comparison with experiments will be performed at a position about 1 m from the kiln inlet end (approximately at the kiln center), at this position the bed depth remains quite flat and constant, as can be seen in Figure 8.1. It has not been possible to measure experimentally the bed depth transient response following the change in operating parameters. However, it is still possible to

Table 8.3: Experimental matrix for the dynamic response measurements using rectangular lifters (RL), straight lifters (SL) and no lifters (NL).

			Fixed operating conditions: $S=3^\circ$, $h_{exit}=33.5$ mm, bed of sand particles											
			Final conditions											
			N [rpm]	2	2	2	2	2	2	2	2	4	8	12
Initial conditions	Lifters		NL	NL	NL	RL	RL	RL	SL	SL	SL	SL	SL	SL
	N [rpm]	\dot{M} [kg.h ⁻¹]	0.9	1.8	2.5	0.9	1.8	2.5	0.9	1.8	2.5	2.5	2.5	2.5
	2	0.9	-	2	1	-	1	1	-	2	2	-	-	-
	2	1.8	-	-	1	-	-	1	1	-	2	-	-	-
	2	2.5	-	-	-	-	-	-	1	1	-	2	2	1
	4	2.5	-	-	-	-	-	-	-	-	1	-	2	-
	8	2.5	-	-	-	-	-	-	-	-	1	-	-	1
	12	2.5	-	-	-	-	-	-	-	-	1	-	-	-

compare the steady state results from the calculated transient response to experimental results obtained at steady state. For example, as presented in Figure 8.1, at a position about 1 m from the kiln inlet, there is a bed depth variation of about 10.6 mm between experiments at 0.9 and 2.7 kg.h⁻¹, while operating at a rotational speed of 2 rpm, a kiln slope of 3°, an exit dam height of 33.5 mm and without lifters. Dynamic simulations between the latter two states are presented in Figure 8.2. The step change was made at $t = 2$ h. A total bed depth variation of about 8.7 mm can be observed for both models presented previously, which is quite close to the experiment value. Note that when solving Eq.8.12, the experimental data presented in Table 8.4 are used.

Figure 8.3 presents results of the simulations of the bed depth transient response following a positive (see Figure 8.3a) and a negative (see Figure 8.3b) step change in the mass flow rate between 1.7 and 2.8 kg.h⁻¹ (at $t = 2$ h), while operating at a rotational speed of 2 rpm, a kiln slope of 3°, an exit dam height of 33.5 mm and with straight lifters. The predictions of the final bed depth from both models agree well within a millimeter. However the transient responses are not similar. The results from Eq.8.12 present a higher transition time (about an hour longer) compared to the results obtained from the dynamic Saeman model. In both cases, the total variation of the bed depth is about 5 mm, but it can be mentioned that the variation is slightly higher in the case of a negative step change in the mass flow rate for both models.

Table 8.4: Experimental values of $d\dot{M}/dt$ used by the model presented for the prediction of the transient response of the bed depth.

\dot{M} [kg.h ⁻¹]		Lifters	t [min]										
init.	fin.			0	20	40	60	80	100	120	140		
0.9	2.7	NL	$d\dot{M}/dt \times 10^9$ [kg.s ⁻²]	0	5.76	150	205	63.3	8.68	0	0		
1.7	2.8	SL		0	0.486	60	130	52.8	10.2	3.89	0		
2.8	1.7	SL		0	-6.18	-53.5	-128	-57.6	-8.26	-1.88	0		

8.2.2 Description of the thermal model

The thermal model developed in this study is a one-dimensional transient thermal model which can be applied to the bulk bed, free-board gas and wall of an indirectly heated rotary kiln

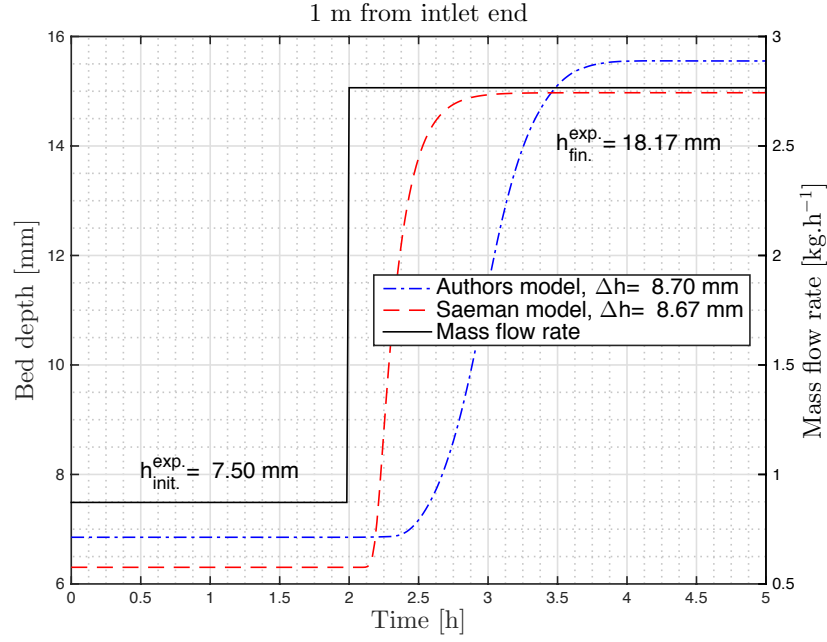
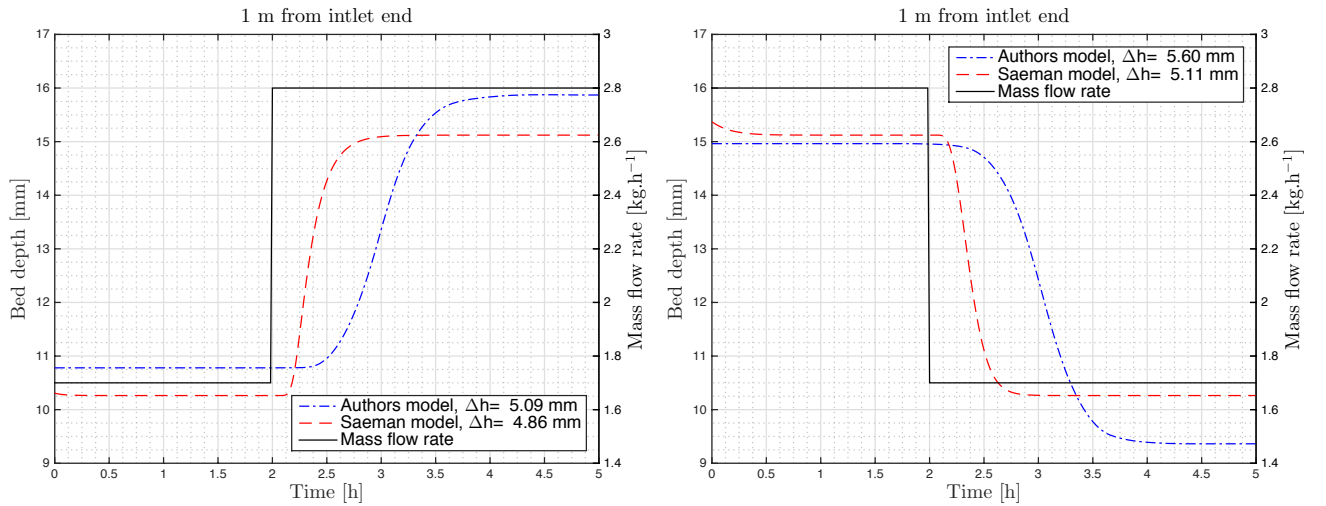


Figure 8.2: Comparison of the predictions from the author's model with those from the [Saeman 1951] model for the transient response of the bed depth 1 m from the inlet end, following a positive step in the mass flow rate between 0.9 and 2.7 kg.h⁻¹, while operating at a rotational speed of 2 rpm, a kiln slope of 3°, an exit dam height of 33.5 mm and without internal fixtures.



(a) Positive step in the mass flow rate.

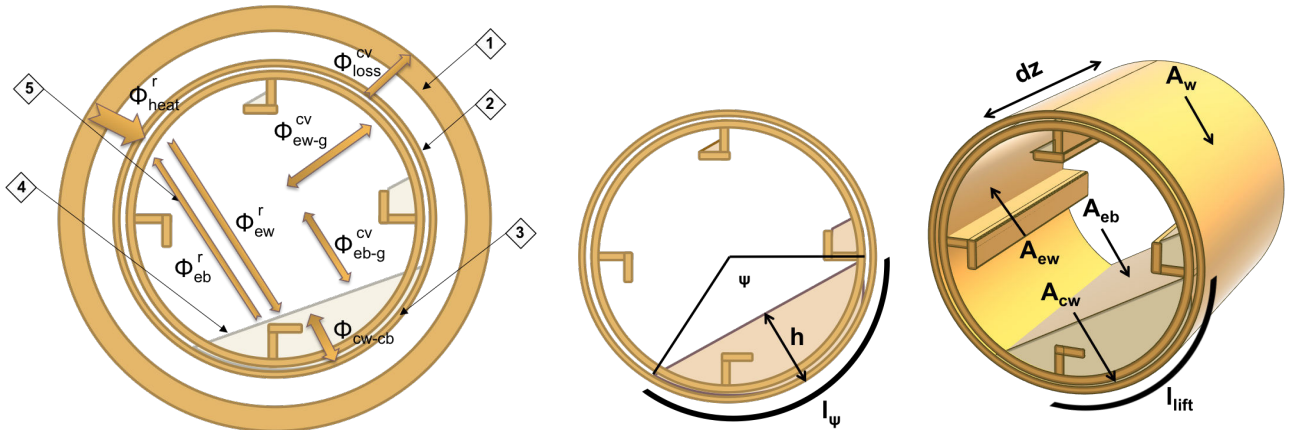
(b) Negative step in the mass flow rate.

Figure 8.3: Comparison of the predictions from the author's model with those from the [Saeman 1951] model for the transient responses of the bed depth 1 m from the inlet end, following: a) a positive and b) a negative step in the mass flow rate between 1.7 and 2.8 kg.h⁻¹, while operating at a rotational speed of 2 rpm, a kiln slope of 3°, an exit dam height of 33.5 mm and with straight lifters.

potentially equipped with lifters. Similar models for the rotary kiln have been proposed for the steady-state calculation of both bed, free-board gas and sometimes wall temperature profiles along the kiln, but they were mostly developed for the case of a directly heated rotary kiln and dedicated to a specific application [Brimacombe 1978, Barr 1989b, Owens 1991, Fan 2015].

8.2.2.1 Heat transfer

As reported in the literature, specifically within an indirectly heated rotary kiln, the heat exchanged between the wall, the bulk bed and the free-board gas involves radiation, convection and conduction as shown in Figure 8.4a. In the case of heating elements, the heat is exchanged through the cross section of the rotary kiln from the heating source by radiation to the kiln external wall, then by conduction within the wall to the inner wall; from the kiln inner wall, the heat transfer then occurs by convection and/or radiation to the freeboard gas, and by radiation and conduction to the bulk bed. Therefore, wall to gas and bed to gas conduction heat transfers are neglected considering the high velocity of the solids phase and the rotational speed of the kiln tube. In the following, in the absence of any chemical reaction or phase transformation, radiation heat transfers to the gas are neglected, as stated by [Howell 2010], since gases with symmetric diatomic molecules, such as N_2 , O_2 , or H_2 , do not emit significantly and are transparent to infrared radiation. Therefore, the gas is assumed to exchange heat only by convection. The small variation of wall temperature between outer and inner surfaces is neglected due to the high thermal conductivity of the wall. This also increases the computational speed.



(a) Heat transfer mechanisms in the cross section of indirectly heated rotary kilns equipped with lifters: 1) heating elements, 2) exposed wall (ew), 3) covered wall (cw), covered bed (cb), 4) exposed bed (eb), 5) freeboard gas (g). (b) Kiln section (left) and slice (right) with nomenclature of the heat transfer areas, the bed depth and the filling angle.

Figure 8.4: (a) Heat transfer mechanisms and (b) definition of heat transfer areas

The definition of the heat transfer fluxes presented in Figure 8.4a is as follows, considering a transverse slice of length ∂z dividing the kiln into 3 separate control volumes of wall, free-board gas and bulk bed as shown in Figure 8.4b:

➤ radiative heat flux emitted from the heating elements to the wall is:

$$\Phi_{heat} = \frac{A_w \sigma (T_{heat}^4 - T_w^4)}{\frac{1}{\varepsilon_w} + \frac{1}{\varepsilon_{heat} - 1} \frac{R_{ext}}{R_{heat}}} \quad (8.14)$$

with $A_w = \alpha (2\pi R_{ext}) \partial z$;

➤ radiative heat flux emitted from the exposed wall to the exposed bed is:

$$\Phi_{ew}^r = \frac{\varepsilon_w}{1 - \varepsilon_w} (\sigma T_w^4 - J_w) A_{ew} \quad (8.15)$$

with $A_{ew} = \alpha \left(R(2\pi - \psi) + 2d_{eff}^{ew} n_{lift}^{ew} \right) \partial z$, $n_{lift}^{ew} = n_{lift}^{total} - \frac{l_\psi}{l_{lift}}$;

➤ radiative heat flux emitted from the exposed bed to the exposed wall is:

$$\Phi_{eb}^r = \frac{\varepsilon_b}{1 - \varepsilon_b} (\sigma T_b^4 - J_b) A_{eb} \quad (8.16)$$

with $A_{eb} = \beta \left(2\sqrt{hD_i - h^2} \right) \partial z$;

➤ heat transfer between the covered wall and covered bed is:

$$\Phi_{cw-cb} = h_{cw-cb} A_{cw} (T_b - T_w) \quad (8.17)$$

with $A_{cw} = \gamma \left(R\psi + 2d_{eff}^{cw} n_{lift}^{cw} \right) \partial z$, $n_{lift}^{cw} = \frac{l_\psi}{l_{lift}}$;

➤ convective heat flux exchanged between the exposed wall and the free-board gas is:

$$\Phi_{ew-g}^{cv} = h_{ew-g}^{cv} A_{ew} (T_g - T_w) \quad (8.18)$$

➤ convective heat flux exchanged between the exposed bed to the free-board gas is:

$$\Phi_{eb-g}^{cv} = h_{eb-g}^{cv} A_{eb} (T_g - T_b) \quad (8.19)$$

➤ convective heat flux that is exchanged between the kiln tube and the surroundings (ambient, insulated and heated zones) is:

$$\Phi_w^{cv} = h_w^{cv} A_w (T_{sur} - T_w) \quad (8.20)$$

➤ radiative heat flux that is exchanged between the kiln tube and the surroundings is:

$$\Phi_w^r = A_w \sigma (T_{sur}^4 - T_w^4) \quad (8.21)$$

In the definition of the heat transfer areas, the coefficients α , β and γ account for the smoothness of the surfaces.

The radiosities J_w and J_b can be determined as detailed in [Bongo Njeng 2015e].

Regarding the convective heat transfer between the exposed wall and the gas, and the that between the exposed bed and the gas, the correlation proposed by [Bongo Njeng 2015d] for the case of no axial forced flow of the gas, is used:

$$Nu = \frac{h_{ew-g/eb-g}^{cv} D_e}{k_g} = 0.1085 Re_w^{0.0275} Pr^{-0.4839} \left(\frac{l_g}{D_i} \right)^{-1.9284} \left(\frac{10^{-10} c_{pg} \rho_g T_g^\infty}{\omega \mu_g} \right)^{-0.2208} \quad (8.22)$$

where the Nusselt number is based on the equivalent diameter, $D_e = \frac{D_i(2\pi - \psi + \sin \psi)}{2(\pi - \psi/2 + \sin \psi/2)}$, which is a function of the filling angle (see Figure 8.4b). The natural convection between the external wall and surrounding is determined as follows in the case of a horizontal cylinder [Welty 1969]:

$$Nu = \frac{h_w^{cv} D_{ext}}{k_g} = A(Ra_f)^m, \quad Ra_f < 10^4 \quad (8.23)$$

Table 8.5: Value of coefficient A and m for Eq.8.23.

Ra_f	A	m
$< 10^{-2}$	0.4	0
10^{-2} to 10^2	1.02	0.148
10^2 to 10^4	0.85	0.188

with A and m as given in Table 8.5. The Rayleigh number, Ra , is determined at the film temperature. The following correlation is used for higher Rayleigh numbers [Welty 1969]:

$$Nu = \frac{h_w^{cv} D_{ext}}{k_g} = \left(0.6 + \frac{0.387 Ra_f^{1/6}}{\left(1 + \frac{0.559}{Pr} \right)^{8/27}} \right)^2, \quad 10^4 \leq Ra_f < 10^{13} \quad (8.24)$$

The heat transfer coefficient between wall and solids is calculated using the correlation proposed by [Bongo Njeng 2015e]:

$$h_{cw-cb} = 2.1371 \frac{k_b}{l_\psi} \left(10^{-3} \frac{\omega D_i^2}{a_b} \right)^{0.4531} \left(10 \frac{l_\psi}{D_i} \right)^{-0.3507} \left(10^{-2} [HU]\% \right)^{0.9693} \left(10^{-4} \frac{T_w k_b^{0.4} c_{pb}^{0.6}}{\rho_b^{0.4} D_i^{2.8}} \right)^{1.4177} \quad (8.25)$$

8.2.2.2 Energy balance

The heat transfer model is based on energy balances within the control volume of the free-board gas, the bulk bed and the wall. The energy balances given below are established in the absence of any chemical reaction or phase transformation. The temperature of the free-board gas, the bulk bed and the wall are assumed to be uniform at any cross-section along the kiln length.

The bulk bed energy balance is given by the following equation:

$$\rho_b c_{pb} \left(\frac{\partial T_b}{\partial t} + V_{ax_b} \frac{\partial T_b}{\partial z} \right) = \frac{\partial}{\partial z} \left(\lambda_b \frac{\partial T_b}{\partial z} \right) + \frac{\Phi_b}{\Omega_b} \quad (8.26)$$

where $\Phi_b = \Phi_{eb}^r + \Phi_{eb-g}^{cv} - \Phi_{cw-cb}$, and $\Omega_b = S_b \partial z$, with $S_b = R^2 \frac{(\psi - \sin \psi)}{2}$; the bed axial velocity is determined depending on the bed motion model. In the present study it can be calculated as $V_{ax_b} = \frac{L}{t}$, or using the Saeman model as $V_{ax_b} = \frac{4\pi NR^3}{3} \left(\frac{\tan(S)}{\sin(\theta)} + \cot(\theta) \frac{\partial h}{\partial z} \right) \left(\frac{2h(z)}{R} - \frac{h(z)}{R^2} \right)^{3/2} / S_b$.

The freeboard gas energy balance is given by the following equation:

$$\rho_g c_{pg} \left(\frac{\partial T_g}{\partial t} - V_{ax_g} \frac{\partial T_g}{\partial z} \right) = \frac{\partial}{\partial z} \left(\lambda_g \frac{\partial T_g}{\partial z} \right) + \frac{\Phi_g}{\Omega_g} \quad (8.27)$$

where $\Phi_g = -\Phi_{eb-g}^{cv} - \Phi_{ew-g}^{cv}$, and $\Omega_g = S_g \partial z$, with $S_g = R^2 \left(\pi - \frac{(\psi - \sin \psi)}{2} \right)$; there is no forced axial air flow, however there is a small flow of the gas induced by the kiln rotation, and promoted by the expansion of gas when heated; this flow is likely counter-current with respect to the solid flow due to kiln inclination. The speed of this flow is evaluated on average by $V_{ax_g} = 10\pi NR \sin(\theta)$ in this study.

Lastly, the wall energy balance is given by the following equation:

$$\rho_w c_{pw} \left(\frac{\partial T_w}{\partial t} \right) = \frac{\partial}{\partial z} \left(\lambda_w \frac{\partial T_w}{\partial z} \right) + \frac{\Phi_w}{\Omega_w} \quad (8.28)$$

where the definition of Φ_w is dependent on the kiln configuration; indeed only some parts of the kiln wall may be insulated, and within these insulated zones only some parts of the wall may

be heated. Therefore in the heated zones, $\Phi_w = \Phi_{ew}^r + \Phi_{ew-g}^{cv} + \Phi_w^{cv} + \Phi_w^r + \Phi_{cw-cb} + \Phi_{heat}$, and in non heated zones, the term related to the heating, Φ_{heat} , is not taken into account. $\Omega_w = S_w \partial z$, with $S_w = 2\pi (R_{ext}^2 - R^2) + d_{eff}^{ew} n_{lift}^{ew} + d_{eff}^{cw} n_{lift}^{cw}$.

8.2.2.3 Boundary and initial conditions

In order to solve the energy balance equations for the free-board gas, the bulk bed and the wall, inlet and outlet boundaries, and initial conditions of the corresponding temperature have to be defined. At initial time the free-board gas, bulk bed and wall are at ambient temperature, so that:

$$T_g(z, t = 0) = T_b(z, t = 0) = T_w(z, t = 0) = T_a \quad (8.29)$$

At any given time, the temperature gradient or the thermal flux at the inlet and outlet ends of the kiln is assumed to be zero regarding the free-board gas, bulk bed and wall. Therefore the simulations were performed using the following boundary conditions:

$$\left. \frac{\partial T_g}{\partial z} \right|_{z=(0,L),t} = 0, \quad \left. \frac{\partial T_b}{\partial z} \right|_{z=(0,L),t} = 0, \quad \left. \frac{\partial T_w}{\partial z} \right|_{z=(0,L),t} = 0 \quad (8.30)$$

8.3 Experimental data for validation of the global model

To validate the predictive ability of the global model, experimental data are required, namely, the free-board gas, the bulk bed and the wall temperature profiles along the kiln. These measurements were performed using a pilot-scale rotary kiln (see Table 8.11 in Appendix 8.6.1) equipped or not with lifters. More details about the experimental procedures can be found in [Bongo Njeng 2015e]. The kiln was equipped in and out with thermocouples, 36 in total, placed

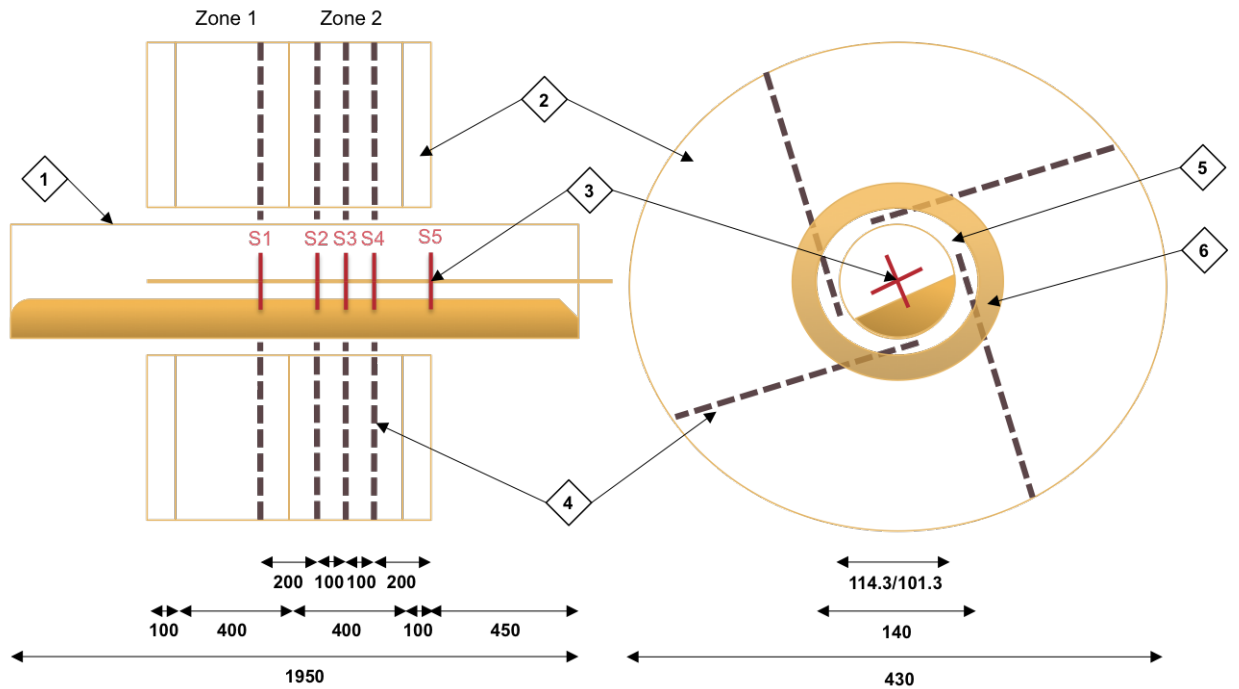


Figure 8.5: Layout of the experimental apparatus heating zones, longitudinal (left side) and transverse (right side) sections: (1) kiln tube, (2) insulation, (3) measuring rod with N-type thermocouples, (4) outer wall K-type thermocouples, (5) air, (6) heating resistors. The dimensions given in the figure are in mm.

along the heated zones at 5 sections, S1 to S5, as illustrated in Figure 8.5, so as to allow measurements of the temperature profile of the free-board gas, bulk bed and at the wall. The solids temperature may be taken as the average bulk temperature at a cross-section. Notice that at each cross-section, the wall and free-board gas temperatures are respectively averaged over the measurements of 4 and 3 thermocouples.

The experiments were performed at atmospheric pressure using nodular sand with an average particle size of 0.55 mm and without any forced axial flow of the air. The thermo-physical properties of the materials used are given in Table 8.6 (at 300°C). These experiments were carried out at low to medium temperatures between 100 and 500°C. They mainly consisted in measuring at steady state flow condition, the transient variation of the temperature at the free-board gas, the bulk bed and the wall, following the heating at the kiln wall.

Table 8.6: Thermal properties of materials at 300°C.

Materials	Sand	Air	Inconel	Remarks
ρ [kg.m ⁻³]	1422	0.616	7950	Density
c_p [J.kg ⁻¹ .K ⁻¹]	835	1045	514	Specific heat capacity
k [W.m ⁻¹ .K ⁻¹]	0.1836	0.0449	18.75	Thermal conductivity
ε [-]	0.76	<0.01	0.9	Emissivity
ϵ_0 [%]	43.36	-	-	Measured porosity

Data from the 3 experiments whose operating conditions are given in Table 8.7 were compared with simulation results. They differed only by the heating temperature setpoint.

Table 8.7: Experimental conditions of the experiments for the study of heat transfer using rectangular lifters (RL), straight lifters (SL) and no lifters (NL).

Operating conditions: Zone 2 heated					
Setpoint Temperature [°C]	N [rpm]	S [°]	M [kg.h ⁻¹]	h [mm]	Lifters [-]
100	2	3	2.5	23.5	Straight lifters
300	2	3	2.5	23.5	Straight lifters
500	2	3	2.5	23.5	Straight lifters

8.4 Results and discussion

As stated previously, a Matlab® environment was chosen for the simulation of the rotary kiln. The global model presented above was described in separate script files and solved with the use of numerical solution methods, namely, PDEPE which is able to solve the differential equation systems defined above within a reasonable computation time. The model parameters other than the operating conditions used for the simulation are given in Appendix 8.6.2. The main input and output data of the global model are presented in Figure 8.6. In developing this model, the main objective was to be able to predict the bed temperature profile and transient response within the heated zone of the rotary kiln in order to validate the transport model as well as the heat transfer sub-models in particular the convective and wall-to-solid heat transfer coefficient models. The model is of general applicability and as shown in Figure 8.6, may require information on: the kiln design, the operating conditions, and gas, solids and wall physical and thermo-physical properties.

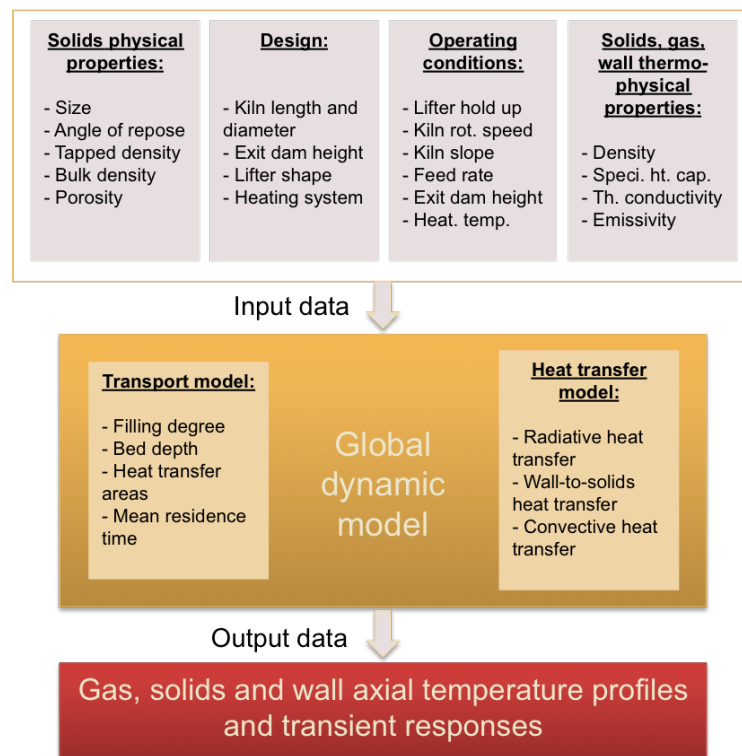


Figure 8.6: Schematic diagram showing input and output data of the global model.

8.4.1 Steady state simulation

8.4.1.1 Simulation results

Figure 8.7 shows the calculated axial profiles for the temperature of free-board gas, bulk bed and wall, and for the bed depth obtained while using for the flow determination the 0-dimension model assuming a constant bed depth presented above and the dynamic Saeman model developed by [Descoins 2005]. The simulations in Figure 8.7 were run for the same operating conditions except for the kiln internal fixtures: no lifters, straight and rectangular lifters. The results are given after 1 and 5 h of heating the kiln wall in Zone 2 at 100°C. The differences between the latter two flow models have been discussed above. As shown in Figure 8.7a, b and c, the Saeman model does not account for the presence of lifters, unlike the 0-dimension model which shows an increasing bed depth in presence of lifters as a function of their hold-up capacity. However the Saeman model bed depth predictions at the kiln outlet end are more realistic. Therefore, different shapes of temperature profiles are expected with regard to the flow model.

A general observation is that the kiln may be divided into three distinct zones: heated zone, insulated zone and non insulated zones. The wall temperature increases slightly at the location about the beginning of the insulated zone, and then increases very rapidly within the heated zone toward the setpoint temperature for the heating, before decreasing again. The bulk bed axial temperature follows a similar trend to the one at the wall but with an axial offset; however, the temperature is lower. The gas axial temperature is slewed to the right and displays a lower value compared to that of the bulk bed and the wall.

Comparing the temperature profiles with regard to the flow model used, some discrepancies can be observed. Using the Saeman model leads to lower bulk bed and gas temperatures. The wall temperature profiles are nearly superimposed, except at the outlet end. Indeed at the outlet end, as expected, there is a remarkably sharp drop in temperature between the 0-dimension and Saeman models. However in the zone of interest, which is around the heated zone, the results from the two models are quite similar.

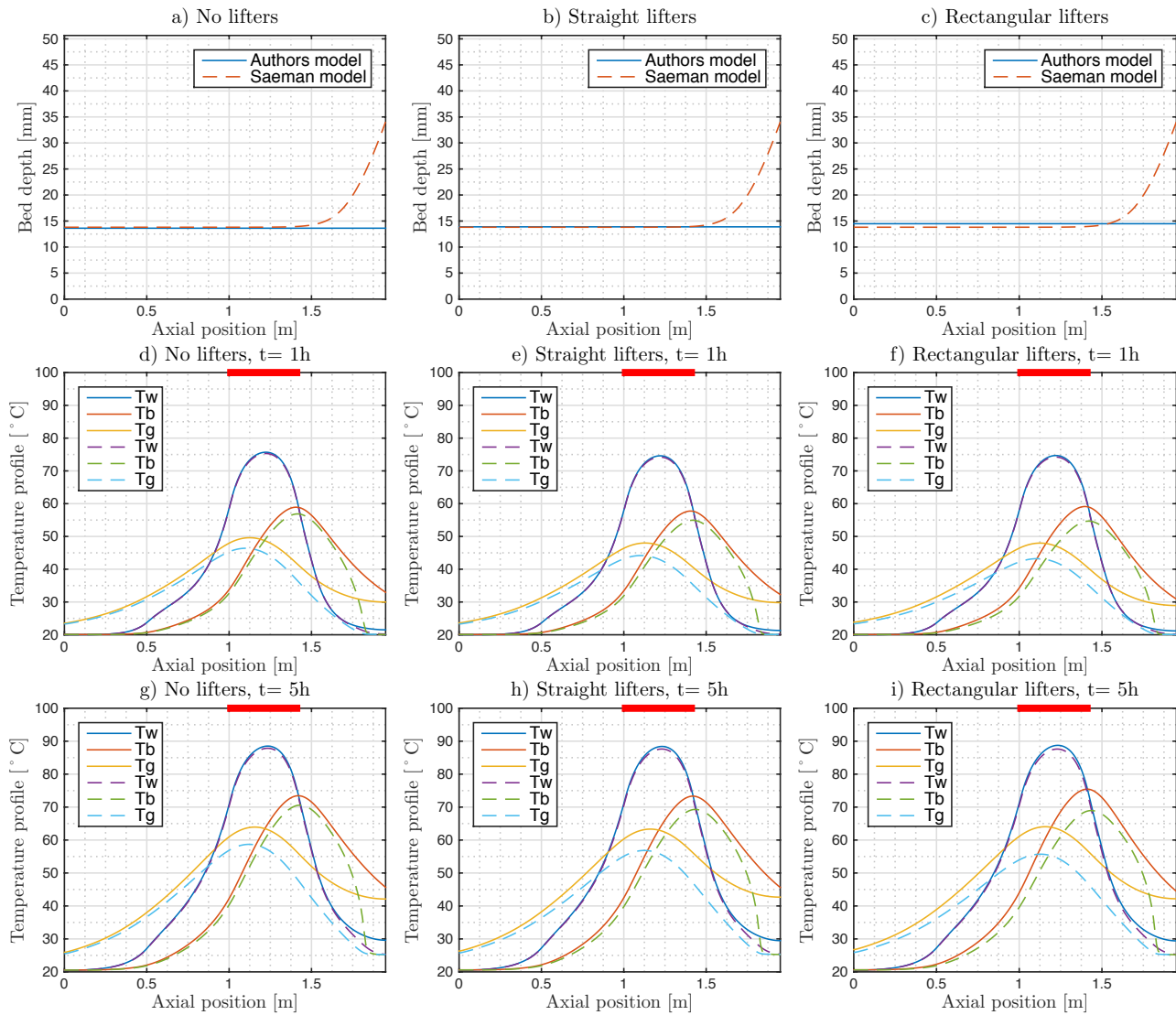


Figure 8.7: Comparison of simulation results namely, the wall, bed and gas axial temperature profiles after 1 and 5 h of heating zone 2 at 100°C, while using the bed depth profile from the author's model, displayed as solid lines, and the Saeman model, displayed as dashed lines. The kiln is equipped with straight, rectangular or no lifters and operated at a rotational speed of 2 rpm, a kiln slope of 3°, an exit dam height of 33.5 mm and a mass flow rate of 2.5 kg.h⁻¹. An ambient temperature of 20°C is used for the simulation. The solid red lines indicate the heating temperature and heated zone.

The simulation shows only very small discrepancies between the case without lifters and those with lifters. In presence of lifters a higher rate of heat transfer could have been expected due to the increase in heat transfer areas. However these effects are not very high: the bed temperature profiles of the cases without lifters and with straight lifters are very close. When using the rectangular lifters, however, the simulations show a higher bulk bed temperature especially when looking at the results from the 0-dimension model.

8.4.1.2 Model validation

For the model validation, the experimental data, namely, free-board gas, bulk bed and wall temperature measured at the position corresponding to sections S1 to S5 (see Figure 8.5), and

obtained for the operating conditions as given in Table 8.7, were compared to the model predictions. Notice that the main difference between the chosen experimental data operating conditions is the heating temperature setpoint. Input data for the model simulation were set at the exact experimental data measured (notably: N , S , h_{exit} , \dot{M} , T_a).

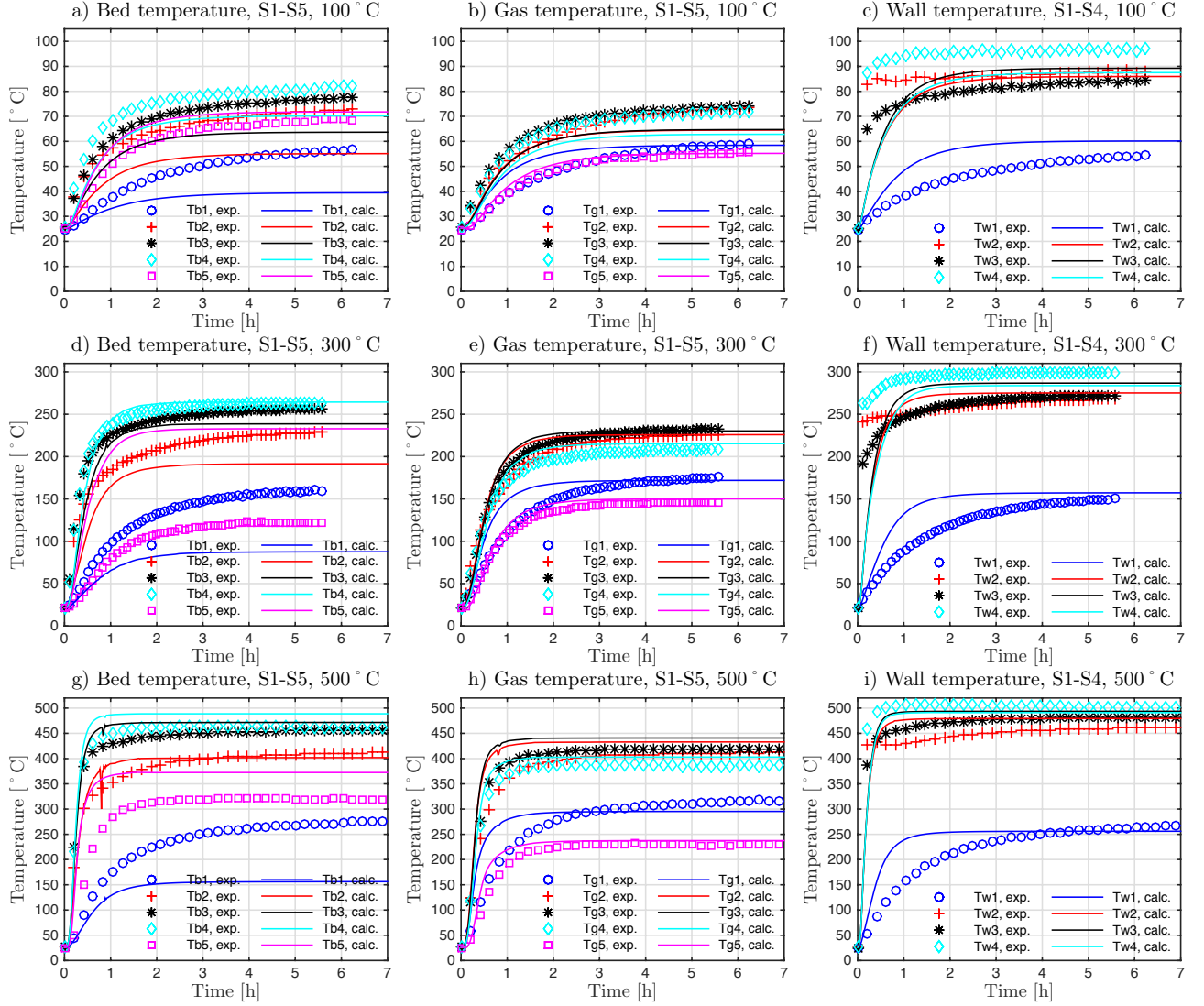


Figure 8.8: Comparison of the bed, gas and wall temperature transient responses at the sections S1 to S5 as given in Figure 8.5 with experimental data whose operating conditions are given in Table 8.7. The labels 1 to 5 refer to the position of sections S1 to S5.

Figure 8.8 compares bulk bed, free-board gas and wall temperature profiles calculated at sections S1 to S5 (see Figure 8.5) to experimentally determined data. In general, at the sections located outside the heated zone, namely, S1 and S5, there is good agreement between the experimental data and the predictions; however some deviations occur between the bulk bed temperature profiles and the experimental data, notably at higher heating temperature setpoints. Within the heated zone, the results are quite mixed; however, considering a $\pm 20\%$ margin of error, only a few discrepancies are observed between theoretical and experimental results, whether in the bulk bed, the gas or the wall. The predictive accuracy of the model is better than what was expected with regard to the uncertainties of the sub-models used either for the flow model or the heat transfer model.

8.4.1.3 Sensitivity analysis

Parameter variations and the uncertainties of models used in particular for the heat transfer modeling, may sometimes cause significant axial displacement or variation in the calculated temperature profiles. Therefore a sensitivity analysis was carried out through the calculation of sensitivity coefficients as defined by [Beck 1977] in order to determine the range of magnitude of change of the bed temperature due to perturbations applied to the values of certain model parameters. Considering $T_b(z, t, \beta)$ with β a parameter vector, the sensitivity coefficients are determined as follows:

$$X_i = \beta_i \frac{\partial T_b}{\partial \beta_i} \sim \frac{T_b(z, t, (1 + \delta) \beta_i) - T_b(z, t, (1 - \delta) \beta_i)}{2\delta} \quad (8.31)$$

The sensitivity coefficient is by definition of the same dimension than the bulk temperature, therefore the comparison can be performed in order to determine the model parameters to which the model is the most sensitive.

Figure 8.9 shows the axial and average sensitivity coefficients calculated at steady state ($t = 5$ h) for a simulation of the kiln without lifters, for a heating temperature in zone 2 of 300°C, a rotational speed of 2 rpm, a kiln slope of 3°, an exit dam height of 33.5 mm, a mass flow rate of 2.5 kg.h⁻¹ and an ambient temperature of 20°C. The sensitivity coefficients were calculated using a value of $\delta = 10\%$. It is clear from the results, and notably from the histogram, that the parameters linked to the gas phase have only a small influence on the bed temperature, which is

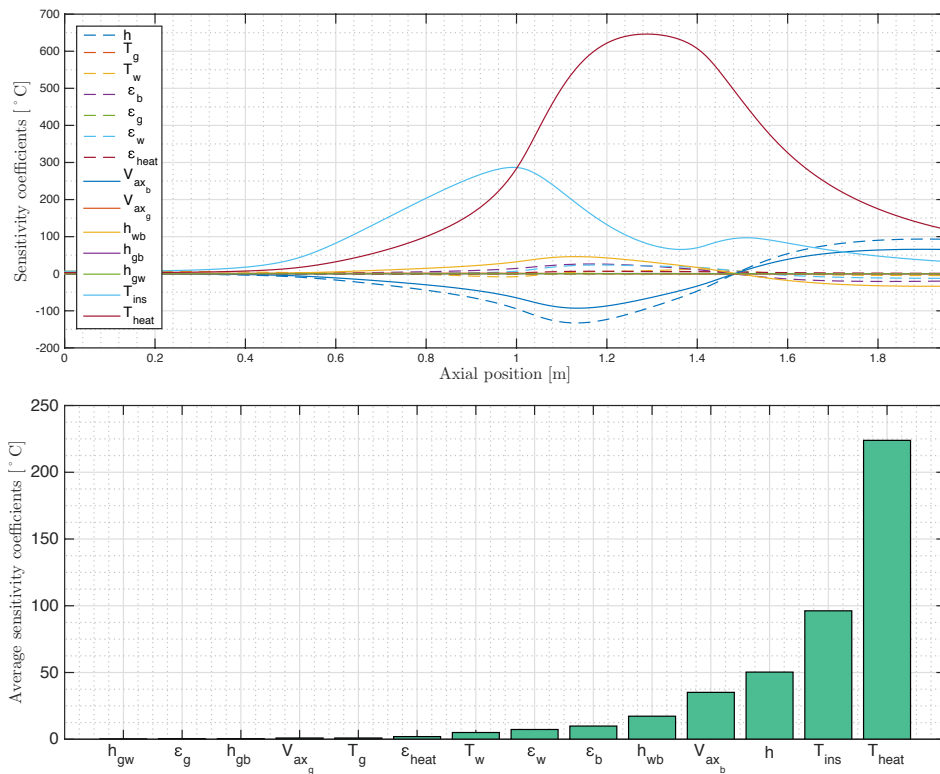


Figure 8.9: Results of the sensitivity analysis of the bed temperature to some model and operating parameters: at the top, the axial sensitivity coefficients and at the bottom the average sensitivity coefficients when the kiln is heated in zone 2 at 300°C, without lifters, and operated at a rotational speed of 2 rpm, a kiln slope of 3°, an exit dam height of 33.5 mm and a mass flow rate of 2.5 kg.h⁻¹. An ambient temperature of 20°C was used for the simulation.

in accordance with theory since the gas is not the heating source, contrary to the case of direct heated rotary kilns. As expected, the temperature setpoint is identified as the most sensitive parameter of the model, followed by the surrounding temperature in the insulated zones. The bed depth also has a significant impact on the model because of the direct dependence of the heat transfer areas on the bed depth. The wall-to-solid heat transfer coefficient and bed axial velocity are also spotted among the most sensitive parameters, indeed, the former sets the rate of heat transfer between the wall and bulk bed, while the latter may impact the residence time of the solids within the heated zone.

8.4.2 Dynamic simulation

8.4.2.1 Simulation results

Dynamic simulations of the model were carried out using the experimental data given in Table 8.4 for a positive (see Figure 8.3a) or a negative (see Figure 8.3b) step change in the mass flow rate between 1.7 and 2.8 $\text{kg}\cdot\text{h}^{-1}$; the step change was set at $t = 5$ h. The simulation was run for the kiln equipped with straight lifters, heated in zone 2 at 300°C , and operated at a rotational speed of 2 rpm, a kiln slope of 3° and an exit dam height of 33.5 mm.

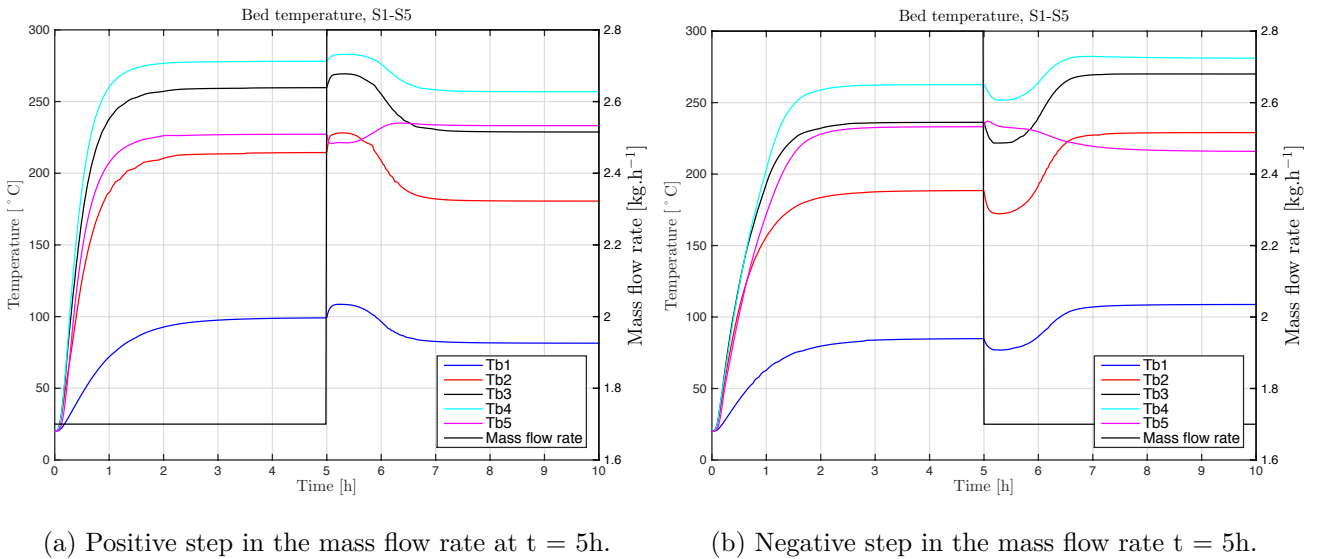


Figure 8.10: Simulation results of the transient responses of the bed temperature at sections S1 to S5 as given in Figure 8.5, following: a) a positive and b) a negative step in the mass flow rate between 1.8 and 2.7 $\text{kg}\cdot\text{h}^{-1}$, while operating at a rotational speed of 2 rpm, a kiln slope of 3° , an exit dam height of 33.5 mm and with straight lifters, when heating zone 2 at 300°C . The corresponding bed depth profiles are given in Figure 8.3. The labels 1 to 5 refer to the position of sections S1 to S5.

Figure 8.10 represents the transient responses of the bulk bed temperature at sections S1 to S5 for a positive (see Figure 8.10a) or a negative (see Figure 8.10b) step change in the mass flow rate. Following the step change, the temperature profile of the bulk bed is significantly disturbed in the case of a positive step, in which case the bed depth increases (see Figure 8.3a). There is a small increase in temperature at sections S1 to S4, followed by a steady decrease down to a plateau, whereas at section S5, the temperature drops slightly before increasing to reach also a plateau. In the case of a negative step change in the mass flow rate, the observed transient responses are reversed, as shown in Figure 8.10b. The shapes displayed by these transient responses for the

bed temperature are, nevertheless, simulation results which may further the understanding of the kiln operation, but still need to be validated with some experimental data. However, these results confirm the finding in the sensitivity analysis of the model showing that the bulk bed axial velocity is a sensitive parameter of the model since it can be correlated to the solid mass flow rate.

8.5 Conclusion

A simple model for indirectly heated flighted rotary kilns has been developed, based on the filling degree and residence time model presented in a previous study [Bongo Njeng 2015c], and the heat transfer correlations for convective and wall-to-solid heat exchanged as defined in previous investigations [Bongo Njeng 2015c, Bongo Njeng 2015d]. Bed depth predictions from the chosen 0-dimension flow model as well as from the Saeman model were compared to the experimental data. While the results demonstrate that the 0-dimension model cannot represent the bed depth properly at the kiln edges, it can give better predictions of the bed depth far from the kiln edges. The overall model simulation of the rotary kiln considered here indicates that the dynamic behavior of the heating mechanisms within the zone of interest (heated zone), can be reproduced with a reasonable quantitative accuracy considering a margin of error, as demonstrated by the calculated axial temperature profiles of the bulk bed, free-board gas and wall at flow steady state conditions. The effects of model parameters uncertainty were analyzed through a sensitivity analysis with regard to the calculated bed temperature. It was found that the model is primarily affected by the surrounding temperature at the wall in particular the heating temperature setpoint, but also some other parameters such as the bed depth and axial velocity or the wall-to-solid heat transfer coefficient. Therefore, a good definition of these parameters may significantly increase the accuracy of the model. Dynamic simulations were also conducted, but the resulting predictions still need to be compared with experimental data to validate the observed dynamic behavior of the kiln in future work.

The present model can be used as the backbone of a global model running specific reactions, to increase understanding and to optimize kiln operation or design. Therefore, the model may give not only information on the axial temperature profiles and transient response but also a wide range of other information depending on the field of application, for various input conditions.

List of symbols

A	Heat transfer area	m^2
a	thermal diffusivity	$[m^2.s^{-1}]$
c_p	Specific heat capacity	$J.kg^{-1}.K^{-1}$
d_{eff}	Length of lifter transferring heat	m
D	Kiln internal diameter	m
D_e	Equivalent diameter	m
d_p	Particle diameter	m
g	Gravitational acceleration	$m.s^{-2}$
h	Bed depth	m, mm
h	Heat transfert coefficient	$W.m^{-2}.K^{-1}$
h_{exit}	Exit dam height	m

HU[%]	hold-up volume fraction or filling degree	-
HU	Hold-up	kg
J	Radiosity	W.m^{-2}
k	Thermal conductivity	$\text{W.m}^{-1}.\text{K}^{-1}$
L	Kiln length	m
l_{ψ}	circumference of the covered wall	m
l_{ctrl}	Length between two sections within the kiln	m
l_g	Effective wall-to-gas contact length along the cross section between	m
l_{lift}	circumference between 2 consecutive lifters	m
\dot{M}	Mass flow rate	kg.h^{-1}
N	Kiln rotational speed	rpm
NA	Not available	-
NL	No lifters	-
n_{lift}	Total number of lifters	-
Pr	Prandtl number	-
Q_v	Volumetric flow rate	$\text{m}^3.\text{h}^{-1}$
R	Kiln radius	m
Ra	Rayleigh number	-
Re_w	Rotational Renolds number	-
rpm	Rotation per minute	-
RL	Rectangular lifters	-
S	Kiln slope	degree
S	Cross-sectional area	m^2
S_0	Power supplied	W
SL	Straight lifters	-
S_{lift}	Area covered by solid particles in a lifter at horizontal position	m^2
t	Time	h
T	Temperature	$^{\circ}\text{C}$
\bar{t}	Mean residence time	s
V	Velocity	m.s^{-1}
X	Sensitivity coefficient	$^{\circ}\text{C}$
z	Axial position	m

Greek letters

$\alpha, \beta, \gamma, \delta, \epsilon, \zeta$	Fitting parameters	-
α, β, γ	Coefficients relative to the smoothness of surface	-
θ	Angle of repose	degrees
ε	Emissivity	-
λ	Thermal conductivity	$\text{W.m}^{-1}.\text{K}^{-1}$
ρ	Density	kg.m^{-3}
σ	Stefan Boltzmann coefficient	$\text{W.m}^{-2}.\text{K}^{-4}$
τ	Time of passage	s
Φ	Heat transfer flux	W
ψ	Filling angle	rad
Ω	Volume	m^3

Subscripts and superscript

a	Ambiant	-
ax	Axial	-
b	Bulk bed of solids	-
calc	Calculated	-
cb	Covered bed	-
ctrl	Control (volume)	-
cv	Convection	-
cw	Covered wall	-
ew	Exposed bed	-
eff	Effective	-
ew	Exposed wall	-
exp	Experimental	-
ext	External wall	-
exit	Exit	-
f	Film	-
fin.	Final	-
G,g	Gas	-
i, init.	Internal wall, initial	-
ins	Insulation	-
lift	Lifters	-
loss	Losses	-
r	Radiation	-
w	Wall	-

8.6 Appendices

8.6.1 Experimental apparatus characteristics

The main characteristics of the rotary kiln used for the model validation and the order of magnitude of the operating conditions are summarized in Table 8.11.

Table 8.11: Main characteristics and order of magnitude of operating conditions of the rotary kiln used.

Subsets	Parameters	Order of magnitude	Remarks
Rotary kiln characteristics	D_i [m]	0.101	Internal diameter
	L [m]	1.95	Kiln length
	Feed hopper [m ³]	5	Capacity
	Heating zones, length [m]	2, 0.4	In a row
	Heating temperature [°C]	1000	Maximum
	TC	36	Thermocouples
Operating conditions	N [rpm]	0.5-12	Rotational speed
	S [°]	0-5	Kiln slope
	\dot{M} [kg.h ⁻¹]	0.5-3	Mass flow rate
	h [mm]	0-33.5	Exit dam height
	Lifters shape	None	Smooth wall
	(configuration),	SL (4 rows), 10	SL: Straight lifter
	height [mm]	RL(4 rows), 10	RL: Rectangular lifter

8.6.2 Model parameters

The model parameters used for the simulation are summarized in Table 8.12.

Note that the heating is gradual: the heating temperature is reached within 5 min, so that the heating temperature if set at T_{heat} will be:

$$\succ \text{ for } t = 0: T_a;$$

$$\succ \text{ for } t < 5 \times 60: T_a + \frac{T_{heat}-T_a}{5 \times 60} t;$$

$$\succ \text{ for } t \geq 5: T_{heat}.$$

The surrounding temperature at the insulated wall, upstream and downstream the heated zone, is assessed as follows:

$$\succ \text{ upstream: } T_{heat} - (T_{heat} - T_a) \left(\frac{z_1 - z}{z} \right)^{1/4}; \text{ where } z_1 \text{ is the inlet location of the heated zone;}$$

$$\succ \text{ downstream: } T_{heat} - (T_{heat} - T_a) \left(\frac{z - z_2}{z} \right)^{1/4}; \text{ where } z_2 \text{ is the outlet location of the heated zone;}$$

Table 8.12: Model parameters used for the simulations.

Subsets	Model parameters	Values	Remarks
Rotary kiln design	L	1.95 m	Kiln length
	D	0.101 m	Internal diameter
	R_{ext}	0.057 m	Kiln external radius
	R_{heat}	0.067 m	Heating elements radius
	Heating zones, length [m]	Zone 2, 0.4 m	
	Heating temperature	100, 300, 500°C	
	Straight lifter	4.5×10	One-section
	Rectangular lifter	$2.15 \times 10 \times 10$	Two-section
Emissivities	ε_b	0.76	Bulk bed emissivity
	ε_g	0.01	Gas emissivity
	ε_w	0.9	Wall emissivity
	ε_{heat}	0.4	Heating elements emissivity
Coefficients relative to the smoothness of surface	α	0.85	
	β	1	
	γ	1	
Thermo-physical properties	ρ_b	1422 kg.m^{-3}	Bulk bed density
	ρ_w	7950 kg.m^{-3}	Gas density
	ρ_g	$1.293 \times 273.15/T \text{ kg.m}^{-3}$	Wall density
	c_{pb}	$835 \text{ J.kg}^{-1}.\text{K}^{-1}$	Bulk bed sp. heat cap.
	c_{pw}	$4.7374 \cdot 10^{-7} T^3 - 1.0958 \cdot 10^{-3} T^2 + 9.9514 \cdot 10^{-1} T + 2.1441 \cdot 10^2 \text{ J/kg.K}$	Gas sp. heat cap.
	c_{pg}	$1.9327 \cdot 10^{-10} T^4 - 7.9999 \cdot 10^{-7} T^3 + 1.1407 \cdot 10^{-3} T^2 - 4.4890 \cdot 10^{-1} T + 1.0575 \cdot 10^3 \text{ J/kg.K}$	Wall sp. heat cap.
	k_b	The model developed by [Bauer 1977] is used	
	k_w	$2.5285 \cdot 10^{-8} T^3 - 5.1235 \cdot 10^{-5} T^2 + 4.8213 \cdot 10^{-2} T + 9.220 \cdot 10^{-1} \text{ W/m.K}$	
	k_g	$1.5207 \cdot 10^{-11} T_g^3 - 4.857 \cdot 10^{-8} T_g^2 + 1.0184 \cdot 10^{-4} T_g - 3.9333 \cdot 10^{-4} \text{ W/m.K}$	

Conclusions and recommendations

The main conclusions of the research findings of the present study are highlighted in the following paragraphs, and some recommendations for future investigations are made. The present research has furthered our knowledge of solids transport and heat transfer mechanisms in inclined indirectly heated rotary kilns, equipped with lifters of different designs, or exit dams of different heights. From this research work, a set of new dimensionless correlations has been developed for the quantitative estimation of the most important solids transport characteristics, and convective and wall-to-solid heat transfer coefficients; a global model has also been established to predict transient axial temperature profiles for indirectly heated rotary kilns.

Conclusions

In the first part of the thesis, a literature review was undertaken in order to identify key research gaps, and therefore, to refine the main objectives of the research work as follows:

- The first objective is the characterization of the solids transport behavior, which is addressed through a comprehensive experimental study at room temperature focusing on the determination and modeling of the residence time distribution, mean residence time, filling degree and axial dispersion coefficient. Effects of lifter shape and number of rows, exit dam height, and usual operating parameters such as rotational speed, inclination, and feed rate are of interest for the study.
- The second one concerns is about the heat transfer mechanisms, in particular the convective and the wall-to-solid heat transfer coefficients. These are tackled through experimental measurements of the heating of the system, which are needed for their determination. From the experimental results, correlations based on dimensional considerations were established for both coefficients.
- The third one is to develop a global dynamic model to determine gas, wall and solids temperature profiles when operating in indirectly heated rotary kilns equipped with lifters.

In the second part of the thesis, the overall methodology employed in this study is described. The methodology is based on dimensional considerations, completed by systematic experimentation. The two pilot-scale rotary kilns, RK1 (at CMGPCE laboratory) and RK2 (at RAPSODEE center), used in the study are presented. They are indirectly heated and their dimensions are suitable to address scaling up issues. The smallest setup, RK1, was used to perform the hot experiments; although some difficulties were encountered, most of them were easily tackled. The

solids selected for the study, namely, sand (hot and cold), broken rice (cold) and beech chips (cold) were characterized. All these solids behave as free-flowing materials. The experimental procedures and modeling technique (dimensional analysis) used are also detailed.

In the third part of the thesis, using RK1 and RK2, the study investigated the effects of operating parameters, namely, the kiln rotational speed and slope, the mass flow rate, the exit dam height, the materials, the shape and number of rows of lifters on the flow characteristics, i.e., the residence time distribution (RTD), the mean (MRT) and variance residence time (VRT), the Peclet number (Pe) and axial dispersion coefficient (D), and the hold-up (HU). The key findings from the present study related to the characterization of the solids transport are as follows:

1. The RTD curves were found to shift towards lower residence time regions with an increase in either the rotational speed, the kiln slope, or the mass flow rate, or a decrease in the exit dam height. Changes in the shape of the curve were linked to the VRT value, which remained quite stable while varying the rotational speed and exit dam height. The smaller the VRT, the higher the peak of the corresponding RTD curves. The use of the axial dispersion model to represent the experimental data has been validated. For RK1, there were no particular effects of segregation or dead volume when processing mono-sized granular solids (sand and rice), while for RK2, which processed beech chips with a wide size distribution, some segregation was observed: the RTD curves had slightly extended tails. However, all the fitted parameters were considered reasonably accurate to characterize the materials transport behavior within the system. Pe were often greater than 100, as usually observed in rotary kiln units, implying plug flow. They were found to be higher in presence of lifters. The exit dam height had no incidence on Pe, whereas an increase in either the rotational speed or the kiln slope induced a decrease in the Pe. It increased with the feed rate. Regarding the axial dispersion coefficient, trends in the results observed were the inverse of those found for Pe.
2. It was found that, an increase in the MRT may result from a decrease in the rotational speed and slope of the kiln, but also to a lesser extent, from an increase in the mass flow rate of solids. The mass flow rate has a remarkable influence on the filling degree: as the flow rate increases, or the kiln rotational speed and slope decrease, the HU increases. With an increase in the exit dam height, both MRT and HU increased slightly. It was found that the shape and number of rows of lifters significantly influenced the flow with regard to the lifters' total hold-up capacity; the use of lifters increases the burden and the residence time of solid particles. Lifters also promote the mixing of particles as suggested by the increase in the axial dispersion coefficient. For the flow of materials with a wide size distribution, by their mixing effect, it was found that lifters reduce the segregation phenomena that may occur.
3. A set of dimensionless correlations have been developed for the mean residence time (\bar{t}), the filling degree (fractional volumetric hold-up, $HU[\%]$) and the axial dispersion coefficient (D). The selected dimensionless groups for these correlations represent the solids characteristics, the dynamic ratio between inertial and gravitational forces, and the geometric ratio of the system. These models are power-law correlations; they were validated by the experimental data from this study. The correlations are expressed as follows (see Chapter 5):

$$\bar{t} = k\sqrt{gL} \left(\frac{N^2 D_i}{g} \right)^\alpha \left(\frac{D_{ex}}{D_i} \right)^\beta \left(\frac{\theta}{S} \right)^\gamma \left(\frac{\dot{M}}{\rho_{bulk} D_i^2 \sqrt{gL}} \right)^\delta \left(\frac{4S_{lift}}{\pi D_i^2} \right)^\epsilon \left(\frac{\rho_{bulk}}{\rho_{tapped}} \right)^\zeta \left(\frac{L}{D_i} \right)^\eta$$

$$HU[\%] = k \frac{\rho_{bulk} L \pi D_i^2}{4} \left(\frac{N^2 D_i}{g} \right)^\alpha \left(\frac{D_{ex}}{D_i} \right)^\beta \left(\frac{\theta}{S} \right)^\gamma \left(\frac{\dot{M}}{\rho_{bulk} D_i^2 \sqrt{gL}} \right)^\delta \left(\frac{4S_{lift}}{\pi D_i^2} \right)^\epsilon \left(\frac{\rho_{bulk}}{\rho_{tapped}} \right)^\zeta \left(\frac{L}{D_i} \right)^\eta$$

$$D = k \sqrt{D_i^2 g L} \left(\frac{N^2 D_i}{g} \right)^\alpha \left(\frac{d_p}{D_i} \right)^\beta (S)^\gamma \left(\frac{\dot{M}}{\rho_{bulk} D_i^2 \sqrt{gL}} \right)^\delta \left(\frac{4S_{lift}}{\pi D_i^2} \right)^\epsilon \left(\frac{\rho_{bulk}}{\rho_{tapped}} \right)^\zeta \left(\frac{L}{D_i} \right)^\eta$$

The fourth part of the thesis concerned the heat transfer mechanisms, in particular the convective and wall-to-solid heat transfer in an indirectly heated rotary kiln. Heating experiments were performed using RK1 for the continuous flow of sand; measurements of the temperature profiles of the bulk bed, the free-board gas and the wall were logged. The effects of operating parameters, namely, the rotational speed, the mass flow rate, the exit dam height, and shape of lifters were investigated. Data analysis of the temperature profile measurements led to the following key findings on heat transfer:

1. When applying the lumped system analysis for the determination of the wall-to-gas and wall-to-solid heat transfer coefficient (HTC):
 - the wall-to-gas HTC was found to be of the order of $10^{-2} \text{ W.m}^{-2}.\text{K}^{-1}$, and to increase with increasing temperature, but to decrease with the kiln rotational speed and in presence of lifters; using the experimental data, the convective coefficient ($h_{ew-g/eb-g}^{cv}$) was correlated as follows (see Chapter 6):

$$h_{ew-g/eb-g}^{cv} = 0.1085 \frac{k_g}{D_e} Re_\omega^{0.0275} Pr^{-0.4839} \left(\frac{l_g}{D_i} \right)^{-1.9284} \left(10^{-10} \frac{c_{pg} \rho_g T_g^\infty}{\omega \mu_g} \right)^{-0.2208}$$

- the wall-to-solid HTC was found to be of the order of $10^2 \text{ W.m}^{-2}.\text{K}^{-1}$, and to increase with the temperature and the rotational speed. This coefficient was also found to increase with an increase of the filling degree following a variation of the solids mass flow rate, exit dam height or lifter capacity; however in the case of lifters this result has been validated only for rectangular lifters, raising the question of a critical lifter design that could better promote heat transfer. For the heat transfer, lifter design thus becomes an open-ended matter of optimizing.
2. The wall-to-solid HTC was also determined through a heat balance, using the power supplied for the heating. The results obtained are of the order of magnitude about $10^2 - 10^3 \text{ W.m}^{-2}.\text{K}^{-1}$. Discrepancies with the previous method of calculations can be attributed to the assumptions. It was found that neglecting radiation may lead to a 24% error. Even if to a lesser degree, the effects of the operating parameters agreed with those given above from the lumped system analysis. Using the experimental data, the wall-to-solid heat transfer coefficient was correlated as follows (see Chapter 7):

$$h_{cw-cb} = 2.1371 \frac{k_b}{l_\psi} \left(10^{-3} \frac{\omega D_i^2}{a_b} \right)^{0.4531} \left(10 \frac{l_\psi}{D_i} \right)^{-0.3507} (10^{-2} [HU]\%)^{0.9693} \left(10^{-4} \frac{T_w k_b^{0.4} c_{pb}^{0.6}}{\rho_b^{0.4} D_i^{2.8}} \right)^{1.4177}$$

3. It has not been possible to establish a fully dynamic global model for the simulation of the operation of indirectly heated rotary kilns equipped or not with lifters. Nevertheless, a steady state axial heat transfer model has been developed for the prediction of axial

temperature profiles of the bulk bed, the free-board gas and wall. This model incorporates the correlations developed in this study for the solid transport, and for the convective and the wall-to-solid heat transfer coefficients. Comparison of the results from the simulation of the global model with experimental data indicates mixed results. However, the overall model simulation of the rotary kiln considered indicates that the dynamic behavior of the heating mechanisms within the zone of interest (heated zone), could be predicted with a reasonable quantitative accuracy considering a certain margin of error. Therefore, a good definition of the model parameters may significantly increase the accuracy of results. The proposed model can be used as the backbone of a global model running specific reactions, to increase understanding and optimize kiln operation or design.

Recommendations

Most of the main objectives of the present research work have been achieved; however, the scope for future research is still quite large. In the following, some recommendations for future work are made:

1. In the present study, a significant amount of experimental data are available for the residence time distribution; the axial dispersion was used for the modeling of these curves. However, in cases of higher dispersion, the characteristic extended tail could not be represented. Based on the results from this work, a stochastic model for the residence time distribution can be developed in a future study, using the Monte Carlo technique.
2. Two main lifters designs were considered in this study: one-section (straight) and two-section (rectangular) lifters. Due to small differences in the hold-up capacity of these two designs, it was sometimes difficult to observe and analyze precisely the differences. Future studies may investigate lifters with a higher hold-up capacity, for example, three-section lifters. In addition, segmented lifters can be also investigated.
3. In this study, free-flowing granular materials were selected for the characterization of solids transport. These investigations should be extended to the case of cohesive materials and even wet materials. However, the feeding systems may require some technical adjustments to allow the inlet flow.
4. The kiln length-to-diameter ratio was not varied in this study. Future work may extend the investigation to this parameter also; without the need for a new setup, a stimulus response test can be performed by means of a spoon-like tool to inject the tracer at different axial positions along the kiln length.
5. The global model described in this study is a foundation which can be consolidated in the future by a refined definition of the most sensitive model parameters in order to increase the accuracy of the model predictions. In addition, experiments were performed to characterize the dynamic response of the solids flow. A preliminary analysis shows that it should be possible, considering the rotary kiln at a macroscopic level to simulate the flow dynamic through a simple stochastic approach based on a Markov chain. Such modeling may extend the global model from steady state flow to dynamic flow simulation.
6. Future study should also consider DEM simulations and coupled DEM-CFD simulations for the investigation of solids transport and heat transfer mechanisms in indirectly heated rotary kilns equipped or not with lifters; the results from such work could be compared to the experimental results from the present study.

Conclusions générales et perspectives

Les principales conclusions issues de la présente étude sont présentées dans les paragraphes qui suivent, et quelques perspectives aux travaux de cette étude sont enfin développées. Cette étude a permis d'améliorer davantage les connaissances sur le transport des particules solides ainsi que les mécanismes de transfert de chaleur dans les fours tournants à chauffage indirect, inclinés, équipés ou non de releveurs, et/ou de diaphragme en sortie du four. Dans ce travail de recherche, un ensemble de corrélations développées par analyse dimensionnelle a été proposé pour l'estimation quantitative des caractéristiques les plus importantes du transport de particules solides ainsi que des coefficients de transfert de chaleur ; un modèle global a également été établi pour prédire les profils de température axiale dans les fours tournants à chauffage indirect.

Conclusions

Dans la première partie de la thèse, une étude bibliographique a été réalisée afin d'identifier les domaines de la recherche sur les fours tournants n'ayant pas été complètement éclaircis ou encore insuffisamment traités, et cela a permis d'affiner les objectifs principaux du présent travail de recherche comme suit :

- Le premier objectif porte sur la caractérisation du transport des particules solides ; cela est réalisé au travers d'une campagne expérimentale assez complète effectuée à température ambiante en mettant l'accent sur la détermination et la modélisation de la distribution des temps de séjour, le temps de séjour moyen, le taux de remplissage et le coefficient de dispersion axiale. Les effets de dispositifs tels que les releveurs (formes et dispositions), le diaphragme en sortie, et divers paramètres opératoires plus usuels tels que la vitesse de rotation et l'inclinaison du four, ou encore le débit massique en entrée présentent un intérêt pour cette étude.
- Le second objet de ce travail se focalise sur les mécanismes de transfert de chaleur, en particulier le coefficient de convection paroi/gaz, et le coefficient de transfert de chaleur paroi/solide. Ces derniers sont déterminés expérimentalement à partir des relevés effectués au cours du chauffage du système. A partir des profils de température et autres données recueillies, et en se fondant sur des considérations dimensionnelles, il a pu être établi des corrélations pour les différents coefficients de transfert de chaleur.
- Le troisième objectif est le développement d'un outil, plus précisément, un modèle global dynamique permettant la détermination de profils de température de la phase gazeuse, du

lit de particules solides et de la paroi du tube pour des fours tournants en chauffage indirect et équipés ou non de releveurs.

Dans la deuxième partie de la thèse, la méthodologie générale employée pour mener cette étude est décrite. Cette méthodologie est basée sur l'analyse dimensionnelle, et marquée par des campagnes expérimentales rigoureuses. Les deux fours tournants à l'échelle pilote, RK1 (au laboratoire CMGPCE) et RK2 (au centre RAPSODEE), utilisés dans l'étude sont présentés. Ces deux pilotes sont indirectement chauffés et leurs dimensions sont favorables à l'étude du changement d'échelle. Le plus petit pilote, RK1, a été utilisé pour réaliser les expériences à températures élevées ; bien que certaines difficultés aient été rencontrées, la plupart d'entre elles ont été facilement contournées. Les particules solides retenues dans cette étude, à savoir, le sable (à chaud et froid), le riz concassé (à froid) et les copeaux de hêtre (à froid), ont été caractérisées. Tous ces solides divisés ont un écoulement fluide. Les procédures expérimentales et la technique de modélisation (analyse dimensionnelle) employées sont également détaillées.

Dans la troisième partie de la thèse, les deux pilotes, RK1 et RK2, sont utilisés pour examiner les effets des différents paramètres opératoires tels que, la vitesse de rotation et l'inclinaison du four, la débit d'alimentation et le type de solides, la hauteur de diaphragme en sortie, la forme et la configuration des releveurs, sur les caractéristiques de l'écoulement, à savoir, la distribution de temps de séjour (DTS), le temps de séjour moyen (TSM) et la variance de la distribution (VD), le nombre de Péclet (Pe) et le coefficient de dispersion axiale (D), et le taux de remplissage (TR). Les principales conclusions de l'étude relative à la caractérisation du transport des particules solides sont comme suit :

1. Il a été établi qu'avec une augmentation soit de la vitesse de rotation, de l'inclinaison ou du débit d'alimentation du four, mais aussi une réduction de la hauteur du diaphragme en sortie du four, les courbes de DTS se déplacent des régions de long temps de séjour vers les régions de plus faible temps de séjour. On relie par ailleurs assez facilement les changements de formes observées sur les courbes de DTS aux valeurs de la variance, ces dernières restant assez stables lors des variations de vitesse de rotation et de la hauteur du diaphragme en sortie. Plus la valeur de la variance est petite, plus le pic des courbes de DTS correspondant est important. La validité du modèle de dispersion axiale pour la représentation des données expérimentales a été vérifiée. Dans le cas du pilote RK1, aucun effet particulier de ségrégation ou de volume mort n'a pu être mis en évidence au cours du traitement des résultats expérimentaux, issus de l'écoulement du sable et du riz qui ont tous deux une distribution de taille assez uniforme. Tandis que dans le pilote RK2, qui a reçu des copeaux de hêtre ayant une distribution de taille plus large, des phénomènes de ségrégation ont pu être observés, notamment au travers des longues traînées observées sur les courbes de DTS déterminées. Malgré cela, les paramètres ajustés utilisés dans le modèle de dispersion axiale ont été considérés comme raisonnablement précis pour caractériser le transport des particules solides dans le système. La valeur des nombres de Péclet déterminés dans cette étude est généralement supérieur à 100, valeur caractéristique d'un écoulement piston, comme c'est très souvent le cas dans les fours tournants. En présence des releveurs, la valeur du nombre de Péclet est d'autant plus élevée. Si le nombre de Péclet est diminué lors d'une augmentation de la vitesse de rotation ou de l'inclinaison du four, la hauteur du diaphragme en sortie du four n'a aucune incidence sur ce dernier. Par contre le nombre de Péclet augmente avec le débit d'alimentation. En ce qui concerne le coefficient de dispersion axiale, les tendances observées sont l'inverse de celles exposées pour le nombre de Péclet.
2. Il est apparu qu'une augmentation du temps de séjour moyen peut résulter d'une diminution de la vitesse de rotation et/ou de l'inclinaison du four, mais aussi dans une moindre mesure, d'une augmentation du débit d'alimentation en entrée du four. Le débit massique en entrée

a une influence significative sur le taux de remplissage : en effet lorsque ce dernier augmente, ou que la vitesse de rotation et/ou l'inclinaison du four diminue, le taux de remplissage augmente. Les temps de séjour moyen et taux de remplissage augmentent légèrement au cours du rehaussement en sortie de la hauteur du diaphragme. Il a été constaté par ailleurs que la forme et la disposition des releveurs influencent de manière conséquente l'écoulement en raison du taux de chargement propre des releveurs ; la présence de releveurs permet ainsi d'accroître la quantité de la charge présente dans le four, mais aussi le temps de résidence des particules solides. Les releveurs favorisent également le mélange des particules solides, comme suggérée par l'augmentation du coefficient de dispersion axiale. En ce qui concerne l'écoulement des particules solides ayant une large distribution de taille, il a été constaté que le mélange induit par les releveurs a pour effet la réduction des phénomènes de ségrégation existants.

3. Un ensemble de corrélations ont été développés par analyse dimensionnelle pour le temps de séjour moyen noté \bar{t} , le taux de remplissage (fraction volumétrique) noté $HU[\%]$, et le coefficient de dispersion axiale noté D . Les groupements sans dimension sélectionnés pour formuler ces corrélations représentent les caractéristiques physiques des particules solides, les ratios dynamiques entre les forces d'inertie et de gravité, et les rapports géométriques du système. Ces modèles sont des corrélations sous forme de loi de puissance ; ils ont été validés à l'aide des données expérimentales issues de cette étude. Les corrélations sont exprimées comme suit (voir Chapitre 5 pour la valeur des paramètres) :

$$\begin{aligned}\bar{t} &= k\sqrt{gL} \left(\frac{N^2 D_i}{g} \right)^\alpha \left(\frac{D_{ex}}{D_i} \right)^\beta \left(\frac{\theta}{S} \right)^\gamma \left(\frac{\dot{M}}{\rho_{bulk} D_i^2 \sqrt{gL}} \right)^\delta \left(\frac{4S_{lift}}{\pi D_i^2} \right)^\epsilon \left(\frac{\rho_{bulk}}{\rho_{tapped}} \right)^\zeta \left(\frac{L}{D_i} \right)^\eta \\ HU[\%] &= k \frac{\rho_{bulk} L \pi D_i^2}{4} \left(\frac{N^2 D_i}{g} \right)^\alpha \left(\frac{D_{ex}}{D_i} \right)^\beta \left(\frac{\theta}{S} \right)^\gamma \left(\frac{\dot{M}}{\rho_{bulk} D_i^2 \sqrt{gL}} \right)^\delta \left(\frac{4S_{lift}}{\pi D_i^2} \right)^\epsilon \left(\frac{\rho_{bulk}}{\rho_{tapped}} \right)^\zeta \left(\frac{L}{D_i} \right)^\eta \\ D &= k\sqrt{D_i^2 g L} \left(\frac{N^2 D_i}{g} \right)^\alpha \left(\frac{d_p}{D_i} \right)^\beta (S)^\gamma \left(\frac{\dot{M}}{\rho_{bulk} D_i^2 \sqrt{gL}} \right)^\delta \left(\frac{4S_{lift}}{\pi D_i^2} \right)^\epsilon \left(\frac{\rho_{bulk}}{\rho_{tapped}} \right)^\zeta \left(\frac{L}{D_i} \right)^\eta\end{aligned}$$

La quatrième partie de la thèse aborde les mécanismes de transfert de chaleur en particulier la convection paroi/gaz et le transfert de chaleur paroi/solide dans les fours tournants à chauffage indirect. Des campagnes expérimentales ont été menées sur le pilote RK1 pour différentes températures de douce à chaude, avec un écoulement continu de sable ; Les profils de température relatifs à la phase gazeuse, au lit de particules solides et à la paroi du four ont ainsi pu être enregistrés. Les effets des paramètres opératoires, tels que, la vitesse de rotation du four, le débit massique d'entrée, la hauteur du diaphragme en sortie, et la forme des releveurs ont été étudiés. L'analyse de données des profils de température mesurés, conduit en matière de transfert de chaleur aux conclusions suivantes :

1. Lors de l'application d'une méthode d'analyse globale des systèmes minces pour la détermination des coefficients de transfert de chaleur entre la paroi et la phase gazeuse d'une part, et la paroi et le lit de particules solides d'autre part :

- Le coefficient de convection paroi/gaz a été estimé de l'ordre de grandeur de $10^{-2} \text{ W.m}^{-2}.\text{K}^{-1}$; par ailleurs il est observé une augmentation du coefficient avec la température, et une diminution avec la vitesse de rotation du four et en présence de releveurs ; en se servant des données expérimentales, le coefficient de convection ($h_{ew-g/eb-g}^{cv}$) a été corrélé comme suit (voir le Chapitre 6) :

$$h_{ew-g/eb-g}^{cv} = 0.1085 \frac{k_g}{D_e} Re_\omega^{0.0275} Pr^{-0.4839} \left(\frac{l_g}{D_i} \right)^{-1.9284} \left(10^{-10} \frac{c_{pg} \rho_g T_g^\infty}{\omega \mu_g} \right)^{-0.2208}$$

- Le coefficient de transfert de chaleur paroi/solide a été estimé de l'ordre de grandeur maximum de $10^2 \text{ W.m}^{-2}.\text{K}^{-1}$; par ailleurs il est observé une augmentation du coefficient avec la température et la vitesse de rotation du four. Ce coefficient est aussi sensible au taux de remplissage, en effet il s'accroît pour toute augmentation du taux de remplissage du four consécutif le plus souvent aux variations de débit d'alimentation, de hauteur de diaphragme, ou encore du taux de chargement propre des relevés. Cependant ce dernier résultat n'a pu clairement être mis en évidence que dans le cas des relevés rectangulaires, soulevant ainsi la question de l'existence d'un certain design optimal des relevés favorisant par leurs forme et taille le transfert thermique. En matière de transfert de chaleur, la question de l'existence d'un design optimal des relevés demeure donc une question à réponse ouverte.
2. Le coefficient de transfert de chaleur paroi/solide a été aussi déterminé par un bilan d'énergie tenant en compte la puissance fournie au système de chauffe. Cela a permis d'estimer des valeurs pour le coefficient de transfert d'un ordre de grandeur de $10^2 - 10^3 \text{ W.m}^{-2}.\text{K}^{-1}$. Les différences d'ordre de grandeur constatées entre les résultats des deux méthodes utilisées peuvent être imputées aux hypothèses de calculs qui sont notamment assez simplificatrices dans le cas de la méthode des systèmes minces utilisés précédemment en calculs préliminaires. Il a par ailleurs été montré que négliger les effets du rayonnement pourrait conduire à une surestimation de près de 24% du coefficient. Même si ce n'est que dans une moindre mesure, les effets des paramètres opératoires sur le coefficient de transfert de chaleur correspondent assez aux observations énoncées précédemment dans le cas de la méthode d'analyse globale des systèmes minces. En utilisant les données expérimentales, le coefficient de transfert de chaleur paroi/solide a été corrélé comme suit (voir le Chapitre 7) :

$$h_{cw-cb} = 2.1371 \frac{k_b}{l_\psi} \left(10^{-3} \frac{\omega D_i^2}{a_b} \right)^{0.4531} \left(10 \frac{l_\psi}{D_i} \right)^{-0.3507} \left(10^{-2} [HU]\% \right)^{0.9693} \left(10^{-4} \frac{T_w k_b^{0.4} c_{pb}^{0.6}}{\rho_b^{0.4} D_i^{2.8}} \right)^{1.4177}$$

3. Il n'a pas été possible d'établir un modèle global spécifiquement dynamique pour la simulation du fonctionnement des fours tournants à chauffage indirect équipés ou non de relevés. Néanmoins, un modèle global non dynamique a été développé pour la prédiction tout le long du four des profils de température du lit de particules solides, de la phase gazeuse et de la paroi du tube. Ce modèle intègre les différentes corrélations développées dans cette étude pour représenter le transport des particules solides, ainsi que les coefficients de transfert de chaleur d'une part convectif et d'autre part entre la paroi et le lit de particules solides. La comparaison des résultats de la simulation du modèle global avec les données expérimentales reste assez mitigée. Toutefois, la simulation du modèle global du pilote considéré indique que le comportement dynamique des mécanismes de chauffage dans la zone d'intérêt, c'est à dire la zone chauffée, serait prédit avec une précision raisonnable en tenant compte d'une certaine marge d'erreur. Par conséquent, une meilleure définition des paramètres du modèle devrait augmenter de manière significative la précision des résultats. Le modèle proposé peut être utilisé comme l'ossature ou la base d'un modèle plus global intégrant des réactions chimiques spécifiques, et visant à améliorer la compréhension du procédé d'une part et d'autre part à optimiser la conception et/ou le fonctionnement des fours tournants.

Perspectives

Bien que la majeure partie des objectifs fixés dans la présente étude ait été atteinte, les opportunités ou perspectives de travaux de recherche dans le domaine des fours tournants n'en sont pas moins nombreuses. En effet, voici quelques pistes de recherche qui pourraient faire suite aux travaux de recherche ici présentés :

1. La présente étude fournie une quantité considérable de données expérimentales en particulier des courbes de distribution de temps de séjour ; ces dernières ont été représentées à l'aide du modèle de dispersion axiale. Cependant, en cas de dispersion plus élevée, la trainée caractéristique de ces distributions ne peut être représentée correctement par ce modèle. Ainsi, basé sur les résultats des travaux de cette étude, un modèle stochastique pourrait être développé dans une étude future pour représenter la distribution des temps de séjour, cela pourrait se faire en utilisant la technique de Monte Carlo par exemple.
2. Deux profils de releveurs ont été considérés dans cette étude : des releveurs plats (une section perpendiculaire à la paroi du tube du four) et des releveurs rectangulaires (deux sections formant un angle droit). En raison de trop faibles écarts des capacités de chargement propre des releveurs mentionnés, il était parfois difficile d'observer et d'analyser précisément leurs effets. Les études futures pourraient examiner des releveurs ayant des capacités de chargement plus importantes, par exemple, des releveurs à trois sections. En outre, les releveurs segmentés pourraient également être étudiés.
3. Pour la caractérisation du transport des particules solides, dans cette étude, des solides divisés ayant un écoulement fluide ont été privilégiés. Les résultats obtenus pourraient être complétés par l'étude du cas de matériaux cohésifs, pâteux ou humides. Cependant, les systèmes d'alimentation des fours tournants utilisés nécessiteraient quelques ajustements techniques spécifiques pour s'adapter à l'écoulement.
4. Le ratio longueur sur diamètre du tube du four tournant n'a pas été varié dans cette étude. Des travaux futurs pourraient étendre l'étude à ce paramètre aussi ; sans forcément avoir besoin de différentes sections de tube, ce qui pourrait s'avérer être assez onéreux, en ce qui concerne la distribution de temps de séjour, l'injection impulsion de traceurs pourrait être réalisée à différentes positions axiales le long du four tournant à l'aide d'un outillage spécifique.
5. Le modèle global décrit dans cette étude est une base qui peut être consolidée à l'avenir par une définition affinée des paramètres du modèle les plus sensibles, ce qui permettrait d'augmenter la précision des prédictions du modèle. En outre, des expériences ont été réalisées afin de caractériser la réponse dynamique de l'écoulement des particules solides. Une analyse préliminaire montre qu'il devrait être possible, en considérant le four tournant comme une unité opératoire, de représenter la dynamique d'écoulement grâce à une approche stochastique simple, basé sur les chaînes de Markov. Cela pourrait étendre la validité du modèle global de four tournant au delà de l'état d'écoulement stationnaire en prenant en compte certaine phase dynamique telle le remplissage ou la vidange.
6. Des travaux futures pourraient également envisager des simulations mettant en œuvre des méthodes à éléments/volumes finis et des couplages de ces derniers avec la dynamique des fluides pour l'étude des mécanismes de transport de solides divisés et de transfert de chaleur dans les fours tournants à chauffage indirect, équipés ou non de releveurs ; les résultats de tels travaux pourraient être comparés aux résultats expérimentaux de la présente étude.

Appendices

Appendix A

Experimental apparatus

The main characteristics of the rotary kilns used, namely RK1 and RK2, and the magnitude of their corresponding operating conditions are resumed in Table A.1.

Table A.1: Comparison of the main characteristics and order of magnitude of operating conditions of the rotary kilns used, RK1 and RK2.

Subsets	Parameters	RK1	RK2	Remarks
Rotary kilns characteristics	D_i [m]	0.101	0.21	Internal diameter
	L [m]	1.95	4.20	Kiln length
	Feed hopper [m ³]	5	30	Capacity
	Heating zones, length [m]	2, 0.4	5, 0.5	In a row
	Heating temperature [°C]	1000	1000	Maximum
	TC	36	16	Thermocouples
Operating conditions	N [rpm]	0.5-12	0.5-21	Rotational speed
	S [°]	0-5	0-7	Kiln slope
	\dot{M} [kg.h ⁻¹]	0.5-3	0.5-10	Mass flow rate
	h [mm]	0-33.5	0	Exit dam height
	Lifters shape	None	None	Smooth wall
	(configuration),	SL (4 rows), 10	Grid (16 rows), 5	SL: Straight lifter
	height [mm]	RL(4 rows), 10	SL (1-6 rows), 30	RL: Rectangular lifter

Appendix B

Solids transport characterization

B.1 Dispersion models: analytical solutions	249
B.1.1 The «open» dispersion model	249
B.1.2 The «closed» dispersion model	249
B.2 Residence time distribution results	250
B.2.1 Results from RK1	250
B.2.2 Results from RK2	255
B.3 Bed depth measurements results	260

B.1 Dispersion models: analytical solutions

B.1.1 The «open» dispersion model

[Levenspiel 1999] published the analytical solution to Eq. 1.32. The solution in a dimensional form is as follows:

$$E(\theta) = \frac{1}{2} \sqrt{\frac{Pe}{\pi\theta}} \exp \left\{ -\frac{Pe(1-\theta)}{4\theta} \right\} \quad (B.1)$$

The mean and variance of this distribution are defined as:

$$\bar{t}_o = 1 + \frac{2}{Pe} \quad (B.2)$$

$$\sigma_o^2 = \frac{2}{Pe} + \frac{8}{Pe^2} \quad (B.3)$$

B.1.2 The «closed» dispersion model

[Thomas 1944] published the analytical solution to Eq. 1.32, it is reproduced here in non dimensional form:

$$E(\theta) = 2 \sum_{n=1}^{n=\infty} \frac{Pe\alpha_n Pe \exp \left[\frac{Pe}{2} \left\{ 1 - \frac{\theta(\alpha_n^2+1)}{2} \right\} \right]}{Pe(\alpha_n^2+1) + 4} \left\{ \alpha_n \cos \left(\frac{Pe}{2} \alpha_n \right) + \sin \left(\frac{Pe}{2} \alpha_n \right) \right\} \quad (B.4)$$

where α_n is given the positive roots of Equation :

$$\tan\left(\frac{Pe}{2}\alpha_n\right) = \frac{2\alpha_n}{(\alpha_n^2 - 1)} \quad (\text{B.5})$$

[Levenspiel 1999] gives expressions for the mean and variance of the «closed» system even if the analytical solution for the RTD itself is not reported:

$$\bar{t}_c = 4 \frac{\sum_{n=1}^{n=\infty} \frac{Kn}{Pe^2(\alpha_n+1)^2}}{\sum_{n=1}^{n=\infty} \frac{Kn}{Pe(\alpha_n+1)}} = 1 \quad (\text{B.6})$$

$$\sigma_c^2 = 32 \frac{\sum_{n=1}^{n=\infty} \frac{Kn}{Pe^3(\alpha_n+1)^3}}{\sum_{n=1}^{n=\infty} \frac{Kn}{Pe(\alpha_n+1)}} = \frac{2}{Pe} + \frac{2}{Pe^2} (1 - \exp(-Pe)) \quad (\text{B.7})$$

B.2 Residence time distribution results

B.2.1 Results from RK1

In this section are presented the experimental RTD curves obtained while processing a bulk of sand with either straight lifters (see Figure B.1) or rectangular lifters (see Figure B.2), and a bulk of broken rice with either no lifters (see Figure B.3), straight lifters (see Figure B.4) or rectangular lifters (see Figure B.5) installed at the kiln inner wall.

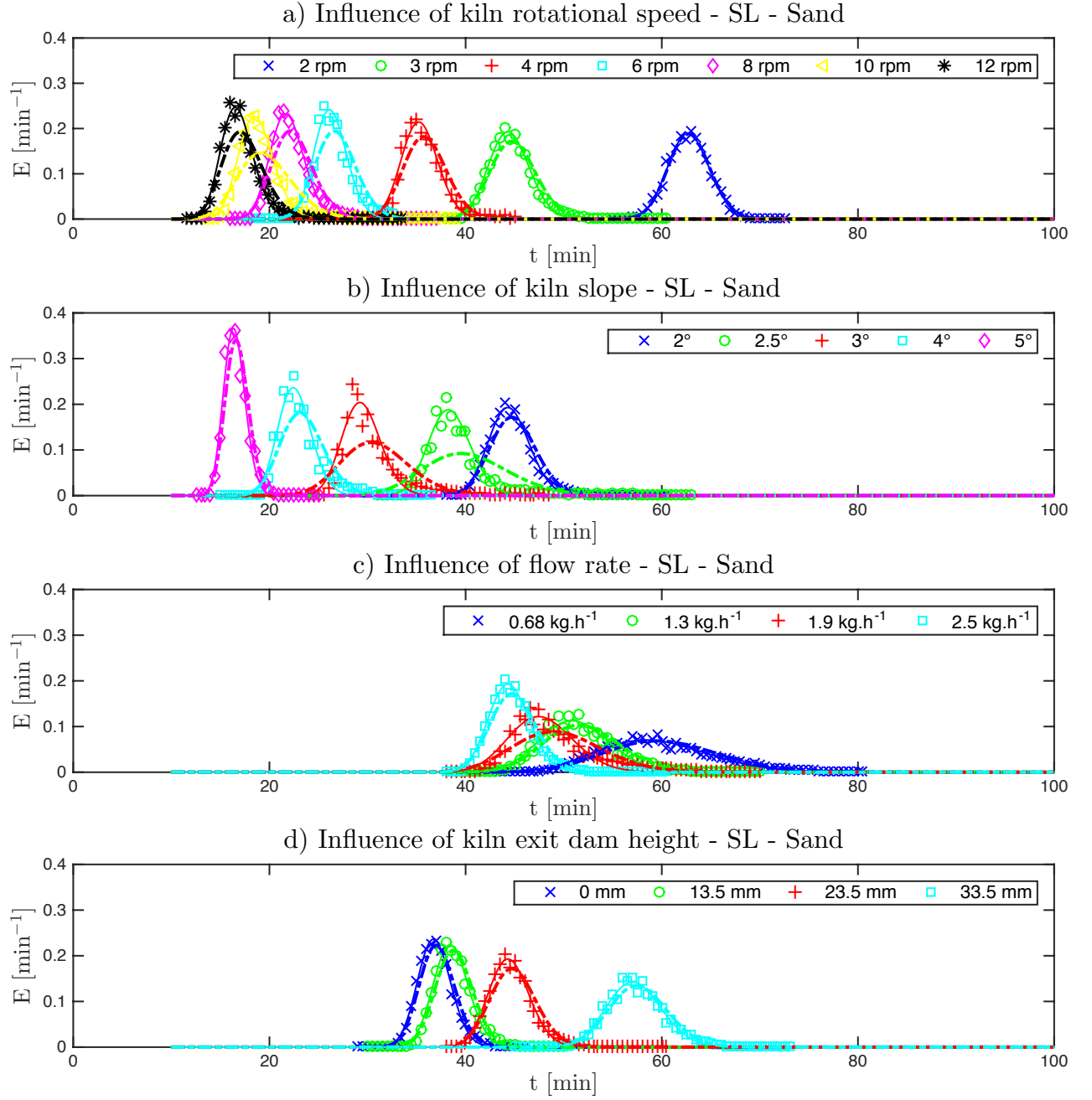


Figure B.1: Influence of operating parameters (N , S , \dot{M} and exit dam height) on the RTD for the flow of sand, when the kiln is equipped with straight lifters. Solid lines represent the axial dispersion model using fitted parameters. Dashed lines represent the axial dispersion model using theoretical parameters.

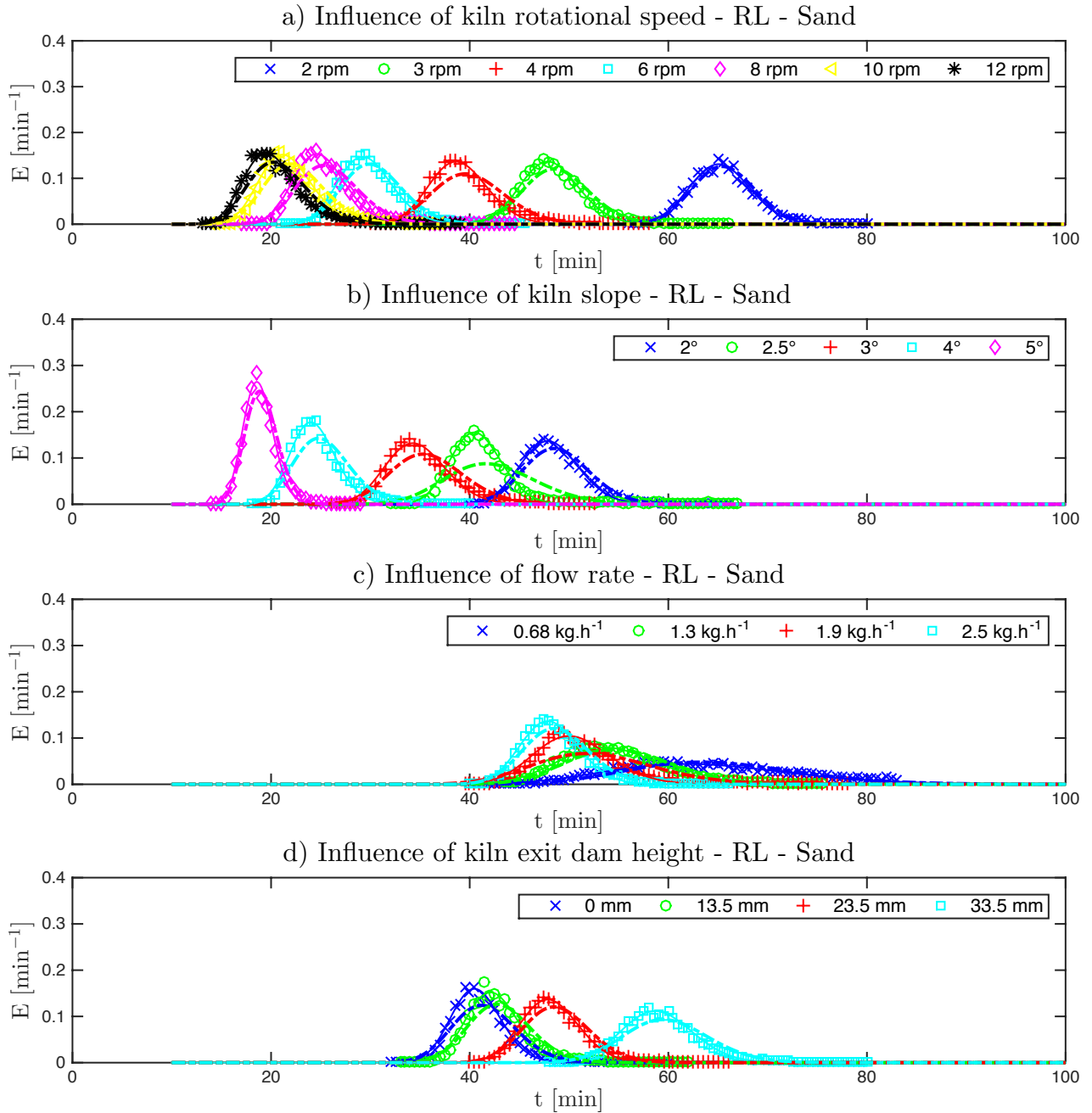


Figure B.2: Influence of operating parameters (N, S, \dot{M} and exit dam height) on the RTD for the flow of sand, when the kiln is equipped with rectangular lifters. Solid lines represent the axial dispersion model using fitted parameters. Dashed lines represent the axial dispersion model using theoretical parameters.

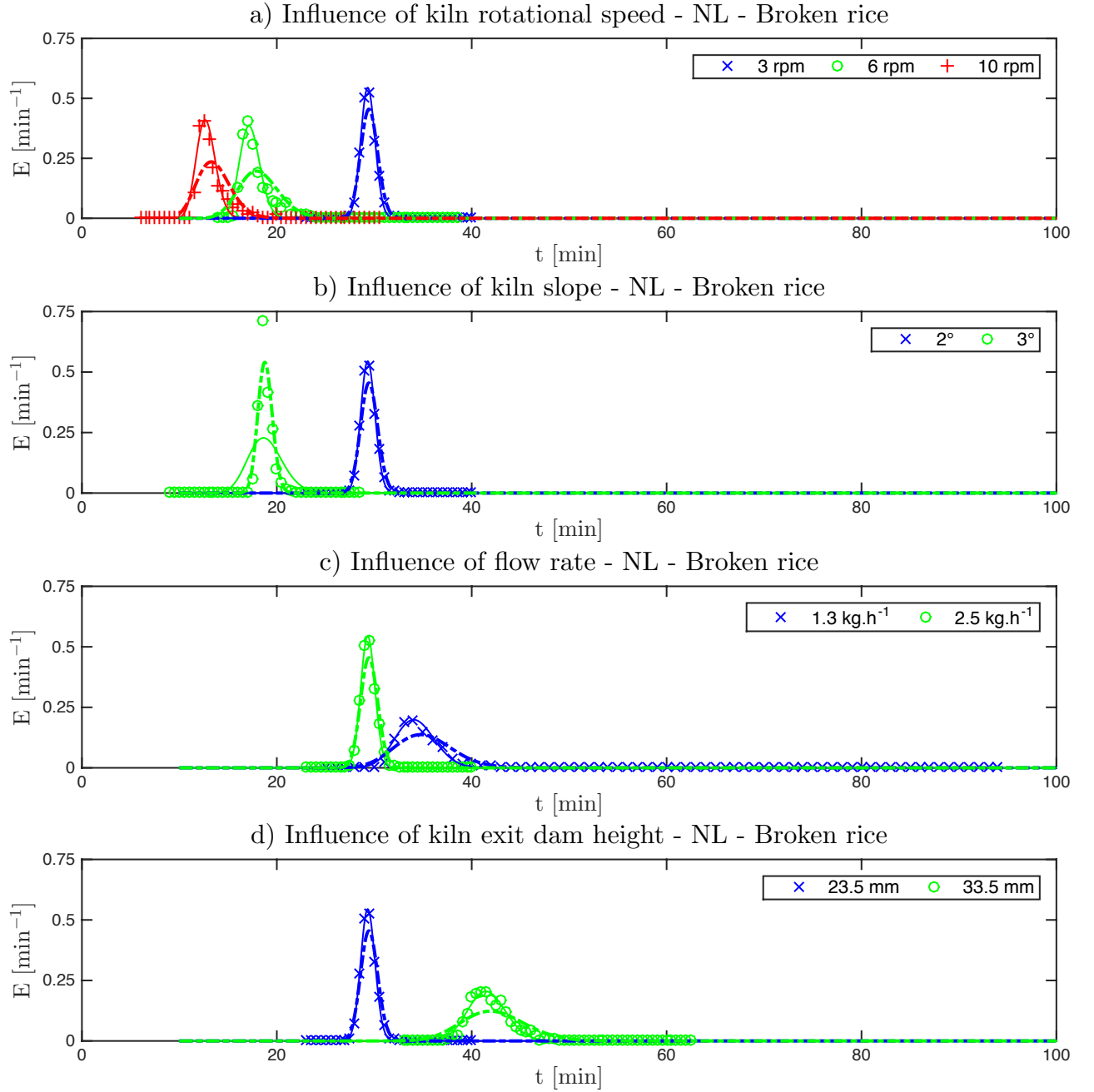


Figure B.3: Influence of operating parameters (N, S, \dot{M} and exit dam height) on the RTD for the flow of broken rice, when there is no internal fixture at the kiln wall. Solid lines represent the axial dispersion model using fitted parameters. Dashed lines represent the axial dispersion model using theoretical parameters.

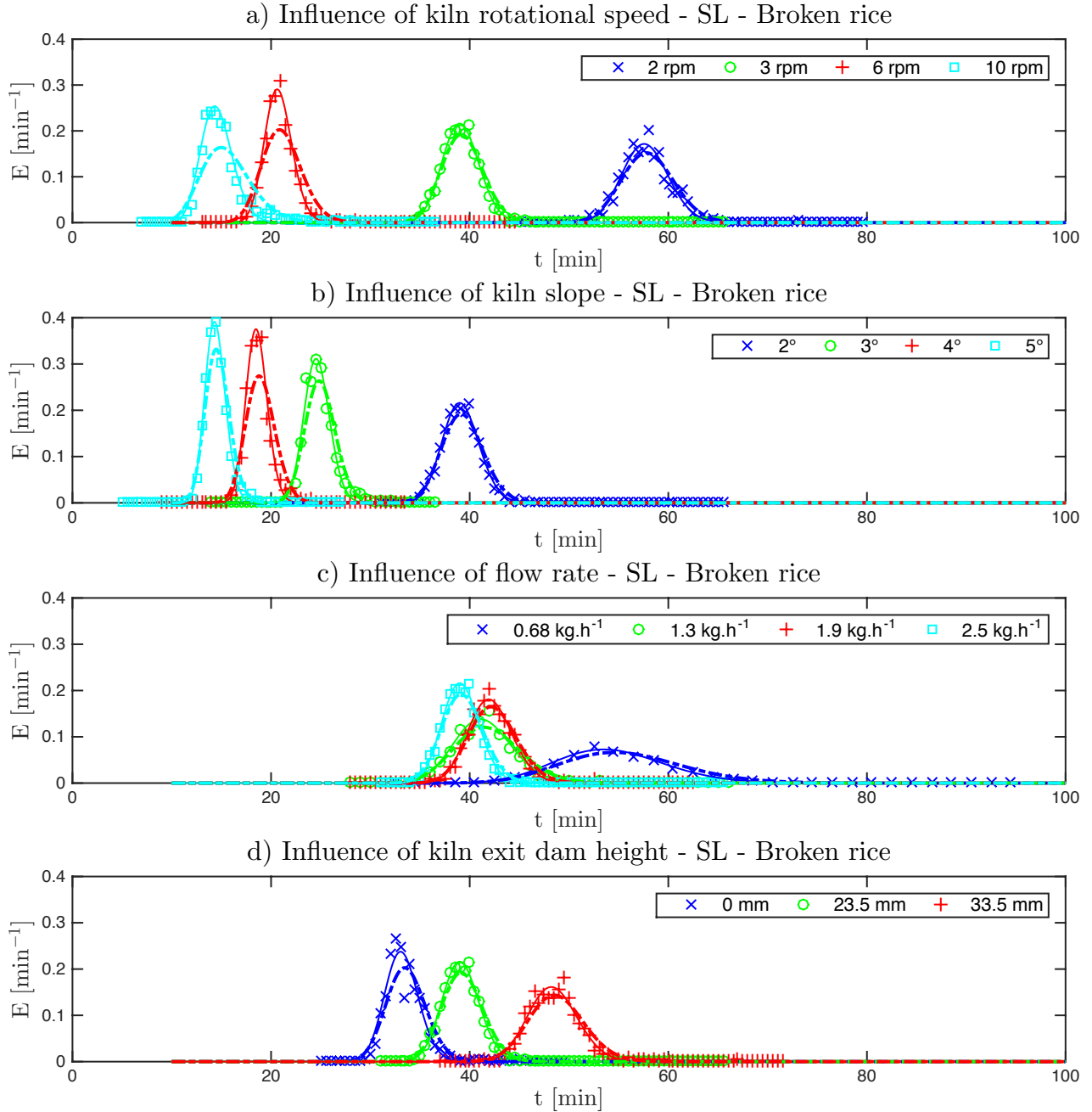


Figure B.4: Influence of operating parameters (N, S, \dot{M} and exit dam height) on the RTD for the flow of broken rice, when the kiln is equipped with straight lifters. Solid lines represent the axial dispersion model using fitted parameters. Dashed lines represent the axial dispersion model using theoretical parameters.

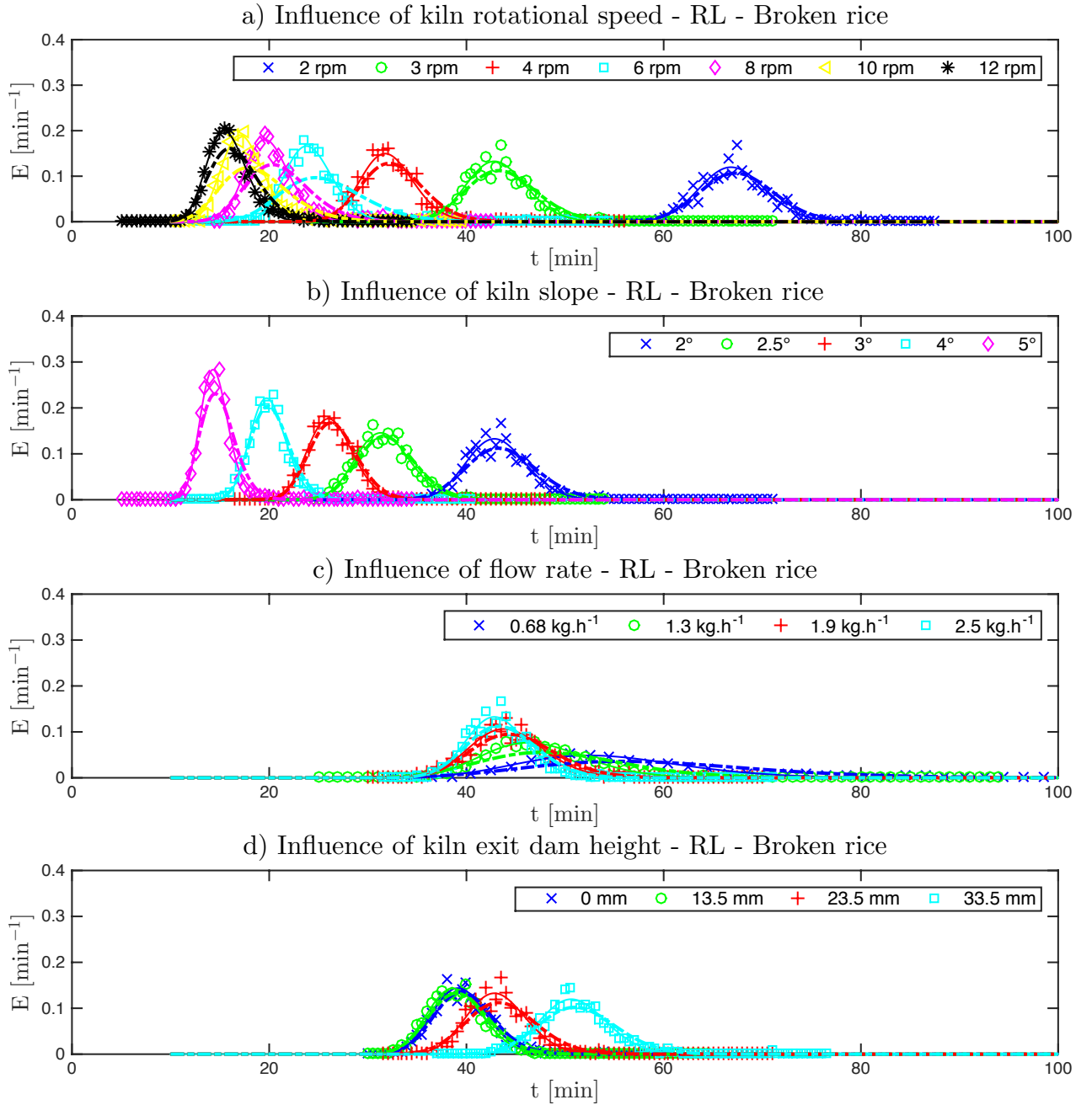


Figure B.5: Influence of operating parameters (N , S , \dot{M} and exit dam height) on the RTD for the flow of broken rice, when the kiln is equipped with rectangular lifters. Solid lines represent the axial dispersion model using fitted parameters. Dashed lines represent the axial dispersion model using theoretical parameters.

B.2.2 Results from RK2

In this section are presented the experimental RTD curves obtained while processing a bulk of beech chips with either no internal fixture (see Figure B.6), a grid (see Figure B.7), 3 rows of straight lifters (see Figure B.8) or 6 rows of straight lifters (see Figure B.9) installed at the kiln inner wall.

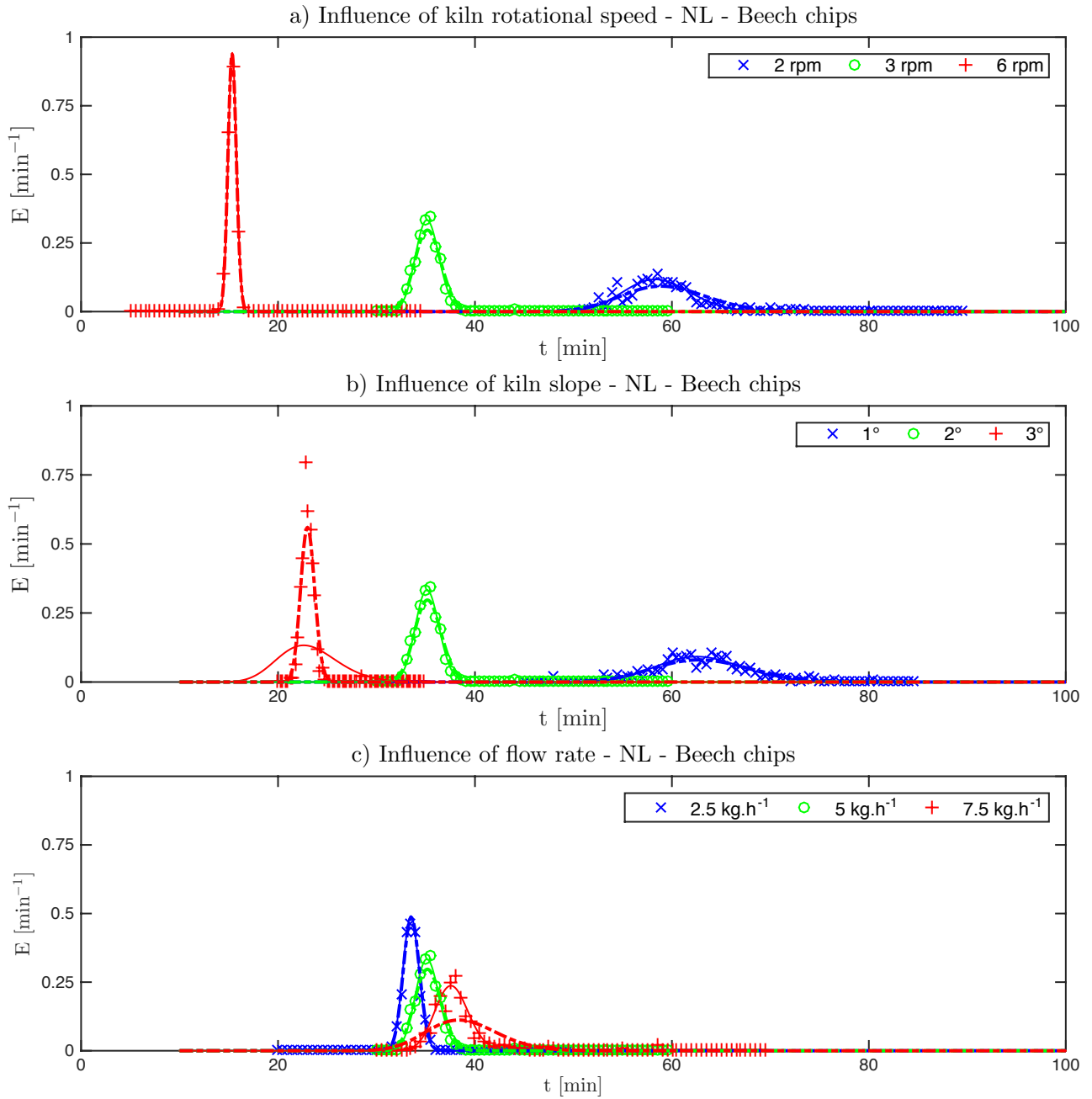


Figure B.6: Influence of operating parameters (N, S and \dot{M}) on the RTD for the flow of beech chips, when there is no internal fixture at the kiln wall. Solid lines represent the axial dispersion model using fitted parameters. Dashed lines represent the axial dispersion model using theoretical parameters.

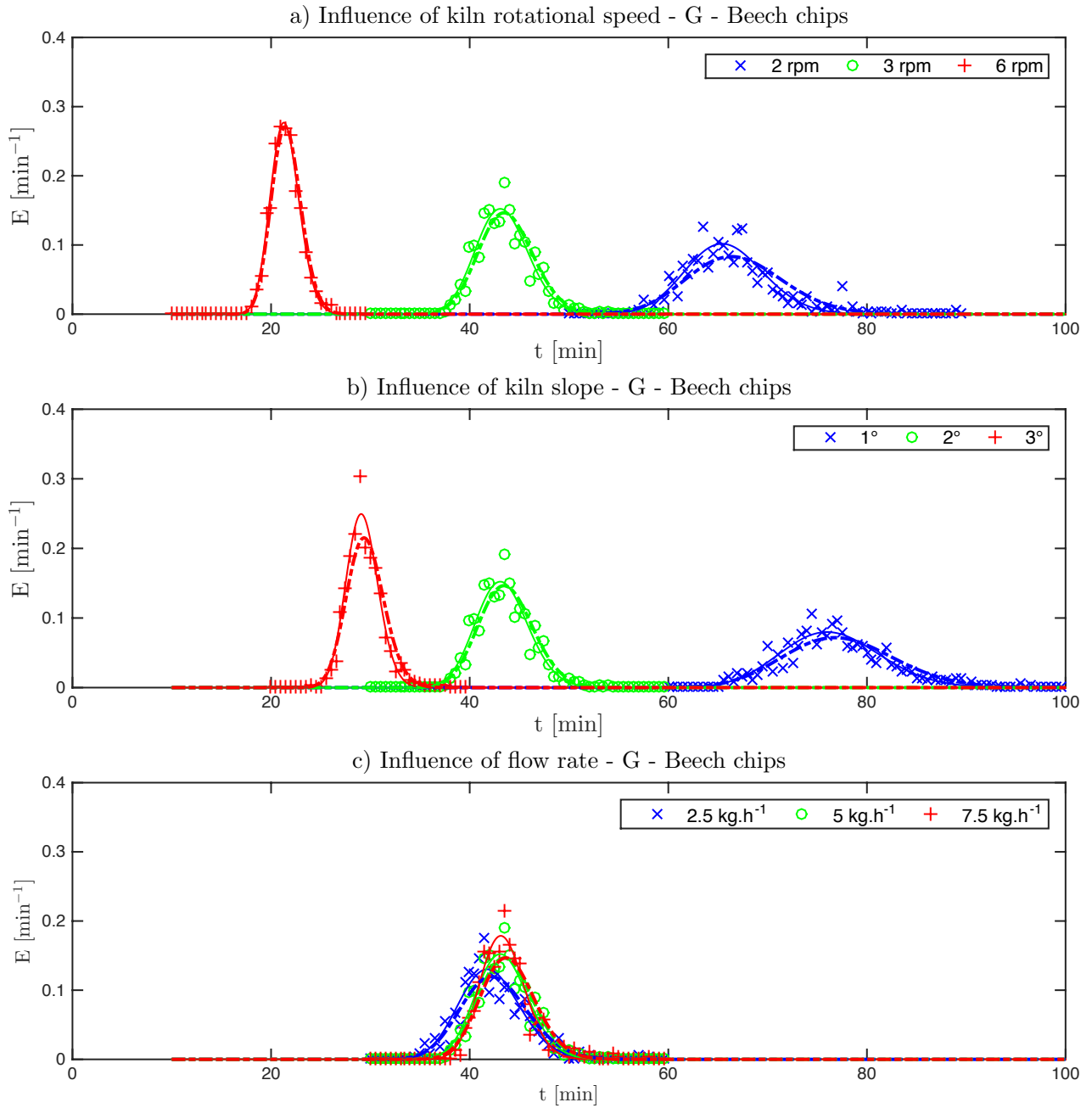


Figure B.7: Influence of operating parameters (N, S and M) on the RTD for the flow of beech chips, when the kiln is equipped with a grid. Solid lines represent the axial dispersion model using fitted parameters. Dashed lines represent the axial dispersion model using theoretical parameters.

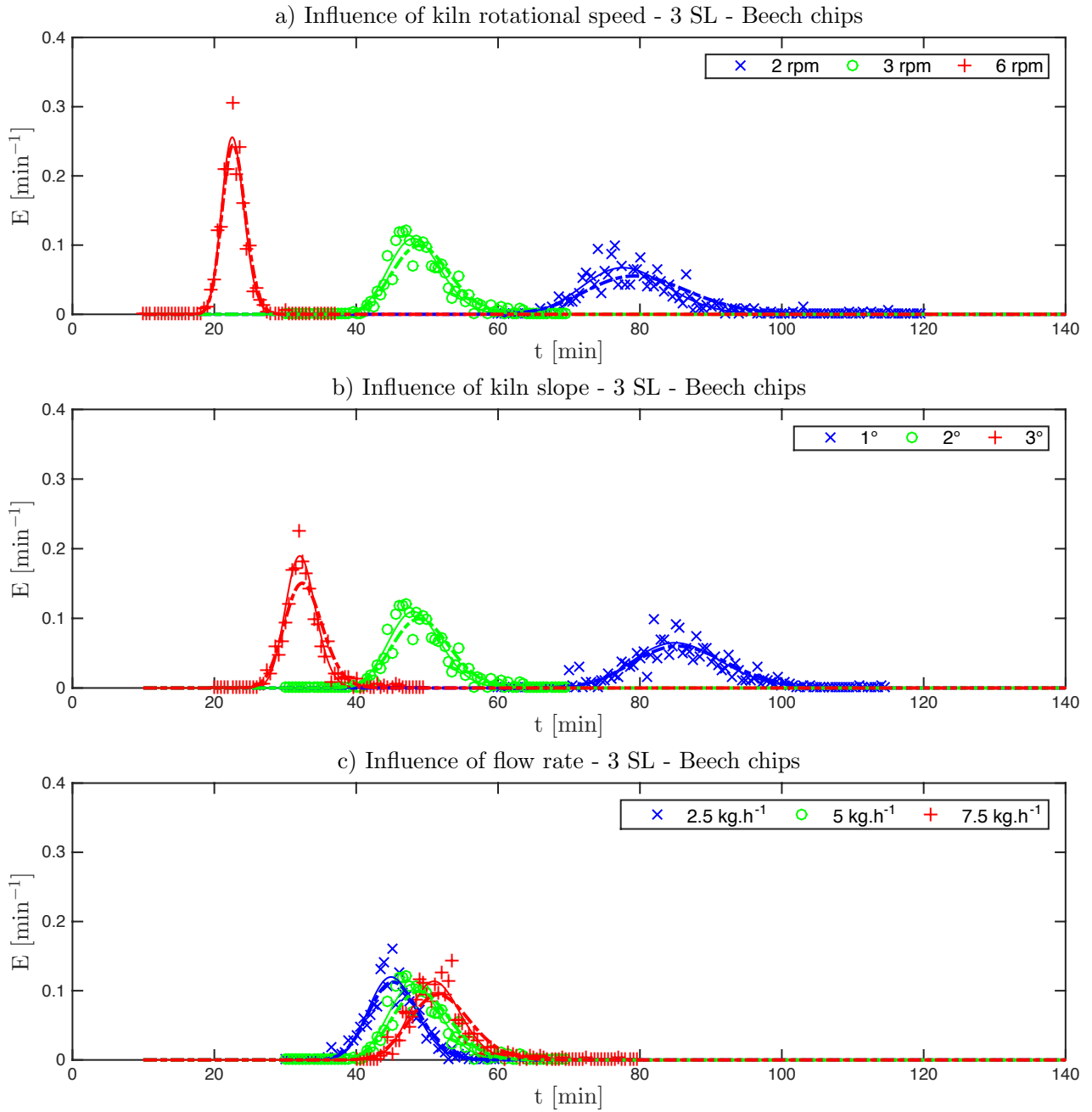


Figure B.8: Influence of operating parameters (N, S and \dot{M}) on the RTD for the flow of beech chips, when the kiln is equipped with 3 rows of straight lifters. Solid lines represent the axial dispersion model using fitted parameters. Dashed lines represent the axial dispersion model using theoretical parameters.

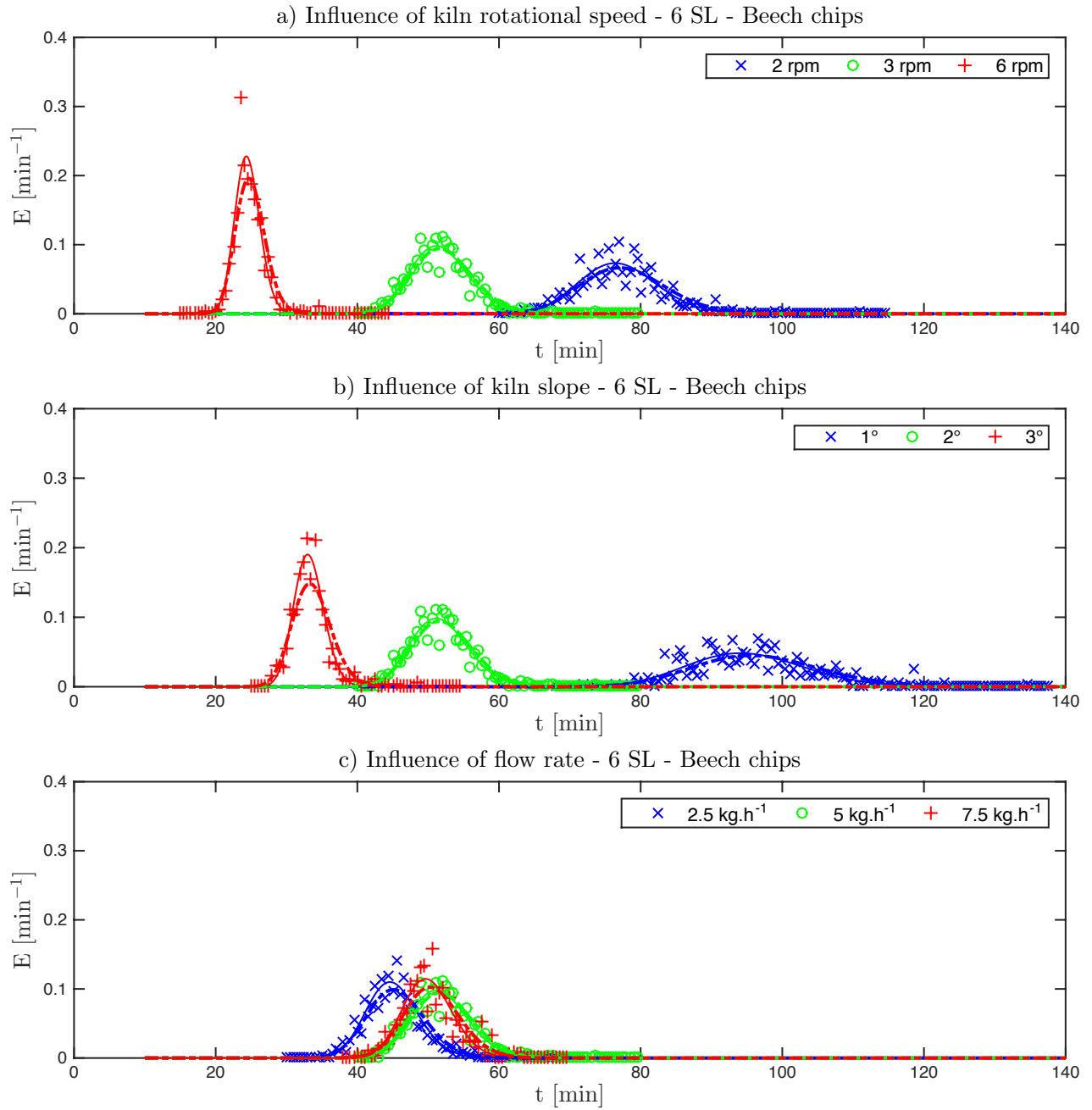


Figure B.9: Influence of operating parameters (N, S and M) on the RTD for the flow of beech chips, when the kiln is equipped with 6 rows of straight lifters. Solid lines represent the axial dispersion model using fitted parameters. Dashed lines represent the axial dispersion model using theoretical parameters.

B.3 Bed depth measurements results

Figure B.10 presents the experimental bed depth measurements performed within RK1 for varying operating conditions without lifters.

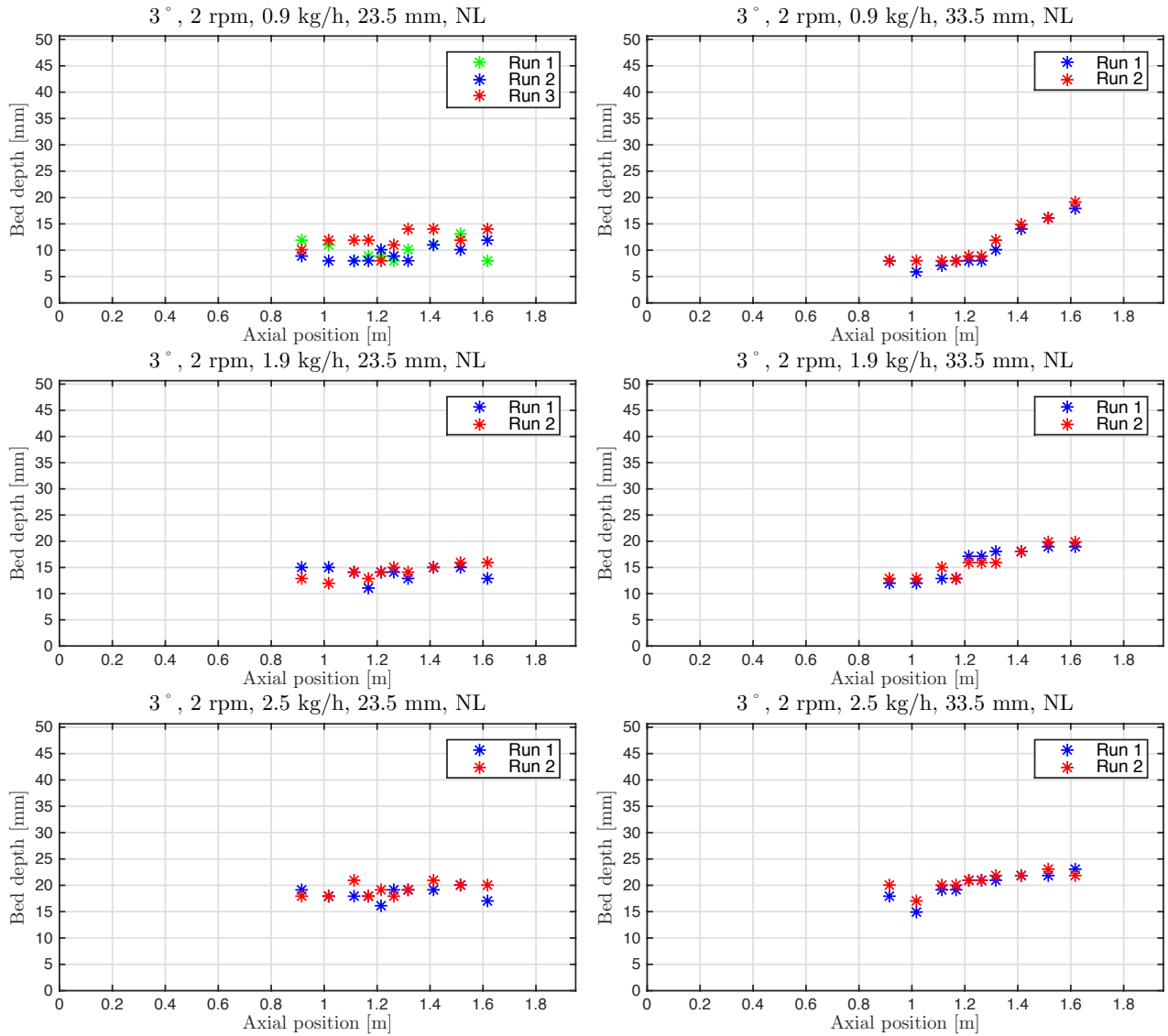


Figure B.10: Bed depth measurements.

Appendix C

Heat transfer

C.1 Experiments with rectangular lifters	262
C.2 Experiments without lifters	265
C.3 Experiments with straight lifters	269
C.3.1 Experiments without solids flow	269
C.3.2 Experiments with solids flow	271

The temperatures measurements of each run as given in Table 2.7, are presented in this part. For reasons of clarity the temperatures will be represented as solid lines.

The wall temperatures are averaged over the 4 thermocouples of each of the 4 series of thermocouples at the wall. Therefore, the wall temperatures along the kiln are represented by Tw1 before the heating zone, and inside the heating zone Tw2, Tw3 and Tw4.

Inside the kiln 5 series of 4 thermocouples are installed. In each of these series 1 thermocouple is embedded. The solids temperatures are measured at 5 positions: Ts1, Ts2, Ts3, Ts4 and Ts5. The remaining (3) thermocouples of each series measured the freeboard gas temperatures (see Figure C.1): at the top Tgu, at the bottom down in left side Tgbd, and the bottom up in right side Tgbu.

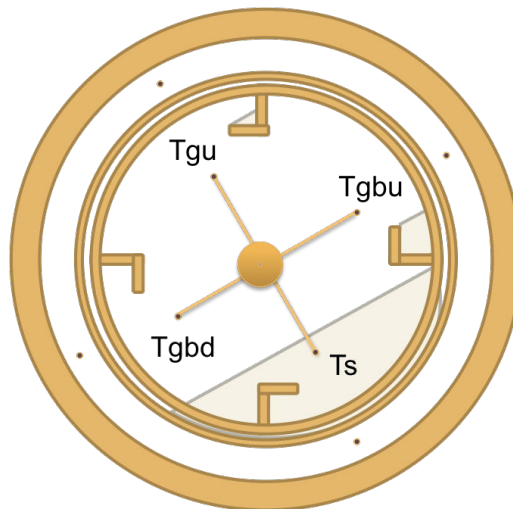


Figure C.1: One series of thermocouples in a cross section of the kiln

C.1 Experiments with rectangular lifters

Examples of temperature profiles for runs operated with rectangular lifters are presented in the Figures C.2, C.3 and C.4.

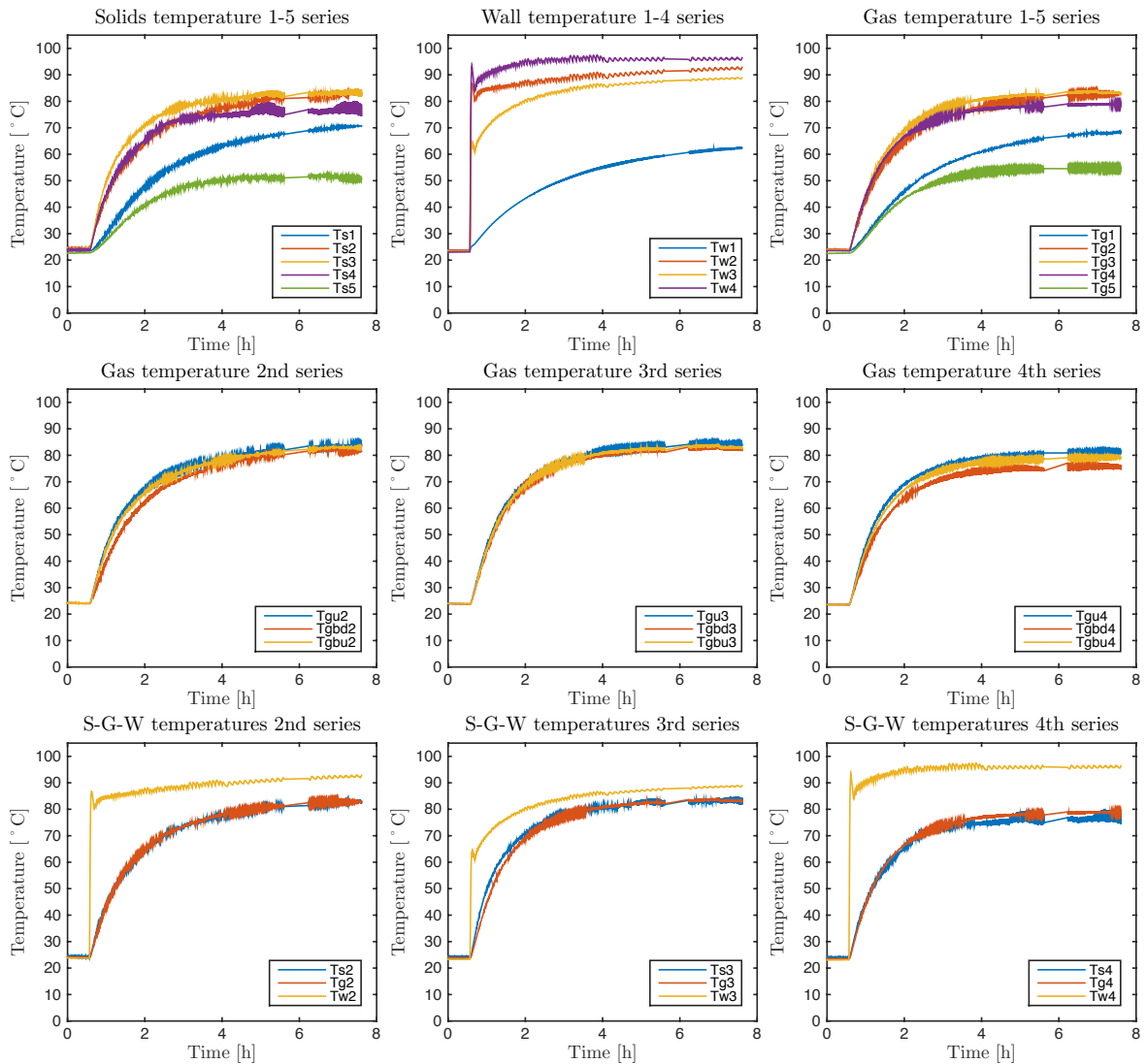


Figure C.2: Temperature profiles of kiln wall, solids and freeboard gas. Operating conditions: 2 rpm rotation speed, 3° slope, 0.9 kg.h⁻¹ MFR, 33.5 mm exit dam height using rectangular lifters, with a setpoint temperature of 100°C in zone 2.

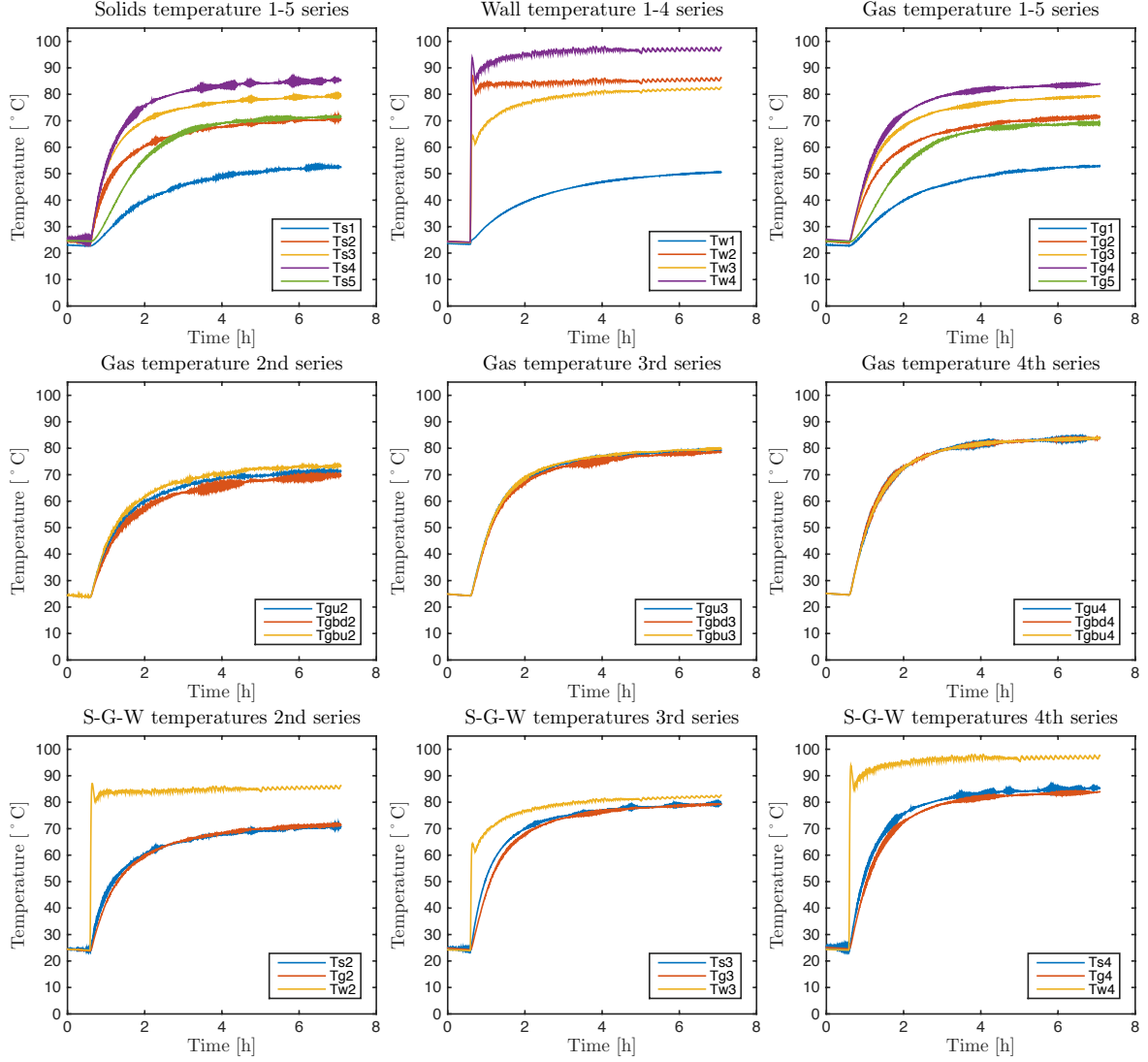


Figure C.3: Temperature profiles of kiln wall, solids and freeboard gas. Operating conditions: 2 rpm rotation speed, 3° slope, 2.5 kg.h⁻¹ MFR, 33.5 mm exit dam height using rectangular lifters, with a setpoint temperature of 100°C in zone 2.

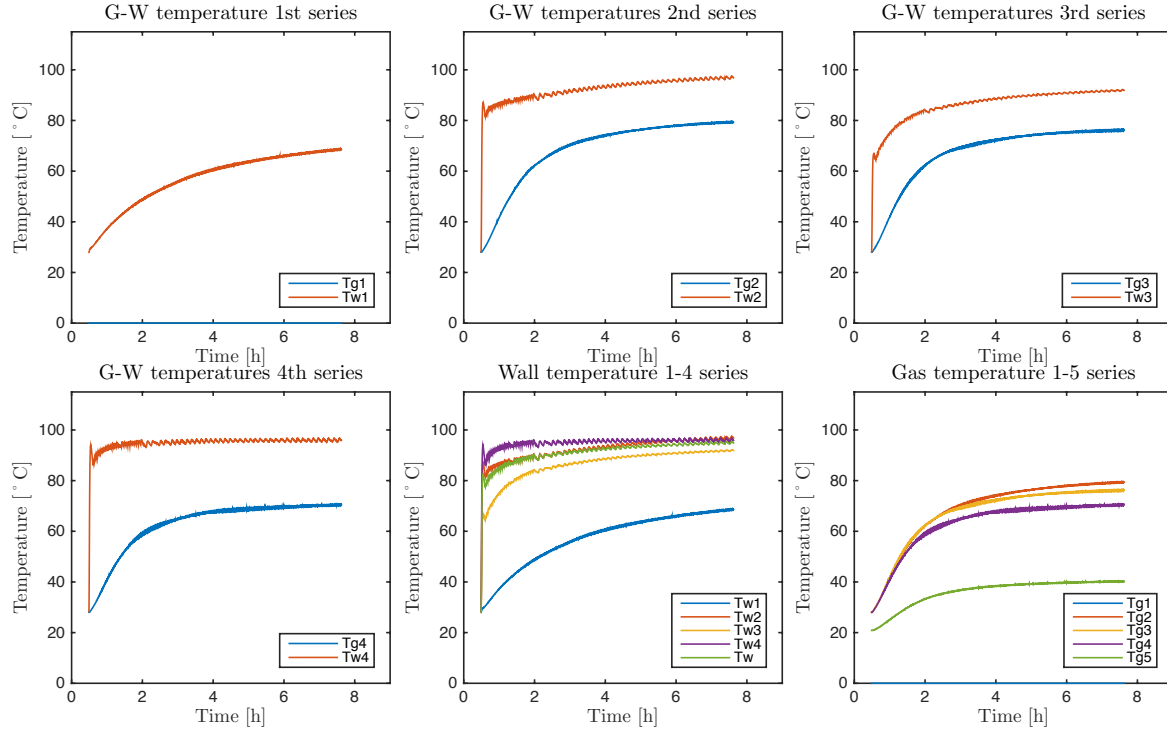


Figure C.4: Temperature profiles of kiln wall and freeboard gas. Operating conditions: 2 rpm rotation speed, 3° slope, no solids flow, 33.5 mm exit dam height using rectangular lifters, with a setpoint temperature of 100°C in zone 2.

C.2 Experiments without lifters

Examples of temperature profiles for runs operated without lifters are presented in the Figures C.5, C.6, C.7, C.8 and C.9.

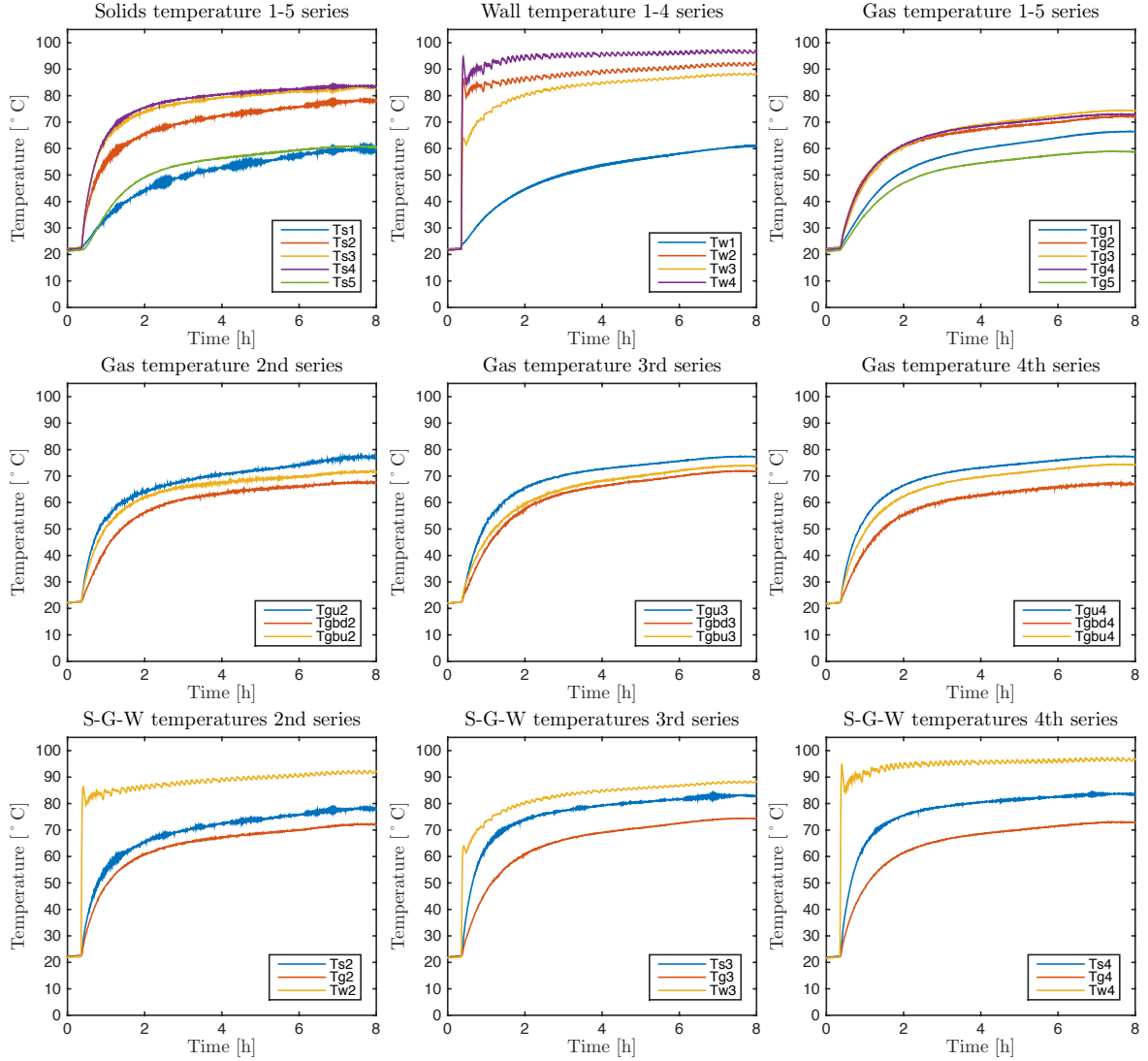


Figure C.5: Temperature profiles of kiln wall, solids and freeboard gas. Operating conditions: 2 rpm rotation speed, 3° slope, 0.9 kg.h⁻¹ MFR, 33.5 mm exit dam height without lifters, with a setpoint temperature of 100°C in zone 2.

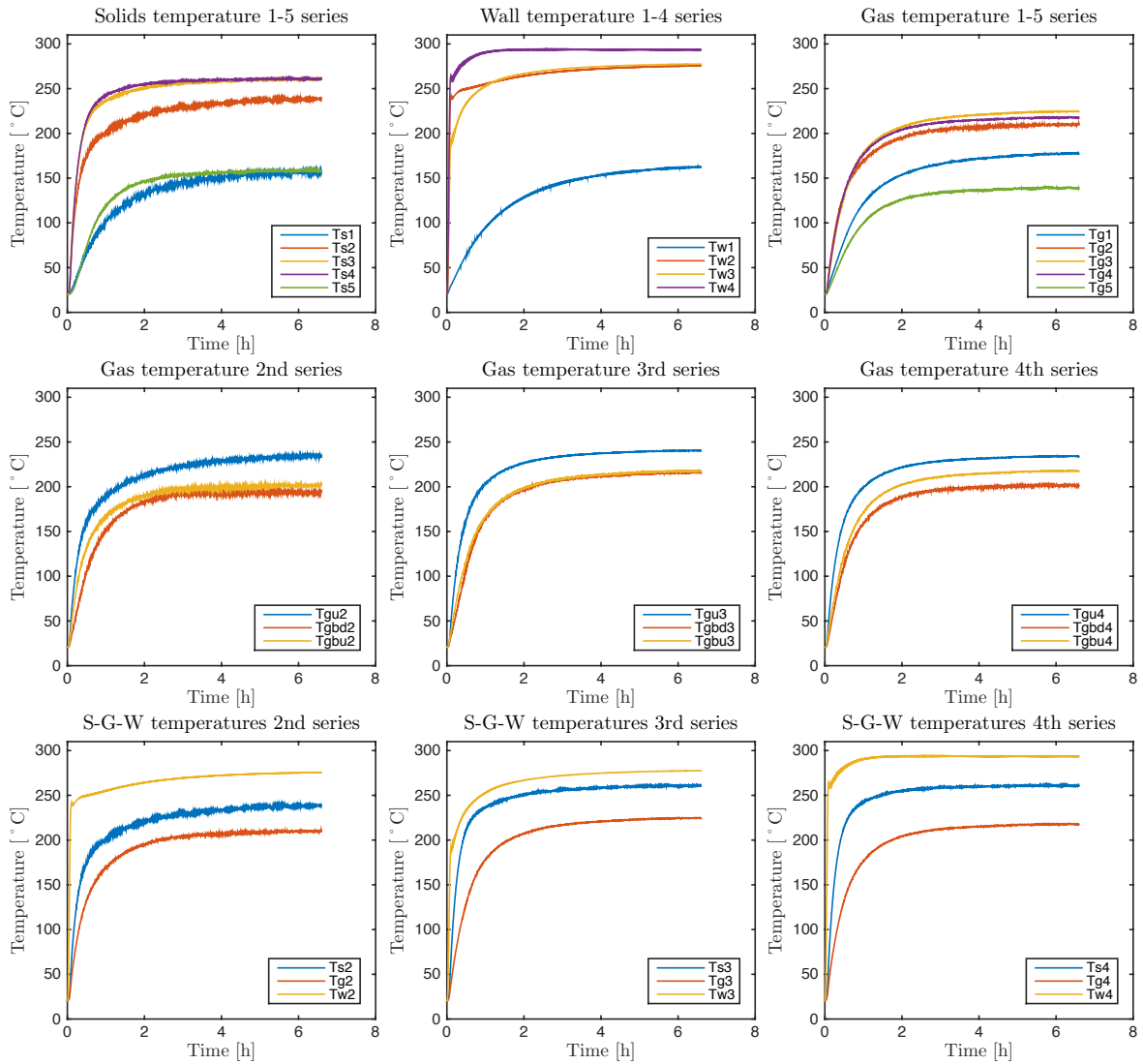


Figure C.6: Temperature profiles of kiln wall, solids and freeboard gas. Operating conditions: 2 rpm rotation speed, 3° slope, 0.9 kg.h⁻¹ MFR, 33.5 mm exit dam height without lifters, with a setpoint temperature of 300°C in zone 2.

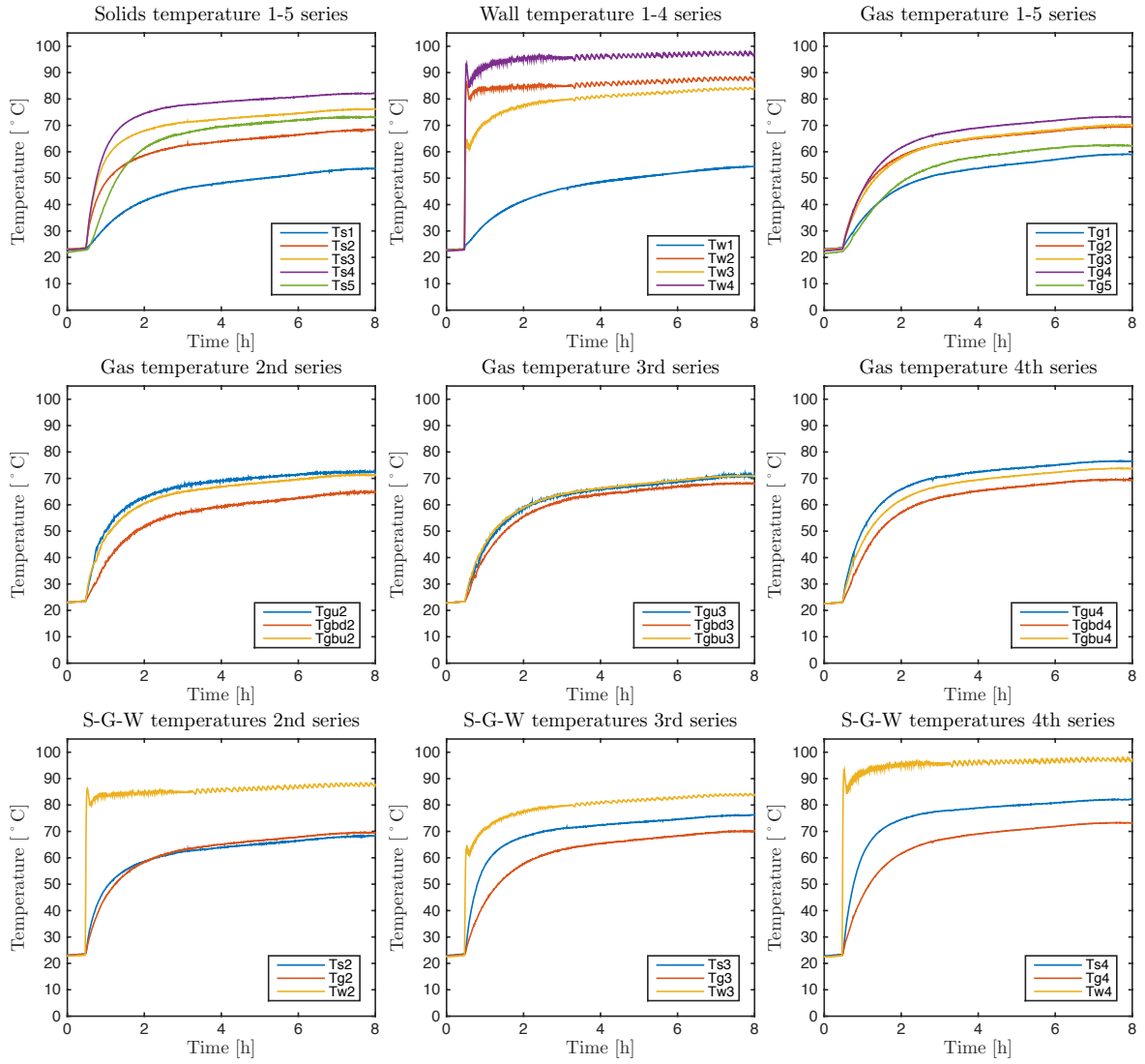


Figure C.7: Temperature profiles of kiln wall, solids and freeboard gas. Operating conditions: 2 rpm rotation speed, 3° slope, 2.5 kg.h⁻¹ MFR, 33.5 mm exit dam height without lifters, with a setpoint temperature of 100°C in zone 2.

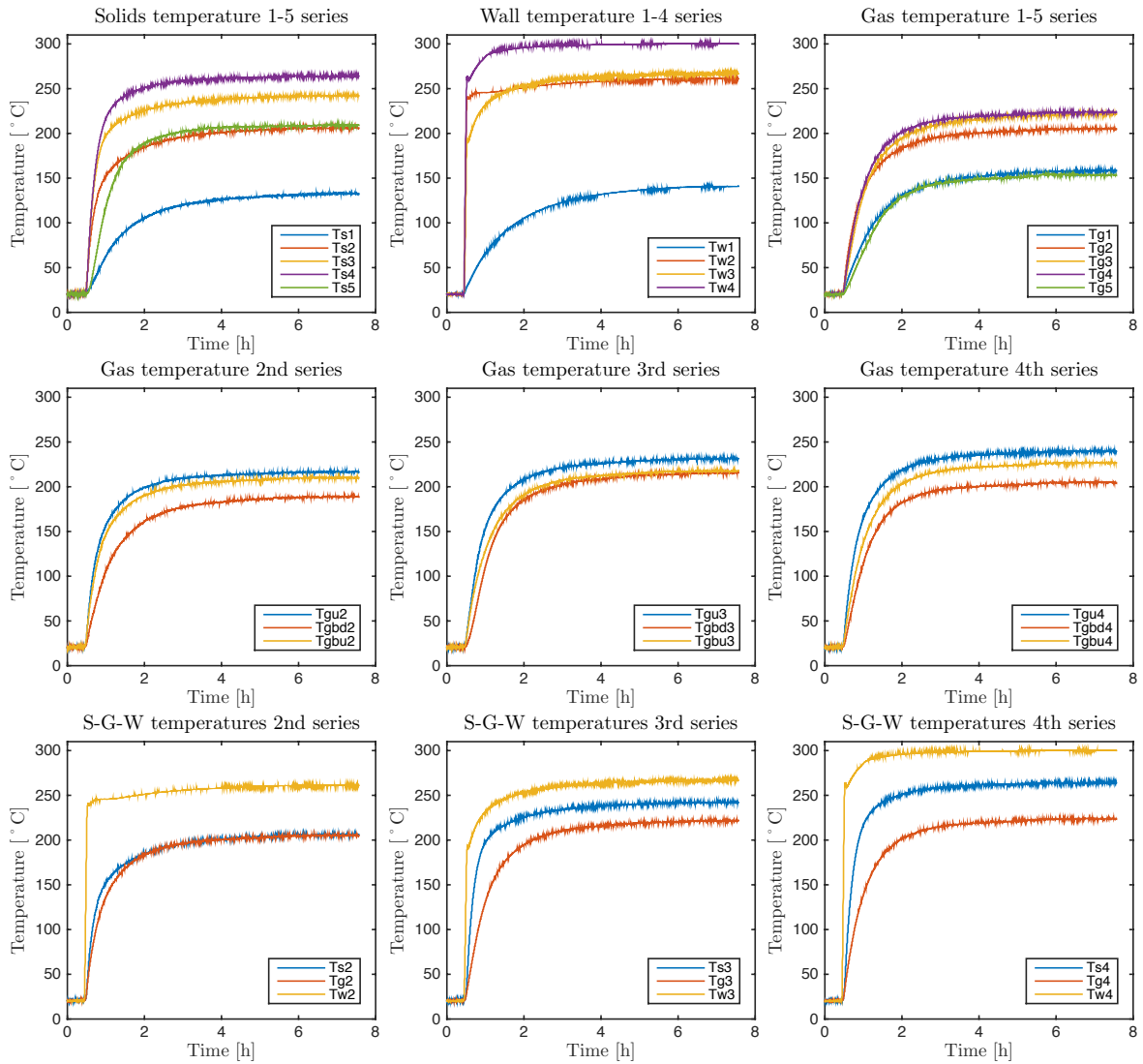


Figure C.8: Temperature profiles of kiln wall, solids and freeboard gas. Operating conditions: 2 rpm rotation speed, 3° slope, 2.5 kg.h⁻¹ MFR, 33.5 mm exit dam height without lifters, with a setpoint temperature of 300°C in zone 2.

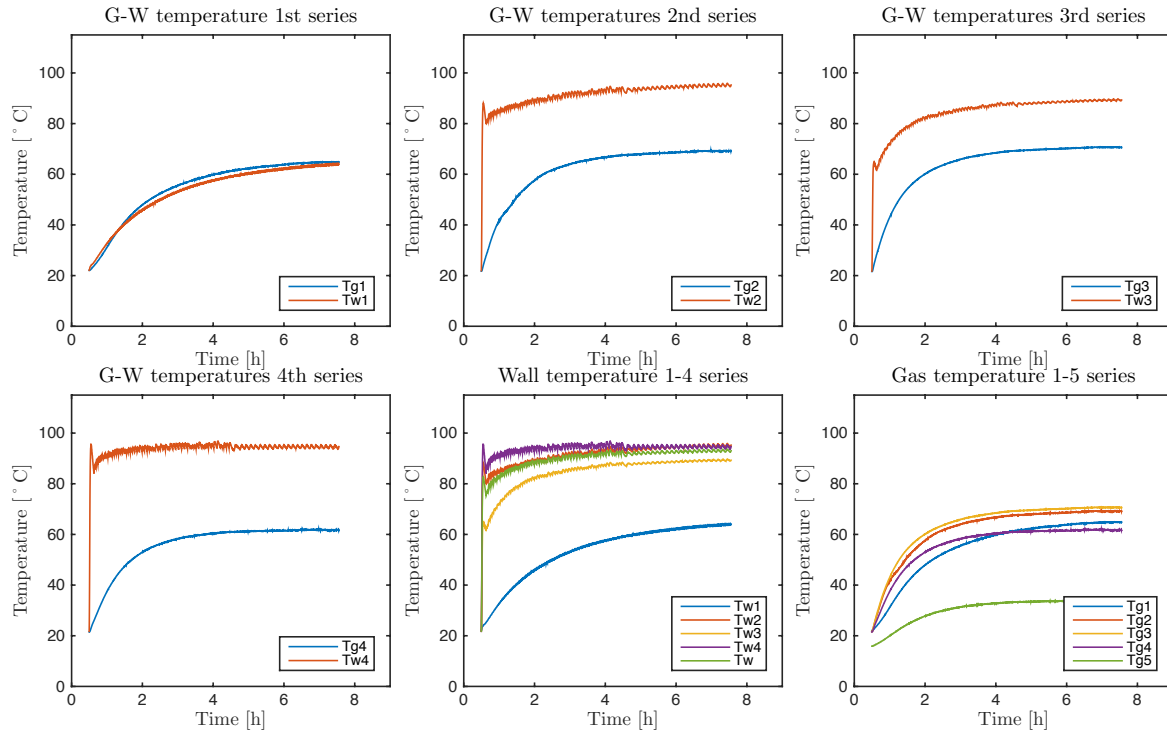


Figure C.9: Temperature profiles of kiln wall and freeboard gas. Operating conditions: 2 rpm rotation speed, 3° slope, no solids flow, 33.5 mm exit dam height without lifters, with a setpoint temperature of 100°C in zone 2.

C.3 Experiments with straight lifters

C.3.1 Experiments without solids flow

Some of the temperature profiles obtained while operating the kiln with straight lifters and without solids flow are presented in Figures C.10, C.11 and C.12.

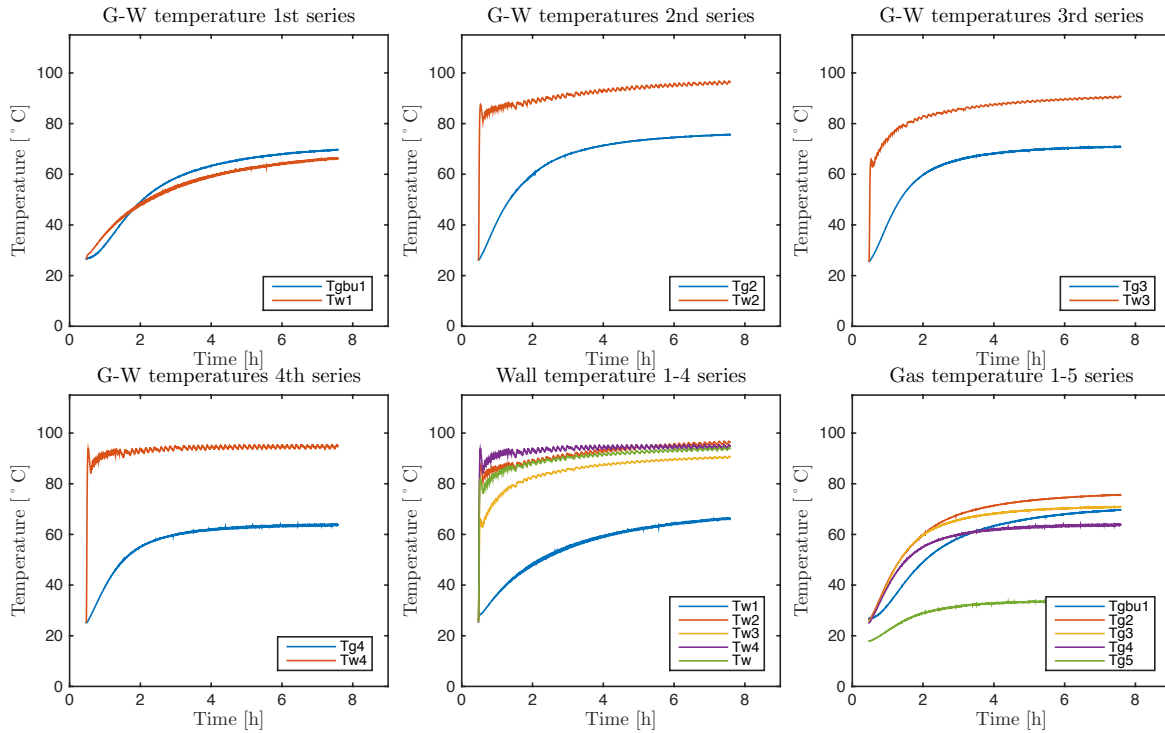


Figure C.10: Temperature profiles of kiln wall and freeboard gas. Operating conditions: 2 rpm rotation speed, 3° slope, no solids flow, 33.5 mm exit dam height with straight lifters, and a setpoint temperature of 100°C in zone 2.

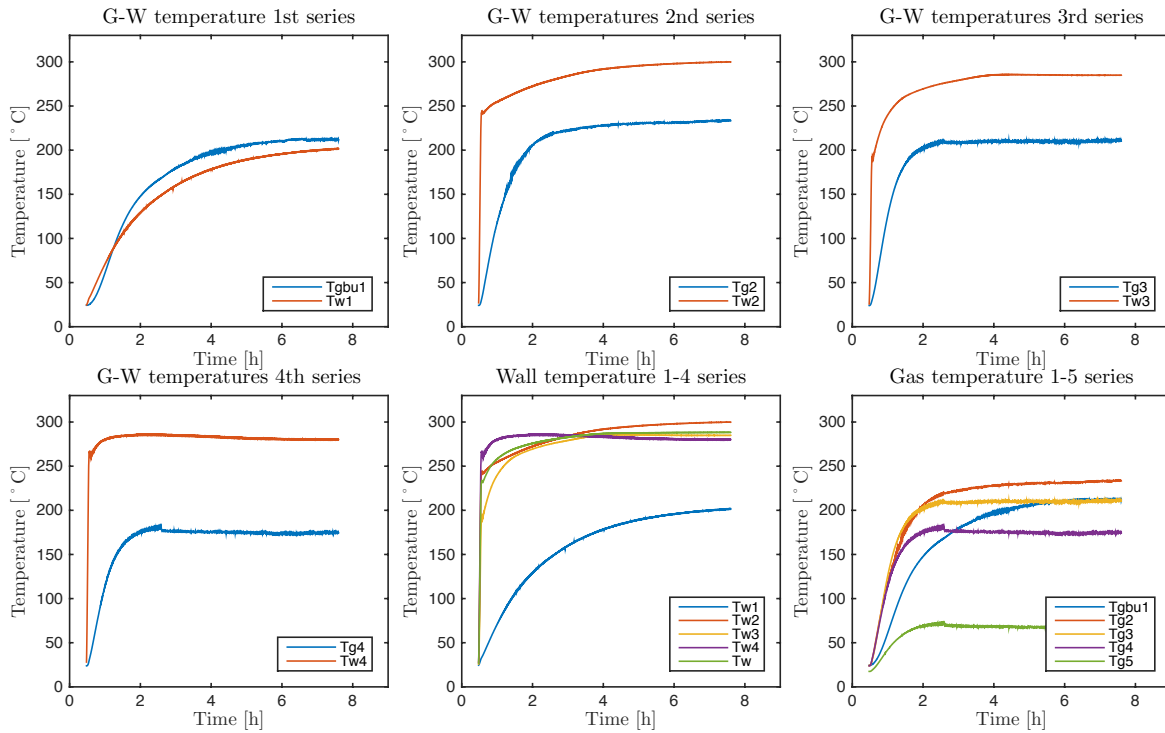


Figure C.11: Temperature profiles of kiln wall and freeboard gas. Operating conditions: 2 rpm rotation speed, 3° slope, no solids flow, 33.5 mm exit dam height with straight lifters, and a setpoint temperature of 300°C in zone 2.

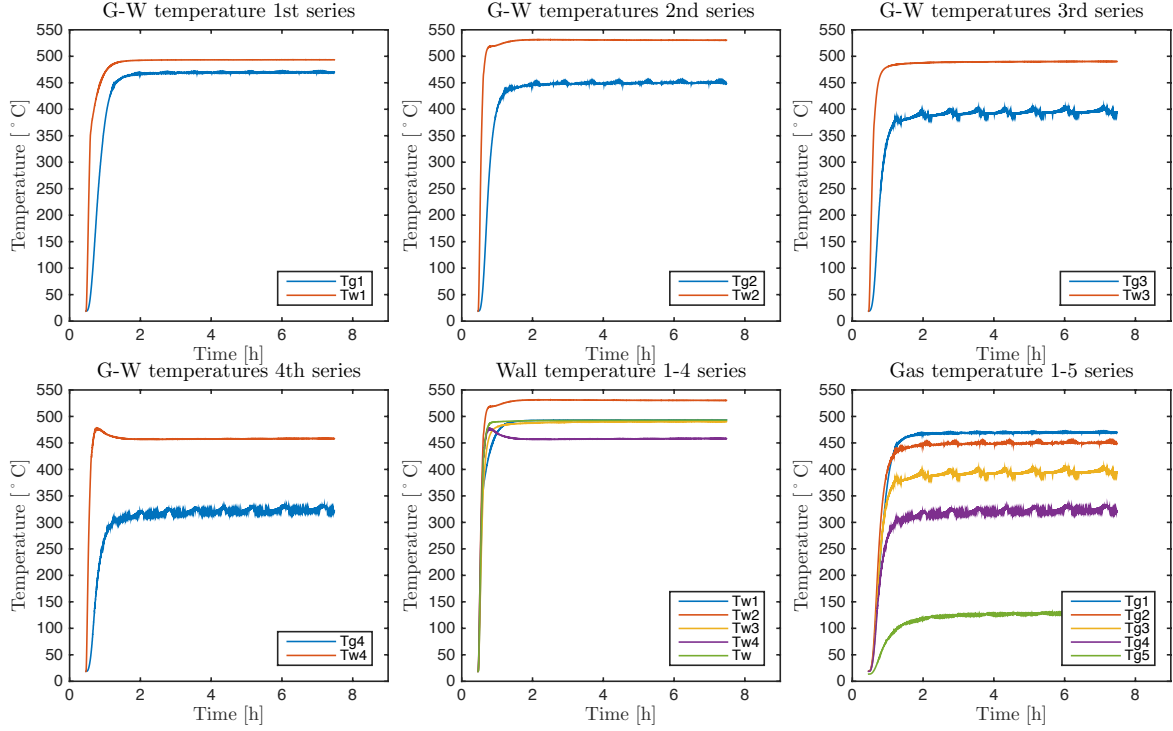


Figure C.12: Temperature profiles of kiln wall and freeboard gas. Operating conditions: 2 rpm rotation speed, 3° slope, no solids flow, 33.5 mm exit dam height with straight lifters, and a setpoint temperature of 500°C in zone 2.

C.3.2 Experiments with solids flow

Some of the temperature profiles obtained while operating the kiln with straight lifters with a solids flow are presented in Figures C.13, C.14, C.15, C.16, C.17, C.18, C.19, C.20 and C.21.

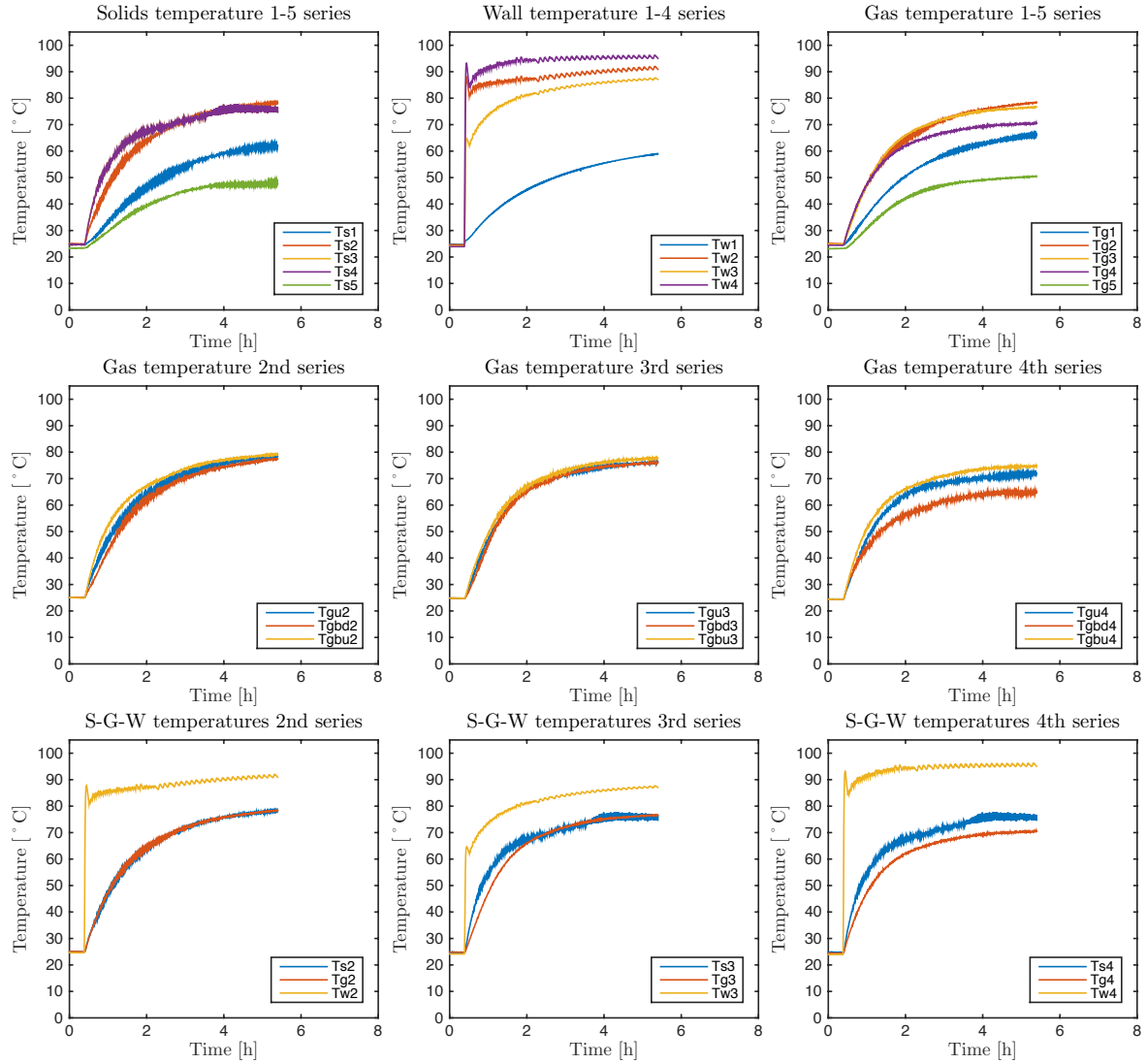


Figure C.13: Temperature profiles of kiln wall, solids and freeboard gas. Operating conditions: 2 rpm rotation speed, 3° slope, 0.9 kg.h⁻¹ MFR, 33.5 mm exit dam height with straight lifters, and a setpoint temperature of 100°C in zone 2.

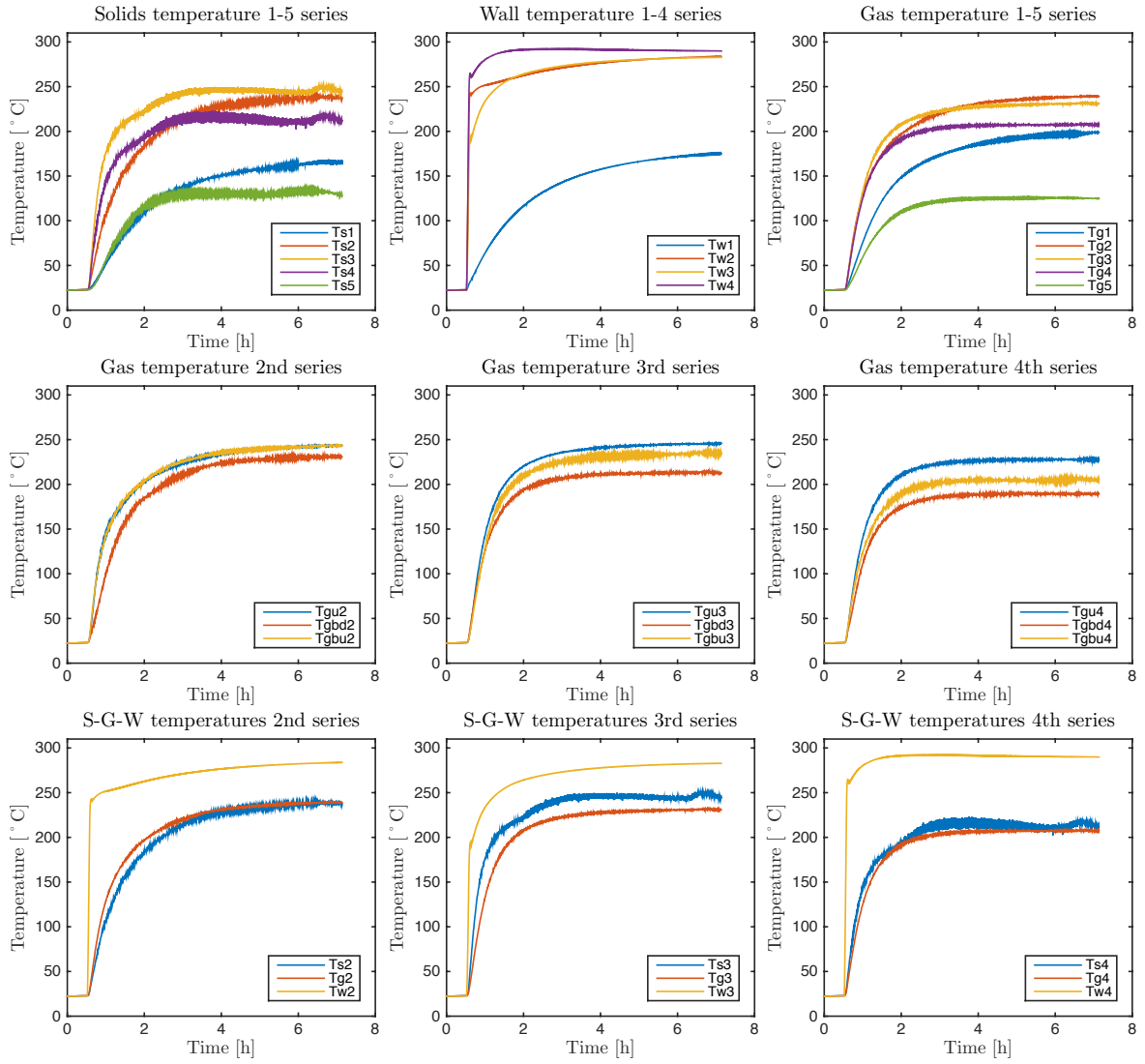


Figure C.14: Temperature profiles of kiln wall, solids and freeboard gas. Operating conditions: 2 rpm rotation speed, 3° slope, 0.9 kg.h⁻¹ MFR, 33.5 mm exit dam height with straight lifters, and a setpoint temperature of 300°C in zone 2.

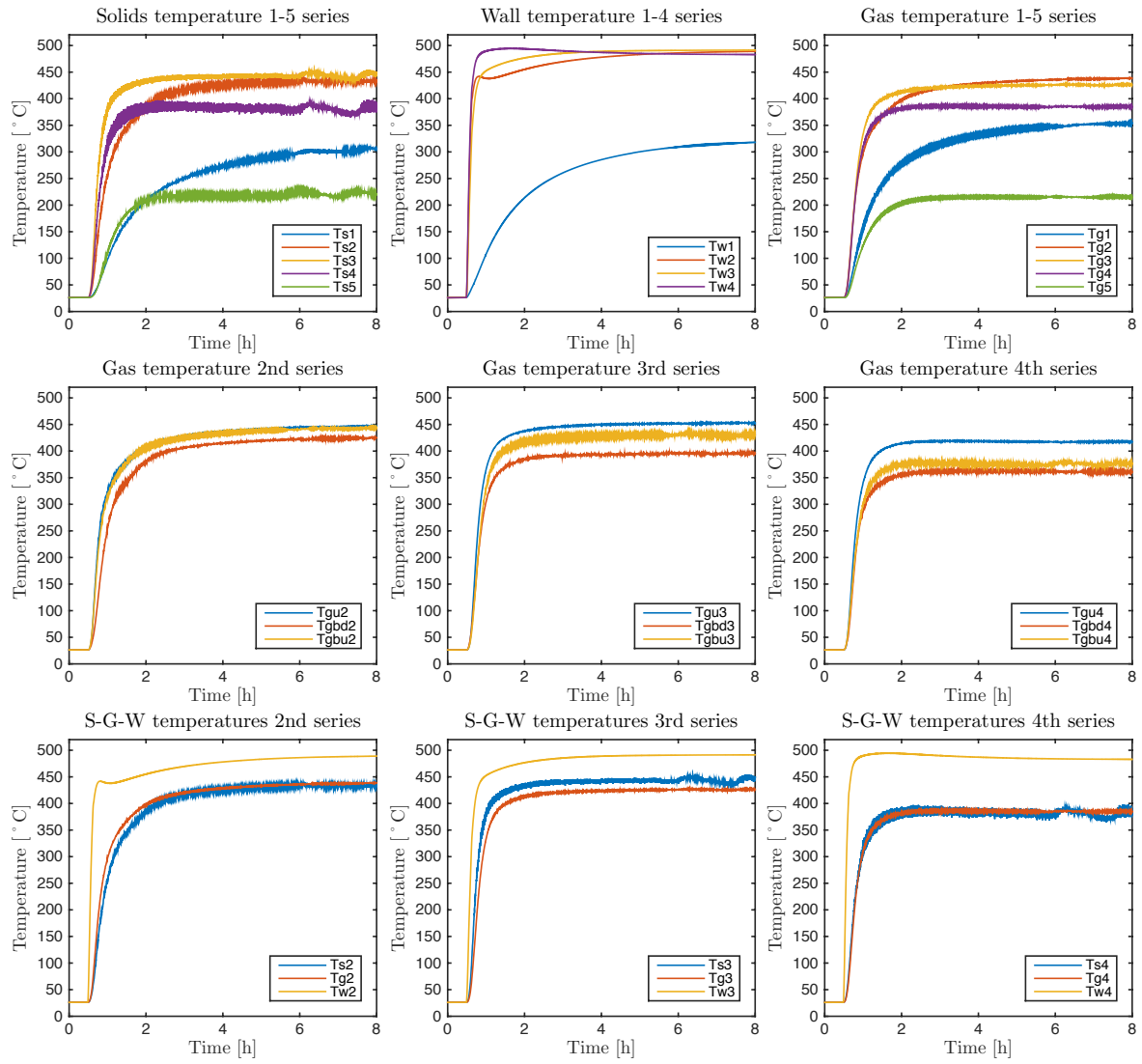


Figure C.15: Temperature profiles of kiln wall, solids and freeboard gas. Operating conditions: 2 rpm rotation speed, 3° slope, 0.9 kg.h⁻¹ MFR, 33.5 mm exit dam height with straight lifters, and a setpoint temperature of 500°C in zone 2.

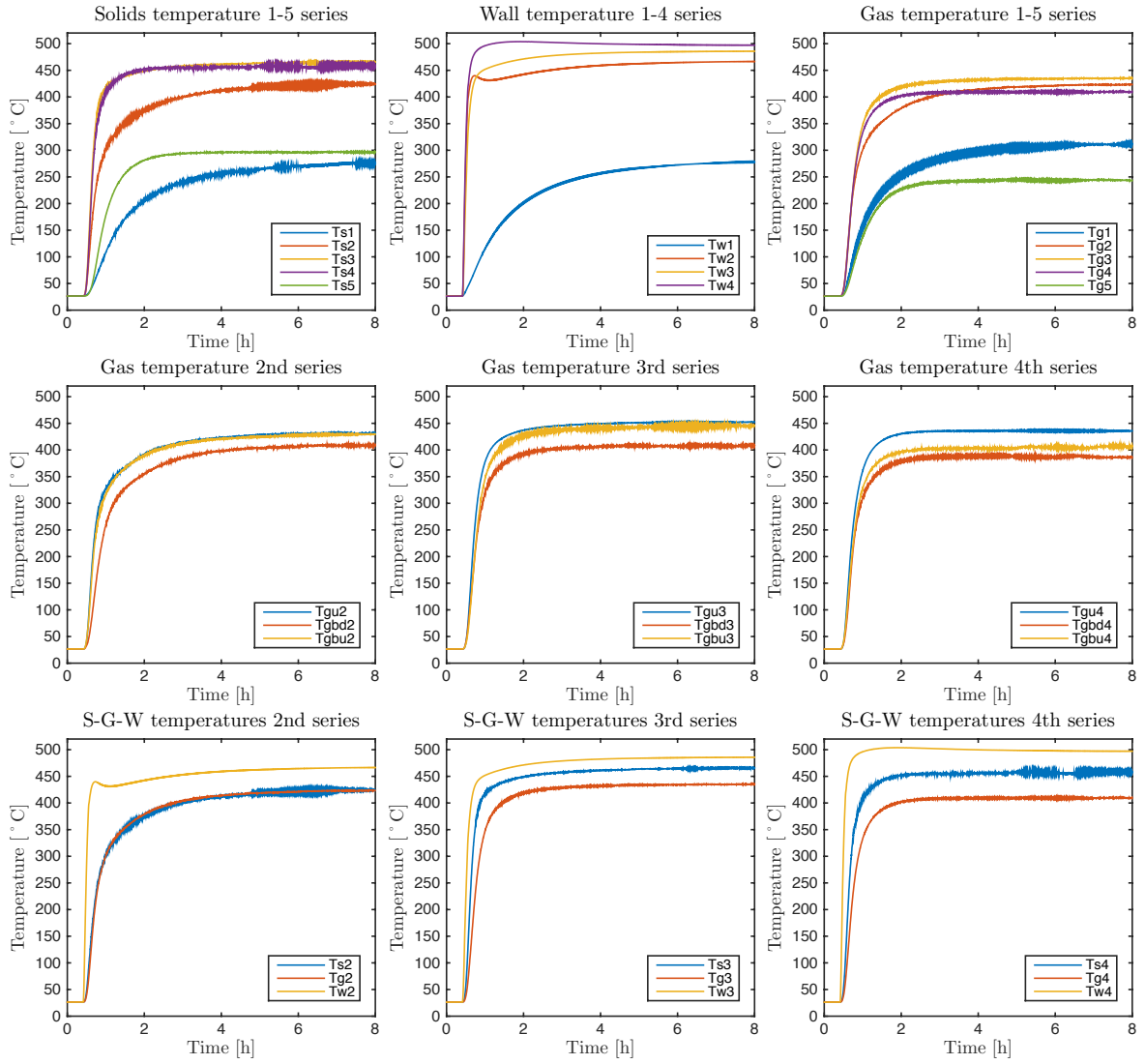


Figure C.16: Temperature profiles of kiln wall, solids and freeboard gas. Operating conditions: 2 rpm rotation speed, 3° slope, 1.8 kg.h⁻¹ MFR, 33.5 mm exit dam height with straight lifters, and a setpoint temperature of 500°C in zone 2.

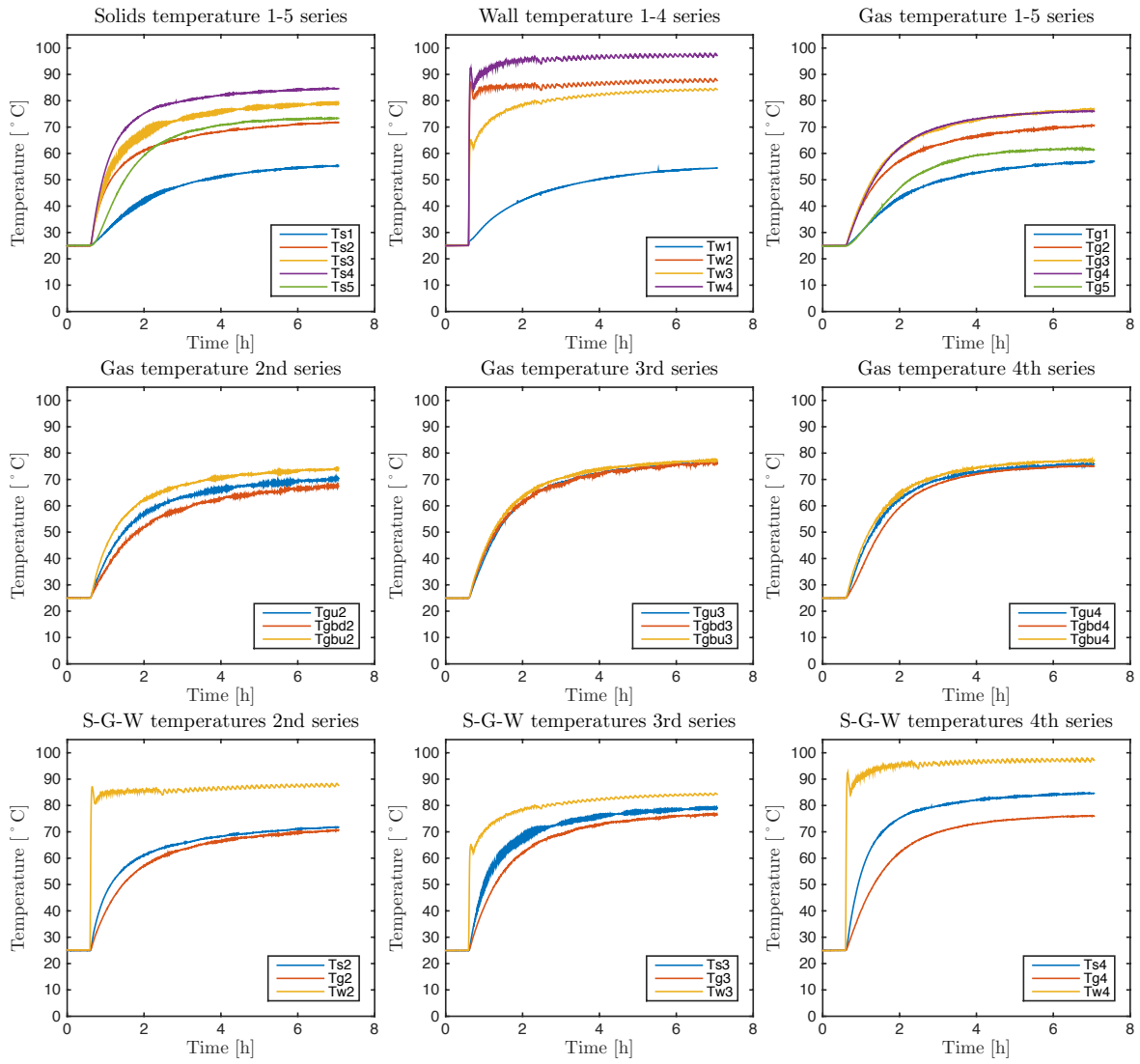


Figure C.17: Temperature profiles of kiln wall, solids and freeboard gas. Operating conditions: 2 rpm rotation speed, 3° slope, 2.5 kg.h⁻¹ MFR, 33.5 mm exit dam height with straight lifters and a setpoint temperature of 500°C in zone 2.

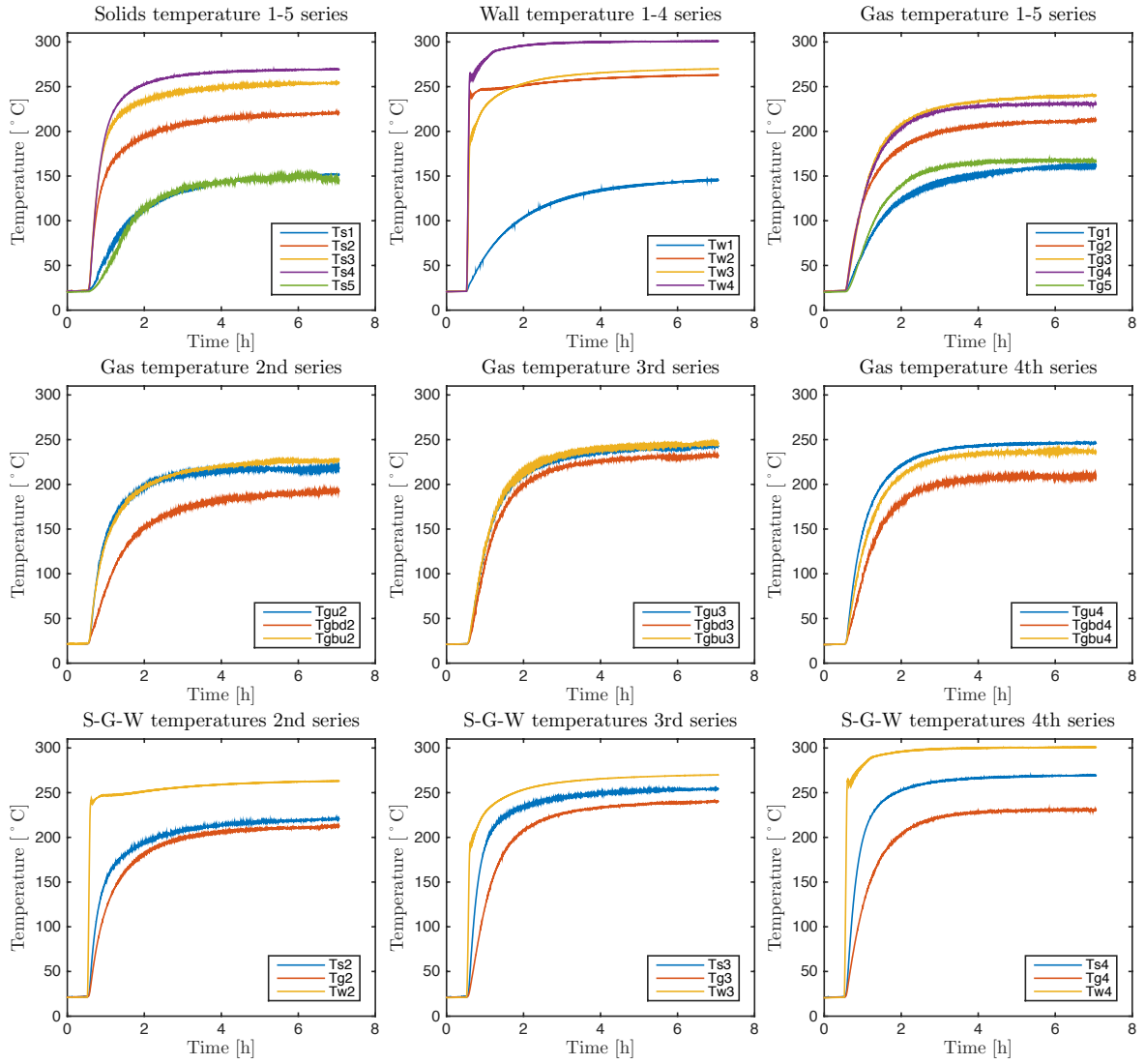


Figure C.18: Temperature profiles of kiln wall, solids and freeboard gas. Operating conditions: 2 rpm rotation speed, 3° slope, 2.5 kg.h⁻¹ MFR, 33.5 mm exit dam height with straight lifters, and a setpoint temperature of 300°C in zone 2.

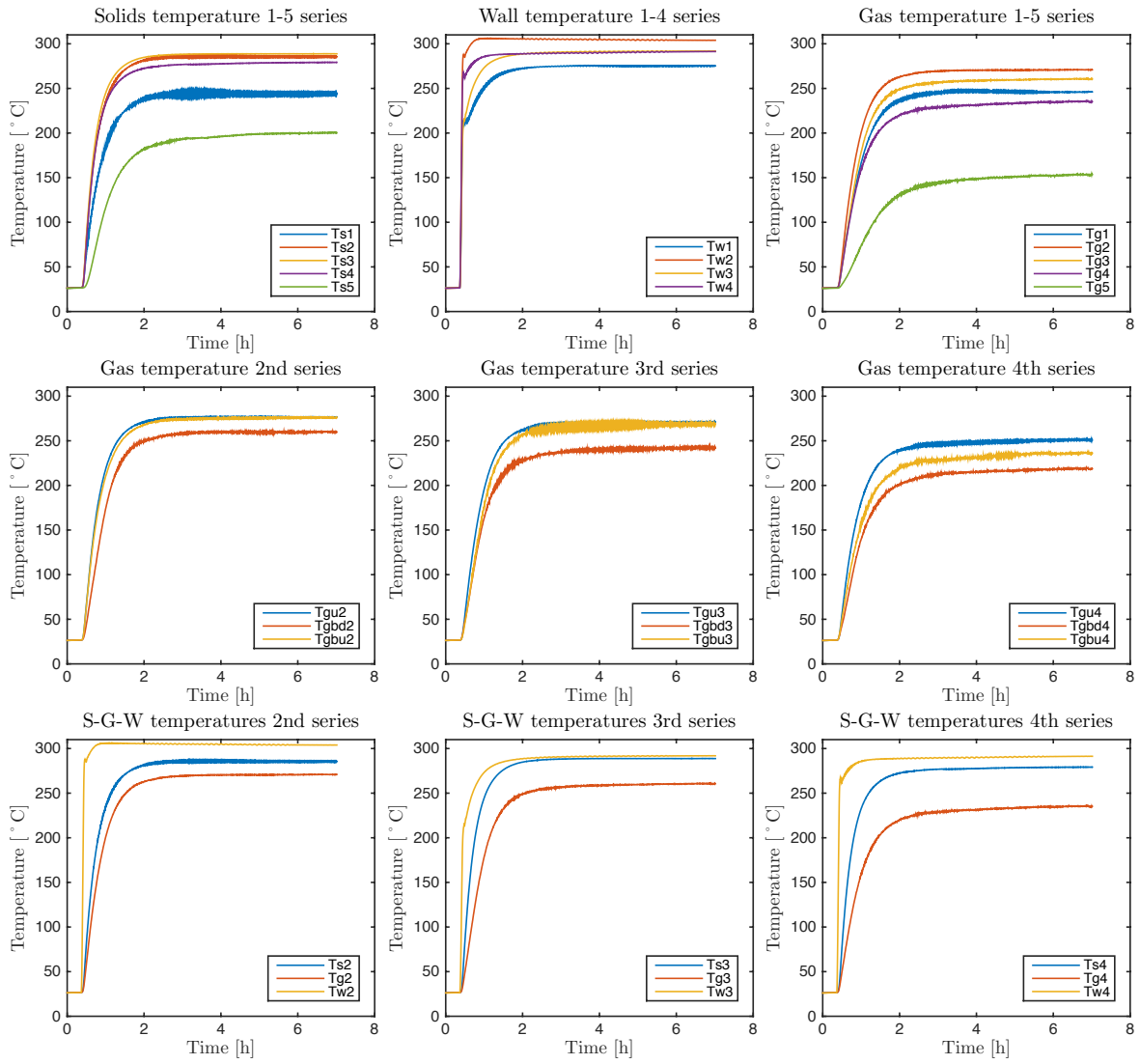


Figure C.19: Temperature profiles of kiln wall, solids and freeboard gas. Operating conditions: 2 rpm rotation speed, 3° slope, 2.5 kg.h⁻¹ MFR, 33.5 mm exit dam height with straight lifters, and a setpoint temperature of 300°C in zones 1 and 2.

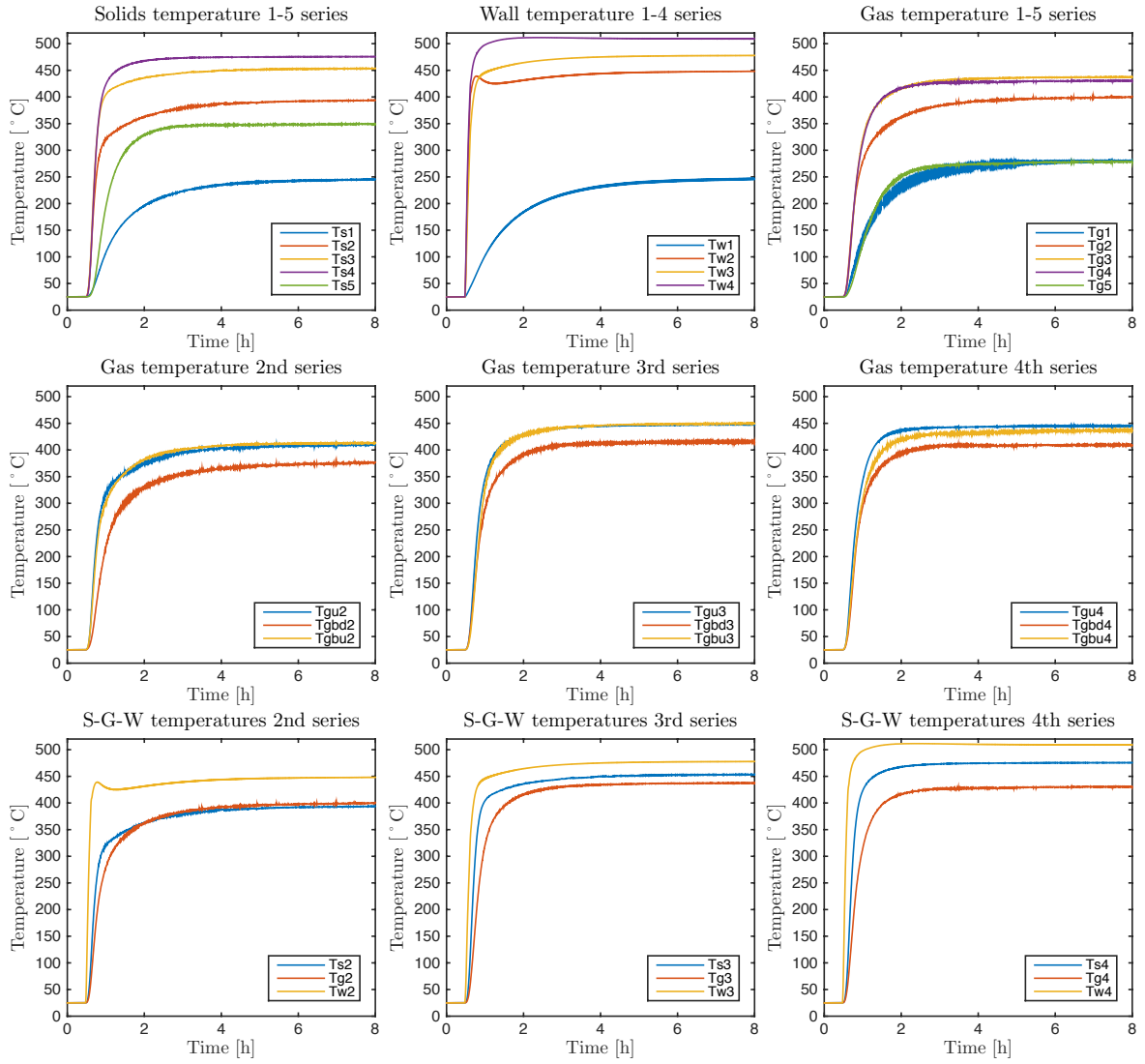


Figure C.20: Temperature profiles of kiln wall, solids and freeboard gas. Operating conditions: 2 rpm rotation speed, 3° slope, 2.5 kg.h⁻¹ MFR, 33.5 mm exit dam height with straight lifters, and a setpoint temperature of 500°C in zone 2.

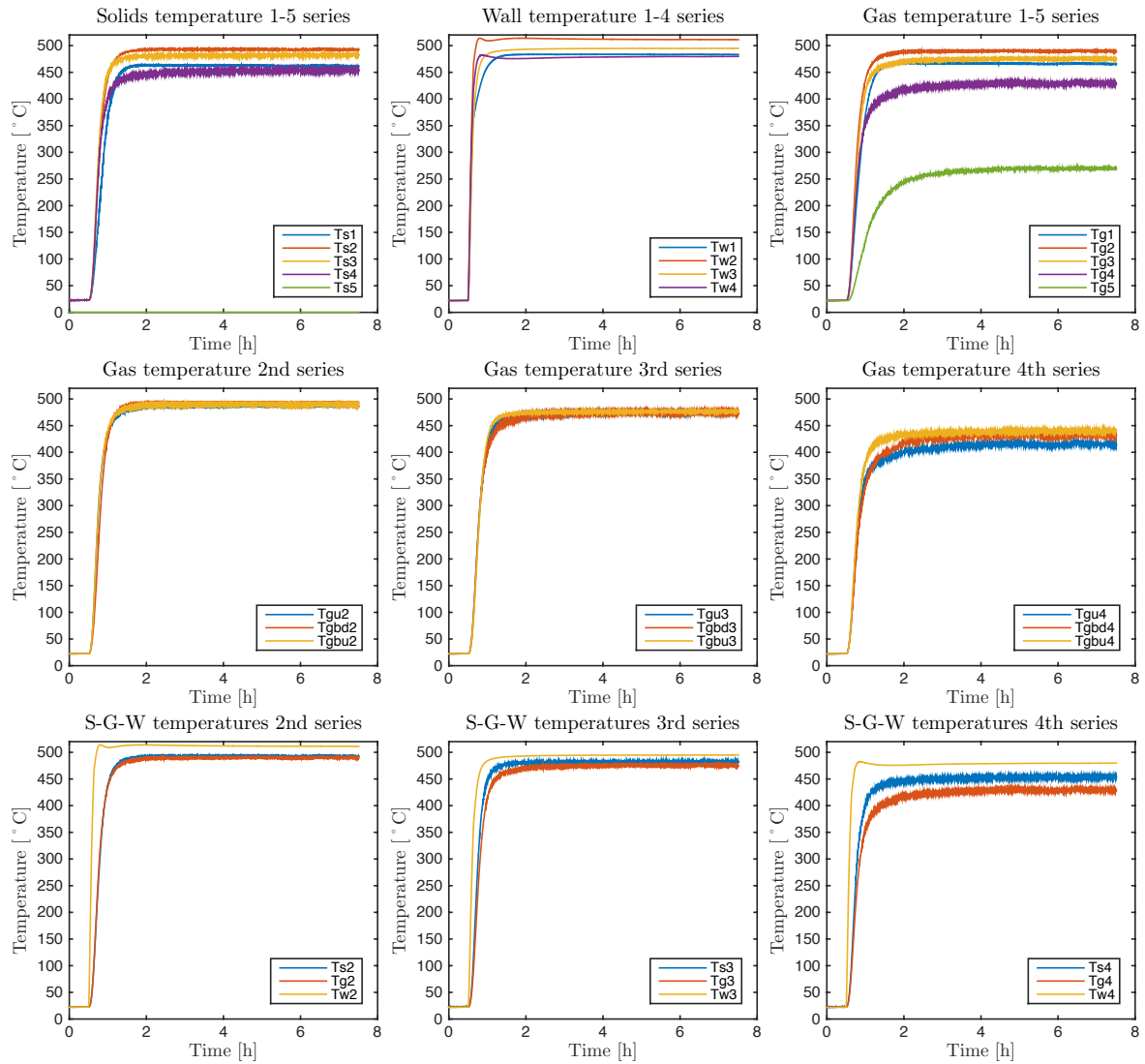


Figure C.21: Temperature profiles of kiln wall, solids and freeboard gas. Operating conditions: 12 rpm rotation speed, 3° slope, 2.5 kg.h⁻¹ MFR, 33.5 mm exit dam height with straight lifters, and a setpoint temperature of 500°C in zones 1 and 2.

Bibliography

- [Ablitzer 2000] Denis Ablitzer & Hani Henein. *A Phenomenological Analysis of Particulate Solids in the Operation of Rotary Reactors*. In Proceedings of the Brimacombe Memorial Symposium, October 2000.
- [Abouzeid 1974] A.-Z.M.A. Abouzeid, T.S. Mika, K.V. Sastry & D.W. Fuerstenau. *The influence of operating variables on the residence time distribution for material transport in a continuous rotary drum*. Powder Technology, vol. 10, no. 6, pages 273–288, 1974
- [Abouzeid 1980] A.-Z.M. Abouzeid, D.W. Fuerstenau & K.V. Sastry. *Transport behavior of particulate solids in rotary drums: scale-up of residence time distribution using the axial dispersion model*. Powder Technology, vol. 27, no. 2, pages 241–250, November 1980
- [Abouzeid 2010] Abdel-Zaher M. Abouzeid & Douglas W. Fuerstenau. *Flow of Non-Homogeneous Particulates in Rotating Drums*. KONA Powder and Particle Journal, no. 28, pages 155–166, 2010.
- [Afacan 1990] A. Afacan & J.H. Masliyah. *Solids hold-up in rotary drums*. Powder Technology, vol. 61, no. 2, pages 179–184, 1990
- [Ajayi 2012] O.O. Ajayi & M.E. Sheehan. *Design loading of free flowing and cohesive solids in flighted rotary dryers*. Chemical Engineering Science, vol. 73, pages 400–411, May 2012
- [Alvarez 1994] P.I. Alvarez & C. Shene. *Experimental Study of Residence Time in a Direct Rotary Dryer*. Drying Technology, vol. 12, no. 7, pages 1629–1651, 1994
- [Ammarcha 2012] C. Ammarcha, C. Gatumel, J. L. Dirion, M. Cabassud, V. Mizonov & H. Berthiaux. *Predicting bulk powder flow dynamics in a continuous mixer operating in transitory regimes*. Advanced Powder Technology, vol. 23, no. 6, pages 787–800, November 2012
- [Ang 1998] H M Ang, M O Tade & M W Sze. *Residence Time Distribution for a Cold Model Rotary Kiln*. The AusIMM, 1998.

- [Atmaca 2014] Adem Atmaca & Recep Yumrutaş. *Analysis of the parameters affecting energy consumption of a rotary kiln in cement industry*. Applied Thermal Engineering, vol. 66, no. 1–2, pages 435–444, 2014
- [Baker 1983] C. G. J. Baker. *Cascading rotary dryers*. In Advances in drying, volume 1, pages 1–51. Hemisphere, New York, USA, mujumdar a. s. edition, 1983.
- [Baker 1988] C.G.J. Baker. *The design of flights in cascading rotary dryers*. Drying Technology, vol. 6, no. 4, pages 631–653, December 1988
- [Bandopadhyay 1986] A. Bandopadhyay, M. P. Srivastava, A. K. Ray & K. K. Prasad. *Mathematical modelling of charge movement in rotary kiln for spong iron making*. Transactions of the Indian Institute of Metals, vol. 39, no. 3, pages 181–186, 1986.
- [Barr 1989a] P. V. Barr, J. K. Brimacombe & A. P. Watkinson. *A heat-transfer model for the rotary kiln: Part I. pilot kiln trials*. Metallurgical Transactions B, vol. 20, no. 3, pages 391–402, June 1989
- [Barr 1989b] P. V. Barr, J. K. Brimacombe & A. P. Watkinson. *A heat-transfer model for the rotary kiln: Part II. Development of the cross-section model*. Metallurgical Transactions B, vol. 20, no. 3, pages 403–419, June 1989
- [Bauer 1977] Ralf Bauer & E. U. Schlunder. *Effective radial thermal conductivity of packed beds with gas flow*. Verfahrenstechnik (Mainz), vol. 11, no. 10, pages 605–614, 1977
- [Beck 1977] James V. Beck & K. J. Arnold. *Parameter Estimation in Engineering and Science*. John Wiley & Sons Inc, New York, first edition edition, July 1977.
- [Bensmann 2010] S. Bensmann, A. Subagyo & P. Walzel. *Residence Time Distribution of Segregating Sand Particles in a Rotary Drum*. Particulate Science and Technology, vol. 28, no. 4, pages 319–331, 2010
- [Boateng 1993] Akwasi A. Boateng. *Rotary kiln transport phenomena: a study of the bed motion and heat transfer*. PhD thesis, 1993
- [Boateng 1996] A.A. Boateng & P.V. Barr. *A thermal model for the rotary kiln including heat transfer within the bed*. International Journal of Heat and Mass Transfer, vol. 39, no. 10, pages 2131–2147, 1996
- [Boateng 2008] Akwasi Acheampong Boateng. *Rotary kilns transport phenomena and transport processes*. Elsevier/Butterworth-Heinemann, Amsterdam; Boston, 2008
- [Bongo Njeng 2015a] A. S. Bongo Njeng, S. Vitu, M. Clausse, J. L. Dirion & M. Debacq. *Effect of lifter shape and operating parameters on the flow of materials in a pilot rotary kiln: Part I. Experimental RTD and axial dispersion study*. Powder Technology, vol. 269, pages 554–565, January 2015
- [Bongo Njeng 2015b] A. S. Bongo Njeng, S. Vitu, M. Clausse, J. L. Dirion & M. Debacq. *Effect of lifter shape and operating parameters on the flow of materials in a pilot rotary kiln: Part II. Experimental hold-up and mean residence time modeling*. Powder Technology, vol. 269, pages 566–576, January 2015

- [Bongo Njeng 2015c] A. S. Bongo Njeng, S. Vitu, M. Clausse, J. L. Dirion & M. Debacq. *Effect of lifter shape and operating parameters on the flow of materials in a pilot rotary kiln: Part III. Up-scaling considerations and segregation analysis*. Powder Technology, vol. To be submitted, September 2015.
- [Bongo Njeng 2015d] A. S. Bongo Njeng, S. Vitu, M. Clausse, J. L. Dirion & M. Debacq. *Evaluation of the wall-to-solids and wall-to-gas heat transfer coefficients in flighted rotary kilns: Lumped system analysis*. International Journal of Heat and Mass Transfer, vol. To be submitted, September 2015.
- [Bongo Njeng 2015e] A. S. Bongo Njeng, S. Vitu, M. Clausse, J. L. Dirion & M. Debacq. *Wall-to-solids heat transfer coefficient in flighted rotary kilns: experimental determination and modeling*. International Journal of Heat and Mass Transfer, vol. To be submitted, September 2015.
- [Brimacombe 1978] J. K. Brimacombe & A. P. Watkinson. *Heat transfer in a direct-fired rotary kiln: I. Pilot plant and experimentation*. Metallurgical Transactions B, vol. 9, no. 2, pages 201–208, June 1978
- [Britton 2006] P.F. Britton, M.E. Sheehan & P.A. Schneider. *A physical description of solids transport in flighted rotary dryers*. Powder Technology, vol. 165, no. 3, pages 153–160, July 2006
- [Bui 1993] R. T. Bui, J. Perron & M. Read. *Model-based optimization of the operation of the coke calcining kiln*. Carbon, vol. 31, no. 7, pages 1139–1147, 1993
- [Bui 1995] R. T. Bui, G. Simard, A. Charette, Y. Kocaefer & J. Perron. *Mathematical modeling of the rotary coke calcining kiln*. The Canadian Journal of Chemical Engineering, vol. 73, no. 4, pages 534–545, 1995
- [Cantelaube 1997] Florence Cantelaube, Daniel Bideau & Stéphane Roux. *Kinetics of segregation of granular media in a two-dimensional rotating drum*. Powder Technology, vol. 93, no. 1, pages 1–11, September 1997
- [Cao 1999] W. F. Cao & T. a. G. Langrish. *Comparison of Residence Time Models for Cascading Rotary Dryers*. Drying Technology, vol. 17, no. 4-5, April 1999
- [Cao 2000] W. F. Cao & T. A. G. Langrish. *The Development and Validation of a System Model for a Countercurrent Cascading Rotary Dryer*. Drying Technology, vol. 18, no. 1-2, pages 99–115, January 2000
- [Chatterjee 1983a] Amit Chatterjee & P. K. Mukhopadhyay. *Flow of materials in rotary kilns used for sponge iron manufacture: Part III. Effect of ring formation within the kiln*. Metallurgical Transactions B, vol. 14, no. 3, pages 393–399, September 1983
- [Chatterjee 1983b] Amit Chatterjee, A. V. Sathe & P. K. Mukhopadhyay. *Flow of materials in rotary kilns used for sponge iron manufacture: Part II. Effect of kiln geometry*. Metallurgical Transactions B, vol. 14, no. 3, pages 383–392, September 1983

- [Chatterjee 1983c] Amit Chatterjee, A. V. Sathe, M. P. Srivastava & P. K. Mukhopadhyay. *Flow of materials in rotary kilns used for sponge iron manufacture: Part I. Effect of some operational variables*. Metallurgical Transactions B, vol. 14, no. 3, pages 375–381, September 1983
- [Chaudhuri 2010] Bodhisattwa Chaudhuri, Fernando J. Muzzio & M. Silvina Tomassone. *Experimentally validated computations of heat transfer in granular materials in rotary calciners*. Powder Technology, vol. 198, no. 1, pages 6–15, 2010
- [Chen 2009] Wen Zhong Chen, Chun Hua Wang, Tie Liu, Chun You Zuo, Yuan Hang Tian & Tian Tian Gao. *Residence time and mass flow rate of particles in carbon rotary kilns*. Chemical Engineering and Processing: Process Intensification, vol. 48, no. 4, pages 955–960, 2009
- [Colin 2013] Baptiste Colin, J.-L. Dirion, Patricia Arlabosse & Sylvain Salvador. *Torrefaction en four tournant: étude de l'écoulement de plaquettes de bois*. volume 104 of *Recents Progres en Genie des Procedes*, Lyon, France, October 2013. SFGP.
- [Colin 2015] B. Colin, J. L. Dirion, P. Arlabosse & S. Salvador. *Wood chips flow in a rotary kiln: experiments and modeling*. Chemical Engineering Research and Design, 2015
- [Cook 1995] Charles A. Cook & Vic A. Cundy. *Heat transfer between a rotating cylinder and a moist granular bed*. International Journal of Heat and Mass Transfer, vol. 38, no. 3, pages 419–432, 1995
- [Corporation 2013] Special Metals Corporation. *Inconel alloy 600*, 2013. www.specialmetals.com
- [Corporation 2014] Special Metals Corporation. *Incoloy alloy 800*, 2014. www.specialmetals.com
- [Cronin 2011] Kevin Cronin, Muammer Catak, Johanna Bour, Aaron Collins & John Smee. *Stochastic modelling of particle motion along a rotary drum*. Powder Technology, vol. 213, no. 1–3, pages 79–91, November 2011
- [Danckwerts 1952] P.V. Danckwerts. *Continuous flow systems. Distribution of residence times*. Chemical Engineering Science, vol. 50, no. 24, pages 3857–3866, October 1952
- [Das Gupta 1991] S. Das Gupta, D. V. Khakhar & S. K. Bhatia. *Axial transport of granular solids in horizontal rotating cylinders. Part 1: Theory*. Powder Technology, vol. 67, no. 2, pages 145–151, 1991
- [Debacq 2001] Marie Debacq. *Étude et modélisation des fours tournants de défluoration et réduction du difluorure d'uranyle*. PhD thesis, Institut National Polytechnique de Lorraine, Nancy, France, 2001.
- [Debacq 2013a] Marie Debacq, Phahath Thammavong, Stéphane Vitu, Denis Ablitzer, Jean-Léon Houzelot & Fabrice Patisson. *A hydrodynamic model for flighted rotary kilns used for the conversion of cohesive uranium powders*. Chemical Engineering Science, vol. 104, pages 586–595, December 2013

- [Debacq 2013b] Marie Debacq, Stéphane Vitu, Denis Ablitzer, Jean-Léon Houzelot & Fabrice Patisson. *Transverse motion of cohesive powders in flighted rotary kilns: Experimental study of unloading at ambient and high temperatures*. Powder Technology, vol. 245, pages 56–63, April 2013
- [Delaplace 2014] Guillaume Delaplace, Karine Loubière, Fabrice Ducept & Romain Jeantet. *Modélisation en génie des procédés par analyse dimensionnelle : Méthode et exemples résolus*. Tec & Doc Lavoisier, Paris, 2014.
- [Descoins 2003] Nicolas Descoins. *Outils de simulation des fours tournants dédiés à la pyrolyse de déchets : modélisation dynamique du couplage transport de la charge-transferts de chaleur-réactions chimiques*. PhD thesis, Institut national polytechnique de Toulouse, Albi, 2003.
- [Descoins 2005] N. Descoins, J.-L. Dirion & T. Howes. *Solid transport in a pyrolysis pilot-scale rotary kiln: preliminary results—stationary and dynamic results*. Chemical Engineering and Processing: Process Intensification, vol. 44, no. 2, pages 315–321, February 2005
- [Dhanjal 2004] S. K. Dhanjal, P. V. Barr & A. P. Watkinson. *The rotary kiln: An investigation of bed heat transfer in the transverse plane*. Metallurgical and Materials Transactions B, vol. 35, no. 6, pages 1059–1070, December 2004
- [Dinesh V 2004] Loni Dinesh V & P. S. T. Sai. *A Model for Residence Time Distribution of Solids in a Rotary Kiln*. The Canadian Journal of Chemical Engineering, vol. 82, no. 2, pages 392–398, 2004
- [Ding 2001] Y. L Ding, R. N Forster, J. P. K Seville & D. J Parker. *Some aspects of heat transfer in rolling mode rotating drums operated at low to medium temperatures*. Powder Technology, vol. 121, no. 2–3, pages 168–181, November 2001
- [Duchesne 1996] Carl Duchesne, Jules Thibault & Claude Bazin. *Modeling of the Solids Transportation within an Industrial Rotary Dryer: A Simple Model*. Industrial & Engineering Chemistry Research, vol. 35, pages 2334–2341, 1996.
- [Fan 1961] Liang-Tseng Fan & Yong-Kee Ahn. *Axial dispersion of solids in rotary solid flow systems*. Applied Scientific Research, vol. 10, no. 1, pages 465–470, January 1961
- [Fan 2015] Xiao-hui Fan, Gui-ming Yang, Xu-ling Chen, Lu Gao, Xiao-xian Huang & Xi Li. *Predictive models and operation guidance system for iron ore pellet induration in traveling grate-rotary kiln process*. Computers & Chemical Engineering, vol. 79, pages 80–90, 2015
- [Fernandes 2009] N. J. Fernandes, C. H. Ataíde & M. A. S. Barrozo. *Modeling and experimental study of hydrodynamic and drying characteristics of an industrial rotary dryer*. Brazilian Journal of Chemical Engineering, vol. 26, no. 2, pages 331–341, June 2009
- [Ferron 1991] John R. Ferron & Dilip K. Singh. *Rotary kiln transport processes*. AIChE Journal, vol. 37, no. 5, pages 747–758, 1991

- [Friedman 1949] S.J. Friedman & W.R. Marshall. *Studies in rotary drying part I-holdup and dusting*. Chemical Engineering Progress, vol. 45, no. 8, pages 482–493, 1949.
- [Gao 2011] Yijie Gao, Aditya Vanarase, Fernando Muzzio & Marianthi Ierapetritou. *Characterizing continuous powder mixing using residence time distribution*. Chemical Engineering Science, vol. 66, no. 3, pages 417–425, 2011
- [Gao 2012] Yijie Gao, Fernando J. Muzzio & Marianthi G. Ierapetritou. *A review of the Residence Time Distribution (RTD) applications in solid unit operations*. Powder Technology, vol. 228, pages 416–423, September 2012
- [Gao 2013] Yijie Gao, Benjamin J. Glasser, Marianthi G. Ierapetritou, Alberto Cuitino, Fernando J. Muzzio, Jean W. Beeckman, Natalie A. Fassbender & William G. Borghard. *Measurement of residence time distribution in a rotary calciner*. AIChE Journal, vol. 59, no. 11, pages 4068–4076, 2013
- [Gibblings 2011] J.C. Gibblings. *Dimensional Analysis*. Springer London, London, 2011
- [Ginsberg 2011a] T. Ginsberg & M. Modigell. *Dynamic modelling of a rotary kiln for calcination of titanium dioxide white pigment*. Computers & Chemical Engineering, vol. 35, no. 11, pages 2437–2446, November 2011
- [Ginsberg 2011b] T. Ginsberg, M. Modigell & W. Wilsmann. *Thermochemical characterisation of the calcination process step in the sulphate method for production of titanium dioxide*. Chemical Engineering Research and Design, vol. 89, no. 7, pages 990–994, July 2011
- [Glikin 1978] P.G. Glikin. *Transport of Solids Through Flighted Rotation Drums*. Transactions of the Institution of Chemical Engineers, vol. 56, pages 120–126, 1978.
- [Gnielinski 1975] Volker Gnielinski. *Neue Gleichungen für den Wärme- und den Stoffübergang in turbulent durchströmten Rohren und Kanälen*. Forschung im Ingenieurwesen A, vol. 41, no. 1, pages 8–16, January 1975
- [Gorog 1981] J. P. Gorog, J. K. Brimacombe & T. N. Adams. *Radiative heat transfer in rotary kilns*. Metallurgical Transactions B, vol. 12, no. 1, pages 55–70, March 1981
- [Gorog 1982] J. P. Gorog, T. N. Adams & J. K. Brimacombe. *Regenerative heat transfer in rotary kilns*. Metallurgical Transactions B, vol. 13, no. 2, pages 153–163, June 1982
- [Gorog 1983] J. P. Gorog, T. N. Adams & J. K. Brimacombe. *Heat transfer from flames in a rotary kiln*. Metallurgical Transactions B, vol. 14, no. 3, pages 411–424, September 1983
- [Grajales 2012] Lina Maria Grajales, Natalia Monteiro Xavier, Joao Paulo Henrique & Joao Claudio Thomeo. *Mixing and motion of rice particles in a rotating drum*. Powder Technology, vol. 222, page 167, 2012. The mixing and motion of particles were analyzed in a rotary drum as part of the developme

- [Hahn 2012] David W. Hahn & M. Necati Ozisik. *Heat Conduction*. John Wiley & Sons, August 2012.
- [Hatzilyberis 1999a] K.S. Hatzilyberis & G.P. Androutsopoulos. *An Rtd Study for the Flow of Lignite Particles Through a Pilot Rotary Dryer Part I: Bare Drum Case*. *Drying Technology*, vol. 17, no. 4-5, pages 745–757, 1999
- [Hatzilyberis 1999b] K.S. Hatzilyberis & G.P. Androutsopoulos. *An Rtd Study for the Flow of Lignite Particles Through a Pilot Rotary Dryer Part II: Flighted Drum Case*. *Drying Technology*, vol. 17, no. 4-5, pages 759–774, 1999
- [Hehl 1978] M. Hehl, H. Kroger, H. Helmrich & K. Schugerl. *Longitudinal mixing in horizontal rotary drum reactors*. *Powder Technology*, vol. 20, no. 1, pages 29–37, 1978
- [Henein 1983] H. Henein, J. K. Brimacombe & A. P. Watkinson. *Experimental study of transverse bed motion in rotary kilns*. *Metallurgical Transactions B*, vol. 14, no. 2, pages 191–205, June 1983
- [Herz 2012] Fabian Herz, Iliyan Mitov, Eckehard Specht & Rayko Stanev. *Experimental study of the contact heat transfer coefficient between the covered wall and solid bed in rotary drums*. *Chemical Engineering Science*, vol. 82, pages 312–318, September 2012
- [Howell 2010] John R. Howell, M. Pinar Menguc & Robert Siegel. *Thermal Radiation Heat Transfer*, 5th Edition. CRC Press, September 2010.
- [Hwan 2009] Iwan Harsono Hwan. *Heat transfer mechanisms in an indirectly heated rotary kiln with lifters and its role in scaling*. PhD thesis, 2009
- [Iguaz 2003] A. Iguaz, A. Esnoz, G. Martinez, A. Lopez & P. Virseda. *Mathematical modelling and simulation for the drying process of vegetable wholesale by-products in a rotary dryer*. *Journal of Food Engineering*, vol. 59, no. 2–3, pages 151–160, September 2003
- [Imber 1962] M. Imber & V. Paschkis. *A new theory for a rotary-kiln heat exchanger*. *International Journal of Heat and Mass Transfer*, vol. 5, pages 623–638, 1962.
- [Incropera 1985] Frank P. Incropera, David P. DeWitt, Theodore L. Bergman & Adrienne S. Lavine. *Fundamentals of Heat and Mass Transfer*. John Wiley & Sons, Hoboken, NJ, 2nd edition edition, 1985.
- [Jenkins 1981] B. G. Jenkins & F. D. Moles. *Modelling of heat transfer from a large enclosed flame in a rotary kiln*. *Chemical Engineering Research and Design*, vol. 59, pages 17–25, 1981.
- [Jeschar 1975] R. Jeschar & W. Schupe. *Simplified calculation of radiant heat transfer in industrial furnaces and comparison with measurements made in an experimental combustion chamber*. *Gas Wärme international*, vol. 2, no. 24, pages 64–74, 1975.
- [Karra 1977] V.K. Karra & D.W. Fuerstenau. *Material transport in a continuous rotary drum. Effect of discharge plate geometry*. *Powder Technology*, vol. 16, no. 1, pages 23–28, January 1977

- [Kelly 1968] J.J. Kelly & J.P. O'Donnell. *Dynamics of granular material rotary dryers and coolers*. In IChemE Symposium Series, volume 29, pages 34–44, 1968.
- [Kelly 1977] J.J. Kelly & J.P. O'Donnell. *Residence Time Model for Rotary Drums*. Transactions of the Institution of Chemical Engineers, vol. 55, no. 243, 1977.
- [Kelly 1992] John Kelly. *Flight design in rotary dryers*. Drying Technology, vol. 10, no. 4, pages 979–993, September 1992
- [Kemp 2004] Ian C. Kemp. *Comparison of Particles Motion Correlations For Cascading Rotary Dryers*. In Proceedings of the 14 th International Drying Symposium (IDS), São Paulo, Brazil, B, pages 790–797, 2004
- [Khan 2004] Zeina S. Khan & Stephen W. Morris. *Subdiffusive axial transport of granular materials in a long drum mixer*, 2004. <http://xxx.lanl.gov/pdf/cond-mat/0408626.pdf>
- [Kohav 1995] Tamar Kohav, James T. Richardson & Dan Luss. *Axial dispersion of solid particles in a continuous rotary kiln*. AIChE Journal, vol. 41, no. 11, pages 2465–2475, November 1995
- [Kramers 1952] H. Kramers & P. Croockewit. *The passage of granular solids through inclined rotary kilns*. Chemical Engineering Science, vol. 1, no. 6, pages 259–265, 1952
- [Kreith 1980] Frank Kreith & William Z. Black. Basic heat transfer. Harper & Row, New York, Etats-Unis, 1980.
- [LANGLAIS 2004] Catherine LANGLAIS & Sorin KLARSFELD. *Isolation thermique à température ambiante. Propriétés*. Techniques de l'ingénieur. Matériaux fonctionnels, vol. 1, no. BE9860, 2004
- [Le Guen 2013] Laurédan Le Guen, Florian Huchet, Jean Dumoulin, Yvan Baudru & Philippe Tamagny. *Convective heat transfer analysis in aggregates rotary drum reactor*. Applied Thermal Engineering, vol. 54, no. 1, pages 131–139, 2013
- [Le Guen 2014] Laurédan Le Guen, Florian Huchet & Jean Dumoulin. *A wall heat transfer correlation for the baffled-rotary kilns with secondary air flow and recycled materials inlet*. Experimental Thermal and Fluid Science, February 2014
- [Lebas 1995a] E. Lebas. *Étude et modélisation de la pyrolyse du charbon en four tournant*. PhD thesis, Institut National Polytechnique de Lorraine, November 1995.
- [Lebas 1995b] E. Lebas, F. Hanrot, D. Ablitzer & J.-L. Houzelot. *Experimental study of residence time, particle movement and bed depth profile in rotary kilns*. The Canadian Journal of Chemical Engineering, vol. 73, no. 2, pages 173–180, April 1995
- [Lee 2008] Andrew Lee. *Modelling the solids transport phenomena within flighted rotary dryers*. phd, James Cook University, May 2008

- [Lee 2010] A. Lee & M.E. Sheehan. *Development of a geometric flight unloading model for flighted rotary dryers*. Powder Technology, vol. 198, no. 3, pages 395–403, March 2010
- [Leger 1993] Christopher B. Leger, Charles A. Cook, Vic A. Cundy, Arthur M. Sterling, Xiao-Xue Deng & Joann S. Lighty. *Bed mixing and heat transfer in a batch loaded rotary kiln*. Environmental Progress, vol. 12, no. 2, pages 101–109, 1993
- [Lehmberg 1977] J. Lehmberg, M. Hehl & K. Schügerl. *Transverse mixing and heat transfer in horizontal rotary drum reactors*. Powder Technology, vol. 18, no. 2, pages 149–163, November 1977
- [Levenspiel 1999] Octave Levenspiel. Chemical reaction engineering. Wiley, 1999.
- [Li 2002a] S.-Q. Li, Y. Chi, R.-D. Li, J.-H. Yan & K.-F. Cen. *Axial transport and residence time of MSW in rotary kilns: Part II. Theoretical and optimal analyses*. Powder Technology, vol. 126, no. 3, pages 228–240, 2002
- [Li 2002b] S.-Q. Li, J.-H. Yan, R.-D. Li, Y. Chi & K.-F. Cen. *Axial transport and residence time of MSW in rotary kilns: Part I. Experimental*. Powder Technology, vol. 126, no. 3, pages 217–227, 2002
- [Li 2005] S.-Q. Li, L.-B. Ma, W. Wan & Q. Yao. *A Mathematical Model of Heat Transfer in a Rotary Kiln Thermo-Reactor*. Chemical Engineering & Technology, vol. 28, no. 12, pages 1480–1489, 2005
- [Lisboa 2007] M. H. Lisboa, D. S. Vitorino, W. B. Delaiba, J. R. D. Finzer & M. A. S. Barrozo. *A study of particle motion in rotary dryer*. Brazilian Journal of Chemical Engineering, vol. 24, no. 3, pages 365–374, September 2007
- [Liu 2006a] Xiao Yan Liu, E. Specht, O. Guerra Gonzalez & P. Walzel. *Analytical solution for the rolling-mode granular motion in rotary kilns*. Chemical Engineering and Processing: Process Intensification, vol. 45, no. 6, pages 515–521, 2006
- [Liu 2006b] Xiao Yan Liu & Eckehard Specht. *Mean residence time and hold-up of solids in rotary kilns*. Chemical engineering science, vol. 61, pages 5176–5181, 2006.
- [Liu 2009] X.Y. Liu, J. Zhang, E. Specht, Y.C. Shi & F. Herz. *Analytical solution for the axial solid transport in rotary kilns*. Chemical Engineering Science, vol. 64, no. 2, pages 428–431, January 2009
- [Lybaert 1985] P. Lybaert. *Contribution à l'étude du transfert de chaleur entre un matériau particulaire et la paroi dans les échangeurs rotatifs indirects*. PhD thesis, Faculté polytechnique de Mons, 1985.
- [Lybaert 1987] P. Lybaert. *Wall-particles heat transfer in rotating heat exchangers*. International Journal of Heat and Mass Transfer, vol. 30, no. 8, pages 1663–1672, 1987

- [Makokha 2011] Augustine B. Makokha & Michael H. Moys. *Characterizing slurry hydrodynamic transport in a large overflow tubular ball mill by an improved mixing cell model based on tracer response data*. Powder Technology, vol. 211, pages 207–214, 2011.
- [Malhotra 1990] Karun Malhotra & Arun S. Mujumdar. *Effect of Particle Shape on Particle-Surface Thermal Contact Resistance*. Journal of Chemical Engineering of Japan, vol. 23, no. 4, pages 510–513, 1990.
- [Martin 2000] AD Martin. *Interpretation of residence time distribution data*. Chemical engineering science, vol. 55, pages 5907–5917, 2000.
- [Martins 2001] Marcio A. Martins, Leandro S. Oliveira & Adriana S. Franca. *Modeling and simulation of petroleum coke calcination in rotary kilns*. Fuel, vol. 80, no. 11, pages 1611–1622, September 2001
- [Matchett 1987] A.J. Matchett & C.G.J. Baker. *Particle residence times in cascading rotary dryers. Part 1 –Derivation of the two-stream model*. Journal of Separation Process Technology. Journal of Separation Process Technology, vol. 8, pages 11–17, 1987.
- [Matchett 1990] A.J. Matchett & M.S. Sheikh. *An Improved Model of Particle Motion in Cascading Rotary Dryers*. Chemical Engineering Research and Design, vol. 68, pages 139–148, 1990.
- [McGlinchey 2008] Don McGlinchey. Bulk solids handling: equipment selection and operation. Blackwell Pub., Oxford; Ames, Iowa, 2008.
- [McTait 1998] G. E. McTait, D. M. Scott & J. F. Davidson. *Residence time distribution of particles in rotary kilns*. In FLUIDIZATION IX, DURANGO, 1998
- [Mellmann 2001] J Mellmann. *The transverse motion of solids in rotating cylinders—forms of motion and transition behavior*. Powder Technology, vol. 118, no. 3, pages 251–270, August 2001
- [Miller 1942] C. O. Miller, B. A. Smith & W. H. Schuette. *Factors Influencing the Performance of Rotary Dryers*. American Institute of Chemical Engineers, pages 841–864, May 1942.
- [Miller 1996] R. S. Miller & J. Bellan. *Analysis of Reaction Products and Conversion Time in the Pyrolysis of Cellulose and Wood Particles*. Combustion Science and Technology, vol. 119, no. 1-6, pages 331–373, October 1996
- [Mousques 2001] Pierre Mousques. Modélisation du couplage réactions chimiques-transferts de chaleur en vue du dimensionnement des réacteurs de pyrolyse. Perpignan, January 2001
- [Mu 1980] Jacob Mu & D. D. Perlmutter. *The mixing of Granular solids in a rotary cylinder*. AIChE Journal, vol. 26, no. 6, pages 928–934, 1980
- [Myklestad 1963] O. Myklestad. *Heat and Mass Transfer in Rotary Dryers*. Chemical Engineering Progress Symposium Series, vol. 41, no. 59, pages 129–137, 1963.

- [Nafsun 2015] Aainaa Izyan Nafsun, Fabian Herz, Eckehard Specht, Viktor Scherer & Siegmund Wirtz. *Heat Transfer Experiments in a Rotary Drum for a Variety of Granular Materials*. Experimental Heat Transfer, pages 0–0, April 2015
- [Nicole 1996] Christophe Nicole. *Étude et modélisation de l'hydrofluorisation du dioxyde d'uranium en four tournant*. PhD thesis, Institut National Polytechnique de Lorraine, Nancy, France, 1996.
- [Niessen 1978] Walter R. Niessen. Combustion and incineration processes: applications in environmental engineering. Numéro v. 7 in Pollution engineering and technology. M. Dekker, New York, 1978.
- [Oppenheim 1956] A. K. Oppenheim. *Radiation analysis by the network method*. Transactions of the ASME, no. 78, pages 725–735, May 1956.
- [Owens 1991] Warren D. Owens, Geoffrey D. Silcox, Joann S. Lighty, Xiao Xue Deng, David W. Pershing, Vic A. Cundy, Christopher B. Leger & Allen L. Jakway. *Thermal analysis of rotary kiln incineration: Comparison of theory and experiment*. Combustion and Flame, vol. 86, no. 1–2, pages 101–114, 1991
- [Pan 2006] Jian-Ping Pan, Ting-Jie Wang, Jun-Jie Yao & Yong Jin. *Granule transport and mean residence time in horizontal drum with inclined flights*. Powder Technology, vol. 162, no. 1, pages 50–58, February 2006
- [Patisson 2006] Fabrice Patisson, Bernard Dussoubs & Denis Ablitzer. *Using Sohn's law of additive reaction times for modeling a multiparticle reactor. The case of the moving bed furnace converting uranium trioxide into tetrafluoride*. San Diego, USA, 2006
- [Perron 1990] J. Perron & R. T. Bui. *Rotary cylinders: Solid transport prediction by dimensional and rheological analysis*. The Canadian Journal of Chemical Engineering, vol. 68, no. 1, pages 61–68, 1990
- [Perron 1992] J. Perron, H. T. Nguyen & R. T. Bui. *Modélisation d'un four de calcination du coke de pétrole: I. Le modèle*. The Canadian Journal of Chemical Engineering, vol. 70, no. 6, pages 1108–1119, 1992
- [Prutton 1942] C. F. Prutton, C. O. Miller & W. H. Schuette. *Factors Influencing the Performance of Rotary Dryers*. American Institute of Chemical Engineers, vol. 38, pages 841–864, 1942.
- [Ranz 1952] W. E. Ranz. *Evaporation from drops: Part I*. Chem. Eng. Prog., vol. 48, page 141, 1952
- [Renaud 2000] M. Renaud, J. Thibault & A. Trusiak. *Solids Transportation Model of an Industrial Rotary Dryer*. Drying Technology, vol. 18, no. 4-5, pages 843–865, 2000
- [Revol 2001] D Revol, C.L Briens & J.M Chabagno. *The design of flights in rotary dryers*. Powder Technology, vol. 121, no. 2-3, pages 230–238, November 2001
- [Riskin 1996] Hannes Riskin. The Fokker-Planck equation: methods of solution and applications. Springer, Berlin, 1996.

- [Rogers 1979] R.S.C. Rogers & R.P. Gardner. *A Monte Carlo method for simulating dispersion and transport through horizontal rotating cylinders*. Powder Technology, vol. 23, no. 2, pages 159–167, 1979
- [Rouaud 2013] Mathieu Rouaud. Calcul d’incertitudes. 2013
- [Rovaglio 1998] M. Rovaglio, D. Manca & G. Biardi. *Dynamic modeling of waste incineration plants with rotary kilns*. Chemical Engineering Science, vol. 53, no. 15, pages 2727–2742, August 1998
- [Rutgers 1965] R. Rutgers. *Longitudinal mixing of granular material flowing through a rotating cylinder: Part II. Experimental*. Chemical Engineering Science, vol. 20, no. 12, pages 1089–1100, 1965
- [Sacadura 1993] J. F. Sacadura. Initiation aux transferts thermiques. Technique et documentation-Lavoisier, Paris, 1993.
- [Saeman 1951] W. C. Saeman. *Passage of solids through rotary kilns. Factors affecting time of passage*. Chemical Engineering Progress, vol. Volume47, pages 508–14, 1951.
- [Saeman 1954] W.C. Saeman & T.R. Mitchell. *Analysis of rotary dryer performance*. Chemical Engineering Progress, vol. 50, no. 9, page 467, 1954.
- [Sai 1990] P. S. T. Sai, G. D. Surender, A. D. Damodaran, V. Suresh, Z. G. Philip & K. Sankaran. *Residence time distribution and material flow studies in a rotary kiln*. Metallurgical Transactions B, vol. 21, no. 6, pages 1005–1011, December 1990
- [Schaefer 1988] C. F. Schaefer & A. A. Anthony. *Rotary Kilns*. In Standard handbook of hazardous waste treatment and disposal. 1988.
- [Schlünder 1984a] E.-U. Schlünder. *Heat Transfer to Packed and Stirred Beds from the Surface of Immersed Bodies*. Chemical Engineering and Processing, vol. 18, pages 31–53, 1984.
- [Schlünder 1984b] E. U Schlünder & N Mollekopf. *Vacuum contact drying of free flowing mechanically agitated particulate material*. Chemical Engineering and Processing: Process Intensification, vol. 18, no. 2, pages 93–111, March 1984
- [Schneider 2003] P Schneider, M Sheehan & S Brown. *Modelling the dynamics of solids transport in flighted rotary dryers*. In Computer Aided Chemical Engineering, volume 14, pages 911–916. Elsevier, 2003
- [Schofield 1962] F.R. Schofield & P.G. Glikin. *Rotary dryers and coolers for granular fertilizers*. Transactions of the Institution of Chemical Engineers, vol. 40, pages 183–190, 1962.
- [Shahhosseini 2000] S. Shahhosseini, I.T. Cameron & F.Y. Wang. *A simple dynamic model for solid transport in rotary dryers*. Drying Technology, vol. 18, pages 867–886, 2000.
- [Shahhosseini 2001] S. Shahhosseini, I. T. Cameron & F. Y. Wang. *A dynamic model with on-line identification for rotary sugar drying processes*. Drying Technology, vol. 19, no. 9, pages 2103–2129, September 2001

- [Sheehan 2002] M. E. Sheehan, P. A. Schneider, A. Monro & S. Vigh. *Transportation and axial dispersion of sugar in flighted rotary dryers*. pages 469–474. PK Editorial Services Pty Ltd, 2002.
- [Sheehan 2005] M.E. Sheehan, P.F. Britton & P.A. Schneider. *A model for solids transport in flighted rotary dryers based on physical considerations*. Chemical Engineering Science, vol. 60, no. 15, pages 4171–4182, 2005
- [Sherritt 1993] Richard G. Sherritt, Rod Caple, Leo A. Behie & Anil K. Mehrotra. *The movement of solids through flighted rotating drums. Part i: Model formulation*. The Canadian Journal of Chemical Engineering, vol. 71, no. 3, pages 337–346, 1993
- [Sherritt 1994] Richard G. Sherritt, Rod Caple, Leo A. Behie & Anil K. Mehrotra. *The movement of solids through flighted rotating drums. Part II solids-gas interaction and model validation*. The Canadian Journal of Chemical Engineering, vol. 72, no. 2, pages 240–248, 1994
- [Sherritt 2003] Richard G. Sherritt, Jamal Chaouki, Anil K. Mehrotra & Leo A. Behie. *Axial dispersion in the three-dimensional mixing of particles in a rotating drum reactor*. Chemical Engineering Science, vol. 58, no. 2, pages 401–415, January 2003
- [Silcox 1990] Geoffrey D. Silcox & David W. Perching. *The Effects of Rotary Kiln Operating Conditions and Design on Burden Heating Rates as Determined by a Mathematical Model of Rotary Kiln Heat Transfer*. Journal of the Air & Waste Management Association, vol. 40, no. 3, pages 337–344, March 1990
- [Song 2003] Yang Song, Jules Thibault & Tadeusz Kudra. *Dynamic characteristics of solids transportation in rotary dryers*. Drying technology, vol. 21, no. 5, pages 755–773, 2003.
- [Spurling 2001] R.J. Spurling, J.F. Davidson & D.M. Scott. *The Transient Response of Granular Flows in an Inclined Rotating Cylinder*. Chemical Engineering Research and Design, vol. 79, no. 1, pages 51–61, January 2001
- [Sudah 2002] Osama S Sudah, A.W Chester, J.A Kowalski, J.W Beeckman & F.J Muzzio. *Quantitative characterization of mixing processes in rotary calciners*. Powder Technology, vol. 126, no. 2, pages 166–173, 2002
- [Sullivan 1927] John D Sullivan, Charles George Maier & Oliver C Ralston. *Passage of solid particles through rotary cylindrical kilns*. Govt. print. off., Washington, 1927.
- [Sunkara 2013a] Koteswara Rao Sunkara, Fabian Herz, Eckehard Specht & Jochen Mellmann. *Influence of flight design on the particle distribution of a flighted rotating drum*. Chemical Engineering Science, vol. 90, pages 101–109, March 2013
- [Sunkara 2013b] Koteswara Rao Sunkara, Fabian Herz, Eckehard Specht, Jochen Mellmann & Richard Erpelding. *Modeling the discharge characteristics of rectangular flights in a flighted rotary drum*. Powder Technology, vol. 234, pages 107–116, January 2013

- [Sunkara 2015] Koteswara Rao Sunkara, Fabian Herz, Eckehard Specht & Jochen Mellmann. *Transverse flow at the flight surface in flighted rotary drum*. Powder Technology, vol. 275, pages 161–171, 2015
- [Suzuki 2008a] Tomoko Suzuki, Teruyuki Okazaki, Kenji Yamamoto, Hiroyuki Nakata & Osamu Fujita. *Improvements in Pyrolysis of Wastes in an Externally Heated Rotary Kiln (Experimental Study on the Heat Transfer Enhancement)*. Transactions of the Japan Society of Mechanical Engineers Series B, vol. 74, no. 743, pages 1586–1592, 2008.
- [Suzuki 2008b] Tomoko Suzuki, Teruyuki Okazaki, Kenji Yamamoto, Hiroyuki Nakata & Osamu Fujita. *Improvements in Pyrolysis of Wastes in an Externally Heated Rotary Kiln (Measurement of the Overall Heat Transfer Coefficient form the Wall to the Wastes)*. Transactions of the Japan Society of Mechanical Engineers Series B, vol. 74, no. 743, pages 1586–1592, 2008. 1st Report, Measurement of the Overall Heat Transfer Coefficient form the Wall to the Wastes.
- [Thammavong 2009] P. Thammavong, M. Debacq, S. Vitu, M. Dupoizat & Alain Delacroix. *Étude expérimentale des échanges paroi/poudre dans des fours tournants munis de releveurs*. Paris, France, 2009. SFGP.
- [Thammavong 2011] P. Thammavong, M. Debacq, S. Vitu & M. Dupoizat. *Experimental Apparatus for Studying Heat Transfer in Externally Heated Rotary Kilns*. Chemical Engineering & Technology, vol. 34, no. 5, pages 707–717, 2011
- [Thibault 2010] Jules Thibault, Pedro I. Alvarez, Roman Blasco & Rolando Vega. *Modeling the Mean Residence Time in a Rotary Dryer for Various Types of Solids*. Drying Technology, vol. 28, no. 10, pages 1136–1141, 2010
- [Thomas 1944] H. A. Thomas & McKee. *Longitudinal mixing in aeration tanks*. Sewage Works Journal, vol. 16, no. 1, pages 42–55, 1944.
- [Tscheng 1979] S. H. Tscheng & A. P. Watkinson. *Convective heat transfer in a rotary kiln*. The Canadian Journal of Chemical Engineering, vol. 57, no. 4, pages 433–443, 1979
- [Van Puyvelde 2000] D.R. Van Puyvelde, B.R. Young, M.A. Wilson & S.J. Schmidt. *Modelling Transverse Segregation of Particulate Solids in a Rolling Drum*. Chemical Engineering Research and Design, vol. 78, no. 4, pages 643–650, May 2000
- [Van Puyvelde 2009] Dennis R. Van Puyvelde. *Modelling the hold up of lifters in rotary dryers*. Chemical Engineering Research and Design, vol. 87, no. 2, pages 226–232, February 2009
- [Venkataraman 1986] K.S. Venkataraman & D.W. Fuerstenau. *Effect of lifter shape and configuration on material transport part I: In rotating drums*. Powder Technology, vol. 46, no. 1, pages 23–32, March 1986
- [Vàhl 1952] L. Vahl & W.G. Kingma. *Transport of solids through horizontal rotary cylinders*. Chemical Engineering Science, vol. 1, no. 6, pages 253–258, 1952

- [Wachters 1964] L.H.J. Wachters & H. Kramers. *The calcining of the sodium bicarbonate in a rotary kiln*. pages 77–87, Amsterdam, 1964.
- [Wang 1995] F.Y. Wang, I.T. Cameron, J.D. Litster & V. Rudolph. *A Fundamental Study on Particle Transport Through Rotary Dryers for Flight Design and System Optimisation*. Drying Technology, vol. 13, no. 5-7, pages 1261–1278, January 1995
- [Watkinson 1978] A. P. Watkinson & J. K. Brimacombe. *Heat transfer in a direct-fired rotary kiln: II. Heat flow results and their interpretation*. Metallurgical Transactions B, vol. 9, no. 2, pages 209–219, June 1978
- [Welty 1969] James R Welty, Charles E Wicks & Robert E Wilson. Fundamentals of momentum, heat, and mass transfer. J. Wiley, New York, 1969.
- [Wes 1976a] G. W. J. Wes, A. A. H. Drinkenburg & S. Stemerding. *Heat transfer in a horizontal rotary drum reactor*. Powder Technology, vol. 13, no. 2, pages 185–192, March 1976
- [Wes 1976b] G. W. J. Wes, A. A. H. Drinkenburg & S. Stemerding. *Solids mixing and residence time distribution in a horizontal rotary drum reactor*. Powder technology, vol. 13, pages 177–184, 1976.
- [White 1988] Frank M White. Heat and mass transfer. Addison-Wesley, Reading, Mass., 1988.
- [Wightman 1998] Carolyn Wightman, Maher Moakher, Fernando J. Muzzio & O. Walton. *Simulation of flow and mixing of particles in a rotating and rocking cylinder*. AIChE Journal, vol. 44, no. 6, pages 1266–1276, 1998
- [Wild 1993] M. B. Wild & T. N. Smith. *A Unified Axial Model for Heat Transfer in a Rotary Kiln*. pages 53–58, Melbourne, 1993. Barton, ACT: Institution of Engineers, Australia
- [Woodcock 1987] C. R Woodcock, J. S Mason & Thames Polytechnic. Bulk Solids Handling Unit. Bulk solids handling: an introduction to the practice and technology. L. Hill ; Chapman and Hall, Glasgow; New York, 1987.
- [Yang 1997] L. Yang & B. Farouk. *Modeling of Solid Particle Flow and Heat Transfer in Rotary Kiln Calciners*. Journal of the Air & Waste Management Association, vol. 47, no. 11, pages 1189–1196, 1997
- [Zheng-ming 2013] Yi Zheng-ming, Xiao Hui, Song Jia-lin, Ma Guang-bai & Zhou Jie-min. *Mathematic simulation of heat transfer and operating optimization in alumina rotary kiln*. Journal of Central South University, vol. 20, no. 10, pages 2775–2780, October 2013
- [Zhu 2011] Wen Kui Zhu, Bin Li, Chuan Fang Yu & Liang Yuan Chen. *Investigation on the Transport Characteristics of Typical Biological Slender Particles in a Pilot-Scale Rotary Dryer*. Advanced Materials Research, vol. 396-398, pages 315–321, November 2011

List of Figures

1.1	Typical residence time distribution for different rotational speeds at a constant feed rate [Hehl 1978].	32
1.2	[Danckwerts 1952] F-diagrams : a) piston flow, b) piston flow with some longitudinal mixing, c) complete mixing, d) dead water.	36
1.3	Cross section of an operating rotary kiln equipped with lifters.	38
1.4	Load conditions within rotary kiln equipped with lifters.	38
1.5	Lifter profiles used by [Hatzilyberis 1999a].	39
1.6	Lifter profiles studied by [Debacq 2001]	39
1.7	Designs and configurations of lifters per row used by [Hwan 2009] in a horizontal rotating kiln with L/D ratio of 7: a) single lifters, b) horizontal straight lifters, c) inclined straight lifters, d) and e) folded lifters.	40
1.8	Tank in series model	46
1.9	Modified Cholette - Cloutier model	46
1.10	Model proposed by [Sheehan 2005]	46
1.11	Model proposed by [Makokha 2011]	47
1.12	Heat transfer mechanisms in the cross section of indirectly (left) and directly (right) heated rotary kilns equipped with lifters.	49
2.1	Research methodology.	66
2.2	Side views of the experimental apparatus.	68
2.3	Feeding systems.	69
2.4	Layout of the experimental apparatus heating zones, longitudinal (left side) and transverse (right side) sections: (1) kiln tube, (2) Insulation, (3) Measuring rod with thermocouples, (4) external thermocouples, (5) air, (6) heating resistors.	70
2.5	Exit dams available for RK1.	72
2.6	Shapes and configurations of lifters used.	72
2.7	RK2 fitted with the grid.	72
2.8	Particle size distribution: sand and rice.	74
2.9	Beech chips size distribution in length, width and thickness.	74
2.10	Thermal conductivity and diffusivity: experiments vs. [Bauer 1977] model predictions.	76
2.11	Effect of the amount of tracer (dyed broken rice) upon the dimensionless RTD in a bulk of broken rice. Operating conditions: 3 rpm rotation speed, 2° slope, 2.5 kg.h ⁻¹ mass flow rate, 23.5 mm exit dam height with rectangular lifters.	79

2.12	Effect of the amount of tracer (dyed beech chips) upon the dimensionless RTD in a bulk of beech chips. Operating conditions: 3 rpm rotation speed, 2° slope, 2.5 kg.h ⁻¹ mass flow rate, with only the lifter structure without lifters.	81
2.13	Bed depth measuring rod and position of the stems.	82
2.14	Experimental procedure for the bed depth measurement.	83
3.1	Layout of the experimental apparatus, including the structure and shapes of lifters.	95
3.2	Effect of the amount of tracer (dyed broken rice) upon the dimensionless RTD in a bulk of broken rice. Operating conditions: 3 rpm rotation speed, 2° slope, 2.5 kg.h ⁻¹ MFR, 23.5 mm exit dam height with rectangular lifters.	97
3.3	Comparison of experimental/theoretical and fitted values of the axial dispersion model parameters, i.e MRT, Pe, and resulting D. Solids lines are ±20% margins.	101
3.4	Effect of presence and shape of lifters on the RTD for the flow of broken rice. Operating conditions: 10 rpm rotation speed, 2° slope, 2.5 kg.h ⁻¹ MFR, 23.5 mm exit dam height. In each case (NL, SL and RL), the experiment was repeated three times. Solid lines are the axial dispersion model of the n°1 replicated run with fitted parameters.	102
3.5	Effect of the bulk materials characteristics on the RTD. Operating conditions for both SL and RL: 3 rpm rotation speed, 2° slope, 2.5 kg.h ⁻¹ MFR, 23.5 mm exit dam height. Solid lines are the axial dispersion model with fitted parameters. . .	103
3.6	Influence of operating parameters (N, S, \dot{M} and exit dam height) on the VRT for the flow of sand and broken rice, when the kiln is equipped with either straight or rectangular lifters.	104
3.7	Influence of operating parameters (N, S, \dot{M} and exit dam height) on the RTD for the flow of broken rice, when the kiln is equipped with rectangular lifters. Solid lines represent the axial dispersion model using fitted parameters. Dashed lines represent the axial dispersion model using theoretical parameters.	105
3.8	Influence of operating parameters (N, S, \dot{M} and exit dam height) on the experimental Peclet number for the flow of sand and broken rice, when the kiln is equipped with either straight or rectangular lifters.	107
3.9	Influence of operating parameters (N, S, \dot{M} and exit dam height) on the experimental axial dispersion coefficient for the flow of sand and broken rice, when the kiln is equipped with either straight or rectangular lifters. The axial dispersion coefficients are obtained from the fitted Pe.	107
3.10	Comparison of axial dispersion coefficient values obtained in the present study with predicted values from a) [Sai 1990], b) [Sherritt 2003], c) Present authors Eq.3.18. Solids lines are ±20% margins.	108
4.1	Experimental Rotary kiln equipped with lifters: a) Rectangular lifters b) Straight lifters. The bulk materials are broken rice.	117
4.2	Influence of operating parameters (N, S, \dot{M} and exit dam height) on the hold-up volume fraction for the flow of sand and broken rice, when the kiln is equipped with either straight or rectangular lifters.	120
4.3	Comparison of experimental MRT and time of passage of solid particles. Solid lines are ±20% margins.	121
4.4	Influence of operating parameters (N, S, \dot{M} and exit dam height) on the MRT for the flow of sand and broken rice, when the kiln is equipped with either straight or rectangular lifters.	122

4.5	Comparison of the experimental MRT while using a) a bulk of sand and b) a bulk of broken rice with predicted values from Eq.4.13 using the 3 sets of parameters as given in Table 4.4. Solid lines are $\pm 20\%$ margins.	125
4.6	Comparison of experimental MRT from [Debacq 2001] with predicted values from Eq.4.13 using the 3 sets of parameters as given in Table 4.4. Solid lines are $\pm 20\%$ margins.	126
4.7	Comparison of experimental MRT from [Colin 2013] with predicted values from Eq.4.13 using the 3 sets of parameters as given in Table 4.4. Solid lines are $\pm 20\%$ margins.	127
4.8	Comparison of experimental MRT from a) [Sai 1990] and b) [Chatterjee 1983b] with predicted values from Eq.4.13 using the 3 sets of parameters as given in Table 4.4. Solid lines are $\pm 20\%$ margins.	128
4.9	Comparison of the experimental MRT with predicted values from Eq.4.2, Eq.4.5 and Eq.4.13 (using "sand & rice-fitted parameters").	128
5.1	Kiln internal fixtures: a) lifter structure and b) grid.	136
5.2	Beech chips size distribution in length, width and thickness.	137
5.3	Comparison of experimental/theoretical and fitted values of the axial dispersion model parameters, i.e MRT, Pe, and resulting D. Solids lines are $\pm 20\%$ margins.	139
5.4	Effect of lifters configurations on the RTD: no lifters (NL), grid (G), 3 and 6 rows of straight lifters (3SL, 6SL). Operating conditions: 3 rpm rotation speed, 2° slope, 5 kg.h^{-1} MFR. For the runs using NL, 3SL and 6SL, there are 2 replicates. Solid lines are the axial dispersion model of the n°1 replicate.	140
5.5	Lifters hold-up for three configurations, from left to right side: 3SL, 6SL and 12SL.	141
5.6	Influence of operating parameters (N, S and \dot{M}) on the MRT, HU[%] and VRT, for the flow of beech chips, when the kiln is equipped without lifters, with a grid, or with 3 and 6 rows of straight lifters.	142
5.7	Influence of operating parameters (N, S and \dot{M}) on the RTD for the flow of beech chips, when the kiln is equipped with 6 rows of straight lifters. Solid lines represent the axial dispersion model using fitted parameters.	143
5.8	Influence of operating parameters (N, S and \dot{M}) on the Pe and D, for the flow of beech chips, when the kiln is equipped with a grid, or with 3 and 6 rows of straight lifters.	146
5.9	Comparison of the experimental MRT, HU[%] and D, while using sand (left), broken rice (middle), and beech chips (right), with the calculated values from Eq.5.9 using the sets of parameters given in Table 5.3. Solid lines are $\pm 20\%$ margins.	148
5.10	Influence of operating parameters N (a-d-g-j), S (b-e-h-k) and \dot{M} (c-f-i-l) on the tracer average weight (function of dimensionless time) for the flow of beech chips, when the kiln is equipped with: NL (1st row), G (2nd row), 3SL (3rd row) and 6SL (4th row). The dimensionless time is defined as $\theta = t/\bar{t}$ and so the red lines represent the time when $t = \bar{t}$	150
5.11	Reproducibility of segregation of beech chips when the kiln is operated within the defined benchmark value for the operating parameter, and equipped with 3 or 6 rows of straight lifters or without lifters.	152
6.1	Layout of the experimental apparatus: (1) feed hopper, (2) screw feeder, (3) feed chute, (4) kiln tube, (5) heating system, (6) external thermocouples, (7) measuring rod with thermocouples, (8) storage tank.	162
6.2	Lifters profiles: a) straight lifters (SL) and b) rectangular lifters (RL).	163

6.3	Exit dam designs.	163
6.4	Layout of the experimental apparatus heating zones, longitudinal (left side) and transverse (right side) sections: (1) kiln tube, (2) insulation, (3) measuring rod with N-type thermocouples, (4) outer wall K-type thermocouples, (5) air, (6) heating resistors. The given dimensions in the drawing are in mm.	164
6.5	Location of thermocouples in a cross section of the kiln.	166
6.6	Experimental temperature profiles measured at the kiln outer wall and in the freeboard gas. Operating conditions: 2 rpm rotation speed, 3° slope, no solids flow, 33.5 mm exit dam height with straight lifters, and a setpoint temperature of 300° C in zone 2. The presented wall and gas temperature profiles are the average of measurements within the sections (S1-S5) defined in Figure 6.4.	166
6.7	Experimental temperature profiles measured at the kiln outer wall, in the solids bed and in the freeboard gas. Operating conditions: 2 rpm rotation speed, 3° slope, 2.5 kg.h ⁻¹ MFR, 33.5 mm exit dam height with straight lifters, and a setpoint temperature of 300° C in zone 2. The presented wall and gas temperature profiles are the average of measurements within the sections (S1-S5) defined in Figure 6.4.	167
6.8	Comparison of the experimental gas temperature profile, with the predictions by Eq.6.6 using the convection HTC resulting from methods 1, 2 and 3.	170
6.9	Values of J, the criterion in performance assessments, for the experimental runs presented in Table 6.2.	171
6.10	Variation of the wall-to-gas heat transfer coefficient with: a) lifter effective length (involved in the heat transfer), b) kiln rotational speed, c) temperature.	172
6.11	Comparison of experimental Nusselt number with predicted values from Eq.6.8 using the set of parameters given in Table 6.3. Solid lines are ±20% margins.	173
6.12	Experimental results obtained for the wall-to-solid heat transfer coefficient for the run which experimental temperature profiles are presented in Figure 6.7.	175
6.13	Variation of the wall-to-solid heat transfer coefficient with the filling degree for different temperatures: a) 100°C and b) 300°C.	176
6.14	Variation of the wall-to-solid heat transfer coefficient with the kiln rotational speed at a) constant flow rate and b) constant filling degree, while using straight lifters and an exit dam (33.5 mm in height).	176
6.15	Biot number calculated for each run using the determined a) wall-to-gas and b) wall-to-solid heat transfer coefficient.	177
6.16	Temperature profile of the internal wall and of the root of straight lifters measured using a pyrometer.	181
7.1	Features equipping the kiln: a) straight lifters (SL), b) rectangular lifters (RL) and c) exit dams.	187
7.2	Layout of the experimental apparatus heating zones, longitudinal (left side) and transverse (right side) sections: (1) kiln tube, (2) insulation, (3) measuring rod with N-type thermocouples, (4) outer wall K-type thermocouples, (5) air, (6) heating resistors. The given dimensions in the drawing are in mm.	188
7.3	Experimental temperature profiles measured at the kiln outer wall, in the solids bed and in the freeboard gas. Operating conditions: 2 rpm rotation speed, 3° slope, 2.5 kg.h ⁻¹ MFR, 33.5 mm exit dam height with straight lifters, and a setpoint temperature of 300°C in zone 2. The given wall and gas temperature profiles are the average of measurements within the sections S1 to S5 defined in Figure 7.2.	190

7.4	Experimental temperature profiles measured at the kiln outer wall, in the solids bed and in the freeboard gas. Operating conditions: 2 rpm rotation speed, 3° slope, 2.5 kg.h ⁻¹ MFR, 33.5 mm exit dam height with straight lifters, and a setpoint temperature of 300°C in zone 1 and 2. The given wall and gas temperature profiles are the average of measurements within the sections (S1-S5) defined in Figure 7.2.	191
7.5	Heat transfer mechanisms in the cross section of indirectly (left) and directly (right) heated rotary kilns equipped with lifters. Herein: 1) exposed wall (ew), 2) heating elements, 3) exposed bed (eb), 4) covered wall (cw), covered bed (cb). In addition: g stands for gas, and fs for falling solids.	192
7.6	Kiln sections with nomenclature of the heat transfer areas, the bed depth and the filling angle.	195
7.7	Experimental and calculated bed depth profiles in zone 2 for varying operating conditions without lifters. Eq.7.17 is used for the determination of the kiln bed depth. The standard deviation of the calculated bed depth with respect to the experimental measurements is also given.	196
7.8	Time variation of the wall-to-solid heat transfer coefficient for both runs, of which the experimental temperature profiles are represented in Figures 7.3 and 7.4. . .	198
7.9	Effect of the convection and radiation heat transfers on the calculated value of the wall-to-solid heat transfer coefficient at different setpoint temperatures in zone 2: a) 100°C, b) 300°C and c) 500°C, while varying the mass flow rate, and operating at a rotational speed of 2 rpm, a kiln slope of 3°, an exit dam height of 33.5 mm and with straight lifters.	199
7.10	Variation of the wall-to-solid heat transfer coefficient with the filling degree at different setpoint temperatures in zone 2: a) 100°C and b) 300°C, while varying the lifters, the exit dam and the mass flow rate, and operating at a rotational speed of 2 rpm, a kiln slope of 3°.	199
7.11	Variation of the wall-to-solid heat transfer coefficient with the kiln rotational speed at a) constant flow rate and b) constant filling degree, while heating in both zones 1 and 2, and operating a slope of 3°, with straight lifters and an exit dam (33.5 mm in height).	200
7.12	Comparison of experimental wall-to-solid heat transfer coefficients with predictions from Eq.7.21 using the set of parameters given in Table 7.3. Solid lines are ±20% margins.	201
7.13	Comparison of the experimental wall-to-solid heat transfer coefficients with the predicted values from the correlations of: a) [Wes 1976a], b) [Tscheng 1979], c) [Li 2005]. Solid lines are ±20% margins.	202
7.14	Bed depth measuring rod and position of the stems.	207
7.15	Experimental procedure for the bed depth measurement.	208
8.1	Comparison of bed depth predictions with experimental measurements. Notice that the mass flow rate is determined within ±0.3 kg.h ⁻¹	216
8.2	Comparison of the predictions from the author's model with those from the [Saeman 1951] model for the transient response of the bed depth 1 m from the inlet end, following a positive step in the mass flow rate between 0.9 and 2.7 kg.h ⁻¹ , while operating at a rotational speed of 2 rpm, a kiln slope of 3°, an exit dam height of 33.5 mm and without internal fixtures.	219

8.3	Comparison of the predictions from the author's model with those from the [Saeman 1951] model for the transient responses of the bed depth 1 m from the inlet end, following: a) a positive and b) a negative step in the mass flow rate between 1.7 and 2.8 kg.h ⁻¹ , while operating at a rotational speed of 2 rpm, a kiln slope of 3°, an exit dam height of 33.5 mm and with straight lifters.	219
8.4	(a) Heat transfer mechanisms and (b) definition of heat transfer areas	220
8.5	Layout of the experimental apparatus heating zones, longitudinal (left side) and transverse (right side) sections: (1) kiln tube, (2) insulation, (3) measuring rod with N-type thermocouples, (4) outer wall K-type thermocouples, (5) air, (6) heating resistors. The dimensions given in the figure are in mm.	223
8.6	Schematic diagram showing input and output data of the global model.	225
8.7	Comparison of simulation results namely, the wall, bed and gas axial temperature profiles after 1 and 5 h of heating zone 2 at 100°C, while using the bed depth profile from the author's model, displayed as solid lines, and the Saeman model, displayed as dashed lines. The kiln is equipped with straight, rectangular or no lifters and operated at a rotational speed of 2 rpm, a kiln slope of 3°, an exit dam height of 33.5 mm and a mass flow rate of 2.5 kg.h ⁻¹ . An ambient temperature of 20°C is used for the simulation. The solid red lines indicate the heating temperature and heated zone.	226
8.8	Comparison of the bed, gas and wall temperature transient responses at the sections S1 to S5 as given in Figure 8.5 with experimental data whose operating conditions are given in Table 8.7. The labels 1 to 5 refer to the position of sections S1 to S5.	227
8.9	Results of the sensitivity analysis of the bed temperature to some model and operating parameters: at the top, the axial sensitivity coefficients and at the bottom the average sensitivity coefficients when the kiln is heated in zone 2 at 300°C, without lifters, and operated at a rotational speed of 2 rpm, a kiln slope of 3°, an exit dam height of 33.5 mm and a mass flow rate of 2.5 kg.h ⁻¹ . An ambient temperature of 20°C was used for the simulation.	228
8.10	Simulation results of the transient responses of the bed temperature at sections S1 to S5 as given in Figure 8.5, following: a) a positive and b) a negative step in the mass flow rate between 1.8 and 2.7 kg.h ⁻¹ , while operating at a rotational speed of 2 rpm, a kiln slope of 3°, an exit dam height of 33.5 mm and with straight lifters, when heating zone 2 at 300°C. The corresponding bed depth profiles are given in Figure 8.3. The labels 1 to 5 refer to the position of sections S1 to S5.	229
B.1	Influence of operating parameters (N, S, \dot{M} and exit dam height) on the RTD for the flow of sand, when the kiln is equipped with straight lifters. Solid lines represent the axial dispersion model using fitted parameters. Dashed lines represent the axial dispersion model using theoretical parameters.	251
B.2	Influence of operating parameters (N, S, \dot{M} and exit dam height) on the RTD for the flow of sand, when the kiln is equipped with rectangular lifters. Solid lines represent the axial dispersion model using fitted parameters. Dashed lines represent the axial dispersion model using theoretical parameters.	252
B.3	Influence of operating parameters (N, S, \dot{M} and exit dam height) on the RTD for the flow of broken rice, when there is no internal fixture at the kiln wall. Solid lines represent the axial dispersion model using fitted parameters. Dashed lines represent the axial dispersion model using theoretical parameters.	253

B.4	Influence of operating parameters (N, S, \dot{M} and exit dam height) on the RTD for the flow of broken rice, when the kiln is equipped with straight lifters. Solid lines represent the axial dispersion model using fitted parameters. Dashed lines represent the axial dispersion model using theoretical parameters.	254
B.5	Influence of operating parameters (N, S, \dot{M} and exit dam height) on the RTD for the flow of broken rice, when the kiln is equipped with rectangular lifters. Solid lines represent the axial dispersion model using fitted parameters. Dashed lines represent the axial dispersion model using theoretical parameters.	255
B.6	Influence of operating parameters (N, S and \dot{M}) on the RTD for the flow of beech chips, when there is no internal fixture at the kiln wall. Solid lines represent the axial dispersion model using fitted parameters. Dashed lines represent the axial dispersion model using theoretical parameters.	256
B.7	Influence of operating parameters (N, S and \dot{M}) on the RTD for the flow of beech chips, when the kiln is equipped with a grid. Solid lines represent the axial dispersion model using fitted parameters. Dashed lines represent the axial dispersion model using theoretical parameters.	257
B.8	Influence of operating parameters (N, S and \dot{M}) on the RTD for the flow of beech chips, when the kiln is equipped with 3 rows of straight lifters. Solid lines represent the axial dispersion model using fitted parameters. Dashed lines represent the axial dispersion model using theoretical parameters.	258
B.9	Influence of operating parameters (N, S and \dot{M}) on the RTD for the flow of beech chips, when the kiln is equipped with 6 rows of straight lifters. Solid lines represent the axial dispersion model using fitted parameters. Dashed lines represent the axial dispersion model using theoretical parameters.	259
B.10	Bed depth measurements.	260
C.1	One series of thermocouples in a cross section of the kiln	261
C.2	Temperature profiles of kiln wall, solids and freeboard gas. Operating conditions: 2 rpm rotation speed, 3° slope, 0.9 kg.h ⁻¹ MFR, 33.5 mm exit dam height using rectangular lifters, with a setpoint temperature of 100°C in zone 2.	262
C.3	Temperature profiles of kiln wall, solids and freeboard gas. Operating conditions: 2 rpm rotation speed, 3° slope, 2.5 kg.h ⁻¹ MFR, 33.5 mm exit dam height using rectangular lifters, with a setpoint temperature of 100°C in zone 2.	263
C.4	Temperature profiles of kiln wall and freeboard gas. Operating conditions: 2 rpm rotation speed, 3° slope, no solids flow, 33.5 mm exit dam height using rectangular lifters, with a setpoint temperature of 100°C in zone 2.	264
C.5	Temperature profiles of kiln wall, solids and freeboard gas. Operating conditions: 2 rpm rotation speed, 3° slope, 0.9 kg.h ⁻¹ MFR, 33.5 mm exit dam height without lifters, with a setpoint temperature of 100°C in zone 2.	265
C.6	Temperature profiles of kiln wall, solids and freeboard gas. Operating conditions: 2 rpm rotation speed, 3° slope, 0.9 kg.h ⁻¹ MFR, 33.5 mm exit dam height without lifters, with a setpoint temperature of 300°C in zone 2.	266
C.7	Temperature profiles of kiln wall, solids and freeboard gas. Operating conditions: 2 rpm rotation speed, 3° slope, 2.5 kg.h ⁻¹ MFR, 33.5 mm exit dam height without lifters, with a setpoint temperature of 100°C in zone 2.	267
C.8	Temperature profiles of kiln wall, solids and freeboard gas. Operating conditions: 2 rpm rotation speed, 3° slope, 2.5 kg.h ⁻¹ MFR, 33.5 mm exit dam height without lifters, with a setpoint temperature of 300°C in zone 2.	268

C.9	Temperature profiles of kiln wall and freeboard gas. Operating conditions: 2 rpm rotation speed, 3° slope, no solids flow, 33.5 mm exit dam height without lifters, with a setpoint temperature of 100°C in zone 2.	269
C.10	Temperature profiles of kiln wall and freeboard gas. Operating conditions: 2 rpm rotation speed, 3° slope, no solids flow, 33.5 mm exit dam height with straight lifters, and a setpoint temperature of 100°C in zone 2.	270
C.11	Temperature profiles of kiln wall and freeboard gas. Operating conditions: 2 rpm rotation speed, 3° slope, no solids flow, 33.5 mm exit dam height with straight lifters, and a setpoint temperature of 300°C in zone 2.	270
C.12	Temperature profiles of kiln wall and freeboard gas. Operating conditions: 2 rpm rotation speed, 3° slope, no solids flow, 33.5 mm exit dam height with straight lifters, and a setpoint temperature of 500°C in zone 2.	271
C.13	Temperature profiles of kiln wall, solids and freeboard gas. Operating conditions: 2 rpm rotation speed, 3° slope, 0.9 kg.h ⁻¹ MFR, 33.5 mm exit dam height with straight lifters, and a setpoint temperature of 100°C in zone 2.	272
C.14	Temperature profiles of kiln wall, solids and freeboard gas. Operating conditions: 2 rpm rotation speed, 3° slope, 0.9 kg.h ⁻¹ MFR, 33.5 mm exit dam height with straight lifters, and a setpoint temperature of 300°C in zone 2.	273
C.15	Temperature profiles of kiln wall, solids and freeboard gas. Operating conditions: 2 rpm rotation speed, 3° slope, 0.9 kg.h ⁻¹ MFR, 33.5 mm exit dam height with straight lifters, and a setpoint temperature of 500°C in zone 2.	274
C.16	Temperature profiles of kiln wall, solids and freeboard gas. Operating conditions: 2 rpm rotation speed, 3° slope, 1.8 kg.h ⁻¹ MFR, 33.5 mm exit dam height with straight lifters, and a setpoint temperature of 500°C in zone 2.	275
C.17	Temperature profiles of kiln wall, solids and freeboard gas. Operating conditions: 2 rpm rotation speed, 3° slope, 2.5 kg.h ⁻¹ MFR, 33.5 mm exit dam height with straight lifters and a setpoint temperature of 500°C in zone 2.	276
C.18	Temperature profiles of kiln wall, solids and freeboard gas. Operating conditions: 2 rpm rotation speed, 3° slope, 2.5 kg.h ⁻¹ MFR, 33.5 mm exit dam height with straight lifters, and a setpoint temperature of 300°C in zone 2.	277
C.19	Temperature profiles of kiln wall, solids and freeboard gas. Operating conditions: 2 rpm rotation speed, 3° slope, 2.5 kg.h ⁻¹ MFR, 33.5 mm exit dam height with straight lifters, and a setpoint temperature of 300°C in zones 1 and 2.	278
C.20	Temperature profiles of kiln wall, solids and freeboard gas. Operating conditions: 2 rpm rotation speed, 3° slope, 2.5 kg.h ⁻¹ MFR, 33.5 mm exit dam height with straight lifters, and a setpoint temperature of 500°C in zone 2.	279
C.21	Temperature profiles of kiln wall, solids and freeboard gas. Operating conditions: 12 rpm rotation speed, 3° slope, 2.5 kg.h ⁻¹ MFR, 33.5 mm exit dam height with straight lifters, and a setpoint temperature of 500°C in zones 1 and 2.	280

List of Tables

1.1	Forms of transverse motion of solids in rotating cylinders [Mellmann 2001]. . . .	30
1.2	Bulk bed and tracer materials used in rotary kiln equipped with internal fixtures from the literature.	33
1.3	Advantages of using lifters [Boateng 2008].	49
1.4	Summary of experimental studies on heat transfer in rotary kilns.	51
1.5	Summary of wall-to-solid heat transfer coefficient correlations.	57
2.1	Selected granular material to be operated at room temperature.	73
2.2	Thermal properties of materials at 300°C.	75
2.3	RK1 Experimental matrix for the RTD measurements using rectangular lifters (RL), straight lifters (SL) and no lifters (NL).	79
2.4	RK2 Experimental matrix for the RTD measurements using no internal fixtures (NL), a grid, 3 rows of straight lifters (3SL), and 6 rows of straight lifters (6SL).	81
2.5	RK1 Experimental matrix for the bed depth measurements without internal fixtures (NL).	83
2.6	RK1 Experimental matrix for the dynamic response measurements using rectangular lifters (RL), straight lifters (SL) and no lifters (NL).	84
2.7	Experimental conditions of experiments within RK1 for the study of heat transfer using rectangular lifters (RL), straight lifters (SL) and no lifters (NL).	86
3.1	Geometrical characteristics of the rotary kiln	95
3.2	Physical properties of materials	96
3.3	Reproducibility of experiments	100
3.4	Parameters for the axial dispersion coefficient in Eq.3.18.	109
4.1	Details of the circular dams at the kiln outlet end	117
4.2	Physical properties of materials	118
4.3	Experimental results	119
4.4	Calculated values of exponents and constant k for the MRT dimensional correlation	124
4.7	Characteristics of differing kilns with their operating parameters range of variation as given in literature.	132
5.1	Geometrical characteristics of the rotary kiln and order of magnitude of operating conditions achieved in this study.	137
5.2	Physical properties of granular materials.	137

5.3	Determined parameters for the models proposed for the mean residence time, the filling degree and the axial dispersion, with associated confidence intervals. . . .	147
5.4	Reproducibility of experiments: experimental hold-up, mean residence time, variance of residence time, Peclet number and axial dispersion.	152
5.8	Results of the experimental matrix set for the RTD measurements.	156
6.1	Thermal properties of materials at 300°C.	164
6.2	Results of the experimental wall-to-gas heat transfer coefficient determined from Methods 1, 2 and 3. NC stands for non convergence, when the numerical fitting from method 1 did not converged.	170
6.3	Estimated parameters for the model proposed for the Nusselt number, with associated confidence intervals.	172
6.7	Experimental conditions of the experiments for the study of heat transfer using rectangular lifters (RL), straight lifters (SL) and no lifters (NL).	182
7.1	Characteristics of the experimental setup and order of magnitude of operating conditions.	187
7.2	Thermal properties of materials at 300°C.	188
7.3	Estimated parameters for the model proposed for the wall-to-solid heat transfer coefficient, with associated confidence intervals.	201
7.7	Calculated uncertainties.	208
7.8	Wall-to-solid heat transfer coefficients ($\text{W.m}^{-2}.\text{K}^{-1}$) calculated from Eq.7.8. . .	209
8.1	Parameters for the models used to calculate of the filling degree and the mean residence time [Bongo Njeng 2015c].	215
8.2	Physical properties of bulk materials	217
8.3	Experimental matrix for the dynamic response measurements using rectangular lifters (RL), straight lifters (SL) and no lifters (NL).	218
8.4	Experimental values of $d\dot{M}/dt$ used by the model presented for the prediction of the transient response of the bed depth.	218
8.5	Value of coefficient A and m for Eq.8.23.	222
8.6	Thermal properties of materials at 300°C.	224
8.7	Experimental conditions of the experiments for the study of heat transfer using rectangular lifters (RL), straight lifters (SL) and no lifters (NL).	224
8.11	Main characteristics and order of magnitude of operating conditions of the rotary kiln used.	233
8.12	Model parameters used for the simulations.	234
A.1	Comparison of the main characteristics and order of magnitude of operating conditions of the rotary kilns used, RK1 and RK2.	247

“Was mich nicht umbringt, macht mich stärker. (What does not destroy me, makes me stronger.)”

(Friedrich Nietzsche, 1844-1900)

Doctorat de l'Université Fédérale de Toulouse Midi-Pyrénées
Délivré par l'École des Mines d'Albi-Carmaux, conjointement avec l'INP Toulouse
École doctorale MEGeP
Spécialité Énergétique et Transferts
Laboratoires RAPSODEE et CMGPCE
Soutenue le 04 novembre 2015
BONGO NJENG Alex

Étude et modélisation de fours tournants équipés de releveurs

Résumé

Ce travail porte sur l'étude de fours tournants équipés de releveurs. Ce sont des contacteurs gaz/solide largement répandus dans de nombreux secteurs industriels mettant en œuvre des solides divisés. Cependant en raison d'une faible connaissance du fonctionnement de ces équipements notamment en matière d'écoulement ou de transfert thermique, leur utilisation repose encore beaucoup sur le savoir faire des opérateurs acquis avec le temps. Ainsi ce travail vise à fournir aux ingénieurs des outils de connaissance et d'extrapolation pour les accompagner dans les phases de dimensionnement, mais aussi d'optimisation de procédés existants, en particulier pour des fours tournants en chauffage indirect et équipés de releveurs.

La première partie de cette étude porte sur l'influence des conditions opératoires sur l'hydrodynamique des solides divisés de forme et taille différentes. Pour ce faire, des procédures expérimentales pour la mesure de distribution des temps de séjours des particules solides ont été mises en œuvres. Deux pilotes de four tournant ont été utilisés. Ces derniers ont un ratio longueur sur diamètre équivalent mais un ratio de taille de 2. L'hydrodynamique des fours a été caractérisée quantitativement à partir des résultats expérimentaux en terme de temps de séjour des solides, taux de remplissage du four ainsi que de la dispersion axiale des particules. Ces derniers ont été modélisés par analyse dimensionnelle dans un souci de généralité en prenant en compte la présence d'éléments internes (releveurs, grille) ou diaphragmes en sortie, mais aussi des paramètres opératoires tels que la vitesse de rotation du tube, son inclinaison ou le débit des particules solides.

La seconde partie de cette étude s'intéresse aux processus de transfert thermique dans les fours tournants en chauffage indirect et équipés de releveurs. Cette étude repose sur la mesure des profils de température à la paroi, dans la phase gazeuse et le lit de particules solides. L'analyse de ces profils de température se focalise sur la détermination des coefficients de transfert de chaleur entre la paroi et le lit de solides d'une part, et entre la paroi et le gaz d'autre part. Une méthode d'analyse globale de système mince et un bilan global intégrant la puissance fournie pour la chauffe sont utilisés pour la détermination de ces coefficients de transfert. Les résultats obtenus permettent d'une part de mettre en évidence l'effet des releveurs ainsi que l'influence des paramètres opératoires sur ces coefficients de transfert de chaleur et d'autres part d'établir par analyse dimensionnelle des modèles pour ces derniers. Enfin, ce travail se termine par la mise en place d'un modèle dynamique simplifié de four tournant en chauffage indirect permettant la détermination des profils de température le long du four et pouvant être facilement adapté à divers procédés.

Mots clés : Fours Tournants, Releveurs, Analyse Dimensionnelle, DTS, Coefficient de Transfert de Chaleur, Modèle Dynamique.

Doctorat de l'Université Fédérale de Toulouse Midi-Pyrénées
Délivré par l'École des Mines d'Albi-Carmaux, conjointement avec l'INP Toulouse
École doctorale MEGeP
Spécialité Énergétique et Transferts
Laboratoires RAPSODEE et CMGPCE
Soutenue le 04 novembre 2015
BONGO NJENG Alex

Experimental study and modeling of hydrodynamic and heating characteristics of flighted rotary kilns

Abstract

The present work addresses a fundamental study on flighted rotary kilns. They are gas-solid reactors, used in a variety of industries to process heterogeneous media. However, operating these kilns mainly relies on the know-how of operators due to insufficient fundamental understanding. The aim of this work is to provide engineers with relevant tools and models to assist in the design stage and the performance improvement of existing operating process units, in particular indirectly heated rotary kilns, inclined and equipped with lifters.

In the first part, we studied the effects of operating parameters on the flow of materials of differing properties and shape. For this purpose, residence time distribution measurements were performed through experimental stimulus response tests. Two pilot-scale rotary kilns with similar length-to-diameter ratios, but a dimension ratio of about two were used in this study. We focused on the effects of lifter shape and configurations. The effects of the rotational speed, the kiln slope, the mass flow rate and the exit dam height were also analyzed. The flow of solids was quantitatively characterized primarily by the experimental mean residence time, hold-up, and axial dispersion coefficient. Using a dimensional analysis, models were established to predict the mean residence time, the filling degree and the axial dispersion coefficient, providing basic information on the kiln design, solid particle properties and operating conditions.

In the second part, we studied the heat transfer mechanisms occurring in the flighted rotary kiln by measuring temperature profiles at the wall, the freeboard gas and the bulk of solids. Analysis of the temperature profiles focused on two main issues : assessment of the heat transfer coefficient between wall and gas, and assessment of the heat transfer coefficient between wall and solid particles. The lumped system analysis and a heat balance using the power supplied for the heating were applied to determine the experimental heat transfer coefficients. The effects of operating conditions and lifting flights were analyzed. Both heat transfer coefficients were then correlated through dimensional considerations. Lastly a global dynamic model mainly based on the models developed in this study can be used to determine wall, gas and bulk solids axial temperature profiles in an indirectly heated flighted rotary kiln. This global model needs to be completed with specific models related to a reaction so as to be used as a framework for the simulation of specific industrial rotary kilns.

Keywords : Rotary Kilns, Lifters, Dimensional Analysis, RTD, Heat Transfer Coefficient, Dynamic Model.